Title

Hydroarylations of C-C Multiple Bonds Catalyzed by Late-Metal Complexes: Mechanistic Investigations

Permalink

https://escholarship.org/uc/item/4gg1m6nv

Author

Suslick, Benjamin Adam

Publication Date

2019

Peer reviewed|Thesis/dissertation

Hydroarylations of C–C Multiple Bonds

Catalyzed by Late-Metal Complexes:

Mechanistic Investigations

by

Benjamin Adam Suslick

A dissertation submitted in partial satisfaction of the
Requirements for the degree of
Doctor of Philosophy
in
Chemistry
in the
Graduate Division
of the
University of California, Berkeley

Committee in charge:

Professor T. Don Tilley, Chair
Professor Robert G. Bergman
Professor Alexis T. Bell

Fall 2019

Abstracts
Hydroarylations of C–C Multiple Bonds Catalyzed by Late-Metal Complexes:
Mechanistic Investigations

Benjamin Adam Suslick
Doctor of Philosophy in Chemistry
University of California, Berkeley
Professor T. Don Tilley, Chair

Chapter One

Undirected and Directed Hydroarylations Catalyzed by Late-Transition Metals: An Introductory Review. Recent investigations into homogeneous catalytic hydroarylations of olefins have focused heavily on catalyst precursors bearing a d^8 electronic configuration. This chapter discusses such cases in the context of olefin hydroarylations with benzene and substituted arenes. More specifically, it discusses three types of olefin hydroarylation by d^8 catalysts: those involving unfunctionalized arenes (e.g., benzene and alkyl arenes), those assisted (and directed) by ortho-arene donor groups, and finally palladium-catalyzed hydroarylations that involve reaction sequences of a Heck-type coupling followed by reduction of the C=C double bond with an exogenous hydrogen source. Since hydroarylation requires both aryl C–H activation and olefin-insertion steps, Pt has proven to be the focus in the early developments of hydroarylation catalysis. There is current interest in the development of homogeneous transition metal catalysts for selective, direct hydroarylation of α-olefins with arenes. Given the history of research in this area, it seems that d^8 precatalysts are promising candidates for future development.

Suslick, B. A.; Tilley, T. D. In *Catalytic Hydroarylation of Carbon-Carbon Multiple Bonds*; Ackermann, L., Gunnoe, T. B., Habgood, L. G., Eds.; Willey-VCH: Weinheim, 2017, p 107–174.

Chapter Two
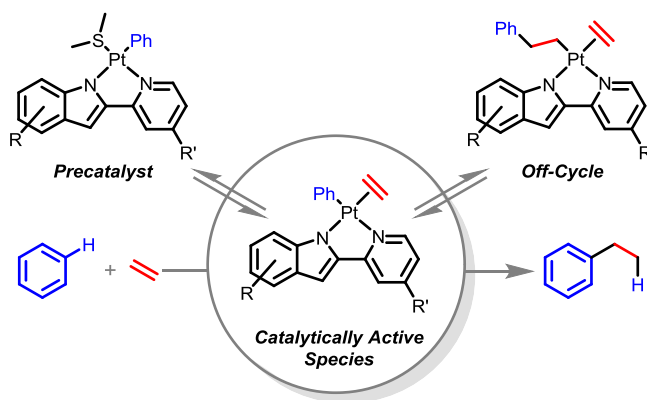
Olefin Hydroarylation Catalyzed by (Pyridyl-Indolate)Pt(II) Complexes: Catalytic Efficiencies and Mechanistic Aspects. A series of Pt(II) complexes of the type (PyInd)PtPh(SR$_2$) (PyInd= 2,2′-pyridyl-indolate) were prepared, and their performance as catalysts for the hydroarylation of olefins was assessed. Evidence that the catalysis is homogeneous and Pt mediated is provided by control experiments with added hindered base (2,6-di-*tert*-butyl-4-methylpyridine) and Hg(0). Two potential catalytic intermediates, (*t*BuPyInd)PtPh(C$_2$H$_4$) and (*t*BuPyInd)Pt(CH$_2$CH$_2$Ph)(C$_2$H$_4$), were synthesized and their catalytic efficacy

was explored. Additionally, decomposition and deactivation pathways, including styrene formation *via β*-hydride elimination and ligand reductive demetallation, were identified.

Suslick, B. A.; Liberman-Martin, A. L.; Wambach, T. C.; Tilley, T. D. *ACS Catal.* **2017**, *7*, 4313–4322.

Chapter Three
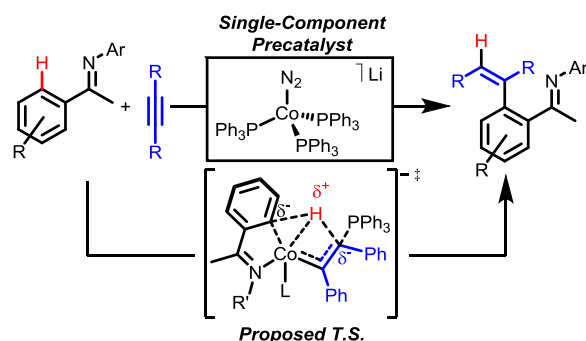
Proposed T.S.

Mechanistic Interrogation of Alkyne Hydroarylations Catalyzed by Highly Reduced, Single-Component Cobalt Complexes. Highly reactive catalysts for *ortho*-hydroarylations of alkynes have previously been reported to result from activation of CoBr$_2$ by Grignard reagents, but the operative mechanism and identity of the active cobalt species remain unidentified. A thorough mechanistic analysis of a related system was performed using isolable reduced Co complexes. Stoichiometric treatment of Co(I) or Co(II) precursors with CyMgCl implicated catalyst initiation via a β-H elimination and deprotonation pathway. The resulting single-component Co(-I) complex is proposed as the direct precatalyst. Michaelis-Menten enzyme kinetic studies elucidated the catalytic dependence on substrate. The (*N*-aryl)aryl ethanimine substrate exhibited saturation-like behavior whereas alkyne demonstrated a complex dependency; rate inhibition and promotion depends on the relative alkyne to imine concentration. Activation of the aryl C–H bond occurred only in the presence of coordinated alkyne, which suggests operation of a concerted metalation-deprotonation (CMD) mechanism. Small primary isotope effects are consistent with a rate-determining C–H cleavage. Off-cycle olefin isomerization catalyzed by the same Co(-I) active species appears to be responsible for the observed *Z*-selectivity.

Chapter Four
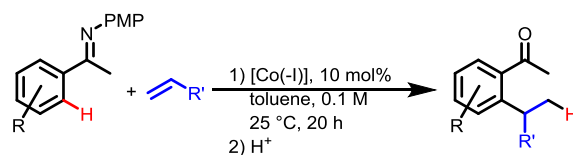
Inexpensive, scalable, single-component catalyst:
- Regioselective
- > 40 examples
- Typical yields > 60%
- Mild conditions

Olefin Hydroarylations Catalyzed by a Single-Component Cobalt(-I) Complex. A single-component Co(-I) catalyst has been developed for olefin hydroarylations with (*N*-aryl)aryl imine substrates. Over 40 examples were examined under mild reaction conditions to afford the desired alkyl-arene product in good to excellent yields. Catalysis occurs in a regioselective manner to afford exclusively branched products with styrene-derived substrates or linear products for aliphatic olefins. Electrophilic functional groups were generally tolerated under the reaction conditions.

Hydroarylations of C–C Multiple Bonds Catalyzed by Late-Metal Complexes: Mechanistic Investigations

Table of Contents

Dedication

For without my wonderful, loving father, Ken, none of this would be possible.

"Christmas time is here, by golly, / Disapproval would be folly / Deck the halls with hunks of holly / Fill the cup and don't say "when." / Kill the turkeys, ducks and chickens, / Mix the punch, drag out the dickens, / Even though the prospect sickens, / Brother, here we go again.

On Christmas day you can't get sore, / Your fellow man you must adore, / There's time to rob him all the more / The other three hundred and sixty-four.

Relations, sparing no expense'll / Send some useless old utensil, / Or a matching pen and pencil. / "just the thing I need! how nice!" / It doesn't matter how sincere it / Is, nor how heartfelt the spirit, / Sentiment will not endear it, / What's important is the price.

Hark the herald tribune sings, / Advertising wondrous things. / God rest ye merry, merchants, / May you make the yuletide pay. / Angels we have heard on high / Tell us to go out and buy!

So let the raucous sleigh bells jingle, / Hail our dear old friend kris kringle, / Driving his reindeer across the sky. / Don't stand underneath when they fly by."
– A Christmas Carol by Tom Lehrer

"It's not time to make a change, / Just relax, take it easy / You're still young, that's your fault, / There's so much you have to know / Find a girl, settle down, If you want you can marry / Look at me, I am old, but I'm happy

I was once like you are now, and I know that it's not easy, / To be calm when you've found something going on / But take your time, think a lot, / Why, think of everything you've got / For you will still be here tomorrow, but your dreams may not

How can I try to explain, when I do he turns away again / It's always been the same, same old story / From the moment I could talk I was ordered to listen / Now there's a way and I know that I have to go away / I know I have to go

It's not time to make a change, / Just sit down, take it slowly / You're still young, that's your fault, / There's so much you have to go through / Find a girl, settle down, / If you want you can marry / Look at me, I am old, but I'm happy

All the times that I cried, keeping all the things I knew inside, / It's hard, but it's harder to ignore it / If they were right, I'd agree, but it's them you know not me / Now there's a way and I know that I have to go away / I know I have to go"
– Father and Son, by Cat Stevens

"Tim Finnegan lived in Walkin Street / A gentle Irishman, mighty odd /He'd a beautiful brogue so rich and sweet /And to rise in the world he carried a hod / You see he'd a sort of the tipp' lin' way / With the love of the liquor, poor Tim was born / And to help him on with his work each day / He'd a drop of the craythur every morn

Whack fol the da, now, dance to your partner / Welt the floor your trotters shake / Wasn't it the truth I tell you Lots of fun at Finnegan's wake

One mornin' Tim was rather full /His head felt heavy, which made him shake / He fell from the ladder and he broke his skull / And they carried him home his corpse to wake / They rolled him up in a nice clean sheet / And laid him out upon the bed / With a gallon of whiskey at his feet / And a barrel of porter at his head
*
His friends assembled at the wake / And Mrs. Finnegan called for lunch / First they brought in tay and cake / Then pipes, tobacco and whiskey punch / Biddy O'Brien began to cry / "Such a nice clean corpse did you ever see? / Tim Mavourneen why did you die?" / "Arrah hold your gob" said Paddy McGee
*
Then Maggie O'Connor took up the job / "O Biddy, " says she "you're wrong I'm sure" / Biddy gave her a belt in the gob / And left her sprawling on the floor / Then the war did soon engage /It was woman to woman and man to man / Shillelagh law was all the rage /And a row and a ruction soon began
*
Then Mickey Maloney raised his head / When a bucket of whiskey flew at him / It missed and falling on the bed / The liquor scattered over Tim / Tim revives, see how he rises / Timothy rising from the bed /Said "Whirl your whiskey around like blazes / Thundering Jesus, do you think I'm dead?""
– Finnegan's Wake by The Dubliners

Acknowledgments

"You are only given one little spark of madness. You mustn't lose it" – Robin Williams

A Ph.D. is not a solo exercise, nor is it a sprint. Much like a marathon, there are many folks who have helped me over the years in numerous and invaluable ways; I owe you my eternal thanks. I have tried to categorize (in no particular order) the various comrades, friends, family, and mentors who have supported me throughout this journey. I offer you, the reader, words of wisdom from some of my favorite witticists, comedians, philosophers, actors, and movie characters.

"I think I am, therefore I am. I think." – George Carlin

"Believe you can do it 'cause you *can* do it" – Bob Ross

<u>Advisor:</u> "Do. Or do not. There is no try." – Yoda, Star Wars Episode V, Lucasfilm, 1980

First and foremost, I would like to thank my advisor, Professor T. Don Tilley. It really has been my pleasure to work with you over the last five and a half years and for that I am in your debt. I have learned so a great deal from my time under your tutelage. I will always look back on graduate school fondly!

"In my experience, there is no such thing as luck." – Obi-wan Kenobi, Star Wars Episode IV, Lucasfilm, 1977

"Don't fear failure. Not failure, but low aim, is the crime. In great attempts it is glorious even to fail." – Bruce Lee

<u>Family</u>: "Time flies like an arrow, fruit flies like a banana" – Groucho Marx

Obviously, I would not have gotten as far as I have without the support of my loving parents: Ken and Patricia. Dad, you have always been there for me whenever I needed it; you always believed in me and I certainly hope that this thesis will make you proud! To my extended family (Suslicks and Mazureks), thank you for always being happy to see me. Having smiling, loving family makes even the darkest times seem bright.

"Take care of yourself, Ken. Thank you for the pen." – Martin Blank, Grosse Point Blank, Buena Vista Pictures, 1997

"I was thinking of the immortal words of Socrates, who said '… I drank what?'" – Chris Knight, Real Genius, TriStar Pictures, 1985

<u>Non-Lab Friends:</u> "Friends help you move. Good friends help you move bodies. Best friends bring their own shovels" – anonymous

There are many friends which I wish to thank. I would like to thank my close group of grad student friends: Chris Kaplan, Steven Lyle, and Thomas "2-chains" Popp. You all have made grad school a lot more fun (and certainly gave me an outlet to vent my frustrations). Chris, you get a second thank you for being a wonderful (and mostly clean) flat mate for the last five years. To my Caltech friends who have been there for me along the way, thanks! Special shout out to my Caltech friends in Berkeley (Dryden Bouamalay, Alison Lui, Megan Jackson, and Linda Chio).

"Lots of my friends have babies, but I don't have any babies. But I have lots of friends; babies don't have any friends. They all have those baby-monitors so they can hear the baby from the other room, which I consider a form of wiretapping. One day, there's gonna be a really smart baby who makes a fake recording of some fake baby noises… gonna crawl out of the window and go to Italy" – Steven Wright

"Michael, I did nothing. I did absolutely nothing, and it was everything I thought it could be." – Peter Gibbons, Office Space, Twentieth Century Fox, 1999

Mentors: "Time is the best teacher; unfortunately, it kills all of its students." – Robin Williams

Needless to say, I have had *many* talented mentors and teachers in my time. Learning is unlike osmosis – you cannot just absorb information from falling asleep on a textbook – it requires a patient teacher to show you the door of knowledge. Only then can one pass the threshold into understanding.

My time in the Suslick group first introduced me to chemistry; as such thank you, Liang Feng, Sung Lim, Jonathon Kemling, Christopher Musto, and Dave Flannigan, for not scaring me away from science when I was in high-school. Also I'd like to thank my high-school chemistry teacher, Dave Bergandine.

In high-school, I was in the Girolami group and had my first taste of inorganic synthesis. Thanks to Prof. Gregory Girolami, Andrew Dunbar, Noel Chang, and Scott Daly for setting me on the path I currently tread.

My nearly three years in the Grubbs group as an undergraduate researcher were perhaps the most exciting time for me. The amount that I learned from my mentors, Prof. Bob Grubbs and Dr. Myles Herbert, is incalculable. Thanks to the group members that I worked with and could call friend: Bill Morandi, Jeff Cannon, Zach Wickens, Garret Miyake, Brendan Quigley, Peter Dornan, Pablo Guzman, Sarah Bronner, Ray Weitekamp, Ben Sveinbjörnsson, John Hartung, Shane Mangold, Lauren Rosebrugh, Alice Chang, Tonia Ahmed, Keith Keitz, and Julian Edwards. I want to also thank some of the influential professors and instructors who taught me when I was attending Caltech: Prof. Harry Gray, Prof. Theo Agapie, Dr. Jeffery Mendez, Prof. Thomas Miller, Prof. John Bercaw, and Prof. Michael Alvarez.

Of course, the bulk of my independent learning has taken place over the course of my Ph.D. at Cal. I would like to thank my close friend and mentor, Allegra Liberman-Martin. To my thesis and qual committees, I owe you my thanks for challenging me: Profs. Robert Bergman, Peter Vollhardt, John Arnold, and Alex Bell. I would also like to thank Bob a second time for teaching me everything I know about physical organic chemistry – your class was, perhaps, the best class I have ever had the pleasure of taking. I would also like to thank the late Prof. Richard Andersen for his words of wisdom; you are sorely missed, Dick.

"In school they told me 'Practice makes perfect.' And then they told me 'Nobody is perfect,' so I stopped practicing" – Steven Wright

"As long as you are learning, you aren't failing" – Bob Ross

Lab Friends: "Basic research is what I am doing when I don't know what I am doing" – Wernher von Braun

I have had the pleasure of working with *many* talented, brilliant individuals in over my Ph.D. career. I want to thank each and everyone one of you for making the Tilley lab as pleasant and educational as it has been (listed in chronological order by year, more or less): Rick Hsueh-Liu, Mike Lipschutz, Allegra Liberman-Martin, Kurt Van Allsburg, Andy Nguyen, John Swierk, Wenjun Liu, Qing Ye, Micah Ziegler, James

"Always go to other people's funerals; otherwise they won't go to yours" – Yogi Berra

"Laughter is involuntary. If it's funny, you laugh" – Tom Lerher

"By the work one knows the workman" – Jean de La Fontaine

"UNLESS someone like you cares a whole awful lot, nothing is going to get better. It's not." Dr. Seuss, The Lorax, Random House, 1971

"What *is* is more important than *what should be*" – Bruce Lee

"Everyone you meet is fighting a battle you know nothing about. Be kind. Always." – Robin Williams

And lastly, this Ph.D. **"was made possible by viewers like you. Thank you." – NPR/PBS**

List of Abbreviations

$(PPh_3)_3RhCl$	Wilkinson's catalyst
$[(PCy_3)(cod)(py)Ir][PF_6]$	Crabtree's catalyst
12-c-4	12-crown-4 or 1,4,7,10-tetraoxacyclododecane
18-c-6	18-crown-6 or 1,4,7,10,13,16-hexaoxacyclooctadecane
acac	acetylacetonate
AgOTf	silver trifluoromethanesulfonate
BPin	4,4,5,5-tetramethyl-1,3,2-dioxaboralane or boronic acid pinacol ester
CMD	concerted metalation deprotonation
cod	cyclooctadiene
coe	cyclooctene
Cp	cyclopentadienyl
Cp*	pentamethylcyclopentadienyl
CyH	cyclohexane
CyMgCl	cyclohexyl magnesium chloride (Cyclohexyl Grignard reagent)
DFT	density functional theory
DHA	9,10-dihydroanthracene
DIPP	2,6-diisopropylphenyl
dme	1,2-dimethoxyethane
dppb	bis(diphenylphosphino)butane
dppe	bis(diphenylphosphino)ethane
dppm	bis(diphenylphosphino)methane
dppp	bis(diphenylphosphino)propane
ee	enantiomeric excess
EI	electron impact ionization
ESI-TOF	electrospray ionization, time of flight
GC-MS	gas chromatography mass spectrometry
HOTf	trifluoromethanesulfonic acid
HOTs	tosylic acid
HRMS	high-resolution mass spectrometry
ICy	N,N-bis(cyclohexyl)imidazolium
IMes	N,N-bis(2,4,6-trimethylphenyl)imidazolium
IPr	N,N-bis(2,6-diisopropylphenyl)imidazolium

IR	infrared
KIE	kinetic isotope effect
LDA	lithium diisopropylamide
Mes	mesityl or 2,4,6-trimethylphenyl
NMR	nuclear magnetic resonance
NTf_2	bis(trifluoromethane)sulfonimide
OAc	acetate
$PCyp_3$	tricyclopentylphosphine
PhCCPh	diphenylacetylene
PHMS	poly(methylhydrosiloxane)
PMP	*para*-methoxyphenyl
PPh_3	triphenylphosphine
py	pyridine
PyInd	pyridyl-indolate
PyPyr	pyridyl-pyrrole
RT	room temperature
^{t}bpy	4,4'-di-tert-buryl-2,2'-bipyridine
TFA	trifluoroacetic acid
TMEDA	N,N,N',N'-tetramethylethylenediamine
TOF	turnover frequency
TON	turnover number
Tp	hydrido-tris(pyrazolyl)borate
triphos	1,1,1-tris(diphenylphosphinomethyl)ethane
T.S.	transition state

Chapter One

Undirected and Directed Hydroarylations Catalyzed by Late-Transition Metals: An Introductory Review

Introduction. Alkylated arenes are essential intermediates in the manufacture of fine chemicals and widely used plastics such as polystyrene. Polystyrene is produced globally on a massive scale and consumed at an annual rate of 1.2×10^7 tons/year.[1-3] En route to polystyrene, styrene is consumed on a comparable scale, at a rate of 2.6×10^7 tons/year.[2,3] A majority of the styrene used in the chemical industry is generated from the dehydrogenation of ethylbenzene (ca. 85%).[1] The synthesis of simple alkyl arenes such as ethylbenzene, therefore, has become a large, profitable industry. While traditional routes to ethylbenzene employ Lewis acid catalysts (e.g., $AlCl_3$/HF) to couple olefins with an arene, current industrial methods typically employ heterogenous catalysts (such as zeolites) to generate ethylbenzene from ethylene and benzene *via* a Friedel-Crafts mechanism.[1,4] Such alkylation systems, however, have drawbacks. The resulting alkyl arene products are often more reactive than the starting materials, which result in undesired polyalkylation. Additionally, catalysis with α-alkene substrates can result in rapid isomerization to an internal olefin, thereby inhibiting generation of the desired anti-Markovnikov, linear alkyl arene.

In academia, synthetic chemists have extensively investigated the process of generating C–C bonds from cheap and abundant feedstocks. While synthetic methods exist to transform simple arenes into more complicated structures (such as the Stille or Suzuki cross-coupling reactions), these routes often require aryl substituents such as SnR_3, BR_2, or ZnX.[5] Installation of these groups can be non-trivial and typically involves additional synthetic steps. Since these substituents are not incorporated into the final product, cross-coupling processes are not atom economical. Moreover, potentially dangerous or toxic waste (*e.g.*, Sn) is generated as a byproduct. As a result, there is a need to directly couple arene C–H bonds with other simple alkyl groups in a selective and efficient manner, using highly active and selective catalysts. In contrast to traditional acid-mediated alkylation catalysis or cross-coupling reactions, transition-metal catalyzed hydroarylation of C–C multiple bonds offer potential advantages.

Recent investigations into homogeneous catalytic hydroarylations of olefins have focused heavily on catalyst precursors bearing a d^8 electronic configuration. This introductory chapter discusses such cases in the context of olefin hydroarylations with benzene and substituted arenes. More specifically, three classes of olefin hydroarylation with late-metal catalysts will be discussed: those involving unfunctionalized arenes (*e.g.*, benzene and alkyl arenes), those assisted (and directed) by *ortho*-arene donor groups, and finally palladium-catalyzed hydroarylations that involve reaction sequences of a Heck-type coupling followed by reduction of the C=C double bond with a hydrogen source. The first two reaction types involve an arene C–H activation and an olefin insertion as key mechanistic steps. The late-transition metals so far identified as hydroarylation catalysis are platinum, rhodium, cobalt, iridium, palladium and nickel. In these studies, the identity of the metal center influences both the operative mechanism as well as the substrate scope.

The simplest (and perhaps most challenging) catalytic hydroarylations involve unfunctionalized arenes and currently only Ni and Pt based systems are known to catalyze such reactions. Research in this area has focused on the coupling of small olefins (*i.e.,* ethylene and propylene) with benzene to generate the corresponding alkyl arene while avoiding over-alkylation (*e.g.,* diethylbenzene formation). For α-olefins such as propylene, Pt catalysts tend to favor branched, Markovnikov alkyl arene products, but new ligand scaffolds exhibit promise for controlling the regioselectivity for production of linear products. Recently reported hydroarylations with nickel complexes indicate that this metal may be promising for the development of new catalyst systems.

With group 9 metals (Co, Rh, and Ir), directed *ortho*-hydroarylation is possible with arenes bearing coordinating functionalities (imines, ketones, aldehydes, etc.). With these substrates, an initial binding of

the aryl directing group orients the *ortho*-aryl hydrogen into a particular position for C–H activation. Alkylation, therefore, only occurs *ortho* to the directing group. Surprisingly, complexes of Rh and Ir appear to inherently impart different regioselectivities for hydroarylation. For Rh complexes, anti-Markovnikov, linear products are favored, whereas branched products are primarily formed with Ir catalysts. In contrast to the well-defined Rh and Ir based systems, Co-based systems involve *in situ* catalyst generation from the treatment of CoX_2 (X = Br, Cl) with Grignard reagents.

In contrast to other late-metal catalyzed hydroarylations, those mediated by Pd have not been reported to promote hydroarylations with unactivated arenes. This difference can perhaps be partially explained by the greater reluctance of palladium to engage in C–H activation processes. However, several studies point to the ability of Pd to mediate hydroarylations with different substrates, namely aryl halides in combination with an olefin. Such reactions resemble Heck couplings, but require an external hydrogen source to accomplish the net addition of aryl and hydrogen groups across the olefin.

Undirected Hydroarylations with Unfunctionalized Arenes Catalyzed by Pt Complexes. Since hydroarylation requires both aryl C–H activation and olefin insertion steps, Pt has proven to be the focus of early developments in hydroarylation catalysis. Significantly, Pt(II) complexes are known to activate aryl and alkyl C–H bonds.[6] In addition, Pt–olefin complexes are known to undergo migratory insertion reactions[7] that functionalize the olefin through an inner sphere pathway. Unlike other transition metal hydroarylation catalysts that require use of a directing aryl substituent or a strained olefin (e.g., norbornene), Pt(II) complexes allow the coupling of simple olefins (e.*g.,* ethylene, propylene) with unfunctionalized arenes (benzene, toluene) to generate alkyl arenes (*e.g.,* ethylbenzene). Several types of supporting ligand systems have been investigated, and in particular complexes bearing neutral and anionic bidentate NN ligands have been described as competent catalysts. Additionally, several other types of non-nitrogen based ligands have been briefly explored.

1: X = H
2: X = F

3

4: X = H
5: X = F

6

7
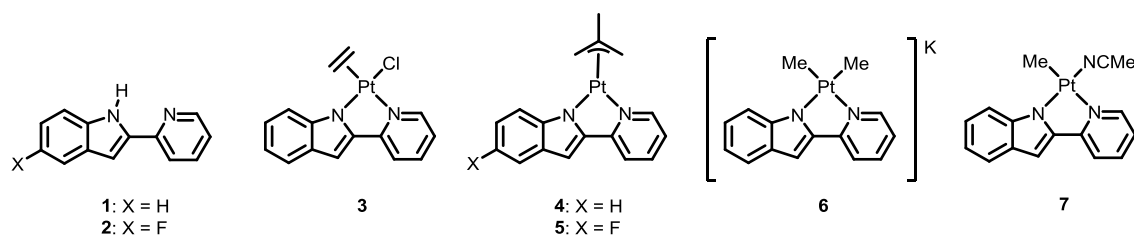
Figure 1.1. PyInd ligated Pt complexes for olefin hydroarylation.[8-10]

Studies of neutral Pt-based catalysts for hydroarylation have employed chelating, nitrogen-donor ligands of the XL type. The first such report, by Tilley and coworkers,[8] involved pyridyl-indolate (PyInd) ligands. These ligands were synthesized by condensation of the appropriate phenyl hydrazine compounds with acetylpyridine, followed by cyclization of the resulting aryl-hydrazone *via* the Fisher-indole reaction to afford the desired PyInd ligand precursors **1** and **2**. The PyInd-based potassium salts were used to obtain various Pt(II) complexes **3-6** (Figure 1.1) by reactions with $[(C_2H_4)PtCl(\mu\text{-Cl})]_2$ (Zeise's dimer), $[(\eta^3\text{-}CH_2CMeCH_2)Pt(\mu\text{-Cl})]_2$, or $[Me_2Pt(\mu\text{-SMe}_2)]_2$, respectively.[8-10] Protonation of the methyl ligand on the anionic complex **6** with $[^iPr_2EtNH][BPh_4]$ in MeCN generated the neutral complex **7**.

The hydroarylation ability of these complexes was examined using norbornene and benzene as substrates (Table 1.1). Complexes **3** and **6** did not exhibit catalytic activity but catalysis was observed with the addition of activating, chloride abstraction reagents such as AgOTf or AgBF$_4$ (for **3**), or the methyl

abstraction reagent $B(C_6F_5)_3$ (for complex **6**). Thus, an empty coordination site is presumably required for substrate activation and functionalization.

Table 1.1. Hydroarylation of norbornene with benzene using (PyInd)Pt^{II} complexes.

Catalyst	Solvent	Ar–H	Temperature (°C)	Time (h)	Yield (%)^a
3 ^{b}	o-$C_6Cl_2H_4$	C_6H_6	115	20	79
3 ^{c}	o-$C_6Cl_2H_4$	C_6H_6	92	2	92
4	C_6H_6	C_6H_6	140	16	38
4	C_6MeH_5	C_6MeH_5	140	16	28
4	C_6ClH_5	C_6ClH_5	140	16	58
4	C_6FH_5	C_6FH_5	140	16	0
4	p-$C_6Me_2H_4$	p-$C_6Me_2H_4$	140	16	0
5	C_6H_6	C_6H_6	140	16	41
6 ^{d}	C_6H_6	C_6H_6	140	16	27
7	C_6H_6	C_6H_6	140	16	26

^{a} % yield refers to the isolated yield of the hydroarylation product. ^{b} Reaction performed with added AgOTf. ^{c} Reaction performed with added AgBF$_4$. ^{d} Reaction performed with added $B(C_6F_6)_3$.[8,9]

Several key differences in activities were observed among these various catalysts. For complexes **4-7**, significant amounts of a norbornene dimer byproduct were identified (yields of 30 ~ 45%), which suggests that vinylic C–H activation is possible with some Pt species. However, this product was not observed with complex **3**. Additionally, high temperatures (140 vs. 110 °C) and long reaction times (16 vs. 5 hours) were required for catalysts **4-7**.[8,9] Minor differences were observed between the activities of complexes bearing PyInd ligand **1** and those involving the fluorinated PyInd ligand **2**. The reduced activity for complexes **6** and **7** versus the ethylene-bound complex **3** or the allylic complexes **4** and **5** is possibly due to the preactivation necessary to replace a methyl ligand by a phenyl ligand. Complex **6** requires the addition of a borane reagent to abstract a methyl ligand to generate an open coordination site for C–H activation to occur; in contrast, complex **7** undergoes a C–H activation step to eliminate methane and generate the corresponding Pt–Ph complex, which presumably is the catalytically active species.[8,9]

The scope of hydroarylation with PyInd complexes was probed with additional substrates. It was found that other cyclic olefins such as cyclohexene and cyclopentene were coupled to benzene at 80 °C providing yields of 65% and 62%, respectively, after 2 hours using 5 mol% of Zeise's dimer and 10 mol%

of AgBF$_4$ to generate an active catalyst. Simple olefins such as propylene underwent hydroarylation in high yield (79%) under the same conditions as described above. With catalyst **4**, hydroarylation of norbornene was observed using benzene, toluene, or chlorobenzene. A mixture of regioisomers was observed for both toluene and chlorobenzene, with an *o:m:p* ratio for toluene of 0.4:1.0:0.6. Interestingly, *p*-xylenes and fluorobenzene were not suitable arene substrates and only norbornene dimers were observed as products. A thorough mechanistic analysis of ethylene hydrophenylation catalyzed by (PyInd)PtPh(SMe)$_2$ was performed and is discussed in greater detail in chapter two.[10]

A pyridyl-pyrrole (PyPyr) ligand set published by Goldberg and colleagues[11-13] illustrates the ability of organoplatinum complexes to promote both C–H activation and olefin coordination. In an initial report,[11] five-coordinate [(PyPyr)Pt^{IV}Me$_3$] complexes **8** and **9** were observed to reductively eliminate ethane in the presence of benzene and ethylene to generate a transient Pt(II) species (Scheme 1.1). This species undergoes a rapid intramolecular C–H activation reaction under ethylene to generate the corresponding Pt^{II}(C$_2$H$_4$) complexes **10** or **11**. Based on these observations, this system was studied in the context of hydroarylation catalysis.

Scheme 1.1. Ethane Elimination and Intermolecular C–H Activation with (PyPyr)Pt^{IV} Complexes at 100 °C for 1 Day.[11]
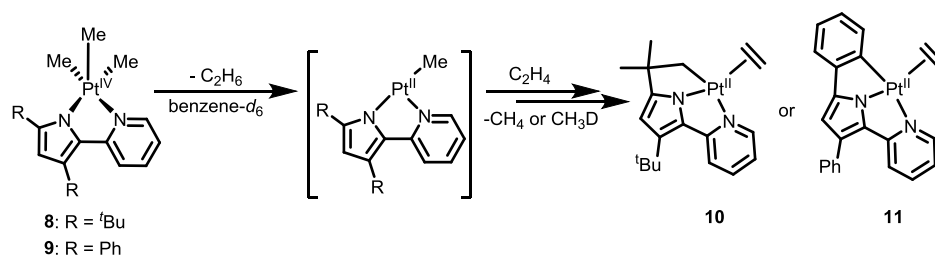
Further investigations[12] with PyPyr complexes indicated that hydroarylation was indeed possible with either Pt(II) or Pt(IV) precatalysts (Figure 1.2). Complexes bearing a dimethyl-substituted pyridyl-pyrrole ligand (PyPyr-Me$_2$) with labile SMe$_2$ and a "pre-activated" phenyl ligand were generated with either a d^6 Pt(IV) (**12**) or d^8 Pt(II) (**13**) metal center. Upon exposure of **13** to ethylene in benzene-*d$_6$*, olefin insertion and subsequent ethylene coordination was observed, to afford [(PyPyr-Me$_2$)Pt^{II}(C$_2$H$_4$)(CH$_2$CH$_2$Ph)] (**14**). Thermolysis of complex **14** at 100 °C in benzene-*d$_6$* generated the hydroarylation product, C$_6$D$_5$CH$_2$CH$_2$D. A similar complex (**15**) bearing an unsubstituted PyPyr ligand was also prepared.
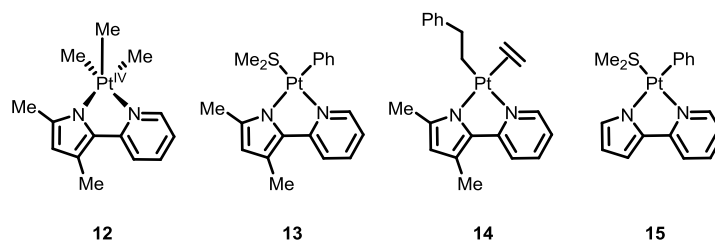
Figure 1.2. Several PyPyr ligated complexes for olefin hydroarylation.

The hydroarylation activity of complexes **12**, **13**, and **15** is summarized in Table 1.2 below.[12,13] Several key differences between these catalysts were observed, and a potentially key observation is an increase in reactivity for Pt(II) versus Pt(IV) precatalysts. With benzene and ethylene, complex **12** gave 26 turnover numbers (TONs) while **13** gave 36 TONs after a similar period of time. More striking, however,

is the difference in regioselectivities during propylene hydroarylation; complex **13** afforded mainly the Markovnikov (branched) product in a 86:14 ratio whereas catalyst **15** generated nearly equivalent amounts of both regioisomers. Finally, substituents on either the aryl or olefin substrate tended to reduce the overall activity of the catalyst, noted by a reduction in TON. While more distal C–H bonds (*i.e.*, *meta-* or *para-*) were easier to activate, a mixture of all three isomers was obtained.

Table 1.2. Hydroarylation substrate scope for (PyPyr)Pt^{II} complexes.
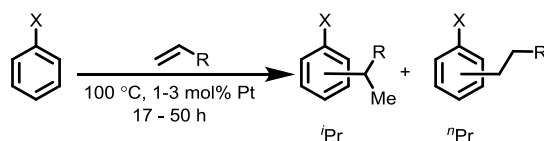

Catalyst	X	R	TON	*o:m:p*	Branched:Linear
12	H	H	26		
		Me	8		86:14
	Me	H	4	7:93*	
		Me	2	10:63:27	85:15
	CF$_3$	H	2	6:62:32	
13	H	H	36		
		Me	18		85:15
		^{n}Bu	12		83:16
	Me	H	12	6:94*	
		Me	3	9:66:25	84:16
15	H	Me	16		51:49
		^{n}Bu	12		43:57

[a] Reactions were performed at either 100 or 120 °C with catalyst loadings between 1 and 3 mol%, for 17 to 50 h. *meta* and *para* isomers were not separated and are instead listed as the sum of the two isomers.[12,13]

With these results, a mechanism was proposed for the hydroarylation of ethylene with benzene (Figure 1.3).[12] In this mechanism, a [(PyPyr)Pt^{II}(C$_2$H$_4$)Ph] complex (**20**) (likely generated by a ligand exchange of SMe$_2$ for C$_2$H$_4$) undergoes ethylene insertion and subsequent ethylene coordination to generate complex **14**. An intramolecular aryl C–H activation produces the Pt(IV)–hydride intermediate **16**, which can undergo reductive elimination and then coordination of benzene (**17**). A reversible oxidative addition of a benzene C–H bond provides a second Pt(IV)–hydride intermediate (**18**), which again can undergo reductive elimination to form the ethylbenzene complex **19**. Ligand substitution with ethylene regenerates

20 and free ethylbenzene. It is possible, however, that the mechanism can proceed *via* a single C–H activation pathway. In this alternative mechanism, dissociation of C_2H_4 from **14** can occur and is followed by C–H activation of solvent to generate the intermediate complex $[(PyPyr)Pt^{IV}(H)(CH_2CH_2Ph)Ph]$ (**18**). Reductive elimination from this species generates complex **19**. It is also possible that complex **14** exists as an off-cycle product (*vide infra*).
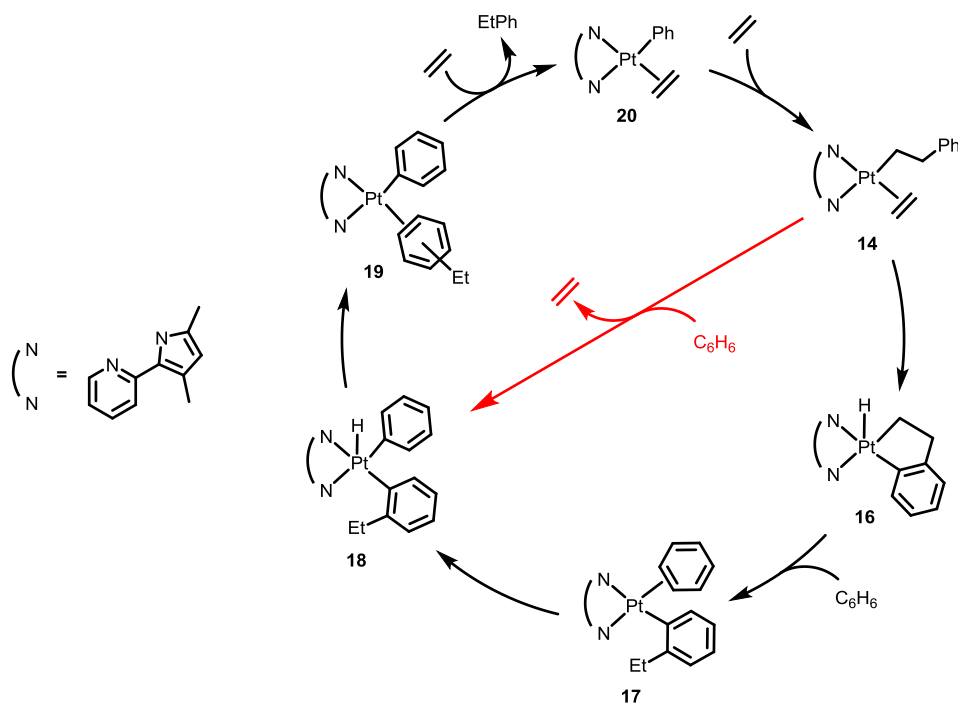

Figure 1.3. Proposed mechanisms for (PyPyr)Pt^{II} catalyzed olefin hydroarylation. The direct pathway (**red**) occurs without internal rearrangement of the phenethyl fragment (**black** pathway).[12]

Initial reports by Tilset and coworkers[14,15] demonstrated that cationic $[L_2Pt^{II}Me(OH)_2]^+$ complexes supported by simple diimine ligands activate the C–H bonds of benzene and other substituted arenes such as toluene or *p*-xylene to generate the corresponding Pt–Ar complexes. Similarly, Bergman and Tilley[16] showed that a dicationic $[(bpy)Pt^{II}(solvent)_2][NTf_2]_2$ complex ($NTf_2 = {}^-N(SO_2CF_3)_2$, bpy = bipyridine) activates allylic C–H bonds. Given their ability to cleave unactivated C–H bonds, cationic Pt complexes have been thoroughly investigated as potential hydroarylation catalysts. An initial investigation by Gunnoe[17] demonstrated that the neutral $[(bpy)Pt^{II}Ph_2]$ complex catalyzes the hydroarylation of ethylene and benzene at elevated temperatures, upon addition of a non-coordinating acid such as $H[BAr'_4]$ ($Ar' = 2,5$-$(CF_3)_2C_6H_3$) as an activator. While catalysis with this platinum-based system gave low yields of product (3.7 and 11.9 TONs after 4 and 16 hours, respectively), it was hypothesized that a cationic complex of the type $[(bpy)Pt^{II}PhL]^+$ might be more active since pre-activation would not be required.

Several cationic complexes were therefore synthesized and isolated (Scheme 1.2).[17,18] A *tert*-butyl substituted ligand (^{t}bpy) was installed onto Pt(II) to afford the neutral complex $[(^t bpy)Pt^{II}PhCl]$ (**21**). Chloride removal with Na[BAr'$_4$] in THF yielded the cationic complex **22** with [BAr'$_4$]$^-$ as the counter ion. This complex, however, proved stable only in the presence of an excess of THF. In the presence of other coordinating solvents such as acetonitrile or perfluoropyridine, ligand exchange occurred to give the

corresponding [(*t*bpy)Pt[II]PhL][BAr'4] complexes (**23** and **24**). Substitution of THF with other ligands, however, was demonstrated to reduce the overall hydroarylation activity. Complexes **22**, **23**, and **24**, exhibited 15.7, 8.1, and 7.4 TONs, respectively, of ethylbenzene after 4 hours. A labile ancillary L ligand, therefore, promotes increased reactivity since ligand loss is required for catalysis to occur.

Scheme 1.2. **Synthesis of Cationic [(*t*bpy)Pt[II]PhL]+ Complexes Bearing Labile Ancillary L-Type Ligands.[17,18]**
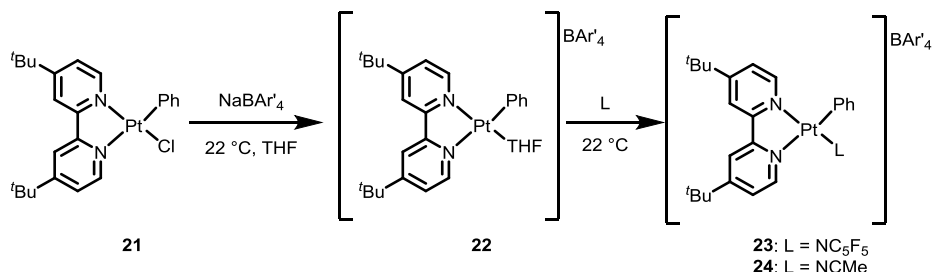
Optimization of initial reaction conditions with precatalyst **22** revealed the effects of temperature and ethylene pressure (using 0.1 mol% catalyst loadings, relative to benzene).[17] It was determined that as the temperature increases from 90 to 140 °C (at 15 psi of ethylene) the overall TON for ethylbenzene after 4 hours increased from 7.2 to 35.8. However, elevated temperatures also increased the amount of dialkylated products. A mixture of *ortho*-, *meta*-, and *para*-diethylbenzene side products were observed with 0.3, 7.3, and 3.3 TON, respectively, after 4 hours at 140 °C. Interestingly, increasing the ethylene pressure reduced the overall activity of the system: an increase in ethylene pressure from 15 to 60 psi (at 100 °C) resulted in a decrease in TON by a factor of almost 50. While the overall activity dropped at higher ethylene pressures, the product ratio of ethylbenzene to the mixture of diethylbenzenes remained relatively constant at 2.3. Hydroarylations of several other substrates (*e.g.*, ethylene with furan or propylene with benzene) were observed with **22** as catalyst.

The operative mechanism for these cationic, Pt-catalyzed hydroarylations was investigated using both experimental evidence and DFT calculations.[18] Attempts to determine a rate law for the hydroarylation of ethylene, with benzene and precatalyst **22**, revealed a first order dependence on the concentration of **22** whereas benzene displayed saturation kinetics as determined in variable concentrations with perfluoropyridine as cosolvent. The kinetics indicate a complex dependence on ethylene, however, as increases in the ethylene pressure result in rapid reduction of the product yield.

DFT calculations were used to explore the free energies of various intermediates and transitions states for multiple possible pathways.[18] The energetics of two different ethylene insertion pathways were investigated, starting from an analogue of **22** without *t*Bu groups. The initial ligand substitution of THF with ethylene can occur either through an associative or dissociative pathway, and DFT calculations indicate that these two routes are energetically similar, with activation energies $\Delta G^{\ddagger}$ of 19.0 and 19.7 kcal mol^{-1}, respectively. Aryl C–H activation can occur through two different pathways: a concerted, one-step σ-bond metathesis route or two-step oxidative addition/reductive elimination route (Figure 1.4). The calculated relative energies (given in Figure 1.4) reveal a 2.3 kcal mol^{-1} energy preference for oxidative addition over σ-bond metathesis.[18]
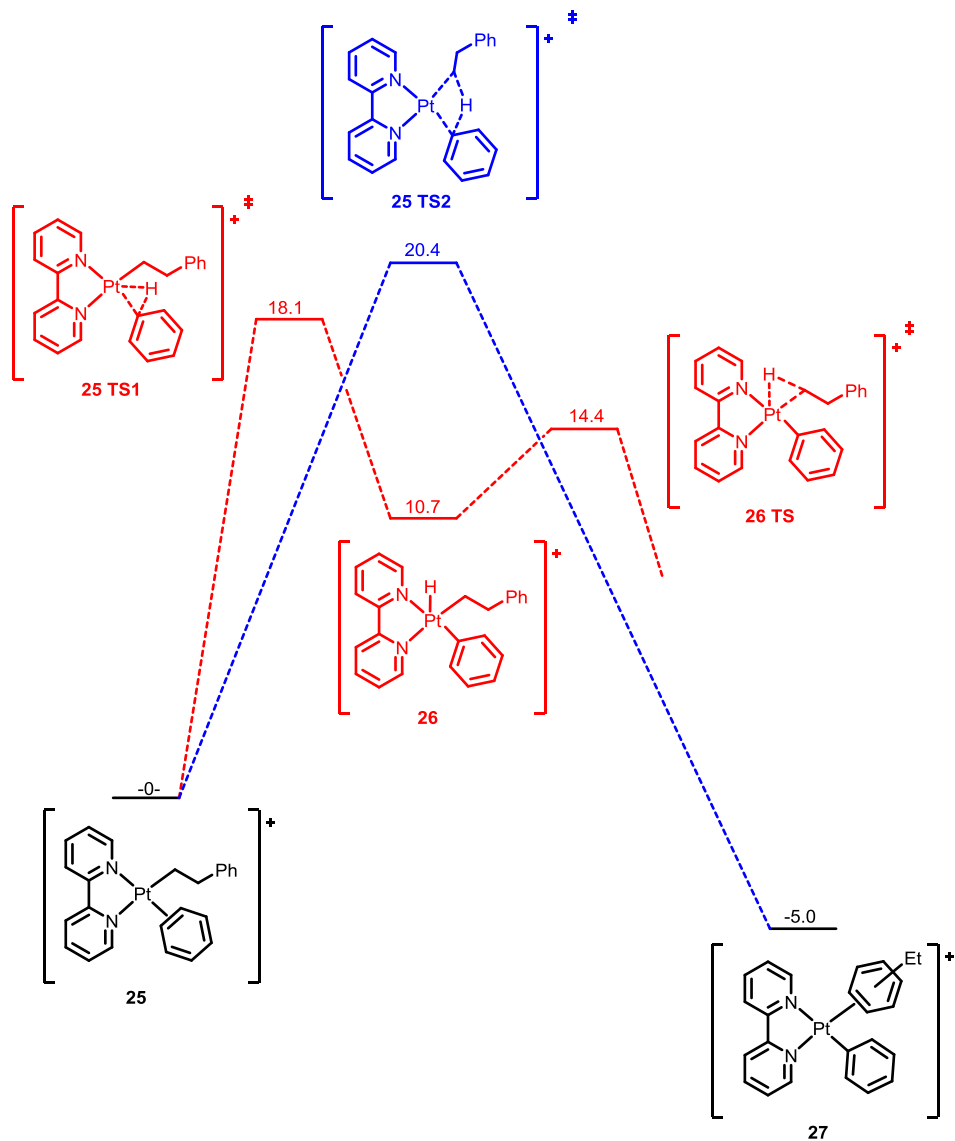
Figure 1.4. Calculated barriers for C–H activation with cationic Pt complexes *via* either a two-step oxidative addition-reductive elimination route (red) or a single-step σ-bond metathesis (blue) pathway. Energies are given in kcal mol^{-1}.[18]

As a further probe of the mechanism, an isotope experiment with catalyst **22** compared the TON for ethylbenzene, using benzene or benzene-d_6 as the arene substrate, to give a TO_H/TO_D (TO = turnovers) ratio of 1.8(4). Given these results from experiment and DFT, two possible mechanisms were proposed (Figure 1.5).[18] In the first mechanism, a [$L_2Pt^{II}(C_2H_4)Ph$] complex (**28**) undergoes ethylene insertion to afford a quasi-three-coordinate Pt(II) species (**29**), likely with either an agostic phenethyl C–H interaction or arene π-coordination to the Pt(II) center. Upon rapid coordination of ethylene (**30**) and reversible exchange with benzene (**31**), C–H activation occurs either as a one- or two-step process as discussed above. Ligand exchange with ethylene regenerates **28** and liberates an equivalent of ethylbenzene. The second proposed mechanism has many similar steps and intermediates, with the exception that complex **30** lies off-cycle in equilibrium with **29**. Given the experimental and DFT evidence, however, both mechanisms are possible and likely indistinguishable.
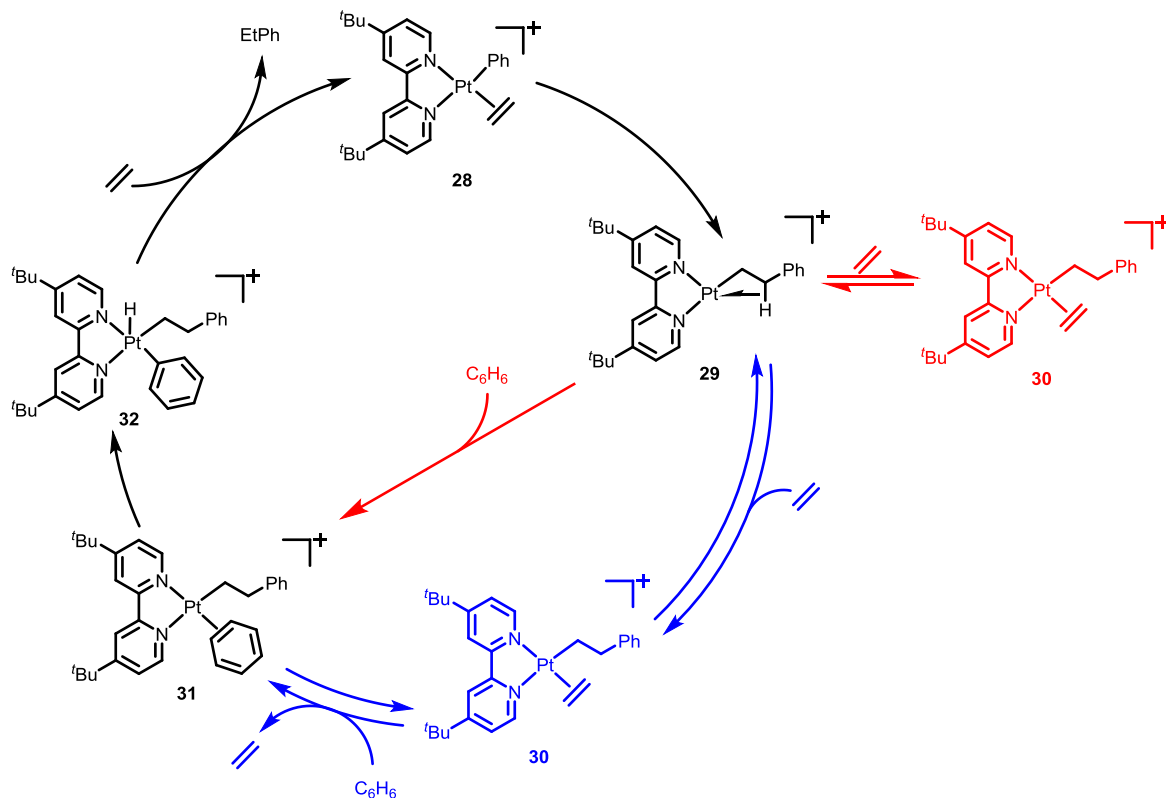
Figure 1.5. Possible mechanisms for cationic Pt(II) catalyzed hydrophenylation of ethylene. Complex **30** is the on-cycle resting state for mechanism one (blue), whereas it is an off cycle resting state in mechanism two (red). Anions have been omitted for clarity.[18]

The selectivities associated with longer chain α–olefins (*e.g.,* propylene) have also been investigated with several (bpy)Pt[II] complexes (Table 1.3).[19] By modifying the substitution on the ligand at the 4 and 4' position, effects on the overall activity and selectivity for anti-Markovnikov products were observed. By changing the substituents from donating groups such as OMe (**33**) or *t*Bu (**22**) to electron-withdrawing groups such as NO₂ (**37**), the amount of anti-Markovnikov product increased. Moreover, a decrease in the overall activity for hydroarylation was noted for most substituents, especially with the Br-substituted complex **35**, and **37**. A slight trend towards branch-selective catalysis was observed with more electron-withdrawing substituents. A Hammett plot was generated from the ratio cumene to *n*-propylbenzene to better illustrate the magnitude of this trend; a linear fit was observed using the σ_p value and the ratio of the two products (*i.e.*, *i*PrPh / *n*PrPh), with a small slope of $\rho = 0.2$. While this may indicate that the ligand substituent affects the overall regioselectivity, it is difficult to confirm that only the rate of C–C bond insertion is perturbed and to rule out changes to other preequilibrium steps.

Table 1.3. Catalytic hydrophenylation of propylene with [(bpy)Pt^{II}Ph(THF)]$^+$ derivatives.
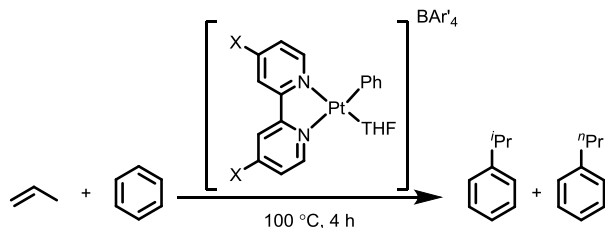

X	σ_p	TON ^{i}PrPh	TON ^{n}PrPh	^{i}PrPh + ^{n}PrPh	^{i}PrPh / ^{n}PrPh
OMe (**33**)	-0.27	10.6	3.7	14.3	2.9
^{t}Bu (**22**)	-0.2	25.0	8.5	33.5	2.9
H (**34**)	0.0	25.8	8.0	33.8	3.2
Br (**35**)	0.23	2.5	0.7	3.2	3.8
CO$_2$Et (**36**)	0.45	12.1	3.3	15.4	3.7
NO$_2$ (**37**)	0.78	4.1	0.9	5.0	4.6

[a] Conditions: 0.01 mol% catalyst loading relative to benzene, 0.1 MPa propylene, 100 °C for 4 hours. σ_p represents the Hammett parameter for *para*-substitutions with negative values representing electron-donating groups and positive values denote electron-withdrawing ability.[19]

Ligand modifications resulted in slight changes in the product selectivity (ethylbenzene vs. styrene) for the hydrophenylation of ethylene (Table 1.4).[20] The ratio of ethylbenzene to styrene for electron withdrawing substituents (**35-37**) was smaller than for electron-donating substituents (**22**, **33**, and **34**), both at 4 and 16 hour time points. It should be noted that the observed TONs for styrene were fairly constant for complexes **22** and **33-37**. The change in ratio, therefore, was attributed to a reduction in overall hydrophenylation activity for complexes bearing ligands with electron-withdrawing substituents.
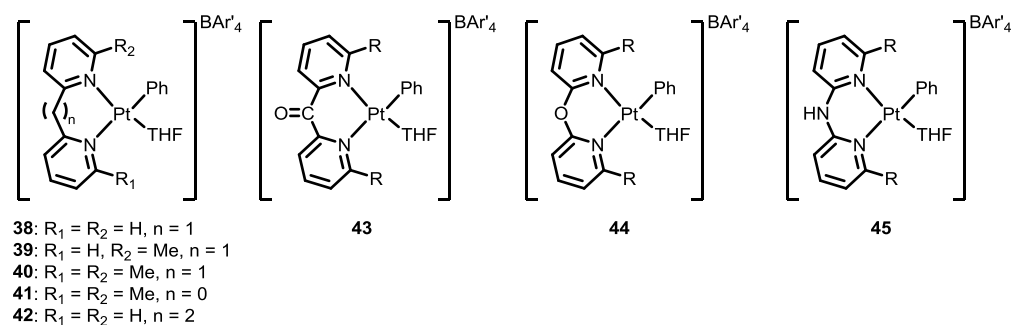
Table 1.4. Catalytic hydrophenylation of ethylene with $[(bpy)Pt^{II}Ph(THF)]^+$ derivatives.
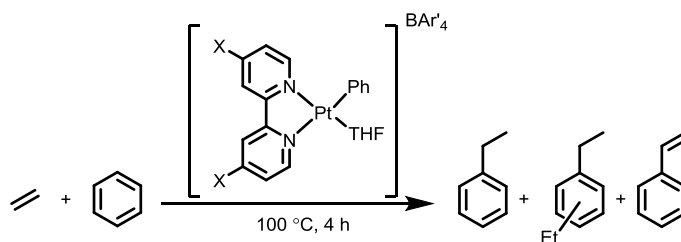
X	TON (EtPh)	TON (Et$_2$C$_6$H$_4$)	TON (styrene)	EtPh / styrene
OMe (**33**)	3.3	0.7	0.4	8.3
^{t}Bu (**22**)	4.0	0.9	0.5	8.0
H (**34**)	5.5	1.4	0.7	7.9
Br (**35**)	0.2	0	1.3	0.2
CO$_2$Et (**36**)	1.9	0.5	1.2	1.6
NO$_2$ (**37**)	0	0	1.0	–

[a] Conditions: 0.01 mol% catalyst loading relative to benzene, 0.3 MPa ethylene, 100 °C for 4 hours.[20]

Alternative pyridine-based, chelating ligands have been employed recently by Gunnoe and coworkers.[21,22] The pyridyl fragments are connected through a linker (*e.g.* CH$_2$), and were used to elucidate the effect of larger ligand bite angles (Figure 1.6). Heteroatom linkers were also used to determine their electronic influence on the catalysis. As with the bpy systems described above, catalysts were generated by reaction of $[L_2Pt^{II}Ph_2]$ complexes with $[H(Et_2O)_2][BAr'_4]$ in THF at -70 °C, to afford the corresponding $[L_2Pt^{II}Ph(THF)]^+$ species.

38: R$_1$ = R$_2$ = H, n = 1
39: R$_1$ = H, R$_2$ = Me, n = 1
40: R$_1$ = R$_2$ = Me, n = 1
41: R$_1$ = R$_2$ = Me, n = 0
42: R$_1$ = R$_2$ = H, n = 2

Figure 1.6. Alternative ligand designs using a linked bpy motif.[21,22]

The differences in catalytic activities for complexes **38-45** in the hydrophenylation of ethylene are summarized in Table 1.5.[22] Increasing the linker length from n = 0 (**22**) to n = 1 (**38**) increased the amount of product generated, with a 55.3 TON observed for ethylbenzene after 4 hours. Unfortunately, a large amount of diethylbenzenes also formed with **38**. By increasing the steric bulk at the metal center with either

6- or 6'-Me substituents on the pyridyl groups (**39-41**), the generation of diethylbenzenes was dramatically reduced while only moderately reducing the overall activity. Complexes bearing longer linkers in the supporting ligand (**42**) or with oxygen containing linkers (**43** and **44**), however, demonstrated very little catalytic activity. The nitrogen linked complex **45** demonstrated comparable activity towards hydroarylation. The selectivity for branched versus linear products with **38-45** was examined with the hydrophenylation of propylene. These catalysts, however, were observed to give mostly branched products (> 4.0 ratio of branched/linear products).

Table 1.5. Catalytic activity in the hydrophenylation of ethylene using linked bis(pyridyl) complexes.
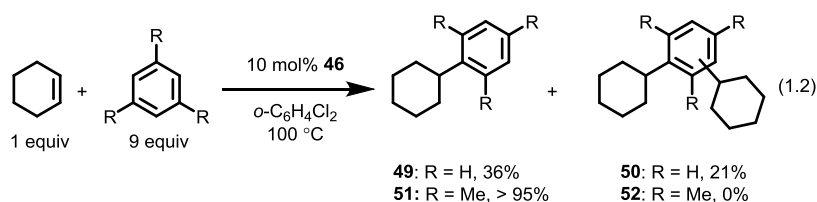
Catalyst	TON (EtC$_6$H$_5$)	TON (Et$_2$C$_6$H$_4$)	TON (styrene)
38	55.3	10.6	0.4
39	31.2	1.3	2.7
40	19.5	0.0	1.7
41	0.0	0.0	0.7
42	0.7	0.0	0.4
43	3.3	0.0	1.9
44	1.6	0.0	2.9
45	18.6	4.0	2.5

[a] The TONs for the mixture of *ortho*-, *meta*-, *para*- diethylbenzene (Et$_2$C$_6$H$_4$) and styrene are also given. Conditions: 0.01 mol% catalyst, at 100 °C with 0.1 MPa of ethylene for 4 hours.[22]

Simple Pt(II) complexes with trifluoromethylsulfonate (OTf) or cyclooctadiene (cod) ligands have been observed to generate alkyl-arenes. In a report by Bergman and Tilley,[23] [(cod)Pt[II](OTf)$_2$] (**46**) was shown to catalyze the coupling of cyclic olefins with non-functionalized arenes such as mesitylene and benzene in an unreactive aromatic solvent. Initial studies with norbornene and benzene demonstrated complete consumption of the olefin after 5 hours using 10 mol% **46** in *ortho*-dichlorobenzene at elevated temperatures, though only 41% of the hydroarylation product **47** was formed (eq 1.1). Interestingly, products containing a dichlorophenyl fragment were not observed, which suggests that electron deficient arenes are not suitable substrates for this type of hydroarylation. To examine the side reactions generated, the reaction was probed at lower temperatures (25 °C) by ^{1}H NMR spectroscopy. It was observed that **46** promoted the isomerization of norbornene to the highly strained nortricyclene **48** without generating **47**. This suggested that this rearrangement was likely competent at elevated temperatures and therefore accounts for the low yields for the desired alkyl-arene.
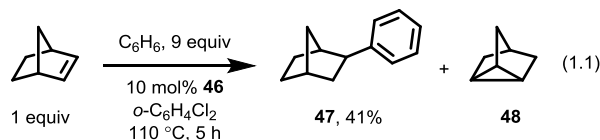
Under conditions similar to those described above, cyclohexene reacts with benzene and mesitylene to generate aryl-substituted cyclohexane products (eq 1.2). Dialkylation occurred with benzene; a yield of 36% for the monoalkylated arene product (**49**) and 21% for the dialkylated species (**50**) was observed after 17 hours. In contrast, bulkier arenes such as mesitylene afforded only the mono-alkylated compound (**51**) in quantitative yield after 4 hours.

$$\text{(1.2)}$$

49: R = H, 36%
51: R = Me, > 95%

50: R = H, 21%
52: R = Me, 0%

1 equiv   9 equiv

10 mol% **46**

$o\text{-}C_6H_4Cl_2$
100 °C

To probe the catalytic mechanisms associated with **46**,[23] the influence of a hindered base (2,6-di-*tert*-butyl-4-methylpyridine) on hydroarylation was examined. Notably, the addition of this non-coordinating base greatly inhibited the reaction of cyclohexene with mesitylene, and complete inhibition was observed in the presence of 20 mol% of the base. In a similar control experiment, **46** was replaced with 10 mol% of HOTf. This resulted in quantitative formation of the hydroarylation product **51** suggesting the possibility of an acid-catalyzed pathway. Thus, the proposed mechanism of catalysis with **46** involves an initial coupling of two cyclohexene molecules to produce a platinum-allyl derivative (**53**) and an equivalent of HOTf. This type of metal-mediated olefin coupling with ethylene and cyclopentene was first identified with electrophilic platinum complexes by Sharp.[24] The acid generated in this coupling chemistry then initiates a Friedel–Crafts–type hydroarylation *via* protonation of cyclohexene to give a carbocation, which then reacts with the arene (Figure 1.7).
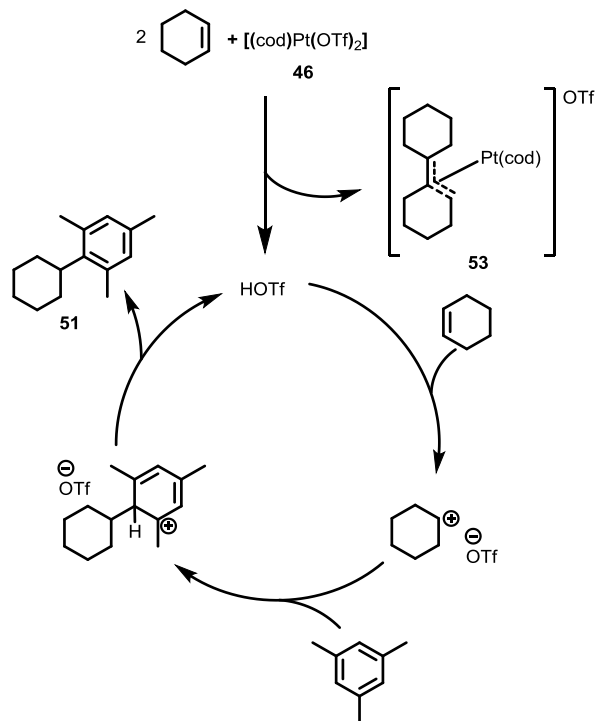

Figure 1.7. Proposed catalytic cycle for the hydroarylation of cyclohexene with mesitylene with complex **46**.[23]

The observation of a metal-initiated acid catalyzed hydroarylation (with **46**) is reminiscent of the platinum-mediated proton-transfer mechanism proposed for hydroaminations of olefins,[25] and raises broader questions regarding the possible role of Brønsted acids in reported, metal-catalyzed hydroarylations. In a study designed to differentiate metal centered C–H activation catalyzed hydroarylation from adventitious acid mediated hydroarylation, Bergman and Tilley[16] described the reactivity of [(bpy)Pt^{II}Ph(NTf$_2$)] **(54)** with the bicyclic olefin substrate spiro-[bicycle[2.2.1]hept-2-ene-7,1'-cyclopropane] (Figure 1.8). It was expected that a mechanism involving direct olefin insertion into a Pt–Ph bond would favor formation of the expected type of hydroarylation product. Alternatively, if an acid-catalyzed mechanism were operative, an acid-mediated Wagner–Meerwein carbocation rearrangement would occur more rapidly than hydroarylation. The resulting rearrangement product could then undergo an acid catalyzed hydroarylation event, yielding a rearranged hydroarylation product. The result of this experiment, however, yielded a surprising result, in that hydroarylation did not occur. Instead a platinum-mediated C–C bond rearrangement reaction induced by a C–H bond activation step occurred to generate 1,2,4,7,7apentahydroindene as the only product. It was postulated by Bergman and Tilley[16] that an intramolecular C–H bond activation of the pendant cyclopropane group occurs instead of solvent activation. Subsequent insertion of the Pt–H hydride into the norbornene olefin generates a norbornyl-centered carbocation, which then undergoes C–C bond rearrangements to produce the observed product.
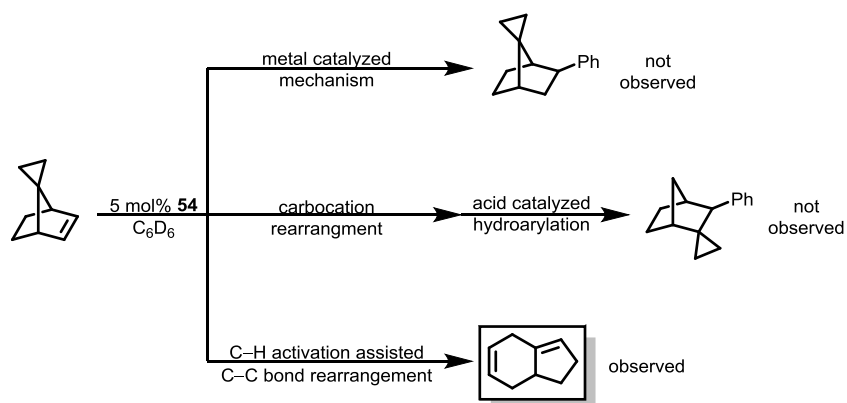
Figure 1.8. Possible reaction pathways for the reaction of a bicyclic olefin with complex **54** in benzene-d_6. No hydroarylation reactions occurred; only the rearrangement product was observed.[16]
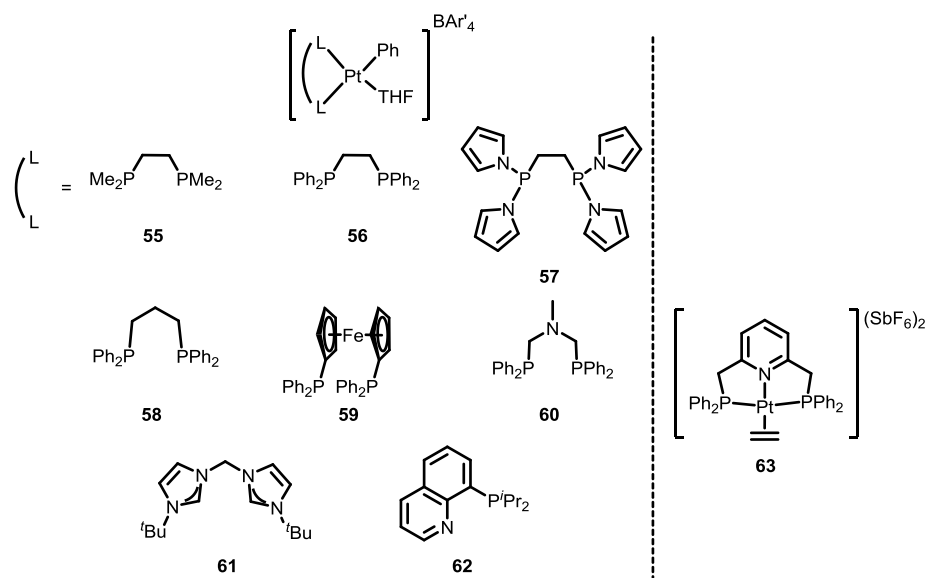
Figure 1.9. Complexes of the type [L$_2$Pt^{II}(THF)Ph][BAr'$_4$] and [L$_3$Pt^{II}(C$_2$H$_4$)] bearing phosphine, mixed phosphine, or bis-*N*-heterocycliccarbene based ligands.[26,27]

Several other ligands for cationic Pt(II) hydroarylation catalysts have also been described, mostly based on chelating bisphosphine donors (**55-62**) (Figure 1.9).[26] Unfortunately, these complexes exhibit poor activities as hydroarylation catalysts. Thus, less than 2.0 equivalents of ethylbenzene were observed for each of these complexes after 4 hours at 100 °C. Interestingly, styrene formation was observed for complexes **55-61,** giving 1-2 turnovers after 4 hours. Additionally, complex **62** bearing a phosphino-quinolyl PN ligand proved to be catalytically inactive. DFT calculations were performed to elucidate the cause for the switch in product formation, and it was determined that a low energy pathway involving β-hydride elimination (8.8 kcal mol^{-1} barrier) followed by benzene C–H activation led to the generation of styrene, along with an equivalent of H$_2$. The tridentate PNP (PNP = 2,6-bis(diphenylphosphinomethyl)pyridine), dicationic complex [(PNP)Pt^{II}(C$_2$H$_4$)][SbF$_6$]$_2$ (**63**) has also been employed in the hydroarylation of ethylene with only electron rich, methoxy-substituted benzene derivatives at elevated temperatures.[27] In this system, however, high yields for the dialkylated product were observed using 3-methylanisole as the arene source.

Undirected Hydroarylations with Electron-Poor Arenes Catalyzed by Ni Complexes. Hydroarylation has been reported for Ni(0) catalyst precursors and Ni(II) species have been implied as intermediates in the catalytic cycle. The Hartwig group[28] recently investigated the hydroarylation of various olefins with electron-deficient bis(trifluoromethyl)benzene substrates using [(cod)$_2$Ni^0] (**64**) and an added carbene ligand (1,3-bis(2,6-diisopropylphenyl)-1,3-dihydro-2H-imidazol-2-ylidene, IPr). While these reaction conditions also catalyze the hydroarylation of 1-hexene with benzene, low yields were observed and highly electron deficient arenes are the preferred substrates in this system. To probe the substrate scope, a variety of terminal and internal olefins were tested (Table 1.6). The complex [(IPr)$_2$Ni^0] (**65**) was used as a precatalyst in large catalyst loadings (20 mol%) with a slight excess of arene. Generally high selectivities were observed for the linear anti-Markovnikov product **66**. While some olefin substrates (R = Me) afford a mixture of both **66** and the branched product **67**, most substrates exhibited greater than 99% selectivity for the linear products. Similarly, moderate yields were generally demonstrated for most olefin substrates.

Several labeling studies were performed with 5-deuterio-1,3-bis(trifluoromethyl)benzene (**68**) using complex **65** as a precatalyst (Figure 1.10).[28] After each reaction, the position of the deuterium atom was determined by ^{2}H NMR spectroscopy. In the first experiment (**A**), 1-octene with added NaO^{t}Bu generated a linear hydroarylation product, for which deuterium incorporation occurred primarily into the β-methylene position. Minimal isomerization of 1-octene was indicated by a lack of deuterium incorporation into the aliphatic chain. Also, observed *ortho*-aryl C–H scrambling suggests a reversible arene-activation step. In a similar reaction without base (**B**), deuterium scrambling into the α-methylene was observed to a greater extent. A similar increase in H(D) exchange into the *ortho*-aryl position was noted. Similarly, very little deuterium incorporation into the aliphatic chain was observed. With the internal olefin *trans*-4-octene (reaction **C**), an increase in deuterium incorporation into the aliphatic chain was observed, likely due to prior isomerization of the olefin. Differences in the initial rates of catalysis with proteo- and deutero-1,3-bis(trifluoromethyl)benzene gave a statistically insignificant kinetic isotope effect of 1.1 ± 0.1.

**Table 1.6.** Hydroarylation substrate scope using Ni(0) with electron deficient arenes.
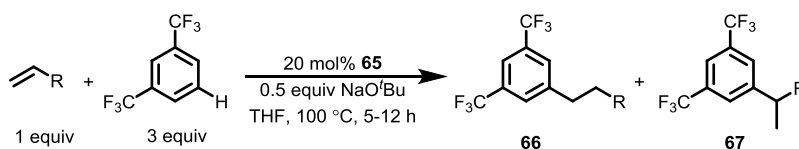
R	Isolated Yield (%)	66:67
Me	57	89:11
^{n}Hex	65	97:3
^{t}Bu	87	> 99:1
Cy	59	> 99:1
CH$_2$CH$_2$Ph	73	97:3
CH$_2$SiMe$_3$	39	> 99:1
SiEt$_3$	78	> 99:1
CH$_2$NBn$_2$	68	> 99:1
O^{t}Bu ^{a}	23	99:1
Cyclohexene	70	–

^{a} Reaction did not include NaO^{t}Bu.[28]
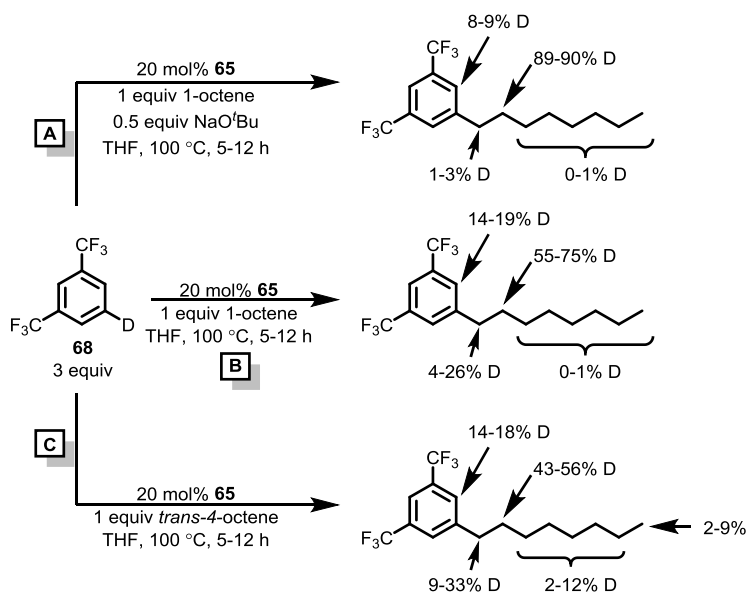
Figure 1.10. Deuterium labeling study with and without NaO^{t}Bu using various octene substrates.[28]

The mechanism of this hydroarylation was probed using DFT calculations (Figure 1.11), which gave activation energies for the proposed transition states and intermediates.[28] This analysis points to [(IPr)Ni^0(olefin)$_2$] (**A** or **A'**) as the resting state. Arene coordinates to this species in an η^2-fashion (**B**), displacing an olefin. Proton transfer from the bound arene to the ancillary olefin ligand occurs to produce two new Ni–C bonds, affording a complex of the type [(IPr)Ni^{II}(R)(Ar)] (**C**) with an agostic C–H interaction. Ligand isomerization from **C** via **D** occurs at a lower transition barrier than the direct isomerization from **C** to **E**. The proposed turnover-limiting step for the formation of both branched and linear products is reductive elimination from the corresponding [(IPr)Ni^{II}(R)(Ar)] (**E**, R = CH(CH$_3$)$_2$ or CH$_2$CH$_2$CH$_3$, respectively) species, with a barrier of 13.1 kcal mol^{-1}. The selectivity of the reaction was attributed to the rate-limiting reductive elimination step; the energy difference between the transition states of the linear and branched products was calculated to be 1.1 kcal mol^{-1}. This difference corresponds to a product ratio of 82:18, which was in good agreement with the experimental data.
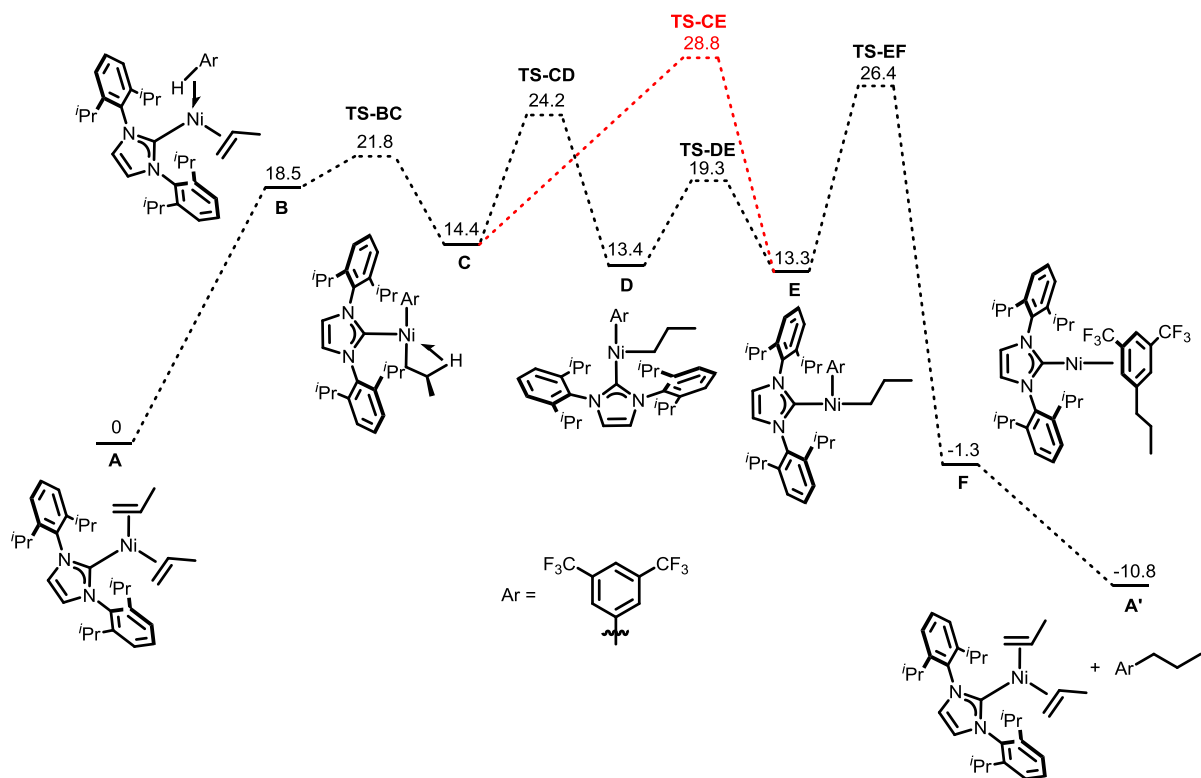
Figure 1.11. DFT calculated catalytic cycle for Ni catalyzed hydroarylation of electron deficient arenes. All energies are given in kcal mol^{-1}. Transition state structures have been omitted for clarity, but are distorted Y-shaped species.[28]

In a similar report by Hiyama and coworkers,[29] the hydroarylation of alkynes and olefins with fluorinated arenes (*e.g.*, C$_6$F$_5$H, 1,2,3,4-C$_6$F$_4$H, etc.) was achieved using [(cod)$_2$Ni^0] with added PCyp$_3$ ligand (Cyp = cyclopentyl). The hydroarylation of 2-vinylnaphthalene with C$_6$F$_5$H yielded the corresponding branched diarylethane product whereby C–H activation occurs preferentially over C–F activation. The resulting [(C$_6$F$_5$)Ni^{II}H] species may coordinate an olefin which then undergoes migratory insertion (into Ni–H) in a Markovnikov fashion. Reductive elimination of the aryl and alkyl ligands generates the alkyl-arene product.

To date, there are no Ni(II) analogues of the well-established Pt(II) hydroarylation catalysts; despite this, a computational study by Cundari and coworkers[30] concludes that species of the type [(κ^2-Tp)Ni^{II}(Ph)(NCMe)] (Tp = hydrido-tris(pyrazolyl)borate) could act as competent hydroarylation catalysts. In this study, the analogous Pt(II) species was also investigated. The energies of various intermediates and transition states in the catalytic cycle for hydroarylation of ethylene with benzene were calculated by DFT. The mechanism is reminiscent of that for Pt(II)-catalyzed hydroarylation, whereby olefin coordination and insertion occur. The resulting M–Ar species may then abstract hydrogen from benzene. It was determined that while the mechanisms for Ni(II) and Pt(II) are similar, the C–H activation steps are different. The Pt(II) species likely undergoes a two-step oxidative addition/reductive elimination pathway, whereas the Ni(II) species undergoes a one-step σ-bond metathesis pathway, with a barrier of 31.6 kcal mol^{-1}.

A recent report by the Lalic group[31] demonstrated that hydroarylation catalyzed with Ni can occur with external hydrogen sources. Specifically, NiCl$_2$(dme) coupled various terminal olefins (e.g., styrene or

vinyl ethers) with a variety of ArI reagents in the presence of excess poly(methylhydrosiloxane) (PHMS) and NaO^{t}Bu. This reaction exploits the relatively weak C–X bond as a means to generate a Ni–C bond capable of undergoing olefin insertion chemistry; PHMS served as the terminal hydrogen source to generate the desired alkyl-arene product. Further mechanistic studies are required to better elucidate the mechanism of this formal hydroarylation by a Ni(II) precatalyst.

Reactions of Unfunctionalized Arenes with Rh(I) Complexes Proceeding *via* Hydroarylation-Like Mechanisms. A recent report by Gunnoe and coworkers[32] highlighted a new method to selectively generate styrene from ethylene and benzene in a one-pot system. Initial synthesis and reactivity studies of a diimine Rh(I) catalyst indicated promising activity towards C–H activation.[33] Complexes **69** and **70** with auxiliary cyclooctene (coe)[33] and ethylene[32] ligands, respectively, were synthesized from the corresponding [L$_2$Rh^I(μ-TFA)]$_2$ dimer (Scheme 1.3).

In the presence of trifluoroacetate-d_1 (TFA-d_1), 1.6 mol% of complex **69** catalyzes arene H(D) exchange at 150 °C.[33] After 2 hours, complex **69** converted benzene to a mixture of C$_6$D$_n$H$_{6-n}$ species with 456 TONs. Using TFA and toluene-d_8, **69** catalyzed H(D) exchange to give a mixture of *ortho-, meta-*, and *para-* H(D) exchanged toluene species with a ratio of 6.9:1.0:6.4, respectively. In a subsequent report, complex **70** also exhibited activity towards arene H(D) exchange.[34] Given this relatively fast rate of C–H(D) activation and exchange, it was hypothesized that [L$_2$Rh^I(TFA)(olefin)] complexes **69** and **70** would be competent hydroarylation and hydrovinylation catalysts.

Using complex **70** and a Cu(II) salt as an external oxidant, the catalytic coupling of ethylene and benzene to generate styrene was achieved at very low catalyst loadings (0.001 mol% relative to neat benzene).[32] After 24 hours at 150 °C, styrene (60 TONs, which is quantitative yield based on Cu(II) as limiting reagent) was produced using 120 equivalents of Cu(OAc)$_2$ relative to **70**. Increasing the amount of Cu(OAc)$_2$ to 240 or 2,400 equivalents resulted in a corresponding increase in product formation, to 115 and 835 TONs, respectively. Moreover, the use of **70** and Cu(OAc)$_2$ selectively generated styrene; hydroarylation to form ethylbenzene was not observed. Other Cu(II) oxidants such as Cu(OHex)$_2$ or Cu(TFA)$_2$ were examined, but Cu(OAc)$_2$ resulted in the most stable system.

Scheme 1.3. Synthesis of Rh(I) Complexes of the Type [L$_2$Rh(olefin)(TFA)].[32,33]
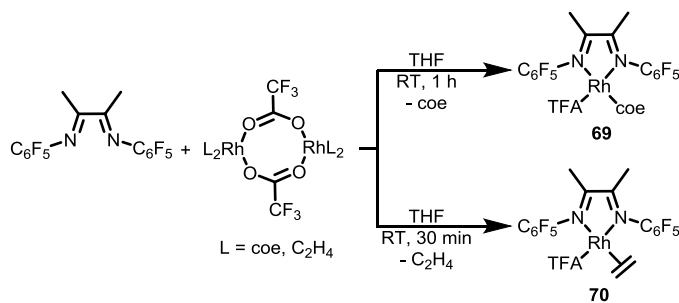
Kinetics experiments probed the effect of ethylene pressure on the rates of reaction (using TOFs).[32,35] The reaction rate was observed to have a first-order dependence on ethylene, which is in contrast to related systems that generally exhibit an inverse dependence on olefin concentration (*e.g.,* Pt(II)-based hydroarylation catalysts; *vide supra* and chapter 2). A competition experiment with equimolar amounts of benzene and benzene-d_6 generated a mixture of styrene and styrene-d_5 in a 3.1(2):1.0 ratio, respectively, and products containing more than five deuterons were not observed. This rate difference appears to

correspond to an isotope effect that is consistent with other C–H activation reactions. On the basis of these data, the mechanism of Figure 1.12 was proposed.[32] The ethylene complex undergoes ligand substitution by benzene which results in C–H bond activation and HX liberation upon ethylene recoordination. The resultant $[L_2Rh^IPh(C_2H_4)]$ complex (**71**) proceeds to a $Rh(CH_2CH_2Ph)$ derivative (**72**) *via* olefin insertion. In other catalytic hydroarylation systems, β-hydride elimination often leads to catalyst decomposition and a reduction in activity. In this system, however, β-hydride elimination appears to be a key step in the formation of styrene *via* a Rh(styrene)H (**73**) intermediate. A secondary catalytic cycle involving a Cu(II) species liberates styrene and regenerates the starting Rh(I) complex. The resulting reduced Cu(I) species can then be reoxidized by O_2 and an equivalent of HX.
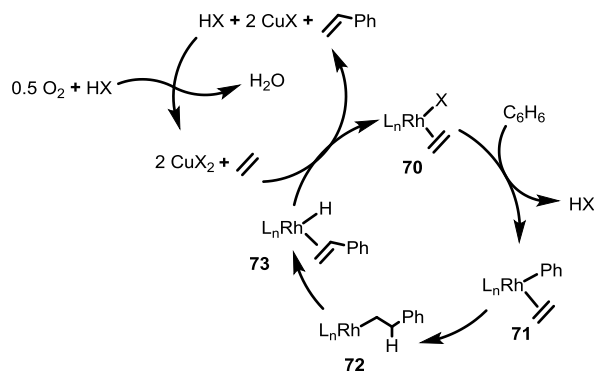
Figure 1.12. Mechanism for styrene formation with a Rh(I) hydroarylation system.[32]

An informative mechanistic investigation of this system has recently been reported by Gunnoe and coworkers.[35] Kinetic data reflect a complex dependence on the concentration of catalyst, which can vary from first- to half-order depending on the reaction temperature and ethylene concentration. The catalysis exhibits saturation like behavior with ethylene concentration (pseudo first-order at low concentrations and zero-order at high concentrations). A zero-order dependence on the concentration of Cu^{II} oxidant was observed. Rate constants were measured in independent reactions with benzene and benzene-d_6, which afforded k_H/k_D values that depend on the catalyst order; in the first-order regime, k_H/k_D was determined to be 6.7(6). In contrast to this, a reduced value of 1.2(6) was observed in the half-order regime, which implicates a change in mechanism. A competition experiment with equimolar amounts of benzene and benzene-d_6 gave the product ratio styrene:styrene-d_5 of 3.0(1). These kinetic isotope effects are consistent with a rate limiting C–H activation step. Computational studies were performed to elucidate activation parameters for individual steps in the proposed catalytic mechanism. A modification of this system, bearing a 1,2-bis(*N*-7-azaindolyl)benzene ligand, has been applied to higher-order olefins (i.e., propylene) to afford a distribution of both linear and branched products (i.e, *cis*/*trans*-β-methylstyrene, allylbenzene, and 2-phenylpropylene).[36]

Key Conclusions from Undirected Hydroarylations. Pt(II) complexes have been employed as catalysts for the hydroarylation of ethylene, using both cationic and neutral complexes. The supporting ligands have most often been chelating, nitrogen-based supporting ligands; bipyridine[17-22] and other nitrogen-containing heterocycles (*i.e.*, indole[8-10] or pyrrole[11-13]) are the most commonly employed ligand motifs. Ligand substituent effects on the few systems investigated so far are relatively minor. While other types of ligands with non-heteroaromatic donors (*e.g.*, phosphines, *N*-heterocycliccarbenes, diimines) have been studied, such complexes exhibit reduced activity towards hydroarylation, and are often completely inactive or

generate primarily styrene.[26,27] This information would seem to suggest that platinum-based catalysts are more effective with hard donors as supporting ligands, but further confirmation of this hypothesis is required.

For Pt(II) species, several related mechanisms[10,12,18] have been proposed. Two key steps are required during catalysis: arene C–H cleavage and olefin insertion into a Pt–Ph bond. Species of the type $[L_2Pt^{II}(C_2H_4)Ph]^+$ have been implicated as intermediates during catalysis. Rapid olefin insertion and subsequent olefin coordination result in a $[L_2Pt^{II}(C_2H_4)(CH_2CH_2Ph)]^+$ species, which is presumed to be the catalytic resting state on the basis of DFT and experimental evidence.[18] It is unclear what, if any, effects the counter anion may have on the hydroarylation mechanism. Aryl C–H activation can then occur to generate a Pt(ethylbenzene) π–complex, either through a single-step σ bond metathesis pathway or through the two-step oxidative addition/reductive elimination route (*via* a Pt(IV)–hydride intermediate). Upon substitution by ethylene, an equivalent of ethylbenzene is liberated along with the regenerated active catalyst. It has also been shown that $[(cod)Pt^{II}(OTf)_2]$ initiates an acid-mediated catalytic cycle with several substrates.[23]

The electrophilic nature of the metal center may play an important role in determining whether a Pt- or acid-based mechanism prevails. Catalyst precursors that can serve as a source of dicationic Pt centers (i.e., the most electrophilic complexes) produce protons likely *via* electrophilic displacement of a proton from the hydrocarbon (e.g., olefin). These species, therefore, catalyze hydroarylation through a Friedel-Crafts mechanism. In contrast, catalyst precursors that initially possess a Pt–aryl bond appear to proceed *via* a pathway that features a metal-centered insertion mechanism. Such catalysts are typically monocationic, and therefore less electrophilic. Current data suggest that catalysts with bidentate NN ligands operate *via* a metal centered insertion mechanism, though further studies are required to rigorously test this hypothesis.

Pt catalysts, nonetheless, do present several unique advantages. Unlike other metal centers employed in hydroarylation, Pt(II) complexes may be used with undirected (unactivated) arene substrates; in contrast, other metal centers (*vide infra*) are often only able to promote hydroarylation *ortho*- to a directing aryl substrate (e.g., imine, ketone). Additionally, the stability of Pt(II) complexes permits the isolation and characterization of a number of proposed intermediates, providing further insight into the operative hydroarylation mechanism and potentially aiding in the development of more active species.

Though Pt-based catalysts seem to offer potential for hydroarylation with unfunctionalized substrates (*i.e.* ethylene and benzene), their productivity is quite low. In many cases, only tens to hundreds of TONs are observed. When compared to other metal centers, Pt(II) catalysts often require neat substrates and exhibit lower yields to achieve hydroarylation catalysis. Moreover, these systems all seem to suffer from competing catalyst deactivation caused either by decomposition to metallic platinum or through unproductive catalysis to generate undesired side products. To make homogeneous Pt(II) catalysis industrially applicable and commercially useful, dramatic improvements are required to be improve their activities, selectivities, and stabilities.

Recent developments in Rh and Ni mediated C–H activations of unfunctionalized arenes towards hydroarylation catalysis may address the current limitations exhibited with Pt-based catalysts, namely irreversible β-hydride eliminations and subsequent ligand reductive eliminations. The development of analogous Ni(II) based systems may be possible given the recent precedents described by the Hartwig group.[28] Given the marked stability of molecular Ni(0) complexes, Ni catalysts likely exhibit enhanced

robustness to irreversible catalyst decomposition. An alternative approach adopted by Gunnoe and coworkers[32-36] exploits β-hydride eliminations with a cooperative Cu(II)/Cu(I) redox cycle. Unfunctionalized arenes such as benzene have been used in a one-step process to generate the corresponding styrene product with over 800 TONs using a bisimine ligated Rh complex.[32] It appears that a key event couples ethylene and benzene to generate a Rh–alkyl complex in a process similar to that operating in many hydroarylation mechanisms.[32,35] However, rather than generating a hydroarylation product by reductive elimination or σ-bond metathesis, a β-hydrogen elimination occurs to generate a hydride species with a bound styrene. With the use of an external Cu oxidant, styrene is eliminated to regenerate the active Rh(I) species. Such direct C–H coupling of benzene and ethylene to styrene is highly desirable industrially as current routes require a two-step Friedel-Crafts alkylation and dehydrogenation pathway.

***Ortho*-Directed Hydroarylations Catalyzed by Rh(I) Complexes.** *Ortho*-directed hydroarylations catalyzed by rhodium have been thoroughly investigated, and reports on Rh(I) catalysts have provided the most information on late-metal systems for this catalysis. This may relate to the well-known ability of Rh(I) complexes to undergo C–H activation chemistry with aryl substrates.[37,38] In 1989, Ghosh and Graham[39] demonstrated that a trispyrazolylborate (HBPz$_3$) complex of Rh(I) binds ethylene and activates a C–H bond in benzene at room temperature under ultraviolet irradiation. The resulting Rh–hydride complex undergoes rapid ethylene insertion, to give the complex [(HBPz$_3$)Rh^{III}(CO)(C$_2$H$_5$)Ph] with both alkyl and aryl ligands bound to the metal center. Upon exposure to CO, insertion into the Rh–alkyl bond occurs to generate the acyl complex [(HBPz$_3$)Rh^{III}(CO)(COC$_2$H$_5$)Ph]. Treatment of this complex with ZnBr$_2$ afforded propiophenone as the final organic product. This work demonstrated that Rh(I) species can mediate both olefin insertions and C–H activations. Subsequent studies[40] confirmed that some Rh(I) complexes (*e.g.*, Wilkinson's catalyst, [(PPh$_3$)$_3$RhCl]) can in fact catalyze olefin hydroarylation. Several reviews have been published on Rh(I)-mediated hydroarylation,[41-44] and these emphasize the versatility of this metal center in this type of catalysis. It is worth noting that [CpRh^{III}] complexes also competently catalyze hydroarylations but will not be discussed further.[45,46]

Most Rh(I) hydroarylation systems have been developed for use with arenes bearing directing or coordinating substituents.[40,47-73] Commercially available catalysts such as Wilkinson's catalyst ([(PPh$_3$)$_3$Rh^{I}Cl], **74**) are typically employed. For this type of hydroarylation, olefin insertion occurs only at aryl C–H bonds that are *ortho*- to the directing group. While slight variations in the operative mechanism have been suggested,[40,47-73] the generalized mechanism of Figure 1.13 seems to be operative for all of the systems discussed here. Initially, pre-coordination of the directing aryl substituent likely occurs to place the *ortho*-proton proximal to the metal center (**75**). Subsequently, C–H activation, assisted by a chelation effect, occurs while also generating a Rh–hydride bond (**76**). Olefin coordination (**77**) and insertion into this Rh–hydride bond generates the corresponding Rh(alkyl)(aryl) complex **78**, which likely is the catalytic resting state. Upon reductive elimination, the desired *ortho*-hydroarylated product is generated. Displacement of product by another arene completes the cycle.
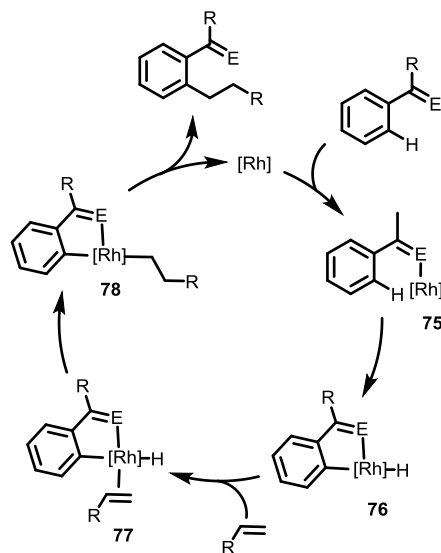
Figure 5.13. Generalized mechanism for Rh(I) catalyzed *ortho*-hydroyarlation (E = NR, O).

Related chemistry reported by Jun and coworkers involves the catalytic hydroacylation of ketones[47] and aldimines[48] using **74** and 2-amino-3-picoline as a chelation cocatalyst. For ketone substrates, an initial condensation with the picoline additive generates an aldimine. Transimination occurs instead with aldimine substrates to replace a phenyl group with a pyridine. The newly installed pyridine fragment is capable of binding to the Rh which anchors the substrate to the metal center. Chelation assisted C–H activation of the aldimine hydrogen then occurs, followed by olefin coordination. Migratory insertion of the olefin followed by C–C reductive elimination produces the hydroacylated product. Condensation of this hydroacylated imine with water regenerates 2-amino-3-picoline and forms the desired ketone.

With a variation of this hydroacylation system, Jun and coworkers[40] observed that **74** catalyzes both the hydroacylation and hydroarylation of *tert*-butylethylene with the aryl aldimine **79** (eq 1.3), in the presence of 2-amino-3-picoline at elevated temperatures. It is worth noting that the initial transamination of **79** with 2-amino-3-picoline affords a new aldimine with two positions available for C–H activation: an imine hydrogen and *ortho*-aryl hydrogen. With this substrate, therefore, both hydroarylation and hydroacylation occur. Upon acid-mediated hydrolysis, the ketone **80** was generated in high yield. In addition, a minor hydroacylation product (**81**) was observed. It was noted that in the absence 2-amino-3-picoline, product formation was not observed with this substrate.
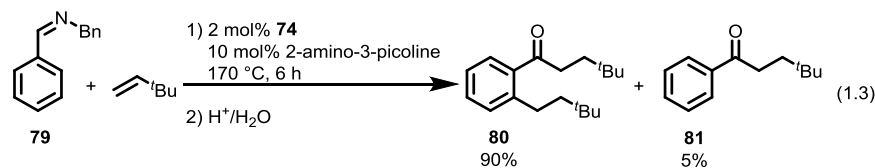

When a ketimine was used in place of an aldimine, only hydroarylation products were obtained. Moreover, the addition of picoline as a reagent was no longer required for catalysis. To further investigate the scope of the system, a wide variety of arene and olefin substrates were tested,[40,49] and the results are summarized in Table 1.7. Three different substituents were varied: the aryl group (R^1), the imine (R^2), and the olefin (R^3). Hydroarylation was achieved with both electron-withdrawing (R^1 = CF$_3$) and -donating (R^1 = OMe) aryl substituents with minimal differences in the isolated yields. Changing the length of the

ketimine substituent had a minimal effect, with a change in yield observed only with longer R^2 groups (*i.e.,* pentyl). Finally, olefins with bulky aliphatic groups (R^3 = ^{t}Bu, ^{n}Bu, ^{n}Hex, Cy, SiMe$_3$) tended to give high (often quantitative) yields. Ester- and amide-containing olefin substituents afforded hydroarylated products in high yield. Electron-withdrawing groups such as SO$_2$Ph or CN resulted in a large reduction in overall activity, to give yields of 43 and 32%, respectively.

A competition experiment with Wilkinson's complex **74**, using various ratios of 1-hexene (**82**) and *N,N*-dimethylacrylamide (**83**) with ketimine **84** afforded a mixture of the corresponding hydroarylated products **85** and **86**, respectively (eq 1.4). With an equimolar amount of **82** and **83**, a product ratio (**85**:**86**) of 10:90 was observed. By increasing the relative ratio of **82** to **83**, a corresponding increase in the product ratio was observed. With an olefin ratio (**85**:**86**) of 5.0:1.2, the product ratio increased to 38:62. Even with a substantial excess of **82**, larger amounts of the products derived from the activated olefin (**86**) were observed, suggesting that functionalized olefins (such as **83**) are preferred substrates. Solvent-free conditions were also reported for the hydroarylation with **74**.[50] Using a microwave reactor, the hydroarylation of various substrates was achieved with high temperatures and short reaction times. Using this method, yields similar to those obtained with high-boiling solvents were achieved after 15 minutes of microwave heating.
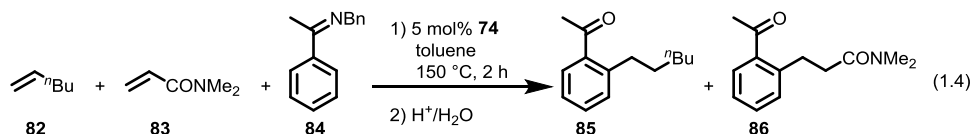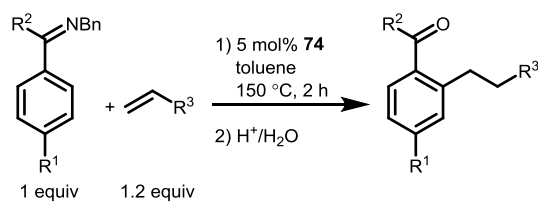

In an effort to develop a recyclable system, Jun and coworkers[51] generated phosphine-containing, extended supramolecular structures to use as ligands. The extended assembly was synthesized from two small molecules, a barbiturate derivative and 2,4,6-triaminopyrimidine, which self-assembled into a larger aggregate (Figure 1.14). [(coe)$_2$Rh^I(μ-Cl)]$_2$ (**87**) was then added to the barbiturate/pyrimidine mixture. The resulting complex readily formed an extended hydrogen-bonding network (depicted below) at room temperature to afford a solid-supported pre-catalyst. At elevated temperatures, however, this hydrogen-bonded network cannot form and liberates the metal complex as a soluble small molecule; the reaction was catalyzed by a homogenous species. Cooling and the addition of *n*-pentane reforms the extended network resulting in the precipitation of the solid supported pre-catalyst. This solid was then isolated by centrifugation and filtration after hydroarylation. The recovered catalyst was then recycled, and it exhibited only a small reduction in overall yield over eight catalytic runs with several substrates.
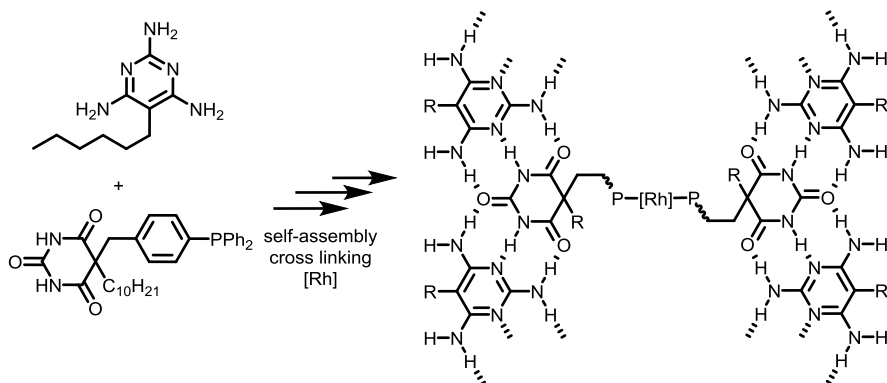
Figure 5.14. Self-Assembly of a barbiturate derivative and 2,4,6-triaminopyrimidine with Rh(I), generating a solid support hydroarylation catalyst.[51]

Table 1.7. Representative *ortho*-hydroarylation substrate scope using **74**.

R¹	R²	R³	Isolated Yield (%)
H	Me	^{t}Bu	97
		^{n}Bu	94
		^{n}Hex	71
		Cy	65
		Si(Me)$_3$	92
		C$_6$F$_5$	91
		CO$_2$Me	94
		CO$_2$Et	93
		CONMe	81
		SO$_2$Ph	43
		CN	32
	Et	Si(Me)$_3$	93
	^{n}Pent	Si(Me)$_3$	73
CF$_3$	Me	^{t}Bu	76*
		CO$_2$Me	95
OMe	Me	^{t}Bu	42[a]
		CO$_2$Me	90

[a] Catalyst loading reduced to 1 mol% of **74** and the reaction was run for 30 min at 130 °C.[40,49]

Bergman, Ellman, and coworkers[52] demonstrated that an intramolecular *ortho*-hydroarylation reaction was achieved for imine-substituted arenes with a pendent C–C double bond. For intramolecular hydroarylation, cyclized products were generated. Upon hydrolysis with acid, acyl-substituted aromatic bicyclic products were isolated in reasonable yields. While the operative mechanism is similar to the general mechanism discussed previously (*vide supra*), a key difference is proposed to selectively generate the cyclized product over intermolecular coupling (Figure 1.15).[53] While the initial pre-coordination (**88**) and oxidative addition (**89**) steps are identical, a rapid coordination of the pendent double bond occurs preferentially over intermolecular olefin binding. This coordination step anchors the substrate through a tridentate binding motif (**90**). Olefin insertion into the Rh–hydride bond (**91**) followed by subsequent reductive elimination affords the cyclized hydroarylation product (in this case, a substituted indane).
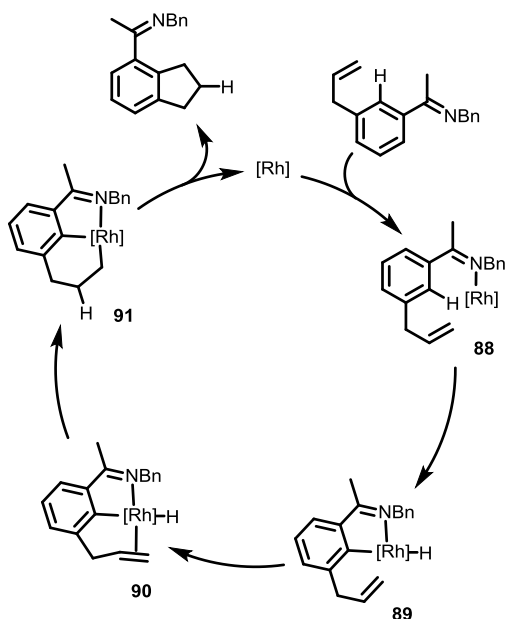
Figure 1.15. Mechanism for intramolecular *ortho*-hydroarylation with Rh(I).[52,53]

To demonstrate the versatility of this intramolecular *ortho*-hydroarylation system, a wide variety of *N*-aryl imine containing olefins were cyclized using conditions similar to those described above and the substrate scope is summarized in Table 1.8.[52,53] Cyclic products were typically isolated in high yields despite the potential for some substrates to isomerize to species incapable of cyclization. Substrates with substituted double bonds (entries 3-7) tended to provide higher yields, potentially due to reduced isomerization. Five-membered cyclized products were observed. Some substrates could potentially generate multiple bicyclic products due to olefin insertion occurring either in a Markovnikov or anti-Markovnikov fashion. The new heterocycles generated were either five- or six-membered. With a longer chain linker (entry 2), for example, both bicyclic products were observed in a 1:1 ratio. Heteroatom-tethered substrates (entries 8-12) in general exhibited higher activity towards ring-closing (*vs.* their aliphatic analogues), producing substituted dihydrobenzofuran and indoline compounds. Overall, cyclization with **74** afforded products with a wide variety of substrates.

Table 1.8. Substrate scope for intermolecular *ortho*-hydroarylation with **74**.

1) 5 mol% **74**
toluene (0.1 M)
2) H⁺/H₂O

n = 0,1   X = CH₂, O, NR
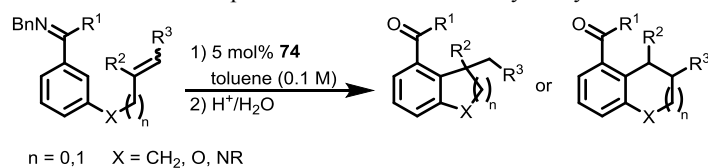
Entry	Substrate	Temp. (°C)	Time (h)	Product	Yield (%)[a]
1		125	1		52
2		150	48		50 (1:1)
3		125	4		71
4		150	36		58
5		150	16		68
6		150	36		50 (7:1 *cis*:*trans*)
7		125	2		85
8		175	0.75		90
9		150	16		59
10		150	3		50
11		125	12		53
12		150	72		41
13		150	6		81

[a] Measured as isolated yields.[52,53]

While Wilkinson's catalyst **74** has been successfully employed in hydroarylation chemistry, the PPh$_3$ ancillary ligands appear to limit its versatility. Since more complex phosphine ligands have exhibited useful properties in other catalytic reactions (*e.g.,* enantioselectivity), additional Rh(I) precatalysts have been explored. Lim and coworkers[54,55] discovered that upon using the phosphine-free Rh(I) precursor **87** ([(coe)$_2$Rh^I(µ-Cl)]$_2$) along with added PCy$_3$ ligands, the *ortho*-hydroarylation of aldimines was achieved. In contrast, complex **74** catalyzed the hydroarylation of aldimines only upon addition of a picoline cocatalyst.[40]

Table 1.9. Substrate scope with **87** and PCy$_3$.[54,55]
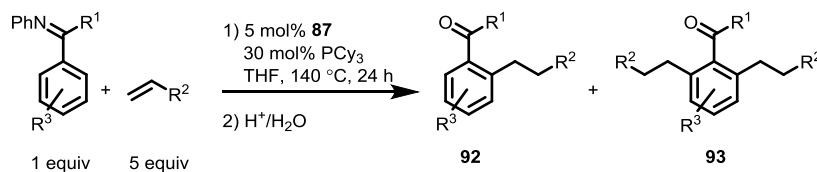
R^1	R^2	R^3	92 : 93	Isolated Yield (%)
H	^{t}Bu	H	11:89	93
		p-OMe	1:99	90
		p-Me	5:95	87
		p-F	1:99	84
		p-Cl	3:97	88
		p-CF$_3$	2:98	90
		p-NO$_2$	88:22	6
		m-OMe	97:3	50
		m-F	26:74	62
		m-Cl	77:23	63
		o-Me	100:0	80
		o-Cl	–	0
		o-NO$_2$	–	0
	^{n}Bu	H	34:66	19
Me	^{t}Bu	H	28:72	99
Et	^{t}Bu	H	97:3	86
	^{n}Pr	H	100:0	65

Using this system, a series of substituted aldimine and ketimine substrates were alkylated (Table 1.9) to generate the corresponding monohydroarylated (**92**) and dihydroarylated (**93**) products.[54,55] Moreover, most aldimines (R^1 = H) exhibited higher yields for **93**, with selectivities generally greater than 95% for dihydroarylated products from *para*-substituted aldimines. With highly electron-withdrawing substituents a switch in selectivity was observed, with *p*-NO$_2$, *m*-F, and *m*-Cl aryl substituents giving reduced selectivities for **93**. Similarly, *meta*- and *ortho*-substituents generally afforded **92** in higher yields. Reducing the steric bulk of the olefin using *n*Bu rather than *t*Bu substituents decreased the amount of **93** formed. However, this was achieved at the expense of reduced overall reactivity. A similar trend towards producing monohydroarylated products was noted for ketimine substrates (R^1 = Me or Et). These conditions were also used in the heterohydroarylation of imine-substituted furan, thiophene, and naphthalene substrates.[55]

In a subsequent publication by Lim and Koo,[56] compound **94** was used as a probe to determine chemoselectivity in *ortho*-hydroarylations. Since each aryl C–H bond in **94** is *ortho* to an imine-directing group, all four positions can potentially undergo hydroarylation. Using an excess of *tert*-butylethylene with **94** under conditions similar to those described above, multiple hydroarylation products were observed (eq 1.5). While the monohydroarylation product **95** was observed, dihydroarylation led to the major product, **96**. With several other olefin substrates (1-butene, 1-pentene, 1-hexene, 3-methyl-1-butene), **97** was formed as a minor product (typically < 3%) and **98** was not observed by ^{1}H NMR spectroscopy. It was suggested, therefore, that the pathway to form **98** proceeds *via* intermediates with sterically hindered Rh(I) centers, for which a second C–H activation at positions *ortho*- to the first alkylation is difficult. The mechanisms for **97** and **98** require additional ligand rearrangements as only *ortho*-aryl C–H bonds can undergo hydroarylation; after the first hydroarylation event, imine decoordination occurs followed by coordination of the *second* imine group. In contrast, C–H activation *meta*- to the first alkylation can occur without imine dissociation and generates a less sterically crowded intermediate. Therefore, compound **96** is observed as the major product.
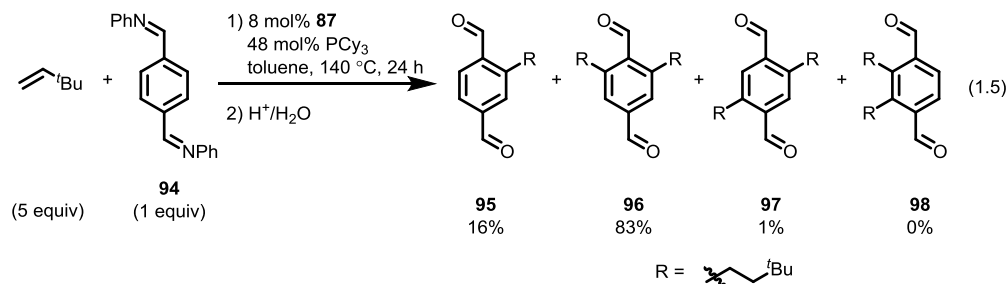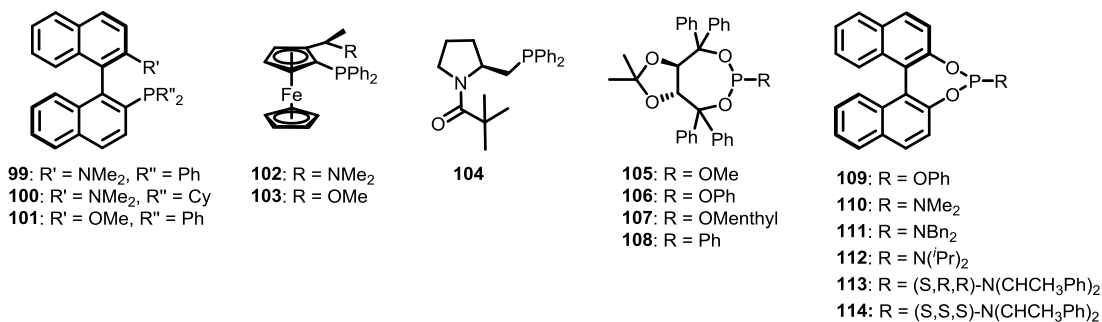

While the **87**/PCy$_3$ catalyst system has been extensively used, other phosphorus-containing ligands have been investigated.[53] In particular, ferrocene-containing phosphine ligands (FpPCy$_2$) demonstrated higher yields and lower reaction times than corresponding alkyl (PCy$_3$) or aryl (PPh$_3$) analogues. Chiral ligands have also been studied by Ellman, Bergman, and colleagues.[57] In these investigations, intramolecular *ortho*-hydroarylation was observed using a series of chiral phosphorus ligands (**99-114**, depicted in Figure 1.16).

Table 1.10. Asymmetric intramolecular *ortho*-hydroarylation using chiral phosphorus ligands.
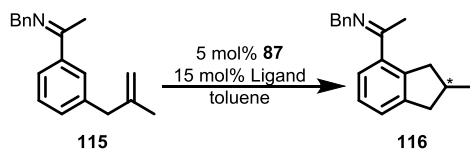
Ligand	Temperature (°C)	Time (h)	Yield (%)	ee (%) [a]
99	125	20	5	–
100	125	20	Trace	–
101	125	20	48	8 (*S*)
102	125	20	9	–
103	75	6	99	35 (*R*)
104	100	6	56	23 (*S*)
105	75	20	93	17 (*R*)
106	75	20	94	9 (*R*)
107	75	20	91	38 (*R*)
108	125	20	34	0
109	125	20	6	–
110	125	2.5	15	19 (*S*)
111	125	2.5	52	58 (*S*)
112	125	< 2	100	83 (*S*)
113	125	< 2	100	88 (*S*)
114	125	< 2	99	87 (*S*)

[a] Major isomer given in parenthesis.[57,58]

99: R' = NMe$_2$, R" = Ph
100: R' = NMe$_2$, R" = Cy
101: R' = OMe, R" = Ph

102: R = NMe$_2$
103: R = OMe

104

105: R = OMe
106: R = OPh
107: R = OMenthyl
108: R = Ph

109: R = OPh
110: R = NMe$_2$
111: R = NBn$_2$
112: R = N(^{i}Pr)$_2$
113: R = (S,R,R)-N(CHCH$_3$Ph)$_2$
114: R = (S,S,S)-N(CHCH$_3$Ph)$_2$

Figure 1.16. Asymmetric, chiral phosphorus containing ligands used for enantioselective hydroarylation.[57,58]

An excess of chiral ligand (**99-114**) relative to **87** was used to determine the yields and enantioselectivities for the intramolecular *ortho*-hydroarylation of **115** to the cyclized product **116** (Table 1.10).[57] Ligands containing P–N bonds (**99**, **100**, and **102**) provided poor yields, likely due to ligand chelation that inhibits substrate binding to the Rh(I) center. In contrast, ligands containing P–O bonds (**101**, **103**, and **105-114**) exhibited enhanced yields with nearly quantitative conversions in many cases. Phosphoramidite ligands **110-114** demonstrated the highest enantioselectivities, producing the *S*-stereoisomer in greater than 50% ee. The (*S*)-binol phosphoramidite ligands (**113-114**) exhibited the highest conversions and enantioselectivities while also requiring the shortest reaction time. Note that both *R*- and *S*-products could be obtained depending on the ligand choice. In a subsequent publication,[58] the optimized conditions for enantioselective intramolecular *ortho*-hydroarylation were described for several other ketimine substrates using a similar set of chiral P–O containing ligands. It is clear that there is much room for improvement in the enantioselectivities of these reactions.

Benzyl and phenyl imines have been extensively employed as hydroarylation substrates due to their simple synthesis.[40,47-58] More recently, Bergman, Ellman, and coworkers[59] have demonstrated that chiral aminoindane-substituted aldimines (**117**) promote enantioselectivity for hydroarylation reactions, even though the aminoindane functionality is ultimately removed by hydrolysis. A series of aminoindane substrates were cyclized using **87** and the phosphine ligand FcPCy$_2$ (**118**) to afford the dihydrobenzofuran **119**. Compared to the achiral ligand **118**, previous studies[57,58] demonstrated that similar chiral ferrocene-based phosphine ligands (**102** and **103**) exhibited reduced enantioselectivities in cyclizations. In contrast to this, catalysis with the chiral aminoindane directing group of **117** and achiral ligand **118** exhibited enhanced enantioselectivity (Table 1.11); the observed selectivity resulted from the chiral directing group and not from any added ancillary ligands. For all substrates tested, yields greater than 60% were observed with high enantiomeric excesses. Temperatures at or below 75 °C resulted in cyclized products (**119**) using aminoindane substituted directing groups, whereas benzyl imine substrates required elevated temperatures for cyclization.

Table 1.11. Substrate scope for enantioselective cyclization using chiral substrates.[59]
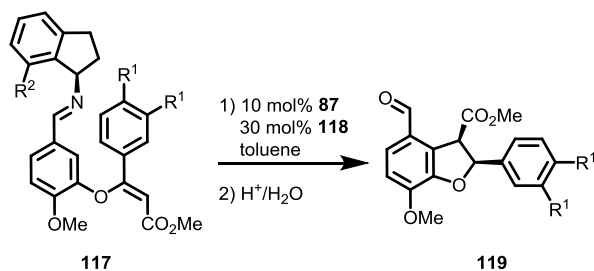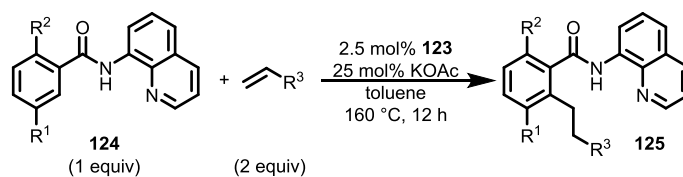

R^1	R^2	Temperature (°C)	Time (h)	Yield (%)	ee (%)
OMe	H	75	16	76	76
	Me	75	16	62	80
	F	60	36	70	90
	Ph	75	16	90	83
H	H	75	16	80	65
	F	75	16	81	70

While ketimines and aldimines have been extensively used to bind the substrate to the Rh(I) center, other coordinating groups have been investigated. Murai and coworkers[60] demonstrated that the pyridine-substituted naphthalene compound **120** could undergo *ortho*-hydroarylation (eq 1.6) using trimethylvinylsilane or ethylene with **87** and added chiral phosphine ligand to generate the corresponding products **121** and **122**, respectively. The yields using a pyridyl directing moiety, however, are generally lower than those derived from imine-based groups.
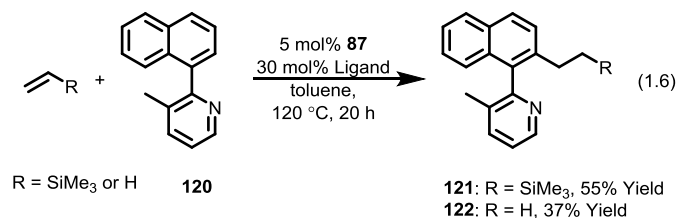
Table 1.12. Substrate scope of *ortho*-hydroarylation using quinolylamide directing substrates.

R¹	R²	R³	Isolated Yield (%) [a]
H	OMe	CO_2Me	77
	Ph	CO_2Me	85
	CF_3	CO_2Me	84
	F	CO_2Me	86
	Me	CO_2Me	86
		$CO_2{}^tBu$	71
		CO_2Bn	81
		$CONMe_2$	68
		SO_2Ph	48
		Ph	86
		p-OMePh	88
		p-^tBuPh	79
		p-tolyl	84
		p-FPh	85
	Me	^nBu	84 (7.3)
		$CH_2(CH_2)_3CH_2OAc$	90 (6.1)
Me	Me	^nBu	56
Me	Me	CO_2Me	91
F	Me	CO_2Me	90
Br	Me	CO_2Me	68

[a] For cases where a mixture of regio-isomers was isolated, the linear to branched ratio is given in parenthesis.[61-63]

A recent series of investigations utilized a bidentate, pre-coordinating scaffold for the *ortho*-hydroarylation of α,β-unsaturated esters,[61] substituted styrenes,[62] and unfunctionalized linear α-oleifns.[63] Specifically, an 8-quinolylamide group directed the hydroarylation to selectively generate *ortho*-hydroarylation products in the presence of the [(cod)Rh^I(μ-Cl)]$_2$ (**123**) and added acetate ligand. Moreover, only anti-Markovnikov products were observed with a variety of substrates, as expected when using Michael Acceptors. The results of the substrate scope using the quinolylamide motif (**124**) are summarized in Table 1.12. For nearly all substrates, alkylated products **125** were isolated in high yields. Interestingly, both α,β-unsaturated esters and substituted styrenes were observed to undergo high conversion, with a minimal effect on yields for a variety of olefins. Similarly, there were minimal effects of arene substituents on the overall yields.

Using deuterium labeling, several key features of the mechanism were elucidated by Chatani and coworkers.[61-63] Deuterated aryl substrate **126** and a naphthalene-containing α,β-unsaturated ester (**127**) were treated with **123** and added acetate (eq 1.7). After heating at 160 °C for 10 minutes, the products were identified and the location of the deuterium atoms was determined. Three separate species were identified after reaction: *ortho*-H(D) exchanged **126**, unreacted **127**, and the hydroarylation product **128**. It was noted that **128** contained 2.87 hydrogen atoms, indicating that on average, nearly one deuterium was incorporated into the product, as expected. The location of this deuterium atom, however, was scrambled across both methylene positions, which suggests that a reversible C–H(D) activation step occurs.

To probe the H(D) exchange further, **126** was only treated with stoichiometric quantities of **123**. Interestingly, proton incorporation into the *ortho*-aryl position of **126** was observed without added acetate, though a higher degree of exchange was noted in the presence of added acetate (0.41 H incorporation after 15 min with added acetate *vs.* 0.19 H incorporation after 12 h without added acetate). This suggests that the role of acetate is to transform **123** into the active catalytic species, likely with a bound acetate. To test this hypothesis, a similar experiment was performed using the acetate-ligated Rh species, [(cod)Rh^I(OAc)]$_2$. Using this catalyst, H(D) exchange was observed with **126** as a substrate, which incorporated the same number of protons either with or without added acetate (c.a. 0.4 H incorporation after 15 min). A similar deuterium-labeling experiment using styrene-d_8[62] or linear α-olefins-d_3[63] with **126**-d_0, revealed that H(D) exchange also occurs from the olefin substrate.

R = naphthalen-1-ylmethyl
Q = quinolyl
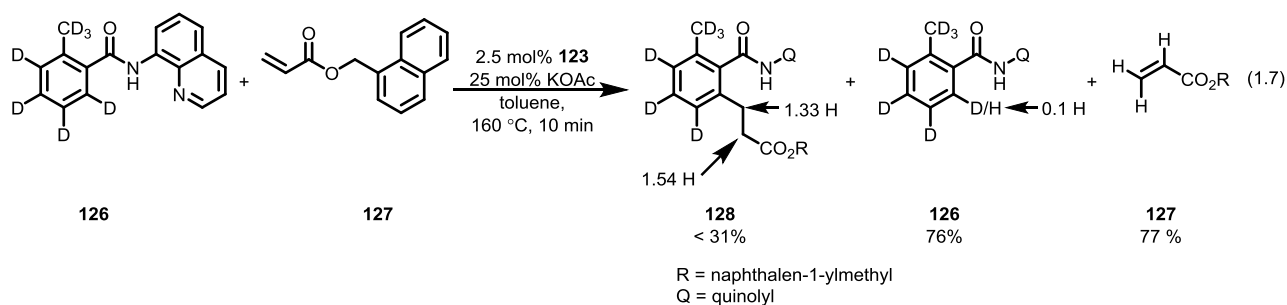
A mechanism for this hydroarylation reaction was proposed (Figure 1.17) to account for both the observed H(D) exchange and the presence of only anti-Markovnikov products.[61] Initially, ligand substitution of a chloride for an acetate ligand occurs. The quinolylamide substrate can bind to this Rh^I(OAc) species (**129**), which anchors it in a bidentate fashion to the Rh center in complex **130**. An *ortho*-aryl C–H activation step can then occur to afford a Rh(III)–hydride species (**131**). Coordination and insertion of an olefin yields the resulting Rh–alkyl fragment. This can occur, however, in either a

Markovnikov (**132**) or anti-Markovnikov (**133**) fashion. According to the authors, steric congestion proximal to the metal center results in a reductive elimination that can only occur with the linear Rh–alkyl fragment thereby generating the anti-Markovnikov products selectively. Therefore, only one regioisomer (**125**) is expected during the reaction. The other regioisomer (**134**) was not observed. Upon reductive elimination of the alkyl and aryl substituents on the Rh(III) center, acetate displaces the product to regenerate the active Rh(I) species (**129**).
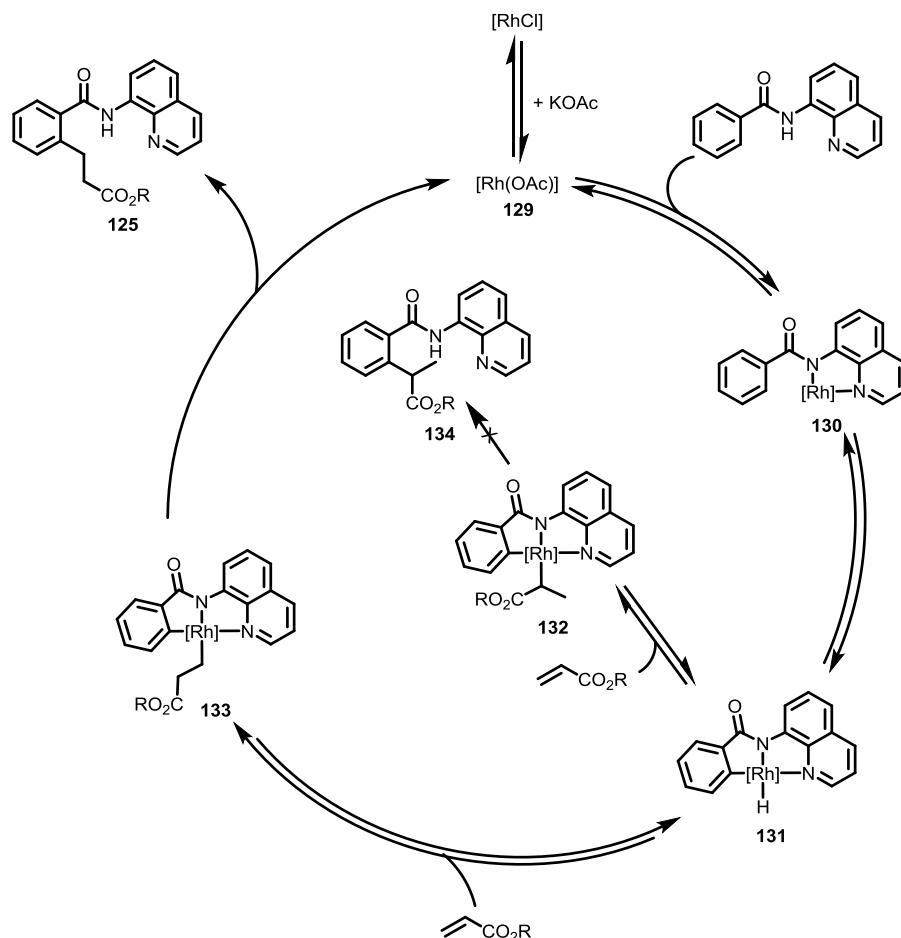
Figure 1.17. Mechanism for quinolylamide directed *ortho*-hydroarylation.[61]

To demonstrate the practicality of intramolecular *ortho*-hydroarylation, Bergman, Ellman, and coworkers reported the total syntheses of (+)-lithospermic acid[59,64] and several mescaline derivatives[53,65] using **87** with added phosphorus-based ligand, **118**. In these total syntheses, hydroarylation was used as a cyclization step, significantly reducing the number of steps required to generate each natural product, in decent yields. (+)-Lithospermic acid (**135**) was synthesized with a 5.9% yield over 10 steps (Scheme 1.4); similarly, the depicted tetrahydrobis(benzofuran) functionalized mescaline derivative (**136**) was isolated in 38% over 6 steps (Scheme 1.5).

Scheme 1.4. Synthesis of (+)-Lithospermic Acid (135) *via* Rh Catalyzed Hydroarylation.[59,64]

135
10 steps, 5.9% overall yield
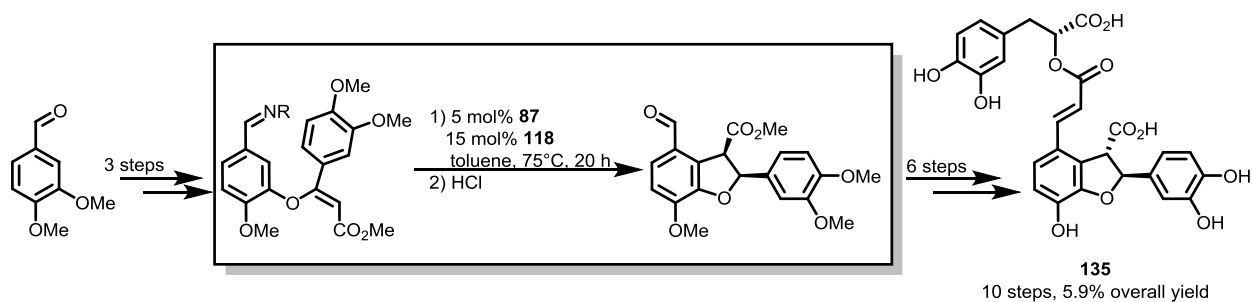
Scheme 1.5. Total Synthesis of Mescaline Derivative 136 *via* Rh Catalyzed Hydroarylation.[53,65]

65% yield

136
6 steps, 38% overall yield
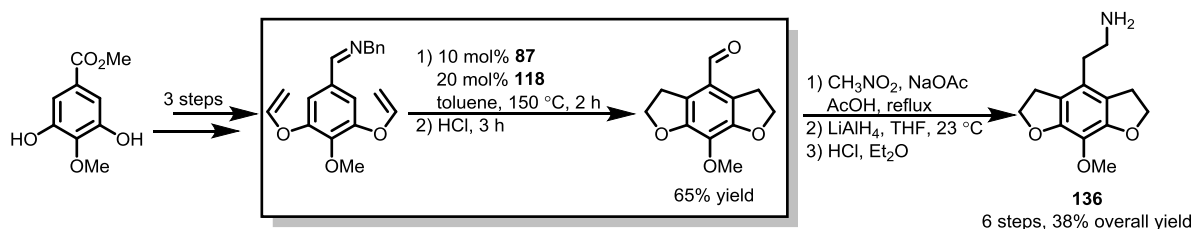
Ortho-hydroarylation has also been successfully employed towards strained olefin substrates such as norbornene. In one such system,[66] several Rh(I) precatalysts were used to catalyze the hydroarylation of norbornene using the biaryl substituted ketone compound **137** (eq 1.8). Using 10 mol% of $[(C_2H_4)_2Rh^I(\mu\text{-}Cl)]_2$ (**138**), two products were observed in the attempted hydroarylation of norbornene with **137**: the desired hydroarylated product (**139**) and a C–C activated product (**140**). This reaction was observed with several different norbornene and biaryl ketone substrates, generating both types of products.
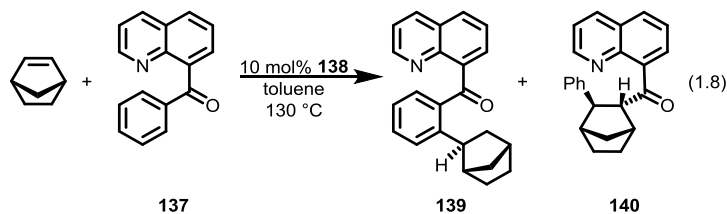
A similar *ortho*-hydroarylation of norbornene with substituted anilines has been reported by Burnet and coworkers[67,68] using $[(PEt_3)_2Rh^I(\mu\text{-}Cl)]_2$ (**141**). With this complex, both hydroamination and hydroarylation were observed (eq 1.9). Using a mixture of aniline and the corresponding lithiated aniline salt, the resulting hydroamination (**142**) and hydroarylation (**143**) products were observed, with **143** as the major product. While the yields using aniline were relatively low, the use of *p*-toluidine increased the overall yield to 90% giving a 10:90 ratio for hydroamination to hydroarylation products.
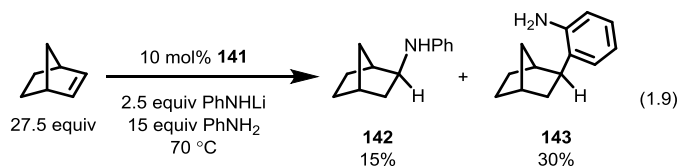
While Rh(I) complexes with phosphorus ligands have been extensively used in *ortho*-hydroarylation, other ligand sets have proven useful. In a report by the Brookhart group,[69] the pentamethylcyclopentadienyl (Cp*) Rh(I) complex [(Cp*)Rh^I(CH$_2$CHSiMe$_3$)$_2$] (**144**) was used as a hydroarylation precatalyst (eq 1.10). Using trimethylvinylsilane and benzophenone substrates, both the monohydroarylated (**145**) and dihydroarylated (**146**) products were observed. Note that only anti-Markovnikov products were formed. Several other olefin substrates were probed with **144**, affording yields of greater than 60% in most cases after 10 hours.

$$(1.10)$$

145
88%

146
11%
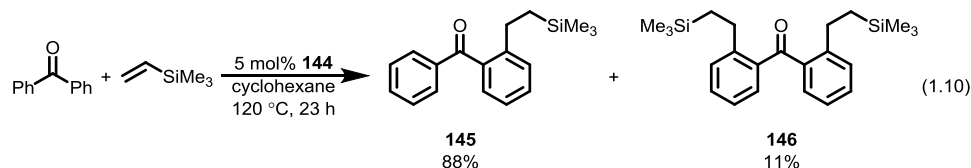
Hydroarylation of highly fluorinated arenes catalyzed by a Rh(I) hydroxide complex was described in a recent report by Zhao and coworkers.[70] It was previously reported by Bercaw and Labinger[71] as well as Goldberg and coworkers[72] that Rh(I) hydroxides undergo stoichiometric aryl C–H bond activations to generate Rh–aryl species. For example, [(cod)Rh^I(μ-OH)]$_2$ (**147**) promotes the C–H activation of indane, to give a [(cod)Rh^I(η^3-indenyl)] complex (**148**) along with an equivalent of water.[71] Moreover, Lautens and coworkers[73] demonstrated that **147** catalyzes the hydroarylation of allyl amines with arylboronic acids in high yields.

Similar C–H bond cleavage reactivity was observed with a Rh(I) complex possessing a 2,6-bis[(di-*tert*-butylphosphino)methyl]pyridine (PNP) pincer ligand, [(PNP)Rh^I(OH)] (**149**).[72] Using **149**, benzene-*d$_6$* or benzene were activated to generate the corresponding Rh–phenyl complexes [(PNP)Rh^I(C$_6$D$_5$)] (**150**) and [(PNP)Rh^{I}Ph] (**151**), respectively (Scheme 1.6). In a control experiment, H(D) scrambling into the methylene bridge of the ligand backbone occurred in benzene upon exposure of **151** to 10 equiv. of D$_2$O. It has been previously demonstrated by Milstein and coworkers[74,75] that (PNP)M complexes (M = Rh, Ir) are susceptible to deprotonation at the PNP methylene bridge as a result of ligand non-innocence. Therefore, it was suggested that adventitious deuterium incorporation occurs between **151** and D$_2$O through an acidic exchange mechanism.[72]

Scheme 1.6. Arene C–H(D) Activations and H(D) Exchange with Complex 149.[72]
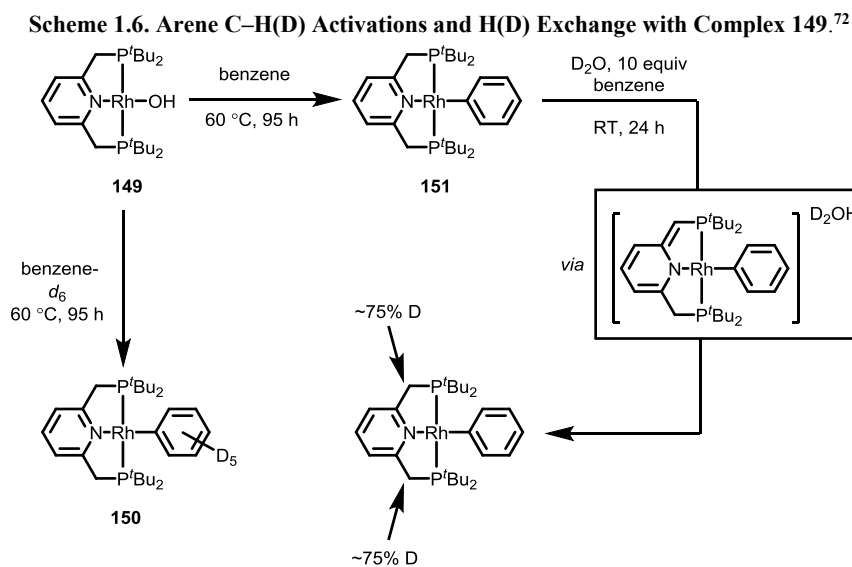
On the basis of these observations, complex **147** with added 1,2-bis(diphenylphosphino)benzene (dppbz) ligand was investigated in hydroarylation.[70] Electron-deficient arenes were examined as coupling partners with α,β-unsaturated carbonyl compounds to generate the desired hydroarylation product (Table 1.13). In this reaction, both the direct, Heck-like C–C coupled (**152**) and the hydroarylation products (**153**) were observed. For ester and ketone substrates, high yields were observed, whereas amide-containing substrates resulted in lower yields. All substrates exhibited high selectivities for generation of **153** over **152**, with nearly quantitative conversion to **153** in some cases. Moreover, only anti-Markovnikov products were observed for all substrates tested.

Table 1.13. Hydroarylation of pentafluorobenzene with α,β-unsaturated esters, amines, and ketones.[70]
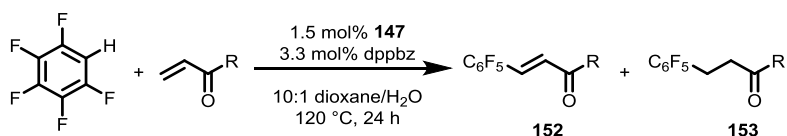
R	152:153	Overall Yield (%)
O^{n}Bu	1:17	88
O^{t}Bu	1:40	87
O^{i}Bu	1:20	91
OEt	1:12	80
NH	1:50	52
NMe	1:11	43
Me	1:50	78
Et	1:50	85

To rationalize the generation of both products, a mechanism was proposed as shown in Figure 1.18. An initial [Rh^I(OH)] complex **154** undergoes hydroxide-assisted C–H activation of the fluorinated arene to generate a Rh–aryl complex (**155**) along with an equivalent of water. Upon coordination and insertion of olefin, the Rh–alkyl fragment **156** is generated. This species can then either undergo β-hydride elimination to produce **152**, or abstract a proton from water to form **153** and the regenerated Rh(I) complex **154**.
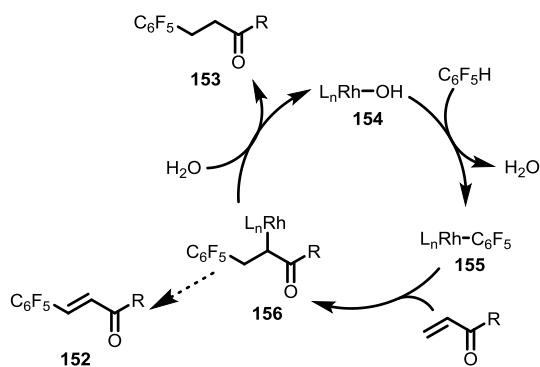
Figure 1.18. Mechanism for hydroarylation and C–C coupling using a [Rh^I(OH)] complex.[70]

***Ortho*-Directed Hydroarylations Catalyzed by Ir(I) Complexes.** For comparative purposes, note that iridium has been featured in several reports by Periana and coworkers on catalytic hydroarylation with catalyst precursors of the type [Ir^{III}(μ-acac-O,O,C^3)(acac-O,O)(acac-C^3)]$_2$ or [(acac)$_2$Ir^{III}(Ph)(L)] (L = H$_2$O, Py).[76-78] In these Ir(III) examples, the catalytic hydroarylation of unactivated arenes (*i.e.* benzene) was achieved with various aliphatic olefins (*i.e.*, ethylene, propylene, 1-hexene, etc.), with activities that exceed those observed for platinum-based catalysts (see sections 4.3 and 5.2). A mechanistic analysis of this catalysis by DFT calculations concludes that olefin insertion into the Ir–aryl bond is energetically significant and likely rate determining.[79-81] The key C–H activation step was calculated to involve a concerted, 4-centered transition state whereby hydrogen is transferred from an arene ligand to the metal-bound carbon of the Ir(CH$_2$CH$_2$Ar) group (σ-bond metathesis or oxidative hydrogen migration). One might expect Ir(I) catalysts to operate by a different mechanism involving C–H oxidative addition, and a few examples of Ir(I)-catalyzed hydroarylation have been reported.[82-89] In contrast to the Ir(III) catalysts, Ir(I) complexes have not been reported to catalyze the hydroarylation of unactivated arenes. For the most part, Ir(I) systems have been used for the directed *ortho*-hydroarylation of arenes bearing directing functionalities, similar to Rh(I) complexes that have been extensively used for this purpose (*vide infra*). Typically, strained cyclic olefins (*i.e.,* norbornene) have been employed as hydroarylation substrates along with arenes bearing directing substituents such as amides or esters. As with many Rh(I) systems, the active Ir(I) species are usually generated *in situ* using commercial or readily synthesized Ir(I) species.

In an initial report by Togni,[82] several Ir(I) complexes were synthesized by treatment of [(coe)$_2$Ir(μ-Cl)]$_2$ (**157**) with chiral bis(phosphine) ligands (**a-d**) to afford the corresponding ligated dimeric complexes **158a-158d** (Scheme 1.7). Subsequent treatment with NaCp in THF resulted in disproportionation to afford complexes of the type [CpIr(L$_2$)] (**159a-159d**; L$_2$ = **a-d**) along with an equivalent of NaCl.
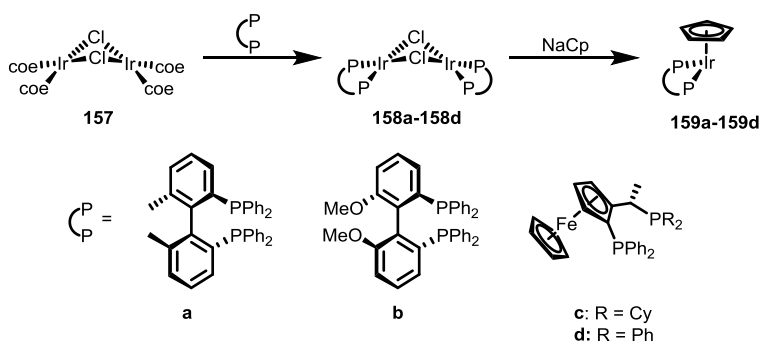
Using 1 mol% of complexes **159a-159d**, the *ortho*-hydroarylation of norbornene with benzamide was observed (eq 1.11).[82] Upon heating at 100 °C for 72 hours, complexes **158a-158d** and **159a-159d** gave either the hydroarylation product **160** or hydroamination product **161** in moderate yields. High enantioselectivities for the exo-norbornyl isomers of **160** and **161** were observed, with enantiomeric excesses larger than 70%. Catalysis with the Cp-ligated complexes **159a-159d** afforded **160** as the only product, though in low yields (ca. 20%). In contrast, the starting dimer species, **158a-158d**, generally produced the hydroamination product **161**. Since these Cp complexes are formally 18-electron species, it is likely that phosphine dissociation or Cp ring slippage occurs to generate the active catalytic species. It was suggested, therefore, that the ability of Cp ligands to change their binding motif from η^5 to η^3 (or even η^1) would provide better access to the Ir center allowing for amide coordination. The resulting Ir(amide) intermediate would then undergo C–H activation and subsequent olefin insertion to produce the hydroarylation product.
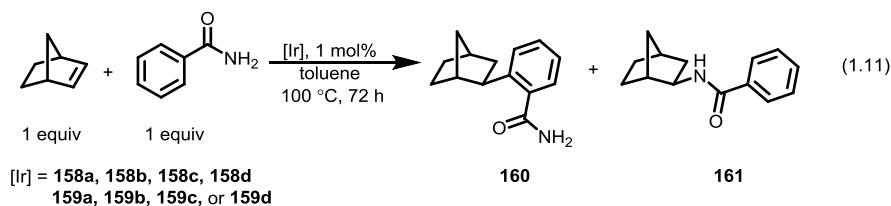
In contrast to benzamide, phenol as a substrate provided only hydroarylation products (**162** and **163**) when treated with neat norbornene and **158d**, even upon heating for several days.[83] However, the dihydroarylation product **163** was also observed (eq 1.12). This reaction is associated with a low stereoselectivity for the exo- and endo-norbornyl products, and a low ee of 4.5%.
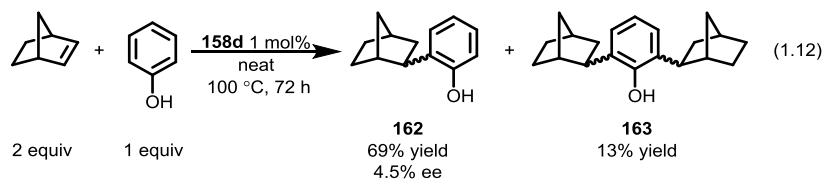
A mechanism was proposed for catalysis with the Ir(I) dimeric precatalyst **158d** (Figure 1.19).[83] An initial coordination of the phenol to the Ir dimer induces a disproportionation to generate the [L₂IrᴵCl(phenol)] intermediate, **164**. Due to the geometry imparted by this anchoring directing group, only *ortho*-aryl C–H bond activation can occur, to give an Ir species with the substrate bound in a bidentate

fashion (**165**). Coordination and insertion of norbornene couples the substrates and generates an Ir(III)–hydride species (**166**). Reductive elimination produces the hydroarylation product and regenerates an active Ir(I) complex, either as the initial dimer (**158d**) or through some other Ir(I) species.
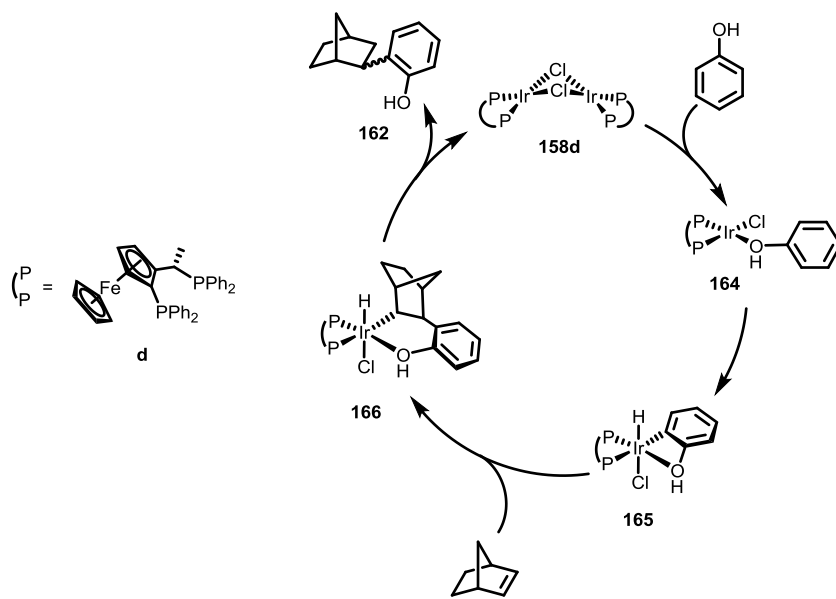

Figure 1.19. Proposed catalytic cycle for the *ortho*-hydroarylation of norbornene and phenol with **158d**.[83]

A report by Yamamoto[84] describes enantioselective *ortho*-hydroarylations of norbornene with carbonyl containing arenes **167** (Table 1.14). For this system, cationic $[(cod)_2Ir^I]^+$ complexes with counterions such as SbF_6^- or $B(C_6F_5)_4^-$ were employed as precatalysts. The active species were generated by addition of a chiral phosphine, and initial ligand screening with $[(cod)_2Ir^I][B(C_6F_5)_4]$ (**168**) showed that the sulfur-linked bis(phosphoramidite) (*R,R*)-S-Me-BIPAM (**169**, Figure 1.20) provided the highest enantioselectivities and overall yields. With this system, a range of arene substrates (**167**) were observed to afford the exo product **170** in high enantiometic excess. Electron-withdrawing aryl substituents (R^2) exhibited reduced conversion to the product, and significantly increased yields were observed with amide- (vs. carbonyl) directing groups. To probe the mechanism, the *N*-cyclohexylbenzamide-d_5 arene substrate was used to provide a kinetic isotope effect (KIE) of 2.08. It was suggested that this small primary KIE indicates a C–H(D) cleavage step in the mechanism. This interpretation of the isotope rate enhancement, however, may be suspect as a rate law has not been determined.

Table 1.14. Substrate scope for *ortho*-hydroarylation of norbornene and **167** with **168** and added **169**.[84]
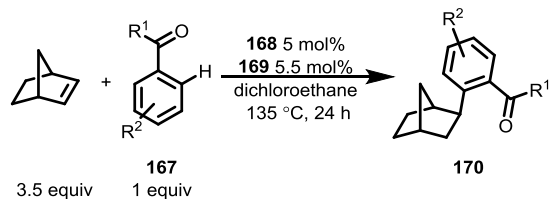
R¹	R²	Isolated Yield (%)	ee (%)
Me	H	40	92
	o-OMe	82	88
	o-F	42	93
	m-Me	50	88
Et	*o*-OMe	61	92
NMe₂	H	90	99
N(*i*Pr)₂	H	90	96
Piperidine	H	91	99
	p-Me	97	99
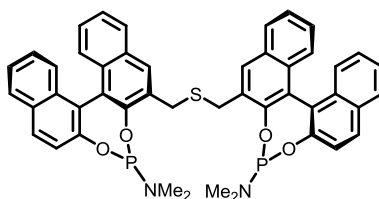
Figure 1.20. Structure of (*R,R*)-S-Me-BIPAM, **169**.

A similar system employing 2,2'-bis(diphenylphosphino)-1,1'-binaphthyl (BINAP) and **168** demonstrated the enantioselective *ortho*-hydroarylation of aryl ketones with norbornene and styrene derivatives.[85] With styrene-based substrates, branched and linear alkyl-arene products were observed. With this bulky BINAP ligand, linear products were preferred for all styrene-containing products. Similarly, exo-norbornyl based products were observed to be favored in the hydroarylation of norbornene with 2'-methylacetophenone, giving an enantiomeric excess of 70%. This system was also successfully used towards the *ortho*-hydroarylation of asymmetric alkynes with substituted acetophenone derivatives.

Bower and coworkers[86,87] examined a variety of chelating diphosphines to further investigate ancillary ligand effects on hydroarylation. These diphosphine ligands contain aliphatic linkers of varying lengths (*i.e.,* CH_2, CH_2CH_2, etc.). It was hypothesized that the bite angle of the diphosphine could potentially influence the regioselectivity of *ortho*-hydroarylation (*i.e.* Markovnikov versus anti-Markovnikov) by changing the steric profile at the metal center. A catalytically active species could be generated *in situ* by addition of a diphosphine to complex **168**. These species catalyzed the hydroarylation of styrene with diethylbenzamide with 5 mol% loading in dioxane at 100 °C for 24 hours to afford the hydroarylation products **171** and **172**. The overall yields and product ratios (branched:linear) were determined by ${}^1H$ NMR spectroscopy and the results are summarized in Table 1.15.

While the racemic-BINAP ligand provided high yields, it gave a high selectively for the linear, anti-Markovnikov product **172**. Surprisingly, the dppm ligand with a small bite angle was very selective for the anti-Markovnikov product (product ratio of 8:92).[86] By increasing the diphosphine bite angle, a switch in selectivity to the branched product **171** was observed. Thus, dppb (a $(CH_2)_4$-linked diphosphine) provided complete selectivity for **171** (branched:linear ratio of 100:0). However, ligands with longer alkyl tethers exhibited significantly reduced overall yield. With dppb only a 28% yield was obtained. Improved yields for **171** were obtained by using fluorinated versions of the diphosphines, as illustrated by d^Fppb and d^Fppe [$(C_6F_5)_2P(CH_2)_nP(C_6F_5)$; n = 4 and 2, respectively] which gave increased yields and retained high branched:linear product ratios compared to the "parent" ligands dppb and dppe, respectively.

Table 1.15. Ligand scope with alkyl tethered diphospine ligands.[86]
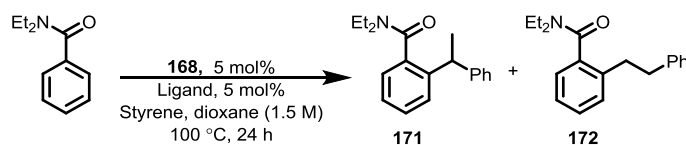
Ligand	Overall Yield (%)	171:172
rac-BINAP	>95	29:71
dppm	73	8:92
dppe	82	23:77
dppp	52	60:40
dppb	28	>95:5
d^Fppe	>95	36:64
d^Fppb	>95	>95:5

To further investigate this system, d^Fppb and **168** were used to probe the substrate scope.[87] High yields and Markovnikov product selectivities were observed for a series of arene substrates containing various carbonyl directing groups (*e.g.,* amides, ketones, esters) and other arene substitutions. Additionally,

various substituted styrene substrates were tested (*i.e., p*-Me, *p*-F, *m*-Cl, and *o*-F), as well as aliphatic olefins. Styrene substituents had a minimal effect on the overall yield and selectivity, typically displaying yields above 70% (and in some cases quantitative conversion). Branch:linear selectivities of >25:1 were observed with all styrene substrates. In contrast, bulky aliphatic olefins gave reduced yields; however, a regioselectivity for branched products was preserved. No reaction was observed with ethyl acrylate. These results suggest that this system is tolerant of many substrates, but likely cannot catalyze the hydroarylation of electron deficient aliphatic olefins. Additionally, it demonstrates that the regioselectivity is likely dictated by the diphosphine bite angle.

To investigate the operative mechanism in this system, a labeling experiment was conducted using deuterated styrene **173** and diethylbenzamide as substrates with the **168**/d^{F}ppb catalyst (eq 1.13).[87] Although this reaction ultimately gives mainly the branched hydroarylation product **174**, the labeling experiment suggests that several reversible steps are involved in the mechanism. Both the methyl and methine positions incorporated deuterium atoms, which is consistent with a reversible olefin insertion step. Additionally, deuterium incorporation into the *ortho*-arene position implies a reversible C–H activation step. As a result of the H(D) exchange, it was suggested that reductive elimination was rate limiting.
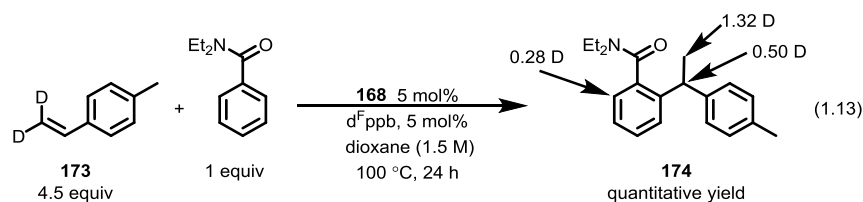
The original mechanism proposed by Bower and coworkers[86,87] involved a mechanism whereby C–H oxidative addition generates an Ir–hydride species. Upon coordination of styrene, a migratory insertion into the Ir–hydride occurs to generate a new Ir–alkyl fragment and C–C reductive elimination then affords the desired alkyl-arene. The operative mechanism has also been explored by Huang and Liu[88] using DFT calculations (Figure 1.21). The results of this study were surprising; the energetically preferred mechanism based on the DFT calculations for this hydroarylation involved several steps different from those of the mechanism proposed by Bower and coworkers.[86,87] Perhaps the most striking difference between the two calculated mechanisms is that a C–H, rather than a C–C, reductive elimination occurs. In the DFT calculated mechanisms, a C–H activation of the arene substrate (**175**) occurs to generate an Ir–hydride, followed by styrene coordination (**176a** or **176b**). Unlike the original mechanism (pathway a), migration of the Ir–aryl bond into the olefin occurs (**178b** *via* **177b** transition state) with a lower calculated kinetic barrier (pathway b). This insertion preserves the Ir–hydride bond and can occur either in a Markovnikov or anti-Markovnikov fashion. A C–H reductive elimination occurs to generate the resulting alkyl-arene product **181**.
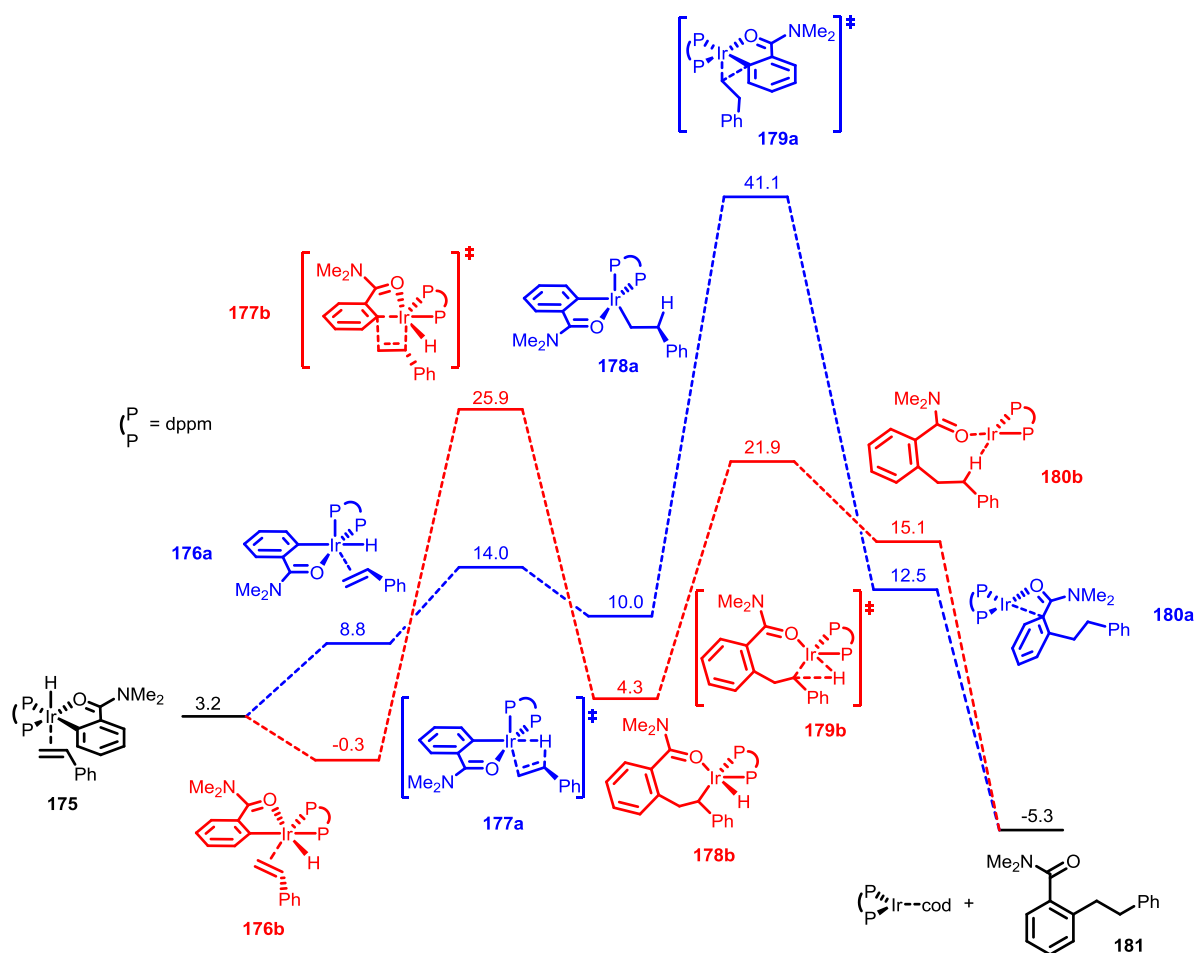
Figure 1.21. Calculated barriers for the two possible insertion and reductive elimination routes in *ortho*-hydroarylation using [(dppm)Ir^I(cod)]$^+$ as the added catalyst. Olefin insertion into the metal–hydride and subsequent C–C reductive elimination pathway (blue) was calculated to have a larger kinetic barrier than the pathway involving arene insertion followed by C–H reductive elimination (red). Only the anti-Markovnikov pathways are depicted. All complexes exist as cationic species and the charge has been omitted for clarity. Energies are given in kcal mol^{-1}.[88]

While added ligands have been successfully employed to probe the selectivity and activity of Ir(I)-based *ortho*-hydoarylation catalysts, a recent report by Nishimura[89] demonstrates that [(cod)Ir^I(μ-Cl)]$_2$ (**182**) with added NaB(C$_6$F$_5$)$_4$ (**183**) is an *ortho*-hydroarylation catalyst, without added ligand. The addition of **183** to **182** likely results in elimination of NaCl to produce a reactive, cationic iridium species. This catalyst couples vinyl ether substrates with pyridyl-substituted arenes, with the pyridine acting as a directing group. These reactions are selective for the branched product for a range of olefins and 2-phenylpyridine as the arene (Table 1.16). Linear products were not observed with any substrates. Instead, only branched hydroarylated products (**184** and **185**) were isolated, generally in yields greater than 85%. While dihydroarylated species (**185**) were occasionally observed, selective conversion to only monohydroarylated products (**184**) occurred for most substrates. This ligand-free system was also applied to arene substrates with different types of directing groups (*e.g.*, imine, oxazole, benzothiazole). A deuterium labeling study using deuterated 2-phenylpyridine (C$_6$D$_5$-2-Py) as a substrate revealed scrambling of hydrogen into the *ortho*-aryl positions. This result, and deuterium incorporation into the methyl and methine positions of the

product suggests reversible C–H activation and olefin insertion steps for hydroarylation catalyzed by Ir(I) species. Nishimura and coworkers[90,91] have also demonstrated that similar [(diene)Ir^I(μ-OH)]$_2$ complexes are competent catalysts for the asymmetric hydroarylation of vinyl ethers or symmetric alkynes with benzamides.

Table 1.16. Substrate scope of ligand free *ortho*-hydroarylation of vinyl ethers.[89]
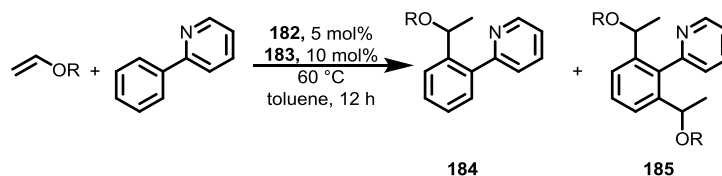
R	Isolated Yield (%)	184:185
Et	90	100:0
^{n}Bu	99	100:0
^{i}Bu	96	95:5
Bn	91	95:5
Ph	91	100:0
p-MePh	98	100:0
p-MeOPh	93	95:5
p-FPh	90	94:6
p-ClPh	93	100:0
m-MePh	91	98:2
o-MePh	98	100:0
SiMe$_3$	88	100:0

***Ortho*-Directed Hydroarylations Catalyzed by Co Complexes.** Cobalt catalyzed hydroarylations and C–H bond activations have emerged as a highly active field of research over the last decade due to low cost of Co compared to Rh and Ir;[92] indeed, several major reviews exist on the topic of Co catalyzed reactions employing C–H activation steps.[93-97] Recent developments have primarily focused on two classes of catalysts: low-[95,98-107] and high-valent.[108-111] {Sanjosé-Orduna, 2019 #276} The first example of Co mediated hydroarylation, as reported by Kisch and coworkers,[98] involved treatment of substituted bis(aryl)diazenes **186** with diphenylacetylene and the diamagnetic Co(I) complex, (PPh$_3$)$_3$Co(N$_2$)H (eq 1.14). A likely first step in the catalytic mechanism involves substrate coordination through the N donor, though a thorough

mechanistic analysis has not yet been performed. Only the addition product **187** with difunctionalization of the *ortho*-C–H bonds existed; moreover, **187** contains an olefin with *Z*-stereochemistry which occurs through an unclear mechanism (see chapter 3).
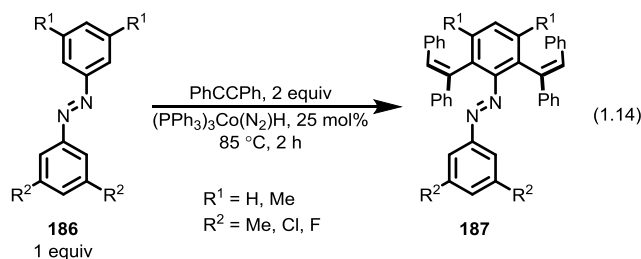
Recent developments in low-valent systems have exclusively involved *in situ* catalyst generation.[95,99-106] An initial report by Yoshikai[100] presented the development of a "one-pot" strategy towards the C–H bond functionalization of phenylpyridine with internal alkynes. The active catalytic species was generated by the addition of a Grignard reagent to $CoBr_2$ (or $CoCl_2$) in the presence of added phosphine ligands and substrates. The reaction conditions were optimized (Table 1.17) by varying the identity of the phosphine ligand, the identity of the Grignard reagent, and the relative Grignard equivalency. In general, both the mono- (**188**) and dialkenylated (**189**) products were observed; typically, **189** was the major product except at reduced RMgX loadings or with bulky R substituents. Interestingly, mixed alkyl-aryl phosphines afforded high yielding catalytic mixtures. In contrast, the use of either PCy_3 and PPh_3 retarded the catalytic activity.

A subsequent report by Yoshikai[104] examined the hydroarylation of (*N*-*p*-methoxylphenyl)-1-aryl ethanimine substrates with internal alkynes under *in situ* conditions similar to those described above (Table 1.18). Similar optimization studies concluded that a mixture of $CoBr_2$ (5 mol%), $P(3\text{-}ClC_6H_4)_3$ (10 mol%), $^tBuCH_2MgBr$ (50 mol%), and pyridine (80 mol%) in THF generated the best performing catalytic mixture; moreover, this catalytic protocol proceeded at ambient temperatures. A broad substrate scope indicated that the reaction conditions were relatively tolerant of a variety of functional groups and aryl substitution patterns. The primary drawback of such catalyst generation methods, however, involves undesired reactions of the Grignard reagent with the substrates themselves. As such, highly electrophilic functionalities (esters, aldehydes, ketones, acids) were not examined as they likely not tolerated.

A cursory kinetic analysis elucidated several mechanistic features.[104] A first order rate dependence on $[CoBr_2]$ was observed; it is unclear, however, whether this dependency results from catalyst initiation or from the catalytic cycle. In a solution of THF, $CoBr_2$ converts to the solvato-complex, $(THF)_2CoBr_2$, which further complicates rate dependence experiments. Interestingly, saturation like kinetics were observed with added ligand, which suggests that phosphine binding is not competitive with either imine or alkyne coordination. Stoichiometric treatment of $CoBr_2$ (0.1 mmol) with $P(3\text{-}ClC_6H_4)_3$ (0.2 mmol) and $^tBuCH_2MgBr$ (0.2 mmol) afforded an equivalent of $^tBuCH_2CH_2^tBu$ which is consistent with a radical-based initiation pathway. The identity of the active catalyst, however, remains elusive under these conditions. Further investigations into the mechanism of low-valent Co catalyzed hydroarylations are described in chapter three.

**Table 1.17.** Hydroarylation of phenylpyridine with 4-octyne.[100]
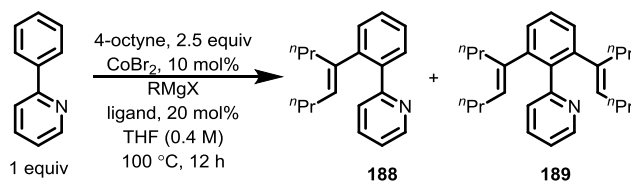
Ligand	RMgX (mol%)	Conversion (%)	Yield 188 (%)	Yield 189 (%)
PMePh$_2$	MeMgCl (100)	80	3	77
	MeMgCl (60)	80	4	76
	MeMgCl (50)	73	54	19
	^{i}PrMgBr (100)	65	29	36
	^{n}BuMgBr (100)	61	41	20
	^{t}BuMgBr (100)	19	19	0
	^{t}BuCH$_2$MgBr (100)	51	42	9
PMe$_2$Ph	MeMgCl (100)	79	45	34
PPh$_3$	MeMgCl (100)	36	36	0
PCy$_3$	MeMgCl (100)	2	2	0

Subsequent reports investigated olefin hydroarylations with similar aryl-imine substrates.[101,103,105-107] In a communication by Nakamura and coworkers,[107] the hydroarylation of substituted benzamides with linear α-olefins (i.e., 1-octene, vinylsilane, 2-methylpentene, etc.) proceeded with a catalyst generated by reduction of Co(acac)$_3$ with an excess of CyMgCl. Interestingly, the hydroarylation of **190** with either *trans*-2-octene or 1-octene afforded the same linear alkylation product **191** which suggests that some degree of chain-walking may occur from reversible insertion steps (eq 1.15). In contrast, no reaction was observed with 3-octene.

(1.15)
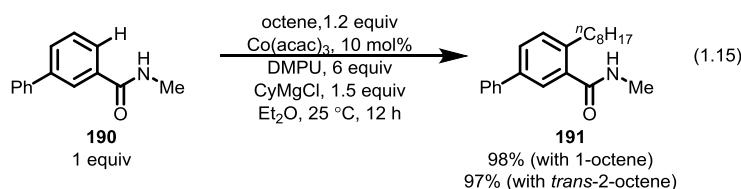
Table 1.18. Hydroarylation of phenylpyridine with internal alkynes.
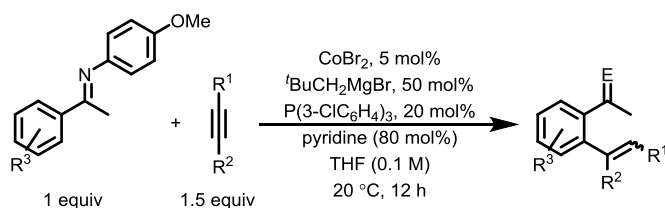
R^1	R^2	R^3	Yield (%)	*E/Z*	Product [a]
^{n}Pr	^{n}Pr	4'-OMe	80	4.9	
		4'-CF$_3$	76	6.7	
		4'-Ph	83	6.1	
		4'-CN	57	6.7	
		3'-Me	94	8.1	
		3'-CF$_3$	85	10.1	
		3'-OMe	87	8.1	
		3'-Cl	85	7.3	
		3'-CN	58	7.3	
		3'-F	92	7.3	
Ph	Ph	H	90	9.0	
		4'-OMe	76	10.1	
		4'-CF$_3$	64	7.3	
		4'-Ph	73	9.0	
		4'-CN	49	6.1	
		4'-Br	37	4.9	
SiMe$_3$	Ph	H	41	–	

[a] E = O resulted from an acidic work up to deprotect the imine which generated the resultant ketone.[104]

While linear selectivities were observed with ketimine directing groups, hydroarylations with aldimine containing substrates and styrene afforded branched products, as illustrated in the example depicted in eq 1.16.[103] The switch in linear to branched selectivity exists primarily as a function of the Grignard reagent employed. With the aldimine substrates, Me$_3$SiCH$_2$MgBr was employed as the catalyst

activator; in contrast, linear products were observed with the use of $^tBuCH_2MgBr$. It was suggested that the choice of Grignard may influence the geometry of styrene coordination, but the details of such a mechanism remain unclear.
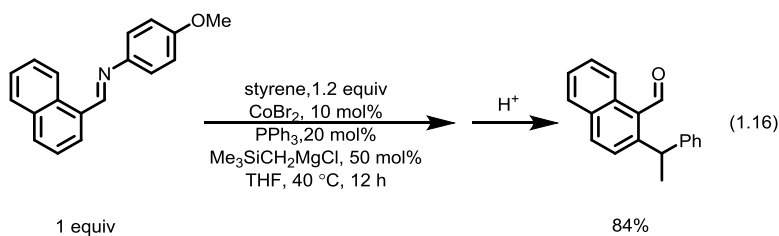
The majority of directing groups in *ortho*-directed hydroarylations involve large, nitrogen-containing functionalities (pyridine, *N*-aryl imine, amides, etc.). These directing groups often require additional steps to install and are atom uneconomical. Recently, Yoshikai and coworkers[106] reported that unsubstituted imine functionalities successfully directed *ortho*-hydroarylations with vinyl silane without loss of catalytic performance, as illustrated in the example depicted in eq 1.17.
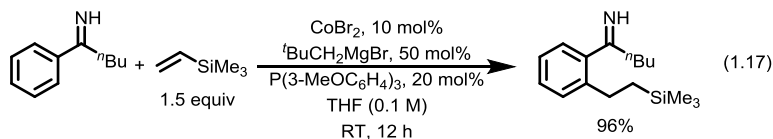
Catalyst generation under Grignard-free conditions were realized in a recent report[105] where a direct reduction of $CoBr_2$ with Mg turnings afforded the active catalytic species. The ligand choice dramatically influenced the selectivity for branched or linear insertion products. Branch selective catalysis occurs with phosphine-based ligands. In contrast, the use of 1,10-phenanthroline affords linear products. Despite being Grignard free, Mg turnings may impart different catalytic constraints; it seems plausible that catalyst reproducibility depends greatly on the batch of Mg turnings that are employed, as the degree of MgO surface coating is highly variant.

In contrast to the low-valent systems described above, several examples of discrete Co(III) catalysts have been described by Kanai and coworkers.[108-110] In an initial report, the cationic sandwich complex $[(Cp^*)Co(\eta^6\text{-}C_6H_6)][PF_6]_2$ (**192**) was employed as a single-component catalyst towards the hydroarylation of substituted phenylpyridines across polar C–E multiple bonds such as Michael acceptors, imines, and aldehydes. Complex **192** could be conveniently prepared in two steps;[112] treatment of $CoCl_2$ with Cp*Li and subsequent oxidation afforded the chloride bridged complex $[(Cp^*)CoCl(\mu\text{-}Cl)]_2$. Chloride abstraction and arene coordination was achieved by treatment of this dimer with $AlCl_3$. A subsequent salt metathesis with NH_4PF_6 afforded complex **192** as an air and moisture stable species in multi-gram scale. The catalytic efficacy of **192** was examined in the hydroarylation of phenylpyridine across substituted (*N*-2-thienylsulfonyl)aryl aldimine substrates (**193**, Table 1.19). Complex **192** was also employed as a catalyst across non-polar C–C multiple bonds in Michael-acceptor substrates. Similar catalytic activities were observed with both linear and cyclic α,β-unsaturated ketone substrates.

Table 1.19. Hydroarylation of phenylpyridine with aryl aldimines (**193**) catalyzed by **192**.[109]
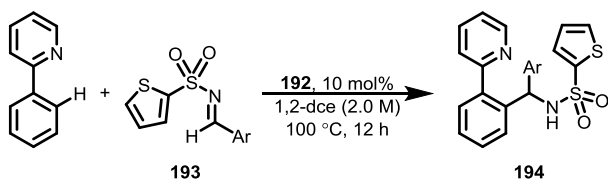
Ar	Yield (%)	Ar	Yield (%)
Ph	80	p-Me-C$_6$H$_4$	76
2-napthyl	79	p-MeO-C$_6$H$_4$	57
p-Cl-C$_6$H$_4$	83	o-Me-C$_6$H$_4$	71
p-Br-C$_6$H$_4$	72	2-thienyl	69
p-CF$_3$-C$_6$H$_4$	64	2-furyl	66
m-Cl-C$_6$H$_4$	76		

In an subsequent study by Kanai,[110] C2-selective hydroarylation of 1-(2-pyrimidyl)imidazole across aryl aldimine substrates (**193**) was achieved with catalyst **192** (Table 1.20). Similar site selective hydroarylations were observed across internal alkynes.[108]

Table 1.20. Hydroarylation of 1-(2-pyrimidyl)indole with aryl aldimines (**193**) catalyzed by **192**.[109]
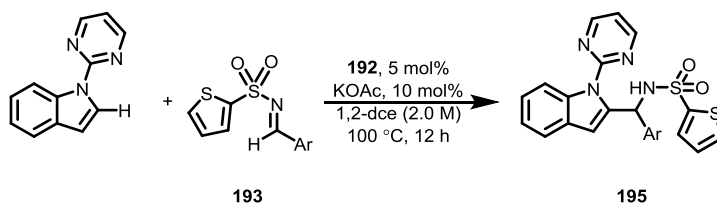
Ar	Yield (%)	Ar	Yield (%)
Ph	83	p-CO$_2$Me-C$_6$H$_4$	90
2-naphthyl	78	p-Me-C$_6$H$_4$	71
p-Cl-C$_6$H$_4$	89	o-Me-C$_6$H$_4$	74
p-Br-C$_6$H$_4$	91	2-furyl	64
p-CF$_3$-C$_6$H$_4$	93	2-thienyl	58
m-Cl-C$_6$H$_4$	90		

Deuterium labeling studies[110] revealed that the C2-selectivity observed with complex **192** occurs *via* a *ortho*-directed pathway and not due to an adventitious Lewis acidic mechanism (Scheme 1.8). As a control, 1-(2-pyrimidyl)indole was treated with a Lewis acid, Sc(OTf)$_3$, and methanol-d_4. Treatment with Lewis acid primarily incorporated deuterium into the C3-site, though C2 deuterium incorporation was also observed to a minor extent. In contrast to this control experiment, treatment with **192** exchanged deuterium only into the C2-position. Similar selectivity and yields were observed by Yoshikai and coworkers[99] employing a low-valent catalyst generated by treatment of CoBr$_2$ with ^{t}BuCH$_2$MgBr and added ligand.

Scheme 1.8. Deuterium Scrambling into the C2- and C3- Positions of 1-(2-pyrimidyl)indole Catalyzed by 192 or Sc(OTf)$_3$.[110]
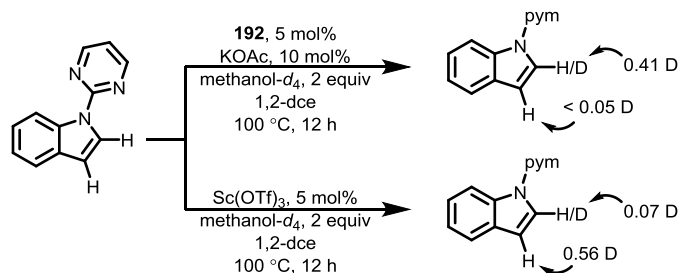
Typical electrophilic aromatic substitutions on indole fragments occur at the more reactive, but perhaps less desirable C3 position. The unusual selectivity observed by Kanai[108,110] originates from initial precoordination of the pyrimidyl functionality to the Co center which positions only the C2 site in close enough proximity for C–H bond activation. The observed C2-selectivity, therefore, appears to be predominantly substrate controlled. The proposed hydroarylation mechanism is reminiscent to that of hydrosilylations of ketones (Figure 1.22). An initial salt metathesis from **192** with KOAc occurs to generate a neutral bis(acetate)Co^{III} complex (**196**). Precoordination of the substrate occurs (**197**) through the pyrimidine directing functionality. A carboxylate-assisted concerted metalation deprotonation (CMD) event occurs to generate the cyclometalated complex **198** as well as an equivalent of HOAc. Imine coordination occurs in a η^1-fashion (**199**) with a subsequent insertion into the Co-aryl bond (**200**); indeed, similar intermediates have been crystallographically identified in the oxidative annulation of alkynes.[111,113] Protonolysis with HOAc occurs to regenerate the active Co(III) catalyst as well as the desired hydroarylation product **195**. It is of note that an oxidation state change at the metal does not appear to occur.
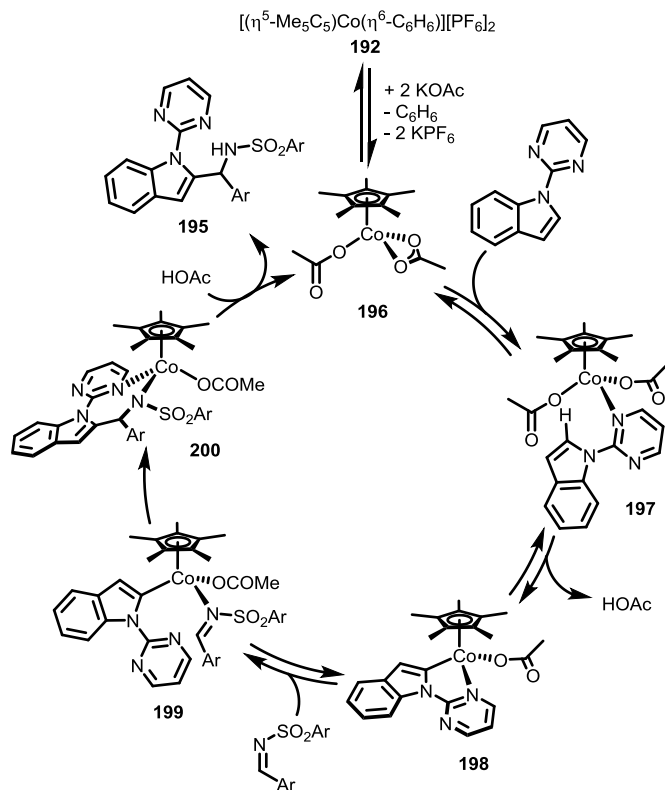
Figure 1.22. Proposed hydroarylation of 1-(2-pyrimidyl)indole with (*N*-thienylsulfonyl)aryl aldimines catalyzed by **192**.[110]

Key Conclusions from *Ortho*-Directed Hydroarylations. Many Rh[I]-based systems have been used as catalysts for olefin hydroarylation. Three major types of arenes have been employed: unfunctionalized arenes,[32-36] arenes with directing substituents,[40,47-62,64-69,73] and highly fluorinated arenes.[70] With these systems, high yields (or TONs) have been observed for the desired products with reasonable catalyst loadings (~5 mol%). The hydroarylation of arenes substituted with a coordinating heteroatom (imines, esters, amides, ketones, pyridines, etc.) has received substantial attention. This strategy has been successfully employed for both inter[40,47-50] and intramolecular[52,53] hydroarylations. It is important to note that with these directing groups, only *ortho*-hydroarylation occurs due to the initial binding step during catalysis. This anchoring of the substrate places the *ortho*-aryl C–H bond in close proximity to the Rh[I] center and allows for subsequent C–H activation to generate a five-membered chelate. Moreover, both *meta*- and *para*- C–H activation do not occur due to the geometry imparted by the directing group which orients these C–H bonds away from the metal center. Additionally, C–H activation through these bonds would generate strained six- or seven-membered chelates. The use of these directing groups, therefore, selectively generates only *ortho*-hydroarylated products. A series of recent publications from the Yu lab, however, indicated that *meta*-[114-123] or *para*-[124] directed C–H bond activations can be achieved with the use of appropriately engineered directing groups which make the *ortho*- position sterically inaccessible. Yu and coworkers[125,126] also developed a method for *meta*-aryl C–H bond functionalization with the use of an olefin cocatalyst, which induces sequential C–H activations mediated by olefin insertion and decoordination of the directing group.

Conveniently, a simple Rh[I] species such as Wilkinson's catalyst serves as a catalyst for this *ortho*-hydroarylation reaction.[40,47-50,52,53] Also, the commonly employed rhodium starting complex [(coe)$_2$Rh[I](μ-

Cl)]$_2$ is useful as a precatalyst, with addition of phosphorus-containing ligands.[54-58] The use of such ligands has demonstrated higher overall yields (*vs.* PPh$_3$), and the flexibility of ligand choice allows for an element of catalyst design. One such benefit is that chiral catalysts are available for enantioselective hydroarylations. Chiral substituents on the aryl-directing group can also improve enantioselectivity.[59] Hydroarylations of α–olefins have also been investigated, and interestingly, only the anti-Markovnikov linear products were observed using Rh^I-based systems. The use of Rh^I in *ortho*-hydroarylation has therefore been used to control both regio- and enantioselectivity during the course of the reaction. Despite this control, dihydroarylation has often been observed with arenes containing multiple *ortho*-aryl C–H bonds.

The Ir(I)-based hydroarylation systems in the literature have provided insights into several aspects of reaction selectivity. With chiral phosphine ligands, the *ortho*-hydroarylation of norbornene with various arenes possessing directing groups enantioselectively produces exo-norbornyl products.[82-85] The *ortho*-hydroarylation of styrenes and vinyl ethers with arenes bearing directing groups was also achieved.[86-88] These studies demonstrate the potential for ligand design to influence the regioselectivity of hydroarylation. Specifically, investigations with diphosphine ligands with varying bite angles illustrate a connection between catalyst structure and olefin insertion regioselectivity,[86] allowing access to both Markovnikov and anti-Markovnikov products. Smaller bite angles lead to increased generation of linear alkyl-arene products, while wider bite angles provide branched alkyl-arenes. The mechanism involving these diphosphine complexes was probed further using DFT calculations.[88] An unexpected mechanism was calculated to be energetically favorable: migration of a Ir–aryl bond into an olefin occurs rather than migration of an Ir–H moiety. While several examples of Ir(I)-catalyzed hydroarylations exist,[82-89] it is a relatively unexplored d^8 metal center for the hydroarylation of olefins. Moreover, the active catalytic species are typically generated *in situ*; it is possible, therefore, that these catalyst systems generate protic species that mediate hydroarylation. Further studies are required to identify likely mechanistic pathways available to these catalysts based on Ir(I) precursors.

Similarly, Co has been demonstrated to competently catalyze both olefin and alkyne hydroarylations. Two distinct reaction manifolds exist with Co: low-[95,98-107] and high-valent.[108-110] Low-valent systems require the addition of reactive Grignard reagents to reduce added CoX$_2$ salts into a catalytically competent complex. The nature of the catalytic mechanism and the identity of the active species remains elusive. Despite this, significant progress has been achieved in the development of an inexpensive and highly active hydroarylation method with potential for dramatic synthetic impacts. High valent Co(III) systems exist with cyclopentadienyl-based ligand scaffolds. In these examples, the Co center does not undergo any direct redox chemistry. Instead, a CMD-like C–H bond transfer occurs, aided by ancillary carboxylate ligands.

Formal Hydroarylation Reactions with Pd(II) Catalysts *via* Heck-Like Mechanisms. Catalysts based on Pd(II) are known to couple olefins with arenes that possess a suitable leaving group (halide, triflate, etc.) or transmetallating substituent (SnR$_3$, B(OH)$_2$, etc.). In these cases, such as the Heck reaction,[127] an olefin product is generated by the formal elimination of HX between the coupling partners. It has been demonstrated that with the addition of a suitable hydrogen source hydroarylation products are generated instead, with formal addition of a hydrogen and an aryl group across the olefin. It is important to note that unlike other hydroarylation catalysts that proceed *via* arene C–H bond activation, Pd(II)-catalyzed hydroarylation reactions occur either through C–X activation or arene transmetallation. Several reviews have been published on such hydroarylation reactions.[128,129] Two categories of conditions have been employed: formate assisted hydroarylation[130-139] and oxidatively coupled hydroarylation.[140-145]

An initial report by Cacchi and coworkers[130] demonstrated that $[(PPh_3)_2Pd^{II}(OAc)_2]$ (**201**) catalyzes the hydroarylation of α,β,γ,δ-dienones (**202a-202d**) with various aryl halides (eq 1.18 reports hydroarylation with 1-iodo-4-methoxybenzene). In contrast to other d^8 metal-based hydroarylation catalysts, an aryl C–H activation step does not occur with this Pd(II) system. Instead, the aryl group is introduced as a ligand by oxidative addition of a C–X bond to generate a Pd(X)(Ar) fragment, and stoichiometric formic acid serves as the source of hydrogen to generate the resulting hydroarylation products **203a-203d**. This system was employed with several dienones and aryl iodide substrates. With some substrates, however, the substituted vinylic Heck products **204a-204d** were observed as a byproduct. This reaction type has also been applied to the formal hydroarylation of alkynes.[131]

	203a-203d	204a-204d
a =	53%	0%
b =	61%	5%
c =	8%	22%
d =	41%	0%

(1.18)
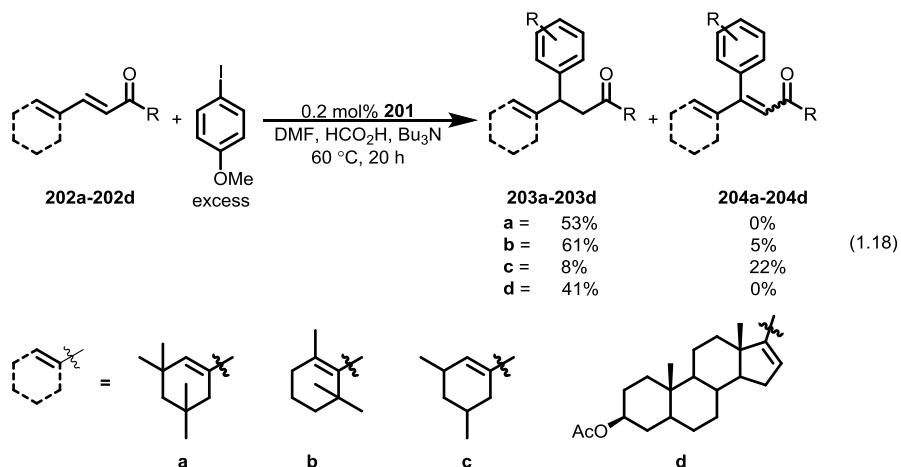
In a subsequent report by Cacchi and colleagues,[132] the scope of this system was explored. In the presence of formic acid and base (either piperidine or tributylamine), modest loadings of **201** catalyzed the hydroarylation of norbornene with a wide variety of aryl iodides (Table 1.21) to selectively generate the aryl-substituted exo-norbornyl product. Arenes containing potentially coordinating groups (*p*-NH₂ or *p*-OH) exhibited reduced yields when compared to noncoordinating substituents (*m*-Me or H). Additionally, electron-deficient norbornenes bearing exo-ester functionalities (**205**) exhibited high activities under the reaction conditions. With all substrates tested, only hydroarylation products (**206**) were isolated and vinylic substituted products (similar to **204**) were not observed, likely due to the strained geometry required for β-hydride elimination.

Table 1.21. Formal hydroarylation of norbornene derivatives with aryl iodides.[132]
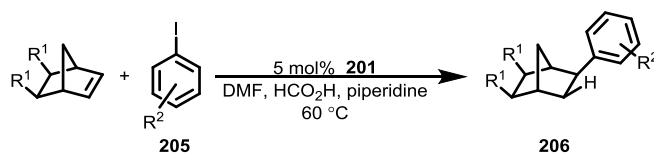
R^1	R^2	Reaction Time	Isolated Yield (%)
H	H	8	83
	p-NHCOMe	4	90
	p-NH$_2$	6	29
	p-OH	6	65
	m-Me	8	72
	o-CH$_2$OH	8	70
CO$_2$Me	H	3	85
	p-Cl	8	83
	o-OMe	8	73

To probe the mechanism, Mayo and Tam[133] used substituted norbornadiene substrates (**207**) to probe stereo- and regioselectivity. Using Pd^{II}(OAc)$_2$ and added PPh$_3$ ligand, catalysis (Table 1.21) was achieved in the presence of formate (either added directly or generated *in situ*). With ester- or silyl-containing norbornene substrates, high yields were observed using formic acid and added piperidine base. Using these conditions, low yields were observed with 2,3-dibromonorbornadiene as a substrate. Adding potassium formate instead of generating formate *in situ* resulted in an increased yield. An additional increase in reactivity was observed upon addition of tetrabutylammonium chloride. Two potentially reactive olefins exist in these substituted norbornadiene substrates, but surprisingly, only one product was identified (**208**). The functionalized olefin remained intact and hydroarylation occurred only across the unfunctionalized olefin.

Table 1.21. Formal hydroarylation of norbornadiene derivatives with phenyliodide.
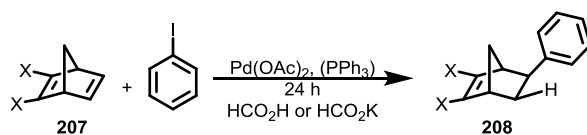
X	Conditions [a]	Isolated Yield (%)
CO$_2$Me	A	91
SiMe$_3$	A	80
Br	A	< 10
	B	33
	C	58

[a] Conditions: **A** = 20 mol% Pd(OAc)$_2$, 40 mol% PPh$_3$, HCO$_2$H, piperidine, THF, 60 °C; **B** = 20 mol% Pd(OAc)$_2$, 40 mol% PPh$_3$, HCO$_2$K, DMF, 25 °C; **C** = 20 mol% Pd(OAc)$_2$, 40 mol% PPh$_3$, HCO$_2$K, Bu$_4$NCl, DMF, 25 °C.[133]

A mechanism was proposed to account for the observed selectivity for preferential hydroarylations across unfunctionalized olefins (Figure 1.23).[133] An initial ligand substitution step generates an active Pd center which oxidatively adds phenyl iodide to generate a Pd^{II}(Ph)(I) species, **209**. Norbornadiene **217** coordinates either through the unfunctionalized or functionalized olefin to generate complexes **210** and **211**, respectively. The steric profile of the metal center for these complexes dictates their overall stability; compound **210** directs the norbornadiene substituents away from the metal center while compound **211** orients them directly into the metal center. Thus, compound **210** either is the favored intermediate during catalysis or proceeds through a lower transition barrier. From this intermediate, olefin insertion can occur in a *syn* fashion, positioning the arene and Pd in exo-positions on the norbornene product. Coordination of formate is then followed by a β-hydride abstraction and then decomplexation affords a Pd–hydride fragment along with an equivalent of CO$_2$. Reductive elimination affords the final exo-norbornyl product **208**. The other regioisomer, **212**, is not observed.
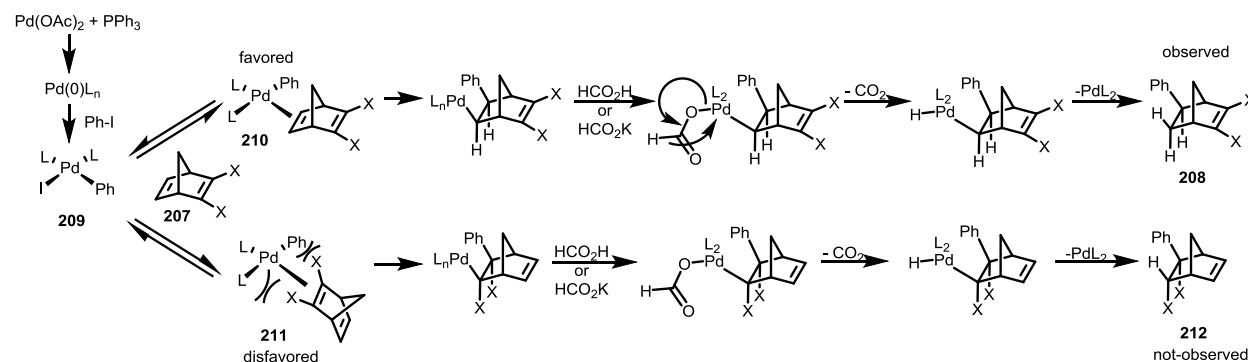
Figure 1.23. Proposed mechanism for formate assisted Pd(II) hydroarylation of substituted norbornenes.[133]

While simple PPh$_3$ ligands have been used in this type of hydroarylation, Brunel and coworkers[134] have investigated several dimeric Pd species as catalysts. These dimeric complexes contain bridging acetate ligands and a bidentate phosphine ligand (see complexes **213-215**, Table 1.22). Complex **213** is a catalyst for hydroarylation of norbornene with aryl halides to generate exo-phenyl substituted norbornane. Formate was produced *in situ* from triethylamine and formic acid. Using this structural motif, the reaction conditions were optimized and other aryl substituents were explored as leaving groups (Table 1.22). Initial optimizations identified dimethylsulfoxide (DMSO) as the preferred solvent; similarly, heating the reaction mixture to 120 °C gave more product. Using this temperature and solvent, catalyst loadings were reduced from 0.5 mol% to 5 x 10^{-9} mol% with little to no reduction in yield as identified by gas chromatography. Similarly, complexes **214** and **215** bearing heterocyclic nitrogen ligands were demonstrated to be competent catalysts. The Br, OTf and I leaving groups gave similar yields, but a Cl leaving group required higher catalyst loadings. The results at such low concentrations seem highly suspect; a control experiment in the absence of a catalyst was not performed. Moreover, a significant loss of reactivity was observed with toluene as solvent upon a 10^{-3} dilution. It seems more plausible, therefore, that adventitious catalysis by DMSO (or perhaps some impurity) occurs in such cases.

Chiral diphosphines,[135] oxazolines,[136,137] and (β-*N*-sulfonylaminoalkyl)phosphines[138] have been employed as ligands (see Figure 1.24) for enantioselective hydroarylation and the results are summarized in Table 1.23. All reactions employed DMSO as the solvent at elevated temperatures using formic acid and triethylamine. Notably, catalysis with the bisphosphine-based ligands (**216-218**) as well as oxazoline containing ligands (**219-226**) provided lower yields than those for the (β-*N*-sulfonylaminoalkyl)phosphine ligands **227-229**. Similarly, compounds **227-229** afforded catalytic mixtures which gave higher enantioselectivities than the nitrogen- or phosphorus-based donors. A related ligand effect study on the hydroarylation of 7-oxybenzonorbornene with PhI or PhOTf was reported by Fiaud.[139] While PhI generally gave higher yields, low enantioselectivity was observed even with chiral ligands such as **216-218**. With PhOTf, however, significantly higher enantioselectivities for the exo-norbornyl product were achieved. Ligand **216** exhibited the highest performance in terms of both yields and enantioselectivities. Overall, these reports demonstrate that chiral, bidentate ligands may be used to induce enantioselectivity.

Table 1.22. Substrate scope of norbornene hydroarylation with dimeric Pd(II) complexes.[134]

213: NR$_2$ = NMe$_2$
214: NR$_2$ = pyrrolidine
215: NR$_2$ = piperidine
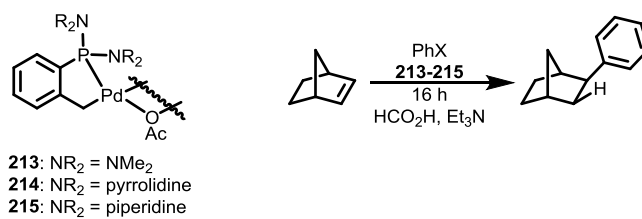
X	Catalyst	Catalyst Loading (mol%)	Solvent	Temperature (°C)	GC Yield (%)
I	**213**	0.5	toluene	25	–
		0.5	toluene	110	72
		5×10^{-4}	toluene	110	–
		0.5	CH$_3$CN	80	–
		0.5	DMF	120	> 95
		0.5	DMSO	120	> 95
		5×10^{-2}	DMSO	120	> 95
		5×10^{-9}	DMSO	120	79
	214	5×10^{-6}	DMSO	120	85
	215	5×10^{-6}	DMSO	120	71
Cl	**213**	0.5	DMSO	120	> 95
		5×10^{-3}	DMSO	120	–
Br	**213**	5×10^{-4}	DMSO	120	> 95
OTf	**213**	5×10^{-4}	DMSO	120	> 95

Table 1.23. Hydroarylation of norbornene catalyzed by Pd(II) bearing chiral ligands.
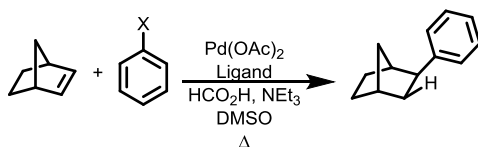
Conditions [a]	X	Ligand	Time (h)	Isolated Yield (%)	ee (%)
A [135]	OTf	**216**	12	9	8
		217	36	18	26
		218	14	58	24
		227	2	37	81
	I	**216**	18	23	15
B [136]	I	**219**	46	44	29
		220	14	47	0
		221	24	51	0
B [137]	I	**222**	14	42	51
		223	58	60	73
		224	43	54	74
		225	14	57	28
		226	14	47	18
C [138]	OTf	**227**	20	74	71
		228	20	89	60
		229	20	75	62

[a] Conditions: **A** = 65 °C, 2 mol% Pd, 4 mol% ligand, excess PhX; **B** = 25 °C, 5 mol% Pd, 10 mol% ligand, excess PhX; **C** = 65 °C, 1.2 mol% Pd, 2.4 mol% ligand, excess norbornene, Ar atmosphere. References are given in brackets.
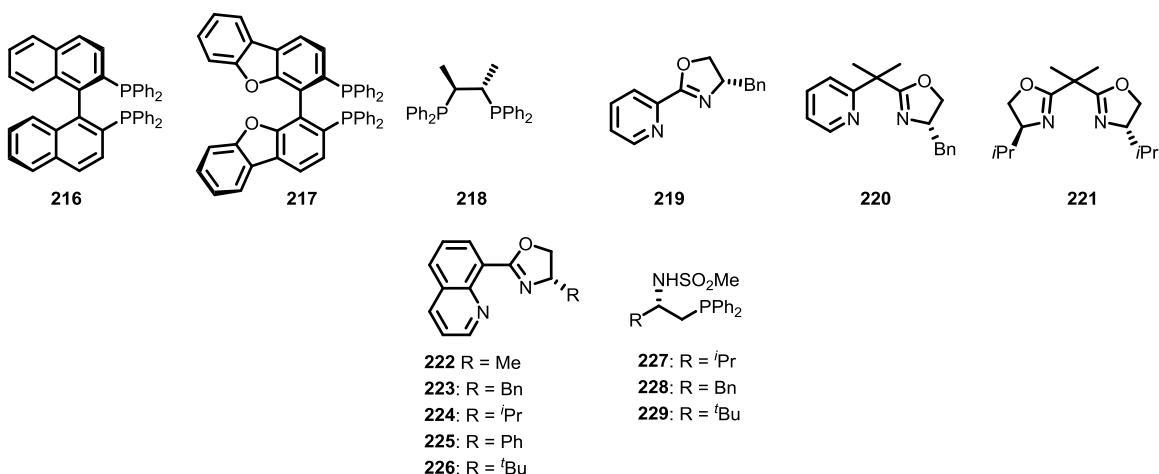
Figure 1.24. Chiral ligands employed in Pd catalyzed hydroarylations of norbornene.

While Pd(II) species have been employed as hydroarylation catalysts with norbornene substrates, several reports describe hydroarylations using stannyl- or boryl-substituted arenes, as typically employed in cross coupling reactions (such as the Stille or Suzuki). A recent report by the Sigman group[140] demonstrates that hydroarylation is achieved in alcohol-containing solvents. In the proposed mechanism (Figure 1.25), a $[L_nPd^{II}X_2]$ (**230**) species mediates oxidation of *iso*-propanol to generate a Pd(II) hydride (**231**) along with acetone and an equivalent of HX. Olefin coordination and Markovnikov-like insertion occurs to produce a Pd–alkyl intermediate (**232**) that undergoes transmetallation with arylboronic esters (or tributylphenyl tin). Reductive elimination from **233** affords the final hydroarylation product along with a Pd^0 species (**234**). Exposure to O_2 and "HX" regenerates the active Pd(II) catalyst along with an equivalent of H_2O_2. A rate decrease over the course of the reaction occurred, likely as a result of adventitious reactivity of the active catalyst with H_2O_2. As a test for this, the catalytic reaction afforded near quantitative yield with added MnO_2, a common H_2O_2 disproportionation reagent.
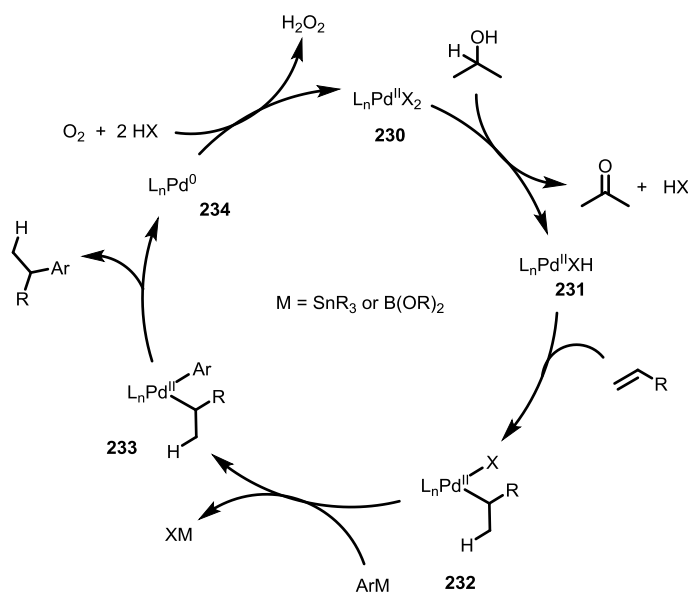
Figure 1.25. Mechanism for aerobic alcohol oxidation coupled to hydroarylation.[140]

To further develop this system, Sigman and coworkers[140] employed Pd(II) complexes with a variety of ligands in the hydroarylation of styrene derivatives with arylboronic esters. The results of the optimization experiments are summarized in Table 1.24. Both the Markovnikov hydroarylation product (**235**) and the classical Heck product (**236**) were observed. Several ligands were tested, containing either nitrogen- (**237**) or carbene-based (**238** and **239**) donors. Additionally, various conditions were employed for the *in situ* generation of the active transmetallation agent (*i.e.* ArB(OR)$_3^-$). Two different bases were used in this study: **237** or a mixture of **237** and K^{t}OBu. Finally, various arylboronic esters were employed (**240-243**). With these conditions, it was determined that an equimolar mixture of **237** and K^{t}OBu achieved the highest activity and selectivity for hydroarylation product **235**. Moreover, the ethylene glycol-derived (**241**) and the pinacol-derived (**242**) phenylboronic esters exhibited the highest activity, generally with quantitative conversion.

Table 1.24. Optimization of Pd hydroarylation using arylboronic esters.[140]
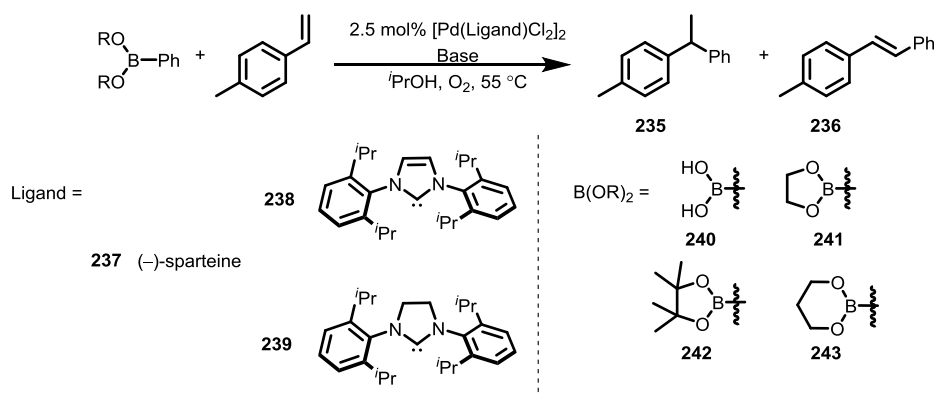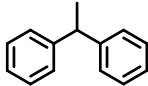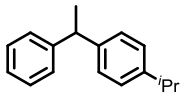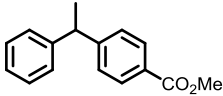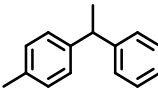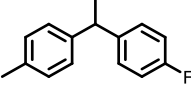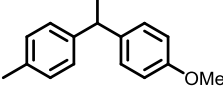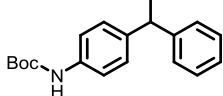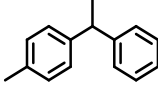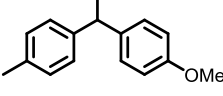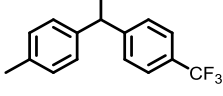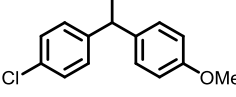
Ligand	PhB(OR)$_2$	Base(s) (mol%)	Time (h)	Conv. (%)	185:186
237	**240**	**237** (40)	24	35	1.4:1
238	**240**	**237** (20)	24	63	3.2:1
	240	**237** (20) + K^{t}OBu (5)	24	18	6.4:1
	241	**237** (7.5) + K^{t}OBu (7.5)	4	> 99	27:1
	242	**237** (5) + K^{t}OBu (5)	24	99	2.7:1
	243	**237** (7.5) + K^{t}OBu (7.5)	24	> 99	17:1
239	**241**	**237** (7.5) + K^{t}OBu (7.5)	8	> 99	> 30:1
	243	**237** (7.5) + K^{t}OBu (7.5)	24	46	> 30:1

The Sigman group has also demonstrated that other arenes can be delivered to olefins using the corresponding arylboronic ester[140] or tributylaryl tin[141] reagents. Added MnO$_2$ was added to reactions using the aryltin reagents, to disproportionate any H$_2$O$_2$ generated during the reaction. A summary of the substrate scope is given below in Table 1.25.

Table 1.25. Substrate scope for reductively coupled hydroarylation.

$$MR^1 \; + \; \diagup\!\!\!\diagdown R^2 \; \xrightarrow[\text{O}_2, \; ^i\text{PrOH}]{\text{[Pd] catalyst}} \; \overset{R^1}{\underset{R^2}{\diagdown}}$$
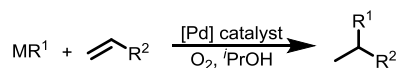
Conditions [a]	M	R^1	R^2	Product	Isolated Yield (%)
A [140]	**241**	Ph	Ph		91
		p-^{i}PrPh	Ph		65
		p-(CO$_2$Me)Ph	Ph		63
		Ph	p-MePh		81
		p-FPh	p-MePh		78
		p-OMePh	p-MePh		58
		Ph	p-NHBocPh		90
B [141]	SnBu$_3$	Ph	p-MePh		76
		p-OMePh	p-MePh		70
		p-CF$_3$Ph	p-MePh		67
		p-OMePh	p-ClPh		65

[a] Conditions: **A** = 1 equiv. alkene, 3 equiv. of MR^1, 0.75 mol% [Pd(**244**)Cl$_2$]$_2$, 6 mol% **237**, 6 mol% K^{t}OBu, 55 °C, 24 h, ^{i}PrOH solvent, O$_2$ atmosphere; **B** = 1 equiv. alkene, 1.5 equiv. of MR^1, 2.5 mol% Pd(**239**)Cl$_2$, 40 mol% **237**, 75 mol% MnO$_2$, 60 °C, 18 h, ^{i}PrOH solvent, 25 psi O$_2$. References are given in brackets.

A deuterium-labeling study with Me$_2$CHOD as the solvent provided information regarding the mechanism of this reaction (Scheme 1.9).[141] Under these conditions, no deuterium was incorporated into the products, which demonstrates that acidic protons are not involved in the mechanism. A similar experiment using Me$_2$CDOH as a solvent, however, demonstrated that a majority (92%) of the product contained deuterium, either at the methyl or methine position; this implies that a Pd(II)–hydride intermediate (**231** in Figure 1.24) likely exists and is generated by reaction with methanol. The existence of multiple isotopomers suggests operation of a reversible β-hydride elimination step, which allows deuterium scrambling into the olefin.

In a subsequent report by Sigman and coworkers,[142] chiral ligands were employed for enatioselective hydroarylations using either arylboronic ester or aryltin reagents. With bulky bis(oxazoline)-based ligands, modest enantioselectivities were achieved for a series of substrates.

Scheme 1.9. Deuterium Labeling Study in Oxidatively Coupled Hydroarylation.[142]
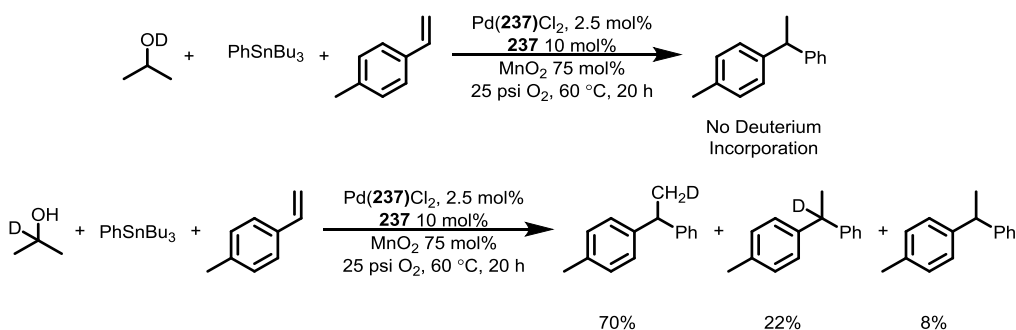
Recent reports by the Sigman group[143,144] describe oxidatively coupled hydroarylations with alkenyl alcohols (eqs 1.19 and 1.20). While the oxidation of added ^{i}PrOH has previously been employed as a hydrogen source, the oxidation of an olefin-containing alcohol has also been explored towards oxidatively-coupled hydroarylations. With alkenyl alcohols, an initial oxidation of the alcoholic group generates a carbonyl and a Pd(II)–hydride. Subsequent coordination and insertion of the olefin can occur. Arylation (eq 1.19) or transmetallation (eq 1.20) followed by reductive elimination generates the desired hydroarylation product. The reaction was made enantioselective with the use of the chiral pyridyl-oxazoline ligand **244**.[143,144] The hydroarylation of nitroalkenes with PdCl$_2$ using aryltin or tetraarylborate as arene sources has also been demonstrated by Sakae.[145]
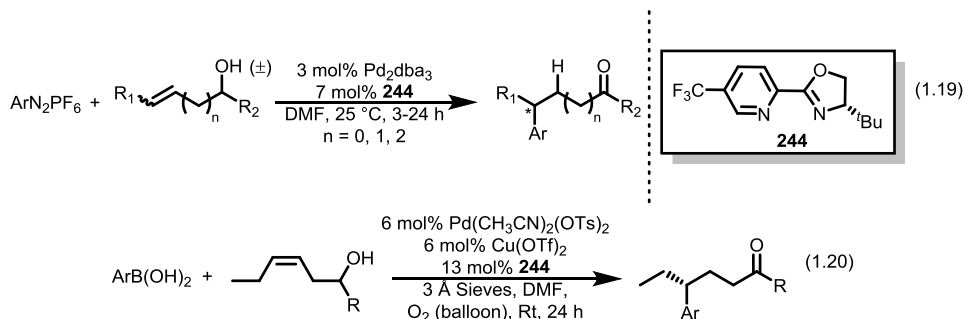
Key Conclusions from Pd Catalyzed Hydroarylations. It has been demonstrated that Pd(II) complexes are catalytically active for hydroarylation.[130-145] In contrast to other commonly employed metals for

hydroarylation, however, aryl C–H activation has not yet been utilized with Pd(II). Instead, a leaving group (I, Br, OTf) or transmetallating substituent such as SnR_3 or $B(OR)_2$ is required; additionally, an external hydrogen source is necessary. Using arenes bearing leaving groups, formate has been employed as a hydrogen source (either *in situ* or as an added salt), to liberate CO_2 as a byproduct.[130-139] For arenes substituted with cross-coupling functionalities, the oxidation of an alcohol to a carbonyl group generates a Pd–hydride intermediate that can reductively eliminate with an alkyl fragment to generate the desired hydroarylation product.[140-144]

While Pd(II) complexes have shown promise as hydroarylation catalysts, further studies are required to explore the possibility of designing species that can access hydroarylation products *via* a C–H activation pathway. Such complexes would allow for hydroarylation to occur without the need to prefunctionalize the arene. Moreover, a C–H activation pathway would eliminate the need for stoichiometric amounts of a hydrogen source (such as formate or ^{i}PrOH). Finally, such C–H activations are more difficult to achieve than C–X activations; as such, accessing this more difficult type of transformation with Pd and applying it towards productive hydroarylation is of interest.

Summary and Outlook. The alkylation of arenes is a massive industrial process that annually generates millions of tons of alkyl arenes. Moreover, these products are typically used as polymer precursors (*e.g.,* for synthesis of polystyrene). While industrial processes typically employ Lewis acids (such as zeolites or $AlCl_3$ with a Brønsted acid) to couple ethylene and benzene *via* a Friedel-Crafts mechanism, this chemistry can lead to over-alkylation. Additionally, for higher olefins, such catalysis affords the less-desired Markovnikov products and often leads to competitive olefin isomerization. As a result, there is current interest in the development of homogenous transition metal catalysts for selective, direct hydroarylation of α-olefins with arenes.

Given the history of research in this area, it seems that late-metal precatalysts are promising candidates for future catalyst development. Many desirable features exist in systems employing a d^8 metal center; for example, hydroarylations of simple unfunctionalized arenes such as benzene or toluene have been demonstrated with Pt(II) complexes.[8-26] While a few examples of Ni(0) hydroarylations exist,[28,29] Ni(II) catalyzed hydroarylations have yet to be investigated. Computational studies employing DFT have suggested that Ni(II) complexes could be competent towards the hydroarylation of ethylene and benzene.[30] Regio- and enantio-selectivity have been achieved in olefin hydroarylations with Rh[32-36,40,47-62,64-73] and Ir[76-90] based catalysts, and have been successfully applied towards complex total syntheses.[53,59,64,65] A wide range of substrates has been identified with Rh catalysts, elucidating the compatibility of the catalyst with various substrate functionalities. Recent developments highlighted Co complexes generated *in situ* are competent analogues to the well-established heavier metal systems.[95,98-107] Additionally, several strategies for the hydroarylation of olefins employing Pd complexes with added external hydrogen sources have been explored.[130-145]

While hydroarylations with d^8 metal centers offer potential benefits when compared to zeolites, several important limitations remain. Overall, d^8 catalysts appear to generally suffer from a lack of activity and catalyst stability issues. Several steps that may lead to catalyst decomposition have been identified, including β-hydride elimination and non-productive reductive elimination. For late transition metals, reduction to elemental states can often be an issue. To address catalytic stability, further research into combating possible decomposition routes is necessary.

References

1. Welch, V. A.; Fallon, K. J.; Gelbke, H.-P. *Ullmann's Encyclopedia of Industrial Chemistry* **2005**, *13*, 451-464.

2. James, D. H.; Castor, W. M. *Ullmann's Encyclopedia of Industrial Chemistry* **2011**, *34*, 529-544.

3. Maul, J.; Frushour, B. G.; Kontoff, J. R.; Eichenauer, H.; Ott, K.-H.; Schade, C. *Ullmann's Encyclopedia of Industrial Chemistry* **2012**, *29*, 475-522.

4. Perego, C.; Ingallina, P. *Catal. Today* **2002**, *73*, 3-22.

5. Hartwig, J. F. *Organotransition Metal Chemistry: From Bonding to Catalysis*; University Science Books: Mill Valley, CA, 2010.

6. Lersch, M.; Tilset, M. *Chem. Rev.* **2005**, *105*, 2471-2526.

7. Chianese, A. R.; Lee, S. J.; Gagné, M. R. *Angew. Chem. Int. Ed.* **2007**, *46*, 4042-4059.

8. Karshtedt, D.; Bell, A. T.; Tilley, T. D. *Organometallics* **2004**, *23*, 4169-4171.

9. Karshtedt, D.; McBee, J. L.; Bell, A. T.; Tilley, T. D. *Organometallics* **2006**, *25*, 1801-1811.

10. Suslick, B. A.; Liberman-Martin, A. L.; Wambach, T. C.; Tilley, T. D. *ACS Catal.* **2017**, *7*, 4313-4322.

11. Luedtke, A. T.; Goldberg, K. I. *Inorg. Chem.* **2007**, *46*, 8496-8498.

12. Luedtke, A. T.; Goldberg, K. I. *Angew. Chem. Int. Ed.* **2008**, *47*, 7694-7696.

13. Clement, M. L.; Grice, K. A.; Luedtke, A. T.; Kaminsky, W.; Goldberg, K. I. *Chem. Eur. J.* **2014**, *20*, 17287-17291.

14. Johansson, L.; Ryan, O. B.; Rømming, C.; Tilset, M. *J. Am. Chem. Soc.* **2001**, *123*, 6579-6590.

15. Johansson, L.; Tilset, M.; Labinger, J. A.; Bercaw, J. E. *J. Am. Chem. Soc.* **2000**, *122*, 10846-10855.

16. Bowring, M. A.; Bergman, R. G.; Tilley, T. D. *J. Am. Chem. Soc.* **2013**, *135*, 13121-13128.

17. McKeown, B. A.; Foley, N. A.; Lee, J. P.; Gunnoe, T. B. *Organometallics* **2008**, *27*, 4031-4033.

18. McKeown, B. A.; Gonzalez, H. E.; Friedfeld, M. R.; Gunnoe, T. B.; Cundari, T. R.; Sabat, M. *J. Am. Chem. Soc.* **2011**, *133*, 19131-19152.

19. McKeown, B. A.; Prince, B. M.; Ramiro, Z.; Gunnoe, T. B.; Cundari, T. R. *ACS Catal.* **2014**, *4*, 1607-1615.

20. McKeown, B. A.; Gonzalez, H. E.; Friedfeld, M. R.; Brosnahan, A. M.; Gunnoe, T. B.; Cundari, T. R.; Sabat, M. *Organometallics* **2013**, *32*, 2857-2865.

21. McKeown, B. A.; Gonzalez, H. E.; Gunnoe, T. B.; Cundari, T. R.; Sabat, M. *ACS Catal.* **2013**, *3*, 1165-1171.

22. McKeown, B. A.; Gonzalez, H. E.; Michaelos, T.; Gunnoe, T. B.; Cundari, T. R.; Crabtree, R. H.; Sabat, M. *Organometallics* **2013**, *32*, 3903-3913.

23. Bowring, M. A.; Bergman, R. G.; Tilley, T. D. *Organometallics* **2011**, *30*, 1295-1298.

24. Szuromi, E.; Sharp, P. R. *Organometallics* **2006**, *25*, 558-559.

25. McBee, J. L.; Bell, A. T.; Tilley, T. D. *J. Am. Chem. Soc.* **2008**, *130*, 16562-16571.

26. Brosnahan, A. M.; Talbot, A.; McKeown, B. A.; Kalman, S. E.; Gunnoe, T. B.; Ess, D. H.; Sabat, M. *J. Organomet. Chem.* **2015**, *793*, 248-255.

27. Cucciolito, M. E.; D'Amora, A.; Tuzi, A.; Vitagliano, A. *Organometallics* **2007**, *26*, 5216-5223.

28. Bair, J. S.; Schramm, Y.; Sergeev, A. G.; Clot, E.; Eisenstein, O.; Hartwig, J. F. *J. Am. Chem. Soc.* **2014**, *136*, 13098-13101.

29. Nakao, Y.; Kashihara, N.; Kanyiva, K. S.; Hiyama, T. *J. Am. Chem. Soc.* **2008**, *130*, 16170-16171.

30. Cundari, T. R.; Gonzalez, H. E. *J. Mol. Catal. A: Chem.* **2012**, *353-354*, 1-6.

31. Nguyen, J.; Chong, A.; Lalic, G. *Chem. Sci.* **2019**, *10*, 3231-3236.

32. Vaughan, B. A.; Webster-Gardiner, M. S.; Cundari, T. R.; Gunnoe, T. B. *Science* **2015**, *348*, 421-424.

33. Webster-Gardiner, M. S.; Fu, R.; Fortman, G. C.; Nielsen, R. J.; Gunnoe, T. B.; Goddard III, W. A. *Catalysis Science & Technology* **2015**, *5*, 96-100.

34. Webster-Gardiner, M. S.; Piszel, P. E.; Fu, R.; McKeown, B. A.; Nielsen, R. J.; Goddard, W. A.; Gunnoe, T. B. *J. Mol. Catal. A: Chem.* **2017**, *426*, 381-388.

35. Vaughan, B. A.; Khani, S. K.; Gary, J. B.; Kammert, J. D.; Webster-Gardiner, M. S.; McKeown, B. A.; Davis, R. J.; Cundari, T. R.; Gunnoe, T. B. *J. Am. Chem. Soc.* **2017**, *139*, 1485-1498.

36. Chen, J.; Nielsen, R. J.; Goddard, W. A.; McKeown, B. A.; Dickie, D. A.; Gunnoe, T. B. *J. Am. Chem. Soc.* **2018**, *140*, 17007-17018.

37. Partridge, M. G.; Field, L. D.; Messerle, B. A. *Organometallics* **1996**, *15*, 872-877.

38. Kawamoto, T. *Inorg. Chim. Acta* **2000**, *300-302*, 512-516.

39. Ghosh, C. K.; Graham, W. A. G. *J. Am. Chem. Soc.* **1989**, *111*, 375-376.

40. Jun, C. H.; Hong, J. B.; Kim, Y. H.; Chung, K. Y. *Angew. Chem. Int. Ed.* **2000**, *39*, 3440-3442.

41. Ritleng, V.; Sirlin, C.; Pfeffer, M. *Chem. Rev.* **2002**, *102*, 1731-1770.

42. Colby, D. A.; Bergman, R. G.; Ellman, J. A. *Chem. Rev.* **2010**, *110*, 624-655.

43. Colby, D. A.; Tsai, A. S.; Bergman, R. G.; Ellman, J. A. *Acc. Chem. Res.* **2012**, *45*, 814-825.

44. Klei, S. R.; Tan, K. L.; Golden, J. T.; Yung, C. M.; Thalji, R. K.; Ahrendt, K. A.; Ellman, J. A.; Tilley, T. D.; Bergman, R. G. In *Activation and Functionalization of C—H Bonds*; American Chemical Society: 2004; Vol. 885, p 46-55.

45. Schipper, D. J.; Hutchinson, M.; Fagnou, K. *J. Am. Chem. Soc.* **2010**, *132*, 6910-6911.

46. Tauchert, M. E.; Incarvito, C. D.; Rheingold, A. L.; Bergman, R. G.; Ellman, J. A. *J. Am. Chem. Soc.* **2012**, *134*, 1482-1485.

47. Jun, C.-H.; Lee, H.; Hong, J.-B. *The Journal of Organic Chemistry* **1997**, *62*, 1200-1201.

48. Jun, C.-H.; Hong, J.-B. *Org. Lett.* **1999**, *1*, 887-889.

49. Lim, S.-G.; Ahn, J.-A.; Jun, C.-H. *Org. Lett.* **2004**, *6*, 4687-4690.

50. Vo-Thanh, G.; Lahrache, H.; Loupy, A.; Kim, I.-J.; Chang, D.-H.; Jun, C.-H. *Tetrahedron* **2004**, *60*, 5539-5543.

51. Yoon, J. H.; Park, Y. J.; Lee, J. H.; Yoo, J.; Jun, C.-H. *Org. Lett.* **2005**, *7*, 2889-2892.

52. Thalji, R. K.; Ahrendt, K. A.; Bergman, R. G.; Ellman, J. A. *J. Am. Chem. Soc.* **2001**, *123*, 9692-9693.

53. Thalji, R. K.; Ahrendt, K. A.; Bergman, R. G.; Ellman, J. A. *The Journal of Organic Chemistry* **2005**, *70*, 6775-6781.

54. Lim, Y.-G.; Han, J.-S.; Yang, S.-S.; Chun, J. H. *Tetrahedron Lett.* **2001**, *42*, 4853-4856.

55. Lim, Y.-G.; Han, J.-S.; Koo, B. T.; Kang, J.-B. *J. Mol. Catal. A: Chem.* **2004**, *209*, 41-49.

56. Lim, Y.-G.; Koo, B. T. *Tetrahedron Lett.* **2005**, *46*, 7997-8001.

57. Thalji, R. K.; Ellman, J. A.; Bergman, R. G. *J. Am. Chem. Soc.* **2004**, *126*, 7192-7193.

58. Harada, H.; Thalji, R. K.; Bergman, R. G.; Ellman, J. A. *The Journal of Organic Chemistry* **2008**, *73*, 6772-6779.

59. Watzke, A.; Wilson, R. M.; O'Malley, S. J.; Bergman, R. G.; Ellman, J. A. *Synlett* **2007**, *2007*, 2383-2389.

60. Kakiuchi, F.; Le Gendre, P.; Yamada, A.; Ohtaki, H.; Murai, S. *Tetrahedron: Asymmetry* **2000**, *11*, 2647-2651.

61. Shibata, K.; Chatani, N. *Org. Lett.* **2014**, *16*, 5148-5151.

62. Shibata, K.; Yamaguchi, T.; Chatani, N. *Org. Lett.* **2015**, *17*, 3584-3587.

63. Yamaguchi, T.; Natsui, S.; Shibata, K.; Yamazaki, K.; Rej, S.; Ano, Y.; Chatani, N. *Chem. Eur. J.* **2019**, *25*, 6915-6919.

64. O'Malley, S. J.; Tan, K. L.; Watzke, A.; Bergman, R. G.; Ellman, J. A. *J. Am. Chem. Soc.* **2005**, *127*, 13496-13497.

65. Ahrendt, K. A.; Bergman, R. G.; Ellman, J. A. *Org. Lett.* **2003**, *5*, 1301-1303.

66. Wentzel, M. T.; Reddy, V. J.; Hyster, T. K.; Douglas, C. J. *Angew. Chem. Int. Ed.* **2009**, *48*, 6121-6123.

67. Brunet, J.-J.; Neibecker, D.; Philippot, K. *J. Chem. Soc., Chem. Commun.* **1992**, 1215-1216.

68. Brunet, J.-J.; Commenges, G.; Neibecker, D.; Philippot, K. *J. Organomet. Chem.* **1994**, *469*, 221-228.

69. Lenges, C. P.; Brookhart, M. *J. Am. Chem. Soc.* **1999**, *121*, 6616-6623.

70. Sun, Z.-M.; Zhang, J.; Manan, R. S.; Zhao, P. *J. Am. Chem. Soc.* **2010**, *132*, 6935-6937.

71. Bercaw, J. E.; Hazari, N.; Labinger, J. A. *Organometallics* **2009**, *28*, 5489-5492.

72. Kloek, S. M.; Heinekey, D. M.; Goldberg, K. I. *Angew. Chem. Int. Ed.* **2007**, *46*, 4736-4738.

73. Tsui, G. C.; Menard, F.; Lautens, M. *Org. Lett.* **2010**, *12*, 2456-2459.

74. Zhang, J.; Leitus, G.; Ben-David, Y.; Milstein, D. *Angew. Chem.* **2006**, *118*, 1131-1133.

75. Ben-Ari, E.; Leitus, G.; Shimon, L. J. W.; Milstein, D. *J. Am. Chem. Soc.* **2006**, *128*, 15390-15391.

76. Matsumoto, T.; Taube, D. J.; Periana, R. A.; Taube, H.; Yoshida, H. *J. Am. Chem. Soc.* **2000**, *122*, 7414-7415.

77. Periana, R. A.; Liu, X. Y.; Bhalla, G. *Chem. Commun.* **2002**, 3000-3001.

78. Bhalla, G.; Oxgaard, J.; Goddard, W. A.; Periana, R. A. *Organometallics* **2005**, *24*, 3229-3232.

79. Oxgaard, J.; Muller, R. P.; Goddard, W. A.; Periana, R. A. *J. Am. Chem. Soc.* **2004**, *126*, 352-363.

80. Oxgaard, J.; Periana, R. A.; Goddard, W. A. *J. Am. Chem. Soc.* **2004**, *126*, 11658-11665.

81. Bhalla, G.; Bischof, S. M.; Ganesh, S. K.; Liu, X. Y.; Jones, C. J.; Borzenko, A.; Tenn, I. I. I. W. J.; Ess, D. H.; Hashiguchi, B. G.; Lokare, K. S.; Leung, C. H.; Oxgaard, J.; Goddard, I. I. I. W. A.; Periana, R. A. *Green Chem.* **2011**, *13*, 69-81.

82. Aufdenblatten, R.; Diezi, S.; Togni, A. *Monatshefte für Chemie / Chemical Monthly* **2000**, *131*, 1345-1350.

83. Dorta, R.; Togni, A. *Chem. Commun.* **2003**, 760-761.

84. Shirai, T.; Yamamoto, Y. *Angew. Chem. Int. Ed.* **2015**, *54*, 9894-9897.

85. Tsuchikama, K.; Kasagawa, M.; Hashimoto, Y.-K.; Endo, K.; Shibata, T. *J. Organomet. Chem.* **2008**, *693*, 3939-3942.

86. Crisenza, G. E. M.; McCreanor, N. G.; Bower, J. F. *J. Am. Chem. Soc.* **2014**, *136*, 10258-10261.

87. Crisenza, G. E. M.; Sokolova, O. O.; Bower, J. F. *Angew. Chem. Int. Ed.* **2015**, *54*, 14866-14870.

88. Huang, G.; Liu, P. *ACS Catal.* **2016**, *6*, 809-820.

89.   Ebe, Y.; Nishimura, T. *J. Am. Chem. Soc.* **2015**, *137*, 5899-5902.

90.   Hatano, M.; Ebe, Y.; Nishimura, T.; Yorimitsu, H. *J. Am. Chem. Soc.* **2016**, *138*, 4010-4013.

91.   Nagamoto, M.; Fukuda, J.-i.; Hatano, M.; Yorimitsu, H.; Nishimura, T. *Org. Lett.* **2017**, *19*, 5952-5955.

92.   Chirik, P.; Morris, R. *Acc. Chem. Res.* **2015**, *48*, 2495-2495.

93.   Wang, S.; Chen, S. Y.; Yu, X. Q. *Chem. Commun.* **2017**, *53*, 3165-3180.

94.   Moselage, M.; Li, J.; Ackermann, L. *ACS Catal.* **2016**, *6*, 498-525.

95.   Gao, K.; Yoshikai, N. *Acc. Chem. Res.* **2014**, *47*, 1208-1219.

96.   Gandeepan, P.; Muller, T.; Zell, D.; Cera, G.; Warratz, S.; Ackermann, L. *Chem Rev* **2019**, *119*, 2192-2452.

97.   Pototschnig, G.; Maulide, N.; Schnürch, M. *Chem. Eur. J.* **2017**, *23*, 9206-9232.

98.   Halbritter, G.; Knoch, F.; Wolski, A.; Kisch, H. *Angew. Chem. Int. Ed.* **1994**, *33*, 1603-1605.

99.   Ding, Z.; Yoshikai, N. *Angew. Chem. Int. Ed.* **2012**, *51*, 4698-4701.

100.   Gao, K.; Lee, P.-S.; Fujita, T.; Yoshikai, N. *J. Am. Chem. Soc.* **2010**, *132*, 12249-12251.

101.   Gao, K.; Yoshikai, N. *J. Am. Chem. Soc.* **2011**, *133*, 400-402.

102.   Gao, K.; Yoshikai, N. *Angew. Chem. Int. Ed.* **2011**, *50*, 6888-6892.

103.   Lee, P. S.; Yoshikai, N. *Angew. Chem. Int. Ed.* **2013**, *52*, 1240-1244.

104.   Lee, P.-S.; Fujita, T.; Yoshikai, N. *J. Am. Chem. Soc.* **2011**, *133*, 17283-17295.

105.   Xu, W.; Pek, J. H.; Yoshikai, N. *Adv. Synth. Catal.* **2016**, *358*, 2564-2568.

106.   Xu, W.; Yoshikai, N. *Angew. Chem. Int. Ed.* **2016**, *55*, 12731-12735.

107.   Ilies, L.; Chen, Q.; Zeng, X.; Nakamura, E. *J. Am. Chem. Soc.* **2011**, *133*, 5221-5223.

108.   Ikemoto, H.; Yoshino, T.; Sakata, K.; Matsunaga, S.; Kanai, M. *J. Am. Chem. Soc.* **2014**, *136*, 5424-5431.

109.   Yoshino, T.; Ikemoto, H.; Matsunaga, S.; Kanai, M. *Angew. Chem. Int. Ed.* **2013**, *52*, 2207-2211.

110.   Yoshino, T.; Ikemoto, H.; Matsunaga, S.; Kanai, M. *Chem. Eur. J.* **2013**, *19*, 9142-9146.

111.   Sanjosé-Orduna, J.; Gallego, D.; Garcia-Roca, A.; Martin, E.; Benet-Buchholz, J.; Pérez-Temprano, M. H. *Angew. Chem. Int. Ed.* **2017**, *56*, 12137-12141.

112.   Koelle, U.; Fuss, B.; Rajasekharan, M. V.; Ramakrishna, B. L.; Ammeter, J. H.; Boehm, M. C. *J. Am. Chem. Soc.* **1984**, *106*, 4152-4160.

113.   Sanjosé-Orduna, J.; Benet-Buchholz, J.; Pérez-Temprano, M. H. *Inorg. Chem.* **2019**.

114.   Jin, Z.; Chu, L.; Chen, Y.-Q.; Yu, J.-Q. *Org. Lett.* **2018**, *20*, 425-428.

115.   Xu, H.-J.; Lu, Y.; Farmer, M. E.; Wang, H.-W.; Zhao, D.; Kang, Y.-S.; Sun, W.-Y.; Yu, J.-Q. *J. Am. Chem. Soc.* **2017**, *139*, 2200-2203.

116.   Xu, H.-J.; Kang, Y.-S.; Shi, H.; Zhang, P.; Chen, Y.-K.; Zhang, B.; Liu, Z.-Q.; Zhao, J.; Sun, W.-Y.; Yu, J.-Q.; Lu, Y. *J. Am. Chem. Soc.* **2019**, *141*, 76-79.

117.   Ding, Q.; Ye, S.; Cheng, G.; Wang, P.; Farmer, M. E.; Yu, J.-Q. *J. Am. Chem. Soc.* **2017**, *139*, 417-425.

118.   Liu, Y.-J.; Xu, H.; Kong, W.-J.; Shang, M.; Dai, H.-X.; Yu, J.-Q. *Nature* **2014**, *515*, 389.

119.   Tang, R.-Y.; Li, G.; Yu, J.-Q. *Nature* **2014**, *507*, 215.

120.   Yang, Y.-F.; Cheng, G.-J.; Liu, P.; Leow, D.; Sun, T.-Y.; Chen, P.; Zhang, X.; Yu, J.-Q.; Wu, Y.-D.; Houk, K. N. *J. Am. Chem. Soc.* **2014**, *136*, 344-355.

121.   Wan, L.; Dastbaravardeh, N.; Li, G.; Yu, J.-Q. *J. Am. Chem. Soc.* **2013**, *135*, 18056-18059.

122.   Dai, H.-X.; Li, G.; Zhang, X.-G.; Stepan, A. F.; Yu, J.-Q. *J. Am. Chem. Soc.* **2013**, *135*, 7567-7571.

123.   Deng, Y.; Yu, J.-Q. *Angew. Chem. Int. Ed.* **2015**, *54*, 888-891.

124.   Li, M.; Shang, M.; Xu, H.; Wang, X.; Dai, H.-X.; Yu, J.-Q. *Org. Lett.* **2019**, *21*, 540-544.

125.   Cheng, G.; Wang, P.; Yu, J.-Q. *Angew. Chem. Int. Ed.* **2017**, *56*, 8183-8186.

126.   Li, G.-C.; Wang, P.; Farmer, M. E.; Yu, J.-Q. *Angew. Chem. Int. Ed.* **2017**, *56*, 6874-6877.

127.   Cabri, W.; Candiani, I. *Acc. Chem. Res.* **1995**, *28*, 2-7.

128.   Cacchi, S. *Pure Appl. Chem.* **1990**, *62*, 713-722.

129.   Namyslo, J. C.; Storsberg, J.; Klinge, J.; Gärtner, C.; Yao, M.-L.; Ocal, N.; Kaufmann, D. E. *Molecules* **2010**, *15*, 3402-3410.

130.   Arcadi, A.; Marinelli, F.; Cacchi, S. *J. Organomet. Chem.* **1986**, *312*, c27-c32.

131.   Arcadi, A.; Bernocchi, E.; Burini, A.; Cacchi, S.; Marinelli, F.; Pietroni, B. *Tetrahedron* **1988**, *44*, 481-490.

132.   Arcadi, A.; Marinelli, F.; Bernocchi, E.; Cacchi, S.; Ortar, G. *J. Organomet. Chem.* **1989**, *368*, 249-256.

133.   Mayo, P.; Tam, W. *Tetrahedron* **2002**, *58*, 9527-9540.

134.   Brunel, J. M.; Heumann, A.; Buono, G. *Angew. Chem. Int. Ed.* **2000**, *39*, 1946-1949.

135.   Namyslo, J. C.; Kaufmann, D. E. *Chem. Ber.* **1997**, *130*, 1327-1331.

136.   Wu, X.-Y.; Xu, H.-D.; Tang, F.-Y.; Zhou, Q.-L. *Tetrahedron: Asymmetry* **2001**, *12*, 2565-2569.

137.   Wu, X.-Y.; Xu, H.-D.; Zhou, Q.-L.; Chan, A. S. C. *Tetrahedron: Asymmetry* **2000**, *11*, 1255-1257.

138.   Sakuraba, S.; Awano, K.; Achiwa, K. *Synlett* **1994**, *1994*, 291-292.

139.   Moinet, C.; Fiaud, J.-C. *Tetrahedron Lett.* **1995**, *36*, 2051-2052.

140.   Iwai, Y.; Gligorich, K. M.; Sigman, M. S. *Angew. Chem. Int. Ed.* **2008**, *47*, 3219-3222.

141.   Gligorich, K. M.; Cummings, S. A.; Sigman, M. S. *J. Am. Chem. Soc.* **2007**, *129*, 14193-14195.

142.   Podhajsky, S. M.; Iwai, Y.; Cook-Sneathen, A.; Sigman, M. S. *Tetrahedron* **2011**, *67*, 4435-4441.

143.   Werner, E. W.; Mei, T.-S.; Burckle, A. J.; Sigman, M. S. *Science* **2012**, *338*, 1455-1458.

144.   Mei, T.-S.; Werner, E. W.; Burckle, A. J.; Sigman, M. S. *J. Am. Chem. Soc.* **2013**, *135*, 6830-6833.

145.   Toshiyuki, O.; Sakae, U. *Bull. Chem. Soc. Jpn.* **2003**, *76*, 1423-1431.

Chapter Two

Olefin Hydroarylation Catalyzed by (Pyridyl-Indolate)Pt(II) Complexes: Catalytic Efficiencies and Mechanistic Aspects

Introduction. Catalytic C–C bond-forming processes are important for efficient utilization of abundant feedstock chemicals. These methods are critical to the industrial-scale syntheses of alkyl arene products, which are incorporated into many plastics and fine chemicals on an enormous scale. For example, polystyrene, which is manufactured from ethylbenzene, was consumed at an annual rate of 1.2 x 10^7 tons/year from 2000-2010.[1-3] While methods exist to couple alkyl and aryl fragments using molecular catalysis (*e.g.* cross coupling[4,5]), such systems often require the use of activated reagents such as ArSnR$_3$ or ArZnX, which generate additional synthetic steps. Moreover, these methods are atom inefficient and generate stoichiometric waste.

Given recent advances in C–H functionalization chemistry,[6-9] reactions that can directly couple aryl C–H bonds and small molecules are feasible. In particular, the hydroarylation of carbon–carbon multiple bonds has garnered considerable attention over the last two decades.[10-12] The initial developments of olefin hydroarylation catalyzed by RuH$_2$(CO)(PPh$_3$)$_3$ were described by Murai and coworkers.[13-15] Further mechanistic investigations with related Ru(II)[16-21] and Ir(III)[22-26] complexes illustrated that olefin insertion into a metal–aryl bond and arene C–H activation are key mechanistic steps.[13-26] Several recent reports have indicated that the hydroarylation of olefins to generate alkyl arenes[10-12] can also be achieved with transition metal catalysts with d^8 electronic configurations (*e.g.*, Ir(I),[27-29] Rh(I),[30-40] and Pd(II)[41,42]); mechanistic features of these systems have not been thoroughly elucidated.

Both cationic and neutral Pt(II) complexes supported by 4,4′-di-*tert*-butyl-2,2′-bipyridine (^{t}bpy)[43] or 2,2′-pyridyl-pyrrole (PyPyr)[44,45] ligands, respectively, have recently been reported as hydroarylation catalysts (see Chapter 1). Unlike other d^8 metal catalysts, these systems operate with unactivated arene substrates that do not contain directing or coordinating functionalities, but the efficiencies of these catalysts are rather limited.[43-45] In the latter context, it has been suggested that modification of the ancillary ligand donating ability could potentially improve the activity of Pt-based catalysts.[46] However, there has not been a thorough study of ligand electronic effects for neutral Pt catalysts, even though these systems appear to exhibit higher selectivities for mono- (vs. poly-) alkylation, relative to cationic catalysts.[45] Moreover, detailed investigations into complex degradation pathways have not been performed for the neutral Pt(II) systems. Determining the primary decomposition routes is necessary to design robust catalysts and elucidate potential additives that suppress unproductive processes.

We have previously reported the use of Pt complexes bearing a parent 2,2′-pyridyl-indolate (PyInd) ligand for the hydroarylation of norbornene.[47,48] Herein, the synthesis and olefin hydroarylation activity of Pt(II) complexes of the type (N–N)PtPh(SR$_2$) are described for a series of pyridyl-indolate complexes. The identification and isolation of several catalytic intermediates provide insight into the operative mechanism for hydroarylation. Additionally, differences in catalytic performance as a function of substituents on the N–N ligand have been determined for a variety of olefin and arene substrates.

Synthesis of Platinum Pyridyl-Indolate Complexes. A parent ligand bearing a 4′-^{t}Bu group on the pyridyl moiety (**4a**) was chosen due to its solubility in hydrocarbons, as well as its diagnostic *tert*-butyl ^{1}H NMR resonance. Several highly-fluorinated derivatives were also synthesized (**4b** and **4c**). To thoroughly probe the electronic effects of this ligand type on catalysis, a series of (N–N) ligands with various electron withdrawing or donating substituents (**4d-4j**) was synthesized using a procedure adapted from Wang and coworkers.[49] Condensation of arylhydrazines **2a-2k** (either purchased commercially or generated from the corresponding aniline, **1**) with acetylpyridine afforded arylhydrazone intermediates **3a-3j**. Treatment with neat polyphosphoric acid generated the desired substituted PyInd ligands (Scheme 2.1).

Scheme 2.1. General PyInd Ligand (4a-4j) Synthetic Route.

1) NaNO$_2$, HCl, 10 °C, 1 h

2) SnCl$_2$, H$_2$O, 10 °C, 50 min

1a-1j

2a-2j

HOAc, EtOH
90 °C, 4 h

polyphosphoric acid

140 °C, 2 h

4a-4j

3a-3j

a: R^{4,5,6,7} = H, R$^{4'}$ = ^{t}Bu
b: R^{4,7} = F, R^{5,6} = H, R$^{4'}$ = ^{t}Bu
c: R^{4,5,6,7} = F, R$^{4'}$ = ^{t}Bu

d: R^{4,6,7} = H, R^5 = H, R$^{4'}$ = H
e: R^{4,6,7} = H, R^5 = OMe, R$^{4'}$ = H
f: R^{4,6,7} = H, R^5 = Me, R$^{4'}$ = H

g: R^{4,6,7} = H, R^5 = F, R$^{4'}$ = H
h: R^{4,6,7} = H, R^5 = Cl, R$^{4'}$ = H
i: R^{4,6,7} = H, R^5 = Br, R$^{4'}$ = H
j: R^{4,5,6} = H, R^7 = Cl, R$^{4'}$ = H
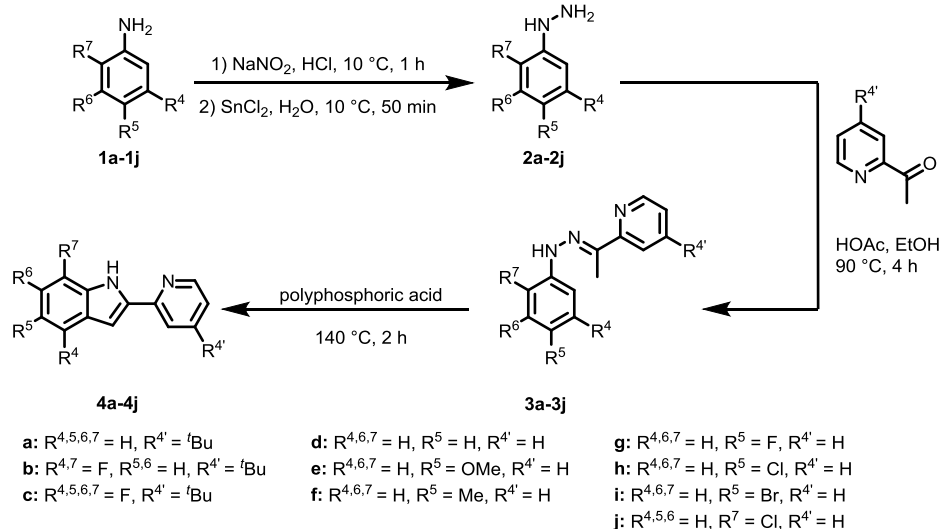
The pyridyl-indolate ligands were incorporated into platinum complexes by reactions with (SMe$_2$)$_2$PtPh$_2$, to afford complexes of the type (N–N)PtPh(SMe$_2$) (**5a-5j**, Scheme 2.1) which were purified by column chromatography. The analogous SEt$_2$ complex, (PyInd)PtPh(SEt$_2$) (**5k**), was generated by treatment of [(μ-SEt$_2$)PtPh$_2$]$_2$ with **4d** in benzene (Scheme 2.2). There are several diagnostic ^{1}H NMR resonances for complexes **5a-5k**. The SMe$_2$ ligand of **5a-5j** appears as a singlet with broad ^{195}Pt satellites (δ ~ 2.30 ppm, J_{PtH} ~ 60 Hz in dichloromethane-d_2). The *o*-aryl protons on the phenyl ligand in complexes **5a-5k** also exhibited ^{195}Pt coupling (δ ~ 7.60, J_{PtH} ~ 35 Hz in dichloromethane-d_2). X-ray diffraction quality single crystals of **5a**, **5b**, and **5c** were obtained by slow diffusion of pentane into a toluene solution of each complex at -35 °C. These complexes display the expected square planar geometry, and the indolate donor is positioned *trans* to the phenyl ligand (Figure 2.1). The bond lengths and angles are consistent with those of related Pt(II) complexes.[46,50]

Scheme 2.2. Synthesis of Catalysts 5a-5k.

(SMe$_2$)$_2$PtPh$_2$

benzene

5a-5c

4a (^{t}BuPyInd); R^4,R^5,R^6,R^7 = H
4b (^{t}BuPyInd-4,7-F$_2$); R^4,R^7 = F; R^5,R^6 = H
4c (^{t}BuPyInd-4,5,6,7-F$_4$); R^4,R^5,R^6,R^7 = F

(SMe$_2$)$_2$PtPh$_2$

benzene

5d-5j

4d (PyInd); R^5,R^7 = H
4e (PyInd-5-MeO); R^5 = MeO; R^7 = H
4f (PyInd-5-Me); R^5 = Me; R^7 = H
4g (PyInd-5-F); R^5 = F; R^7 = H
4h (PyInd-5-Cl); R^5 = Cl; R^7 = H
4i (PyInd-5-Br); R^5 = Br; R^7 = H
4j (PyInd-7-Cl); R^5 = H; R^7 = Cl

4d

[(μ-SEt$_2$)PtPh$_2$]$_2$

benzene

5k

4c

[(μ-SMe$_2$)PtMe$_2$]$_2$

benzene

5l
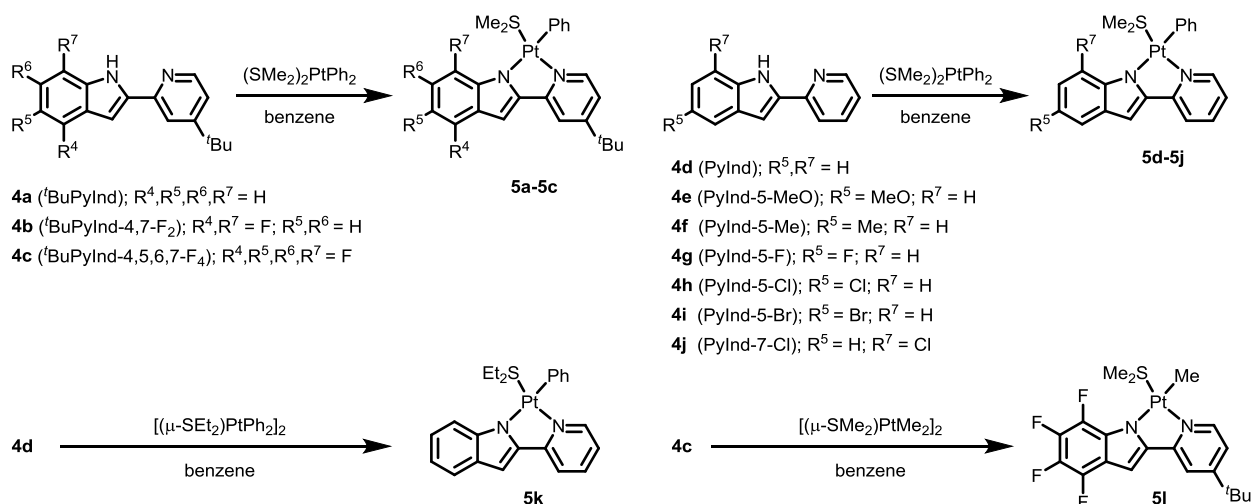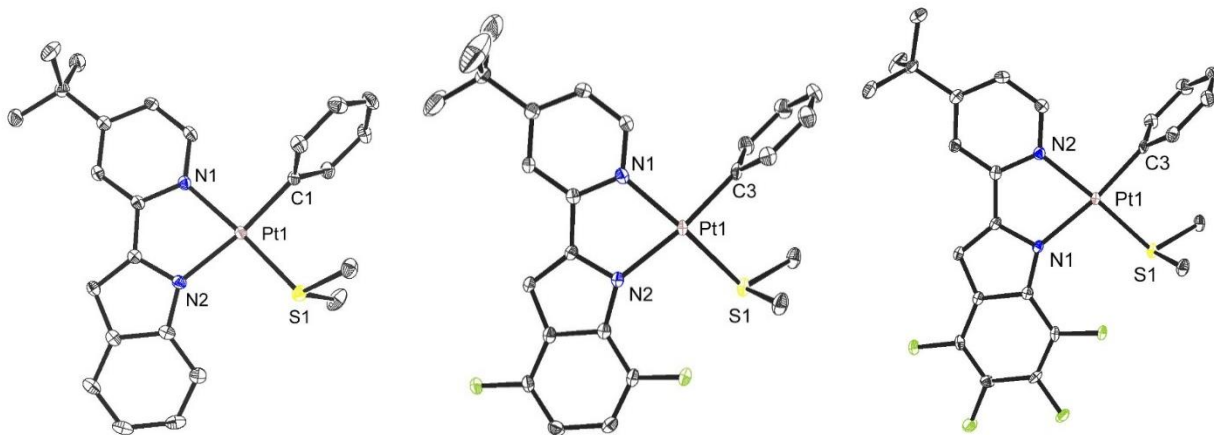
Figure 2.1. Left: Crystal structure of **5a**, with hydrogen atoms omitted and thermal ellipsoids at 50% probability. Selected bond lengths (Å) and angles (°) for **5a**: C(1)–Pt(1): 2.014(2), N(1)–Pt(1): 2.0529(18), N(2)–Pt(1): 2.1030(17), S(1)–Pt(1): 2.2580(5), C(1)–Pt(1)–N(1): 93.41(8), C(1)–Pt(1)–S(1): 90.57(6), N(1)–Pt(1)–N(2): 79.32(7), N(2)–Pt(1)–S(1): 96.70(5). **Middle:** Crystal structure of **5b**, with thermal ellipsoid at 50% probability. For clarity, hydrogen atoms have been omitted. Selected bond length (Å) and angles (°) for **5b**: C(3)–Pt(1): 2.009(3), N(1)–Pt(1): 2.049(2), N(2)–Pt(1): 2.125(2), S(1)–Pt(1): 2.2611(7), C(3)–Pt(1)–N(1): 93.16(10), C(3)–Pt(1)–S(1): 90.10(8), N(1)–Pt(1)-N(2): 79.19(9), N(2)–Pt(1)–S(1): 97.56(6). **Right:** Crystal structure of **5c**, with thermal ellipsoid at 50% probability. For clarity, hydrogen atoms have been omitted. Selected bond length (Å) and angles (°) for **5c**: C(3)–Pt(1): 2.008(2), N(2)–Pt(1): 2.0522(17), N(1)–Pt(1): 2.1244(16), S(1)–Pt(1): 2.2619(5), C(3)–Pt(1)–N(2): 93.64(7), C(3)–Pt(1)–S(1): 89.83(6), N(2)–Pt(1)–N(1): 79.16(6), N(1)–Pt(1)–S(1): 97.36(5).

Alternatively, complexes **5a** and **5b** were accessible from treatment of [(μ-SMe$_2$)PtMe$_2$] with **4a** or **4b**, respectively, in benzene at ambient temperature with concurrent generation of two equivalents of methane. It is presumed that the first equivalent of methane resulted from ligand deprotometallation. The second equivalent of methane likely occurs from benzene C–H activation which affords the observed phenyl complexes. In contrast, treatment with tetrafluorinated ligand **4c** in benzene at ambient temperature afforded (^{t}BuPyInd-4,5,6,7-F$_4$)PtMe(SMe$_2$) (**5l**) and a single equivalent of methane. A solid-state structure of **5l** (Figure 2.2) as well as ^{1}H NMR spectroscopy in benzene-d_6 (δ 1.38 (s, J_{PtH} = 73.8 Hz, 3H, Pt–Me), 2.53 (s, J_{PtH} = 59.7 Hz, 6H, Pt–SMe$_2$)) confirmed the assignment as a PtMe complex. Methyl-phenyl exchange occurred under thermolysis at 60 °C in benzene (or benzene-d_6). Given the relatively facile C–H activation observed with complexes of the type (N–N)PtMe(SMe$_2$), it was hypothesized such complexes (as well as the resultant PtPh complexes) may also be competent hydroarylation catalysts.
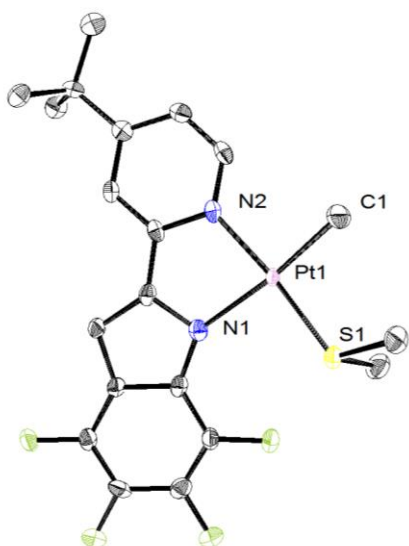
Figure 2.2. Crystal structure of **5l**, with hydrogen atoms omitted and thermal ellipsoids at 50% probability. Selected bond lengths (Å) and angles (°) for **5l**: C(1)–Pt(1): 2.053(5), N(1)–Pt(1): 2.149(4), N(2)–Pt(1): 2.044(4), S(1)–Pt(1): 2.2482(12), C(1)–Pt(1)–N(2): 94.57(18), N(2)–Pt(1)–N(1): 79.25(14), N(1)–Pt(1)–S(1): 95.46(10), S(1)–Pt(1)–C(1): 90.62(15).

Catalytic Hydroarylation with (N–N)Pt(SMe₂)Ph Complexes. Olefin hydroarylation studies were performed to determine the catalytic efficacy of complexes **5a-5k**. In the simplest hydroarylation reaction, neat benzene-d_6 and ethylene (1 atm) were heated to 100 °C in the presence of the catalyst (**5a-5k**; 3.7 mM). The formation of the product, ethylbenzene-d_6 ($C_6D_5CH_2CH_2D$),[45] was monitored by ^{1}H NMR spectroscopy over the course of 46 h (Figure 2.3). With all catalysts tested, over-alkylation to form polyethylbenzenes was negligible (< 1 turnover for all examples) as determined by ^{1}H NMR spectroscopy and GC-MS (Figure 2.4). Moreover, H(D) scrambling occurs to a minor extent as indicated in the mass spectrum (Figure 2.4 C and D). Note that while multiple isotopomers of ethylbenzene-d_n (n = 2, 3, 4, 5, 6, 7) were observed, the primary product was indeed ethylbenzene-d_6.
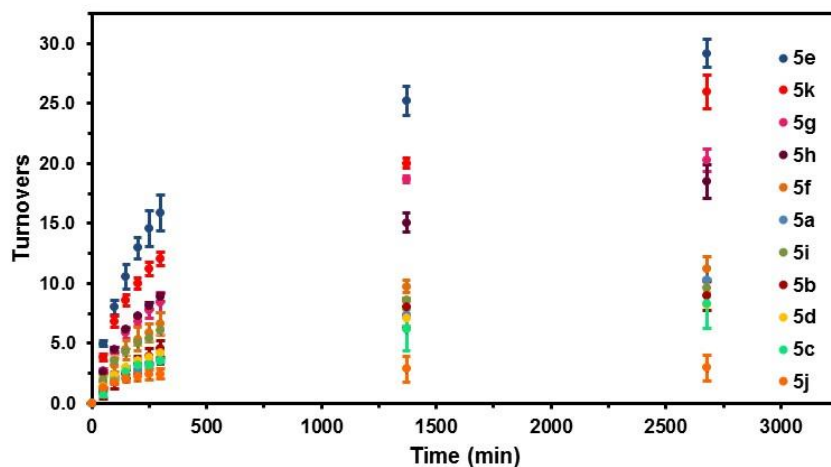
Figure 2.3. Monitored hydroarylation of ethylene (1 atm) with benzene-d_6 at 100 °C over 46 h by ^{1}H NMR spectroscopy using catalysts **5a-5k** (3.7 mM). Turnovers are given as the average of triplicate experiments with error calculated as the standard deviation.
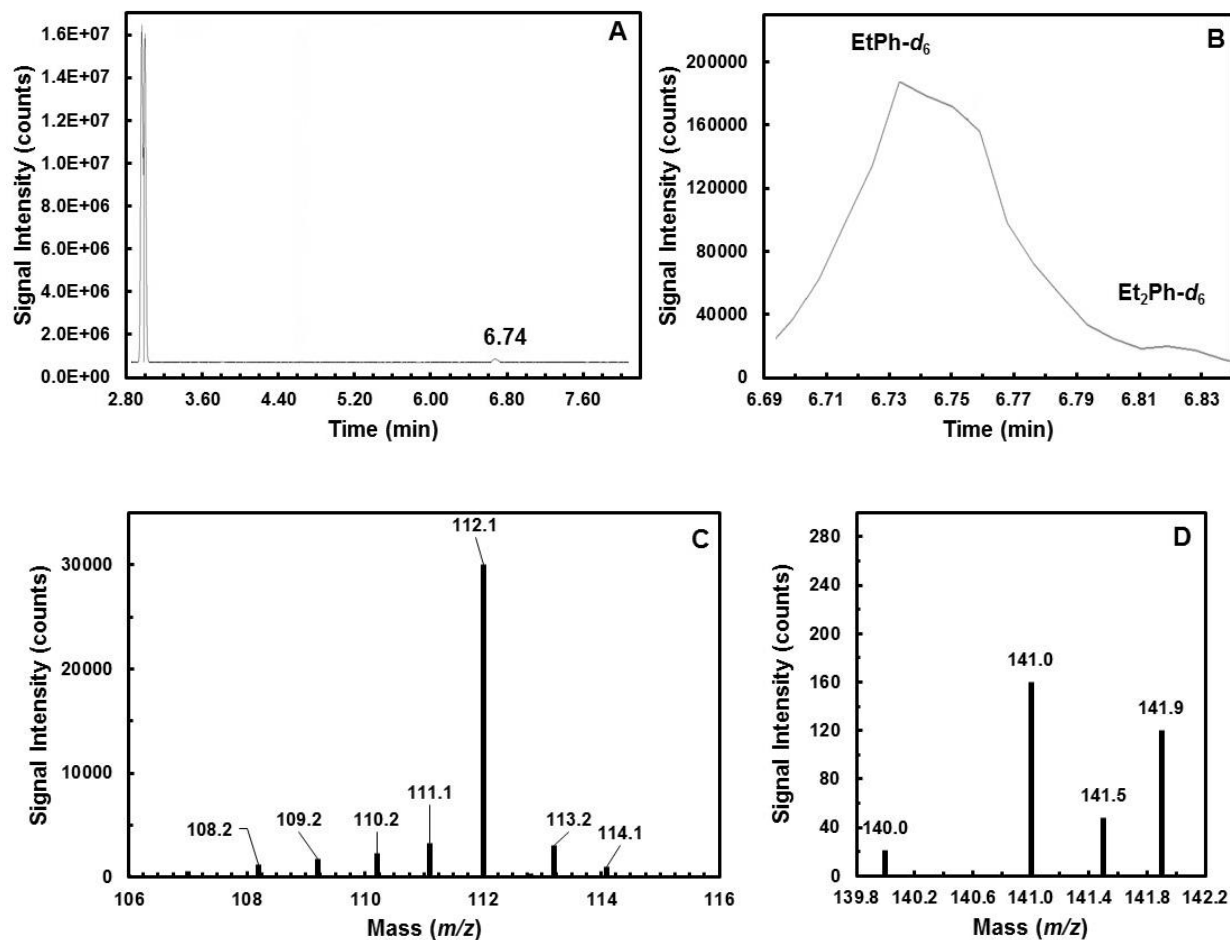
Figure 2.4. A: Representative vapor phase chromatogram of catalytic ethylene hydroarylation with benzene-d_6 using catalysts **5a-5k**. Note that the sample was diluted in benzene as a carrier solvent in the GC-MS experiement and is observed with a retention time ca. 2.89 min. **B:** Expansion of the chromatogram which exhibits partially overlapping peaks coresponding to ethylbenzene-d_n (6.70-6.79 min) and diethylbenzenes-d_n (6.78-6.84 min). Additionally, note that the *ortho-, meta-, para-*isomers of diethylbenzene could not be resolved. **C**: Averaged mass spectrum from 6.70-6.79 min. Note that multiple isotopomers were observed for ethylbenzene-d_n (n = 2, 3, 4, 5, 6, 7). **D**: Averaged mass spectrum from 6.80-6.84 min. Note that multiple isotopomers were observed for diethylbenzene-d_n (n = 6, 7).

Comparisons of total turnovers (after 24 h) and initial rates (as approximated by the number of turnovers after 1 h) for catalysts **5a-5k** are presented in Table 2.1. In general, no catalyst decomposition was observed after 1 h, by ^{1}H NMR spectroscopy. However at longer reaction times (> 24 h), elemental Pt(0) was observed as a black precipitate as well as a thin film coating the walls of the reaction vessel. Moreover, minimal additional ethylbenzene production was observed beyond 24 h even upon exposure to additional ethylene, suggesting that this time point represents the catalysts' maximum lifespan. Unfortunately, a clear trend of ethylbenzene formation as a function of the substitution pattern on the indolate fragment did not exist. In particular, substitution of the 5-position resulted in an inconclusive trend: both electron withdrawing (F, Cl) and electron donating (OMe) substituents resulted in an increase in initial rate and turnovers when compared to the parent catalyst **5d**; however, a few notable patterns are discernible.

The inclusion of a 4′-^{t}Bu moiety on the pyridyl fragment (**5a** *vs.* **5d**) appeared to have no effect on product formation. The position of indolate substitution with Cl appeared to have a slight effect; complex **5j** rapidly decomposed (resulting in reduced turnovers) whereas **5h** was still catalytically active after 24 h. Interestingly, replacing the ancillary SMe$_2$ ligand (**5d**) for the slightly bulkier SEt$_2$ donor (**5k**) resulted in a faster initial rate and higher turnover numbers. This superior performance may be attributed to the more labile SEt$_2$ ligand being easier to exchange for ethylene, which is a key step in the hydroarylation mechanism.

Table 2.1. Catalytic ethylene hydroarylation with **5a-5k**.
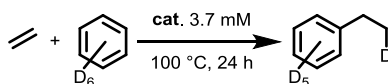
Catalyst [a]	Total Turnovers [b]	Initial Rate (TO / h) [c]
5a	7.4 ± 1.1	1.0 ± 0.02
5b	8.0 ± 0.7	0.7 ± 0.4
5c	6.2 ± 1.8	0.7 ± 0.2
5d	7.1 ± 0.7	1.4 ± 0.1
5e	25.2 ± 1.2	5.0 ± 0.2
5f	9.7 ± 0.6	1.8 ± 0.5
5g	18.7 ± 0.3	2.7 ± 0.2
5h	15.1 ± 0.8	2.6 ± 0.1
5i	8.6 ± 0.2	2.0 ± 0.2
5j	2.9 ± 0.6	1.3 ± 0.1
5k	20.0 ± 0.4	3.8 ± 0.3

[a] Reaction conditions: Ethylene (1 atm), catalyst (0.0026 mmol, 3.7 mM), and Si(SiMe$_3$)$_4$ (internal standard) in benzene-d_6 (0.7 mL) at 100 °C. [b] Total turnovers at 24 h (average of triplicate experiments with standard deviations) determined by ^{1}H NMR spectroscopy. [c] Initial rate given as the turnover numbers after 1 h.

To elucidate the relative influence of catalyst decomposition on catalytic efficiency, the relationship between ethylbenzene-d_6 production (total turnovers, at 24 h) and initial rate (turnovers at 1 h) was compared (Figure 2.5). The data were fit to a linear regression with a slope of ca. 5.4. Ethylene concentration in solution (as determined by ^{1}H NMR spectroscopy) was relatively constant since the reaction vessel's head-space contained a significant excess of ethylene relative to catalyst loading. The linearity of this relationship, and the low value of the slope (far less than 24), implies that the product yield is mainly influenced by the initial reaction rate, and that the decomposition rate is roughly the same for all catalysts.
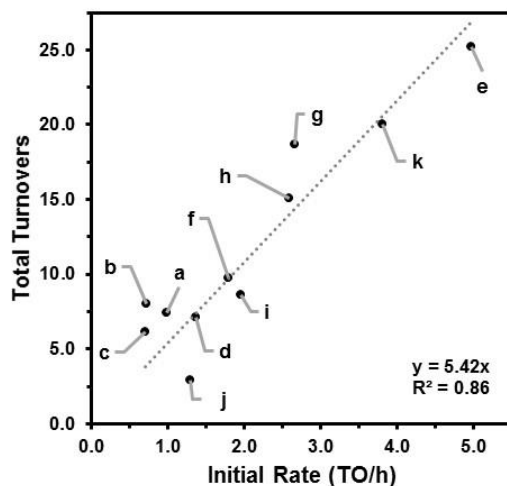
Figure 2.5. Plot of total turnovers of ethylbenzene-d_6 for catalysts **5a-5k** (measured at 24 h) *vs.* the initial rate of ethylbenzene-d_6 formation (approximated as the turnovers after 1 h). Error bars have been omitted for clarity. The dashed line is a linear fit of the data.

Propylene hydroarylation was surveyed using catalysts **5a-5k** to determine the influence of ligand substitution on the ratio of anti-Markovnikov (linear) *vs.* Markovnikov (branched) products (Table 2.2). Reactions were performed for 24 h at 100 °C, and product formation was monitored by ^{1}H NMR spectroscopy (Figure 2.6). Minimal variation in catalytic activity was observed for complexes **5a-5k**, and the overall activity of propylene hydroarylation was reduced compared to ethylene. Interestingly, complex **5e** proved to be significantly more active than any of the other complexes tested, affording nearly 20 turnovers of propylene hydroarylation products after 24 h.
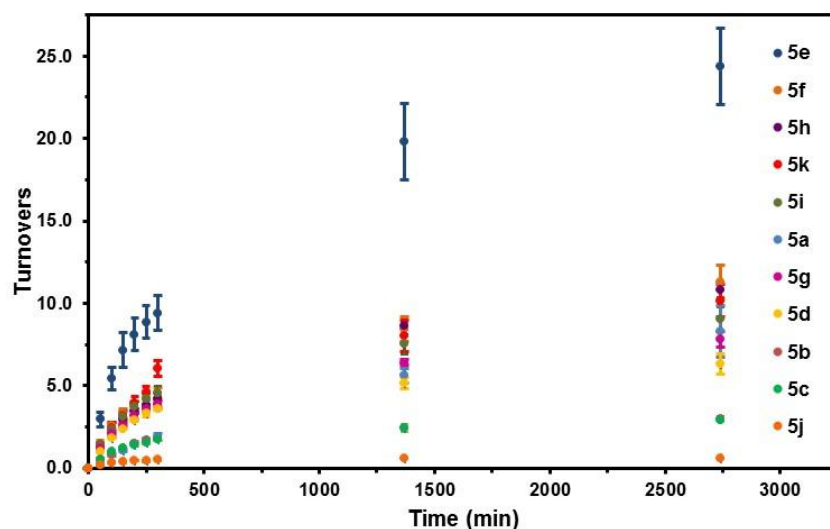
Figure 2.6. Monitored hydroarylation of propylene (1 atm) with benzene-d_6 at 100 °C over 46 h by ^{1}H NMR spectroscopy using catalysts **5a-5k** (3.7 mM). Turnovers are given as the average of triplicate experiments with error calculated as the standard deviation.

Table 2.2. Catalytic propylene hydroarylation with **5a-5k**.
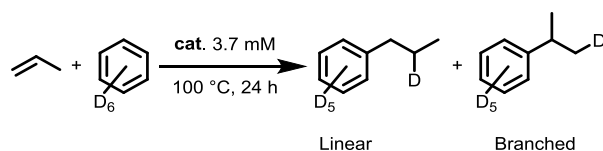
Catalyst [a]	Total Turnovers [b]	Linear:Branched [c]
5a	5.6 ± 0.4	0.40 ± 0.03
5b	2.4 ± 0.1	0.36 ± 0.02
5c	2.5 ± 0.2	0.31 ± 0.02
5d	5.2 ± 0.4	0.43 ± 0.04
5e	19.8 ± 2.3	0.40 ± 0.03
5f	8.5 ± 0.7	0.44 ± 0.05
5g	6.4 ± 0.2	0.38 ± 0.03
5h	8.6 ± 0.2	0.36 ± 0.02
5i	7.5 ± 0.6	0.37 ± 0.02
5j	0.6 ± 0.03	0.70 ± 0.09
5k	8.0 ± 1.0	0.40 ± 0.02

[a] Reaction conditions: Propylene (1 atm), catalyst (0.0026 mmol, 3.7 mM), and $Si(SiMe_3)_4$ (internal standard) in benzene-d_6 (0.7 mL) at 100 °C. [b] Total turnovers at 24 h (average of triplicate experiments with standard deviations) determined by ^1H NMR spectroscopy and refers to the sum of the turnovers of n-propylbenzene-d_6 and cumene-d_6. [c] Determined as the ratio of TO$_{Linear}$:TO$_{Branched}$.

Only a minimal variation in regioselectivity was observed for complexes **5a-5k**; the catalysts tended to form cumene-d_6 preferentially to n-propylbenzene-d_6 (*i.e.* Markovnikov selectivity), with a linear:branched ratio of ca. 0.40. This selectivity is similar to that observed previously for other platinum hydroarylation catalysts.[45,46,51-53] The linear/branched ratio remained constant over the course of the reaction (Figure 2.7), which suggested that the product formation rates for the two regioisomers are similar. Lastly, a comparison of total turnovers *vs.* initial rate for the hydroarylation of propylene with benzene-d_6 suggested that the decomposition rates of catalysts **5a-5k** are similar (Figure 2.8).
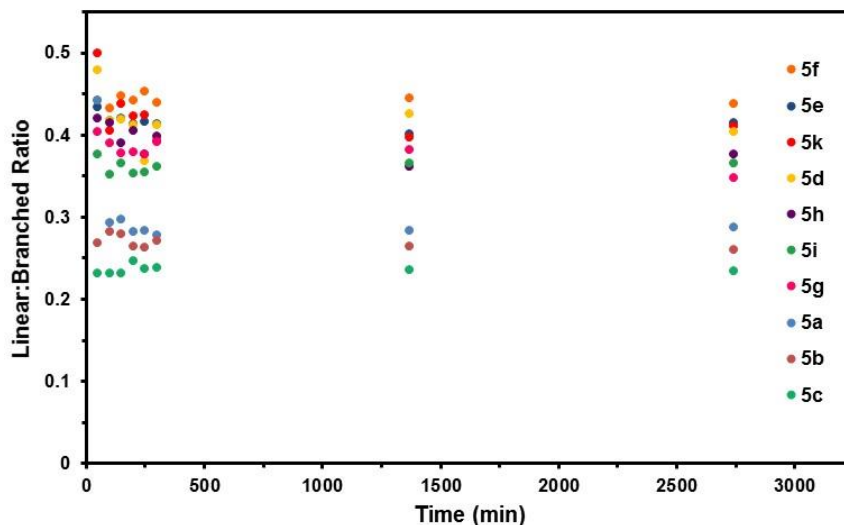
Figure 2.7. Monitored product regioselectivity during hydroarylation of propylene (1 atm) with benzene-d_6 at 100 °C over 46 h by ^{1}H NMR spectroscopy using catalysts **5a-5k** (3.7 mM) [note: catalyst **5j** is omitted; error bars have been omitted for clarity]. Selectivities determined as the ratio of $TO_{Linear}:TO_{Branched}$ and values are given as the average of triplicate experiments.
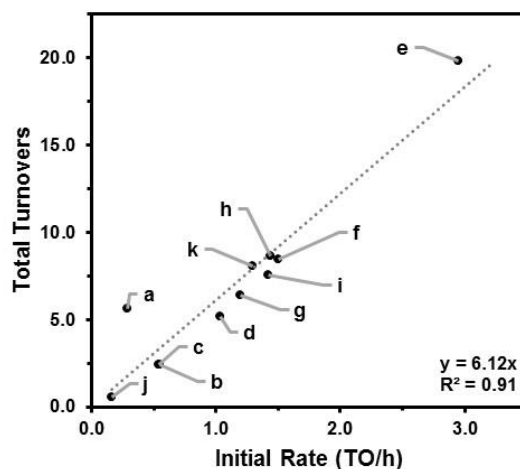
Figure 2.8. Plot of total turnovers from the hydroarylation of propylene with benzene-d_6 using catalysts **5a-5k** (measured at 24 h) vs. the initial product formation rate (measured as the turnovers after 1 h). Turnovers represent the sum of turnovers for cumene-d_6 and n-propylbenzene-d_6. The dashed line is a linear fit of the data.

Attempted catalytic hydroarylations of other substituted olefins with complex **5a** were unsuccessful. While *tert*-butylethylene reacted with complex **5a** in benzene-d_6, the rate of product formation was far slower than was observed for reactions with propylene or ethylene (ca. 1 turnover of the hydroarylation products after 24 h). Unfortunately, other olefins did not undergo hydroarylation: 1-octene rapidly isomerized to 2-octene, and cyclohexene did not undergo conversion over 24 h. This suggests that the rate of isomerization catalyzed by these complexes is faster than the rate of productive hydroarylation, and internal olefins (2-octene and cyclohexene) are inert under the catalytic conditions.

The regiochemistry of C–H bond cleavage during catalysis was probed with substituted arene substrates. Treatment of ethylene with catalyst **5a** in neat toluene yielded 8.4 ± 0.3 equivalents of ethyltoluenes after 24 h at 100 °C, with 98% selectivity for *meta-* and *para*-products (as analyzed by GC; *meta-* and *para*-ethyltoluene isomers could not be resolved). By ^{1}H NMR spectroscopy, overlapping benzylic peaks were observed thereby preventing resolution of the *meta-* to *para*-ratio. This suggests that the steric properties of the arene largely direct the C–H activations. Mesitylene was employed as a substrate to determine whether more highly substituted arenes could also be functionalized. Indeed, catalyst **5a** converted mesitylene into the corresponding hydroarylation product (8.8 ± 0.4 turnovers after 24 h at 100 °C), indicating that *ortho*-functionalization is viable.

Isotope Effects. To gain insight into the rate-determining step for catalysis, isotope effects on turnover numbers were examined. First, in separate experiments, the hydroarylation of ethylene using catalyst **5a** in either benzene or benzene-d_6 gave 18.1 ± 1.1 and 7.4 ± 1.1 turnovers, respectively, after 24 hours at 100 °C. The ratio of these two values (TO$_H$/TO$_D$ = 2.4 ± 0.39) suggests that C–H(D) activation is important in the turnover-limiting step.[54] However, note that this comparison does not reflect a kinetic isotope effect as it is not calculated using rate constants and a rate law for this catalytic system has not been quantitatively determined.

Given that catalysis only occurs in neat benzene, saturation-like kinetics are expected in [arene]. A high ethylene pressure experiment illustrated the qualitative effect of ethylene concentration on catalytic activity. The turnover number of ethylbenzene-d_6 using **5a** under a constant stream of ethylene at 3 atm was measured to be 4.1 and is the same, within error, as the turnovers measured with 1 atm of ethylene (3.6 ± 0.4). The similar activity at higher ethylene pressure implies an observed zeroth order in [ethylene] which may arise from a complicated dependence on the concentration of ethylene; it likely both inhibits and promotes fundamental steps during the catalysis, as has been observed by Gunnoe and coworkers[46] for cationic Pt hydroarylation catalysts. It is likely that a first-order dependence on [catalyst] exists in this system akin to the analogous cationic system reported by Gunnoe.[46]
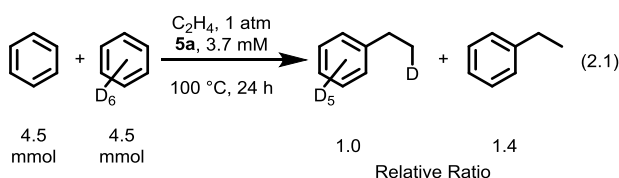
In a separate experiment, equimolar amounts of benzene and benzene-d_6 were used as neat substrates for ethylene hydroarylation with **5a** as the catalyst (eq 2.1). In this experiment, hydroarylation could occur either through C–H or C–D activation to generate ethylbenzene or ethylbenzene-d_6, respectively, assuming that intermolecular isotopic scrambling does not occur. The product ratio was determined by quantitative, long-pulse delay ^{13}C{^{1}H} NMR spectroscopy after 24 hours at 100 °C (Figure 2.9). The terminal methyl carbons of the two products have different coupling patterns; for ethylbenzene, the CH$_3$ resonance appears as a singlet, whereas the CH$_2$D resonance appears as a triplet due to C–D coupling. The ratio of these resonances provided a product ratio of ethylbenzene:ethylbenzene-d_6 of 1.4:1.0, which is consistent with hydroarylation occurring faster with benzene than with benzene-d_6. The discrepancy in these values (1.4 *vs.* 2.4) results from the fact that catalyst TON is a composite metric influenced by both reaction and decomposition rates and therefore is not a direct measure of k_H or k_D. On

the other hand, the isotopologue distribution as measured in the intermolecular competition experiment provides direct mechanistic information about the C–H activation step.[54]
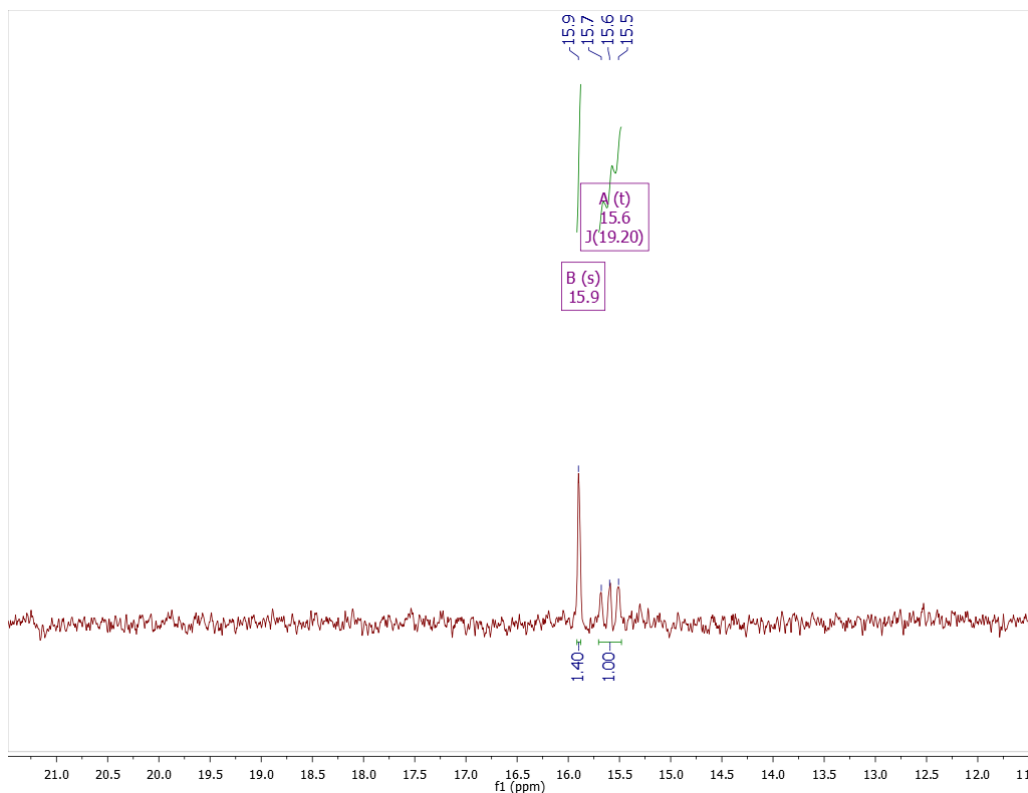
Figure 2.9. Quantitative, long-pulse delay (D_1 = 60 s) $^{13}C\{^1H\}$ NMR spectrum of the resulting products [$C_6H_5(CH_2CH_3)$ at 15.9 ppm and $C_6D_5(CH_2CH_2D)$ at 15.6 ppm] from competitive hydroarylation of ethylene with **5a** in an equimolar mixture of benzene and benzene-d_6. Note that methyl resonances in ethylbenzene-d_6 appear as an equal height t due to C–D coupling (J_{2H13C} = 19.2 Hz).

Synthesis and Isolation of Potential Catalytic Intermediates. It has been suggested that complexes of the type [$L_2Pt(CH_2CH_2Ph)(C_2H_4)$]$^+$ are either catalytic intermediates in hydroarylation or off-cycle species formed by the trapping of a 3-coordinate [$L_2Pt(CH_2CH_2Ph)$]$^+$ intermediate with ethylene.[43,46,51-53] To elucidate the role of such species during catalysis, several stoichiometric reactions with ethylene were performed to generate potential catalytic intermediates. Using a low-pressure J-Young NMR tube (3 mL volume) as a reaction vessel, complex **5a** was treated with ethylene (1 atm) in benzene-d_6 at ambient temperatures over a 4 d period and the reaction was monitored by ^1H NMR spectroscopy. During the course of the ligand substitution reaction, a mixture of **5a**, the ligand substitution product ($^tBuPyInd$)PtPh(C_2H_4) (**6**), and the olefin insertion product ($^tBuPyInd$)Pt(CH_2CH_2Ph)(C_2H_4) (**7**) was observed by ^1H NMR spectroscopy after 3 days in a ratio of ca. 1.1:1.0:0.2, respectively (Figure 2.10).
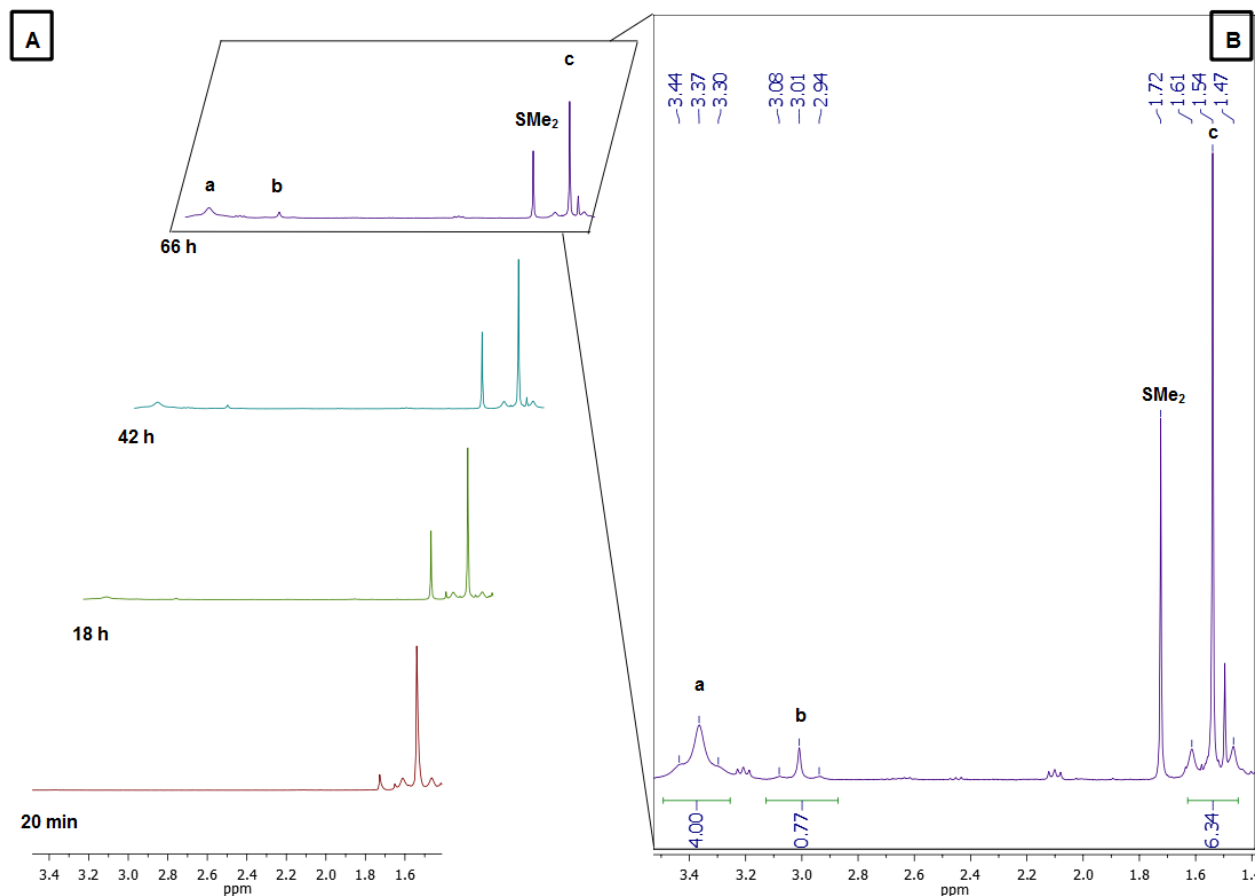
Figure 2.10. ^{1}H NMR spectra of Pt speciation during ligand substitution reaction after exposure of **5a** to ethylene (1 atm) at ambient temperature. Resonance **a** (3.37 ppm, J_{PtH} = 59 Hz) is the C_2H_4 fragment of complex **6**. Resonance **b** (3.01 ppm, J_{PtH} = 54 Hz) is the C_2H_4 fragment of complex **7**. Resonance **c** (1.54 ppm, J_{PtH} = 53 Hz) is the SMe_2 fragment of complex **5a**. Free SMe_2 is observed at 1.72 ppm. **Insert A**: Monitored ^{1}H NMR spectra of the substitution reaction over the course of 3 days. Note that resonances **a**, **b**, and **SMe₂** grow in intensity over time while resonance **c** decays. **Insert B**: Expansion of the ^{1}H NMR spectra after 66 h of exposure to C_2H_4. Note the relative ratio of the integrations of resonances **c**, **a**, and **b** are ca. 6.3:4.0:0.8, respectively. This corresponds to the observed product ratio of **5a**:**6**:**7** of 1.1:1.0:0.2, respectively.

Compound **6** could be purified from the reaction mixture by column chromatography in low yield (isolated yield: 9 mg, 29%). An independent and scalable synthesis of **6** (Scheme 2.3) was accomplished by (i) metallation of Zeise's dimer, $[(C_2H_4)Pt(\mu\text{-Cl})Cl]_2$, with [t]BuPyInd in the presence of NaO[t]Bu, followed by (ii) treatment with AgOTf, and (iii) phenylation with PhLi (isolated yield: 25 mg, 20%). The X-ray structure of **3** (Figure 2.11) reveals a square planar geometry similar to that of complex **5a**, except that in **6** the phenyl ligand is *cis* to the indolate group. Overall, the Pt–N and Pt–C distances are similar in **5a** and **6**. The C–C bond of the bound ethylene ligand in **6** (1.386(6) Å) is slightly elongated compared to free ethylene (1.3305(10) Å).[55] A broad ethylene resonance with [195]Pt satellites was observed in the ^{1}H NMR spectrum of **6** in dichloromethane-d_2 (δ = 3.84 ppm, J_{PtH} = 60 Hz).
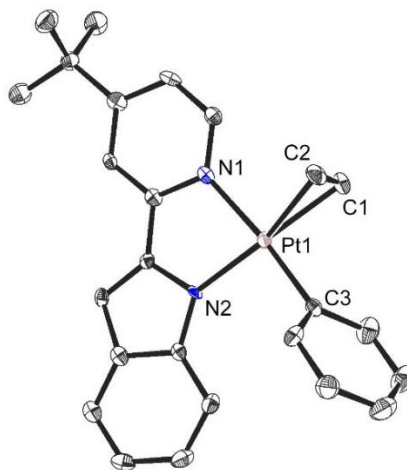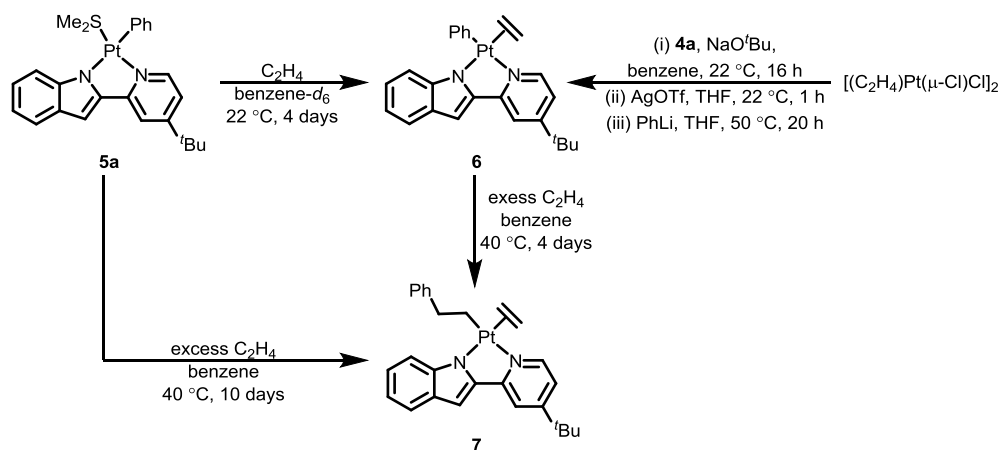
Figure 2.11. Crystal structure of **6**, with thermal ellipsoids at 50% probability and hydrogen atoms omitted. Selected bond lengths (Å) and angles (°) for **6**: C(1)–C(2): 1.386(6), C(1)–Pt(1): 2.115(4), C(2)–Pt(1): 2.130(4), C(3)–Pt(1): 2.013(4), N(1)–Pt(1): 2.121(3), N(2)–Pt(1): 2.023(3), C(3)–Pt(1)–N(2): 96.37(14), N(1)–Pt(1)–N(2): 79.52(12).

Exposure of **5a** to an excess of ethylene at 40 °C for 10 days cleanly afforded the insertion product **7** after purification *via* column chromatography in an overall yield of 22% (Scheme 2.3). In the ^{1}H NMR spectrum, diagnostic resonances were observed for the two sets of phenethyl methylene protons of **7** at 3.21 ppm (t, J = 8.1 Hz) and 2.10 ppm (t, J_{HH} = 8.2 Hz, J_{PtH} = 67 Hz). Additionally, the bound ethylene protons displayed a diagnostic, broadened singlet ^{1}H NMR resonance with ^{195}Pt coupling at 3.00 ppm (s, J_{PtH} = 54 Hz). The crystal structure of **7** (Figure 2.12) is similar to those of **5a** and **6**, with the phenethyl ligand positioned *cis* to the indolate donor.
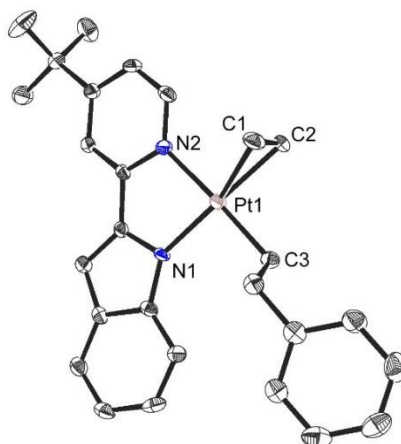
Figure 2.12. Crystal structure of **7**, with thermal ellipsoids at 50% probability and hydrogen atoms omitted. Selected bond lengths (Å) and angles (°) for **7**: C(1)–C(2): 1.375(6), C(1)–Pt(1): 2.108(4), C(2)–Pt(1): 2.104(4), C(3)–Pt(1): 2.051(4), N(1)–Pt(1): 2.038(3), N(2)–Pt(1): 2.134(3), N(1)–Pt(1)–N(2): 76.69(12), N(1)–Pt(1)–C(3): 97.17(14).

Thermolysis and Hydroarylation Reactions with Complexes 5a, 6, and 7. The stability of complexes **5a**, **6**, and **7** in the absence of olefin was assessed by heating these complexes to 100 °C in benzene-d_6 and monitoring changes by ^{1}H NMR spectroscopy. Complex **5a** was stable; after 4 h, no change in the ^{1}H NMR spectrum was observed. However, after 46 h isomerization to a mixture of **5a** and *cis*-**5a** was observed by the formation of a second SMe$_2$ resonance as a singlet with ^{195}Pt–H coupling (Figure 2.13). Surprisingly, activation of benzene-d_6 to form (^{t}BuPyInd)Pt(C$_6$D$_5$)(SMe$_2$) did not occur. Decomposition to elemental Pt was not visually observed after 46 h.
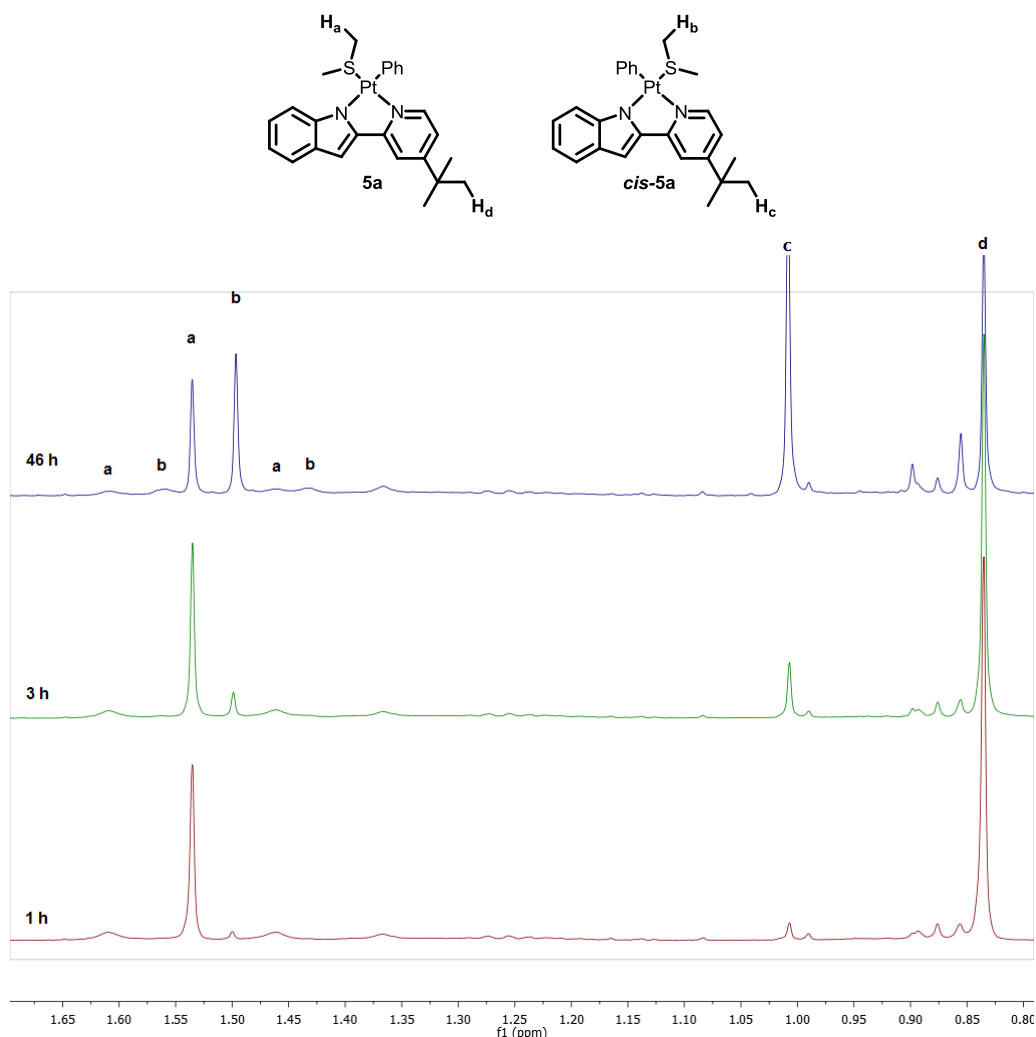
Figure 2.13. Monitored thermolysis of complex **5a** at 100 °C in benzene-d_6. Lower: ^{1}H NMR spectrum after 1 h of heating. Middle: ^{1}H NMR spectrum after 3 h of heating. Upper: ^{1}H NMR spectrum after 46 h of heating. Selected resonances shown above for compound **5a**: δ 1.54 (s, J_{PtH} = 60 Hz, **a**), 0.84 (s, **d**). Selected resonances above for compound *cis*-**5a**: δ 1.50 (s, J_{PtH} = 52 Hz, **b**), 1.01 (s, **c**). Aryl protons for **5a** and *cis*-**5a** overlap, making individual peak assignment difficult.

At 100 °C in benzene-d_6, complex **6** rapidly decomposed to elemental Pt, and free ethylbenzene-d_1 (1 equiv. *vs.* **6**) was observed by ^{1}H NMR spectroscopy after 1 h (Figure 2.14). In contrast, heating **7** at 100 °C for 2 h resulted in the formation of free ethylene and ethylbenzene-d_1, 0.06 and 0.3 equiv relative to Pt, respectively (Figure 2.15). After 24 h, larger quantities of ethylbenzene-d_1 were observed, along with the disappearance of resonances corresponding to free ethylene and complex **7**. Additionally, elemental Pt was visually observed. This suggests that prior to hydroarylation, the ancillary ethylene ligand of **7** must dissociate to provide an open coordination site for C–H activation to occur. Complex **7**, therefore, is not the active species on the catalytic cycle and is instead an off-cycle intermediate.
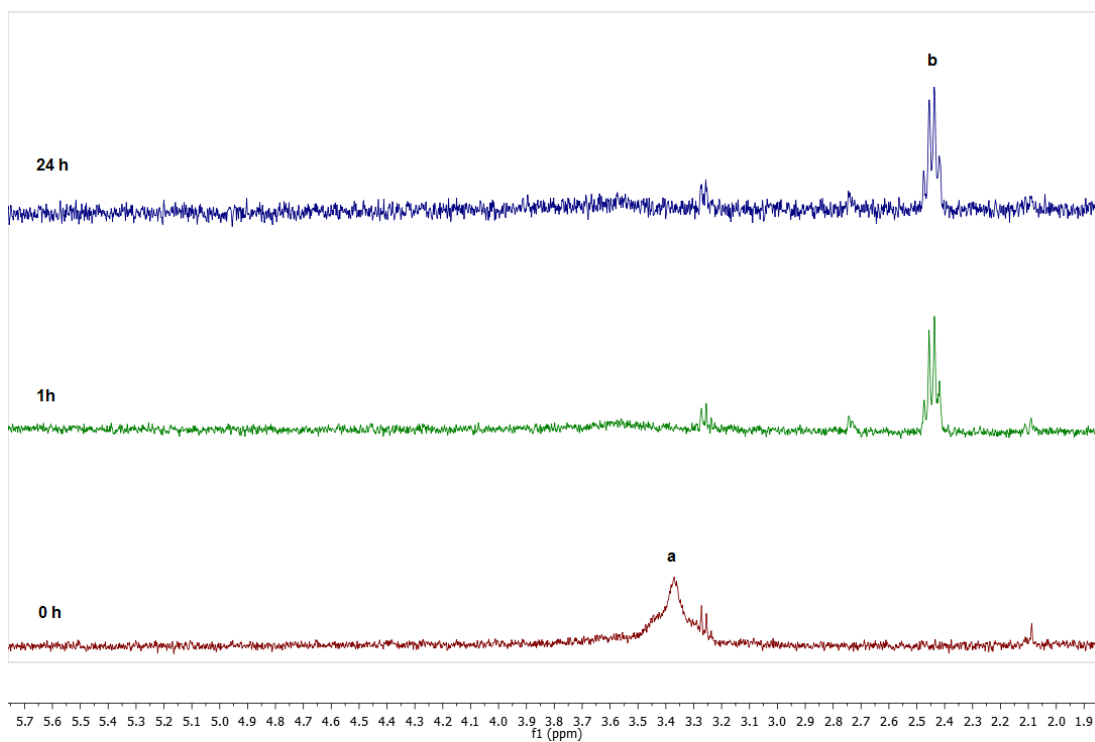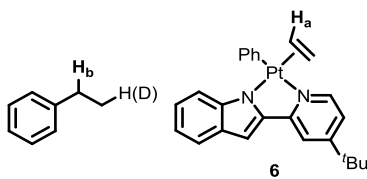
Figure 2.14. Monitored thermolysis of complex **6** at 100 °C in benzene-d_6. Lower: initial ^{1}H NMR spectrum prior to heating. Middle: ^{1}H NMR spectrum after 1 h of heating. Upper: ^{1}H NMR spectrum after 24 h of heating. Selected resonances shown above for compound **6**: 3.83 (s, J_{PtH} = 59 Hz, **a**). Rapid decomposition of **6** occurs with concurrent ethylbenzene formation. Note that H(D) exchange appears to occur to produce a mixture of ethylbenzene-d_1 and ethylbenzene-d_0.
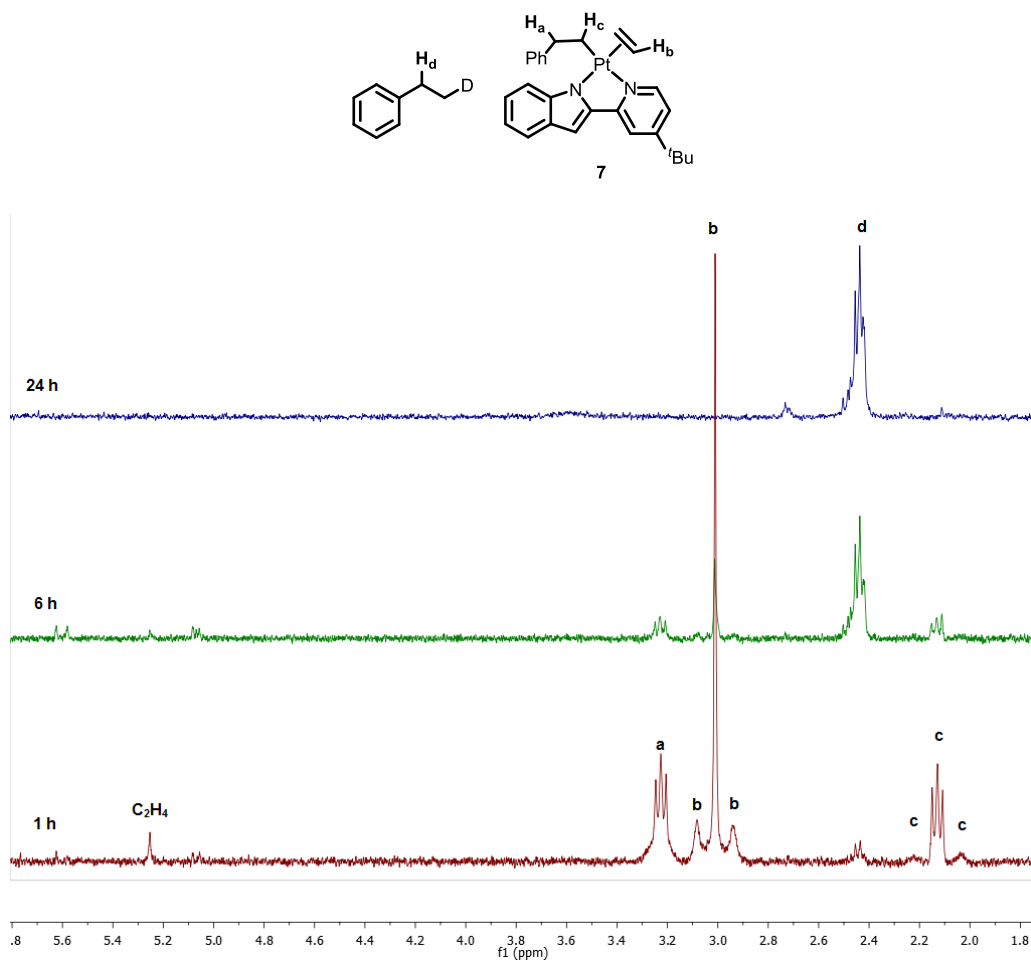
Figure 2.15. Monitored thermolysis of complex **7** at 100 °C in benzene-d_6. Lower: ^{1}H NMR spectrum after 1 h of heating. Middle: ^{1}H NMR spectrum after 3 h of heating. Upper: ^{1}H NMR spectrum after 24 h of heating. Selected resonances shown above for compound **7**: δ 3.22 (t, J = 8.1 Hz, **a**), 3.01 (s, J_{PtH} = 54 Hz, **b**), 2.12 (t, J_{HH} = 8.2 Hz, J_{PtH} = 67 Hz, **c**). Ethylene resonance at 5.25 noted during early time points of heating. Ethylbenzene benzylic resonance (**d**) noted after 1 h and rapidly increased as **7** decomposed.

The ethylene hydroarylation activities of complexes **6** and **7** were monitored over 46 h by ^{1}H NMR spectroscopy to determine the catalytic efficacy of these potential intermediates (Figure 2.16). Since these complexes lack a strongly coordinating SMe$_2$ ligand, an enhancement in turnovers in comparison to complex **5a** was expected. Under catalytic conditions, complexes **5a** and **7** displayed similar reaction profiles, with complex **5a** generating ethylbenzene-d_6 at a slightly faster initial rate. At 24 h, catalytic turnover for complexes **5a** and **7** were, within error, identical (7.4 ± 1.1 and 7.2 ± 1.0 turnovers, respectively). In contrast, complex **6** exhibited significantly enhanced initial product formation rates and afforded 12.2 ± 0.7 turnovers at 24 h. Interestingly, both **6** and **7** appeared to be completely inactive after 24 h whereas **5a** was still minimally competent as a catalyst (albeit at a significantly slower rate). After 46 h, formation of elemental Pt was observed from all three complexes.
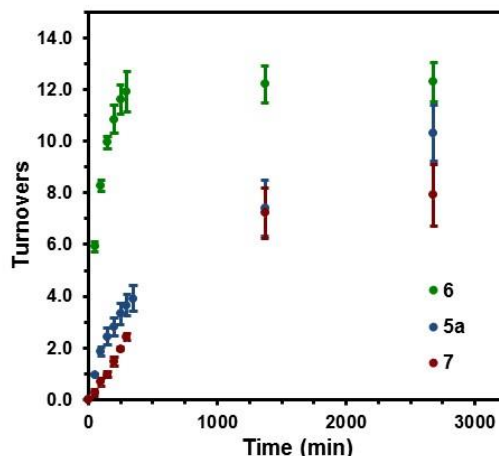
Figure 2.16. Plot of turnovers of ethylbenzene-d_6 *vs.* time for catalysts **5a**, **6**, and **7**. Error bars are given as the standard deviation from triplicate experiments.

The effect of L-type ligand concentration on catalysis was explored. Ethylene hydroarylation with benzene-d_6 using complexes **5a** or **7** with 10 equiv of added SMe$_2$ (relative to catalyst) was monitored over 46 h (Figure 2.17). While both **5a** and **7** exhibited minimal turnovers of ethylbenzene-d_6 after 24 hours, the effect was greater for **5a** than **7** (0.2 and 1.6 turnovers, respectively).
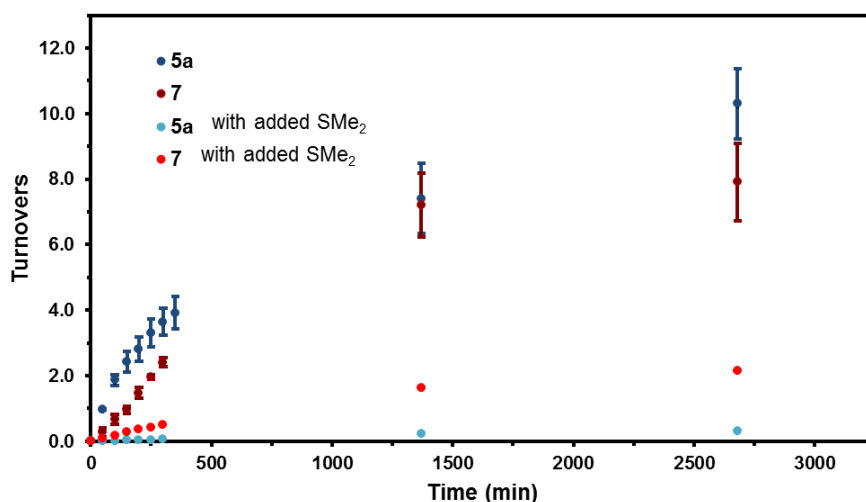
Figure 2.17. Monitored hydroarylation of ethylene (1 atm) with benzene-d_6 at 100 °C over 144 h by ^{1}H NMR spectroscopy using catalysts **5a** and **7** (3.7 mM) with and without added SMe$_2$ in the reaction mixture. Turnovers are given as the average of triplicate experiments with error calculated as the standard deviation.

Since catalysis with **5a**, **6**, and **7** likely proceeds through a common intermediate, variable temperature ^{1}H NMR spectroscopy experiments at 80 °C were performed in the presence of 1 atm of ethylene to elucidate the platinum complex speciation during catalysis (Figures 2.18-2.20). At the initial time point (ca. 3 min of heating; catalysis does not occur at RT) using complex **5a** as the precatalyst, complexes **5a** and **6** were observed in a 0.83:1.00 ratio, implying that the exchange of SMe$_2$ for ethylene occurs rapidly under catalytic conditions. Interestingly, the insertion product **7** was not observed to any

appreciable extent over the course of 3 h at 80 °C. This suggests that C–H activation occurs more rapidly than trapping with ethylene, perhaps due to low concentrations of ethylene relative to benzene-d_6. While the amount of ethylbenzene-d_6 increased over time, the amount of observed **6** remained relatively constant.
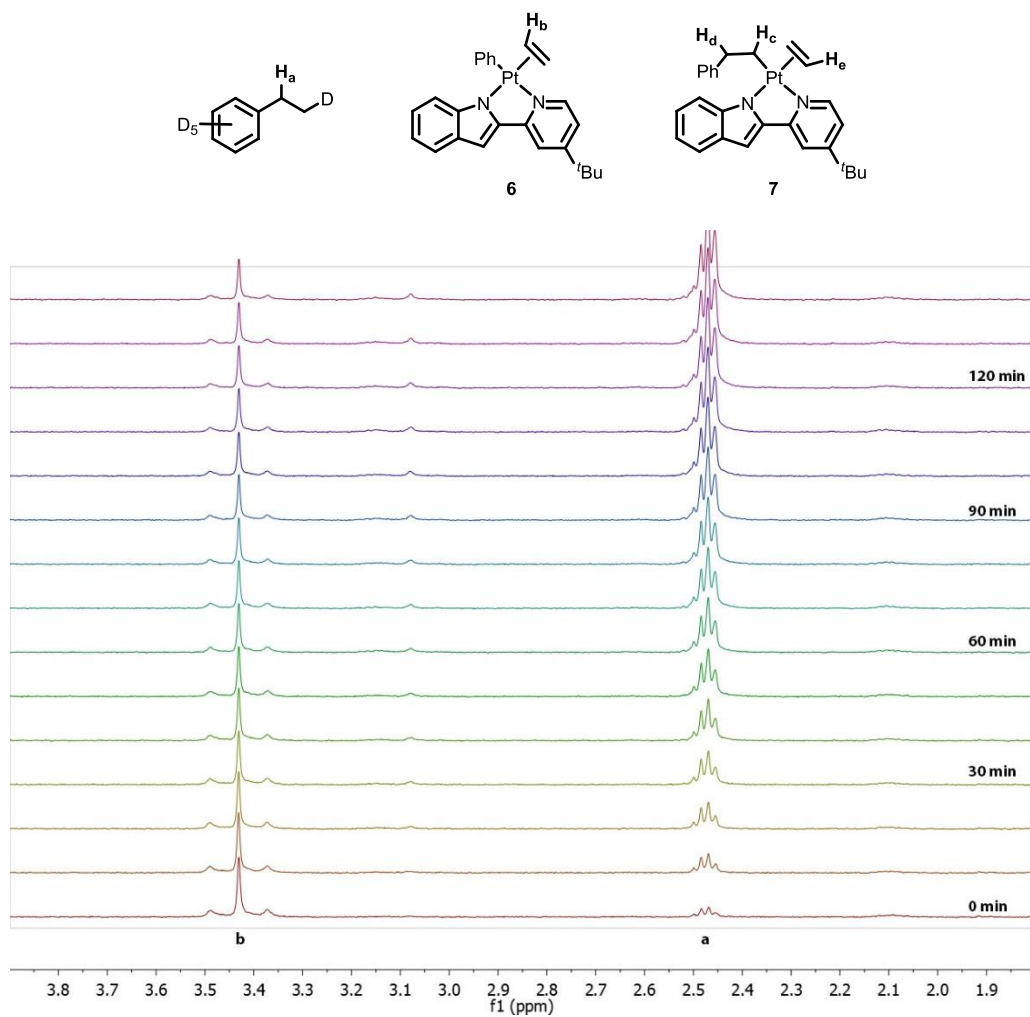
Figure 2.18. Variable temperature ^{1}H NMR spectrum of **5a** at 80 °C in benzene-d_6. Scans were taken once every 10 min during the course of the reaction (over a 2 h period). The resonance corresponding to bound ethylene in **6** (**b**) was observed at the first scan after being heated in the NMR spectrometer. Additionally, free SMe$_2$ was noted as well as bound SMe$_2$ (not shown). Full conversion of **5a** to **6**, therefore, was not observed. Rapid conversion of ethylene and benzene-d_6 to ethylbenzene-d_6 was observed, as noted by the formation of the ethlbenzene-d_6 benzylic peak (**a**). Complex **7** was not observed to a major extent during the course of the variable temperature ^{1}H NMR experiment.
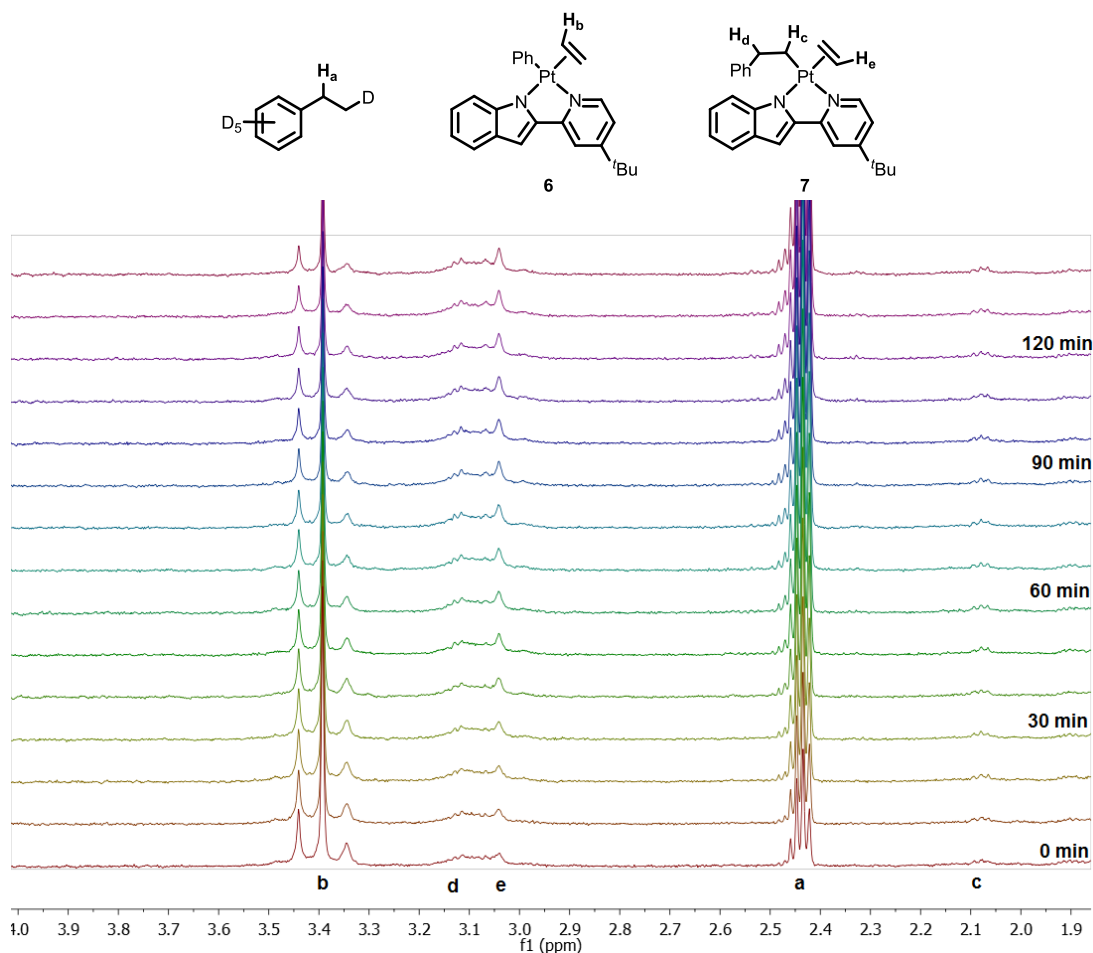
Figure 2.19. Variable temperature ^{1}H NMR spectrum of **6** at 80 °C in benzene-d_6. Scans were taken once every 10 min during the course of the reaction (over a 2 h period). Bound ethylene resonances (**b**) for complex **6** were noted in every time point of the experiment, and only slowly reduced in intensity over time. Resonances corresponding to complex **7** (**c**, **d**, and **e**) only slowly grew in intensity during the reaction. Rapid formation of ethylbenzene-d_6 (**a**) was noted during the course of the reaction.

In an analogous experiment with **6** as the added precatalyst, rapid ethylbenzene-d_6 formation was observed, which was accompanied by a slow conversion of **6** to **7**. In a similar experiment using complex **7**, reduced activity towards the generation of ethylbenzene-d_6 was observed. Concurrent formation of complex **6** occurred at a slower rate compared to the analogous reaction using **5a** as the precatalyst. These results suggest that ethylene dissociation from complex **7** to form a catalytically active species is not rapid.
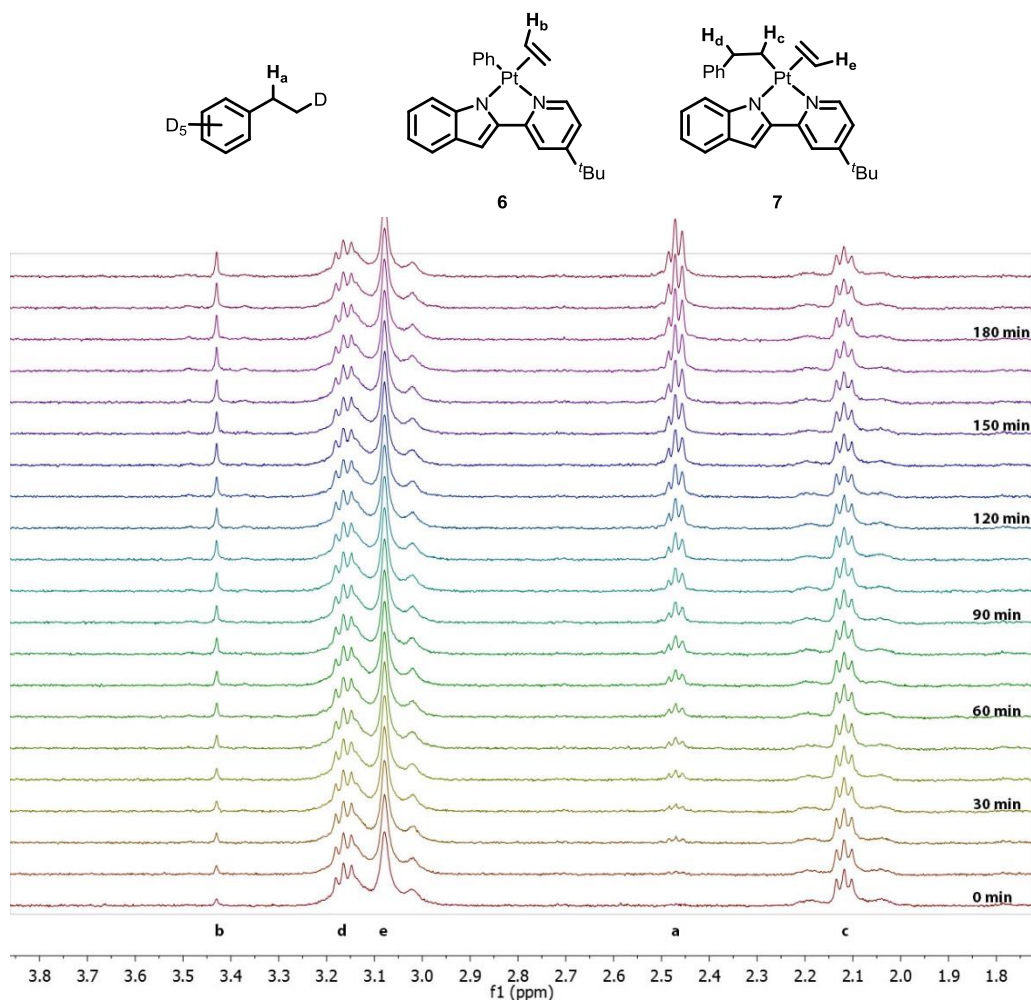
Figure 2.20. Variable temperature ^{1}H NMR spectrum of **7** at 80 °C in benzene-d_6. Scans were taken once every 10 min during the course of the reaction (over a 3 h period). Bound ethylene resonances (**b**) for complex **6** only slowly grew in intensity during the reaction. Resonances corresponding to complex **7** (**c**, **d**, and **e**) were present during the entirety of the experiment, and only decreased in intensity slowly during the reaction. Slow formation of ethylbenzene-d_6 (**a**) was noted during the course of the reaction.

Testing the Active Catalyst Identity: Base and Hg(0) Poisoning Experiments. A recent report from this laboratory[56] demonstrated that the hydroarylation of cyclohexene with mesitylene catalyzed by (COD)Pt(OTf)$_2$ proceeds by an acid-catalyzed mechanism, despite the lack of acid as an initial reagent. For this system, an initial metal-mediated olefin coupling[57] occurs to generate olefin dimers as well as an equivalent of HOTf, which can catalyze hydroarylation via a Friedel-Crafts mechanism. The addition of a bulky, non-coordinating base (2,6-di-*tert*-butyl-4-methylpyridine) reduced catalysis, with complete catalytic inhibition observed upon addition of only two equivalents of base relative to Pt.

To determine whether *in situ* acid generation caused the observed catalysis with complexes **5a-5k**, hydroarylation of ethylene with benzene-d_6 was performed in the presence of 20 equiv of 2,6-di-*tert*-butyl-4-methylpyridine relative to catalyst **5a**. Catalytic activity was monitored by ^{1}H NMR spectroscopy over

46 h at 100 °C (Figure 2.21). No change in catalytic behavior was observed at any point during catalysis, which suggests that hydroarylation is not the result of adventitious acid-catalysis.
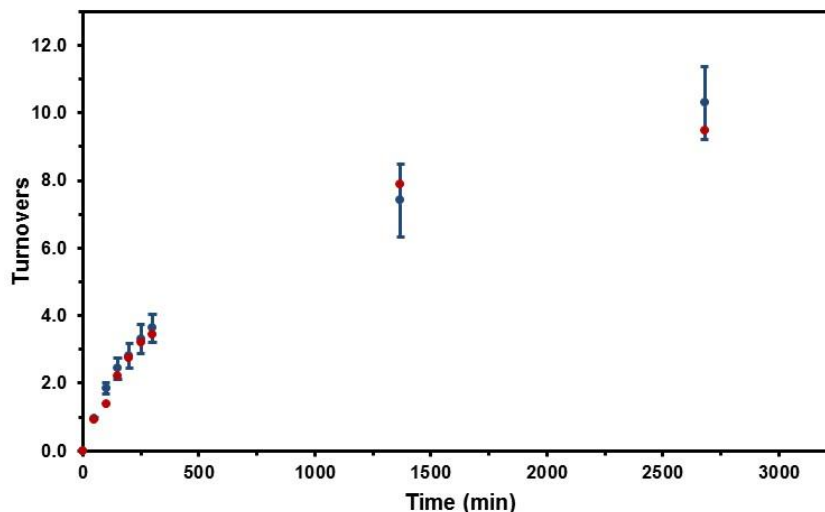
Figure 2.21. Monitored hydroarylation of ethylene (1 atm) with benzene-d_6 at 100 °C over 46 h by ^{1}H NMR spectroscopy using catalyst **5a** (3.7 mM) with (**red**) and without added 2,6-di-*tert*-butyl-4-methylpyridine (**blue**). Turnovers are given as the average of triplicate experiments with error calculated as the standard deviation.

Hydroarylation experiments in the presence of added Hg(0) were used to elucidate whether the reaction was catalyzed by a soluble species or by a heterogeneous Pt(0) material formed by *in situ* decomposition of the molecular precatalysts.[58-64] Mercury readily forms amalgams with Group 10 metals, which should trap any catalytically active heterogeneous species, assuming the rate of amalgamation is fast relative to catalysis.[58] To this end, addition of Hg(0) has been employed as a poison for adventitious nanoparticle catalyzed reactions.[59-61] As a result, if nanoparticles are indeed the catalytically active species then the inclusion of Hg(0) into the reaction mixture should inhibit product formation (assuming a fast rate of amalgamation).[58-61]

An initial indication that homogeneous catalysis occurs was observed in a hydroarylation experiment of ethylene and benzene-d_6 with catalyst **5a**. After 24 h, the catalytic mixture was filtered through Al_2O_3 to remove decomposed Pt(0) products and the resultant filtrate was charged with an additional 1 atm of ethylene. Additional ethylbenzene formation was observed from this recovered catalytic mixture, albeit with a reduced TOF. As a test for heterogeneous catalysis, the hydroarylation of ethylene with benzene-d_6, with **5a** or **6** as catalysts, was performed in the presence of Hg(0) and product formation was monitored over a 5 day period (Figure 2.22). Surprisingly, catalytic activity for both **5a** and **6** was improved with the addition of Hg (15.7 and 24.3 turnovers after 24 h at 100 °C in the presence of Hg(0) *vs* 7.8 and 12.2 turnovers in its absence, respectively). Moreover, decomposition rates were reduced in the presence of Hg. To elucidate the cause for the improved performance, several further control experiments were performed.
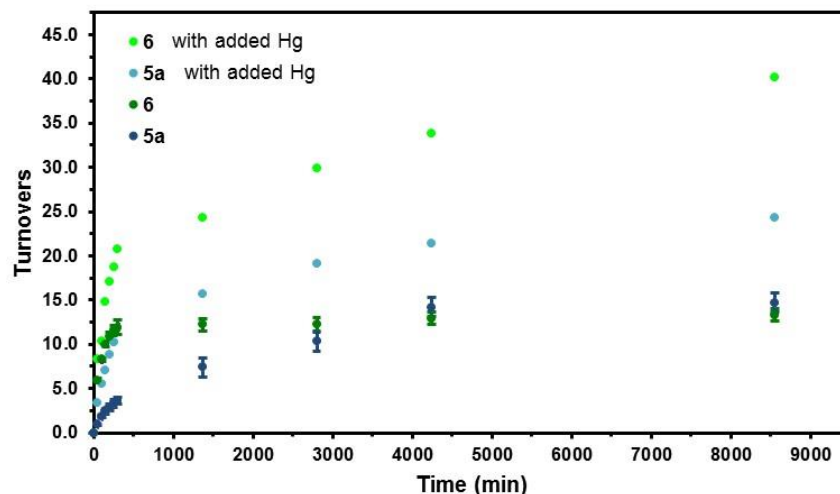
Figure 2.22. Monitored hydroarylation of ethylene (1 atm) with benzene-d_6 at 100 °C over 144 h by ^{1}H NMR spectroscopy using catalysts **5a** and **6** (3.7 mM) with and without the presence of Hg(0) in the reaction mixture. Turnovers are given as the average of triplicate experiments with error calculated as the standard deviation.

To probe the existence of possible molecular Hg-Pt adducts which could be more catalytically active than the initial precatalysts, complex **5a** was heated to 100 °C in benzene-d_6 with added mercury in the absence of ethylene. No change in the ^{1}H NMR spectrum was observed, which suggests that in the absence of olefin, Hg and **5a** do not interact to form a detectable species. Additionally, catalysts **5a** or **6** were prestirred in benzene-d_6 with Hg(0), carefully filtered, and then subjected to standard hydroarylation conditions (Figure 2.23). Catalyst **6** did not exhibit a change in activity compared to catalysis without prestirring with Hg(0). In contrast, complex **5a** demonstrated a slight improvement in catalytic activity (albeit less so than in the presence of Hg). It has been reported that metallic nanoparticles can grow by an autocatalytic mechanism involving an acceleration of the conversion rate for molecular precursors after nucleation.[62-64] Therefore, we propose that sequestration of Pt(0) seed particles *via* amalgamation with Hg(0) results in reduced competitive decomposition rates and therefore an improvement to catalyst stability and longevity.
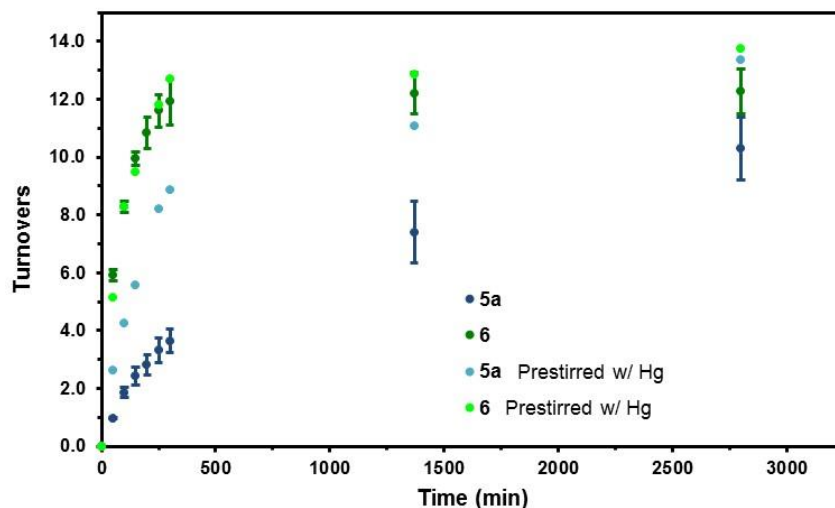
Figure 2.23. Monitored hydroarylation of ethylene (1 atm) with benzene-d_6 at 100 °C over 46 h by ^{1}H NMR spectroscopy using catalysts **5a** and **6** (3.7 mM) with and without prestirring the catalysts with Hg(0) prior to olefin addition. Mercury was removed prior to substrate addition and heating. Turnovers are given as the average of triplicate experiments with error calculated as the standard deviation.

Proposed Hydroarylation Mechanism. Given the observations above, a mechanism for ethylene hydroarylation similar to those reported by Gunnoe[46] and Goldberg[45] is proposed (Figure 2.24). An equilibrium between the dimethylsulfide precatalyst **5a** and the active species **6** occurs via a rapid ligand exchange with ethylene. Olefin insertion into the Pt–Ph bond yields a coordinatively unsaturated (ᵗBuPyInd)Pt(CH$_2$CH$_2$Ph) species (**A**), likely stabilized by either an agostic interaction of the β-phenethyl C–H bond or a π-interaction of the phenethyl arene with the Pt center. Computations for analogous cationic Pt complexes suggest that a π-interaction is more stable than an agostic interaction, resulting in a larger kinetic barrier for C–H activation from the π-complex ($\Delta\Delta G^\ddagger$ = 5.0 kcal/mol).[46] Therefore, it is quite possible that the agostic complex is the catalytically relevant intermediate, **A**.

Intermediate **A** induces arene C–H activation of solvent by an oxidative addition reaction to form a five-coordinate, Pt^{IV}-hydride intermediate (**B**). Subsequent reductive elimination from **C**, and exchange of the bound ethylbenzene ligand for ethylene, regenerates **6**. Alternatively, C–H activation can occur by a σ–bond metathesis mechanism to form ethylbenzene in a single step. Recent precedent for this type of mechanism has been published by the Gunnoe[43,46,52,53] and Cundari[51] groups. For cationic Pt species, DFT calculations suggest that a two-step oxidative addition/reductive elimination pathway is only slightly preferred over a σ-bond metathesis route ($\Delta\Delta G^\ddagger$ = 2.3 kcal/mol).[46,43,51-53]

It has been suggested by Gunnoe and coworkers[46] that complexes of the type [(bpy)Pt(CH$_2$CH$_2$Ph)(C$_2$H$_4$)]$^+$ are either catalytic intermediates or off-cycle species. Since complex **7** exhibits reduced hydroarylation activity compared to **5a** or **6**, and releases ethylene upon heating in benzene, it seems likely that this complex exists as an off-cycle intermediate in equilibrium with **A** *via* ethylene dissociation.
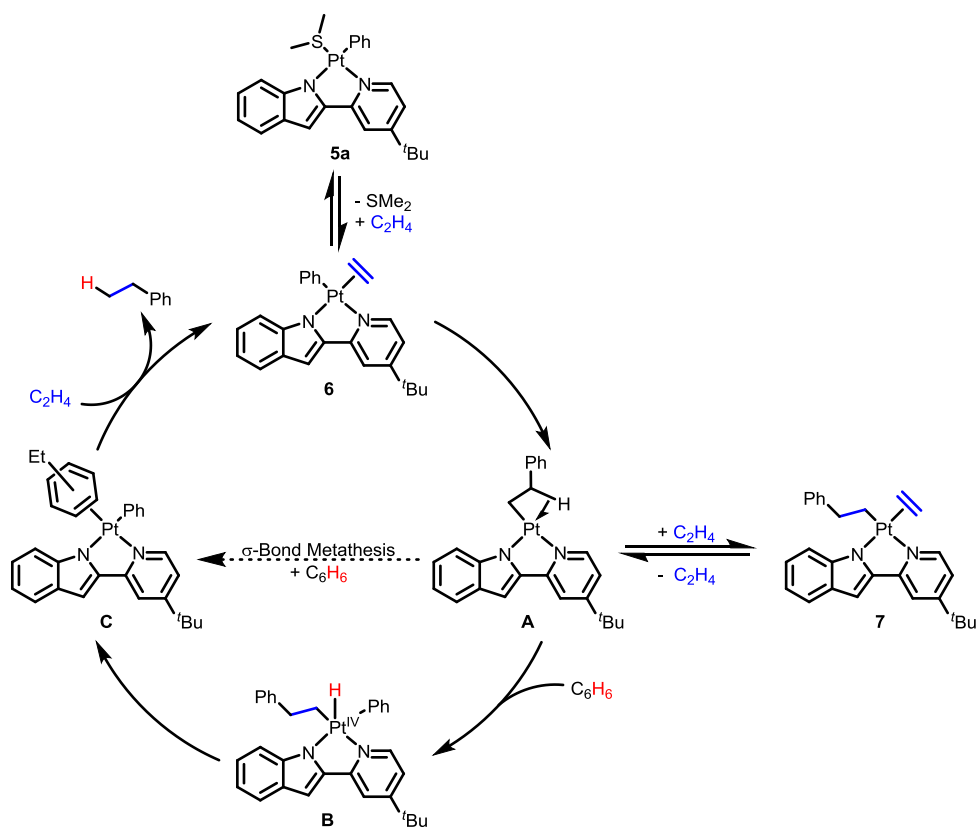
Figure 2.24. Proposed mechanism for productive catalytic ethylene hydroarylation with **5a**. Note that C–H bond activation can occur *via* either an oxidative addition/reductive elimination or σ-bond metathesis pathway.
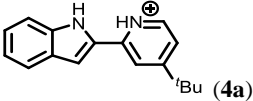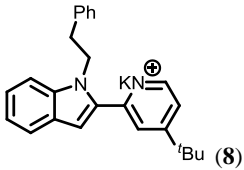
Catalyst Decomposition Studies. While olefin hydroarylation is catalyzed by (N–N)-ligated Pt complexes, the stability of these catalytic species appears to be the major factor in defining catalytic efficiency (*vide supra*). In an effort to understand the decomposition pathways available during catalysis, a sample of **5a** was exposed to benzene and ethylene (1 atm) at 100 °C for 20 h, and products were separated from elemental Pt by preparative thin-layer chromatography. Several species were identified by high resolution mass spectrometry (Table 2.3). Organic species with m/z values consistent with free ligand (**4a**) and phenethyl substituted ^{t}BuPyInd (**8**) were identified. Complexes **5a** and **6** were also observed. Surprisingly, m/z values that correspond to previously unobserved organometallic compounds were also detected: [(^{t}BuPyInd)Pt(CH$_2$CH$_2$Ph)(SMe$_2$)] (**9**), [(^{t}BuPyInd)PtEt(SMe$_2$)] (**10**), and [(^{t}BuPyInd)PtPh(H$_2$C=CHPh)] (**11**). While relative amounts could not be quantified with high resolution mass spectrometry, the existence of these species suggests possible decomposition pathways.

Since styrene has been implied as a major decomposition product,[45,46,50] a separate ethylene hydroarylation experiment was performed at 100 °C for 24 h and styrene content was determined by ^{1}H NMR spectroscopy. Unreacted ethylene was removed by a freeze/pump/thaw cycle, since ethylene and styrene vinylic resonances overlap. Multiple sets of vinylic resonances are consistent with styrene, β-(*E*)-deuterostyrene, and β-(*Z*)-deuterostyrene. The relative ratio of these three species (with respect to the initial catalyst loading) was ca. 10%:8%:12%, respectively. Given that styrene is slightly volatile, a control experiment consisting of a mixture of styrene and Si(SiMe$_3$)$_4$ as an internal standard in benzene-d_6 was

subjected to the same freeze/pump/thaw procedure; by ^{1}H NMR spectroscopy, styrene loss was not observed.

Table 2.3. Decomposition products identified by HRMS (ESI-TOF).[a]

Found *m/z*	Theoretical *m/z* [b]	Assignment (Compound Number)
251.1559	[M + H]$^+$ Calcd for C$_{17}$H$_{19}$N$_2$, 251.154.	(**4a**)
393.2098	[M + K]$^+$ Calcd for C$_{25}$H$_{26}$N$_2$K, 393.1728.	(**8**)
536.1706	[M + H]$^+$ Calcd for C$_{21}$H$_{29}$N$_2$PtS, 536.1694	[(^{t}BuPyInd)PtEt(SMe$_2$)]H$^+$ (**10**)
550.1831	[M + H]$^+$ Calcd for C$_{25}$H$_{27}$N$_2$Pt, 550.1816.	[(^{t}BuPyInd)PtPh(C$_2$H$_4$)]H$^+$ (**6**)
584.1706	[M + H]$^+$ Calcd for C$_{25}$H$_{29}$N$_2$PtS, 584.1694.	[(^{t}BuPyInd)PtPh(SMe$_2$)]H$^+$ (**5a**)
612.2007	[M + H]$^+$ Calcd for C$_{27}$H$_{33}$N$_2$PtS, 612.2007.	[(^{t}BuPyInd)Pt(CH$_2$CH$_2$Ph)(SMe$_2$)]H$^+$ (**9**)
626.1817	[M + H]$^+$ Calcd for C$_{31}$H$_{31}$N$_2$Pt, 626.2129.	[(^{t}BuPyInd)PtPh(H$_2$C=CHPh)]H$^+$ (**11**)

[a] Decomposition products were determined after the ethylene hydroarylation with catalyst **5a** in benzene at 100 °C for 20 h. [b] Masses of proposed structures (as the H$^+$ or K$^+$ species) are given under the Theoretical *m/z*.
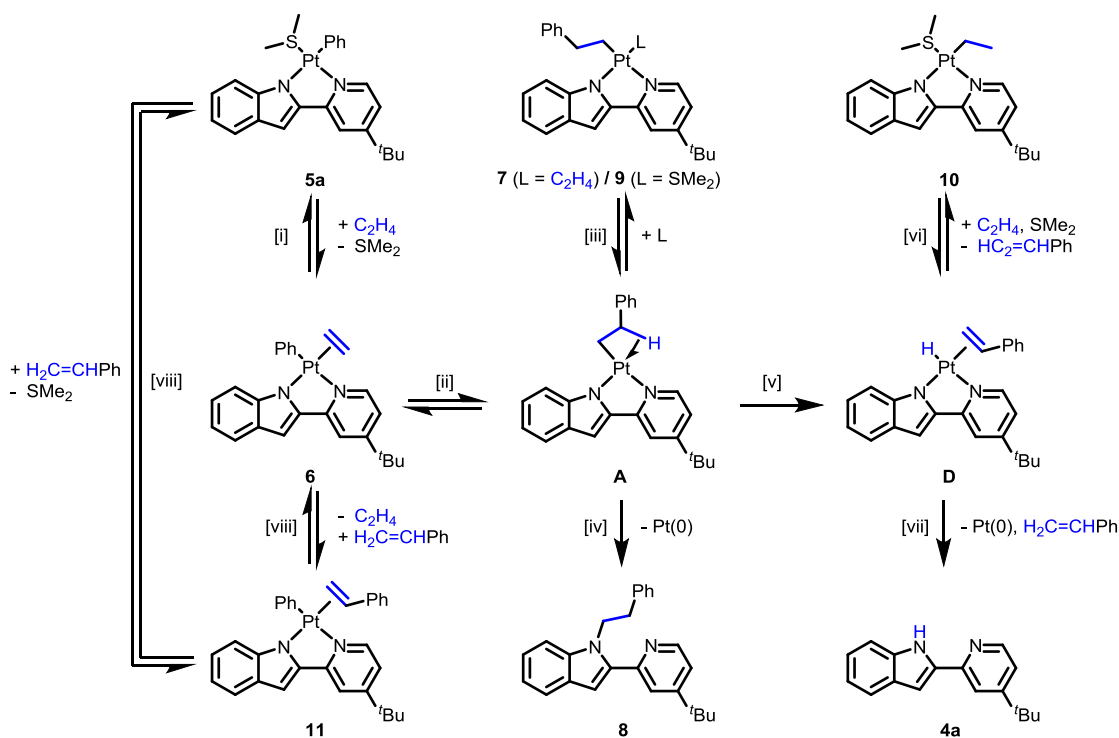
Figure 2.25. Organometallic speciation and decomposition pathways in ethylene hydroarylation with benzene and catalyst **5a**. [i]: ligand substitution for ethylene; [ii]: olefin insertion; [iii]: coordination of either SMe$_2$ or ethylene; [iv]: reductive elimination of phenethyl and ^{t}BuPyInd; [v]: β-hydride elimination; [vi]: ligand substitution of styrene for ethylene, followed by olefin insertion and coordination of SMe$_2$; [vii]: reductive elimination of hydride and ^{t}BuPyInd; [viii]: ligand substitution of SMe$_2$ for styrene.

Given these data, possible catalyst decomposition pathways are described in Figure 2.25. As in the productive hydroarylation mechanism (Figure 2.24), ligand exchange with ethylene from complex **5a** affords the ethylene complex **6** and subsequent insertion yields intermediate **A**. This intermediate is undoubtedly trapped by available L-type ligands (*i.e.* ethylene or SMe$_2$) to afford complexes **7** and **9.** These species can reenter the catalytic cycle, but as shown above they are less effective than **6** and do not directly participate in the major catalytic cycle.

While **A** can undergo reaction to produce ethylbenzene (Figures 2.24 and 2.25), it may also be a key intermediate in catalyst decomposition. Intermediate **A** can undergo irreversible decomposition by reductive elimination of the phenethyl fragment with the ^{t}BuPyInd ligand, which results in the formation of Pt(0) and **8**. Alternatively, β-hydride elimination from the phenethyl fragment can occur to generate a transient Pt–hydride complex **D** bearing a styrene ligand. Precedent for this decomposition route exists and has been supported by DFT calculations for cationic Pt systems.[46] β-Agostic intermediates of the type [(^{t}bpy)Pt(CH$_2$CH$_2$Ph)]$^+$ have been calculated to contain a shortened C$_{sp3}$–C$_{sp3}$ bond distance, which is consistent with partial [(^{t}bpy)PtH(styrene)]$^+$ character. Therefore, it is unsurprising that the Pt–hydride intermediate **A** likely undergoes a facile β-hydride elimination to afford **D**. Reductive elimination can occur from **D** to generate free ligand (**4a**) as well as an equivalent of styrene and Pt(0). Goldberg and coworkers[44,45,50] have observed styrene formation *via* β-hydride elimination as the primary decomposition pathway for a similar pyridyl-pyrrole ligated Pt(II) system. Given the existence of multiple styrene

isotopomers and that the catalysis primarily affords ethylbenzene-d_6, H(D) scrambling likely occurs from complex **D** and not a catalytically active species.

In a recent publication by Nozaki,[65] complexes of the type [(P–O)PtPh(L)] supported by a 2-(di-*tert*-butylphosphanyl)benzenesulfonate (P–O) ligand were employed as precursors in the generation of stable Pt–hydride species by treatment with ethylene. Olefin insertion from these PtPh complex was suggested to generate a Pt(CH$_2$CH$_2$Ph) fragment, although such species were not directly observed. Moreover, C–H activation to form ethylbenzene was not observed. Instead, a favorable β–hydride elimination event occurred to generate [(P–O)PtH(styrene)] as an isolable species capable of catalytic olefin polymerization. This suggests that the donating properties of the supporting ligand greatly affect the stabilities of intermediates during productive hydroarylation and catalyst decomposition processes; stabilization of Pt–hydride species prevents irreversible ligand reductive elimination while also favoring unproductive β-hydride elimination over C–H activation.

Complex **D** can also undergo ligand substitution of styrene for ethylene. Hydride migration to the bound ethylene can occur followed by coordination of an L-type ligand to generate the Pt(II)–ethyl complex **10**. Similar Pt–ethyl complexes have been identified as off-cycle organometallic products by the Gunnoe group,[46] for cationic (^{t}bpy)Pt complexes. Finally, complex **5a** can also undergo ligand substitution with any styrene generated during the course of decomposition to afford the styrene-bound complex **11**. These data suggest that a series of common mechanistic steps occur to produce the observed organometallic side-products, organic decomposition species, and elemental Pt: β-hydride elimination, olefin (or residual sulfide) binding at platinum, and reductive elimination involving the (N–N) ligand.

Conclusions. In summary, a series of Pt(II) catalysts featuring bidentate pyridyl-indolate ligands with varying substituents has been successfully synthesized. These complexes demonstrated the ability to catalyze olefin hydroarylation on a range of arene and olefin substrates. In general, complexes of the type (N–N)PtPh(SR$_2$) exhibited reasonable activity compared to other reported Pt complexes.[45,46] Additionally, reduced over-alkylation was observed using the current catalysts.

Two potential intermediates (**6** and **7**) were isolated and their activities were compared with that of precatalyst **5a**. Complex **6**, bearing Ph and C$_2$H$_4$ as ancillary ligands, rapidly catalyzed olefin hydroarylation. In contrast to complexes **5a** and **6**, the aforementioned complex (^{t}BuPyInd)Pt(CH$_2$CH$_2$Ph)(C$_2$H$_4$) exhibited reduced activity and therefore is not a direct catalytic intermediate in this system: ethylene dissociation is required for catalysis to occur. Interestingly, complex **5a** exhibited improved catalytic stability when compared to **6** or **7**, which suggests that the ancillary SMe$_2$ ligand retards decomposition at the expense of reduced activity.

Several studies were designed to probe the operative mechanism for catalysis. We have shown that efficiency in this platinum system is determined primarily by competing, irreversible catalyst decomposition. The competitive decomposition routes were studied to better understand how to combat poor catalytic stability. Many different organometallic and organic species were identified after completion of the catalysis; the organometallic complexes could potentially reenter the catalytic cycle while the organic fragments arise from irreversible reductive eliminations. Additional experiments are required to demonstrate whether these organometallic complexes are indeed active precatalysts. Unproductive β-hydride elimination is a major issue for catalytic stability due to the ease with which irreversible reductive elimination occurs from Pt–hydride species to form free ligand and elemental Pt. Moreover, the competing processes of catalyst turnover and decomposition involve (^{t}BuPyInd)Pt(CH$_2$CH$_2$Ph) as a key, common

intermediate. Therefore, further improvements in efficiencies of Pt-based hydroarylation catalysts should focus on improving the stabilities of catalytic intermediates, especially toward β-hydride eliminations.

External base and Hg(0) tests revealed that hydroarylation is metal mediated rather than adventitiously catalyzed either by acid generated *in situ* or elemental Pt nanoparticles. Interestingly, this study uncovered a potential additive in catalysis (elemental Hg) that seemingly suppresses catalyst decomposition and allows for longer catalyst lifetimes.[58-64] This surprising inhibition of catalytic decomposition is an interesting feature of this system, which provides a potential solution to one of the major dilemmas in Pt catalyzed hydroarylation: competitive catalytic decomposition. While only Hg(0) has been employed in this study towards decomposition suppression, it may be possible that other additives can effectively sequester nucleating Pt nanoparticles and thereby prevent autocatalytic decay of hydroarylation catalysts.

Experimental

General Considerations

All reactions and experiments, unless otherwise noted, were performed using standard Schlenk techniques under N_2 atmosphere or inside a N_2 glovebox. Schlenk glassware was oven dried overnight before use and N-N$^-$ ligated metal complexes were stored at ambient temperature in a N_2 glovebox. Solvents were stored over 3 Å molecular sieves after drying with a JC Meyers Phoenix SDS solvent purification system. Solvents for organic syntheses were used without further purification. Deuterated NMR solvents were purchased from Cambridge Isotope Laboratory. Benzene-d_6 was degassed by three freeze/pump/thaw cycles and then dried over 3 Å molecular sieves.

Ethylene (99.9%) was purchased in a gas cylinder from Praxair Technology and used as received. Propylene (99.99%) was purchased in a gas cylinder from Matheson Tri-Gas and used as received. *o*-Ethyltoluene, *m*-ethyltoluene, *p*-ethyltoluene, NaO^{t}Bu, AgOTf, PhLi, 2,6-di-*tert*-butyl-4-methylpyridine, and tridecane were purchased from commercial sources and used without further purification. Si(SiMe$_3$)$_4$ was purchased from a commercial source, sublimed before use, and stored in a N_2 glovebox. Phenyl hydrazine (**2a**), 4-methoxyphenyl hydrazine hydrochloride (**2e**), 4-methylphenyl hydrazine hydrochloride (**2f**), 4-fluorophenyl hydrazine hydrochloride (**2g**), 4-chlorophenyl hydrazine hydrochloride (**2h**), 4-bromophenyl hydrazine hydrochloride (**2i**), and 2-chlorophenyl hydrazine hydrochloride (**2j**) were purchased from commercial sources and used without further purification. 2,5-Difluorophenyl hydrazine (**2b**),[49] 2,3,4,5-tetrafluorophenyl hydrazine (**2c**),[49] 4-*tert*-butyl-2-acetylpyridine,[66] *cis*-(SMe$_2$)$_2$PtPh$_2$,[67,68] [(μ-SEt$_2$)PtPh$_2$]$_2$,[69] and [(C$_2$H$_4$)Pt(μ-Cl)Cl]$_2$ (Zeise's Dimer)[70] were prepared according to published literature procedures.

All ^{1}H, ^{13}C{^{1}H}, and ^{19}F NMR experiments were carried out using Bruker AV-300, AVB-400, AVQ-400, AV-500, AV-600 MHz, or AV-900 MHz (equipped with a TCI cryoprobe) spectrometers at ambient temperatures (unless otherwise noted). ^{1}H and ^{13}C{^{1}H} NMR experiments were internally calibrated to residual solvents relative to tetramethylsilane. ^{19}F NMR was calibrated externally to hexafluorobenzene. Quantitative GC experiments were performed on an Agilent 7890 GC equipped with an HP-5 column (25 m x 0.20 mm x 0.33 μm film) and an FID detector. High resolution mass spectrometry (HRMS) experiments were carried out by the QB3/Chemistry Mass Spectrometry Facility at the University of California, Berkeley. ESIHR experiments were performed on a LTQ-FT instrument (from Thermo-Finnigan) with direct injection using Excalibur software. EIHR experiments were performed on an Autospec Premier instrument (from Waters) using MassLynx software.

Elemental analyses were performed at the Microanalytical Laboratory at the University of California, Berkeley using a Perkin Elmer 2400 Series II combustion analyzer equipped for determination of %C, %H and %N (as well as %S). Single crystal X-ray diffraction experiments were performed at the CheXray crystallography facility at the University of California, Berkeley with a Bruker APEX-II CCD area detector using Mo Kα radiation (λ = 0.71073 Å) monochromated by QUAZAR multilayer mirrors. Crystals were kept at 100(2) K during data collection. Data collection was performed using Bruker APEX2 software. Unit cell refinement and data reduction were performed using Bruker SAINT software. Structures were solved in WinGX using SHELXT-2014 software and refined with SHELXL-2014 software using anisotropic parameters. All thermal ellipsoid graphics were rendered using ORTEP-32 software. Selected details can be found in Table 2.4.

Synthesis of Ligand Precursors, Ligands, and Metal Complexes

Synthesis of (*E*)-4-(*tert*-butyl)-2-(1-(2-phenylhydrazono)ethyl)pyridine (3a). Aryl hydrazine **2a** (0.60 mL, 5.7 mmol, 1 equiv) and 4-*tert*-butyl-2-acetylpyridine (1.0 g, 5.7 mmol, 1 equiv) were dissolved in absolute ethanol (10 mL) with catalytic glacial acetic acid (ca. 2 pipette drops) and refluxed at 90 °C for 4 h under air until judged complete by TLC (10% ethyl acetate/hexanes). Upon completion, the reaction mixture was cooled to ambient temperature and then diluted with water (50 mL). The crude mixture was extracted with dichloromethane (3 x 50 mL). The organic layers were combined, washed with brine (50 mL), dried over Na_2SO_4, and filtered. Volatile components were removed under reduced pressure yielding the title compound as a spectroscopically pure orange solid (1.3 g, 87 %).

^{1}H NMR (dichloromethane-d_2, 600.1 MHz): δ 8.44 (d, *J* = 5.3 Hz, 1H), 8.19 (s, 1H, N–H), 7.63 (s, 1H), 7.30 (t, *J* = 7.7 Hz, 2H), 7.22 (d, *J* = 7.4 Hz, 3H), 6.90 (t, *J* = 7.2 Hz, 1H), 2.38 (s, 3H, N=CCH₃), 1.37 (s, 9H, *t*Bu).

^{13}C{^{1}H} NMR (dichloromethane-d_2, 150.9 MHz): δ 160.5, 156.5, 148.4, 143.4, 129.7, 120.8, 120.3, 116.8, 113.6, 112.9, 35.1, 30.7, 10.3.

HRMS (EI) *m/z*: [M]$^+$ Calcd for $C_{17}H_{21}N_3$ 267.1735; Found 267.1729.

Synthesis of 2-(4-(*tert*-butyl)pyridin-2-yl)-1*H*-indole (4a, *t*BuPyInd). Hydrazone **3a** (1.3 g, 4.9 mmol, 1 equiv) was heated to 140 °C in neat polyphosphoric acid (3 mL) under air for 1.5 h using a large stir bar to ensure thorough mixing. After completion, the reaction mixture was cooled to ambient temperature and quenched with $NaOH_{(aq)}$ (150 mL, 20 wt%). The crude mixture was extracted with dichloromethane (4 x 50 mL). The organic layers were combined, washed with brine (50 mL), dried over $MgSO_4$, and filtered. Volatile components were removed under reduced pressure to afford an orange solid. Purification by SiO_2 column chromatography (eluting with 10% ethyl acetate/hexanes) afforded the title compound as a spectroscopically pure off-white powder (0.59 g, 48%).

^{1}H NMR (benzene-d_6, 400.1 MHz): δ 9.57 (s, 1H), 8.42 (dd, *J* = 5.3, 0.6 Hz, 1H), 7.76 – 7.71 (m, 1H), 7.69 (dd, *J* = 1.8, 0.6 Hz, 1H), 7.21 – 7.18 (m, 2H), 7.08 – 7.02 (m, 1H), 6.95 (dd, *J* = 2.0, 0.8 Hz, 1H), 6.77 (dd, *J* = 5.3, 1.9 Hz, 1H), 1.08 (s, 9H).

^{1}H NMR (dichloromethane-d_2, 400.1 MHz): δ 9.83 (s, 1H, N–H), 8.48 (d, J = 5.3 Hz, 1H), 7.82 (d, J = 1.9 Hz, 1H), 7.64 (d, J = 7.9 Hz, 1H), 7.43 (d, J = 8.3 Hz, 1H), 7.23 – 7.16 (m, 2H), 7.09 (t, J = 7.8 Hz, 1H), 7.05 (d, J = 2.1 Hz, 1H), 1.38 (s, 9H, ^{t}Bu).

^{13}C{^{1}H} NMR (dichloromethane-d_2, 150.9 MHz): 161.3, 150.6, 149.4, 137.7, 136.9, 129.6, 123.3, 121.4, 120.4, 120.1, 117.1, 111.7, 100.2, 35.2, 30.7.

HRMS (EI) m/z: [M]$^+$ Calcd for $C_{17}H_{18}N_2$ 250.1470; Found 250.1470.

Synthesis of (^{t}BuPyInd)PtPh(SMe$_2$) (5a). Cis-(SMe$_2$)$_2$PtPh$_2$ (200 mg, 0.42 mmol, 1.1 equiv) and **4a** (100 mg, 0.40 mmol, 1 equiv) were dissolved in benzene (20 mL). The reaction mixture was allowed to stir at ambient temperature for 5 h. Volatile components were then removed under reduced pressure. Under ambient atmosphere, SiO$_2$ column chromatography (eluting with 10% ethyl acetate/hexanes) provided the title compound as an analytically pure yellow solid (220 mg, 95%). X-Ray quality crystals were obtained by slow diffusion of pentane into toluene at -35 °C.

^{1}H NMR (benzene-d_6, 600.1 MHz): δ 8.31 (d, J = 8.3 Hz, 1H), 8.03 (d, J = 7.8 Hz, 1H), 7.74 (d with ^{195}Pt satellites, J_{HH} = 7.2 Hz, J_{PtH} = 33 Hz, 2H), 7.67 (d, J = 6.3 Hz, 1H), 7.55 (s, 1H), 7.45 (t, J = 7.4 Hz, 1H), 7.33 (t, J = 7.2 Hz, 1H), 7.27 – 7.17 (m, 3H), 7.15 – 7.12 (m, 1H), 5.83 (d, J = 5.9 Hz, 1H), 1.54 (s with ^{195}Pt satellites, J_{PtH} = 53 Hz, 6H, SMe$_2$), 0.84 (s, 9H, ^{t}Bu).

^{1}H NMR (dichloromethane-d_2, 400.1 MHz): δ 7.88 (dd, J = 8.3, 0.8 Hz, 1H), 7.78 (d, J = 2.0 Hz, 1H), 7.62 – 7.56 (m, 3H), 7.53 (d, J = 6.6 Hz, 1H), 7.10 (t, J = 7.2 Hz, 2H), 7.05 – 6.97 (m, 3H), 6.89 (t, J = 7.7 Hz, 1H), 6.80 (dd, J = 6.4, 2.2 Hz, 1H), 2.31 (s with ^{195}Pt satellites, J_{PtH} = 56 Hz, 6H, SMe$_2$), 1.31 (s, 9H, ^{t}Bu).

^{13}C{^{1}H} NMR (benzene-d_6, 150.9 MHz): δ 162.0, 160.0, 149.9, 148.6, 147.1, 146.8, 139.1, 138.0, 132.6, 123.7, 122.6, 122.3, 118.3, 118.1, 116.4, 115.1, 103.2, 34.7, 29.8, 22.9.

Anal. Calcd for $C_{25}H_{28}N_2PtS$: C, 51.45; H, 4.84; N, 4.80; S, 5.49. Found: C, 51.13; H, 4.92; N, 4.55; S, 5.35.

Synthesis of (E)-4-($tert$-butyl)-2-(1-(2-(2,5-difluorophenyl)hydrazono)ethyl) pyridine (3b). Aryl hydrazine **2b** (0.66 g, 4.5 mmol, 1.3 equiv) and 4-$tert$-butyl-2-acetylpyridine (0.64 g, 3.6 mmol, 1 equiv) were dissolved in absolute ethanol (10 mL) with catalytic glacial acetic acid (ca. 2 pipette drops) and refluxed at 90 °C for 4 h under air until judged complete by TLC (10% ethyl acetate/hexanes). Upon completion, the reaction mixture was cooled to ambient temperature. Volatile components were removed under reduced pressure to afford an orange solid. Recrystallization from hexanes yielded the title compound as a spectroscopically pure yellow solid (0.88 g, 81%).

^{1}H NMR (dichloromethane-d_2, 600.1 MHz): δ 8.47 (dd, J = 5.2, 0.6 Hz, 1H), 8.18 (d, J = 1.3 Hz, 1H), 7.68 (s, 1H, N–H), 7.37 (ddd, J = 10.0, 6.6, 3.1 Hz, 1H), 7.26 (dd, J = 5.3, 1.9 Hz, 1H), 7.02 (ddd, J = 11.1, 8.9, 4.9 Hz, 1H), 6.55 – 6.44 (m, 1H), 2.41 (s, 3H, N=CCH$_3$), 1.38 (s, 9H, ^{t}Bu).

^{13}C{^{1}H} NMR (dichloromethane-d_2, 150.9 MHz): δ 161.2, 160.7, 159.6, 156.2, 148.9, 147.7, 147.0, 146.2, 135.2, 135.1, 135.0, 121.0, 117.2, 116.1, 116.0, 115.9, 105.8, 105.7, 105.6, 102.3, 102.1, 35.3, 30.9, 10.8 (fluorinated carbons difficult to observe and assign due to complicated C–F couplings).

^{19}F NMR (dichloromethane-d_2, 376.4 MHz): δ -116.23 (br s), -141.45 (br s).

HRMS (EI) *m/z*: [M]$^+$ Calcd for $C_{17}H_{19}N_3F_2$, 303.1547; Found, 303.1549.

Synthesis of 2-(4-(*tert*-butyl)pyridin-2-yl)-4,7-difluoro-1*H*-indole (4b, ^{t}BuPyInd-4,5-F$_2$). Hydrazone **3b** (0.75 g, 2.5 mmol, 1 equiv) was heated to 110 °C in neat polyphosphoric acid (10 mL) for 4 h under air using a large stir bar to ensure thorough mixing. After completion, the reaction mixture was cooled to ambient temperature and quenched with NaOH$_{(aq)}$ (200 mL, 20 wt%). The crude mixture was extracted with diethyl ether (3 x 100 mL). The organic layers were combined, washed with brine (50 mL), dried over MgSO$_4$, and filtered. Volatile components were removed under reduced pressure to afford an orange/yellow solid. Purification by SiO$_2$ column chromatography (eluting with 10% ethyl acetate/hexanes) afforded the title compound as a spectroscopically pure yellow powder (0.11 g, 15%).

^{1}H NMR (dichloromethane-d_2, 600.1 MHz): δ 10.08 (s, 1H, N–H), 8.50 (d, *J* = 5.3 Hz, 1H, Py), 7.85 (d, *J* = 1.7 Hz, 1H, Py), 7.27 (dd, *J* = 5.3, 1.8 Hz, 1H, Py), 7.17 – 7.09 (m, 1H, Ind), 6.82 (ddd, *J* = 10.3, 8.7, 3.5 Hz, 1H, Ind), 6.67 (ddd, *J* = 9.6, 8.6, 3.1 Hz, 1H, Ind), 1.38 (s, 9H, ^{t}Bu).

^{13}C{^{1}H} NMR (dichloromethane-d_2, 150.9 MHz): δ 161.8, 153.8, 152.2, 149.7, 147.3, 145.7, 139.0, 127.1, 127.0, 126.9, 121.7, 121.6, 121.5, 120.9, 117.6, 107.8, 107.7, 107.6, 104.6, 104.5, 104.4, 104.3, 96.9, 35.4, 30.8 (fluorinated carbons difficult to observe and assign due to complicated C–F couplings).

^{19}F NMR (dichloromethane-d_2, 376.4 MHz): δ -127.61 (dd, *J* = 22.5, 9.5 Hz), -139.43 (dd, *J* = 22.2, 10.3 Hz).

HRMS (EI) *m/z*: [M]$^+$ Calcd for $C_{17}H_{16}N_2F_2$ 286.1282; Found, 286.1284.

Synthesis of (^{t}BuPyInd-4,7-F$_2$)PtPh(SMe$_2$) (5b). In a manner similar to that used above for **5a**, *cis*-(SMe$_2$)$_2$PtPh$_2$ (175 mg, 0.37 mmol, 1 equiv) and **4b** (110 mg, 0.39 mmol, 1.1 equiv) were dissolved in benzene (20 mL). Purification by SiO$_2$ column chromatography (eluting with 10% ethyl acetate/hexanes) yielded the title compound as an analytically pure yellow solid (202 mg, 88%). X-Ray quality crystals were obtained by slow diffusion of pentane into toluene at -35 °C.

^{1}H NMR (dichloromethane-d_2, 600.1 MHz): δ 7.85 (d, *J* = 1.5 Hz, 1H), 7.56 (d, *J* = 7.2 Hz, 2H), 7.52 (d, *J* = 6.3 Hz, 1H), 7.19 (d, *J* = 2.6 Hz, 1H), 7.10 (t, *J* = 7.4 Hz, 2H), 7.03 (t, *J* = 7.3 Hz, 1H), 6.87 (dd, *J* = 6.2, 1.9 Hz, 1H), 6.63 (ddd, *J* = 12.2, 8.3, 3.9 Hz, 1H), 6.47 (td, *J* = 9.2, 2.5 Hz, 1H), 2.18 (s with ^{195}Pt satellites, *J*$_{PtH}$ = 58 Hz, 6H, SMe$_2$), 1.32 (s, 9H, ^{t}Bu).

^{13}C{^{1}H} NMR (dichloromethane-d_2, 150.9 MHz): δ 163.8, 158.5, 154.6, 153.0, 152.9, 149.9, 149.8, 148.8, 148.5, 148.2, 148.1, 143.5, 137.5, 136.9, 136.8, 136.7, 136.76, 128.8, 124.0, 123.8, 123.7, 123.6, 123.5, 119.8, 117.5, 105.8,

105.7, 105.6, 101.04, 100.99, 100.90, 100.8, 99.0, 35.8, 30.4, 24.3 (fluorinated carbons difficult to observe and assign due to complicated C–F couplings).

^{19}F NMR (dichloromethane-d_2, 376.4 MHz): δ -127.70 (ddd, J = 23.3, 9.5, 4.0 Hz), -129.99 (dd, J = 23.3, 12.3 Hz).

Anal. Calcd for $C_{25}H_{26}F_2N_2PtS$: C, 48.46; H, 4.23; N, 4.52. Found: C, 48.66; H, 4.31; N, 4.50.

Synthesis of (*E*)-4-(*tert*-butyl)-2-(1-(2-(2,3,4,5-tetrafluorophenyl)hydrazono)ethyl) pyridine (3c). Aryl hydrazine **2c** (1.8 g, 9.7 mmol, 1.3 equiv) and 4-*tert*-butyl-2-acetylpyridine (1.4 g, 7.8 mmol, 1 equiv) were dissolved in absolute ethanol (40 mL) with catalytic glacial acetic acid (ca. 2 pipette drops) and refluxed at 90 °C for 4 h under air until judged complete by TLC (10% ethyl acetate/hexanes). Upon completion, the reaction mixture was cooled to ambient temperature. Volatile components were removed under reduced pressure to afford an orange/yellow solid. Purification by SiO_2 column chromatography (eluting with 10% ethyl acetate/hexanes and then 50% ethyl acetate/hexanes) afforded the title compound as a spectroscopically pure yellow powder (1.6 g, 61%).

^{1}H NMR (dichloromethane-d_2, 600.1 MHz): δ 8.46 (d, J = 5.7 Hz, 1H, Py), 8.11 (d, J = 1.4 Hz, 1H, Py), 7.55 (s, 1H, N–H), 7.32 – 7.28 (m, 1H, C_6F_4H), 7.27 (dd, J = 5.2, 1.9 Hz, 1H, Py), 2.41 (s, 3H, N=CCH$_3$), 1.37 (s, 9H, ^{t}Bu).

^{13}C{^{1}H} NMR (dichloromethane-d_2, 150.9 MHz): δ 160.6, 155.7, 148.8, 148.2, 148.0, 141.3, 135.1, 132.9, 121.1, 117.0, 97.1, 96.9, 35.1, 30.7, 10.8 (fluorinated carbons difficult to observe and assign due to complicated C–F couplings).

^{19}F NMR (dichloromethane-d_2, 376.4 MHz): -139.50 (dt, J = 22.0, 11.0 Hz), -157.73 (t, J = 20.3 Hz), -162.77 – -163.04 (m), -170.46 – -170.94 (m).

HRMS (EI) *m/z*: [M]$^+$ Calcd for $C_{17}H_{17}N_3F_4$ 339.1539; Found 339.1358.

Synthesis of 2-(4-(*tert*-butyl)pyridin-2-yl)-4,5,6,7-tetrafluoro-1*H*-indole (4c, ^{t}BuPyInd-4,5,6,7-F$_4$). Hydrazone **3c** (1.0 g, 2.9 mmol, 1 equiv) was heated to 110 °C in neat polyphosphoric acid (7 mL) for 4 h under air using a large stir bar to ensure thorough mixing. After completion, the reaction mixture was cooled to ambient temperature and quenched with NaOH$_{(aq)}$ (150 mL, 10 wt%). The crude mixture was extracted with dichloromethane (4 x 50 mL). The organic layers were combined, washed with brine (100 mL), dried over $MgSO_4$, and filtered. Volatile components were removed under reduced pressure to afford an orange/yellow solid. Purification by SiO_2 column chromatography (eluting with 5% ethyl acetate/hexanes) afforded the title compound as a spectroscopically pure yellow powder (0.25 g, 27%).

^{1}H NMR (dichloromethane-d_2, 600.1 MHz): δ 10.08 (s, 1H, N–H), 8.50 (dd, J = 5.3, 0.9 Hz, 1H, Py), 7.82 (dd, J = 1.9, 0.9 Hz, 1H, Py), 7.29 (dd, J = 5.3, 1.8 Hz, 1H, Py), 7.14 (d, J = 2.7 Hz, 1H, Ind), 1.38 (s, 9H, ^{t}Bu).

$^{13}C\{^1H\}$ NMR (dichloromethane-d_2, 150.9 MHz): δ 161.3, 149.1, 148.5, 139.6, 138.9, 138.8, 137.9, 136.4, 136.3, 136.2, 136.0, 135.8, 134.4, 134.3, 134.2, 133.6, 133.5, 120.9, 120.5, 116.9, 115.4, 115.2, 96.1, 34.8, 30.1 (fluorinated carbons difficult to observe and assign due to complicated C–F couplings).

^{19}F NMR (dichloromethane-d_2, 376.4 MHz): δ -150.12 (dd, J = 19.6, 17.1 Hz), -160.95 (ddt, J = 19.8, 16.7, 3.5 Hz), -165.11 (td, J = 19.4, 1.7 Hz), -169.64 (td, J = 19.7, 3.9 Hz).

HRMS (EI) *m/z*: [M]$^+$ Calcd for $C_{17}H_{14}N_2F_4$ 322.1093; Found, 322.1093.

Synthesis of (^{t}BuPyInd-4,5,6,7-F$_4$)PtPh(SMe$_2$) (5c). In a manner similar to that used above for **5a**, *cis*-(SMe$_2$)$_2$PtPh$_2$ (121 mg, 0.26 mmol, 1.1 equiv) and **4c** (75 mg, 0.23 mmol, 1 equiv) were dissolved in benzene (20 mL). Purification by SiO$_2$ column chromatography (eluting with 10% ethyl acetate/hexanes) yielded the title compound as an analytically pure yellow solid (131 mg, 86%). X-Ray quality crystals were obtained by slow diffusion of pentane into toluene at -35 °C.

^1H NMR (benzene-d_6, 600.1 MHz): δ 7.58 (d, J = 7.4 Hz, 2H), 7.53 (d, J = 6.3 Hz, 1H), 7.40 (s, 1H), 7.21 (s, 1H), 7.17-7.10 (m, 3H), 7.07 (t, J = 7.1 Hz, 1H), 5.86 (d, J = 5.8 Hz, 1H), 1.49 (s with ^{195}Pt satellites, J_{PtH} = 55 Hz, 6H, SMe$_2$), 0.80 (s, 9H, ^{t}Bu).

$^{13}C\{^1H\}$ NMR (benzene-d_6, 150.9 MHz): δ 162.3, 157.9, 149.0, 148.9, 148.8, 148.2, 143.2, 137.0, 136.5, 136.4, 134.4, 134.3, 134.2, 132.8, 132.7, 132.6, 131.5, 131.4, 131.3, 123.6, 119.9, 118.7, 117.8, 117.7, 117.6, 117.6, 116.3, 99.3, 34.4, 29.3, 22.6. (fluorinated carbons difficult to observe and assign due to complicated couplings).

^{19}F NMR (dichloromethane-d_2, 376.4 MHz): δ -151.69 (td, J = 20.6, 18.6, 4.6 Hz), -153.35 (dd, J = 20.8, 15.2 Hz), -169.26 (td, J = 20.2, 3.9 Hz), -173.48 (td, J = 20.1, 4.0 Hz).

Anal. Calcd for $C_{25}H_{24}F_4N_2PtS$: C, 45.80; H, 3.69; N, 4.27; S, 4.89. Found: C, 45.99; H, 3.69; N, 4.08; S, 5.05.

Synthesis of (*E*)-2-(1-(2-phenylhydrazono)ethyl)pyridine (3d). A mixture of aryl hydrazine **2a** (2.0 mL, 20 mmol, 1 equiv) and 2-acetylpyridine (2.3 mL, 20 mmol, 1 equiv) in absolute ethanol (20 mL) with catalytic glacial acetic acid (ca. 2 pipette drops) was heated to 90 °C for 2 h under air until reaction was judged complete by TLC (10% ethyl acetate/hexanes). Upon completion, the reaction mixture was cooled to 0 °C, resulting in the formation of orange needles. The solution was filtered and the solid was washed with cold absolute ethanol. Residual volatile components were removed under reduced pressure to afford the title compound as analytically pure orange needles (3.1 g, 73%).

^1H NMR (dimethyl sulfoxide-d_6, 600.1 MHz): δ 9.49 (s, 1H, NH), 8.52 (d, J = 4.7 Hz, 1H, Py), 8.11 (d, J = 8.1 Hz, 1H, Py), 7.76 (td, J = 7.7, 1.9 Hz, 1H, Py), 7.31 – 7.22 (m, 5H, C$_6$H$_5$), 6.80 (tt, J = 7.2, 1.3 Hz, 1H, Py), 2.34 (s, 3H, N=CCH$_3$).

$^{13}C\{^1H\}$ NMR (dimethyl sulfoxide-d_6, 150.9 MHz): δ 156.2, 148.3, 145.5, 141.4, 136.1, 128.9, 122.2, 119.4, 119.2, 113.0, 11.0.

HRMS (ESI) m/z: [M + H]$^+$ Calcd for C$_{13}$H$_{14}$N$_3$ 212.1182; Found 212.1177.

Synthesis of 2-(pyridin-2-yl)-1*H*-indole (4d, PyInd). Hydrazone **3d** (1.0 g, 4.7 mmol, 1 equiv) was heated to 140 °C in neat polyphosphoric acid (3 mL) for 2 h under air using a large stir bar to ensure thorough mixing. After completion, the reaction mixture was cooled to ambient temperature and quenched with NaOH$_{(aq)}$ (50 mL, 20 wt%). The crude mixture was extracted with dichloromethane (4 x 50 mL). The organic layers were combined, washed with brine (50 mL), dried over MgSO$_4$, and filtered. Volatile components were removed under reduced pressure to afford an orange solid. Purification by SiO$_2$ column chromatography (eluting with 10% ethyl acetate/hexanes) afforded the title compound as a spectroscopically pure yellow powder (0.32 g, 35%).

^{1}H NMR (dichloromethane-d_2, 600.1 MHz): δ 9.68 (s, 1H, N–H), 8.58 (d, J = 4.8 Hz, 1H), 7.83 (d, J = 8.0 Hz, 1H), 7.75 (td, J = 7.7, 1.8 Hz, 1H), 7.64 (d, J = 7.9 Hz, 1H), 7.42 (d, J = 8.2 Hz, 1H), 7.24 – 7.15 (m, 2H), 7.09 (t, J = 7.5 Hz, 1H), 7.04 – 7.03 (m, 1H).

^{13}C{^{1}H} NMR (dichloromethane-d_2, 150.9 MHz): δ 150.7, 149.6, 137.2, 137.0, 136.9, 129.6, 123.5, 122.5, 121.5, 120.5, 120.2, 111.7, 100.7.

HRMS (ESI) m/z: [M + H]$^+$ Calcd for C$_{13}$H$_{11}$N$_2$ 195.0917; Found 195.0913.

Synthesis of (PyInd)PtPh(SMe$_2$) (5d). In a manner similar to that used above for **5a**, *cis*-(SMe$_2$)$_2$PtPh$_2$ (75 mg, 0.16 mmol, 1 equiv) and **4d** (39 mg, 0.20 mmol, 1.3 equiv) were dissolved in benzene (20 mL). The crude product was washed with 10% ethyl acetate/hexanes solution (20 mL) to afford the title compound as an analytically pure yellow solid (81 mg, 97%).

^{1}H NMR (dichloromethane-d_2, 600.1 MHz): δ 7.88 (d, J = 8.4 Hz, 1H), 7.81 (d, J = 8.1 Hz, 1H), 7.71 (td, J = 7.7, 1.6 Hz, 1H), 7.67 (dd, J = 5.9, 1.3 Hz, 1H), 7.65 – 7.55 (m, 3H), 7.11 (t, J = 7.4 Hz, 2H), 7.05 – 6.96 (m, 3H), 6.90 (ddd, J = 7.9, 6.7, 1.0 Hz, 1H), 6.77 (ddd, J = 7.3, 6.0, 1.6 Hz, 1H), 2.31 (s with ^{195}Pt satellites, J_{PtH} = 61 Hz, 6H, SMe$_2$).

^{13}C{^{1}H} NMR (dichloromethane-d_2, 150.9 MHz): δ 159.9, 149.3, 149.1, 147.9, 147.6, 138.6, 137.6, 134.6, 128.6, 123.8, 122.3, 121.7, 121.0, 120.4, 117.9, 114.7, 102.7, 23.8.

Anal. Calcd for C$_{21}$H$_{20}$N$_2$PtS: C, 47.81; H, 3.82; N, 5.31. Found: C, 47.99; H, 3.56; N, 5.29.

Synthesis of (*E*)-2-(1-(2-(4-methoxyphenyl)hydrazono)ethyl)pyridine (3e). A mixture of aryl hydrazine **2e** (as the HCl salt, 3.6 g, 20 mmol, 1 equiv) and 2-acetylpyridine (2.3 mL, 20 mmol, 1 equiv) in absolute ethanol (20 mL) with catalytic glacial acetic acid (ca. 2 pipette drops) was heated to 90 °C for 3 h under air until reaction was judged complete by TLC (10% ethyl acetate/hexanes). Upon completion, the reaction mixture was cooled to 0 °C, resulting in the formation of an orange/red solid. The solution was filtered and the solid was washed with cold absolute ethanol.

Residual volatile components were removed under reduced pressure to afford the title compound as a spectroscopically pure dark orange powder (4.2 g, 85%).

^{1}H NMR (dimethyl sulfoxide-d_6, 600.1 MHz): δ 10.47 (s, 1H, N–H), 8.69 (d, J = 5.6 Hz, 1H), 8.41 (t, J = 7.7 Hz, 1H), 8.21 (d, J = 8.3 Hz, 1H), 7.73 (t, J = 6.5 Hz, 1H), 7.60 (d, J = 8.8 Hz, 2H), 6.88 (d, J = 8.9 Hz, 2H), 3.72 (s, 3H, OMe), 2.39 (s, 3H, N=CCH$_3$).

^{13}C{^{1}H} NMR (dimethyl sulfoxide-d_6, 150.9 MHz): δ 154.4, 149.7, 144.9, 142.0, 137.9, 130.6, 123.2, 122.6, 115.7, 114.3, 55.2, 11.9.

HRMS (EI) m/z: [M]$^+$ Calcd for C$_{14}$H$_{15}$N$_3$O 241.1215; Found 241.1212.

Synthesis of 5-methoxy-2-(pyridin-2-yl)-1H-indole (4e, PyInd-5-MeO). Hydrazone **3e** (0.70 g, 2.9 mmol, 1 equiv) was dissolved in glacial acetic acid (10 mL). The reaction mixture was heated to 115 °C under a flow of N$_2$ for 28 h, after which the reaction mixture was cooled to ambient temperature. The reaction mixture was quenched with KOH$_{(aq)}$ (100 mL, 20 wt%). The crude mixture was extracted with dichloromethane (3 x 50 mL). The organic layers were combined, washed with brine, dried over MgSO$_4$, and filtered. The crude mixture was purified by SiO$_2$ column chromatography (eluting with 50% chloroform/toluene and then chloroform) to afford the title compound as a spectroscopically pure yellow solid (0.084 g, 13%).

^{1}H NMR (dichloromethane-d_2, 600.1 MHz): δ 9.65 (s, 1H, N–H), 8.57 (dt, J = 4.9, 1.3 Hz, 1H), 7.80 (dt, J = 8.1, 1.1 Hz, 1H), 7.74 (td, J = 7.7, 1.8 Hz, 1H), 7.29 (d, J = 8.8 Hz, 1H), 7.18 (ddd, J = 7.4, 4.8, 1.2 Hz, 1H), 7.09 (d, J = 2.4 Hz, 1H), 6.96 (dd, J = 2.0, 0.9 Hz, 1H), 6.85 (dd, J = 8.8, 2.4 Hz, 1H), 3.84 (s, 3H, OMe).

^{13}C{^{1}H} NMR (dichloromethane-d_2, 150.9 MHz): δ 154.9, 150.7, 149.6, 137.8, 137.0, 132.2, 130.0, 122.4, 120.1, 114.1, 112.5, 102.6, 100.5, 56.0.

HRMS (EI) m/z: [M]$^+$ Calcd for C$_{14}$H$_{12}$N$_2$O 224.0950; Found 224.0951.

Synthesis of (PyInd-5-MeO)PtPh(SMe$_2$) (5e). Cis-(SMe$_2$)$_2$PtPh$_2$ (40 mg, 0.08 mmol, 1 equiv) and **5e** (19 mg, 0.08 mmol, 1 equiv) were dissolved in benzene (20 mL). The reaction mixture was allowed to stir at 50 °C for 20 h. Volatile components were then removed under reduced pressure. The crude product was triturated with 10% ethyl acetate/hexanes solution (20 mL) to afford the title compound as a spectroscopically pure yellow solid (36 mg, 77%).

^{1}H NMR (dichloromethane-d_2, 600.1 MHz): δ 7.77 (d, J = 9.0 Hz, 1H), 7.75 (d, J = 8.6 Hz, 1H), 7.68 (ddd, J = 8.5, 5.8, 1.5 Hz, 1H), 7.64 (d, J = 6.0 Hz, 1H), 7.62 – 7.57 (m, 2H), 7.10 (t, J = 7.5 Hz, 2H), 7.05 – 7.01 (m, 1H), 7.00 (d, J = 2.6 Hz, 1H), 6.93 (s, 1H), 6.74 (ddd, J = 7.4, 6.0, 1.6 Hz, 1H), 6.69 (dd, J = 8.9, 2.6 Hz, 1H), 3.82 (s, 3H, OMe), 2.30 (s with ^{195}Pt satellites, J_{PtH} = 58 Hz, 6H, SMe$_2$).

^{13}C{^{1}H} NMR (dichloromethane-d_2, 150.9 MHz): δ 153.1, 149.2, 147.0, 146.9, 146.6, 145.8, 138.5, 137.5, 137.0, 128.5, 123.7, 120.6, 120.2, 115.5, 113.9, 102.2, 101.5, 55.8, 23.7.

Anal. Calcd for $C_{22}H_{22}N_2OPtS$ • 0.5 CD_2Cl_2: C, 44.96; H, 4.02; N, 4.66. Found: C, 45.15; H, 3.74; N, 4.40.

Synthesis of *(E)*-2-(1-(2-(*p*-tolyl)hydrazono)ethyl)pyridine (3f). A mixture of aryl hydrazine **2f** (as the HCl salt, 2.2 g, 14 mmol, 1 equiv) and 2-acetylpyridine (1.6 mL, 14 mmol, 1 equiv) in absolute ethanol (30 mL) with catalytic glacial acetic acid (ca. 2 pipette drops) was heated to 90 °C for 2 h under air until reaction was judged complete by TLC (10% ethyl acetate/hexanes). Upon completion, the reaction mixture was cooled to 0 °C, resulting in the formation of an orange solid. The solution was filtered and the solid was washed with cold absolute ethanol. Residual volatile components were removed under reduced pressure to afford the title compound as a spectroscopically pure orange powder (2.5 g, 78%).

^{1}H NMR (dimethyl sulfoxide-d_6, 600.1 MHz): δ 10.26 (s, 1H, N–H), 8.67 (d, J = 5.6 Hz, 1H), 8.37 (t, J = 8.1 Hz, 1H), 8.23 (d, J = 8.2 Hz, 1H), 7.71 (t, J = 6.6 Hz, 1H), 7.45 (d, J = 8.0 Hz, 2H), 7.11 (d, J = 8.0 Hz, 2H), 2.37 (s, 3H, N=CCH$_3$), 2.25 (s, 3H, Me).

^{13}C{^{1}H} NMR (dimethyl sulfoxide-d_6, 150.9 MHz): δ 149.9, 144.7, 142.4, 141.9, 131.8, 130.1, 129.4, 123.4, 122.7, 114.4, 20.4, 11.9.

HRMS (ESI) m/z: [M + H]$^+$ Calcd for $C_{14}H_{16}N_3$ 226.1339; Found 226.1334.

Synthesis of 5-methyl-2-(pyridin-2-yl)-1*H*-indole (4f, PyInd-5-Me). Hydrazone **3f** (1.0 g, 4.4 mmol, 1 equiv) was heated to 140 °C in neat polyphosphoric acid (3 mL) for 1 h under air using a large stir bar to ensure thorough mixing. After completion, the reaction mixture was cooled to ambient temperature and quenched with NaOH$_{(aq)}$ (150 mL, 10 wt%). The crude mixture was extracted with dichloromethane (4 x 50 mL). The organic layers were combined, washed with brine (50 mL), dried over MgSO$_4$, and filtered. Volatile components were removed under reduced pressure to afford an orange solid. Purification by SiO$_2$ column chromatography (eluting with 10% ethyl acetate/hexanes) afforded the title compound as a spectroscopically pure white powder (0.31 g, 33%).

^{1}H NMR (dichloromethane-d_2, 600.1 MHz): δ 9.49 (s, 1H, N–H), 8.56 (dt, J = 5.0, 1.4 Hz, 1H), 7.80 (dt, J = 8.3, 1.2 Hz, 1H), 7.73 (td, J = 7.7, 1.8 Hz, 1H), 7.42 (s, 1H), 7.32 (d, J = 8.3 Hz, 1H), 7.18 (ddd, J = 7.4, 4.9, 1.3 Hz, 1H), 7.04 (d, J = 8.3 Hz, 1H), 6.94 (d, J = 1.8 Hz, 1H), 2.43 (s, 3H, Me).

^{13}C{^{1}H} NMR (dichloromethane-d_2, 150.9 MHz): δ 150.8, 149.6, 137.3, 137.0, 135.3, 129.9, 129.8, 125.3, 122.3, 121.0, 120.1, 111.4, 100.2, 21.6.

HRMS (ESI) m/z: [M + H]$^+$ Calcd for $C_{14}H_{13}N_2$ 209.1073; Found 209.1069.

Synthesis of (PyInd-5-Me)PtPh(SMe₂) (5f). In a manner similar to that used above for **5a**, *cis*-(SMe₂)₂PtPh₂ (75 mg, 0.16 mmol, 1 equiv) and **4f** (42 mg, 0.20 mmol, 1.3 equiv) were dissolved in benzene (10 mL). The crude product was triturated with 10% ethyl acetate/hexanes solution (20 mL) to afford the title compound as an analytically pure yellow solid (75 mg, 88%).

¹H NMR (dichloromethane-d_2, 600.1 MHz): δ 7.76 (dd, J = 8.9, 2.2 Hz, 2H), 7.72 – 7.64 (m, 2H), 7.60 (d with ¹⁹⁵Pt satellites, J_{HH} = 6.7 Hz, J_{PtH} = 31, 2H), 7.35 (s, 1H), 7.11 (t, J = 7.5 Hz, 2H), 7.02 (td, J = 7.2, 1.5 Hz, 1H), 6.92 (s, 1H), 6.86 (dd, J = 8.4, 1.8 Hz, 1H), 6.73 (ddd, J = 7.2, 5.8, 1.5 Hz, 1H), 2.38 (s, 3H, Me), 2.30 (s with ¹⁹⁵Pt satellites, J_{PtH} = 59 Hz, 6H, SMe₂).

¹³C{¹H} NMR (dichloromethane-d_2, 150.9 MHz): δ 159.9, 149.2, 147.6, 146.3, 146.0, 138.5, 137.6, 132.2, 128.6, 126.9, 124.5, 123.8, 121.0, 120.7, 120.3, 114.4, 102.2, 23.8, 21.7.

Anal. Calcd for $C_{22}H_{22}N_2PtS$: C, 48.79; H, 4.09; N, 5.17. Found: C, 49.07; H, 3.89; N, 4.80.

Synthesis of (*E*)-2-(1-(2-(4-fluorophenyl)hydrazono)ethyl)pyridine (3g). A mixture of aryl hydrazine **2g** (as the HCl salt, 2.0 g, 12 mmol, 1 equiv) and 2-acetylpyridine (1.4 mL, 12 mmol, 1 equiv) in absolute ethanol (30 mL) with catalytic glacial acetic acid (ca. 2 pipette drops) was heated to 90 °C for 3 h under air until reaction was judged complete by TLC (10% ethyl acetate/hexanes). Upon completion, the reaction mixture was cooled to 0 °C, resulting in the formation of an orange/yellow solid. The solution was filtered and the solid was washed with cold absolute ethanol. Residual volatile components were removed under reduced pressure to afford the title compound as a spectroscopically pure yellow powder (2.7 g, 83%).

¹H NMR (dimethyl sulfoxide-d_6, 600.1 MHz): δ 10.48 (s, 1H, N–H), 8.71 (d, J = 5.3 Hz, 1H), 8.41 (t, J = 8.3 Hz, 1H), 8.25 (d, J = 8.3 Hz, 1H), 7.75 (t, J = 6.6 Hz, 1H), 7.63 (dd, J = 8.8, 4.7 Hz, 2H), 7.13 (t, J = 8.9 Hz, 2H), 2.40 (s, 3H, N=CCH₃).

¹³C{¹H} NMR (dimethyl sulfoxide-d_6, 150.9 MHz): δ 158.1, 156.5, 149.9, 144.5, 142.8, 140.8, 132.9, 123.7, 122.7, 115.6, 115.5, 115.4, 12.0 (fluorinated carbons difficult to observe and assign due to complicated C–F couplings).

¹⁹F NMR (dimethyl sulfoxide-d_6, 376.4 MHz, DMSO): δ -122.5 (br s).

HRMS (ESI) m/z: [M + H]⁺ Calcd for $C_{13}H_{13}N_3F$ 230.1088; Found 230.1084.

Synthesis of 5-fluoro-2-(pyridin-2-yl)-1*H*-indole (4g, PyInd-5-F). Hydrazone **3g** (1.0 g, 4.4 mmol, 1 equiv) was heated to 140 °C in neat polyphosphoric acid (3 mL) for 1.5 h under air using a large stir bar to ensure thorough mixing. After completion, the reaction mixture was cooled to ambient temperature and quenched with NaOH₍aq₎ (150 mL, 10 wt%). The crude mixture was extracted with dichloromethane (4 x 50 mL). The organic layers were combined, washed with brine (50 mL), dried over MgSO₄, and filtered. Volatile components were removed under reduced pressure to afford a tan solid. Purification by SiO₂ column chromatography (eluting with 10% ethyl acetate/hexanes) afforded the title compound as a spectroscopically pure white powder (0.58 g, 62%).

^{1}H NMR (dichloromethane-d_2, 600.1 MHz): δ 9.73 (s, 1H, N–H), 8.59 (d, J = 4.7 Hz, 1H), 7.82 (d, J = 7.9 Hz, 1H), 7.76 (td, J = 7.8, 1.8 Hz, 1H), 7.35 (dd, J = 8.8, 4.4 Hz, 1H), 7.29 (dd, J = 9.7, 2.5 Hz, 1H), 7.25 – 7.19 (m, 1H), 7.00 (d, J = 2.1 Hz, 1H), 6.96 (td, J = 9.1, 2.5 Hz, 1H).

^{13}C{^{1}H} NMR (dichloromethane-d_2, 150.9 MHz): δ 158.8, 157.2, 149.8, 149.2, 138.5, 136.7, 133.0, 129.4, 129.3, 122.3, 119.8, 112.1, 112.0, 111.4, 111.2, 105.5, 105.3, 100.2, 100.1 (fluorinated carbons difficult to observe and assign due to complicated C–F couplings).

^{19}F NMR (dichloromethane-d_2, 376.4 MHz): δ -124.2 (br s).

HRMS (ESI) m/z: [M + H]$^+$ Calcd for $C_{13}H_{10}N_2F$ 213.0823; Found 213.0817.

Synthesis of (PyInd-5-F)PtPh(SMe$_2$) (5g). In a manner similar to that used above for **5a**, *cis*-(SMe$_2$)$_2$PtPh$_2$ (75 mg, 0.16 mmol, 1 equiv) and **4g** (42 mg, 0.20 mmol, 1.3 equiv) were dissolved in benzene (10 mL). The crude product was triturated with hexanes (10 mL) then 10% ethyl acetate/hexanes solution (15 mL) to afford the title compound as an analytically pure yellow solid (63 mg, 73%).

^{1}H NMR (dichloromethane-d_2, 600.1 MHz): δ 7.84 (dd, J = 9.1, 4.8 Hz, 1H), 7.80 (d, J = 8.0 Hz, 1H), 7.76 – 7.70 (m, 1H), 7.67 (d, J = 5.9 Hz, 1H), 7.59 (d with ^{195}Pt satellites, J_{HH} = 6.9 Hz, J_{PtH} = 37, 2H), 7.20 (dd, J = 10.2, 2.7 Hz, 1H), 7.11 (t, J = 7.4 Hz, 2H), 7.03 (t, J = 7.4 Hz, 1H), 6.98 (s, 1H), 6.82 – 6.75 (m, 2H), 2.31 (s with ^{195}Pt satellites, J_{PtH} = 60 Hz, 6H, SMe$_2$).

^{13}C{^{1}H} NMR (dichloromethane-d_2, 150.9 MHz): δ 159.5, 157.8, 156.3, 149.3, 147.9, 145.8, 145.3, 138.7, 137.5, 128.6, 123.9, 121.3, 120.5, 115.4, 111.0, 110.8, 105.1, 104.9, 102.5, 102.4, 23.7 (fluorinated carbons difficult to observe and assign due to complicated C–F couplings).

^{19}F NMR (dichloromethane-d_2, 376.4 MHz): δ -127.04 (td, J = 9.6, 4.7 Hz).

Anal. Calcd for $C_{21}H_{19}FN_2PtS$: C, 46.24; H, 3.51; N, 5.14. Found: C, 46.50; H, 3.45; N, 4.99.

Synthesis of (*E*)-2-(1-(2-(4-chlorophenyl)hydrazono)ethyl)pyridine (3h). A mixture of aryl hydrazine **2h** (as the HCl salt, 3.6 g, 20 mmol, 1 equiv) and 2-acetylpyridine (2.3 mL, 20 mmol, 1 equiv) in absolute ethanol (20 mL) with catalytic glacial acetic acid (ca. 2 pipette drops) was heated to 90 °C for 2 h under air until the reaction was judged complete by TLC (10% ethyl acetate/hexanes). Upon completion, the reaction mixture was cooled to 0 °C, resulting in the formation of an orange solid. The solution was filtered and the solid was washed with cold absolute ethanol. Residual volatile components were removed under reduced pressure to afford the title compound as a spectroscopically pure light orange powder (3.9 g, 77%).

^{1}H NMR (dimethyl sulfoxide-d_6, 600.1 MHz): δ 10.69 (s, 1H, N–H), 8.75 (d, J = 5.2 Hz, 1H), 8.44 (t, J = 7.4 Hz, 1H), 8.26 (d, J = 8.2 Hz, 1H), 7.79 (t, J = 6.3 Hz, 1H), 7.69 (d, J = 8.7 Hz, 2H), 7.29 (d, J = 8.8 Hz, 2H), 2.43 (s, 3H, N=CCH$_3$).

^{13}C{^{1}H} NMR (dimethyl sulfoxide-d_6, 150.9 MHz): δ 149.6, 144.7, 143.2, 142.6, 133.6, 128.6, 124.6, 123.9, 122.9, 115.9, 12.3.

HRMS (EI) m/z: [M]$^+$ Calcd for C$_{13}$H$_{12}$N$_3$Cl 245.0720; Found 245.0720.

Synthesis of 5-chloro-2-(pyridin-2-yl)-1H-indole (4h, PyInd-5-Cl). Hydrazone **3h** (1.0 g, 4.1 mmol, 1 equiv) was heated to 140 °C in neat polyphosphoric acid (3 mL) for 1.5 h under air using a large stir bar to ensure thorough mixing. After completion, the reaction mixture was cooled to ambient temperature and quenched with NaOH$_{(aq)}$ (100 mL, 10 wt%). The crude mixture was extracted with dichloromethane (4 x 50 mL). The organic layers were combined, washed with brine (50 mL), dried over MgSO$_4$, and filtered. Volatile components were removed under reduced pressure to afford a yellow solid. Purification by SiO$_2$ column chromatography (eluting with 10% ethyl acetate/hexanes and then 30% ethyl acetate/hexanes) afforded the title compound as a spectroscopically pure white powder (0.49 g, 52%).

^{1}H NMR (dichloromethane-d_2, 600.1 MHz): δ 9.97 (s, 1H, N–H), 8.59 (d, J = 4.7 Hz, 1H), 7.82 (d, J = 7.9 Hz, 1H), 7.76 (td, J = 7.7, 1.8 Hz, 1H), 7.61 (d, J = 2.2 Hz, 1H), 7.32 (d, J = 8.6 Hz, 1H), 7.23 (dd, J = 7.4, 4.9 Hz, 1H), 7.15 (dd, J = 8.7, 2.0 Hz, 1H), 6.98 (d, J = 2.3 Hz, 1H).

^{13}C{^{1}H} NMR (dichloromethane-d_2, 150.9 MHz): δ 150.2, 149.7, 138.7, 137.2, 135.3, 130.6, 125.9, 123.6, 122.9, 120.7, 120.4, 112.9, 100.2.

HRMS (EI) m/z: [M]$^+$ Calcd for C$_{13}$H$_9$N$_2$Cl 228.0454; Found 228.0455.

Synthesis of (PyInd-5-Cl)PtPh(SMe$_2$) (5h). In a manner similar to that used above for **5a**, *cis*-(SMe$_2$)$_2$PtPh$_2$ (45 mg, 0.10 mmol, 1 equiv) and **4h** (27 mg, 0.12 mmol, 1.2 equiv) were dissolved in benzene (10 mL). The crude product was triturated with 10% ethyl acetate/hexanes solution (15 mL) to afford the title compound as a spectroscopically pure yellow solid (50 mg, 94%).

^{1}H NMR (dichloromethane-d_2, 600.1 MHz): δ 7.85 (d, J = 8.9 Hz, 1H), 7.81 (dd, J = 7.7, 1.4 Hz, 1H), 7.73 (td, J = 7.7, 1.6 Hz, 1H), 7.68 (d, J = 5.7 Hz, 1H), 7.59 (d with ^{195}Pt satellites, J_{HH} = 6.8 Hz, J_{PtH} = 36 Hz, 2H), 7.54 (d, J = 2.2 Hz, 1H), 7.15 – 7.09 (m, 2H), 7.05 – 7.00 (m, 1H), 6.97 (s, 1H), 6.95 (dd, J = 8.9, 2.1 Hz, 1H), 6.81 (ddd, J = 7.5, 5.9, 1.5 Hz, 1H), 2.30 (s with ^{195}Pt satellites, J_{PtH} = 60 Hz, 6H, SMe$_2$).

^{13}C{^{1}H} NMR (dichloromethane-d_2, 150.9 MHz): δ 159.3, 149.4, 147.8, 147.3, 145.2, 138.8, 137.4, 132.7, 128.7, 123.9, 123.2, 122.4, 121.5, 120.6, 120.5, 115.8, 102.0, 23.7.

Anal. Calcd for C$_{21}$H$_{19}$ClN$_2$PtS • 1.2CD$_2$Cl$_2$: C, 40.02; H, 3.60; N, 4.20. Found: C, 40.01; H, 3.60; N, 4.22.

Synthesis of (*E*)-2-(1-(2-(4-bromophenyl)hydrazono)ethyl)pyridine (3i). A mixture of aryl hydrazine **2i** (as the HCl salt, 3.2 g, 14 mmol, 1 equiv) and 2-acetylpyridine (1.6 mL, 14 mmol, 1 equiv) in absolute ethanol (30 mL) with catalytic glacial acetic acid (ca. 2 pipette drops) was heated to 90 °C for 2 h under air until reaction was judged complete by TLC (10% ethyl acetate/hexanes). Upon completion, the reaction mixture was cooled to 0 °C, resulting in the formation of a light orange solid. The solution was filtered and the solid was washed with cold absolute ethanol. Residual volatile components were removed under reduced pressure to afford the title compound as a spectroscopically pure orange powder (3.6 g, 87%).

^{1}H NMR (dimethyl sulfoxide-d_6, 600.1 MHz): δ 10.59 (s, 1H, N–H), 8.74 (d, *J* = 5.0 Hz, 1H), 8.42 (t, *J* = 7.0 Hz, 1H), 8.26 (d, *J* = 6.7 Hz, 1H), 7.78 (t, *J* = 5.3 Hz, 1H), 7.60 (d, *J* = 6.0 Hz, 2H), 7.43 (d, *J* = 6.4 Hz, 2H), 2.42 (s, 3H, N=CCH$_3$).

^{13}C{^{1}H} NMR (dimethyl sulfoxide-d_6, 150.9 MHz): δ 148.7, 148.5, 144.6, 143.6, 142.9, 131.5, 123.9, 122.9, 116.3, 112.4, 12.2.

HRMS (ESI) m/z: [M + H]$^+$ Calcd for C$_{13}$H$_{13}$N$_3$Br 290.0287; Found 290.0286.

Synthesis of 5-bromo-2-(pyridin-2-yl)-1*H*-indole (4i, PyInd-5-Br). Hydrazone **3i** (1.0 g, 3.5 mmol, 1 equiv) was heated to 140 °C in neat polyphosphoric acid (3 mL) for 1.5 h under air using a large stir bar to ensure thorough mixing. After completion, the reaction mixture was cooled to ambient temperature and quenched with KOH$_{(aq)}$ (100 mL, 20 wt%). The crude mixture was extracted with dichloromethane (4 x 50 mL). The organic layers were combined, washed with brine (50 mL), dried over MgSO$_4$, and filtered. Volatile components were removed under reduced pressure to afford an orange oily solid. Purification by SiO$_2$ column chromatography (eluting with 10% ethyl acetate/hexanes) afforded an oily white solid. Recrystallization from hexanes layered onto a benzene solution afforded the title compound as a spectroscopically pure white solid (0.19 g, 20%).

^{1}H NMR (benzene-d_6, 600.1 MHz): δ 9.42 (s, 1H, N–H), 8.30 (d, *J* = 4.6 Hz, 1H), 7.85 – 7.74 (m, 1H), 7.25 (dd, *J* = 8.6, 1.9 Hz, 1H), 7.22 (d, *J* = 7.9 Hz, 1H), 7.01 (td, *J* = 7.7, 1.7 Hz, 1H), 6.61 (d, *J* = 8.6 Hz, 1H), 6.57 (d, *J* = 1.6 Hz, 1H), 6.55 (dd, *J* = 7.5, 4.8 Hz, 1H).

^{13}C{^{1}H} NMR (benzene-d_6, 150.9 MHz): δ 150.3, 149.2, 138.1, 136.4, 135.5, 131.4, 126.4, 124.0, 122.1, 120.0, 113.8, 113.3, 100.4.

HRMS (ESI) m/z: [M + H]$^+$ Calcd for C$_{13}$H$_{10}$N$_2$Br 273.0022. Found 273.0018.

Synthesis of (PyInd-5-Br)PtPh(SMe$_2$) (5i). In a manner similar to that used above for **5a**, *cis*-(SMe$_2$)$_2$PtPh$_2$ (63 mg, 0.13 mmol, 1 equiv) and **4i** (36 mg, 0.13 mmol, 1 equiv) were dissolved in benzene (10 mL). The crude product was triturated with 10% ethyl acetate/hexanes solution (15 mL) to afford the title compound as an analytically pure yellow solid (60 mg, 75%).

^{1}H NMR (dichloromethane-d_2, 600.1 MHz): δ 7.82 – 7.79 (m, 2H), 7.74 (td, J = 7.7, 1.5 Hz, 1H), 7.70 (d, J = 2.1 Hz, 1H), 7.68 (dd, J = 6.1, 1.3 Hz, 1H), 7.59 (dd with ^{195}Pt satellites, J_{HH} = 7.7, 1.4 Hz, J_{PtH} = 31 Hz, 2H), 7.11 (t, J = 7.6 Hz, 2H), 7.07 (dd, J = 8.9, 2.1 Hz, 1H), 7.03 (tt, J = 7.3, 1.2 Hz, 1H), 6.97 (d, J = 1.0 Hz, 1H), 6.82 (ddd, J = 7.4, 6.0, 1.5 Hz, 1H), 2.30 (s with ^{195}Pt satellites, J_{PtH} = 59 Hz, 6H, SMe$_2$).

^{13}C{^{1}H} NMR (dichloromethane-d_2, 150.9 MHz): δ 159.3, 149.4, 147.6, 147.4, 138.8, 137.4, 133.5, 128.6, 124.8, 123.9, 123.7, 121.5, 120.7, 120.6, 116.2, 110.9, 101.9, 23.7.

Anal. Calcd for C$_{21}$H$_{19}$BrN$_2$PtS • 0.7CD$_2$Cl$_2$: C, 39.06; H, 3.29; N, 4.20. Found: C, 39.24; H, 3.02; N, 4.09.

Synthesis of (*E*)-2-(1-(2-(2-chlorophenyl)hydrazono)ethyl)pyridine (3j). A mixture of aryl hydrazine **2j** (as the HCl salt, 3.1 g, 20 mmol, 1 equiv) and 2-acetylpyridine (2.3 mL, 20 mmol, 1 equiv) in absolute ethanol (20 mL) with catalytic glacial acetic acid (ca. 2 pipette drops) was heated to 90 °C for 2 h under air until reaction was judged complete by TLC (10% ethyl acetate/hexanes). Upon completion, the reaction mixture was cooled to 0 °C, resulting in the formation of a light yellow solid. The solution was filtered and the solid was washed with cold absolute ethanol. Residual volatile components were removed under reduced pressure to afford the title compound as a spectroscopically pure light-yellow powder (3.8 g, 77%).

^{1}H NMR (dimethyl sulfoxide-d_6, 600.1 MHz): δ 8.90 (s, 1H, N–H), 8.74 (d, J = 5.4 Hz, 1H), 8.34 – 8.28 (m, 2H), 7.98 (d, J = 8.3 Hz, 1H), 7.73 (t, J = 7.0 Hz, 1H), 7.44 (d, J = 8.0 Hz, 1H), 7.35 (t, J = 7.8 Hz, 1H), 6.98 (t, J = 7.7 Hz, 1H), 2.46 (s, 3H, N=CCH$_3$).

^{13}C{^{1}H} NMR (dimethyl sulfoxide-d_6, 150.9 MHz): δ 144.5, 140.1, 129.3, 128.1, 124.3, 123.1, 122.8, 122.3, 122.1, 118.5, 117.6, 116.4, 11.2.

HRMS (EI) m/z: [M]$^+$ Calcd for C$_{13}$H$_{12}$N$_3$Cl 245.0720; Found 245.0717.

Synthesis of 7-chloro-2-(pyridin-2-yl)-1*H*-indole (4j, PyInd-7-Cl). Hydrazone **3j** (1.0 g, 4.1 mmol, 1 equiv) was heated to 140 °C in neat polyphosphoric acid (3 mL) for 1.5 h under air using a large stir bar to ensure thorough mixing. After completion, the reaction mixture was cooled to ambient temperature and quenched with KOH$_{(aq)}$ (100 mL, 20 wt%). The crude mixture was extracted with dichloromethane (4 x 50 mL). The organic layers were combined, washed with brine (50 mL), dried over MgSO$_4$, and filtered. Volatile components were removed under reduced pressure to afford an orange solid. Purification by SiO$_2$ column chromatography (eluting with 10% ethyl acetate/hexanes) afforded the title compound as a spectroscopically pure white powder (0.18 g, 19%).

^{1}H NMR (dichloromethane-d_2, 600.1 MHz): δ 9.74 (s, 1H, N–H), 8.61 (d, J = 4.7 Hz, 1H), 7.81 (d, J = 7.9 Hz, 1H), 7.75 (td, J = 7.8, 1.8 Hz, 1H), 7.57 (d, J = 7.9 Hz, 1H), 7.28 – 7.20 (m, 2H), 7.10 – 7.00 (m, 2H).

^{13}C{^{1}H} NMR (dichloromethane-d_2, 150.9 MHz): δ 150.1, 149.7, 138.1, 137.1, 134.2, 131.0, 122.9, 122.7, 121.3, 120.3, 120.2, 117.1, 101.5.

HRMS (ESI) m/z: [M + H]$^+$ Calcd for $C_{13}H_{10}N_2Cl$ 229.0527; Found 229.0527.

Synthesis of (PyInd-7-Cl)PtPh(SMe₂) (5j). C*is*-(SMe₂)₂PtPh₂ (40 mg, 0.08 mmol, 1 equiv) and **4j** (23 mg, 0.10 mmol, 1.2 equiv) were dissolved in benzene (10 mL). The reaction mixture was stirred at 50 °C for 22 h. Volatile components were removed under reduced pressure. The crude product was triturated with 25% ethyl acetate/hexanes solution (15 mL) to afford the title compound as a spectroscopically pure yellow solid (23 mg, 49%).

^{1}H NMR (dichloromethane-d_2, 600.1 MHz): δ 7.80 (d, J = 8.6 Hz, 1H), 7.75 (td, J = 7.7, 1.5 Hz, 1H), 7.57 – 7.54 (m, 2H), 7.52 (ddd, J = 8.0, 3.2, 1.2 Hz, 2H), 7.13 (s, 1H), 7.10 – 7.04 (m, 3H), 7.03 – 6.98 (m, 1H), 6.86 (t, J = 7.6 Hz, 1H), 6.82 (ddd, J = 7.4, 5.9, 1.6 Hz, 1H), 2.15 (s with ^{195}Pt satellites, J_{PtH} = 62 Hz, 6H, SMe₂).

^{13}C{^{1}H} NMR (dichloromethane-d_2, 150.9 MHz): δ 160.9, 159.5, 149.6, 149.1, 139.2, 138.8, 137.7, 134.4, 128.6, 124.0, 123.0, 121.5, 120.8, 120.7, 120.4, 118.9, 103.7, 24.6.

Anal. Calcd for $C_{21}H_{19}ClN_2PtS$: C, 44.88; H, 3.41; N, 4.98. Found: C, 44.85; H, 3.37; N, 4.67.

Synthesis of (PyInd)PtPh(SEt₂) (5k). [(μ-SEt₂)PtPh₂]₂ (45 mg, 0.05 mmol, 1 equiv) and **4d** (42 mg, 0.10 mmol, 2 equiv) were dissolved in benzene (10 mL). The reaction mixture was stirred at 50 °C for 20 h. Volatile components were removed under reduced pressure. The crude product was triturated with hexanes (10 mL) then 15% ethyl acetate/hexanes solution (15 mL) to afford the title compound as an analytically pure yellow solid (41 mg, 72%).

^{1}H NMR (dichloromethane-d_2, 600.1 MHz): δ 8.11 (d, J = 8.5 Hz, 1H), 7.81 (d, J = 8.1 Hz, 1H), 7.70 (td, J = 7.7, 1.6 Hz, 1H), 7.66 – 7.55 (m, 4H), 7.10 (t, J = 7.5 Hz, 2H), 7.03 (s, 1H), 7.03 – 6.98 (m, 2H), 6.89 (t, J = 7.4 Hz, 1H), 6.75 (ddd, J = 7.3, 5.9, 1.6 Hz, 1H), 2.75 (dq with ^{195}Pt satellites, J_{HH} = 14.8, 7.6 Hz, J_{PtH} = 60 Hz, 2H, S**CH₂**CH₃), 2.55 (dq with ^{195}Pt satellites, J_{HH} = 14.1, 7.4 Hz, J_{PtH} = 71 Hz, 2H, S**CH₂**CH₃), 1.43 (t, J = 7.4 Hz, 6H, SCH₂**CH₃**).

^{13}C{^{1}H} NMR (dichloromethane-d_2, 150.9 MHz): δ 160.8, 150.3, 150.0, 147.5, 145.9, 139.5, 138.5, 133.0, 129.5, 124.6, 123.0, 122.5, 121.8, 121.4, 118.8, 116.5, 103.6, 32.6, 14.2.

Anal Calcd for $C_{23}H_{24}N_2PtS$ • 0.4 CD_2Cl_2: C, 47.61; H, 4.37; N, 4.75. Found: C, 47.85; H, 4.02; N, 4.71.

Synthesis of (ᵗBuPyInd-4,5,6,7-F₄)PtMe(SMe₂) (5l). [(μ-SMe₂)PtMe₂]₂ (86 mg, 0.15 mmol, 0.6 equiv) and **4c** (80 mg, 0.25 mmol, 1 equiv) were dissolved in benzene (20 mL). The reaction mixture was stirred at ambient temperatures for 2 h. Volatile components were removed under reduced pressure to afford an orange solid. Purification by SiO₂ column chromatography (eluting with 10% ethyl acetate/hexanes) afforded the title compound as a yellow solid (30

mg, 20%, purity ca. 70% with residual [(μ-SMe$_2$)PtMe$_2$]$_2$ identified). Recrystallization by slow diffusion of pentane into a fluorobenzene solution of **5l** yielded X-ray quality crystals.

^{1}H NMR (dichloromethane-d_2, 400.1 MHz): δ 8.48 (d with ^{195}Pt satellites, J_{PtH} = 44.6 Hz, J_{HH} = 5.9 Hz, 1H), 7.84 (s, 1H), 7.19 (dd, J = 5.8, 2.7 Hz, 1H), 7.16 (d, J = 2.7 Hz, 1H), 2.53 (s with ^{195}Pt satellites, J_{PtH} = 59 Hz, 6 H), 0.86 (s with ^{195}Pt satellites, J_{PtH} = 75 Hz, 3H).

^{19}F NMR (dichloromethane-d_2, 376.4 MHz): δ -151.9, -152.6, -169.7, -173.8.

Synthesis of (^{t}BuPyInd)PtPh(C$_2$H$_4$) (6) *via* Ligand Exchange with 5a. Inside a glovebox, **5a** (30 mg, 0.05 mmol) was dissolved in benzene-d_6 (0.7 mL) in a low pressure/vacuum J. Young NMR tube (4 mm outer diameter, 3 mL). On a Schlenk line, the solution was thoroughly degassed by three freeze/pump/thaw cycles after which ethylene (1 atm) was added at ambient temperature. After 1 day at ambient temperature, the volatile components were removed under reduced pressureto remove SMe$_2$ in order to prevent back reactions. Inside a glovebox, fresh benzene-d_6 was added and degassed as described previously. Additional ethylene (1 atm) was added and the mixture was left for 1 day. This process was repeated a total of four times. The reaction mixture was concentrated under reduced pressure and passed through a SiO$_2$ column under ambient atmosphere (eluting with 5% ethyl acetate/hexanes and then 10% ethyl acetate/hexanes) to yield the title compound as an analytically pure yellow solid (8 mg, 29%). Recrystallization by slow diffusion of pentane into a toluene solution of **3** yielded X-ray quality crystals.

^{1}H NMR (benzene-d_6, 600.1 MHz): δ 7.76 (t, J = 6.4 Hz, 1H), 7.69 (t, J = 6.5 Hz, 1H), 7.56 – 7.43 (m, 2H), 7.31 – 7.22 (m, 3H), 7.10 – 7.02 (m, 2H), 6.94 (d, J = 5.1 Hz, 1H), 6.76 (t, J = 5.7 Hz, 1H), 6.45 (t, J = 6.8 Hz, 1H), 6.31 (dt, J = 5.9, 2.9 Hz, 1H), 3.40 (s with ^{195}Pt satellites, J_{PtH} = 59 Hz, 4H, C$_2$H$_4$), 0.99 (s, 9H, ^{t}Bu).

^{1}H NMR (dichloromethane-d_2, 400.1 MHz): δ 7.87 (d, J = 1.7 Hz, 1H), 7.69 (d, J = 6.0 Hz, 1H), 7.55 – 7.40 (m, 3H), 7.23 (dd, J = 6.0, 2.0 Hz, 1H), 7.15 – 7.04 (m, 3H), 7.01 (d, J = 0.8 Hz, 1H), 6.78 (tt, J = 7.5, 0.9 Hz, 1H), 6.56 (ddd, J = 8.3, 6.9, 1.3 Hz, 1H), 5.64 (dd, J = 8.6, 0.7 Hz, 1H), 3.83 (s with ^{195}Pt satellites, J_{PtH} = 59 Hz, 4H, C$_2$H$_4$), 1.39 (s, 9H, ^{t}Bu).

^{13}C{^{1}H} NMR (benzene-d_6, 150.9 MHz): δ 162.1, 157.5, 153.9, 148.8, 147.8, 142.2, 139.1, 137.7, 128.9, 124.6, 124.0, 121.0, 120.0, 118.8, 117.5, 116.3, 104.0, 63.9, 34.8, 29.9.

Anal. Calcd for C$_{25}$H$_{26}$N$_2$Pt: C, 54.64; H, 4.77; N, 5.10. Found: C, 54.98; H, 4.54; N, 5.09.

Synthesis of (^{t}BuPyInd)PtPh(C$_2$H$_4$) (6) *via* Ligation and Phenylation of Zeise's Dimer. A mixture of Zeise's dimer (91 mg, 0.15 mmol, 1 equiv), **4a** (77 mg, 0.31 mmol, 2 equiv), and NaO^{t}Bu (35 mg, 0.31 mmol, 2 equiv) were dissolved in benzene (20 mL). A bright orange solid rapidly precipitated from solution. The mixture was stirred for 16 h at ambient temperature. Volatile components were removed under reduced pressure. Recrystallization from hexanes afforded *cis*/*trans*-(PyInd)PtCl(C$_2$H$_4$) as an orange solid (114 mg, 72%) which was identified by ^{1}H NMR spectroscopy and used without further purification.

^{1}H NMR (dichloromethane-d_2, 300.1 MHz): δ 8.60 (d, J = 8.5 Hz, 1H), 7.78 (d, J = 2.3 Hz, 1H), 7.56 (d, J = 8.1 Hz, 1H), 7.41 (d, J = 6.6 Hz, 1H), 7.19 – 7.06 (m, 2H), 7.04 – 6.93 (m, 2H), 4.67 – 4.36 (m, 2H, C_2H_4), 4.42 – 3.97 (m, 2H, C_2H_4), 1.38 (s, 9H, ^tBu).

In THF (10 mL), *cis/trans*-(PyInd)PtCl(C_2H_4) (114 mg, 0.22 mmol, 1 equiv) was treated with AgOTf (60 mg, 0.24 mmol, 1.1 equiv) at ambient temperature and stirred for 1 h. A solution of PhLi in THF (5 mL, 0.24 mmol, 47 mM, 1.1 equiv) was slowly added. The reaction mixture was then heated to 50 °C for 20 h in the dark. The reaction mixture was filtered over Celite and the filtrate was concentrated under reduced pressure. Purification by SiO_2 column chromatography (eluting with 5% ethyl acetate/hexanes) afforded the title compound as a spectroscopically pure yellow solid (25 mg, 20% yield).

^{1}H NMR (dichloromethane-d_2, 600.1 MHz): δ 7.87 (d, J = 1.9 Hz, 1H), 7.69 (d, J = 6.2 Hz, 1H), 7.55 – 7.40 (m, 3H), 7.24 (dd, J = 6.0, 2.1 Hz, 1H), 7.15 – 7.05 (m, 3H), 7.01 (d, J = 0.9 Hz, 1H), 6.78 (td, J = 7.5, 1.0 Hz, 1H), 6.56 (ddd, J = 8.3, 6.9, 1.3 Hz, 1H), 5.64 (dd, J = 8.6, 1.1 Hz, 1H), 3.84 (s with ^{195}Pt satellites, J_{PtH} = 60 Hz, 4H, C_2H_4), 1.39 (s, 9H, ^tBu).

Synthesis of (^{t}BuPyInd)Pt(CH$_2$CH$_2$Ph)(C$_2$H$_4$) (7). *Caution: working with high pressures is a potential safety hazard, and the reaction vessel should be tested above working pressures prior to usage*. Inside a glovebox, **5a** (140 mg, 0.24 mmol) was dissolved in benzene (10 mL) in a 50 mL Teflon stoppered Schlenk flask equipped with a stir bar. On a Schlenk line, the solution was thoroughly degassed by three freeze/pump/thaw cycles, then ethylene was added while the reaction flask was still cool (ca. 10 °C, 1 atm). The reaction vessel was heated to 40 °C for 5 days. Volatile components were removed under reduced pressure to prevent back reactions. The reaction vessel was brought back into a glovebox and fresh benzene (10 mL) was added. Outside the glovebox, the solution was degassed and ethylene (> 1 atm) was added as described above. The reaction vessel was then heated to 40 °C for an additional 5 days. Volatile components were removed under reduced pressure, and purification by SiO_2 column chromatography (eluting with 5% ethyl acetate/hexanes and then 10% ethyl acetate/hexanes) yielded the title compound as an analytically pure yellow solid (30 mg, 22%). X-Ray quality crystals were obtained by slow diffusion of pentane into toluene at -35 °C.

^{1}H NMR (benzene-d_6, 600.1 MHz): δ 8.36 (d, J = 8.5 Hz, 1H), 7.90 (d, J = 7.8 Hz, 1H), 7.52 (d, J = 1.7 Hz, 1H), 7.45 (d, J = 7.3 Hz, 2H), 7.40 (t, J = 7.7 Hz, 1H), 7.27 (t, J = 7.7 Hz, 3H), 7.19 – 7.11 (m, 1H), 7.02 (s, 1H), 6.76 (d, J = 5.9 Hz, 1H), 6.29 (dd, J = 5.9, 1.9 Hz, 1H), 3.21 (t, J = 8.1 Hz, 2H, PtCH$_2$**CH$_2$**Ph), 3.00 (s with ^{195}Pt satellites, J_{PtH} = 54 Hz, 4H, C_2H_4), 2.10 (t with ^{195}Pt satellites, J_{HH} = 8.2 Hz, J_{PtH} = 67 Hz, 2H, Pt**CH$_2$**CH$_2$Ph), 0.97 (s, 9H, ^tBu).

^{13}C{^{1}H} NMR (benzene-d_6, 150.9 MHz): δ 161.7, 157.1, 149.9, 147.7, 146.0, 141.8, 132.3, 128.9, 128.7, 128.4, 125.7, 124.2, 121.6, 119.9, 119.1, 116.5, 116.4, 104.0, 60.2, 39.1, 34.8, 29.9.

Anal. Calcd for $C_{27}H_{30}N_2Pt$: C, 56.14; H, 5.24; N 4.85. Found: C, 56.05; H, 5.41; N, 4.83.

Catalytic Methods

General Procedure for Ethylene Hydroarylation with Benzene-d_6 Using Catalysts 5a-5k, 6, and 7. Inside a glovebox, catalysts **5a-5k**, **6**, or **7** (0.0026 mmol, 3.7 mM), benzene-d_6 (0.7 mL), and a known amount of Si(SiMe$_3$)$_4$ as an internal standard, were added to a low pressure/vacuum (4 mm outer diameter, 3 mL) J. Young NMR tube. On a Schlenk line, the solution was thoroughly degassed by three freeze/pump/thaw cycles and ethylene (1 atm) was added at ambient temperature. The reaction vessel was submerged in a 100 °C bath. Product formation was monitored over a 24 h by ^{1}H NMR spectroscopy after 50, 100, 150, 200, 250, 300, 1370 min of heating. Product formation was determined by identifying new benzylic and methyl resonances in the ^{1}H NMR spectrum and comparing them to literature values.[45] Overall TON was determined by comparing the benzylic peak to the internal standard peak.

Selected ^{1}H NMR resonances for benzylic/methyl protons for C$_6$D$_5$C**H$_2$**C**H$_2$**D: ^{1}H NMR (benzene-d_6, 400.1 MHz): δ 2.44 (tt, J_{HH} = 7.5 Hz, J_{HD} = 1.1 Hz, 2H), 1.06 (tt, J_{HH} = 7.5 Hz, J_{HD} = 2.0 Hz, 2H). Polyethylbenzene formation was qualitatively identified by GC-MS after filtering through Al$_2$O$_3$ (Figure 2.4).

High Pressure Ethylene Hydroarylation with Benzene Using Catalyst 5a. *Caution: working with high pressures is a potential safety hazard, and the reaction vessel should be tested above working pressures prior to usage.* In a glovebox, a Fischer-Porter apparatus (50 mL) equipped with a stir bar was charged with catalyst **5a** (4.5 mg, 7.7 µmol, 3.7 mM) in benzene-d_6 (2.1 mL) with a known amount Si(SiMe$_3$)$_4$ as an internal standard. The apparatus was transferred onto a Schlenk line and attached to a high-pressure ethylene inlet. The reaction vessel was then purged with ethylene, pressurized to 3 atm, and then heated to 100 °C with vigorous stirring for 6 h. After this time, the reaction vessel was depressurized and cooled to ambient temperature. A ^{1}H NMR spectrum of the reaction mixture was acquired to determine ethylbenzene turnovers.

Propylene Hydroarylation with Benzene-d_6 Using Catalysts 5a-5k. In a similar manner to that described in the general procedure above, catalysts **5a-5k** (0.0026 mmol, 3.7 mM), benzene-d_6 (0.7 mL), propylene (1 atm), and a known amount of Si(SiMe$_3$)$_4$ as an internal standard were added to a low pressure/vacuum (4 mm outer diameter, 3 mL) J. Young NMR tube. The reaction vessel was submerged in a 100 °C bath. Product formation was monitored over a 24 h period by ^{1}H NMR spectroscopy after 50, 100, 150, 200, 250, 300, 1370 min of heating. Product formation was determined by identifying new benzylic and methyl resonances in the ^{1}H NMR spectrum and comparing them to literature values of cumene-d_6 (C$_6$D$_5$CHCH$_3$CH$_2$D)[71] and n-propylbenzene-d_6 (C$_6$D$_5$CH$_2$CHDCH$_3$)[72]. For product selectivity ratios, the ratio of the benzylic peaks for the two isomers was calculated by ^{1}H NMR spectroscopy. Overall TON was determined by comparing the benzylic peak to the internal standard peak for Si(SiMe$_3$)$_4$.

Selected ^{1}H NMR resonance for the benzylic proton for cumene-d_6 (C$_6$D$_5$C**H**(CH$_3$)(CH$_2$D)): ^{1}H NMR (benzene-d_6, 400.1 MHz): δ 2.70 (h, J_{HH} = 6.6 Hz, J_{HD} = 1.3 Hz).

Selected ^{1}H NMR peak for the benzylic protons for n-propylbenzene-d_6 (C$_6$D$_5$C**H$_2$**CHDCH$_3$): ^{1}H NMR (benzene-d_6, 400.1 MHz): δ 2.42 (dt, J_{HH} = 7.3 Hz, J_{HD} = 1.0 Hz).

Selected ^{1}H NMR peak for the benzylic protons for *n*-propylbenzene-d_0 (C$_6$H$_5$C**H$_2$**CH$_2$CH$_3$): ^{1}H NMR (benzene-d_6, 400.1 MHz): δ 2.43 (t, J_{HH} = 7.4 Hz).

Hydroarylation of *tert*-Butylethylene with Benzene-d_6 Using Catalyst 5a. Inside a glovebox, catalyst **5a** (0.0026 mmol, 0.3 mol% catalyst loading relative to olefin, 3.7 mM), benzene-d_6 (0.7 mL), *tert*-butylethylene (100 μL, 0.78 mmol), and a known amount of Si(SiMe$_3$)$_4$ as an internal standard, were heated to 100 °C for 24 h. A ^{1}H NMR spectrum was acquired and new benzylic peaks were identified for 2-*tert*-butyl-1-phenylethane and 1-*tert*-butyl-1-phenylethane. These peaks were in agreement with literature values.[73,74] The overall TON was determined by comparing the integration of the benzylic peaks to the standard peak, and product selectivity was determined as the ratio of the two new benzylic peaks.

Selected ^{1}H NMR resonances for the benzylic protons for 2-*tert*-butyl-1-phenylethane and 1-*tert*-butyl-1-phenylethane: ^{1}H NMR (300.1 MHz): δ 2.46 (dt, J_{HH} = 9.2 Hz, J_{HD} = 1.4 Hz), 2.41 (tt, J_{HH} = 6.3 Hz, J_{HD} = 1.3 Hz).

Attempted Hydroarylation of Cyclohexene with Benzene-d_6 Using Catalyst 5a. The general procedure was followed with **5a** (0.0026 mmol, 0.3 mol% catalyst loading relative to olefin, 3.7 mM), benzene-d_6 (0.7 mL), cyclohexene (8.0 μL, 0.082 mmol), and a known amount of Si(SiMe$_3$)$_4$ as a standard were heated to 100 °C for 24 h. A ^{1}H NMR spectrum was acquired. No new products were identified and cyclohexene was not consumed.

Attempted Hydroarylation of 1-Octene with Benzene-d_6 Using Catalyst 5a. Catalyst **5a** (0.0026 mmol, 0.3 mol% catalyst loading relative to olefin, 3.7 mM), benzene-d_6 (0.7 mL), 1-octene (100 μL, 0.64 mmol), and a known amount of Si(SiMe$_3$)$_4$ as a standard were heated to 100 °C for 24 h. A ^{1}H NMR spectrum indicated only isomerization to 2-octene. No other products were identified.

Ethylene Hydroarylation with Benzene Using Catalyst 5a. In a similar manner to that described in the general procedure above, catalyst **2a** (1.5 mg, 0.0026 mmol, 3.7 mM), benzene (0.7 mL), ethylene (1 atm), and a known amount of Si(SiMe$_3$)$_4$ as a standard were added to a low pressure/vacuum (4 mm outer diameter, 3 mL) J. Young NMR tube. The reaction vessel was submerged in a 100 °C bath for 24 h. The reaction mixture was then cooled to ambient temperature and an aliquot of the reaction mixture was diluted in chloroform-d_1. Product formation was determined by identifying new benzylic and methyl resonances in the ^{1}H NMR spectrum and comparing them to known literature values in chloroform-d_1.[75] TON was determined by comparing the benzylic peak to the internal standard peak.

Selected ^{1}H NMR resonances for benzylic/methyl protons for C$_6$H$_5$C**H$_2$**C**H$_3$**: ^{1}H NMR (chloroform-d_1, 400.1 MHz): δ 2.65 (q, *J* = 7.6 Hz, 2H), 1.22 (t, *J* = 7.6, 3H).

Competitive Ethylene Hydroarylation with Equimolar Benzene and Benzene-d_6 Using Catalyst 5a. In a similar manner to that described in the general procedure above, catalyst **5a** (1.5 mg, 0.0026 mmol, 3.3 mM), benzene (0.4 mL), benzene-d_6 (0.4 mL), ethylene (1 atm), and a known amount of Si(SiMe$_3$)$_4$ as a standard were added to a low pressure/vacuum (4 mm outer diameter, 3 mL) J. Young NMR tube. The reaction vessel was submerged in a 100 °C bath for 24 h. The ratio of C$_6$H$_5$CH$_2$CH$_3$ to C$_6$D$_5$CH$_2$CH$_2$D was determined by ^{1}H and ^{13}C{^{1}H} NMR spectroscopy (Figure S15). In the ^{1}H NMR spectrum, the ratio was calculated by integration of the benzylic proton resonances. In ^{13}C{^{1}H} NMR spectrum, the ratio was calculated by integration of the methyl CH$_3$ and CH$_2$D resonances [selected NMR value for mixture of C$_6$D$_5$CH$_2$CH$_3$ and C$_6$D$_5$CH$_2$CH$_2$D: ^{13}C{^{1}H} NMR (benzene-d_6, 226.4 MHz, D_1 = 60.0 s, temp = 298.0 K): δ 15.9 (s, measure T_1 = 3.9 s), 15.5 (t, J_{CD} = 19.2 Hz, measured T_1 = 4.3 s)].[76]

Hydroarylation of Ethylene with Toluene Using Catalyst 5a. Inside a glove box, catalyst **5a** (0.0026 mmol, 3.7 mM), toluene (0.7 mL) and tridecane as an internal standard (7 µL, 0.029 mmol) were added to a low pressure/vacuum (4 mm outer diameter, 3 mL) J. Young NMR tube. On a Schlenk line, the solution was thoroughly degassed by three freeze/pump/thaw cycles and then ethylene (1 atm) was added at ambient temperature. The reaction vessel was submerged in a 100 °C bath for 24 h. GC calibration curves and response factors were generated for authentic samples of *o*-ethyltoluene, *m*-ethyltoluene, and *p*-ethyltoluene versus a tridecane standard using known concentrations in ethyl acetate. The signals corresponding to *m*- and *p*-ethyltoluene could not be resolved and were integrated as a single peak. A 300 µL aliquot of the reaction mixture was dissolved in 1.5 mL ethyl acetate and filtered over a short plug of Al$_2$O$_3$ to remove any residual metal complexes. Using the response factor, this sample was then analyzed by GC to determine overall TON and product selectivity for *o*-ethyltoluene versus the mixture of *m*- and *p*-ethyltoluene.

Ethylene Hydroarylation with Mesitylene Using Catalyst 5a. In a similar manner to that described in the general procedure above, catalyst **5a** (0.0026 mmol, 3.7 mM), mesitylene (0.7 mL), ethylene (1 atm), and a known amount of Si(SiMe$_3$)$_4$ were added to a low pressure/vacuum (4 mm outer diameter, 3 mL) J. Young NMR tube. The reaction vessel was submerged in a 100 °C bath for 24 h. The reaction mixture was cooled to ambient temperature and an aliquot was diluted in chloroform-d_1. Product formation was determined by identifying new benzylic and methyl resonances in the ^{1}H NMR spectrum and comparing them to known literature values of 1-ethyl-2,4,6-trimethylbenzene.[77] Overall TON was determined by comparing the benzylic peak to the internal standard peak for Si(SiMe$_3$)$_4$.

Selected ^{1}H NMR resonances for benzylic/methyl protons for 1-ethyl-2,4,6-trimethylbenzene: ^{1}H NMR (chloroform-d_1, 400.1 MHz): δ 2.60 (q, J = 7.4 Hz, 2H), 2.29 (s, 6H), 2.25 (s, 3H), 1.08 (t, J = 7.6 Hz, 3H).

Ethylene Hydroarylation with Benzene-d_6 Using 5a with Added Base. In a similar manner to that described in the general procedure above, catalyst **5a** (0.0026 mmol, 3.7 mM), benzene-d_6 (0.7 mL), 2,6-di-*tert*-butyl-4-methylpyridine (11 mg, 0.054 mmol, 20 equiv relative to **5a**), ethylene (1 atm) and a known amount of Si(SiMe$_3$)$_4$ as an internal standard were added to a low pressure/vacuum (4 mm outer diameter, 3 mL) J. Young NMR tube. The reaction vessel was submerged in a 100 °C bath. Product formation was monitored over a 24 h period by ^{1}H NMR spectroscopy after 50, 100, 150, 200, 250, 300, 1370 min of heating.

Ethylene Hydroarylation with Benzene-*d₆* Using Catalyst 5a or 7 with Added Dimethyl Sulfide. In a similar manner to that described in the general procedure above, **5a** or **7** (0.0026 mmol, 3.7 mM), benzene-*d₆* (0.7 mL), dimethyl sulfide (2.0 μL, 0.026 mmol, 10 equiv. relative to [Pt]), ethylene (1 atm), and a known amount of a $Si(SiMe_3)_4$ internal standard were added to a low pressure/vacuum (4 mm outer diameter, 3 mL) J. Young NMR tube. The reaction vessel was submerged in a 100 °C bath. Product formation was monitored over a 24 h period by ^{1}H NMR spectroscopy after 50, 100, 150, 200, 250, 300, 1370 min of heating.

Ethylene Hydroarylation with Benzene-*d₆* Using Catalysts 5a or 6 in the Presence of Hg(0). In a similar manner to that described in the general procedure above, catalyst **5a** or **6** (0.0026 mmol, 3.7 mM), benzene-*d₆* (0.7 mL), ethylene (1 atm), a known amount of $Si(SiMe_3)_4$ as an internal standard, and Hg(0) (ca. 1 pipette drop) were added to a low pressure/vacuum (4 mm outer diameter, 3 mL) J. Young NMR tube. The reaction mixture was submerged in a 100 °C bath. Product formation was monitored over a 24 h period by ^{1}H NMR spectroscopy after 50, 100, 150, 200, 250, 300, 1370 min of heating.

Ethylene Hydroarylation with Benzene-*d₆* Using Catalysts 5a or 6, Pre-Stirring with Hg(0). In a glovebox, catalyst **5a** or **6** (0.0026 mmol, 3.7 mM) and a known amount $Si(SiMe_3)_4$ as a standard were dissolved in benzene-*d₆* (0.7 mL). This solution was stirred at ambient temperature with Hg(0) (ca. 1 pipette drop) for 30 min. The solution was decanted and then filtered over Celite to remove residual Hg(0) from the reaction mixture. This solution was then added to a low pressure/vacuum (4 mm outer diameter, 3 mL) J. Young NMR tube. On a Schlenk line, the solution was thoroughly degassed by three freeze/pump/thaw cycles and then ethylene (1 atm) was added at ambient temperature. The reaction vessel was submerged in a 100 °C bath. Product formation was monitored over a 24 h period by ^{1}H NMR spectroscopy after 50, 100, 150, 200, 250, 300, 1370 min of heating.

Thermolysis Reactions using Compounds 5a, 6 or 7 in Benzene-*d₆*. Inside a glovebox, **5a**, **6**, or **7** (0.0086 mmol, 8.6 mM) and a known amount of $Si(SiMe_3)_4$ as an internal standard were dissolved in benzene-*d₆* (1 mL) and added to a low pressure/vacuum (4 mm outer diameter, 3 mL) J. Young NMR tube. The reaction vessel was submerged in a 100 °C bath for 48 h. The reaction mixture was monitored by ^{1}H NMR spectroscopy after 50, 100, 1370, 2810 min of heating.

Thermolysis of 5a in Benzene-*d₆* in the Presence of Hg(0). In a glovebox, catalyst **5a** (0.0026 mmol, 3.7 mM), benzene-*d₆* (0.7 mL), a known amount of $Si(SiMe_3)_4$ as a standard, and Hg(0) (ca. 1 pipette drop) were added to a low pressure/vacuum (4 mm outer diameter, 3 mL) J. Young NMR tube. The reaction vessel was submerged in a 100 °C bath. Product formation was monitored over a 24 h period by ^{1}H NMR spectroscopy after 50, 100, 150, 200, 250, 300, 1370 min of heating.

Variable Temperature ^{1}H NMR Spectroscopy with Compounds 5a, 6 or 7. In a similar manner to that described in the general procedure above, catalysts **5a**, **6** or **7** (0.0026 mmol, 3.7 mM), benzene-d_6 (0.7 mL), ethylene (1 atm), and a known amount of Si(SiMe$_3$)$_4$ as a standard were added to a low pressure/vacuum (4 mm outer diameter, 3 mL) J. Young NMR tube. An NMR spectrometer (500.2 MHz) was preheated to 80 °C. The temperature was separately calibrated using the peak-to-peak separation of resonances in neat ethylene glycol (measured temp = 353 K). Once the spectrometer reached temperature, the J. Young reaction vessel was injected into the spectrometer. Scans were taken every 10 min over a 3 h time span. Products were quantified versus the internal standard. The identity of Pt based species was identified versus authentic samples (*vide supra*).

Styrene Determination in Ethylene Hydroarylation with Benzene Using Catalyst 5a. In a similar manner to that described in the general procedure above, catalyst **5a** (1.5 mg, 0.0026 mmol, 3.7 mM), benzene-d_6 (0.7 mL), ethylene (1 atm), and a known amount of Si(SiMe$_3$)$_4$ as a standard were added to a low pressure/vacuum (4 mm outer diameter, 3 mL) J. Young NMR tube. The reaction vessel was submerged in a 100 °C bath for 24 h. The reaction mixture was then cooled to ambient temperature and degassed by three freeze/pump/thaw cycles. Vinylic resonances for styrene,[78] β-(*E*)-deuterostyrene,[79] and β-(*Z*)-deuterostyrene[79] were identified in the ^{1}H NMR spectrum and were in agreement with reported literature values. Products were quantified versus the internal standard.

Selected ^{1}H NMR resonances for the vinylic protons in styrene (PhC**H**=C**H$_2$**): ^{1}H NMR (benzene-d_6, 400.1 MHz): δ 6.57 (dd, *J* = 18.3, 11.0 Hz), 5.59 (dd, *J* = 17.6, 1.3 Hz), 5.06 (dd, *J* = 10.9, 1.2 Hz).

Selected ^{1}H NMR resonances for the vinylic protons in β-(*E*)-deuterostyrene (PhC**H**=C**H**D: ^{1}H NMR (benzene-d_6, 400.1 MHz): δ 6.64 (bd, *J* = 17.9 Hz), 5.69 (bd, *J* = 17.9 Hz).

Selected ^{1}H NMR resonances for the vinylic protons in β-(*Z*)-deuterostyrene: ^{1}H NMR (benzene-d_6, 400.1 MHz): 6.67 (bd, *J* = 10.5 Hz), 5.16 (bd, *J* = 10.9 Hz).

Determination of Decomposition Products and Organometallic Speciation in Ethylene Hydroarylation with Benzene Using Catalyst 5a. In a glovebox, catalyst **5a** (21 mg, 0.036 mmol, 7.2 mM) was dissolved in benzene (5 mL) in a 100 mL Teflon stoppered Schlenk flask equipped with a stir bar. On a Schlenk line, the solution was thoroughly degassed by three freeze/pump/thaw cycles and then ethylene (1 atm) was added at ambient temperature. The reaction mixture was heated to 100 °C for 20 h. The reaction mixture was then cooled to ambient temperature and volatile components were removed under reduced pressure. Dichloromethane was added to the residue. The resultant solution was spotted onto a preparatory SiO$_2$ TLC plate (eluting with 10% ethyl acetate/hexanes) in order to separate Pt(0) from organometallic and ligand species. Two broad bands (R_f = 0.40-0.55, and 0.02-0.10) were observed. The top band was physically removed and the products were extracted with dichloromethane (2 x 10 mL). The solution was filtered to remove residual SiO$_2$. An aliquot of the resultant solution was filtered over Al$_2$O$_3$ and a HRMS (ESI-TOF) was acquired. The results are summarized in Table 2.3.

Table 2.4. Summary of crystallographic data for complexes **5a-5c**, **5l**, **6**, and **7**.

Compound	5a	5b	5c	5l	6	7
Formula	$C_{25}H_{28}N_2PtS$	$C_{25}H_{26}F_2N_2PtS$	$C_{25}H_{24}F_4N_2PtS$	$C_{20}H_{22}F_4N_2PtS$	$C_{25}H_{26}N_2Pt$	$C_{27}H_{30}N_2Pt$
Formula Mass	583.64	619.64	655.62	593.55	549.58	577.62
Crystal System	Monoclinic	Triclinic	Triclinic	Monoclinic	Monoclinic	Monoclinic
Space Group	C2/c	P-1	P-1	P2$_1$/c	C2/c	P2$_1$/c
a (Å)	25.6857(8)	9.0052(4)	8.9213(5)	12.7623(12)	30.2380(10)	9.0700(3)
b (Å)	11.6427(4)	10.3193(5)	10.1362(5)	18.0135(17)	12.4961(4)	22.5628(8)
c (Å)	18.7609(6)	13.9951(6)	14.7554(8)	8.8929(9)	13.1254(4)	10.8200(4)
α (°)	90	90.135(2)	97.236(3)	90	90	90
β (°)	116.0020(10)	92.418(2)	90.819(3)	100.840(4)	106.172(2)	96.155(2)
γ (°)	90	94.402(2)	94.146(3)	90	90	90
Unit Cell Volume (Å^3)	5042.6(3)	1295.52(10)	1319.84(12)	2007.9(3)	4763.3(3)	2201.49(13)
Z	8	2	2	4	8	4
Crystal Size (mm^3)	0.07 x 0.05 x 0.01	0.10 x 0.05 x 0.01	0.11 x 0.10 x 0.03	0.10 x 0.09 x 0.02	0.06 x 0.04 x 0.01	0.09 x 0.04 x 0.01
Reflections Collected	35910	29536	35194	3638	30377	34268
Independent Reflections	4634	4718	4860	3638	4379	4007
R$_{int}$	0.0267	0.0276	0.0266	0.0000	0.0536	0.0398
Completeness to θ = 25.000° (%)	100.0	99.4	99.9	98.5	100.0	99.6
Final R indices (I > 2σ(I))	0.0139	0.0172	0.0131	0.0475	0.0264	0.0230
Final R indices (all data)	0.0147	0.0178	0.0142	0.0490	0.0381	0.0298
Goodness-of-Fit of F^2	1.041	1.050	1.047	1.055	1.066	1.090

Note: Complete crystallographic data can be found in the CIF files in Appendix A as well as the supplemental information of Suslick, B. A.; Liberman-Martin, A. L.; Wambach, T. C.; Tilley, T. D. *ACS Catal.* **2017**, *7*, 4313–4322.

References

1. Welch, V. A.; Fallon, K. J.; Gelbke, H.-P. *Ullmann's Encyclopedia of Industrial Chemistry* **2005**, *13*, 451-464.

2. James, D. H.; Castor, W. M. *Ullmann's Encyclopedia of Industrial Chemistry* **2011**, *34*, 529-544.

3. Maul, J.; Frushour, B. G.; Kontoff, J. R.; Eichenauer, H.; Ott, K.-H.; Schade, C. *Ullmann's Encyclopedia of Industrial Chemistry* **2012**, *29*, 475-522.

4. Hartwig, J. F. *Organotransition Metal Chemistry: From Bonding to Catalysis*; University Science Books: Mill Valley, CA, 2010.

5. Kambe, N.; Iwasaki, T.; Terao, J. *Chem. Soc. Rev.* **2011**, *40*, 4937-4947.

6. Goldman, A. S.; Goldberg, K. I. In *Activation and Functionalization of C—H Bonds*; American Chemical Society: 2004; Vol. 885, p 1-43.

7. Lersch, M.; Tilset, M. *Chemical Reviews* **2005**, *105*, 2471-2526.

8. Colby, D. A.; Tsai, A. S.; Bergman, R. G.; Ellman, J. A. *Acc. Chem. Res.* **2012**, *45*, 814-825.

9. DeMott, J. C.; Bhuvanesh, N.; Ozerov, O. V. *Chem. Sci.* **2013**, *4*, 642-649.

10. Andreatta, J. R.; McKeown, B. A.; Gunnoe, T. B. *J. Organomet. Chem.* **2011**, *696*, 305-315.

11. Chianese, A. R.; Lee, S. J.; Gagné, M. R. *Angew. Chem. Int. Ed.* **2007**, *46*, 4042-4059.

12. Moselage, M.; Li, J.; Ackermann, L. *ACS Catalysis* **2016**, *6*, 498-525.

13. Kakiuchi, F.; Murai, S. *Acc. Chem. Res.* **2002**, *35*, 826-834.

14. Murai, S.; Kakiuchi, F.; Sekine, S.; Tanaka, Y.; Kamatani, A.; Sonoda, M.; Chatani, N. *Nature* **1993**, *366*, 529.

15. Kakiuchi, F.; Kochi, T.; Mizushima, E.; Murai, S. *J. Am. Chem. Soc.* **2010**, *132*, 17741-17750.

16. Foley, N. A.; Lee, J. P.; Ke, Z.; Gunnoe, T. B.; Cundari, T. R. *Acc. Chem. Res.* **2009**, *42*, 585-597.

17. Lee, J. P.; Jimenez-Halla, J. O. C.; Cundari, T. R.; Gunnoe, T. B. *J. Organomet. Chem.* **2007**, *692*, 2175-2186.

18. Foley, N. A.; Lail, M.; Lee, J. P.; Gunnoe, T. B.; Cundari, T. R.; Petersen, J. L. *J. Am. Chem. Soc.* **2007**, *129*, 6765-6781.

19. Foley, N. A.; Lail, M.; Gunnoe, T. B.; Cundari, T. R.; Boyle, P. D.; Petersen, J. L. *Organometallics* **2007**, *26*, 5507-5516.

20. Kumar, N. Y. P.; Bechtoldt, A.; Raghuvanshi, K.; Ackermann, L. *Angew. Chem. Int. Ed.* **2016**, *55*, 6929-6932.

21. Schinkel, M.; Wallbaum, J.; Kozhushkov, S. I.; Marek, I.; Ackermann, L. *Org. Lett.* **2013**, *15*, 4482-4484.

22. Matsumoto, T.; Taube, D. J.; Periana, R. A.; Taube, H.; Yoshida, H. *J. Am. Chem. Soc.* **2000**, *122*, 7414-7415.

23. Periana, R. A.; Liu, X. Y.; Bhalla, G. *Chem. Commun.* **2002**, 3000-3001.

24. Bhalla, G.; Oxgaard, J.; Goddard, W. A.; Periana, R. A. *Organometallics* **2005**, *24*, 3229-3232.

25. Oxgaard, J.; Muller, R. P.; Goddard, W. A.; Periana, R. A. *J. Am. Chem. Soc.* **2004**, *126*, 352-363.

26. Oxgaard, J.; Periana, R. A.; Goddard, W. A. *J. Am. Chem. Soc.* **2004**, *126*, 11658-11665.

27. Crisenza, G. E. M.; McCreanor, N. G.; Bower, J. F. *J. Am. Chem. Soc.* **2014**, *136*, 10258-10261.

28. Ebe, Y.; Nishimura, T. *J. Am. Chem. Soc.* **2015**, *137*, 5899-5902.

29. Sevov, C. S.; Hartwig, J. F. *J. Am. Chem. Soc.* **2013**, *135*, 2116-2119.

30. Vaughan, B. A.; Webster-Gardiner, M. S.; Cundari, T. R.; Gunnoe, T. B. *Science* **2015**, *348*, 421-424.

31. Webster-Gardiner, M. S.; Fu, R.; Fortman, G. C.; Nielsen, R. J.; Gunnoe, T. B.; Goddard III, W. A. *Catalysis Science & Technology* **2015**, *5*, 96-100.

32. Webster-Gardiner, M. S.; Piszel, P. E.; Fu, R.; McKeown, B. A.; Nielsen, R. J.; Goddard, W. A.; Gunnoe, T. B. *J. Mol. Catal. A: Chem.* **2017**, *426*, 381-388.

33. Vaughan, B. A.; Khani, S. K.; Gary, J. B.; Kammert, J. D.; Webster-Gardiner, M. S.; McKeown, B. A.; Davis, R. J.; Cundari, T. R.; Gunnoe, T. B. *J. Am. Chem. Soc.* **2017**, *139*, 1485-1498.

34. Filloux, C. M.; Rovis, T. *J. Am. Chem. Soc.* **2015**, *137*, 508-517.

35. Harada, H.; Thalji, R. K.; Bergman, R. G.; Ellman, J. A. *The Journal of Organic Chemistry* **2008**, *73*, 6772-6779.

36. Jun, C. H.; Hong, J. B.; Kim, Y. H.; Chung, K. Y. *Angew. Chem. Int. Ed.* **2000**, *39*, 3440-3442.

37. Lim, S.-G.; Ahn, J.-A.; Jun, C.-H. *Org. Lett.* **2004**, *6*, 4687-4690.

38. Ryu, J.; Cho, S. H.; Chang, S. *Angew. Chem. Int. Ed.* **2012**, *51*, 3677-3681.

39. Sun, Z.-M.; Zhang, J.; Manan, R. S.; Zhao, P. *J. Am. Chem. Soc.* **2010**, *132*, 6935-6937.

40. Tsui, G. C.; Menard, F.; Lautens, M. *Org. Lett.* **2010**, *12*, 2456-2459.

41. Podhajsky, S. M.; Iwai, Y.; Cook-Sneathen, A.; Sigman, M. S. *Tetrahedron* **2011**, *67*, 4435-4441.

42. Cacchi, S. *Pure Appl. Chem.* **1990**, *62*, 713-722.

43. McKeown, B. A.; Foley, N. A.; Lee, J. P.; Gunnoe, T. B. *Organometallics* **2008**, *27*, 4031-4033.

44. Luedtke, A. T.; Goldberg, K. I. *Inorg. Chem.* **2007**, *46*, 8496-8498.

45.   Luedtke, A. T.; Goldberg, K. I. *Angew. Chem. Int. Ed.* **2008**, *47*, 7694-7696.

46.   McKeown, B. A.; Gonzalez, H. E.; Friedfeld, M. R.; Gunnoe, T. B.; Cundari, T. R.; Sabat, M. *J. Am. Chem. Soc.* **2011**, *133*, 19131-19152.

47.   Karshtedt, D.; Bell, A. T.; Tilley, T. D. *Organometallics* **2004**, *23*, 4169-4171.

48.   Karshtedt, D.; McBee, J. L.; Bell, A. T.; Tilley, T. D. *Organometallics* **2006**, *25*, 1801-1811.

49.   Liu, Q. D.; Mudadu, M. S.; Thummel, R.; Tao, Y.; Wang, S. *Adv. Funct. Mater.* **2005**, *15*, 143-154.

50.   Clement, M. L.; Grice, K. A.; Luedtke, A. T.; Kaminsky, W.; Goldberg, K. I. *Chemistry – A European Journal* **2014**, *20*, 17287-17291.

51.   Cundari, T. R.; Gonzalez, H. E. *J. Mol. Catal. A: Chem.* **2012**, *353-354*, 1-6.

52.   McKeown, B. A.; Gonzalez, H. E.; Michaelos, T.; Gunnoe, T. B.; Cundari, T. R.; Crabtree, R. H.; Sabat, M. *Organometallics* **2013**, *32*, 3903-3913.

53.   McKeown, B. A.; Gonzalez, H. E.; Gunnoe, T. B.; Cundari, T. R.; Sabat, M. *ACS Catalysis* **2013**, *3*, 1165-1171.

54.   Simmons, E. M.; Hartwig, J. F. *Angew. Chem. Int. Ed.* **2012**, *51*, 3066-3072.

55.   Craig, N. C.; Groner, P.; McKean, D. C. *The Journal of Physical Chemistry A* **2006**, *110*, 7461-7469.

56.   Bowring, M. A.; Bergman, R. G.; Tilley, T. D. *Organometallics* **2011**, *30*, 1295-1298.

57.   Szuromi, E.; Sharp, P. R. *Organometallics* **2006**, *25*, 558-559.

58.   Widegren, J. A.; Finke, R. G. *J. Mol. Catal. A: Chem.* **2003**, *198*, 317-341.

59.   Whitesides, G. M.; Hackett, M.; Brainard, R. L.; Lavalleye, J. P. P. M.; Sowinski, A. F.; Izumi, A. N.; Moore, S. S.; Brown, D. W.; Staudt, E. M. *Organometallics* **1985**, *4*, 1819-1830.

60.   Bayram, E.; Linehan, J. C.; Fulton, J. L.; Szymczak, N. K.; Finke, R. G. *ACS Catalysis* **2015**, *5*, 3876-3886.

61.   Hagen, C. M.; Widegren, J. A.; Maitlis, P. M.; Finke, R. G. *J. Am. Chem. Soc.* **2005**, *127*, 4423-4432.

62.   Naqvi, K. R.; Marsh, J.; Chechik, V. *Dalton Trans.* **2014**, *43*, 4745-4751.

63.   Kent, P. D.; Mondloch, J. E.; Finke, R. G. *J. Am. Chem. Soc.* **2014**, *136*, 1930-1941.

64.   Besson, C.; Finney, E. E.; Finke, R. G. *J. Am. Chem. Soc.* **2005**, *127*, 8179-8184.

65.   Pal, S.; Kusumoto, S.; Nozaki, K. *Organometallics* **2017**, *36*, 502-505.

66.   Perera, S.; Li, X.; Guo, M.; Wesdemiotis, C.; Moorefield, C. N.; Newkome, G. R. *Chem. Commun.* **2011**, *47*, 4658-4660.

67.   Rashidi, M.; Fakhroeian, Z.; Puddephatt, R. J. *J. Organomet. Chem.* **1991**, *406*, 261-267.

68.   Hill, G. S.; Irwin, M. J.; Redina, L. M.; Puddephatt, R. J.; Andersen, R. A.; McLean, L. In *Inorg. Synth.*; Darensbourg, M. Y., Ed.

69.   Steele, B. R.; Vrieze, K. *Transition Metal Chemistry* **1977**, *2*, 140-144.

70.   Grice, K. A., University of Washington, Seattle 2010.

71.   Calvo, B.; Wuttke, J.; Braun, T.; Kemnitz, E. *ChemCatChem* **2016**, *8*, 1945-1950.

72.   Simonneau, A.; Friebel, J.; Oestreich, M. *Eur. J. Org. Chem.* **2014**, *2014*, 2077-2083.

73.   Le Bailly, B. A. F.; Greenhalgh, M. D.; Thomas, S. P. *Chem. Commun.* **2012**, *48*, 1580-1582.

74.   Andersson, S.; Drakenberg, T. *Organic Magnetic Resonance* **1983**, *21*, 730-744.

75.   Carter, T. S.; Guiet, L.; Frank, D. J.; West, J.; Thomas, S. P. *Adv. Synth. Catal.* **2013**, *355*, 880-884.

76.   Borovik, A. S.; Barron, A. R. *Main Group Chem.* **2005**, *4*, 135-144.

77.   Hartgers, W. A.; Damaste, J. S. S.; Koopmans, M. P.; de Leeuw, J. W. *J. Chem. Soc., Chem. Commun.* **1993**, 1715-1716.

78.   Hommeltoft, S. I.; Berry, D. H.; Eisenberg, R. *J. Am. Chem. Soc.* **1986**, *108*, 5345-5347.

79.   Kapeller, D.; Barth, R.; Mereiter, K.; Hammerschmidt, F. *J. Am. Chem. Soc.* **2007**, *129*, 914-923.

Chapter Three

Mechanistic Interrogation of Alkyne Hydroarylations Catalyzed by Highly Reduced, Single-Component Cobalt Complexes

Introduction. Chelation-assisted C–H activations allow selective functionalization of unreactive C–H bonds, thereby accessing atom-economical, late-stage molecular modifications without the installation of wasteful cross-coupling partners.[1-9] In this context, hydroarylation has emerged as an attractive method to form C–C bonds *via* the addition of activated aryl C–H bonds across olefins or alkynes. In the past two decades, catalyst development for such reactions has been aided by mechanistic investigations.[2,8-10] The first report of olefin hydroarylation from the Murai group[11,12] described RuH$_2$(CO)(PPh$_3$)$_3$ as the precatalyst and more recent advances in hydroarylations are based on precatalysts bearing a metal center with a square-planar, d^8 configuration (e.g., Rh(I),[13-18] Ir(I)[19-21] Pd(II),[22] and Pt(II)[23-25]). Significantly, mechanistic studies with these second- and third-row transition metal catalysts implicate a rate-limiting C–H addition.[23-26] By comparison, far fewer first-row transition metal hydroarylation catalysts have been identified, despite recent efforts to exploit the high abundance and low costs[27] of Fe,[28] Co,[3,29] and Ni.[30-34] Future catalyst designs should rely on mechanistic information that is largely nonexistent, and notably, first-row metals often engage in mechanisms that are distinctly different from those of heavier transition metals.[2,5,35]

Recent developments in Co-catalyzed *ortho*-hydroarylations illustrate the potential for highly active first-row transition metal complexes to participate in C–H activation chemistry.[29,36-46] Two distinct classes of Co precatalysts have been discovered, based on either high- or low-valent cobalt. For well-defined, high-valent Co(III) complexes, DFT calculations suggest that a redox-neutral C–H activation step is plausible.[36-38,47,48] Additionally, the isolation of cyclometalated intermediates implicate the operation of alkyne insertion and C–H reductive elimination steps in the catalytic cycle.[37,47] In comparison, mechanisms for low-valent Co catalysis remain elusive.

Low-valent cobalt catalysts for the hydroarylation of alkynes have been generated *in situ* and have been extensively studied by the Yoshikai group.[29,39-45] The uncharacterized, active catalytic species is generated by treatment of CoBr$_2$ with certain Grignard reagents (e.g., ^{t}BuCH$_2$MgBr and Me$_3$SiCH$_2$MgBr) in the presence of added ligands and substrates. Additionally, the resultant hydroarylation products form as a mixture of *E*- and *Z*-olefins and this aspect of the mechanism is also not understood.

Several plausible catalytic cycles have been proposed for the catalytic hydroarylation of (*N*-aryl)aryl ethanimines with internal alkynes;[29] however, specific details about the nature of the catalytic intermediates (e.g., oxidation states, ligand sphere, etc.) or the initiation pathway have remained unclear. The Grignard reagent has been proposed to reduce the Co(II) precatalyst to a Co(I) or Co(0) active species, possibly *via* a radical-based, one-electron reductive coupling.[2,3] While metal-hydride complexes are implicated as key intermediates, such species have yet to be observed. The work described here addresses the mechanism of alkyne hydroarylation by low-valent cobalt, with reactivity studies that provide insight into the nature of the catalytically active species, the catalytic cycle, and the concurrent olefin isomerization.

Conditions for Catalytic Hydroarylation. Investigations began with examination of a particular "one-pot" transformation closely related to those described by Yoshikai and coworkers[29] involving hydroarylation of diphenylacetylene by an (*N*-aryl)aryl ethanimine, with a CoCl$_2$/RMgCl (R = -CH$_2$CMe$_3$, -CH$_2$SiMe$_3$)/P(3-Cl-C$_6$H$_4$)/pyridine catalyst system. For these reactions, reported yields range from 60-95% and favor the *E*-isomer as the product (*Z/E* ratios of ca. 0.1-0.2). The reaction chosen for study also utilized and *in situ*-generated catalyst from a CoCl$_2$/CyMgCl/PPh$_3$ mixture. In this case, the hydroarylation of **1a** was found to proceed in 33% yield, but surprisingly with *Z*-selectivity and a relatively high *Z/E* ratio of 5.7 after hydrolysis (eq 3.1). It is worth noting that *Z*-selective catalysis has also been observed by the Petit group[49] using Co(I)-PMe$_3$ precatalysts and microwave conditions.

1) CoCl$_2$, 10 mol%
   CyMgCl, 40 mol%
   PPh$_3$, 30 mol%
   PhCCPh, 1 equiv
   THF (0.1 M), 65 °C, 20 h
2) H$^+$

1a
PMP = *p*-methoxyphenyl

Z/E-2a
33%
Z/E = 5.7

(3.1)
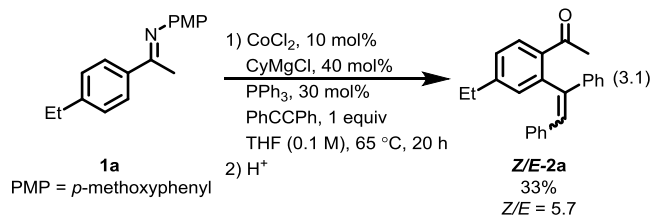
Previous reports of such reactions speculated that the reducing conditions likely give rise to a low-valent catalytically active species formed by the reduction of Co(II) precursors by the Grignard reagent.[2,3,29,39] To more thoroughly probe the nature of the active catalyst, the well-defined Co(I) complex (PPh$_3$)$_3$CoCl[50] (**Co-Cl**) was investigated as a catalyst precursor. Complex **Co-Cl** is not a competent single-component hydroarylation catalyst (Table 3.1); however, treatment of **Co-Cl** with two equivs of CyMgCl produced a catalytic species giving yields similar to those observed with CoCl$_2$/PPh$_3$ in the presence of activators (eq 3.1). Since previous reports have indicated a dramatic effect associated with the nature of the Grignard reagent,[29,39] catalysis with **Co-Cl** was examined with a range of organometallic activators (Table 3.1). The best results were obtained with CyMgCl, and in general it appears that β-hydrogens in the alkyl group of the magnesium reagent lead to better results.

In general, organomagnesium reagents were observed to out-perform more reactive organolithium reagents. In some cases, no catalysis resulted from treatment of **Co-Cl** with an organolithium. In contrast to results reported by the Yoshikai group[29,39-45] where *E*-products are favored (*vide supra*), the *Z*-isomer (formally a *trans*-insertion product) is the major species with all the activators tested. Additionally, the degree of *Z*-selectivity was found to vary with the organometallic activator employed. Activators bearing β-CH$_2$ fragments (e.g., EtMgCl, CyMgCl, or ^{n}Bu$_2$Mg) successfully activated **Co-Cl** towards productive catalysis.

Table 3.1. Effects of Organometallic Activator Identity.
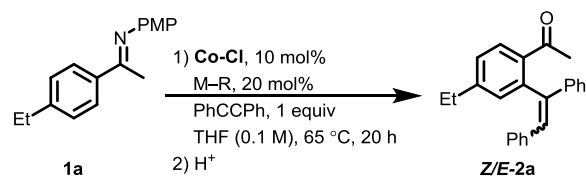
M–R	^{1}H NMR Yield (%) [a]	Z/E [a]
–	0	–
^{n}BuLi	5	4.4
PhLi	< 2	–
MesLi	12	33
MeMgCl	< 2	–
EtMgCl	32	5.1
H$_2$C=CHMgBr [b]	33	27
CyMgCl	33	> 100
CyMgCl [b]	84	> 100
^{n}Bu$_2$Mg	55	> 100
Mes$_2$Mg	10	14
Bn$_2$Mg	41	5.2
Ph$_2$Zn	5	23

[a] As measured by ^{1}H NMR spectroscopy of the crude reaction mixture vs Si(SiMe$_3$)$_4$ as an internal standard. [b] An equivalent of pyridine was added.

Optimization of catalytic conditions with **Co-Cl** and CyMgCl revealed several insights. First, Yoshikai and coworkers[29] observed that addition of an equivalent of pyridine greatly improved yields (a two-fold increase in some cases). Similarly, addition of 1 equiv of pyridine (relative to substrates) to a catalytic mixture derived from **Co-Cl**/CyMgCl improved ^{1}H NMR yields from 33 to 84% (Table 3.2). Also, catalytic efficiencies modestly improved with addition of 5% v/v TMEDA or 1,4-dioxane to 45 and 42%, respectively (Table 3.2). The possible role of adventitious acid in this catalysis (e.g., to facilitate Friedel-Crafts processes) was addressed by addition of one equivalent (relative to Co) of a proton scavenger. Thus, the non-coordinating base 2,6-di-*tert*-butyl-4-methylpyridine was added in lieu of pyridine to the catalytic mixture. This experiment illustrates that the catalytic yield is unaffected by the presence of this compound (Table 3.2). However, stoichiometric addition (relative to Co) of strongly coordinating *N*-heterocyclic carbene ligands (e.g., IMes or IPr) in the presence or absence of pyridine resulted in complete catalytic inhibition (Table 3.2).

Table 3.2. Effects of Added Reagents on the Catalytic Hydroarylation of 1a with Diphenylacetylene.
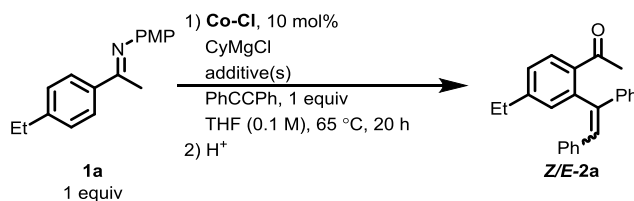
Additive(s)	CyMgCl (mol%)	^{1}H NMR Yield (%) [a]
–	20	33
pyridine (35 µL, 0.4 mmol, 1 equiv)	–	0
pyridine (35 µL, 0.4 mmol, 1 equiv)	20	84
TMEDA (0.2 mL, 5% v/v)	20	45
1,4-dioxane (0.2 mL, 5% v/v)	20	42
2,6-di-*tert*-butyl-4-methylpyridine (16 mg, 80 µmol, 20 mol%)	–	0
2,6-di-*tert*-butyl-4-methylpyridine (16 mg, 80 µmol, 20 mol%)	20	31
PPh$_3$ (42 mg, 0.16 mmol, 40 mol%)	40	30
IPr (32 mg, 80 µmol, 20 mol%)	20	< 5
dppe (64 mg, 0.16 mmol, 40 mol%)	20	0
pyridine (35 µL, 0.4 mmol, 1 equiv), IMes (25 mg, 80 µmol, 20 mol%)	20	5
9,10-dihydroanthracene (72 mg, 0.4 mmol, 1 equiv)	–	0
9,10-dihydroanthracene (72 mg, 0.4 mmol, 1 equiv)	40	62

[a] As measured by ^{1}H NMR spectroscopy of the crude reaction mixture vs Si(SiMe$_3$)$_4$ as an internal standard.

Inhibition of catalysis also occurred in coordinating solvents (e.g., Py or MeCN). On the other hand, ethereal solvents (THF, 2-methyl-THF, dioxane, Et$_2$O) resulted in the highest catalytic conversions (Table 3.3). The CyMgCl/**Co-Cl** ratio (in THF with pyridine) was found to impact both conversion and selectivity in catalysis (Table 3.4).

Table 3.3. Effect of Solvent Choice on the Catalytic Hydroarylation of 1a with Diphenylacetylene.
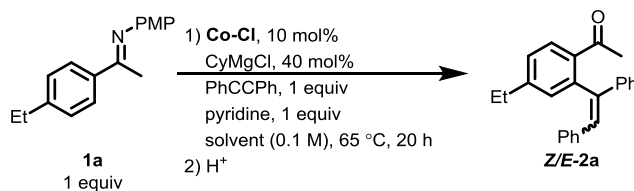
Solvent	Pure Solvent Dielectric Constant (ε)	^{1}H NMR Yield (%) [a]	Z/E [a]
MeCN	37.5	22	26
pyridine	12.4	20	4.2
THF	7.58	87	> 50
THF [b]	7.58	33	5.7
2-MeTHF	6.97	57	> 50
Et$_2$O	4.33	77	> 50
toluene	2.38	73	> 50
1,4-dioxane	2.25	82	> 50
1,4-dioxane [b]	2.25	77	> 50
1,4-dioxane/THF (1:1) [b]	–	48	40

[a] As measured by ^{1}H NMR spectroscopy of the crude reaction mixture vs Si(SiMe$_3$)$_4$ as an internal standard. [b] an equivalent of pyridine was not added.

Table 3.4. Effect of CyMgCl Stoichiometry (Relative to Co-Cl) on the Hydroarylation of 1a with Diphenylacetylene.
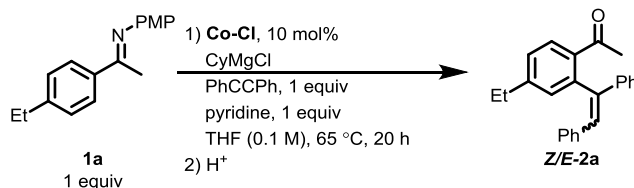
CyMgCl (mol%)	Volume CyMgCl Added (μL) [a]	^{1}H NMR Yield (%) [b]	Z/E [a]
0	–	0	–
10	20	25	> 50
20	40	84	> 50
40	80	87	> 50
50	100	81	45
100	200	36	2.1

[a] CyMgCl was used as a 2.0 M solution in Et_2O. [b] As measured by ^{1}H NMR spectroscopy of the crude reaction mixture vs $Si(SiMe_3)_4$ as an internal standard.

While at least two equivalents of CyMgCl relative to Co were required for reasonable conversion, an excess of ca. 5 equiv of CyMgCl greatly reduced activity. Finally, the concentration of the substrate influenced the overall conversion (Table 3.5); dilute catalytic conditions provided the highest yielding *in situ* catalyst, and yields decreased as a function of substrate concentration (e.g., 83% for 0.05 M vs. 66% for 1.0 M, as measured by ^{1}H NMR spectroscopy).

Table 3.5. Effect of Substrate Concentration on the Hydroarylation of 1a with Diphenylacetylene.
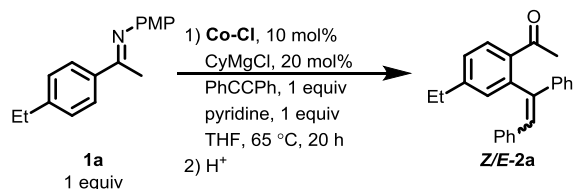
Concentration (M)	Volume THF (mL)	^{1}H NMR Yield (%) [a]	Z/E [a]
0.05	8	83	> 50
0.1	4	84	> 50
0.2	2	72	45
0.4	1	70	31
1.0	0.5	66	29

[a] As measured by ^{1}H NMR spectroscopy of the crude reaction mixture vs. $Si(SiMe_3)_4$ as an internal standard.

Formation and Identity of Catalytically Active Species. The activation of cobalt by the organomagnesium reagent would seem to occur *via* formation of a reactive alkyl complex of the type $(PPh_3)_3CoR$. Interestingly, treatment of **Co-Cl** with 1 equiv of CyMgCl (eq 3.2) cleanly produced cyclohexene and the diamagnetic hydride $(PPh_3)_3Co(N_2)H$ (**Co-H**), first reported by Sacco and Rossi[51,52] in 1967.

$$(PPh_3)_3CoCl \xrightarrow[\text{THF, 25 °C}]{\text{CyMgCl, 1 equiv}} (PPh_3)_3Co(N_2)H \; + \; \bigcirc \quad (3.2)$$

Co-Cl   **Co-H**
                                        2.6 g, 51%
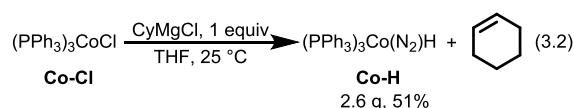
It has been previously reported by Kisch and coworkers[53] that **Co-H** catalyzes the hydroarylation of diphenylacetylene with diaryl-substituted diazo compounds as a neat melt at 85 °C. However, in our hands, 10 mol% of complex **Co-H** did not promote catalysis with diphenylacetylene and **1a** in a solution of THF and pyridine heated to 65 °C for 1 d. However, the addition of an equiv (relative to Co) of CyMgCl or a similarly strong base (e.g., *n*BuLi, LDA) gave catalysis (Table 3.6). Activation of the cobalt hydride species under the latter conditions suggests that the active catalyst results from deprotonation.

Table 3.6. **Effect of Base on the Hydroarylation of 1a with Diphenylacetylene Catalyzed by Co-H.**
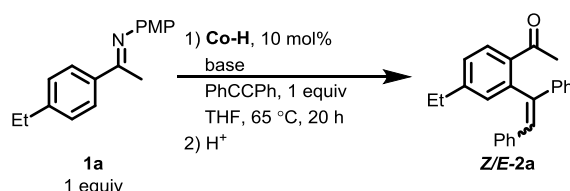
Base (mol%)	^{1}H NMR Yield (%) [a]	Z/E [a]
–	0	–
MeMgBr (40)	10	> 100
CyMgCl (10)	30	79
CyMgCl (20)	25	83
MeLi (10)	16	> 100
*n*BuLi (10)	24	> 100
LDA (10)	20	52

[a] As measured by ^{1}H NMR spectroscopy of the crude reaction mixture vs $Si(SiMe_3)_4$ as an internal standard.

The organic byproducts created by treatment of complexes **Co-Cl** and **Co-H** (as well as $CoCl_2/3PPh_3$) with CyMgCl were quantified by ^{1}H NMR spectroscopy (Table 3.7 and Figure 3.1). With two equivalents of CyMgCl, equimolar amounts of cyclohexene and cyclohexane were observed for both $CoCl_2$ (with PPh_3) and **Co-Cl**. An excess of CyMgCl with **Co-Cl** did not result in the evolution of additional cyclohexane or cyclohexene. In contrast, stoichiometric treatment of **Co-H** with CyMgCl afforded only a single equivalent of cyclohexane.

Table 3.7. Quantification of Cyclohexene and Cyclohexane from Activation of Cobalt Species.
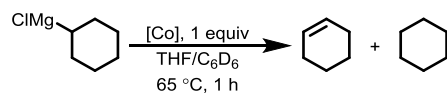
CyMgCl (equiv)	[Co]	Cyclohexene (equiv) [a]	Cyclohexane (equiv) [a]
1		0.7	0.3
2	CoCl$_2$ / 3PPh$_3$	1	1
4		2	2
1		0.7	0.3
2	**Co-Cl**	1	1
4		1	1
1	**Co-H**	0	1

[a] Volatile organic products were separated from [Co] via vacuum transfer and quantified by ^{1}H NMR spectroscopy vs *p*-xylene as an internal standard.
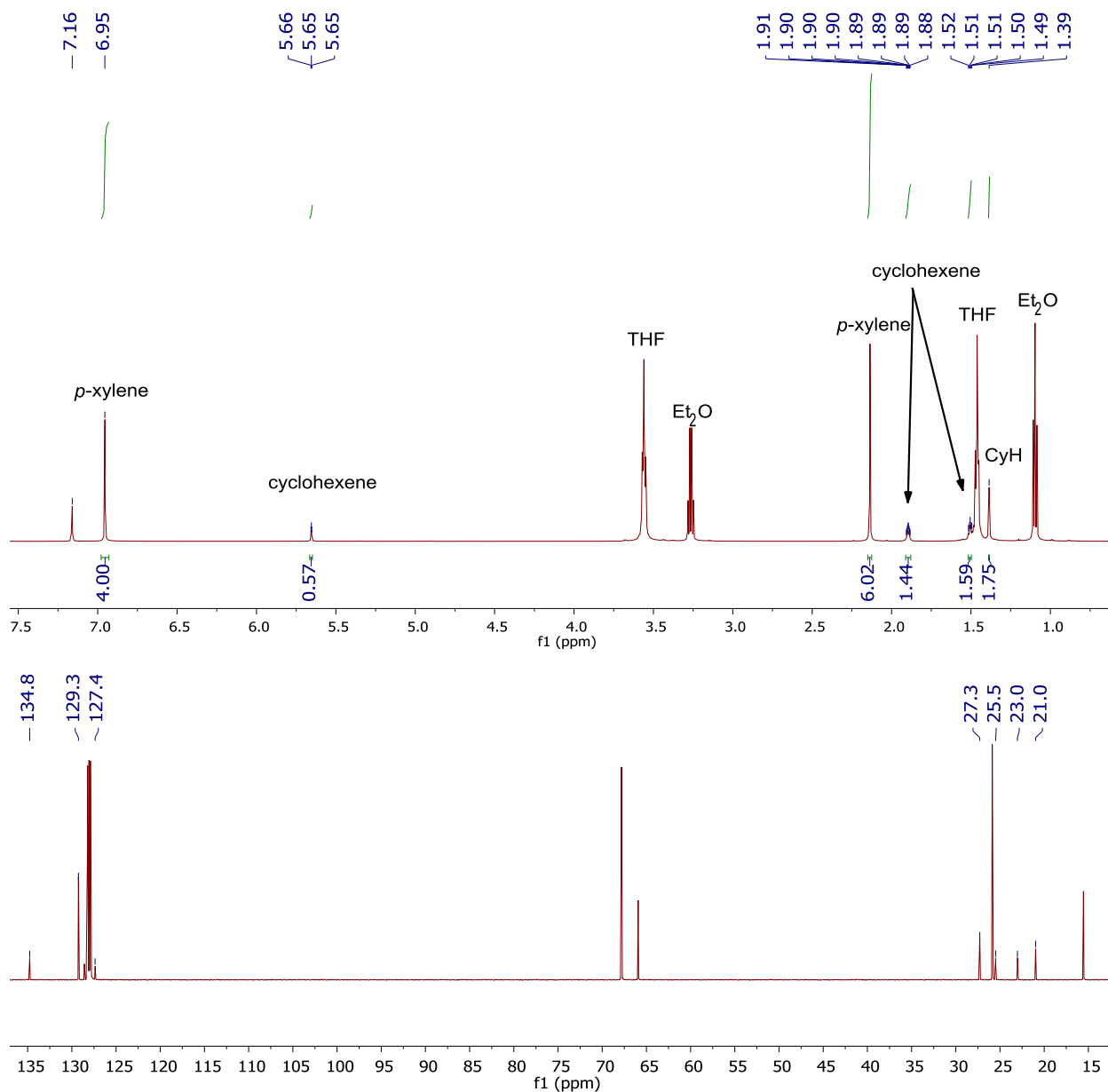
Figure 3.1. Representative ^{1}H (top) and ^{13}C{^{1}H} (bottom) NMR spectra of the volatile components resulting from treatment of **Co-Cl** with CyMgCl in benzene-d_6. Note that THF and Et$_2$O exist as impurities from the reaction conditions.

Upon first inspection, it is perhaps surprising that deprotonation of **Co-H** occurs given the ancillary ligand environment; cobalt hydride complexes bearing only σ-donating phosphine co-ligands display hydridic character (e.g., pK_a^{MeCN} [HCo(dppe)$_2$] = 38.1). The introduction of π-acidic ligands considerably reduces the pK_a value (e.g., pK_a^{MeCN} [HCo(CO)$_4$] = 8.3; [HCo(CO)$_3$(PPh$_3$)] = 15.4).[54,55] Given the slight π-acidic behavior of end-on N$_2$ ligands, it seems plausible that **Co-H** is deprotonated with a strong base such as a RMgX or R$_2$Mg (e.g., pK_a^{THF} [EtMgCl] = 30.1; pK_a^{THF} [Et$_2$Mg] = 30.5).[56] Indeed, stoichiometric treatment of **Co-H** with MeLi, ^{n}BuLi, Bn$_2$Mg, or CyMgCl generated an equivalent of the corresponding alkane (i.e., MeH, ^{n}BuH, toluene, and CyH, respectively) as determined by ^{1}H NMR spectroscopy in benzene-d_6. Gram-scale deprotonation of **Co-H** with ^{n}BuLi or ^{n}Bu$_2$Mg in THF (eqs 3.3 and 3.4) afforded

Co(-I) complexes of the type $[(PPh_3)_3Co(N_2)]_nM$ (M = Li(THF)$_3$, n = 1, **Co-Li**; M = Mg(THF)$_4$, n = 2, **Co$_2$-Mg**) as reported by Yamamoto and coworkers.[57]

$$\textbf{Co-H} \xrightarrow[\text{THF, -78 °C}]{^n\text{BuLi, 1 equiv}} \underset{\substack{\textbf{Co-Li}\\ \text{2.3 g, 75\%}}}{[(PPh_3)_3Co(N_2)][Li(THF)_3]} + {}^n\text{BuH} \qquad (3.3)$$

1 equiv

$$\textbf{Co-H} \xrightarrow[\text{THF, -78 °C}]{^n\text{Bu}_2\text{Mg, 1 equiv}} \underset{\substack{\textbf{Co}_2\text{-Mg}\\ \text{0.65 g, 56\%}}}{[(PPh_3)_3Co(N_2)]_2[Mg(THF)_4]} + 2\,{}^n\text{BuH} \qquad (3.4)$$

2 equiv
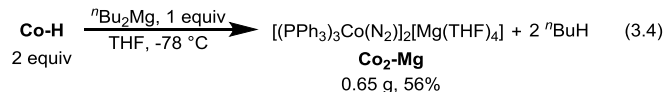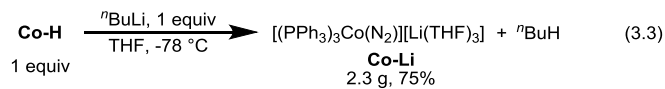
Complexes **Co-Li** and **Co$_2$-Mg** exhibit red-shifted N_2 stretching modes at 1898 and 1860 cm^{-1}, respectively (for comparison, ν_{N-N} (**Co-H**) = 2092 cm^{-1}; KBr). **Co-Li** exhibited a broad ^{7}Li{^{1}H} NMR resonance at -3.8 ppm in benzene-d_6, which is consistent with solvent-separated ion pairs.[58-60] Hydrolysis of **Co-Li** resulted in liberation of three equivalents of both THF and PPh$_3$ as determined by ^{1}H NMR spectroscopy (Figure 3.2) versus Si(SiMe$_3$)$_4$ as an internal standard, which is in agreement with the solid-state composition of **Co-Li** as determined by elemental analysis. However, both complexes appear to exhibit ligand dissociation in benzene-d_6, as indicated by the existence of a ^{31}P{^{1}H} NMR resonance at -5.24 ppm (unbound PPh$_3$), along with those for **Co-Li** (48.14) or **Co$_2$-Mg** (48.26).
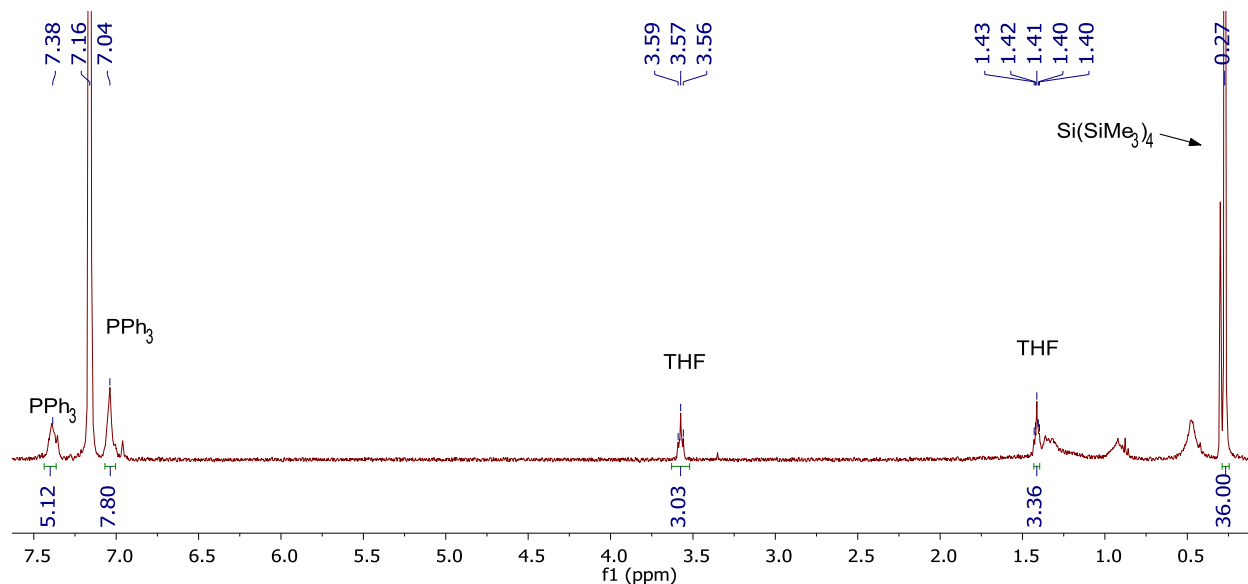
Figure 3.2. Representative ^{1}H NMR spectrum of the organic byproducts of protonolysis of **Co-Li**.

For comparative purposes, a structural analogue to **Co$_2$-Mg** was prepared according to the procedure described by Long and coworkers.[61] Treatment of CoCl$_2$ with Zn and the tridentate ligand triphos, MeC(CH$_2$PPh$_2$)$_3$, afforded the intermediate species [(triphos)CoCl], which upon further reduction with Mg afforded **Co'$_2$-Mg** (eq 3.5). This complex exhibits a similarly red-shifted N_2 stretch at 1846 cm^{-1} (KBr). In contrast to complexes bearing PPh$_3$, **Co'$_2$-Mg** does not engage in solution-state ligand exchange dynamics, as illustrated by a single ^{31}P{^{1}H} NMR resonance at 31.20 ppm.

$$\text{CoCl}_2 \xrightarrow[\substack{\text{2) Mg(0)}\\\text{THF, 3 d}}]{\substack{\text{1) triphos}\\\text{Zn(0)}\\\text{THF, 1 d}}} \quad \textbf{Co'}_2\textbf{-Mg} \qquad (3.5)$$

Co'₂-Mg
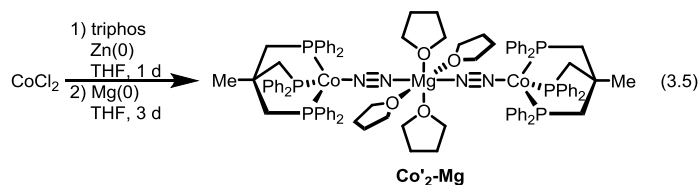
While complexes of Co(-I) are relatively uncommon, a recent report by Deng and coworkers[62] described the synthesis and reactivity of a Co(-I) dinitrogen complex, $[(ICy)_2Co(N_2)_2][K(18\text{-c-}6)]$, in the context of nitrogen fixation. DFT calculations indicate that the formally d^{10} Co center engages in extensive back-bonding into the $N_2 \, \pi^*$ orbital, which may activate the N_2 ligand of this complex for functionalization. An example of such reactivity is borne out in the catalytic silylation of N_2 to $N(SiMe_3)_3$ in the presence of excess KC_8 and Me_3SiCl.[62] Long and coworkers[61] described similar N_2 functionalization chemistry with **Co'₂-Mg**; stoichiometric treatment of this complex with Me_3SiCl afforded the silyldiazenido complex, $[(triphos)Co(N_2SiMe_3)]$, likely as a result of N_2 activation by the electron rich metal center. Given this notable reactivity toward N_2, investigations into interactions of highly-reduced Co complexes with unsaturated substrates (i.e., olefins and alkynes) are of interest, particularly in the context of hydroarylations.

Table 3.8 compares the catalytic hydroarylation activity of cobalt complexes **Co-Cl**, **Co-H**, **Co-Li**, **Co₂-Mg**, and **Co'₂-Mg** with those of a catalyst generated *in situ* as described above in eq 3.1. TMEDA or 1,4-dioxane were employed as co-solvents in place of pyridine since higher activities were observed with the anionic complexes as the catalysts, presumably by enhanced Li or Mg sequestration, respectively. While neither **Co-Cl** nor **Co-H** are single-component catalysts, competent catalysis occurs after addition of CyMgCl (1 and 2 equiv, respectively). In contrast to the Co(I) precursors, the Co(-I) species **Co-Li** and **Co₂-Mg** catalytically coupled (*N*-aryl)aryl ethanimine **1a** and diphenylacetylene without the addition of Grignard. Additionally, catalytic yields observed for **Co-Li** and **Co₂-Mg** are comparable to those obtained using $CoCl_2/3PPh_3$, **Co-Cl**, or **Co-H** with a corresponding quantity of CyMgCl, which implicates $[(PPh_3)_3Co(N_2)]^-$ as the catalytically active Co fragment. Interestingly, **Z-2a** was the major isomer observed regardless of precatalyst, which suggests that a common species capable of *E*- to *Z*-olefin isomerization exists as a result of activation with CyMgCl.

Table 3.8. Activity Comparison of Added Catalysts.
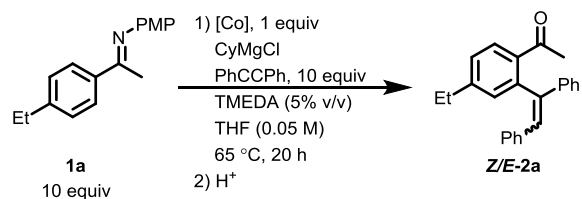
[Co]	CyMgCl (equiv)	^{1}H NMR Yield (%) [a]	Z/E [a]
CoCl$_2$ / 3PPh$_3$	4	41	40
Co-Cl	0	0	–
	2	45	59
Co-H	0	0	–
	1	44	65
Co-Li	0	58 (50) [b]	> 100
Co$_2$-Mg [c,d]	0	64 (48) [b]	44
Co'$_2$-Mg [c,d]	0	0	–

[a] Determined by comparison to a known quantity of Si(SiMe$_3$)$_4$ as an internal standard. [b] Isolated yield given in parenthesis. [c] 0.5 equiv of complex was added. [d] 1,4-dioxane (5% v/v) was used instead of TMEDA.

Unlike the PPh$_3$-ligated complexes, the triphos analogue **Co'$_2$-Mg** did not catalyze hydroarylation. Stoichiometric reactions with either diphenylacetylene or **1a** did not consume the organic substrate and instead afforded a common, unknown paramagnetic species consistent with broadened ^{1}H NMR resonances at δ 15.10 (br s, 18H), -1.17 (br s, 6H), -2.54 (br s, 2H) in benzene-d_6 (Figures 3.3 and 3.4). The lack of reactivity with alkyne or aryl-imine observed with **Co'$_2$-Mg** implies that a catalytic intermediate with fewer than three ancillary phosphine ligands is required for catalysis.
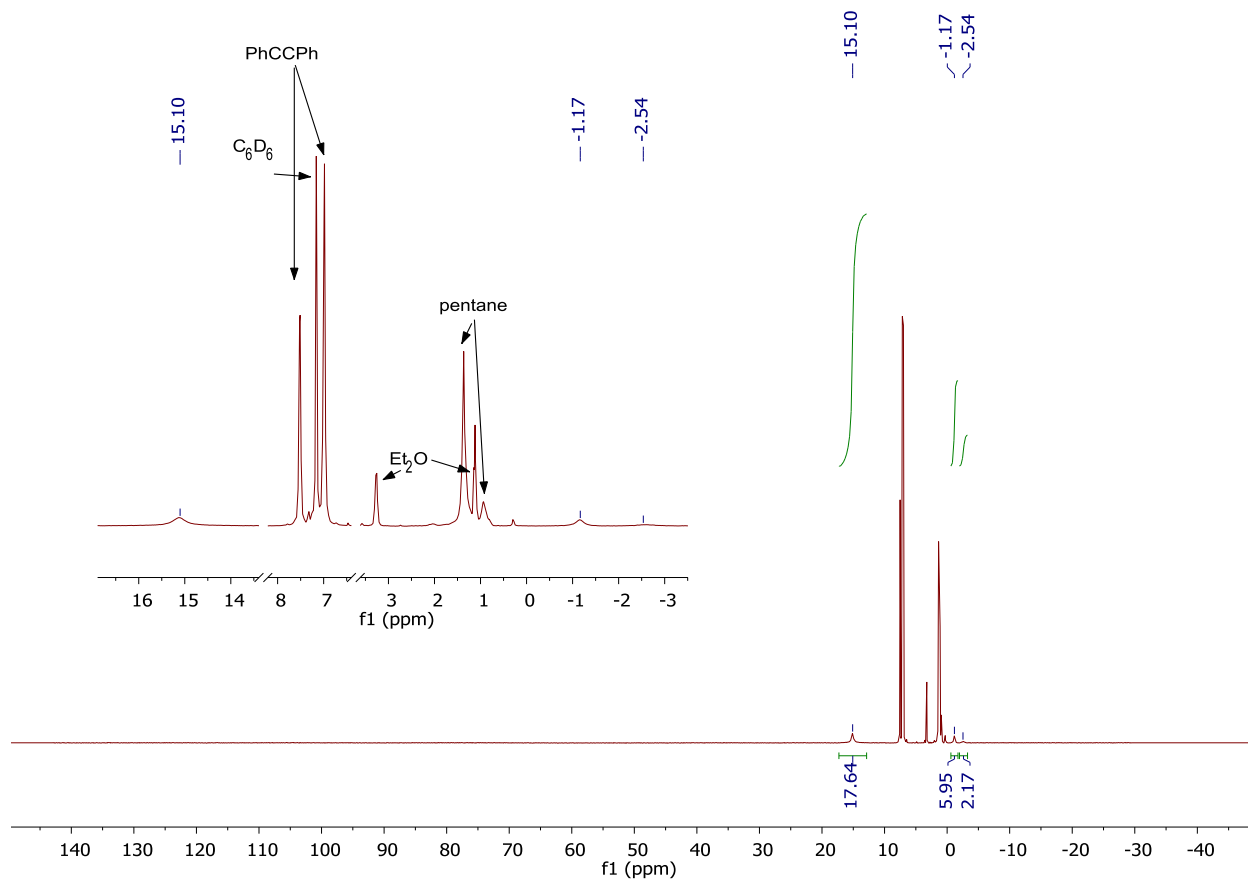
Figure 3.3. Crude ^{1}H NMR spectrum (benzene-d_6) of the reaction of diphenylacetylene (4 equiv) with **Co'$_2$-Mg** (1 equiv). Note that residual Et$_2$O and pentane were observed as well as unreacted diphenylacetylene. Three new broad features exist at 15.10 (18H), -1.17 (6H), and -2.54 (2H) ppm, which are attributed to a new, unidentified paramagnetic species.
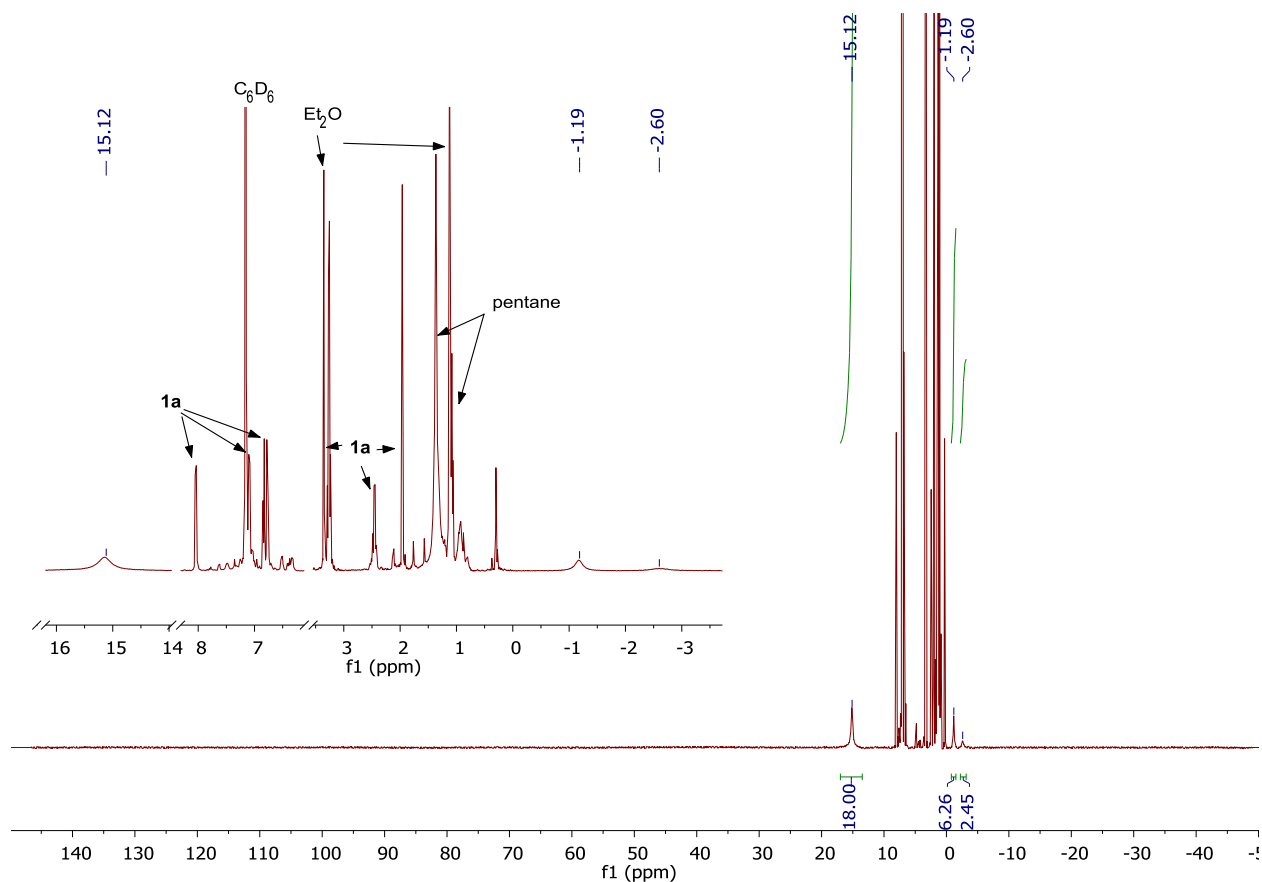
Figure 3.4. Crude ^{1}H NMR spectrum (benzene-d_6) of the reaction of **1a** (4 equiv) with **Co'$_2$-Mg** (1 equiv). Note that residual Et$_2$O and pentane were observed as well as unreacted diphenylacetylene. Three new broad features exist at 15.10 (18H), -1.17 (6H), and -2.54 (2H) ppm, which are attributed to a new, unidentified paramagnetic species.

While hydroarylations reported by the Yoshikai group[29] have focused on Mg containing activators, **Co-Li** proved to be a more convenient for mechanistic investigations. The charge matching of the Co(-I) fragment and Li^{+} reduced the number of ion dissociation equilibria compared to the dicationic Mg counterion present in **Co$_2$-Mg**. All subsequent mechanistic studies, therefore, employed **Co-Li** as the catalyst.

Comparisons of the functional group tolerance of the single-source catalyst **Co-Li** vs. the *in situ* CoCl$_2$/3PPh$_3$/CyMgCl catalyst were made for several substrates as shown in Table 3.9. These results illustrate a potential advantage to "Grignard-free" hydroarylations. Electrophilic groups (e.g., esters, ketones, aldehydes) are often not compatible with nucleophilic organomagnesium reagents that can undergo rapid, competing reactions with the substrate. This problem may be circumvented to some extent by addition of the Grignard to the catalyst mixture prior to introduction of the substrate, but *in situ* catalyst generations of this type often employ a slight excess of activator. Note that the Yoshikai group[44] has developed "Grignard-free" catalysis by use of Mg turnings as the terminal reductant, but these reducing conditions may also lead to undesired reactions of various functional groups (e.g., halides).

Significantly, with complex **Co-Li** as the catalyst substrates bearing an ester (**1b**) or a nitrile (**1c**) group are tolerated in modest yields; only the desired product was observed. In contrast, *in situ* reactions did not cleanly catalyze hydroarylation since products derived from nucleophilic addition of CyMgCl to

the carbonyl or nitrile fragments were produced, as observed by ^{1}H NMR spectroscopy. The existence of such species requires more difficult purification procedures. Moderate catalytic conversion occurred with substrates bearing electron withdrawing CF_3 (**1d**) or donating OMe (**1e**) functionalities. These data suggest that complex **Co-Li** may be useful for substrates that are not tolerated by the catalysts generated *in situ* despite being mildly acid-sensitive.

Table 3.9. Arene Functional Group Tolerance.

1b: R = CO_2Me
1c: R = CN
1d: R = CF_3
1e: R = OMe

Z/E-**2b-2e**
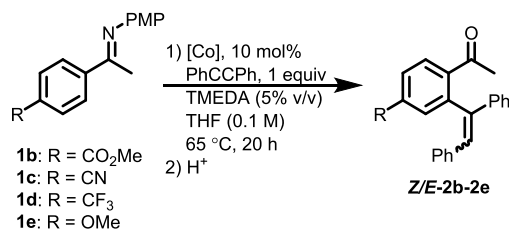
Imine	[Co]	Yield (%) [a,b]	Conv. (%) [a,c]	Z/E [a]
1b	$CoCl_2$ / 3PPh$_3$ / 4CyMgCl	30	68	8.8
	Co-Li	36 (33)	36	8.0
1c	$CoCl_2$ / 3PPh$_3$ / 4CyMgCl	11	36	> 100
	Co-Li	86 (70)	86	6.7
1d	**Co-Li**	43 (29)	43	15
1e	**Co-Li**	47 (27)	47	20

[a] ^{1}H NMR yield and *Z/E* ratios were determined by comparison to a known quantity of Si(SiMe$_3$)$_4$ as an internal standard. [b] Isolated yield given in parenthesis. [c] Conversion was determined from the quantity of substituted acetophenone derived from hydrolysis of unreacted imine substrate.

Given the observations described above, it appears that catalyst generation occurs by treatment of precatalyst **Co-Cl** with an organometallic transmetalation reagent bearing a β–H substituent (e.g., EtMgCl, CyMgCl, etc; Scheme 3.1). The resultant Co–R complex (**A**) undergoes rapid β–H elimination under an N$_2$ atmosphere to generate (PPh$_3$)$_3$Co(N$_2$)H (**Co-H**) and an equivalent of olefin (e.g., ethylene, cyclohexene, etc.). Deprotonation by the basic organometallic activator then results in formation of stoichiometric alkane (e.g., ethane or cyclohexane) and the active Co(-I) anion. Indeed, similar activation pathways have been reported by Koszinowski and coworkers[63] in the context of Co-catalyzed Heck-type reactions.

Scheme 3.1. Proposed Catalyst Activation Mechanism.
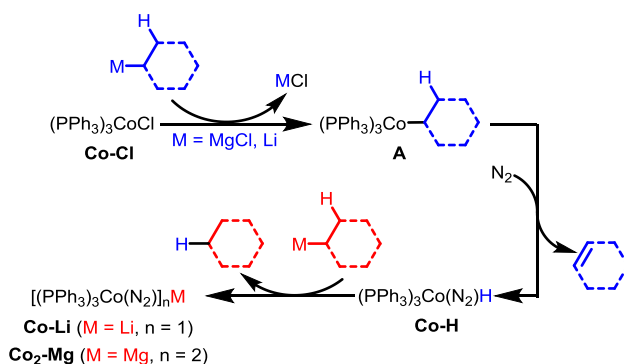
Substrate Coordination and Implications for the Catalytic Cycle. To probe interactions of the alkyne substrate with the cobalt center, **Co-Li** was treated with an excess of the alkyne bis(*para*-tolyl)acetylene (*p*-TolCC*p*-Tol; Figure 3.5). For varying quantities of added alkyne, the ratio of free to bound alkyne was quantified after equilibration by ^{1}H NMR spectroscopy (Figure 3.6) versus an internal standard. The existence of multiple distinct tolyl-CH_3 resonances suggests the presence of a mixture of several alkyne-ligated complexes. On the basis of the initial concentration of **Co-Li**, an average number of bound alkynes per Co (x) was determined for various [*p*-TolCC*p*-Tol]$_0$/[**Co-Li**]$_0$ ratios and temperatures, and the results are plotted in Figure 3.5. The addition of alkyne results in displacement of ligated PPh$_3$; under catalytic conditions (~10 equivs relative to Co), each Co coordinates 2 alkynes on average, which corresponds to displacement of the N$_2$ ligand and one PPh$_3$. Surprisingly, this ratio appears to be temperature invariant.
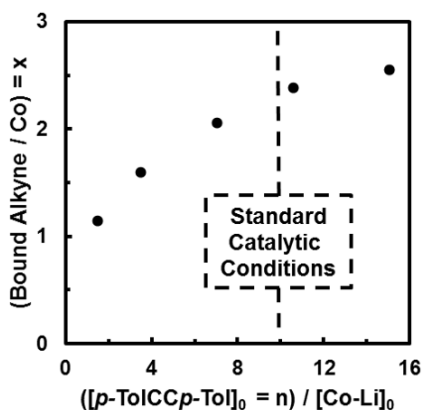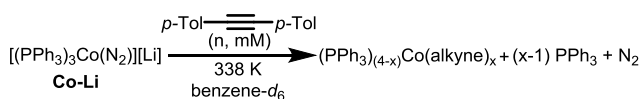
Figure 3.5. Average bound alkyne per Co as a function of alkyne equivalents. Reaction conditions: [**Co-Li**]$_0$ = 13 mM; [bis(*p*-tolyl)acetylene]$_0$ = 19, 44, 90, 135, and 190 mM. Average bound alkyne per Co measured by ^{1}H NMR spectroscopy in benzene-d_6 versus Si(SiMe$_3$)$_4$ as an internal standard with the NMR probe temperature calibrated and set to 338 K.
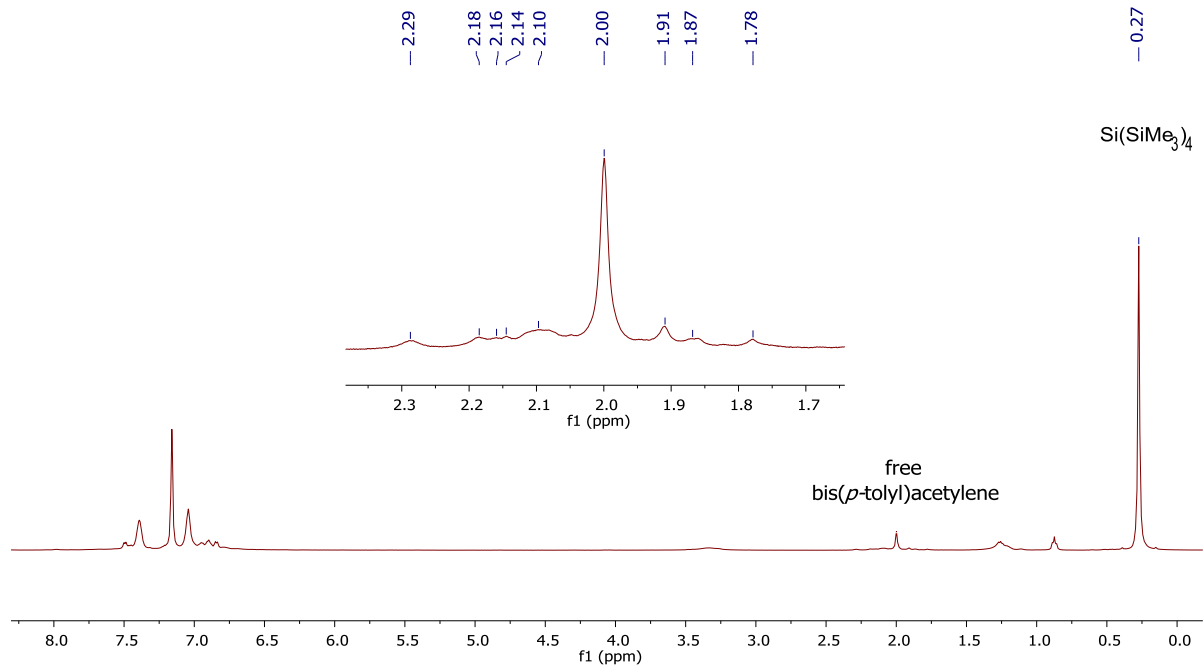
Figure 3.6. Representative ¹H NMR spectrum of treatment of **Co-Li** with excess bis(*p*-tolyl)acetylene. Note that the large peak at 2.00 ppm is free alkyne; several new species were observed, corresponding to a large variety of alkyne-bound Co complexes.

While similar ligand substitution behavior was observed with (*N*-aryl)aryl ethanimine, productive C–H activation did not occur. Stoichiometric treatment of **Co-Li** with **1a** in benzene-d_6 at 65 °C did not result in the generation of a new cyclometallated species; instead, only broadened ¹H NMR resonances for **1a**, likely the result of rapid ligand exchange with PPh₃, were observed.

Reactant Order and Catalytic Kinetics. The reaction profile (Figure 3.7) with complex **Co-Li** as catalyst was monitored by ¹H NMR spectroscopy at 65 °C (Figure 3.8). Initial time points reveal that the *E*-isomer is the kinetic product; conversion to **Z-3a** occurred only after the formation of **E-3a**. These data are consistent with an off-cycle isomerization process to generate the *Z*-isomer as the thermodynamic product.
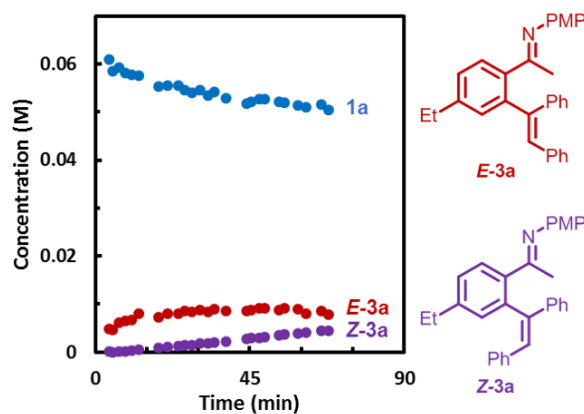
Figure 3.7. Representative initial reaction kinetic profile of the hydroarylation of **1a** ([**1a**]$_0$ = 67 mM) with diphenylacetylene ([alkyne]$_0$ = 67 mM) catalyzed by **Co-Li** ([**Co-Li**]$_0$ = 2 mM, 3 mol%). Reaction was monitored by ¹H NMR spectroscopy in benzene-d_6 versus Si(SiMe₃)₄ as an internal standard with the NMR probe temperature calibrated and set to 339 K.
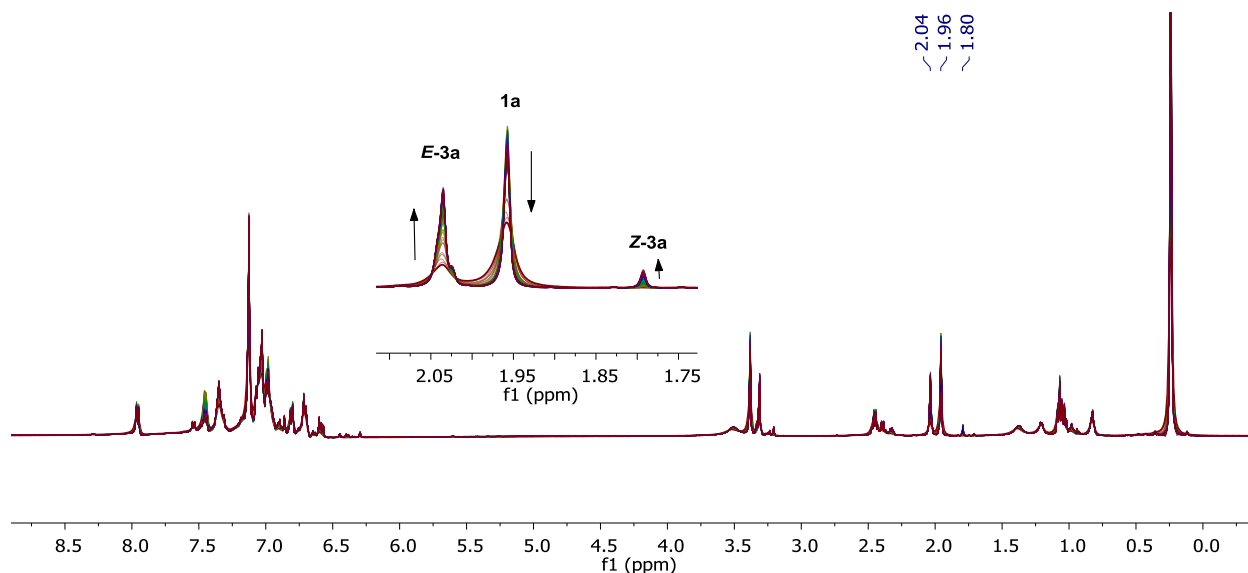
Figure 3.8. Representative kinetic profile of the hydroarylation of **1a** with diphenylacetylene catalyzed by **Co-Li**.

With **Co-Li** as the catalyst, an initial catalytic rate constant was calculated to be $k_{obs} = 9.4(19)$ x 10^{-4} s^{-1} (Figure 3.9A) with a first-order dependence on $[\textbf{Co-Li}]_0$ (Figure 3.9B). No observable difference in initial rate occurred when 12-crown-4 was added to the catalytic mixture. This result rules out participation of the Li counterion as a Lewis-acid in the catalysis. Significantly slower catalysis occurred with the bimetallic complex **Co₂-Mg** (Figure 3.10A), with a calculated catalytic rate constant of $k_{obs} = 3.0(3)$ x 10^{-5} s^{-1}, which implicates slow decoordination of the active L_3Co^{-1} fragment from the Mg^{2+} counterion. Surprisingly, a first-order dependence on $[\textbf{Co}_2\textbf{-Mg}]_0$ (Figure 3.10B) suggests that only a single catalytically active Co fragment exists along with an inert $[L_3Co(N_2)]Mg^+$ counterion, which implicates Li^+ as a better dissociating counter cation than Mg^{2+}.
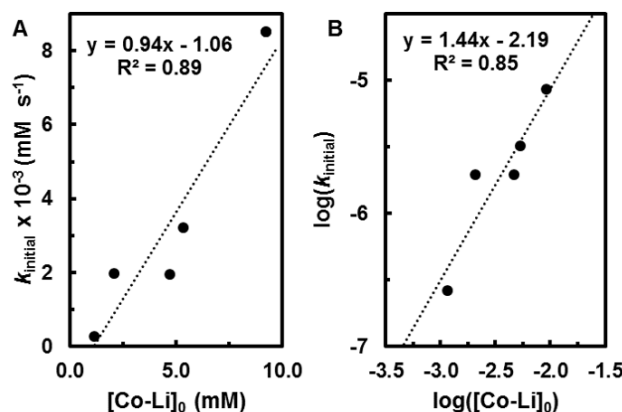
Figure 3.9. A: Dependence of $[\textbf{Co-Li}]_0$ on the hydroarylation of **1a** ($[\textbf{1a}]_0 = 67$ mM) with diphenylacetylene ($[\text{alkyne}]_0 = 67$ mM). Initial rates ($k_{initial}$) were determined by ^{1}H NMR spectroscopy in benzene-d_6 vs Si(SiMe₃)₄ as an internal standard with the NMR probe temperature calibrated and set to 338 K. The dashed line is a linear fit of the data with a slope of $k_{obs} = 9.4(19)$ x 10^{-4} s^{-1}. Error determined as the standard error of the linear regression ($R^2 = 0.89$, $S_x = 1.9$ x 10^{-4} s^{-1}). **B:** log-log plot depiction of the first-order dependence of $[\textbf{Co-Li}]_0$ on the initial rate (slope ca. 1.1 when the highest concentration value is omitted). Error determined as the standard error of the linear regression ($R^2 = 0.85$, $S_x = 0.3$).
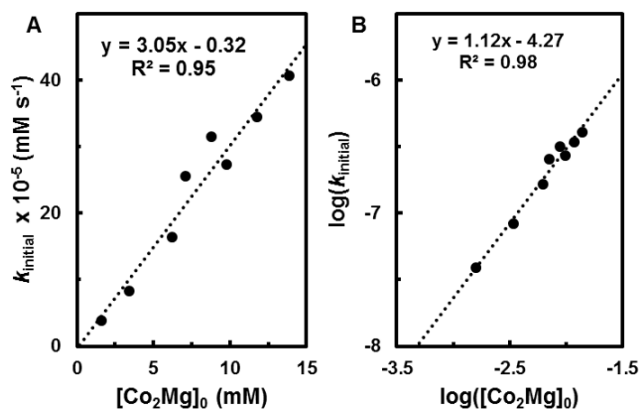
Figure 3.10. A: Dependence of [**Co₂-Mg**]₀ on the hydroarylation of **1a** ([**1a**]₀ = 67 mM) with diphenylacetylene ([alkyne]₀ = 67 mM). Initial rates ($k_{initial}$) were determined by ^{1}H NMR spectroscopy in benzene-d_6 vs Si(SiMe₃)₄ as an internal standard with the NMR probe temperature calibrated and set to 339 K. The dashed line is a linear fit of the data with a slope of k_{obs} = 3.0(3) x 10^{-5} s^{-1}. Error determined as the standard error of the linear regression (R^2 = 0.95, S_x = 0.3 x 10^{-5} s^{-1}). **B:** log-log depiction of the first-order dependence of [**Co₂-Mg**]₀ on the initial rate (slope ca. 1.1). Error determined as the standard error of the linear regression (R^2 = 0.98, S_x = 0.06).

Each of the substrates displayed saturation-type kinetics, with pseudo-first order dependencies at low substrate concentrations. Given these results, a Michaelis-Menten analysis was used to further examine the catalytic mechanism. Typically, such studies are performed to elucidate the origin of saturation behavior, using various models for enzyme inhibition.[64,65] By presenting the data in a Lineweaver-Burk double-reciprocal plot, two key mechanistic features can be extracted from a linear fit, namely the maximum achievable rate (v_{max} = 1/intercept$_y$) and a modified binding constant (K_M = -1/intercept$_x$). Three main classes of enzymatic inhibition mechanisms exist, which result from competitive (K_M increases), uncompetitive (both V_{max} and K_M decrease), and non-competitive (v_{max} decreases) binding of the inhibitor.[65]

With these mechanistic factors in mind, an enzymatic-like kinetic analysis was applied to the cobalt-catalyzed hydroarylations described herein. The hydroarylations of diphenylacetylene with **1a** at various initial substrate concentrations were monitored by ^{1}H NMR spectroscopy in benzene-d_6 at 338 K using complex **Co-Li** as the catalyst (7 mM; Figure 3.11). The initial catalytic rate constants ($k_{initial}$) were determined for each of these catalytic reactions (i.e., at each [alkyne]₀ and [**1a**]₀); at a fixed alkyne concentration, saturation-like imine dependence was observed and is reflected in a linear fit in the main double reciprocal plot. A series of such linear fits was generated at a variety of initial alkyne concentrations (see Experimental Section, Tables 3.17-3.19). Each fit passed through the same y-intercept from which an average v_{max} was calculated to be 1.2(2) x 10^{-5} M s^{-1}. Interestingly, the slope of each fit (K_M/v_{max}) depends on the initial alkyne concentration, as illustrated in the expansion of Figure 3.11. This secondary Michaelis-Menten plot was fit to a hyperbolic function which contains a linear and an inverse dependence on alkyne concentrations.
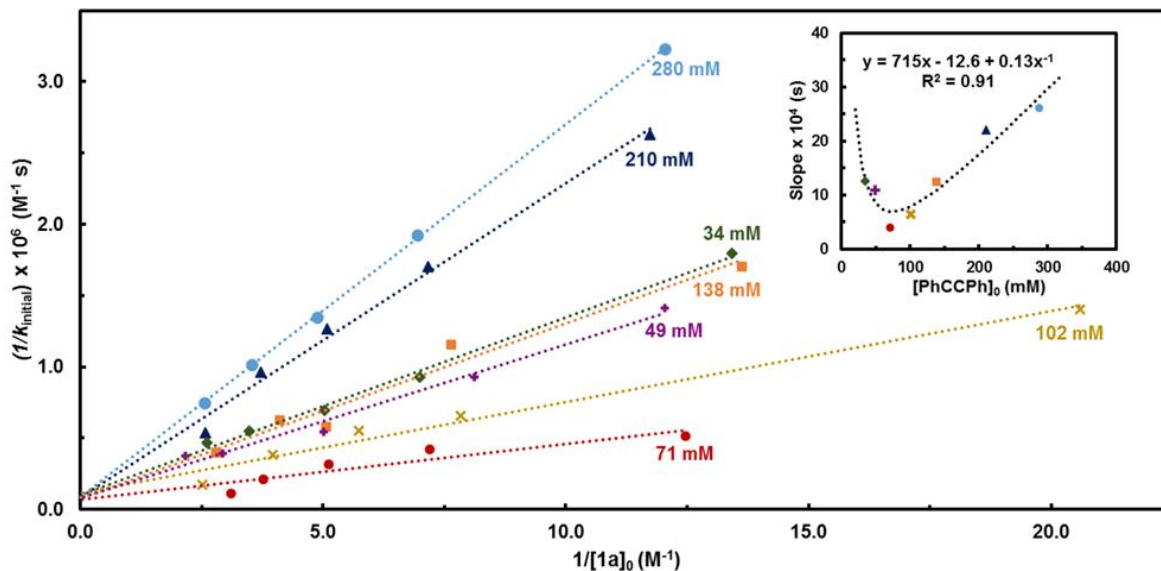
Figure 3.11. Lineweaver-Burk (double-reciprocal) plot of the hydroarylation of diphenylacetylene and **1a** catalyzed by **Co-Li** (7 mM). Initial rates ($k_{initial}$) were determined by ^1H NMR spectroscopy in benzene-d_6 with Si(SiMe$_3$)$_4$ as an internal standard with the NMR spectrometer probe calibrated and set to 338 K. Each experiment within a data set was performed at identical [diphenylacetylene]$_0$ as follows: **34 mM** (♦), **49 mM** (✚), **71 mM** (●), **102 mM** (✖), **138 mM** (▪), **210 mM** (▲), and **280 mM** (●). The colored dashed lines are the linear fits for each corresponding data set. Each fit has the same y-intercept which corresponds to a $V_{max} = 1.2(2)$ x 10^{-5} M s^{-1}. Error determined as the standard deviation of the average of y-intercepts from all 7 data sets. **Inset:** Plot of the slope of the linear fits from the main plot versus [diphenylacetylene]$_0$. The black dashed line represents a hyperbolic fit of the data.

A model of the catalytic rate law was derived to account for the hyperbolic fit and the full derivation is described in the Experimental Section below.[66] This Michaelis-Menten model (eq 3.6) relates the observed rate (v) to a function of the catalytic rate (where $v_{max} = k_{cat}$[**Co-Li**]$_0$) and substrate binding equilibria (where K_d and K_d' are the dissociation constants for **1a** and diphenylacetylene, respectively; K_a' is an off-cycle association constant). The observed alkyne kinetics result from the role of **1a** both as a substrate and a competitive inhibitor. That is, two discrete regimes exist: at low concentrations, the presence of alkyne increases the reaction rate, whereas high alkyne concentrations result in competitive inhibition, which is consistent with the formation of inactive bis(alkyne) off-cycle species.

$$\frac{1}{v} = \frac{1}{v_{max}} + \frac{1}{v_{max}\,[\mathbf{1a}]}\left(K_d + \frac{K_d'}{[\text{PhCCPh}]} + [\text{PhCCPh}]K_a' \right) \quad (3.6)$$

Given the lability of the ancillary phosphine ligands under catalytic conditions, the influence of added PAr$_3$ on catalysis with **Co-Li** was investigated (Figure 3.12) with PPh$_3$, PMes$_3$ and P(C$_6$F$_5$)$_3$. Surprisingly, additional PPh$_3$ promoted catalytic activity until saturation at ca. 50 equivs relative to **Co-Li**. A similar rate enhancement occurred with added PMes$_3$, which achieved saturation-like behavior at ca. 10 equivs relative to **Co-Li**. In contrast, the perfluorinated analogue, P(C$_6$F$_5$)$_3$, displayed a complex rate dependency; a modest rate increase was only observed at ca. 1-3 equiv of added P(C$_6$F$_5$)$_3$ relative to Co. It may be possible that added phosphine promotes the reaction rate either by stabilization of the active catalytic species or by changing the operative mechanism. Similar saturation behavior for ancillary ligands

has been observed by Yoshikai and coworkers.[29] It is of note that C–H activation of the *ortho*-aryl position of PPh$_3$ does not occur (as determined by ^{1}H NMR spectroscopy), even at excess phosphine loadings.
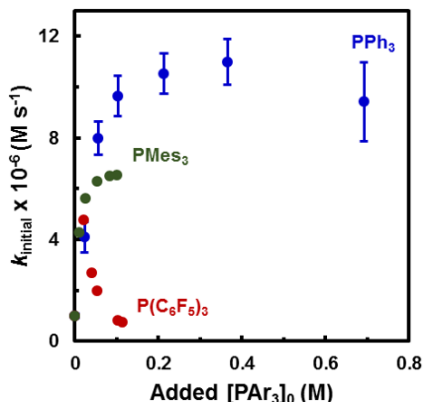
Figure 3.12. Dependence of added [PAr$_3$]$_0$ (**PPh$_3$**, **PMes$_3$**, or **P(C$_6$F$_5$)$_3$**) on the hydroarylation of **1a** ([**1a**]$_0$ = 67 mM) with diphenylacetylene ([alkyne]$_0$ = 67 mM) catalyzed by **Co-Li** ([**Co-Li**]$_0$ = 7 mM, 10 mol%). The reaction in benzene-d_6 was monitored by ^{1}H NMR spectroscopy versus Si(SiMe$_3$)$_4$ as an internal standard with the NMR probe temperature calibrated and set to 338 K. Error determined for reactions with added PPh$_3$ as the standard deviation of triplicate runs except at [**PPh$_3$**]$_0$ = 0.7 M, which was performed in pentaplicate.

Monitored catalysis by time-resolved ^{31}P{^{1}H} NMR spectroscopy probed the speciation of PPh$_3$ (Figure 3.13). Given the relatively low [PPh$_3$] under catalytic conditions, a high-field NMR spectrometer equipped with a liquid N$_2$ cryoprobe broadband channel was used to facilitate direct observation of potential phosphorus-containing intermediates. Two new resonances were observed over the course of the catalysis (in addition to free PPh$_3$); the first at 69.27 ppm is attributed to a new, Co-bound PPh$_3$ ligand, given the similar shift for **Co-Li** (48.14 ppm). A second resonance at 9.90 ppm exists in a range similar to that of a phosphonium-ylide, which typically exhibits resonances between 5 to 20 ppm.[67] However, it is unclear whether this species might exist as a free "ylide" or is complexed by a Co fragment.[68-74]
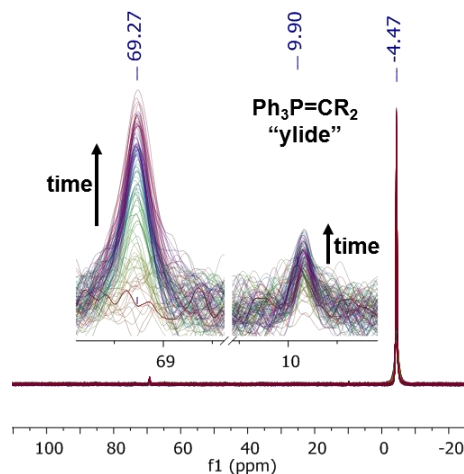
Figure 3.13. Time-resolved $^{31}P\{^1H\}$ NMR spectra (benzene-d_6, 242.94 MHz) during the hydroarylation of **1a** ([**1a**]$_0$ = 67 mM) with diphenylacetylene ([alkyne]$_0$ = 67 mM) catalyzed by **Co-Li** ([**Co-Li**]$_0$ = 7 mM, 10 mol%). Spectra were acquired on a 600 MHz NMR spectrometer equipped with a liquid N_2 cryoprobe broadband channel with the NMR probe temperature calibrated to 339 K. All spectra over the course of the reaction are displayed atop one another as a stack. Time points were acquired every 20 s as the average of 8 scans (d1 = 1s, d20 = 20 s, ns = 8). **Inset:** expansion of two new peaks observed at 69.27 and 9.90 ppm, which grow in over the course of the reaction. These peaks are attributed to a new bound PPh$_3$ complex and a phosphonium-ylide-like species, respectively.

Rate Limiting C–H Activation and Isotope Effects. Deuteron-quenching experiments were utilized to probe the nature of the C–H activation step (Scheme 3.2). In a control experiment (Scheme 3.2A), a solution of imine **1a** in chloroform-d was treated with a slight excess of acetic acid-d_4 to afford a mixture of p-anisidine, 4'-ethylacetophenone, and residual **1a**. Deuteron incorporation into the *ortho*-C–H bond was not observed; however, ca. 1.4 D were observed in the acetyl -C(O)CH$_3$ fragment of 4'-acetophenone and in the iminyl -C(N)CH$_3$ positions of 1a, which resulted from acid-catalyzed enol and enamine tautomerization, respectively. To probe the interaction of *ortho*-C–H bonds with the catalyst in the absence of alkyne, an equimolar mixture of **1a** and **Co-Li** in THF was heated to 65 °C for 2 h (Scheme 3.2B). Subsequent treatment with benzoic acid-d (C$_6$H$_5$COOD) afforded **1a** with D incorporation only in the iminyl fragment. An analogous experiment with equimolar quantities of **1a**, **Co-Li**, and diphenylacetylene (Scheme 3.2C) resulted in the formation of **Z/E-2a** and **Z/E-3a**. Interestingly, only acid-catalyzed exchange into the acetyl or iminyl groups occurred. That is, no *ortho*-H(D) exchange was observed. The existence of these hydroarylation products as well as the lack of *ortho*-deuterium incorporation in Scheme 3.2 suggests two possibilities. First, the C–H bond activation event may require the presence of alkyne to occur. Alternatively, the concentration of any intermediates derived from substrate deprotometalation may not build up to an appreciable extent, thereby precluding interception by the added deuterium source.

Scheme 3.2. Stoichiometric Deuteron-Quenching Reactions.

A) D⁺ Quench of 1a, Control
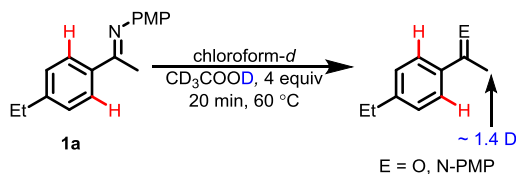
B) D⁺ Quench of 1a and Co-Li, Control
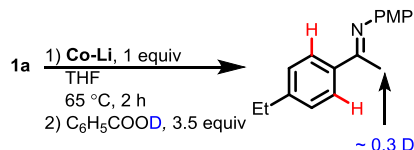
C) D⁺ Quench of 1a, Alkyne, and Co-Li
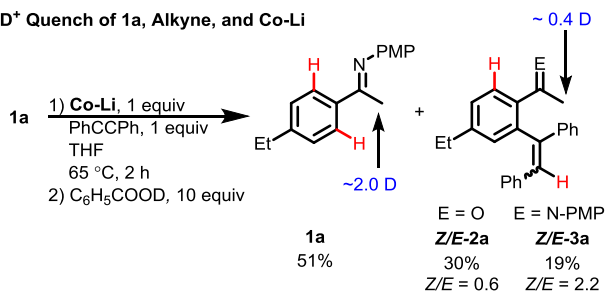
Further investigation of catalysis with isotopically enriched substrates probed the C–H activation step. *Ortho*-dideuterated imine **1a-d_2** was synthesized by selective deuteration of 4'-ethylacetophenone with D₂ and Crabtree's catalyst followed by condensation with *p*-anisidine (eq 3.7). In addition, *ortho*-monodeuterated substrate **1f-d_1** was synthesized from 2'-bromoacetophenone (eq 3.8).
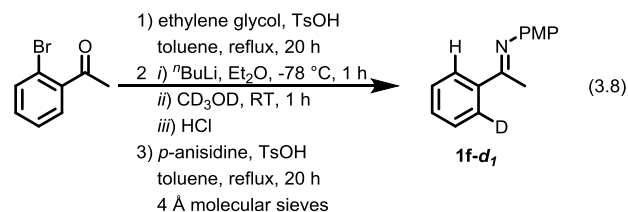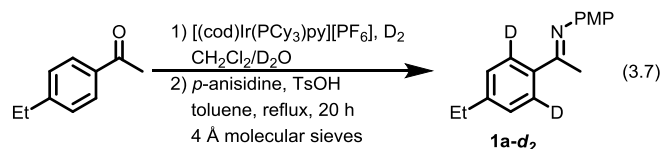
Monitoring the hydroarylation of **1a-d_2** with **Co-Li** as the catalyst (14 mol%) by ¹H NMR spectroscopy provided an isotope effect on both the catalytic rate as well as the rate of isomerization (Figure 3.14). The replacement of C–H for C–D greatly diminished the observed rate of *Z*-olefin formation and implicates a C–H(D) cleavage step as being key to the isomerization. Analysis of the **Z/E-3a-d_2** products

by ^{2}H NMR spectroscopy confirmed deuterium incorporation into the vinylic position (6.60 ppm and 7.06 ppm, respectively) and retention of deuterium at the *ortho*-aryl position (7.86 ppm).
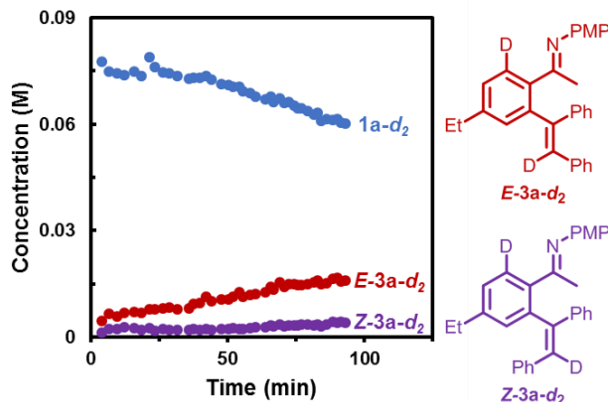
Figure 3.14. Representative initial reaction kinetic profile of the hydroarylation of **1a-d_2** ([**1a-d_2**]$_0$ = 72 mM) with diphenylacetylene ([alkyne]$_0$ = 72 mM) catalyzed by **Co-Li** ([**Co-Li**]$_0$ = 10 mM, 14 mol%). The reaction in benzene-d_6 was monitored by ^{1}H NMR spectroscopy versus Si(SiMe$_3$)$_4$ as an internal standard with the NMR probe temperature calibrated and set to 336 K.

Scheme 3.3. Kinetic Isotope Effect Studies.
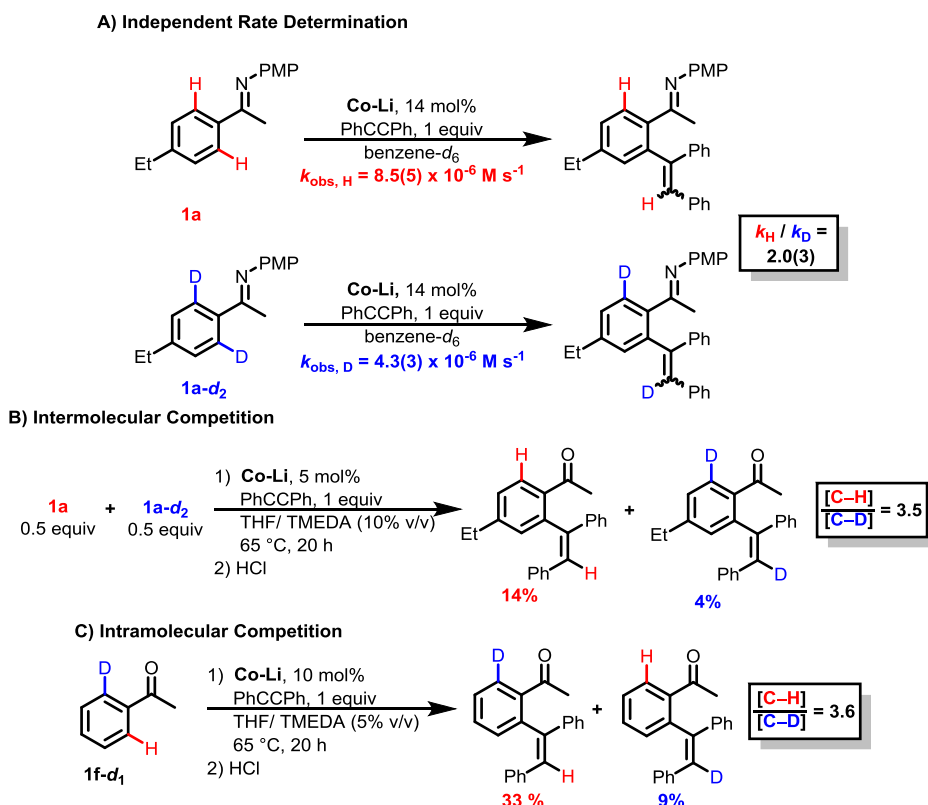
In separate reactions performed at identical concentrations of catalyst and substrates, the observed initial catalytic reaction rate constants $k_{H,obs}$ and $k_{D,obs}$ were determined to be 8.5(5) x 10^{-6} M/s and 4.3(3) x 10^{-6} M/s, respectively (Scheme 3.3A). The calculated KIE ($k_{H,obvs}/k_{D,obs}$) of 2.0(3) is consistent with a rate-

determining C–H cleavage.[75] Additional KIE experiments with equimolar amounts of **1a** and **1a-d_2** are consistent with this result; this intermolecular competition (Scheme 3.3B) resulted in an isotopic distribution corresponding to a KIE of 3.5, which is larger than that determined in the independent rate experiments due to slightly different reaction conditions (*i.e.,* catalyst loading and solvent). The mixed products resulting from H(D)-crossover were not observed in this competition, which supports the C–H cleavage as a non-reversible step. Similarly, an intramolecular KIE was calculated to be 3.6 using imine **1f-d_1** bearing both an *ortho*-deuterium and *ortho*-proton (Scheme 3.3C).

Substrate competition experiments further examined the nature of the C–H transfer step. In four separate experiments, equimolar amounts of electron rich and electron poor (*N*-aryl)aryl ethanimine substrates were subjected to catalytic conditions. The competition of **1a** and **1b** (eq 3.9) illustrates a representative trend that electron-poor arenes (e.g., CO_2Me) are favored over electron-rich substrates (e.g., Et) in the catalysis, which suggests that a proton-like transfer occurs in the C–H bond activation event.[76] Additional substrate competition experiments are given in eqs 3.10 - 3.14.
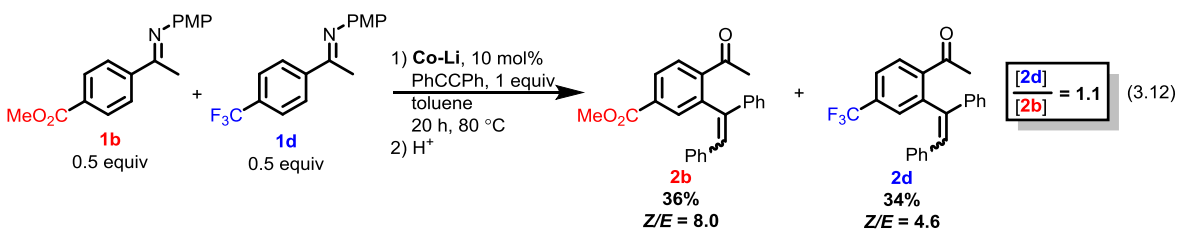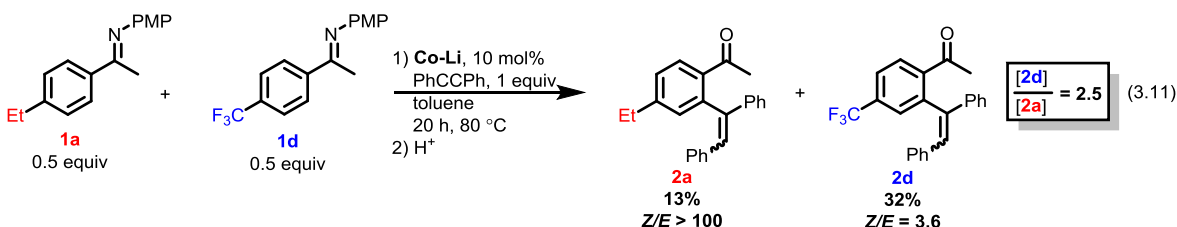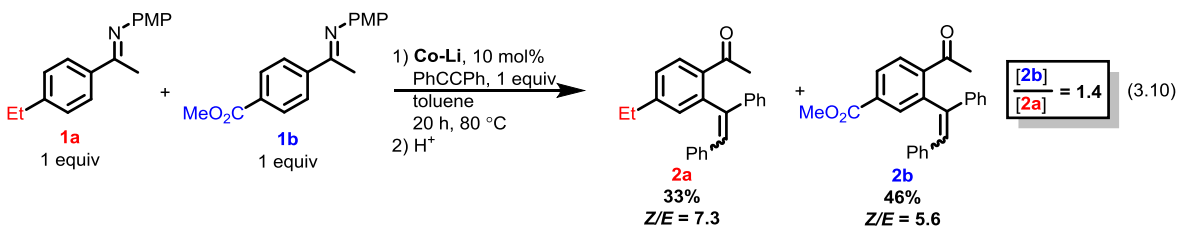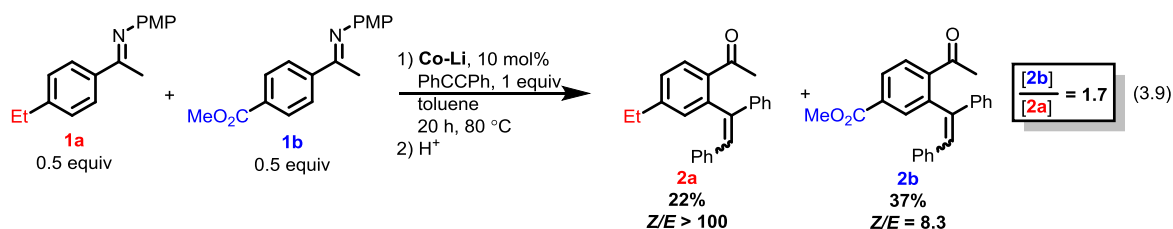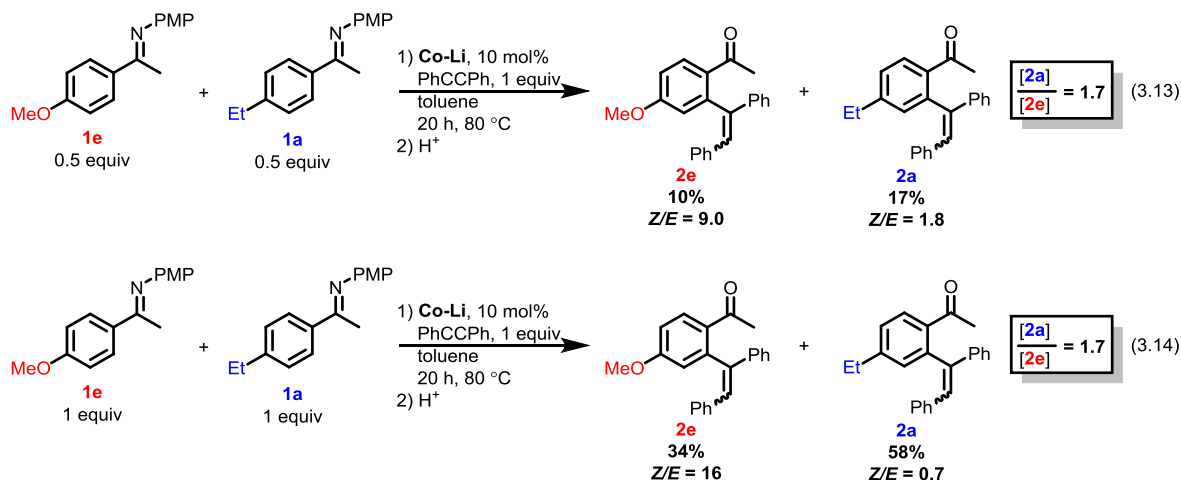
Independent rate measurements for the hydroarylations of the substituted (*N*-aryl)aryl ethanimines with **Co-Li** corroborated the competition experiments. The initial catalytic rates were determined for **1a**, **1b**, **1d**, and **1e** and appear to correlate to the σ_{para} parameter, as illustrated in the correlation plot (Figure 3.15A). A Hammett plot (Figure 3.15B) was generated by the normalization of the measured rates by the rate observed for **1a** (k_X/k_{Et}); the small, but positive slope ($\rho' = 0.36(6)$) of this plot indicates that the arene and metal center accumulate negative charge during the C–H activation. That is, the observed rate of catalysis may have a weak correlation with the pK_a of the arene C–H bond. However, the relatively small rate enhancements observed in this series of substrates preclude the proposal of any unambiguous rationale.
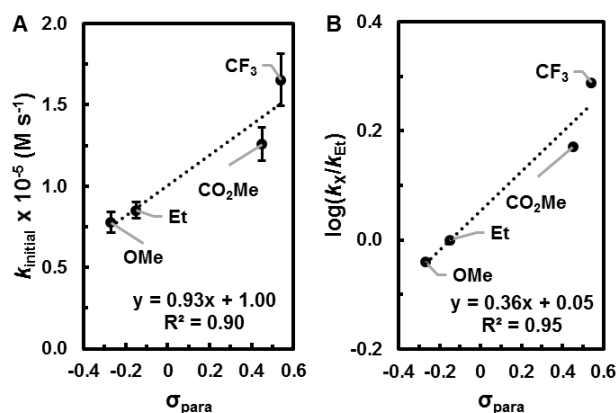
Figure 3.15. A: Hammett parameter versus the initial rate of hydroarylation for **1a** (Et), **1b** (CO$_2$Me), **1d** (CF$_3$), and **1e** (OMe). Catalytic conditions: (*N*-aryl)aryl ethanimine ([**1**]$_0$ = 72 mM) with diphenylacetylene ([PhCCPh]$_0$ = 72 mM) catalyzed by **Co-Li** ([**Co-Li**]$_0$ = 10 mM). The reactions in benzene-d_6 were monitored by ^{1}H NMR spectroscopy versus Si(SiMe$_3$)$_4$ as an internal standard with the NMR probe temperature calibrated to 340 K. Error bars determined as the standard deviation of triplicate runs. **B:** Normalized Hammett plot, which depicts the log(k_X/k_{Et}) as a function of the Hammett parameter with a slope of $\rho' = 0.36(6)$, with error determined as the standard error of the linear regression ($R^2 = 0.95$, $S_x = 0.06$).

Scheme 3.4. Proposed Mechanism for Alkyne Hydroarylation Catalyzed by Co-Li. [a]
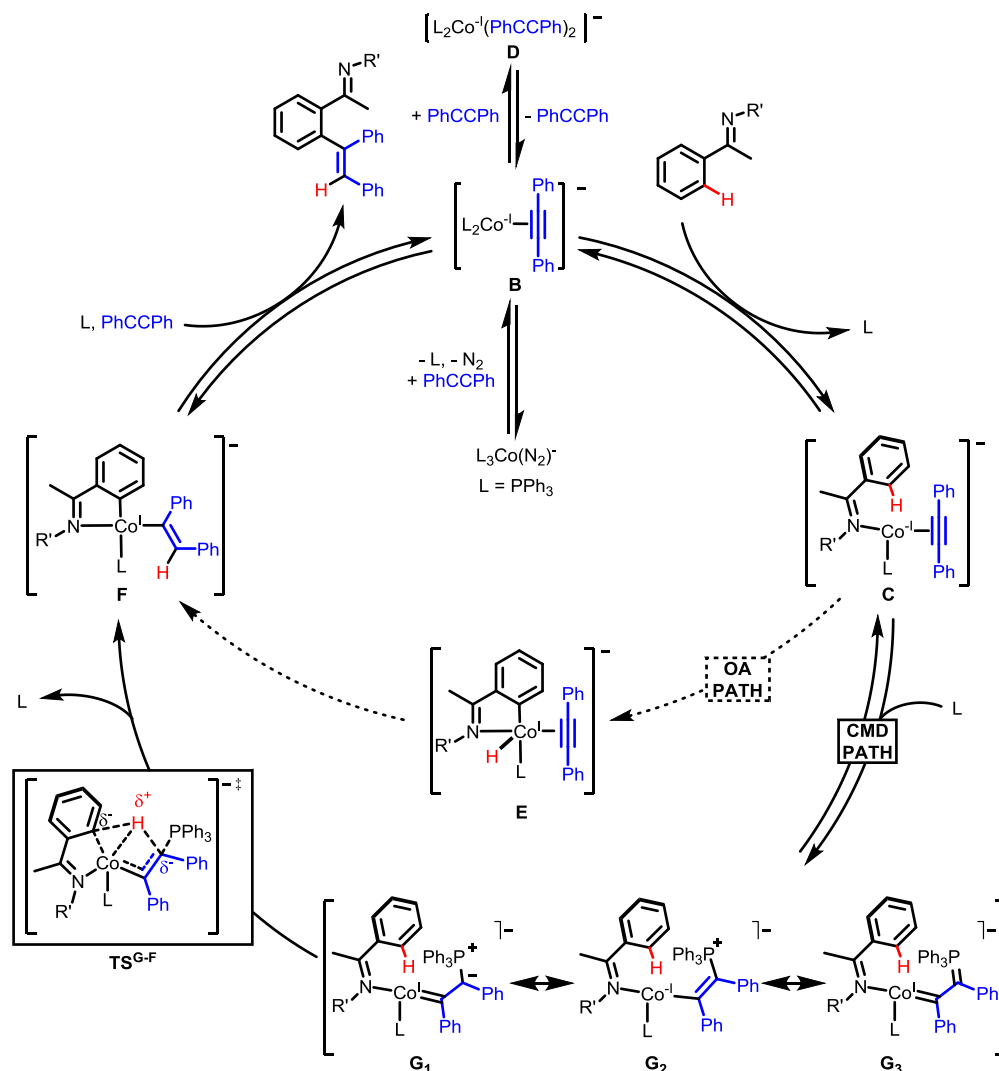
[a] Mg or Li counterions have been omitted for clarity in all catalytic steps.

Proposed Mechanism for the Catalytic Cycle. Cumulatively, the results described above allow postulation of a reasonable mechanism for this catalysis (Scheme 3.4). The anionic complex **Co-Li** appears to be a direct precursor to the active catalytic species. Alkyne coordination occurs prior to the rate determining C–H activation step by displacement of PPh_3 and N_2 to generate the Co(alkyne) complex **B** which undergoes reversible imine precoordination to form complex **C**. It is also possible that multiple, non-productive alkyne ligation steps occur to form the off-cycle species **D**. This type of complex is apparently not catalytically active based on the observed competitive inhibition described in the Michaelis-Menten study (Figure 3.11). Presumably, such complexes possess less activated alkyne ligands due to competitive π-backbonding.

In catalytically productive steps, complex **C** may undergo C–H bond activation. One possible pathway (dashed) involves an intramolecular aryl C–H oxidative addition (OA) in **C** to afford a hydrido-Co(I) intermediate **E**; subsequent hydride insertion affords a (C,N)-chelated complex **F** bearing a

diphenylvinyl fragment. Reductive elimination and substrate coordination afford the hydroarylation product as the *E*-isomer and regenerates **B**. However, this mechanism does not explain the rate enhancement observed with added PPh$_3$.

An alternative C–H bond activation route (bold) involves an initial nucleophilic attack of exogeneous PPh$_3$ onto the bound alkyne in **C** to afford the zwitterionic intermediate **G**. This species may be described by resonance structures involving charge localization exists on the alkyne β-carbon (**G$_1$**), the Co metal center (**G$_2$**), or across the entire alkyne (**G$_3$**). If addition of L to the cobalt center occurs instead at **C** or **G**, the resultant coordinatively saturated 18 e$^-$ species would lack a requisite open coordination site for the H transfer step to occur. This should lead to a rate inhibition and not the observed rate enhancement.

Indeed, precedent exists for phosphine addition to metal bound alkyne complexes.[68-74] One example reported by Chin and coworkers[68] demonstrated that such additions occur upon exposure of [(CO)Ir(PPh$_3$)$_4$]$^+$ to phenylacetylene (eq 3.15). The resultant metalo-phosphonium-ylide complex exhibits a ^{31}P NMR resonance at 20.11 ppm (chloroform-*d*), which is similar to that observed for the Co intermediate described above (9.90 ppm, benzene-*d$_6$*, Figure 3.13).
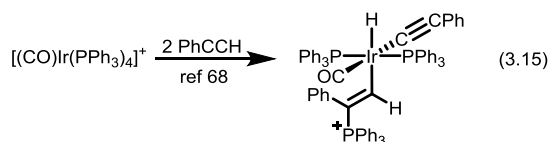
An example of a first-row transition metal complex which undergoes phosphine assisted alkyne insertion was described by Huggins and Bergman.[69] In this report, (acac)Ni(PPh$_3$)R complexes were observed to react with internal alkynes of the type R'CCR" to afford (acac)Ni(CR'=CR"R)(PPh$_3$) species with an unusual distribution of *syn*- and *anti*-insertion products. They postulated that PPh$_3$ played a role in both the insertion process and off-cycle isomerizations by direct attack on Ni(alkyne) or Ni(vinyl) intermediates. While analogous reactivity with monometallic cobalt complexes has yet to be described, a bimetallic Co$_2$(alkyne) complex undergoes an intramolecular rearrangement to generate a new P–C$_{alkyne}$ bond (eq 3.16) that is reminiscent of a formal insertion (^{31}P resonances observed at 31.3 and 4.7 ppm in dichloromethane).[70] Phosphine-alkyne couplings have also been reported for Mo,[71] Re,[72] Pd,[73] and Rh/Os heterobimetallic[74] complexes.
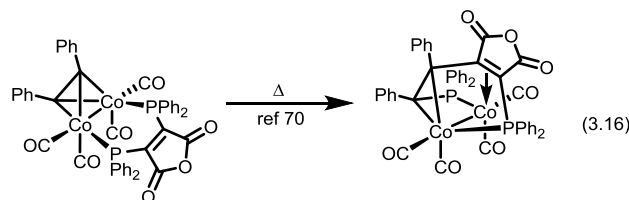
We propose that PPh$_3$ imparts Wittig-like character (and nucleophilicity) to the Co-bound carbon, as illustrated by resonance structure **G$_1$**, and thereby accesses a more facile C–H cleavage though a direct, H$^+$ transfer to afford **F** (via **TS^{G-F}**). Indeed, concerted metalation deprotonation (CMD) mechanisms have considerable theoretical precedence[4,6,76-78] and have been invoked in the context of hydroarylation, specifically towards relevant arene-to-alkyne or arene-to-olefin H-transfer steps.[32,33,49,79-81]

A related, low-valent cobalt system has been described by the Petit group[49] which employed (PMe$_3$)$_4$Co as the precatalyst and microwave conditions for alkyne hydroarylation. For this system, it was

postulated that multiple phosphine dissociations occur to generate a monophosphine Co(PMe$_3$) intermediate. On the basis of this assumption, computational studies indicated that a direct, ligand-to-ligand hydride transfer (similar to **TS^{G-F}**, Scheme 3.4) could account for the C–H activation event.[49] The barrier for this concerted H-transfer was calculated to be $\Delta G^{\ddagger} = 15.9$ kcal mol^{-1} for the transition state corresponding to a Co(0) center bearing imine, alkyne, and PMe$_3$ ligands. The CMD mechanism[4,6,76-78] is now well recognized as an important class of bond activation steps, and it seems likely that the hydroarylation catalysis with **Co-Li** involves such a C–H activation pathway. In this context, we favor the direct, CMD-like mechanism (bold) over the classical oxidative bond cleavage path (dashed).

Origin of Observed Olefin *Z/E*-Selectivity: Off-Cycle Isomerization. To investigate the off-cycle isomerization process, a series of disubstituted olefins was treated with catalytic quantities of complex **Co-Li** in the dark to avoid adventitious photoisomerization (eqs 3.17 and 3.18).
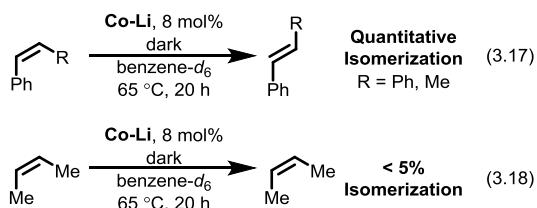
Quantitative isomerization occurred after 20 h at 65 °C for mono- or diaryl substituted *cis*-olefins (i.e., *cis*-stilbene and *cis*-β-methylstyrene, eq 3.17 and Figures 3.16 and 3.17) to afford the corresponding *trans*-olefin. The reverse isomerization (i.e., *trans*- to *cis*-) did not occur to an appreciable extent; after 20 h at 65 °C with added **Co-Li**, *trans*-stilbene remained stereometrically pure (Figure 3.18). Surprisingly, complex **Co-Li** was unreactive towards dialkyl olefins (i.e., *cis*-2-butene, eq 3.18 and Figure 3.19). Upon stoichiometric addition of a hydrogen-atom source (i.e, 9,10-dihydroanthracene, DHA), *cis*-2-butene was converted to *trans*-2-butene with a half-life of ca. 5 h at 65 °C (quantitative after 20 h; Figure 3.20).
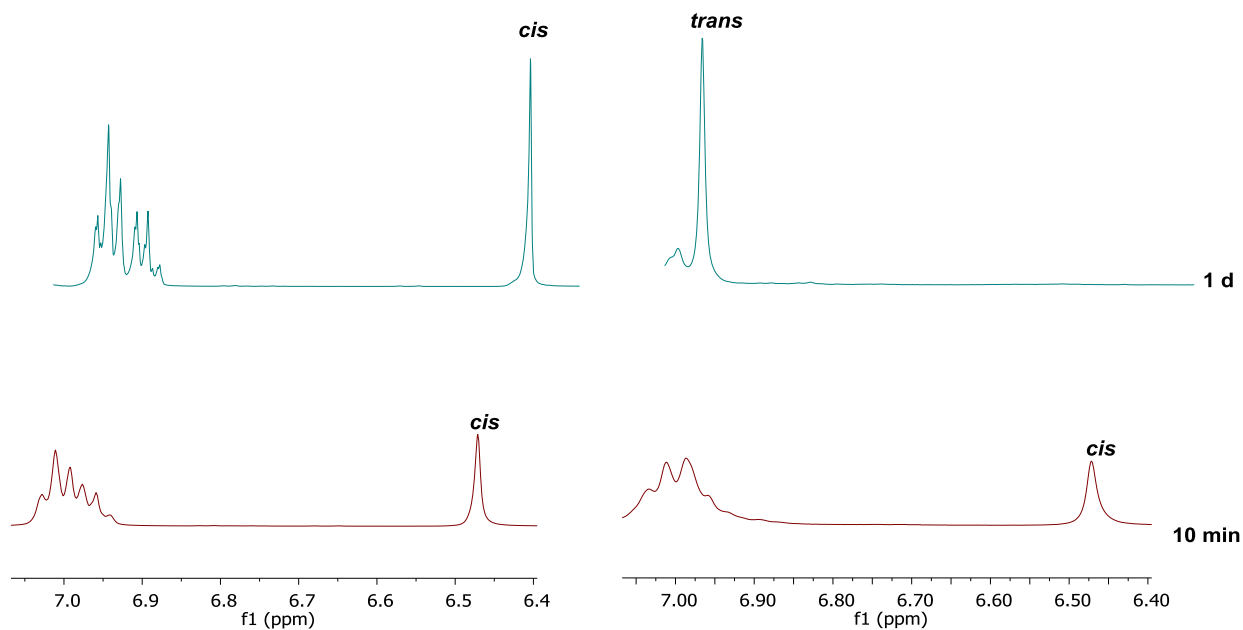
Figure 3.16. Left: Control experiment exhibits no isomerization after heating *cis*-stilbene to 65 °C in the absence of **Co-Li** and in the dark. **Right**: Quantitative isomerization of *cis*-stilbene to the *trans*-isomer after 1 d of heating at 65 °C in the presence of **Co-Li** and in the dark.
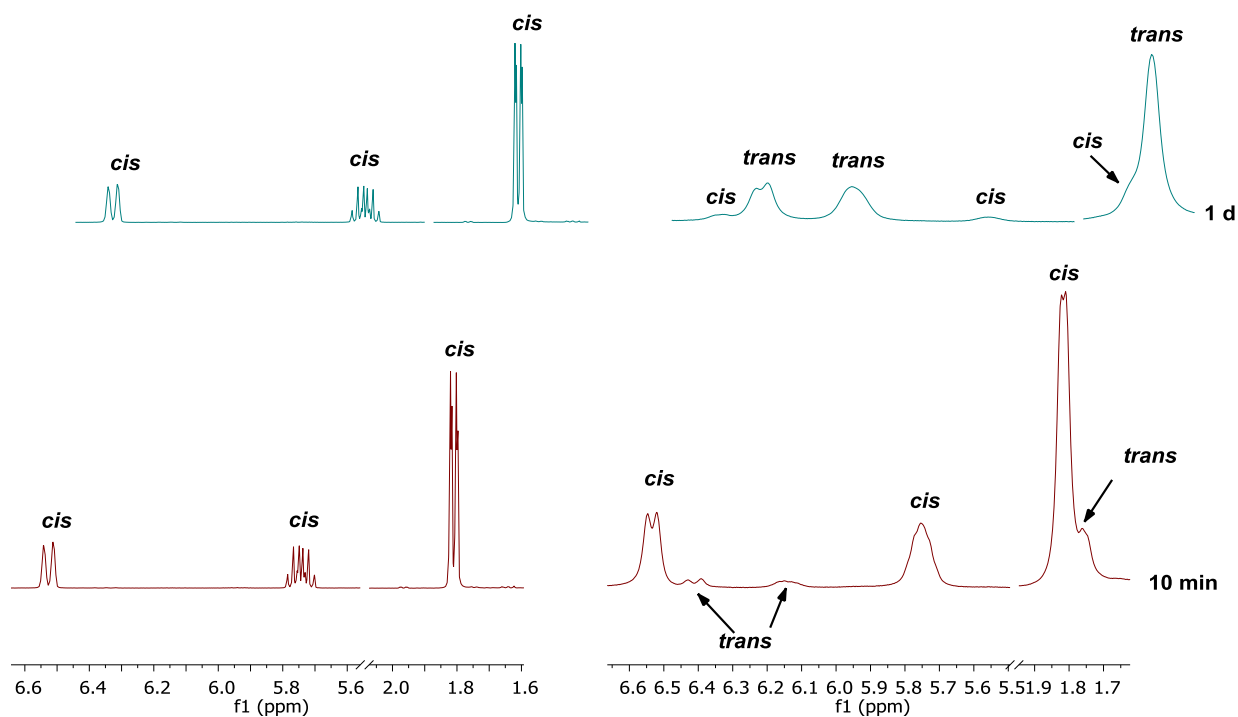
Figure 3.17. Left: Control experiment exhibits no isomerization after heating *cis*-β-methylstyrene to 65 °C in the absence of **Co-Li** and in the dark. **Right**: Quantitative isomerization of *cis*-β-methylstyrene to the *trans*-isomer after 1 d of heating to 65 °C in the presence of **Co-Li** and in the dark.
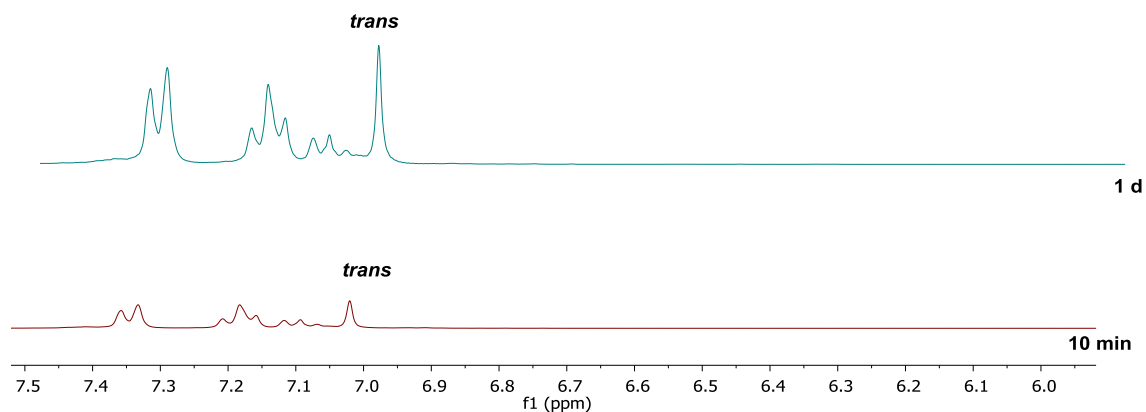
Figure 3.18. Attempted isomerization of *trans*-stilbene with **Co-Li** at 65 °C for 1 d. Note that no detectable isomerization occurred as indicated by the absence of any new *cis*-stilbene resonances.
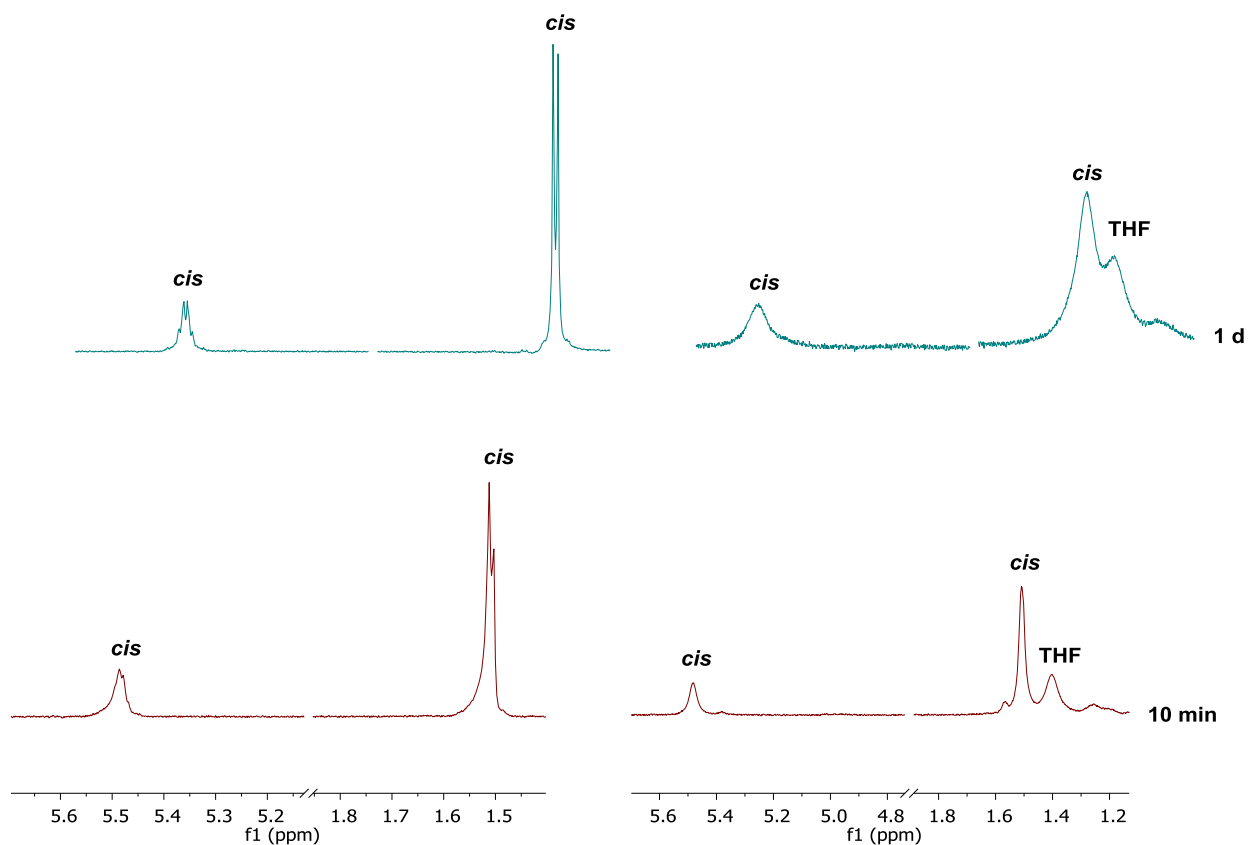
Figure 3.19. Left: Control experiment of heating *cis*-2-butene in the absence of **Co-Li** and in the dark **Right:** Attempted isomerization of *cis*-2-butene with **Co-Li** at 65 °C for 1 d. Note that no detectable isomerization occurred as indicated by the absence of any new *trans*-2-butene resonances.
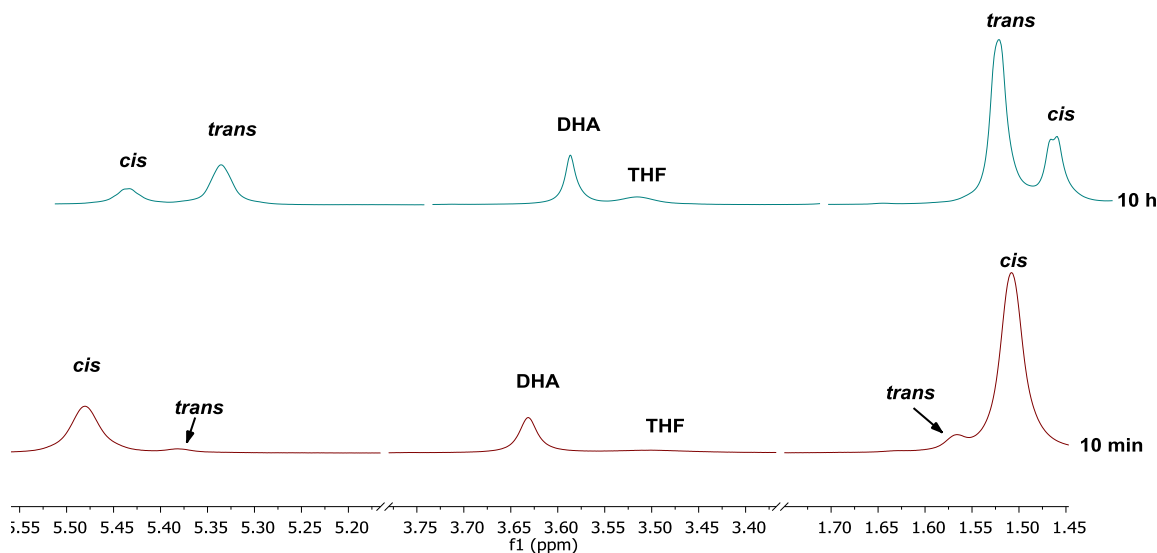
Figure 3.20. Isomerization of *cis*-2-butene with **Co-Li** at 65 °C with the addition of 1 equiv of 9,10-dihydroanthracene (DHA). Note that the reaction occurs with a half-life of ca. 5 h.

The kinetic profiles of the isomerization process with *cis*-stilbene (Figure 3.21A) and *cis*-β-methylstyrene (Figure 3.23A) as the substrates were investigated by ^{1}H NMR spectroscopy in benzene-d_6 at 22 °C (see Figures 3.22 and 3.24 for representative spectra). The dependence of the isomerization rate on [olefin] revealed a first-order rate dependence for the case of *cis*-stilbene (Figure 3.21B; k_{obs} = 3.1(2) x 10^{-6} s^{-1}), but an inverse first-order dependence for *cis*-β-methylstyrene (Figure 3.23B; k_{obs} = 1.3(1) x 10^{-7} M^{-1} s^{-1}). After ca. 3 days at 22 °C, near quantitative conversion (~ 95%) to the *trans*-isomer was observed for both olefin substrates.
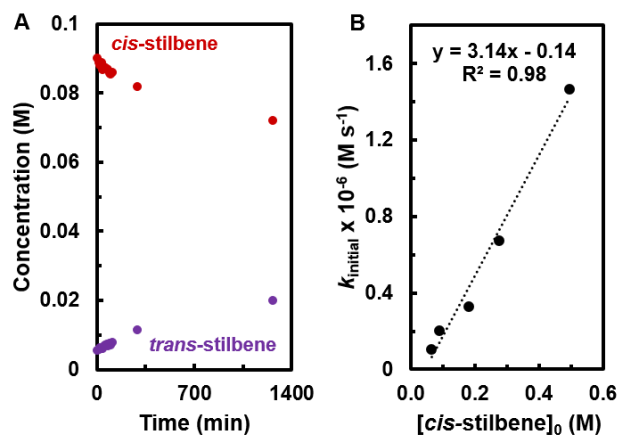
Figure 3.21. A: Representative kinetic profile of *cis*-stilbene ([*cis*-stilbene]$_0$ = 95 mM) isomerization catalyzed by **Co-Li** (10 mol%, [**Co-Li**]$_0$ = 7 mM) as determined by ^{1}H NMR spectroscopy in benzene-d_6 vs Si(SiMe$_3$)$_4$ as an internal standard with the NMR probe temperature calibrated and set to 295 K. **B:** Dependence of isomerization rate on [*cis*-stilbene]$_0$. The dashed line is a linear fit of the data with a slope of k_{obs} = 3.1(2) x 10^{-6} s^{-1}. Error determined as the standard error of the linear regression (R^2 = 0.98, S$_x$ = 0.2 x 10^{-6} s^{-1}).
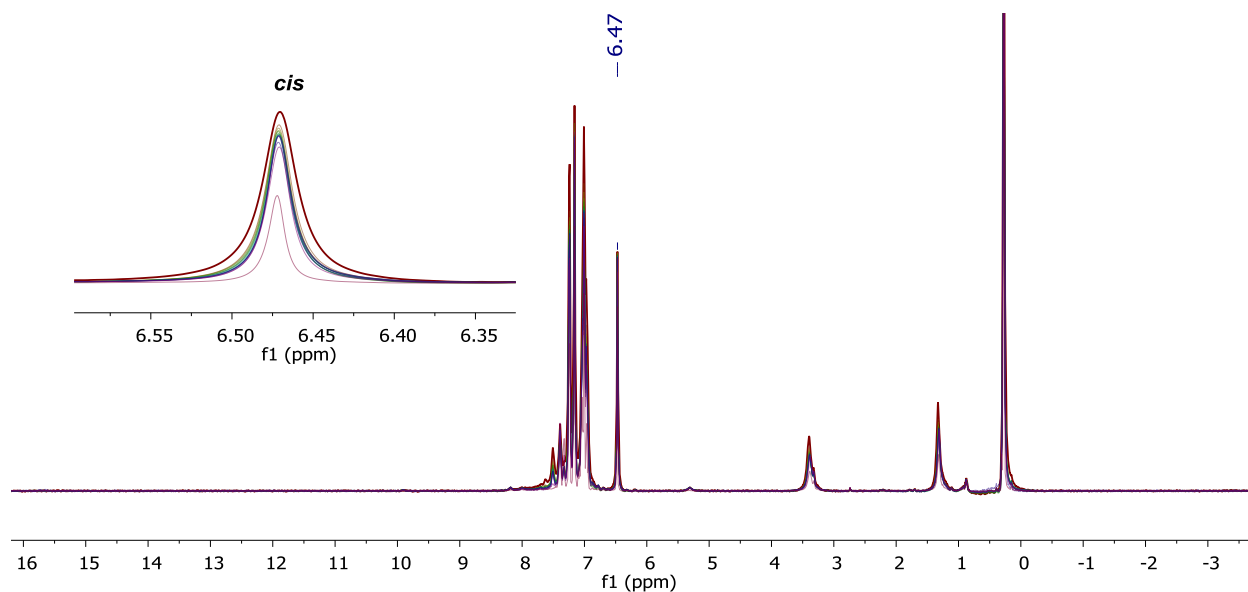
Figure 3.22. Representative kinetic profile of the isomerization of *cis*-stilbene catalyzed by **Co-Li** (7 mM).
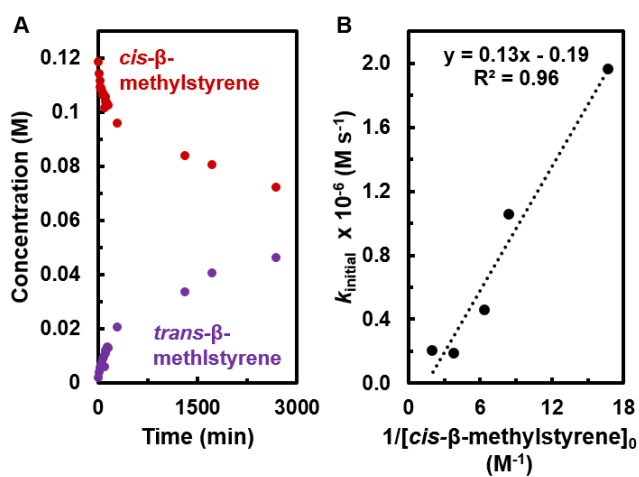
Figure 3.23. A: Representative kinetic profile of *cis*-β-methylstyrene ([*cis*-stilbene]$_0$ = 120 mM) isomerization catalyzed by **Co-Li** (10 mol%, [**Co-Li**]$_0$ = 7 mM) as determined by ^{1}H NMR spectroscopy in benzene-d_6 vs Si(SiMe$_3$)$_4$ as an internal standard with the NMR probe temperature calibrated and set to 295 K. **B:** Dependence of isomerization rate on [*cis*-β-methylstyrene]$_0$. The dashed line is a linear fit of the data with a slope of k_{obs} = 1.3(1) x 10^{-7} M^{-1} s^{-1}. Error determined as the standard error of the linear regression (R^2 = 0.96, S$_x$ = 0.1 x 10^{-7} M^{-1} s^{-1}).
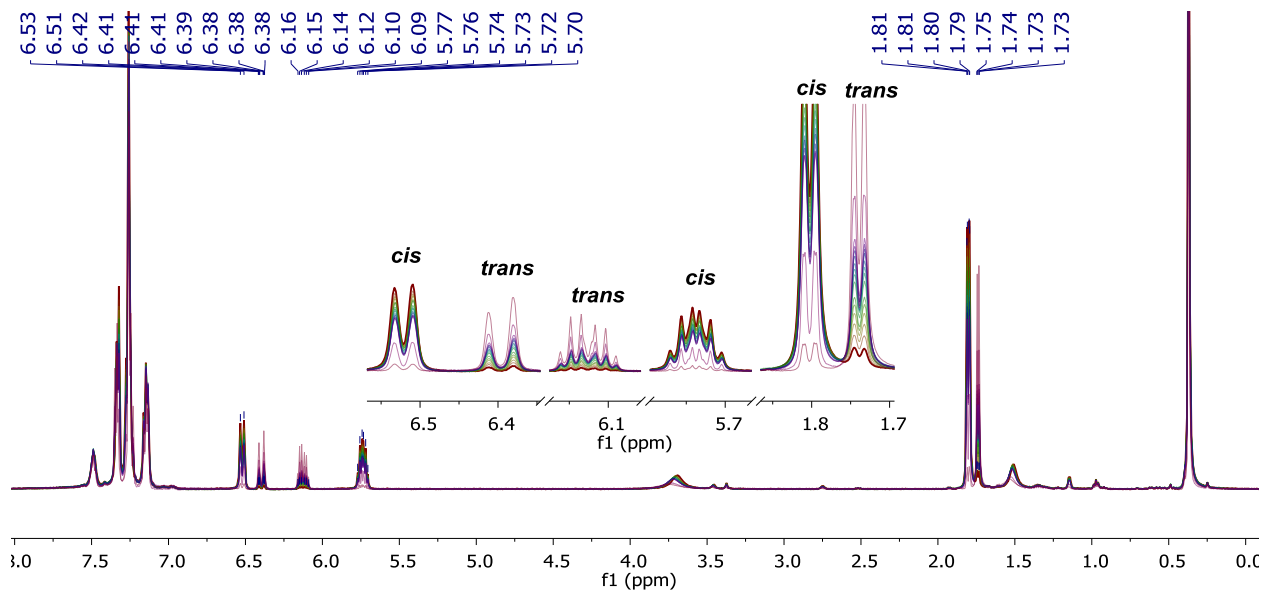
Figure 3.24. Representative kinetic profile of the isomerization of *cis*-β-methylstyrene catalyzed by **Co-Li** (7 mM).

Cobalt-catalyzed olefin isomerizations have recently been reported by Hilt and coworkers.[82] Isomerization of terminal olefins of the type $H_2C=CHCH_2R$ into a mixture of *E*- and *Z*-internal olefins was observed upon treatment with a mixture of $CoBr_2(PR_3)_2$, Zn, ZnI_2, and Ph_2PH. Isomerization required the use of Ph_2PH, presumably because the key mechanistic step involves reversible H-transfer to the olefin to generate the cobalt intermediate, $L_2Co(H_3C-CHCH_2R)(=PPh_2)$. Free rotation about the previously olefinic **C–C** bond in the resultant saturated alkyl fragment may occur, which results in formation of the observed mixture of *E*- and *Z*-olefin products. In contrast to the system described by Hilt,[82] complex **Co-Li** isomerizes internal diarylolefins without the addition of a reagent that might produce a cobalt hydride species. However, it seems likely that a Co–H species, formed under the reaction conditions, may be responsible for the observed isomerization.

These results point to a catalytic, off-cycle isomerization event that accounts for the observed *Z*-selectivity in the hydroarylation process (Scheme 3.5). Initial coordination of *cis*-olefin to complex **Co-Li** occurs to give intermediate **H**. A formal C–H oxidative addition of the bound olefin of **H** could produce the hydride species **I** bearing a *cis*-vinyl fragment. Cobalt-vinyl intermediates, such as **F** (Scheme 3.4) and **I** (Scheme 3.5), may undergo olefin isomerization in a manner similar to that postulated by Huggins and Bergman[69] for analogous *trans*-isomerization in vinylic complexes derived from *cis*-insertions of aryl-substituted alkynes into a Ni–H bond. It was posited by these authors[69] that such Ni-based alkyne complexes exhibit charge localization on the diaryl-vinyl ligand, thereby reducing the double-bond character and allowing C–C bond rotation.

Anionic character in the analogous Co–vinyl complex **I** should concentrate negative charge on the benzylic β–C as indicated in resonance structure **J**, which is stabilized in the presence of aryl substituents (e.g., R = Ph). This aryl-group resonance stabilization of a carbanionic center would account for the observation that *cis*-stilbene and *cis*-β-methylstyrene are rapidly isomerized by **Co-Li**, whereas *cis*-2-butene is unreactive under comparable conditions. A low-energy C–C bond rotation from **J** would result in formation of a cobalt-bound *trans*-vinyl ligand (**K**). Reductive elimination and ligand substitution would

then liberate the observed *trans*-olefin and regenerate **H**. It is possible that PPh₃ addition (akin intermediate **G** proposed above in Scheme 3.4) may play a role in the observed isomerization process.

It is plausible that a second olefin may bind to **H** to form the bis(olefin) complex **L**, which may be catalytically incompetent. It is likely that olefin size may suppress the formation of such off-cycle species, which is consistent with observation of the first-order dependence on *cis*-stilbene and inverse first-order dependence on *cis*-β-methylstyrene.

Scheme 3.5. Proposed Olefin Isomerization Mechanism. [a]
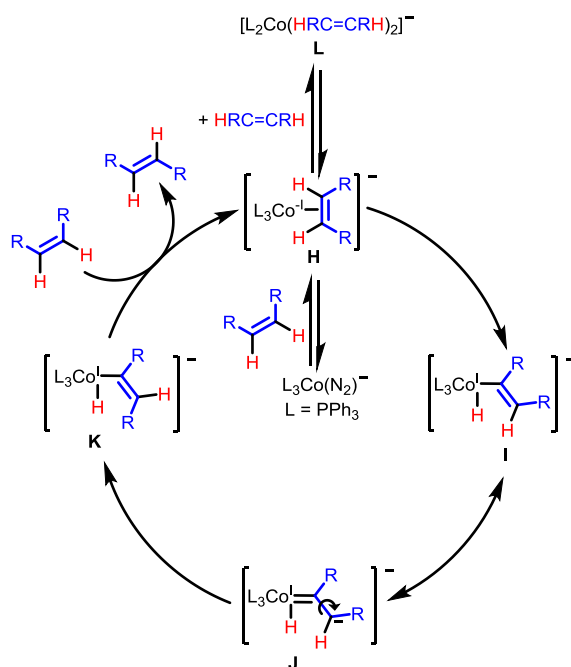
[a] Mg or Li counterions have been omitted for clarity in all catalytic steps.

The apparent lack of appreciable isomerization in the Yoshikai system[29] may implicate alternative isomerization pathways that are operative with different initiation reagents. For example, activation of CoBr₂ with bulky Grignard reagents without β-hydrogens may result in reduction to a Co(0) species as the active catalyst. Such species may not be as active for olefin isomerization as **Co-Li**, as illustrated by the observation of primarily *E*-isomers in the Yoshikai system.[29]

Conclusions. Significantly, this mechanistic study has developed a highly reduced, single-component cobalt catalyst for alkyne hydroarylations. Initiation of catalysis occurs via a three-step pathway (i.e., transmetallation, β-H elimination, deprotonation) to afford a dinitrogen Co(-I) complex, **Co-Li**. Evidence for the catalytic mechanism, such as the moderate primary isotope effect and the observed requirement that alkyne binds prior to the C–H activation, implicates a CMD mechanism.[4,6,32,33,49,79,80] Modified Michaelis-Menten enzyme kinetic analysis revealed a complex dependency of the substrates on the observed reaction rate; while both substrates display saturation-like kinetics, competitive substrate inhibition occurs at non-equimolar concentrations of (*N*-aryl)aryl ethanimine and alkyne. This may be a result of an additional alkyne coordination to formation of an off-cycle bis(alkyne) complex. Interestingly, rate enhancements were observed with additional ancillary ligand, which implicates PAr₃ as a non-innocent reactant in this

system. The observed *Z*-selectivity occurs by an off-cycle olefin isomerization catalyzed by **Co-Li**. Interestingly, only aryl-substituted olefins (i.e., stilbene, β-methylstyrene) undergo *cis*-to-*trans* isomerization, which may implicate free rotation about the C–C bond within a metallo-carbanion intermediate.

These mechanistic insights should prove useful in the design of new first row transition metal catalysts that utilize C–H activations and C–C bond hydroarylations. In particular, the identity of the active species and the mechanism of initiation provide insight into structural requirements for competent catalysis. Highly reduced species exhibit catalytic activity, and such species appear to be generated *in situ* when cobalt dihalide species are activated with organometallic reagents (e.g, RMgBr, RLi, AlR$_3$, etc.). This information provides concepts for developing first row-metal, single-component catalysts that are storable in solid-state, which circumvents the need for multiple, solution-state reagents.

Experimental

General Considerations

All reactions and experiments, unless otherwise noted, were performed using standard Schlenk techniques under N$_2$ atmosphere or inside a N$_2$ glovebox. Schlenk glassware was oven dried overnight before use. Solvents were stored over 3 Å molecular sieves after drying with a JC Meyers Phoenix SDS solvent purification system. Solvents for organic syntheses were used without further purification. Deuterated NMR solvents were purchased from Cambridge Isotope Laboratory. Benzene-*d$_6$* was degassed by three freeze/pump/thaw cycles and then dried over 3 Å molecular sieves. Substituted acetophenones, CoCl$_2$(H$_2$O)$_6$, NaBH$_4$, PPh$_3$, diphenylacetylene, *p*-anisidine, Grignard reagents, *n*BuLi, tosylic acid monohydrate, CuI, (PPh$_3$)$_2$PdCl$_2$, *p*-iodotoluene, 4-ethynyltoluene, *cis*-stilbene, *trans*-stilbene, *cis*-β-methylstyrene, *cis*-2-butene, and Crabtree's catalyst were purchased from commercial suppliers (Sigma-Aldrich, Alfa Aesar, TCI) and used without further purification. MeLi was purchased from a commercial source and desolvated under reduced pressure prior to usage. D$_2$ (99.7%) was purchased in a lecture bottle sized gas cylinder from Praxair Technology and used as recieved. Si(SiMe$_3$)$_4$ was purchased from a commercial source, sublimed, and stored in a N$_2$ glovebox prior to usage.

All ^{1}H, ^{2}H, ^{7}Li{^{1}H}, ^{13}C{^{1}H}, and ^{31}P{^{1}H} NMR experiments were carried out using Bruker AV-300, AVB-400, AVQ-400, AV-500, DRX-500, NEO-500, or AV-600 MHz spectrometers at ambient temperatures (unless otherwise noted). ^{1}H and ^{13}C{^{1}H} NMR spectra were internally calibrated to residual solvents relative to tetramethylsilane. ^{31}P{^{1}H} NMR spectra were calibrated externally to trimethyl phosphate. ^{7}Li{^{1}H} NMR spectra were calibrated externally to LiCl/D$_2$O. ^{19}F NMR spectra were calibrated externally to CFCl$_3$. Variable temperature NMR experiments were calibrated versus ethylene glycol as an external NMR thermometer.[83]

High resolution mass spectrometry (HRMS) experiments were carried out by the QB3/Chemistry Mass Spectrometry Facility at the University of California, Berkeley. ESIHR experiments were performed on a LTQ-FT instrument (from Thermo-Finnigan) with direct injection using Excalibur software. EIHR experiments were performed on an Autospec Premier instrument (from Waters) using MassLynx software. Elemental analyses were performed at the Microanalytical Laboratory at the University of California, Berkeley using a Perkin Elmer 2400 Series II combustion analyzer equipped for determination of %C, %H and %N. Rate law modeling was performed using Mathematica 11 software.

Synthesis of Metal Complexes

Synthesis of (PPh₃)₃CoCl (Co-Cl). The synthesis of **Co-Cl** has been described by Wakatsuki and coworkers[50] and an adaptation is described below. A slurry of $CoCl_2 \cdot 6\ H_2O$ (9.6 g, 40.5 mmol, 1 equiv) and PPh_3 (32 g, 122 mmol, 3 equiv) in EtOH (200 mL) was thoroughly sparged with N_2. Under a flow of N_2, the reaction mixture was heated to reflux for 30 min with a concurrent color change to deep blue. The reaction mixture was cooled to ambient temperature and $NaBH_4$ (1.3 g, 33.7 mmol, 0.8 equiv) was added slowly over ca. 10 min. *Note: decomposition occurs if NaBH₄ is added too quickly.* A color change from dark blue to dark green-blue and then to light brown was observed during $NaBH_4$ addition. The reaction mixture was stirred for an additional 10 min to allow for complete reduction. Upon completion, the mixture was filtered to afford a light brown solid which was washed thoroughly with EtOH (ca. 0.5 L) to remove residual Co^{II} starting materials. After EtOH washes appeared colorless, the solids were washed with H_2O (ca. 0.2 L) and then EtOH (ca. 0.1 L). A final hexane wash afforded the title compound as a light brown powder (27.2 g, 76%). Note: **Co-Cl** is mildly air-sensitive and decomposes after ca. 1-2 days in solid-state. Therefore, **Co-Cl** should be stored in an inert atmosphere glovebox for long-term storage.

Anal. Calcd for $C_{54}H_{45}ClCoP_3$: C, 73.6; H, 5.15. Found: 73.4; H, 5.20.

Synthesis of (PPh₃)₃Co(N₂)H, (Co-H). Alternative syntheses of **Co-H** from $Co(acac)_3$ and $AlEt_2(OEt)$ have been described previously[51,52] and a milder synthesis is described below. To a slurry of **Co-Cl** (5.0 g, 5.7 mmol, 1 equiv) in THF (ca. 50 mL), CyMgCl (3.7 mL, 2.0 M in Et_2O, 7.4 mmol, 1.3 equiv) was added dropwise. Rapid color change from brown to red-brown was observed. The reaction mixture was allowed to stir at ambient temperatures for 16 h, upon which dioxane (2 mL) was added to trap residual $MgCl_2$ as the insoluble coordination polymer, $[MgCl_2(dioxane)]_n$. The reaction mixture was then filtered and the volatile components were removed under reduced pressure. The residue was dissolved in Et_2O (ca. 50 mL) and the solution was cooled to -30 °C to afford orange crystals of the title compound (2.6 g, 51 %) with spectroscopic features matching literature values.[51,52]

^{1}H NMR (benzene-d_6, 400.1 MHz): δ 7.40 (br s, 18 H), 6.91 (br s, 27 H), -19.94 (q, $^2J_{HP}$ = 50.2 Hz, 1H).

^{31}P{^{1}H} NMR (benzene-d_6, 162.0 MHz): δ 48.33 (br s).

Anal. Calcd for $C_{54}H_{46}CoN_2P_3$: C, 74.1; H, 5.30; N, 3.20. Found: C, 73.9; H, 5.12; N, 2.90.

IR (KBr) $\bar{\nu}_{max}$: 3053 (m), 2970 (w), 2862 (w), 2092 (vs, N_2), 1583 (m), 1477 (s), 1432 (s) cm^{-1}.

Synthesis of [(PPh₃)₃Co(N₂)][Li(THF)₃] • LiBr(THF)₂ from Deprotonation with MeLi (Co-Li). To a solution of **Co-H** (400 mg, 0.46 mmol, 1 equiv) in THF (3 mL), a solution of MeLi$_{(s)}$ (27 mg, 1.2 mmol, 2.6 equiv) in THF (3 mL) was added. *Note: commercial solutions of MeLi often contain LiBr as a common impurity.* Rapid methane generation was observed during addition. The reaction mixture was allowed to stir for 16 h and subsequently filtered to remove insoluble solids. Volatile components were removed under reduced pressure to afford a dark-red/black film, which was triturated with pentane (3 x 10 mL) to afford the title compound as a deep maroon/black solid (320 mg, 63 %).

Anal Calcd for $C_{66}H_{69}CoLiN_2O_3P_3 \cdot LiBr \cdot 2C_4H_8O$: C, 66.9; H, 6.45; N, 2.11. Found: C, 67.0; H, 6.43; N, 2.18.

Synthesis of [(PPh₃)₃Co(N₂)][Li(THF)₃] from Deprotonation with ⁿBuLi (Co-Li). An alternate (and scalable) synthesis of **Co-Li** has been adapted from the procedure described by Yamamoto et al.[57] To a solution of **Co-H** (2.4 g, 2.74 mmol, 1 equiv) in THF (10 mL), ⁿBuLi (1.9 mL, 1.7 M in heptane, 3.02 mmol, 1.1 equiv) was added dropwise at ambient temperature resulting in a rapid color change to deep red. The reaction mixture was allowed to stir for 16 h and volatile components were removed under reduced pressure to afford a dark-red/black solid. The solid was triturated with pentane (5 x 10 mL) to afford the title compound as a deep maroon/black solid (2.26 g, 75%), with spectroscopic features matching literature reported values.[57]

Note: While the solid-state characterization for this compound is consistent the formula assigned, dynamic ligand exchange in solution likely occurs giving rise to broadened NMR spectral features as well as resonances consistent with unbound PPh₃.

^{1}H NMR (benzene-d_6, 400.1 MHz): δ 7.50 – 7.30 (m, 27H), 7.05 – 6.95 (m, 18H), 6.89 (br s, 9H), 3.34 (br s, 12H, THF), 1.29 (br s, 12H, THF).

^{1}H NMR (tetrahydrofuran-d_0 with benzene-d_6 as an internal reference, 400.1 MHz): δ 7.37 (b s, 18H), 7.05 (br s, 27H).

^{7}Li{^{1}H} NMR (benzene-d_6, 233.2 MHz): δ -3.82 (br s, FWHM ~ 400 Hz or 1.8 ppm).

^{13}C{^{1}H} NMR (tetrahydrofuran-d_0 with benzene-d_6 as an internal reference, 125.6 MHz): δ 137.7 (d, J_{CP} = 12.3 Hz, unbound PPh₃), 133.7 (d, J_{CP} = 19.7 Hz, unbound PPh₃), 133.3 (overlapping d, J_{CP} = 8.1 Hz, bound PPh₃), 128.6 (s, bound PPh₃), 128.4 (s, unbound PPh₃), 128.4 (d, J_{CP} = 6.8 Hz, unbound PPh₃), 128.1 (s, bound PPh₃), 127.1 (overlapping m, bound PPh₃).

^{31}P{^{1}H} NMR (tetrahydrofuran-d_0, 242.9 MHz): δ 48.14 (br s, bound PPh₃), -5.24 (br s, unbound PPh₃).

IR (KBr) $\bar{\nu}_{max}$: 3047 (br), 2980 (br), 2877 (br), 1897 (vs, N₂), 1578 (vs), 1474 (vs), 1431 (vs) cm^{-1}.

Anal Calcd for $C_{66}H_{69}CoLiN_2O_3P_3$: C, 72.3; H, 6.34; N, 2.55. Found: C, 72.1; H, 6.21; N, 2.35.

Synthesis of [(PPh₃)₃Co(N₂)]₂Mg(THF)₄ from Deprotonation with ⁿBu₂Mg (Co₂-Mg). An alternate (and scalable) synthesis of **Co₂-Mg** has been adapted from the procedure described by Yamamoto et al.[57] To a solution of **Co-H** (1 g, 1.14 mmol, 1 equiv) in THF (5 mL), ⁿBu₂Mg (3.8 mL, 0.6 M in heptane, 2.3 mmol, 2 equiv) was added dropwise at ambient temperature resulting in a rapid color change to deep red. The reaction mixture was allowed to stir for 16 h and volatile components were removed under reduced pressure to afford a dark-red/black solid. The solid was triturated with pentane (5 x 10 mL) to afford the title compound as a deep maroon/black solid (0.65 g, 56%), with spectroscopic features matching literature reported values.[57]

Note: Dynamic ligand exchange in solution likely occurs giving rise to broadened NMR spectral features as well as resonances consistent with unbound PPh₃.

^{1}H NMR (benzene-d_6, 600.13 mHz): δ 7.44 – 7.38 (m, 36 H), 7.05 – 6.80 (m, 54 H), 3.43 (br s, THF, 16H), 1.82 – 1.34 (overlapping s, THF, 17H).

^{31}P{^{1}H} NMR (benzene-d_6, 242.95): δ 48.26 (br s, bound PPh₃), -5.30 (br s, unbound PPh₃).

IR (KBr) $\bar{v}_{max}$: 3049 (br), 2858 (vbr), 1951 (ms),1850 (vs, N$_2$), 1583 (m) cm^{-1}

Synthesis of [(triphos)Co(N$_2$)]$_2$Mg(THF)$_4$ (Co'$_2$-Mg). The original synthesis was described in a procedure by Long et al.[61] and an adaptation is given below. Under an N$_2$ atmosphere, CoCl$_2$ (0.12 g, 0.93 mmol, 1 equiv), and triphos (0.5 g, 0.93 mmol, 1 equiv) were slurried in THF (5 mL) for 1 h at ambient temperature, which resulted in a green-blue solution. After this, Zn powder (0.13 g, 1.86 mmol, 2.2 equiv) was added and allowed to stir for 1 d which resulted in a tan-green slurry. The mixture was filtered to remove residual salts and afforded an orange solution of (triphos)CoCl (260 mg, 39%) which was used without further purification.

To a solution of (triphos)CoCl (260 mg, 0.36 mmol, 1 equiv) in THF (5 mL) under an N$_2$ atmosphere, Mg powder was slurried (130 mg, 5.4 mmol, 15 equiv). The reaction mixture was allowed to stir at ambient temperatures for 2 d which resulted in a deep red solution; after this time, the mixture was filtered through celite to remove residual solids. A second filtration through a 0.2 µm PTFE syringe filter afforded a red film after solvent was removed under reduced pressure. This film was triturated with pentane (3 x 10 mL) to afford the title compound as a deep red solid (210 mg, 67%, purity ca. 80% by ^{1}H NMR) with spectroscopic features matching that of literature reported values.[61]

^{1}H NMR (benzene-d_6, 600.16 mHz): δ 7.80 – 7.51 (m, 12H), 7.47 –7.25 (m 18 H), 7.08 – 6.96 (m, 12H), 6.94 – 6.74 (m, 18H), 3.74 (THF), 2.25 – 2.08 (m, 9H), 1.41 (THF), 1.22 – 1.15 (m, 6H).

^{31}P{^{1}H} NMR (benzene-d_6, 242.95): 31.20 (s) with small impurities at 40.73 and 38.15.

IR (KBr) $\bar{v}_{max}$: 3398 (br), 3050 (br), 2979 (br), 2878 (br), 1846 (vs, N$_2$), 1640 (wv), 1432 (s) cm^{-1}

Synthesis of (*N*-Aryl)Aryl Ethanimine Substrates and Precursors
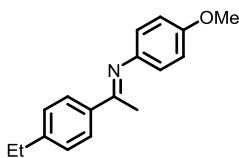
Synthesis of (*E*)-1-(4-ethylphenyl)-*N*-(4-methoxyphenyl)ethan-1-imine (1a). To a round bottom flask equipped with a Dean Stark apparatus and 4 Å molecular sieves (ca. 10 g), a solution of 4'-ethylacetophenone (6.1 mL, 41 mmol, 1 equiv), *p*-anisidine (5.0 g, 41 mmol, 1 equiv), and tosylic acid monohydrate (0.9 g, 4.2 mmol, 0.1 equiv) in toluene (40 mL) was heated to reflux for 16 h. Upon completion, the reaction mixture was allowed to cool to ambient temperature and was filtered to remove residual solids. Volatile components were removed under reduced pressure to afford an orange oil. Crystallization from toluene/pentane at -30 °C afforded the title compound as a yellow solid (6.0 g, 59%).

^{1}H NMR (chloroform-*d*, 400.1 MHz): δ 7.93 (d, *J* = 7.9 Hz, 2H), 7.28 (d, *J* = 8.3 Hz, 2H), 6.91 (d, *J* = 8.9 Hz, 2H), 6.65 (d, *J* = 8.6 Hz, 2H), 3.82 (s, 3H), 2.71 (q, *J* = 7.7 Hz, 2H), 2.23 (s, 3H), 1.27 (t, *J* = 7.6 Hz, 3H).

^{1}H NMR (benzene-d_6, 400.1 MHz): δ 8.04 (d, *J* = 8.2 Hz, 2H), 7.09 (d, *J* = 8.2 Hz, 2H), 6.87 – 6.82 (m, 2H), 6.79 – 6.74 (m, 2H), 3.36 (s, 3H), 2.46 (q, *J* = 7.6 Hz, 2H), 1.97 (s, 3H), 1.08 (t, *J* = 7.6 Hz, 3H).

$^{13}C\{^1H\}$ NMR (benzene-d_6, 125.6 MHz): δ 164.4, 156.5, 146.8, 145.7, 137.9, 128.3, 127.8, 121.2, 114.6, 55.0, 29.0, 16.7, 15.7.

Anal. Calcd for $C_{17}H_{19}NO$: C, 80.6; H, 7.56; N, 5.53. Found: C, 80.6; H, 7.54; N, 5.54.
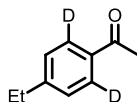
Synthesis of 4'-Ethylacetophenone-(2',6'-d_2). *Caution: working with high pressures is a potential safety hazard, and the reaction vessel should be tested above working pressures prior to usage.* Following an adaptation of a reported literature procedure,[84] 4'-ethylacetophenone (1 mL, 6.8 mmol, 1 equiv) and Crabtree's catalyst ($[(PCy_3)(cod)(py)Ir][PF_6]$, 55 mg, 0.7 mmol, 1 mol%) were dissolved in CH_2Cl_2 (5 mL) with a catalytic quantity of D_2O (ca. 0.3 mL) in a 250 mL Teflon stoppered Schlenk flask equipped with a stir bar. On a Schlenk line, the solution was thoroughly degassed by three freeze/pump/thaw cycles; then, D_2 was added while the reaction flask was still cool (ca. 10 °C, 1 atm). The reaction vessel was then allowed to stir at ambient temperature for 16 h. The solution was then degassed and additional D_2 was added as described above. After an additional 16 h, Et_2O was added to precipitate out residual Ir-containing complexes and the solids were removed via filtration. Volatile components were removed under reduced pressure to afforded the title compound as a pale-yellow oil (0.83 g, 82%). Note: ca. 85% deuterium incorporation at the 2',6'-positions was observed with 4'-ethylacetophenone-(2'-d) as the detectable impurity.

^1H NMR (chloroform-d, 300.1 MHz): δ 7.28 (t, J_{HD} = 1.5 Hz, 2 H), 2.71 (q, J = 7.6 Hz, 2H), 2.58 (s, 3H), 1.26 (t, J = 7.6 Hz, 3H).
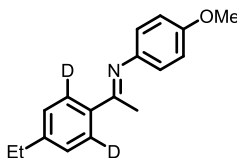
Synthesis of (E)-1-(4-ethylphenyl-2,6-d_2)-N-(4-methoxyphenyl)ethan-1-imine (1a-d_2). To a round bottom flask equipped with a Dean Stark apparatus and 4 Å molecular sieves (ca. 2 g), a solution of 4'-ethylacetophenone-(2',6'-d_2) (0.32 g, 2.1 mmol, 1 equiv), p-anisidine (0.26 mg, 2.1 mmol, 1 equiv), and tosylic acid monohydrate (40 mg, 0.2 mmol, 0.1 equiv) in toluene (5 mL) was heated to reflux for 16 h. Upon completion, the reaction mixture was allowed to cool to ambient temperature and was filtered to remove residual solids. Volatile components were removed under reduced pressure to afford an orange oil. Crystallization from toluene/pentane at -30 °C afforded the title compound as a yellow solid (0.40 g, 47%). Note that trace **1a-d_1** was observed.

^1H NMR (benzene-d_6, 500.2 MHz): δ 7.09 (br s, 2H), 6.87 – 6.80 (m, 2H), 6.80 – 6.75 (m, 2H), 3.36 (s, 3H), 2.46 (q, J = 7.6 Hz, 2H), 1.96 (s, 3H), 1.08 (t, J = 7.6 Hz, 3H).

^2H NMR (benzene-d_0, referenced to added dichloromethane-d_2, 92.1 MHz): δ 8.04 (s).

$^{13}C\{^1H\}$ NMR (benzene-d_6, 125.8 MHz): δ 164.4, 156.5, 146.8, 145.8, 137.8, 128.4, 127.5, 121.2, 114.7, 55.0, 29.0, 16.7, 15.7.

Anal. Calcd for $C_{17}H_{17}D_2NO$: C, 80.0; H, 8.29; N, 5.49. Found: C, 79.6; H, 7.90; N, 5.36.
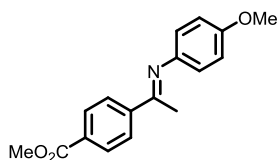
Synthesis of Methyl (*E*)-4-(1-((4-methoxyphenyl)imino)ethyl)benzoate (1b). To a round bottom flask equipped with a Dean Stark apparatus and 4 Å molecular sieves (ca. 2 g), a solution of methyl-4-acetylbenzoate (2.0 g, 11 mmol, 1 equiv), *p*-anisidine (1.4 g, 11 mmol, 1 equiv), and tosylic acid monohydrate (0.2 g, 1.1 mmol, 0.1 equiv) in toluene (40 mL) was heated to reflux for 16 h. Upon completion, the reaction mixture was allowed to cool to ambient temperature and was filtered to remove residual solids. Petroleum ether was then layered for crystallization at -30 °C to afford the title compound as yellow needles (2.3 g, 72%), with spectroscopic features matching literature reported values.[85]

^{1}H NMR (chloroform-*d*, 400.1 MHz): δ 8.10 (d, *J* = 8.5 Hz, 2H), 8.02 (d, *J* = 8.5 Hz, 2H), 6.92 (d, *J* = 8.8 Hz, 2H), 6.77 (d, *J* = 8.9 Hz, 2H), 3.94 (s, 3H), 3.82 (s, 3H), 2.28 (s, 3H).
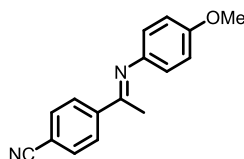
Synthesis of (*E*)-4-(1-((4-methoxyphenyl)imino)ethyl)benzonitrile (1c). To a round bottom flask equipped with a Dean Stark apparatus and 4 Å molecular sieves (ca. 2 g), a solution of 4-acetylbenzonitrile (1 g, 6.9 mmol, 1 equiv), *p*-anisidine (0.9 g, 6.9 mmol, 1 equiv), and tosylic acid monohydrate (0.13 g, 0.7 mmol, 0.1 equiv) in toluene (20 mL) was heated to reflux for 16 h. Upon completion, the reaction mixture was filtered hot to remove residual solids. Upon cooling to ambient temperature, a bright yellow solid precipitated out from solution. The resultant solids were washed with hexanes and volatile components were removed under reduced pressure to afford the title compound as a bright yellow powder (1.5 g, 88%), with spectroscopic features matching literature reported values.[86]

^{1}H NMR (chloroform-*d*, 300.1 MHz): δ 8.12 – 8.01 (m, 2H), 7.78 – 7.70 (m, 2H), 6.98 – 6.89 (m, 2H), 6.80 – 6.72 (m, 2H), 3.83 (s, 3H), 2.29 (s, 3H).
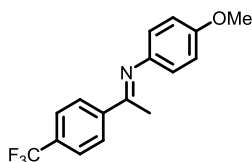
Synthesis of (*E*)-*N*-(4-methoxyphenyl)-1-(4-(trifluoromethyl)phenyl)ethan-1-imine (1d). To a round bottom flask equipped with a Dean Stark apparatus and 4 Å molecular sieves (ca. 2 g), a solution of 4'-(trifluoromethyl)acetophenone (1.0 g, 5.3 mmol, 1 equiv), *p*-anisidine (0.65 g, 5.3 mmol, 1 equiv), and tosylic acid monohydrate (0.13 g, 0.7 mmol, 0.1 equiv) in toluene (20 mL) was heated to reflux for 16 h. Upon completion, the reaction mixture was filtered hot to remove residual solids. Upon cooling to ambient temperature, a bright-yellow needles precipitated out from solution. The resultant solids were washed with

hexanes and volatile components were removed under reduced pressure to afford the title compound as bright-yellow needles (0.86 g, 55%), with spectroscopic features matching literature reported values.[29,86]

^{1}H NMR (chloroform-d, 400.1 MHz): δ 8.08 (d, J = 8.2 Hz, 2H), 7.70 (d, J = 8.2 Hz, 2H), 7.07 – 6.87 (m, 2H), 6.82 – 6.72 (m, 2H), 3.83 (s, 3H), 2.29 (s, 3H).

^{19}F{^{1}H} NMR (chloroform-d, 376.5 MHz): δ -61.92.
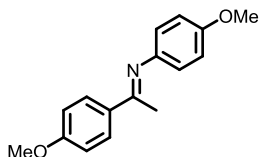
Synthesis of (E)-N,1-bis(4-methoxyphenyl)ethan-1-imine (1e). To a round bottom flask equipped with a Dean Stark apparatus and 4 Å molecular sieves (ca. 2 g), a solution of 4'-methoxyacetophenone (1.0 g, 6.7 mmol, 1 equiv), p-anisidine (0.82 g, 6.7 mmol, 1 equiv), and tosylic acid monohydrate (0.13 g, 0.7 mmol, 0.1 equiv) in toluene (20 mL) was heated to reflux for 16 h. Upon completion, the reaction mixture was filtered hot to remove residual solids. Upon cooling to ambient temperature, a tan-orange powder precipitated out from solution. The resultant solids were washed with hexanes and volatile components were removed under reduced pressure. Further purification by SiO$_2$ column chromatography (eluting with toluene) afforded the title compound as a dull-orange powder (0.57 g, 34%), with spectroscopic features matching literature reported values.[29,86]

^{1}H NMR (chloroform-d, 400.1 MHz): δ 8.01 – 7.84 (m, 2H), 6.99 – 6.93 (m, 2H), 6.92 – 6.89 (m, 2H), 6.75 (m, 2H), 3.87 (s, 3H), 3.82 (s, 3H), 2.23 (s, 3H).
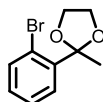
Synthesis of 2-(2-bromophenyl)-2-methyl-1,3-dioxolane. To a round bottom flask equipped with a Dean Stark apparatus, a solution of 2'-bromoacetophenone (3.1 g, 16 mmol, 1 equiv), ethylene glycol (1.8 mL, 31 mmol, 2 equiv) and tosylic acid monohydrate (0.3 g, 1.6 mmol, 0.1 equiv) in toluene (50 mL) was heated to reflux for 16 h. Upon completion, the reaction mixture was quenched with saturated NaHCO$_3$ (50 mL), and extracted with Et$_2$O (3 x 50 mL). The organic layers were combined and washed with brine (50 mL), dried with Na$_2$SO$_4$, and filtered. Volatile components were removed under reduced pressure to afford a colorless oil. Purification by SiO$_2$ column chromatography (eluting with 5% EtOAc/hexanes) afforded the title compound as a colorless oil (3.2 g, 85%), with spectroscopic features matching literature reported values.[87,88]

^{1}H NMR (chloroform-d, 300.1 MHz): δ 7.66 (dd, J = 7.8, 1.8 Hz, 1H), 7.60 (dd, J = 7.9, 1.4 Hz, 1H), 7.28 (ddd, J = 7.9, 7.5, 1.3 Hz, 1H), 7.14 (ddd, J = 7.8, 7.6, 1.8 Hz, 1H), 4.19 – 3.99 (m, 2H), 3.83 – 3.67 (m, 2H), 1.81 (s, 3H).
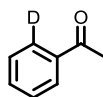
Synthesis of acetophenone-(2'-_d_). In a 100 mL Schlenk tube, 2-(2-bromophenyl)-2-methyl-1,3-dioxolane (3.2 g, 13 mmol, 1 equiv) was degassed under reduced pressure, after which THF (20 mL) was added. The resultant solution was then cooled to -78 °C and ^{n}BuLi (9 mL, 1.6 M in heptane, 15 mmol, 1.1 equiv) was added dropwise over 10 min. The reaction mixture was allowed to stir cold for 1 h and then CD_3OD (2 mL) was added in one portion resulting in immediate precipitation of a white solid. The reaction mixture was then warmed to ambient temperature and let stir for an additional 2 h. The reaction mixture was then diluted with H_2O (40 mL) and Et_2O (50 mL). The organic layer was separated from the aqueous layer and then concentrated under reduced pressure. The organic layer was treated with aqueous HCl (5M, 30 mL) and allowed to stir for 16 h. Organic components were extracted with Et_2O (2 x 50 mL) and the organic layers were washed with H_2O, dried with Na_2SO_4, and filtered. Volatile components were removed under reduced pressure; subsequent purification by SiO_2 column chromatography (eluting with 5% EtOAc/hexanes) afforded the title compound as a pale-yellow oil (1.1 g, 71%), with spectroscopic features matching literature reported values.[87,89]

^{1}H NMR (chloroform-_d_, 600.1 MHz): δ 7.96 (dd, J_{HH} = 7.9, 1.3 Hz, 1H), 7.57 (ddd, J_{HH} = 7.9, 7.4, 1.2 Hz, 1H), 7.49 – 7.45 (m, 2H), 2.61 (s, 3H).

^{2}H NMR (chloroform-d_0, referenced to added chloroform-_d_, 92.1 MHz): δ 8.00 (s), 2.58 (s, corresponding to trace acetophenone-2-_d_).
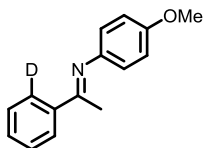
Synthesis of (_E_)-1-(phenyl-2-_d_)-_N_-(4-methoxyphenyl)ethan-1-imine (1f-d_1). To a round bottom flask equipped with a Dean Stark apparatus and 4 Å molecular sieves (ca. 2 g), a solution of acetophenone-(2'-_d_) (1.1 g, 9.3 mmol, 1 equiv), _p_-anisidine (1.3 g, 10 mmol, 1.1 equiv), and tosylic acid monohydrate (0.2 g, 1.1 mmol, 0.1 equiv) in toluene (20 mL) was heated to reflux for 16 h. Upon completion, the reaction mixture was allowed to cool to ambient temperature and was filtered to remove residual solids. Hexanes was then layered for crystallization at -30 °C to afford the title compound as orange crystals (1.6 g, 78%).

^{1}H NMR (chloroform-_d_, 600.1 MHz): δ 8.03 – 7.88 (m, 1H), 7.53 – 7.41 (m, 3H), 6.99 – 6.86 (m, 2H), 6.84 – 6.70 (m, 2H), 3.82 (s, 3H), 2.26 (s, 3H).

^{2}H NMR (chloroform-d_0, referenced to added chloroform-_d_, 92.1 MHz): δ 8.01 (s).

^{13}C{^{1}H} NMR (chloroform-_d_, 125.8 MHz): δ 165.9, 156.1, 144.9, 139.8, 130.5, 128.5, 128.4, 127.2, 127.0 (t, J_{CD} = 24.4 Hz), 120.9, 114.4, 55.6, 17.5.

Anal. Calcd for $C_{15}H_{14}DNO$: C, 79.6; H, 7.13; N, 6.19. Found: C, 79.6; H, 6.92; N, 6.07.

HRMS (ESI) _m/z_: [M+H]$^+$ Calcd for $C_{15}H_{14}DNO$ 227.1289. Found 227.1286.
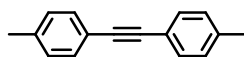
Synthesis of bis(_p_-tolyl)acetylene. In a 100 mL Schlenk tube, _p_-iodotoluene (1.6 g, 7 mmol, 1 equiv), PPh$_3$ (0.3 g, 1.1 mmol, 0.3 equiv), CuI (0.15 g, 0.8 mmol, 10 mol%), and (PPh$_3$)$_2$PdCl$_2$ (0.3 g, 0.4 mmol, 5 mol%)

were deoxygenated under reduced pressure. After three N_2/vacuum cycles, dry THF (10 mL) and $^iPr_2NH$ (6 mL) were added to afford a deep orange solution. After 5 min of stirring, 4-ethynyltoluene (1 mL, 7.5 mmol, 1.1 equiv) was added which resulted in a rapid color change to yellow and then to yellow-grey. The reaction mixture was heated to 45 °C for 16 h. Upon cooling to ambient temperature, CH_2Cl_2 (50 mL) diluted the reaction mixture and 5M HCl (ca. 50 mL) was added to quench residual base. The organic components were extracted with CH_2Cl_2 (3 x 50 mL), washed with H_2O, dried with Na_2SO_4, and filtered. Subsequent purification by SiO_2 column chromatography (eluting with petroleum ether) afforded the title compound as a flocculent white powder (1.3 g, 86%), with spectroscopic features matching literature reported values.[90]

^{1}H NMR (benzene-d_6, 300.1 MHz): δ 7.50 (d, J = 8.1 Hz, 4H), 6.83 (d, J = 8.2 Hz, 4H), 1.99 (s, 6H).

Characterization Data for Hydroarylation Products
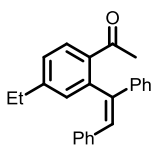
Synthesis of (Z)-1-(2-(1,2-diphenylvinyl)-4-ethylphenyl)ethan-1-one (Z-2a). Prepared according to the general catalytic procedure described below. Purification by SiO_2 column chromatography (eluting with 1% EtOAc/Hexane) afforded the title compound as a yellow oil (76 mg, 58 %, Z/E > 100 as determined by ^{1}H NMR spectroscopy).

^{1}H NMR (chloroform-d, 500.1 MHz): δ 7.64 (d, J = 7.9 Hz, 1H), 7.32 – 7.28 (m, 3H), 7.27 – 7.15 (m, 3H), 7.14 – 7.07 (m, 3H), 7.04 (s, 1H), 7.01 (s, 1H, Ar_2C=CHAr), 6.94 (d, J = 6.6 Hz, 2H), 2.60 (q, J = 7.5 Hz, 2H), 2.20 (s, 3H, -C(O)**CH₃**), 1.13 (t, J = 7.5 Hz, 3H).

^{1}H NMR (benzene-d_6, 500.0): δ 7.46 (d, J = 7.9 Hz, 1H), 7.41 – 7.31 (m, 2H), 7.13 – 7.02 (m, 6H), 7.00 (s, 1H, Ar_2C=CHAr), 6.96 (t, J = 7.6 Hz, 2H), 6.92 – 6.83 (m, 2H), 2.22 (q, J = 7.6 Hz, 2H), 2.00 (s, 3H, -C(O)**CH₃**), 0.88 (t, J = 7.6 Hz, 3H).

Selected ^{1}H NMR resonances corresponding E-isomer (minor product): ^{1}H NMR (chloroform-d, 500.1 MHz): δ 6.57 (s, Ar_2C=CHAr), 2.62 (q, J = 7.5 Hz, -**CH₂**CH₃), 2.34 (s, -C(O)**CH₃**)

^{13}C{^{1}H} NMR (chloroform-d, 125.8 MHz): δ 200.7, 148.8, 142.6, 142.3, 139.9, 137.6, 137.2, 131.8, 129.9, 129.5, 128.4, 128.2, 128.1, 127.6, 127.3, 127.2, 127.0, 28.8, 28.7, 15.4.

HRMS (EI) m/z: [M]$^+$ Calcd for $C_{24}H_{22}O$ 326.1671; Found 326.2012.
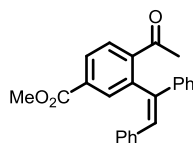
Synthesis of methyl (Z)-4-acetyl-3-(1,2-diphenylvinyl)benzoate (Z-2b). Prepared according to the catalytic procedure described below. Purification by SiO_2 column chromatography (eluting with 2% EtOAc/Hexane) afforded the title compound as a yellow oil (23 mg, 36%, Z/E = 8.0 as determined by [1]H

NMR spectroscopy). Note: both isomers are resolvable by ^{1}H NMR spectroscopy but not by SiO$_2$ column chromatography. The NMR data for each is given below.

^{1}H NMR (chloroform-d, 500.1 MHz): δ 8.07 (dd, J = 8.1, 1.5 Hz, 1H), 7.91 (d, J = 1.3 Hz, 1H), 7.64 (d, J = 8.1 Hz, 1H), 7.36 – 7.28 (m, 6H), 7.13 – 7.1 (m, 2H), 7.06 (s, 1H, Ar$_2$C=C**H**Ar), 6.92 (dd, J = 6.5, 2.7 Hz, 2H), 3.89 (s, 3H), 2.14 (s, 3H, -C(O)C**H$_3$**).

Selected ^{1}H NMR resonances corresponding E-isomer (minor product): ^{1}H NMR (chloroform-d, 500.1 MHz): δ 8.13 (dd, J = 8.3, 1.2 Hz, 1H), 8.04 – 8.00 (m, 2H), 7.94 (d, J = 1.7 Hz, 1H), 7.50 (d, J = 8.0 Hz, 1H), 7.19 – 7.15 (m, 6H), 7.11 – 7.08 (m, 2H), 6.64 (s, Ar$_2$C=C**H**Ar), 3.90 (s, 3H), 2.32 (s, 3H, -C(O)C**H$_3$**).

^{13}C{^{1}H} NMR corresponding to both Z- and E-isomers: ^{13}C{^{1}H} NMR (chloroform-d, 125.8 MHz): 201.1, 166.2, 144.6, 143.4, 142.2, 140.7, 140.6, 139.7, 139.3, 136.9, 136.7, 133.3, 132.8, 132.6, 132.0, 131.8, 131.0, 130.9, 130.0, 129.6, 129.6, 129.4, 129.0, 128.7, 128.6, 128.5, 128.4, 128.4, 128.3, 128.1, 128.0, 127.7, 127.6, 127.5, 127.3, 52.6, 52.5, 52.5, 29.1, 28.9.

HRMS (EI) m/z: [M]$^+$ Calcd for C$_{24}$H$_{20}$O$_3$ 356.1412. Found 356.1414.
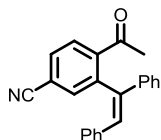
Synthesis of (Z)-4-acetyl-3-(1,2-diphenylvinyl)benzonitrile (Z-2c). Prepared according to the catalytic procedure described below. Purification by SiO$_2$ column chromatography (eluting with 2% EtOAc/Hexane) afforded the title compound as a yellow oil (180 mg, 70%, Z/E = 6.7 as determined by ^{1}H NMR spectroscopy). Note: both isomers are resolvable by ^{1}H NMR spectroscopy but not by SiO$_2$ column chromatography. Note that some peaks for the Z- and E-isomers overlap, and have been noted below. The NMR data for each is given below.

^{1}H NMR (chloroform-d, 500.1 MHz): δ 7.69 (d, J = 1.6 Hz, 1H), 7.65 (overlapping d, J = 7.7 Hz, 1H), 7.54 – 7.52 (overlapping m, 1H), 7.34 – 7.28 (m, 3H), 7.25 – 7.22 (overlapping m, 2H), 7.18 – 7.16 (overlapping m, 3H), 7.08 (s, 1H, Ar$_2$C=C**H**Ar), 6.95 – 6.91 (m, 2H), 2.14 (s, 3H, -C(O)C**H$_3$**).

Selected ^{1}H NMR resonances corresponding to the E-isomer (minor product) match literature reported[29] values: ^{1}H NMR (chloroform-d, 500.2 MHz): δ 7.70 (d, J = 1.6 Hz, 1H), 7.63 (overlapping dd, J = 8.0, 1.8 Hz, 1H), 7.54 – 7.52 (overlapping m, 1H), 7.36 – 7.33 (m, 3H), 7.19 – 7.15 (overlapping m, 5H), 7.10 – 7.08 (m, 2H), 6.61 (s, 1H, Ar$_2$C=C**H**Ar), 2.36 (s, 3H, -C(O)C**H$_3$**).

^{13}C{^{1}H} NMR corresponding to both Z- and E-isomers: ^{13}C{^{1}H} NMR (chloroform-d, 125.8 MHz): 202.9, 200.3, 145.3, 144.7, 144.1, 141.6, 140.7, 139.5, 139.3, 138.8, 136.4, 136.3, 136.0, 134.4, 133.8, 131.4, 131.0, 130.8, 130.3, 129.6, 129.5, 128.9, 128.9, 128.8, 128.6, 128.5, 128.4, 128.3, 128.3, 128.0, 127.8, 127.5, 118.1, 117.9, 115.2, 114.1, 30.0, 28.7.

HRMS (EI) m/z: [M]$^+$ Calcd for C$_{23}$H$_{17}$NO 323.1310. Found 323.1311.
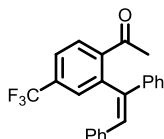
Synthesis of (Z)-1-(2-(1,2-diphenylvinyl)-4-(trifluoromethyl)phenyl)ethan-1-one (Z-2d). Prepared according to the catalytic procedure described below. Purification by SiO_2 column chromatography (eluting with 1% EtOAc/Hexane) afforded the title compound as a yellow oil (48 mg, 29%, Z/E = 15, purity = 95% with residual *p*-anisidine as determined by ^{1}H and ^{13}C{^{1}H} NMR spectroscopy).

^{1}H NMR (chloroform-*d*, 500.2 MHz): δ 7.66 (d, *J* = 2.3 Hz, 1H), 7.53 – 7.36 (m, 1H), 7.40 – 7.27 (m, 5H), 7.24 – 7.12 (m, 5H), 7.07 (s, 1H, Ar$_2$C=C**H**Ar), 6.91 – 6.87 (m, 1H), 2.13 (s, 3H, -C(O)C**H₃**).

Selected ^{1}H NMR resonance corresponding to the *E*-isomer (minor product) match literature reported[29] values: ^{1}H NMR (chloroform-*d*, 500.2 MHz): 2.33 (s, -C(O)C**H₃**).

^{13}C{^{1}H} NMR (chloroform-*d*, 125.8 MHz): δ 201.0, 144.3, 142.2, 140.5, 136.8, 133.5 (q, $^2J_{C-F}$ = 32.9 Hz), 130.2, 130.1, 129.8, 129.6 (q, $^3J_{C-F}$ = 3.5 Hz), 129.1, 129.0, 128.8, 128.7, 128.6, 128.5, 128.1, 127.9, 127.8, 125.0 (q, $^3J_{C-F}$ = 3.7 Hz), 122.8 (q, $^1J_{C-F}$ = 273.7 Hz), 29.1.

^{19}F{^{1}H} NMR (chloroform-*d*, 376.5 MHz): δ -62.03 (s, 1F, *E*-isomer), -62.18 (s, 15.3F, *Z*-isomer).

HRMS (EI) *m/z*: [M]$^+$ Calcd for $C_{23}H_{17}F_3O$ 366.1232. Found 366.1236.
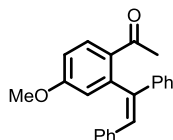
Synthesis of (Z)-1-(2-(1,2-diphenylvinyl)-4-methoxyphenyl)ethan-1-one (Z-2e). Prepared according to the catalytic procedure described below. Purification by SiO_2 column chromatography (eluting with a mixture of dichloromethane/EtOAc/Hexane in a ratio of 1:5:94) afforded the title compound as a yellow oil (40 mg, 27%, Z/E = 20 as determined by ^{1}H NMR spectroscopy).

^{1}H NMR (chloroform-*d*, 500.1 MHz): δ 7.79 (d, *J* = 8.5 Hz, 1H), 7.17 – 7.09 (m, 5H), 7.05 (s, 1H, Ar$_2$C=C**H**Ar), 7.04 – 6.95 (m, 5H), 6.93 (dd, *J* = 8.3, 1.7 Hz, 1H), 6.71 (d, *J* = 2.2 Hz, 1H), 3.76 (s, 3H, -OC**H₃**), 2.25 (s, 3H, -C(O)C**H₃**).

Selected ^{1}H NMR resonance corresponding to the *E*-isomer (minor product) match literature reported[29] values: ^{1}H NMR (chloroform-*d*, 500.2 MHz): 6.58 (s, Ar$_2$C=C**H**Ar), 3.78 (s, -OC**H₃**), 2.37 (s, -C(O)C**H₃**).

^{13}C{^{1}H} NMR (chloroform-*d*, 125.8 MHz): δ 199.0, 162.5, 142.5, 142.3, 142.2, 137.1, 132.4, 132.0, 129.5, 128.5, 128.3, 128.0, 127.7, 127.1, 127.0, 117.3, 113.2, 55.6, 28.7.

HRMS (EI) *m/z*: [M]$^+$ Calcd for $C_{23}H_{20}O_2$ 328.1463. Found 328.1465.
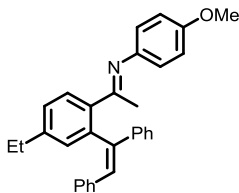
Synthesis of (E)-1-(2-((Z)-1,2-diphenylvinyl)-4-ethylphenyl)-N-(4-methoxyphenyl)ethan-1-imine (Z-3a). Prepared according to the catalytic procedure described below. Purification by SiO_2 column chromatography (gradient eluting with 1% EtOAc/Hexane to 5% EtOAc/Hexane) afforded the title compound as an orange solid (132 mg, 40%, Z/E > 50 as determined by ^{1}H NMR spectroscopy).

^{1}H NMR (benzene-d_6, 600.1 MHz): δ 7.56 (d, J = 7.8 Hz, 1H), 7.41 (d, J = 7.2 Hz, 2H), 7.29 (s, 1H), 7.26 (d, J = 7.6 Hz, 2H), 7.11 – 7.05 (m, 4H), 7.02 (s, 1H), 7.00 (t, J = 7.6 Hz, 2H), 6.91 (t, J = 7.5 Hz, 1H), 6.77 (d, J = 8.7 Hz, 2H), 6.44 (d, J = 8.6 Hz, 2H), 3.31 (s, 3H), 2.30 (q, J = 7.9 Hz, 2H), 1.83 (s, 3H, -C(O)**CH₃**), 0.94 (t, J = 7.6 Hz, 3H).

Selected ^{1}H NMR resonances corresponding E-isomer (minor product): ^{1}H NMR (benzene-d_6, 500.2 MHz): δ 6.61 (s, Ar₂C=C**HAr**), 2.05 (s, -C(O)**CH₃**)

^{1}H NMR (chloroform-d, 600.1 MHz): δ 7.55 (d, J = 7.7 Hz, 1H), 7.37 – 7.28 (m, 5H), 7.20 – 7.14 (m, 2H), 7.11 (t, J = 7.3 Hz, 3H), 7.06 (s, 1H), 7.03 (s, 1H), 6.84 (t, J = 5.9 Hz, 1H), 6.73 (d, J = 8.4 Hz, 2H), 6.19 (d, J = 8.3 Hz, 2H), 3.75 (s, 3H), 2.59 (q, J = 7.4 Hz, 2H), 1.87 (s, 3H, -C(O)**CH₃**), 1.12 (t, J = 7.5 Hz, 3H).

^{13}C{^{1}H} NMR (chloroform-d, 150.9 MHz): δ 155.8, 145.8, 142.9, 142.4, 138.1, 137.5, 131.6, 131.5, 129.7, 128.9, 128.5, 128.4, 128.2, 127.7, 127.7, 127.7, 127.1, 126.7, 125.3, 120.4, 114.0, 55.5, 28.7, 20.1, 15.8.

HRMS (ESI) m/z: [M+H]$^+$ Calcd for $C_{31}H_{30}NO$ 432.2322; Found 432.2320.

Stoichiometric Reactivity of Co-Cl, Co-H, Co-Li, and Co'₂-Mg

Quantitative Cyclohexene and Cyclohexane Determination. General procedure: CyMgCl (2.0 M in Et_2O, 80 μL, 0.14 mmol, 4 equiv) was added to a solution of **Co-Cl** (30 mg, 0.034 mmol, 1 equiv) in THF (0.1 mL) and C_6D_6 (0.7 mL) in a Teflon capped J-Young NMR tube with p-xylene as an internal standard. A rapid color change to red/red-brown was observed upon CyMgCl addition. The reaction mixture was heated to 65 °C for 2 h; upon completion, the volatile components were vacuum transferred to an empty J-Young tube under static vacuum. Cyclohexene and cyclohexane content in the reaction mixture was quantified by ^{1}H NMR spectroscopy versus the p-xylene internal standard, and the ^{1}H NMR chemical shifts were in agreement with literature values.[91-94] The ^{13}C{^{1}H} NMR spectrum further corroborated the presence of cyclohexene and cyclohexane. See Figure 3.1 for representative NMR spectrum.

The general procedure was repeated with 1, 2, or 4 equiv of CyMgCl and with **Co-Cl**, **Co-H** or $CoCl_2$ (with 3 equiv of PPh_3) as the metal precursor.

Selected ^{1}H and ^{13}C{^{1}H} NMR resonances for cyclohexene:[91]

^{1}H NMR (benzene-d_6, 499.5 MHz): δ 5.64 (t, J = 1.6 Hz, 2H), 1.90 (tp, J = 3.7, 1.8 Hz, 4H), 1.50 (p, J = 3.7 Hz, 4H). ^{13}C{^{1}H} NMR (benzene-d_6, 150.92 MHz): δ 127.4, 25.5, 23.0.

Selected ^{1}H and ^{13}C{^{1}H} NMR resonances for cyclohexane:[92]

^{1}H NMR (benzene-d_6, 400.1 MHz): δ 1.40 (s, 12H). ^{13}C{^{1}H} NMR (benzene-d_6, 150.92 MHz): δ 27.3.

Selected ^{1}H and ^{13}C{^{1}H} NMR resonances for *p*-xylene:[93,94]

^{1}H NMR (benzene-d_6, 400.1 MHz): δ 6.96 (s, 4H), 2.14 (s, 6H). ^{13}C{^{1}H} NMR (benzene-d_6, 150.92 MHz): δ 134.8, 129.3, 21.0.

^{1}H NMR Identification *via in situ* Deprotonation of Co-H with RMgCl, R$_2$Mg, or RLi. A solution of **Co-H** (10 mg, 11 μmol, 1 equiv) in benzene-d_6 (1 mL) was treated with R–M (0.1 mmol, 10 equiv) in a Teflon capped J-Young NMR tube (see Table 3.10, below). A ^{1}H NMR spectrum was then acquired and the organic byproducts were identified. The ^{1}H NMR chemical shifts were in agreement with literature reported values.

Table 3.10. Identification of Organic Byproducts Resulting from Deprotonation of **Co-H**.

R–M	Observed ^{1}H NMR Shifts of Organic Byproduct in C$_6$D$_6$ (ppm) [a]	Assignment (Reported ^{1}H NMR Shifts in C$_6$D$_6$, ppm) [b]
EtMgCl	0.80	EtH (0.80) [92]
CyMgCl	1.39	CyH (1.40) [92]
MeLi	0.16	MeH (0.16) [92]
MesLi	6.73, 2.16	MesH (6.63, 2.16) [95,c]
*n*BuLi	0.77 [d]	BuH (0.81, 0.74) [96]
Bn$_2$Mg	7.13, 7.05, 2.12	BnH (7.13, 7.02, 2.11) [92]

[a] Measured on a 300.13 MHz instrument. [b] Reference for the reported chemical shift. [c] reported value measured in neat mesitylene. [d] observed shift is a set of overlapping multiplets.

Protonolysis of Co-Li with HCl. A solution of **Co-Li** (2 mg, 2 μmol) in benzene-d_6 (1 mL) with Si(SiMe$_3$)$_4$ (2 mg, 6 μmol) as an internal standard was treated with concentrated HCl (1 mL), which resulted in rapid decomposition. The resultant biphasic mixture was dried with MgSO$_4$ and filtered. A ^{1}H NMR spectrum was acquired to determine THF and PPh$_3$ content versus the internal standard and then normalized to the initial Co content (see Figure 3.2 for a representative ^{1}H NMR spectrum). Observed THF: 2.7 ± 0.4 equiv; observed PPh$_3$: 3.0 ± 0.4 equiv. Error was determined as the standard deviation of triplicate hydrolysis experiments.

Treatment of Co-Li with Excess Alkyne: Variable Concentration and Temperature NMR Experiments. A metal-complex containing stock solution of **Co-Li** (54 mg, 13 mM), Si(SiMe$_3$)$_4$ as an internal standard (19 mg, 15 mM) in benzene-d_6 (3.9 mL) was prepared. In five separate Teflon capped J-Young NMR tubes, 0.7 mL of the stock solution was added to bis(*p*-tolyl)acetylene (2.7/6.4/12.9/19.4/27.6 mg, 19/44/90/140/190 mM, respectively) and were stored at -78 °C to prevent adventitious background

reactivity prior to injection into a 500 MHz NMR spectrometer. The NMR spectrometer probe temperature was initially set to 303 K and the sample was injected. After the probe temperature equilibrated, a ^{1}H NMR spectrum was acquired (after properly locking/tuning/shimming the instrument). This process was repeated at 309, 318, 329, and 339 K for every sample. The ratio of bound alkyne to Co was calculated versus the Si(SiMe$_3$)$_4$ standard and normalized versus the initial concentration of [**Co-Li**], as described in the equation below. The CH$_3$ fragment of bis(p-tolyl)acetylene (1.99 ppm) was used to determine the quantity of free alkyne. Additionally, the sum of all CH$_3$ resonances was equal to the initial amount of alkyne added (Figure S3). The initial concentrations were determined theoretically based on the mmol added / total volume. A plot of the data is given in Figure 3.5 and a representative ^{1}H NMR spectrum is illustrated in Figure 3.6:

$$\frac{\text{Bound Alkyne}}{\text{Co}} = \frac{[\text{bis(p-tolyl)acetylene}]_{\text{initial}} - [\text{bis(p-tolyl)acetylene}]_{\text{T}}}{[\textbf{Co-Li}]_{\text{initial}}}$$

Table 3.11. Measured concentrations of free alkyne at various temperatures versus the initial alkyne loading.

Entry	[bis(*p*-tolyl)acetylene]$_{\text{initial}}$	[alkyne]$_{303K}$	[alkyne]$_{309K}$	[alkyne]$_{318K}$	[alkyne]$_{329K}$	[alkyne]$_{339K}$
1	19	6.3	5.1	4.2	3	3
2	44	26	25	24	23	23
3	90	64	65	63	62	58
4	140	108	107	104	103	110
5	190	160	160	159	154	154

[a] All values reported in mM.

Table 3.12. Bound alkyne/Co ratios (BA/Co) at various temperatures as computed from the above equation and Table 3.11.

Entry	[bis(*p*-tolyl)acetylene]$_{\text{initial}}$	BA/Co 303K	BA/Co 309K	BA/Co 318K	BA/Co 329K	BA/Co 339K
1	19	1.0	1.1	1.2	1.2	1.2
2	44	1.5	1.6	1.6	1.6	1.6
3	90	2.0	2.0	2.1	2.1	2.1
4	140	2.1	2.2	2.4	2.4	2.4
5	190	2.5	2.6	2.6	2.6	2.6

[a] All values reported in mM.

Treatment of Co'$_2$-Mg with Stoichiometric Alkyne or (*N*-aryl)aryl Ethanimine. In a N$_2$ glovebox, diphenylacetylene (10 mg, 0.048 mmol, 4 equiv) or **1a** (14 mg, 0.048 mmol, 4 equiv) were treated with **Co'$_2$-Mg** (20 mg, 0.012 mmol, 1 equiv) in Et$_2$O. After stirring at ambient temperatures for 20 h, a color change from deep-red/brown to tan was observed. Volatile components were removed under reduced pressure and the resultant residue was extracted with benzene-*d$_6$* and added to a Teflon capped J-Young NMR tube. In the ^{1}H NMR spectrum, no new substrate containing resonances existed (only unreacted diphenylacetylene or **1a** were observed). A new set of broadened, paramagnetic features were observed at 15.10, -1.17, and -2.54 ppm for both reactions (Figures 3.3 and 3.4, respectively).

Catalytic Methods, Optimizations, and Procedures

General Optimized Hydroarylation Procedure with Precatalysts Co-Cl or Co-H Activated by CyMgCl. In a N$_2$ glovebox, a 100 mL Teflon stoppered Schlenk tube equipped with a stir bar was charged with a solution of **Co-Cl** (35 mg, 40 µmol, 10 mol%) or **Co-H** (35 mg, 40 µmol, 10 mol%), diphenylacetylene (71 mg, 0.4 mmol, 50 mM, 1 equiv), and *N*-Aryl imine **1a** (100 mg, 0.4 mmol, 50 mM, 1 equiv) in THF (7.6 mL) with Si(SiMe$_3$)$_4$ as an internal standard. On a Schlenk line, TMEDA (0.4 mL) and then CyMgCl (2.0 M in Et$_2$O, 40 µL, 80 µmol, 20 mol% for **Co-Cl** or 20 µL, 40 µmol, 10 mol% for **Co-H**) were added, which resulted in a rapid color change to red/brown. The reaction mixture was then sealed and allowed to heat at 65 °C for 20 h. Upon completion, the reaction mixture was cooled to ambient temperature and the catalyst was quenched with 5M HCl (10 mL). After stirring for 1 h, the organic components were extracted with CH$_2$Cl$_2$ (2 x 50 mL), washed with H$_2$O, dried with Na$_2$SO$_4$, and filtered. Volatile components were removed under reduced pressure to afford the crude product as an orange oil. ^{1}H NMR yields were determined in chloroform-*d* by integration of the acyl CH$_3$ resonances corresponding to the hydroarylation products ***Z/E*-2a** (*vide supra*) versus the internal standard. The *Z/E*-ratios were calculated as the ratio of the aforementioned acyl resonances. Purification by SiO$_2$ column chromatography afforded the isolated yield (*vide supra* for specific eluent conditions).

Hydroarylation of 1a Catalyzed by Complex Co-Li. The general procedure described above was performed with the following modifications: complex **Co-Li** (44 mg, 40 µmol, 10 mol%) was employed as the active precatalyst. CyMgCl was not added; **Co-Li** was catalytically active without the addition of any co-catalysts/activators.

Hydroarylation of 1a Catalyzed by Complex Co$_2$-Mg. The general procedure described above was performed with the following modifications: complex **Co$_2$-Mg** (41 mg, 20 µmol, 5 mol% per **Co$_2$-Mg**, 10 mol% per Co) was employed as the active precatalyst. CyMgCl was not added; **Co$_2$-Mg** was catalytically active without the addition of any co-catalysts/activators.

Attempted Hydroarylation of 1a Catalyzed by Complex Co'$_2$-Mg. The general procedure described above was performed with the following modifications: complex **Co'$_2$-Mg** (10 mg, 6 µmol, 5 mol%) was employed as the active precatalyst with diphenylacetylene (22 mg, 0.12 mmol, 1 equiv) and **1a** (30 mg, 0.12 mmol, 1 equiv) in THF with 5% v/v 1,4-dioxane. CyMgCl was not added; **Co'$_2$-Mg** was catalytically inactive.

Hydroarylation of 1a Catalyzed by Complex Co-Li without Acid Workup. The general procedure described above was performed with the following modifications: complex **Co-Li** (44 mg, 40 µmol, 10 mol%) was employed as the active precatalyst. CyMgCl was not added; **Co-Li** was catalytically active without the addition of any co-catalysts/activators. The reaction mixture was not quenched with HCl;

instead, the crude mixture was passed through Al_2O_3 and the volatile components were removed from the filtrate. Purification by SiO_2 (*vide supra* for specific eluent conditions) afforded ***Z/E*-3a**.

Hydroarylation of 1a Catalyzed by CoCl₂ Activated by CyMgCl. The general procedure described above was performed with the following modifications: $CoCl_2$ (5 mg, 40 μmol, 10 mol%) and PPh_3 (31 mg, 0.12 mmol, 30 mol%) were employed as the precatalysts instead of **Co-Cl** or **Co-H**. CyMgCl (2.0 M in Et_2O, 80 μL, 0.16 mmol, 40 mol%) was added to activate the precatalyst.

Hydroarylation of 1b Catalyzed by Complex Co-Li. The general procedure described above was performed with the following modifications: the catalytic mixture contained *N*-aryl imine **1b** (200 mg, 0.71 mmol, 0.1 M, 1 equiv), diphenylacetylene (126 mg, 0.71 mmol, 0.1 M, 1 equiv), **Co-Li** (77 mg, 70 μmol, 10 mol%), THF (7.6 mL), and TMEDA (0.4 mL). $Si(SiMe_3)_4$ was used as an internal standard and the ^1H NMR yield were determined in chloroform-*d* by integration of the acyl CH_3 resonances corresponding to the hydroarylation products ***Z/E*-2b** (*vide infra*) versus the internal standard. Conversion was determined by integration of new acyl CH_3 resonances compared the acyl CH_3 resonance corresponding to methyl-4-acetylbenzoate. Purification by SiO_2 column chromatography afforded the isolated yield (*vide infra* for specific eluent conditions).

Hydroarylation of 1b Catalyzed by CoCl₂ Activated with CyMgCl. The general procedure described above was performed with the following modifications: the catalytic mixture contained *N*-aryl imine **1b** (50 mg, 0.18 mmol, 0.1 M, 1 equiv), diphenylacetylene (32 mg, 0.18 mmol, 0.1 M, 1 equiv), $CoCl_2$ (4 mg, 18 μmol, 10 mol%), PPh_3 (14 mg, 54 μmol, 30 mol%), CyMgCl (2.0 M in Et_2O, 40 μL, 80 μmol, 40 mol%), THF (1.9 mL), and TMEDA (0.1 mL). $Si(SiMe_3)_4$ was used as an internal standard and the ^1H NMR yield were determined in chloroform-*d* by integration of the acyl CH_3 resonances corresponding to the hydroarylation products ***Z/E*-2b** (*vide infra*) versus the internal standard. Conversion was determined by integration of all new acyl CH_3 resonances compared the acyl CH_3 resonance corresponding to methyl-4-acetylbenzoate.

Hydroarylation of 1c Catalyzed by Complex Co-Li. The general procedure described above was performed with the following modifications: the catalytic mixture contained *N*-aryl imine **1c** (200 mg, 0.8 mmol, 0.1 M, 1 equiv), diphenylacetylene (140 mg, 0.8 mmol, 0.1 M, 1 equiv), **Co-Li** (85 mg, 80 μmol, 10 mol%), THF (7.6 mL), and TMEDA (0.4 mL). $Si(SiMe_3)_4$ was used as an internal standard and the ^1H NMR yield were determined in chloroform-*d* by integration of the acyl CH_3 resonances corresponding to the hydroarylation products ***Z/E*-2c** (*vide infra*) versus the internal standard. Conversion was determined by integration of new acyl CH_3 resonances compared the acyl CH_3 resonance corresponding to 4-acetylbenzonitrile. Purification by SiO_2 column chromatography afforded the isolated yield (*vide infra* for specific eluent conditions).

Hydroarylation of 1c Catalyzed by CoCl₂ Activated with CyMgCl. The general procedure described above was performed with the following modifications: the catalytic mixture contained *N*-aryl imine **1c** (50 mg, 0.2 mmol, 0.1 M, 1 equiv), diphenylacetylene (36 mg, 0.2 mmol, 0.1 M, 1 equiv), $CoCl_2$ (4 mg, 18 μmol, 10 mol%), PPh_3 (16 mg, 60 μmol, 30 mol%), CyMgCl (2.0 M in Et_2O, 40 μL, 80 μmol, 40 mol%), THF (1.9 mL), and TMEDA (0.1 mL). $Si(SiMe_3)_4$ was used as an internal standard and the ^1H NMR yield were determined in chloroform-*d* by integration of the acyl CH_3 resonances corresponding to the hydroarylation products ***Z/E*-2c** (*vide infra*) versus the internal standard. Conversion was determined by integration of all new acyl CH_3 resonances compared the acyl CH_3 resonance corresponding to 4-acetylbenzonitrile.

Hydroarylation of 1d Catalyzed by Complex Co-Li. The general procedure described above was performed with the following modifications: the catalytic mixture contained *N*-aryl imine **1d** (135 mg, 0.46 mmol, 0.1 M, 1 equiv), diphenylacetylene (82 mg, 0.46 mmol, 0.1 M, 1 equiv), **Co-Li** (50 mg, 50 μmol, 10 mol%), THF (4.3 mL), and TMEDA (0.3 mL). Si(SiMe$_3$)$_4$ was used as an internal standard and the ^{1}H NMR yield were determined in chloroform-*d* by integration of the acyl CH$_3$ resonances corresponding to the hydroarylation products **Z/E-2d** (*vide infra*) versus the internal standard. Conversion was determined by integration of new acyl CH$_3$ resonances compared the acyl CH$_3$ resonance corresponding to 4'-(trifluoromethyl)acetophenone. Purification by SiO$_2$ column chromatography afforded the isolated yield (*vide infra* for specific eluent conditions).

Hydroarylation of 1e Catalyzed by Complex Co-Li. The general procedure described above was performed with the following modifications: the catalytic mixture contained *N*-aryl imine **1e** (117 mg, 0.46 mmol, 0.1 M, 1 equiv), diphenylacetylene (82 mg, 0.46 mmol, 0.1 M, 1 equiv), **Co-Li** (50 mg, 50 μmol, 10 mol%), THF (4.3 mL), and TMEDA (0.3 mL). Si(SiMe$_3$)$_4$ was used as an internal standard and the ^{1}H NMR yield were determined in chloroform-*d* by integration of the acyl CH$_3$ resonances corresponding to the hydroarylation products **Z/E-2e** (*vide infra*) versus the internal standard. Conversion was determined by integration of new acyl CH$_3$ resonances compared the acyl CH$_3$ resonance corresponding to 4'-methoxyacetophenone. Purification by SiO$_2$ column chromatography afforded the isolated yield (*vide infra* for specific eluent conditions).

Catalyst Optimization: Effects of Organometallic Activator Identity. The general procedure described above was performed with the following modifications. Complex **Co-Cl** (35 mg, 40 μmol, 10 mol%) was activated with one of the following reagents: *^{n}*BuLi (1.6 M in heptane, 50 μL, 80 μmol, 20 mol%), PhLi (1.8 M in Bu$_2$O, 44 μL, 80 μmol, 20 mol%), MesLi (10 mg, 80 μmol, 20 mol%), MeMgCl (3M in THF, 30 μL, 80 μmol, 20 mol%), EtMgCl (3M in Et$_2$O, 30 μL, 80 μmol, 20 mol%), H$_2$C=CHMgBr (1M in Et$_2$O, 80 μL, 80 μmol, 20 mol%), *^{n}*Bu$_2$Mg (1M in heptane, 80 μL, 80 μmol, 20 mol%), Mes$_2$Mg (18 mg, 80 μmol, 20 mol%), Bn$_2$Mg (15 mg, 80 μmol, 20 mol%), or Ph$_2$Zn (18 mg, 80 μmol, 20 mol%). TMEDA was not added as a cosolvent. The substrate concentrations were increased to 0.1 M (in 4 mL THF). The results are summarized in Table 3.1.

Catalyst Optimization: Additive Study. The general procedure described above was performed with the following modifications: the substrate concentrations were increased to 0.1 M (in 4 mL THF). TMEDA was not added as a cosolvent, except were otherwise noted. Additives were included as co-reagents and the details are summarized in Table 3.2.

Catalyst Optimization: Solvent Effects. The general procedure described above was performed with the following modifications: the substrate concentrations were increased to 0.1 M (in 4 mL THF) and the catalytic solvents used are listed in Table 3.3. Pyridine (35 μL, 0.4 mmol, 1 equiv) was used instead of TMEDA as a cosolvent. A slight excess of CyMgCl (2.0 M in Et$_2$O, 0.16 mL, 0.16 mmol, 40 mol%) was used to activated the catalyst.

Catalyst Optimization: Stoichiometry of CyMgCl vs Co-Cl. The general procedure described above was performed with the following modifications: the substrate concentrations were increased to 0.1 M (in 4 mL THF) and the stoichiometry of CyMgCl (2.0 M in Et$_2$O) added was varied as summarized in Table 3.4. Pyridine (35 μL, 0.4 mmol, 1 equiv) was used instead of TMEDA as a cosolvent.

Catalyst Optimization: Concentration Effects. The general procedure described above was performed with the following modifications: the substrate concentrations were varied by changing the total reaction volume as summarized in Table 3.5. Pyridine (35 μL, 0.4 mmol, 1 equiv) was used instead of TMEDA as a cosolvent.

Catalyst Optimization: Catalysis with Co-H and Added Bases. The general procedure described above was performed with the following modifications: the substrate concentrations were increased to 0.1 M (in 4 mL THF) and no co-solvents were added. The identity and quantity of added base are summarized in Table 3.6.

Isotope Effects and Labelling Studies

Deuteron-Quench Experiment A (Control): Treatment of 1a with Acetic Acid-d_4
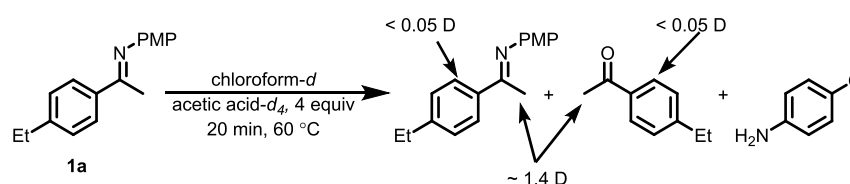
A solution of **1a** (25 mg, 0.1 mmol, 1 equiv) and acetic acid-d_4 (25 μL, 0.4 mmol, 4 equiv) in chloroform-d (ca. 1 mL) was heated to 60 °C in a sealed Teflon capped J-Young NMR tube for 20 min. After heating, a long relaxation delay ^{1}H NMR spectrum was acquired ($d1 = 60$ s; Figure 3.25). Three major species were identified: 4'-ethylacetophenone, residual **1a**, and *p*-anisidine. Deuterium incorporation was determined by relative integrations (*vide infra*).

Selected ^{1}H NMR resonances for 4'-ethylacetophenone:[97]

^{1}H NMR (chloroform-d, 400 MHz): δ 7.88 (d, $J = 8.0$ Hz, 2'/6'-H, 2H), 7.28 (d, $J = 8.0$ Hz, 3'/5'-H, 2H), 2.70 (q, $J = 7.4$ Hz, -CH$_2$, 2H), 2.57 (s, -COCH$_3$, 3H), 1.25 (t, $J = 7.4$ Hz, -CH$_3$, 3H).
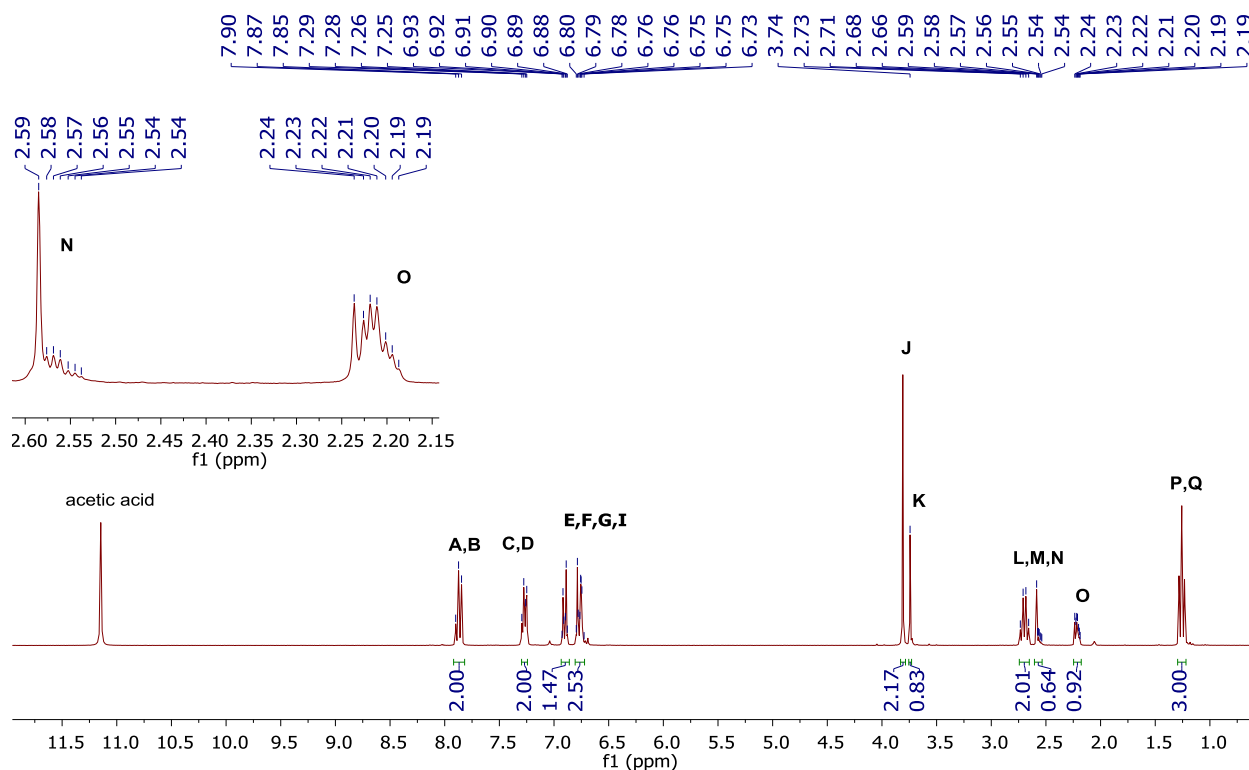
Figure 3.25. ^{1}H NMR spectrum of **1a** in chloroform-*d* with 4 equiv of acetic acid-*d$_4$*. Both imine hydrolysis as well as iminyl/acetyl H(D) exchange occurs with solvent as evidenced by the existence of multiple isotopomers (resonances N and O) as well as the formation of CD$_3$COOH.

Deuteron-Quench Experiment B (Control): 1a with Co-Li Quenched by C$_6$H$_5$COOD
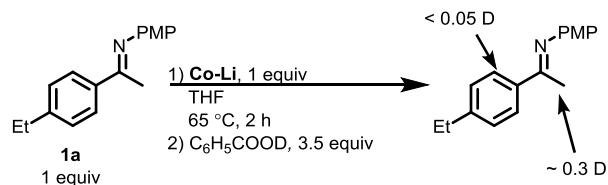
Inside an N$_2$ glovebox, a solution of **1a** (12 mg, 47 µmol, 1 equiv) and **Co-Li** (50 mg, 46 µmol, 1 equiv) in THF (0.7 mL) was added to a sealed Teflon capped J-Young NMR tube and heated to 65 °C for 2 h. After heating, the reaction mixture was cooled to room temperature. Inside an N$_2$ glovebox, benzoic acid-*d* (C$_6$H$_5$COOD, 20 mg, 0.16 mmol, 3.5 equiv) was added to the reaction mixture. A ^{2}H NMR spectrum of the crude reaction mixture was acquired (Figure 3.26), which indicates the presence of H(D) exchange at the iminyl -C(N)CH$_3$ fragment of **1a**. Under ambient atmosphere, the reaction mixture was passed through a plug of Al$_2$O$_3$. The volatile components were removed under reduced pressure to afford a brown oily film. The organic products were further purified by SiO$_2$ column chromatography (eluting with hexanes then 2% EtOAc/hexanes; Figure 3.27). Deuterium incorporation was determined by relative integrations from a long relaxation-delay ^{1}H NMR spectrum ($d1$ = 60 s).
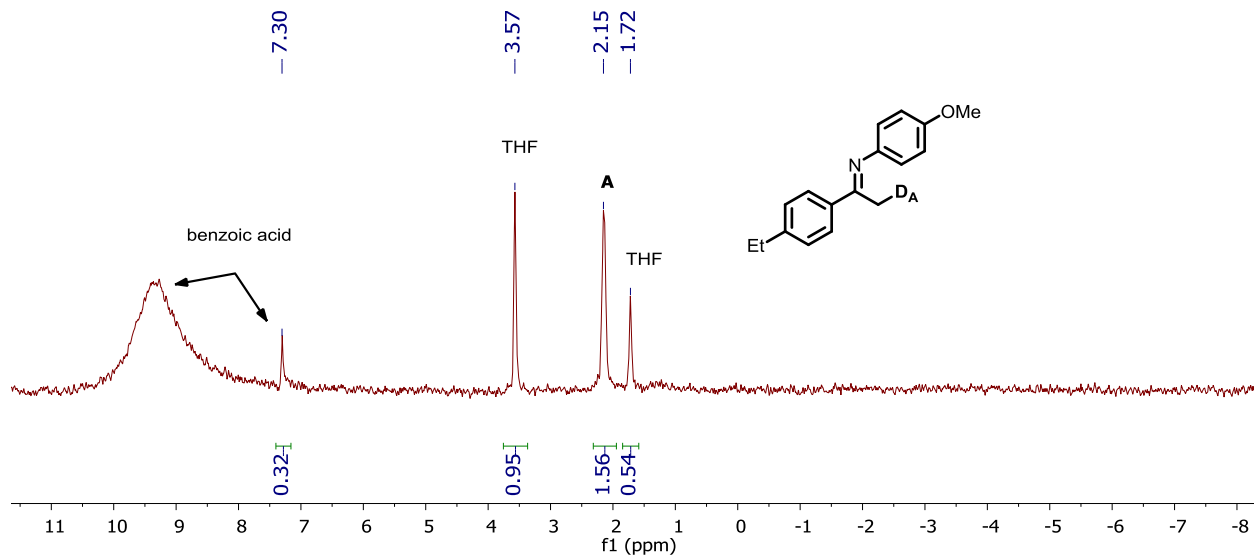
Figure 3.26. ^{2}H NMR spectrum in THF-d_0 of the crude reaction mixture resulting from a heated mixture of **1a** and **Co-Li** that was quenched by benzoic acid-d. Only iminyl H(D) exchange was observed.
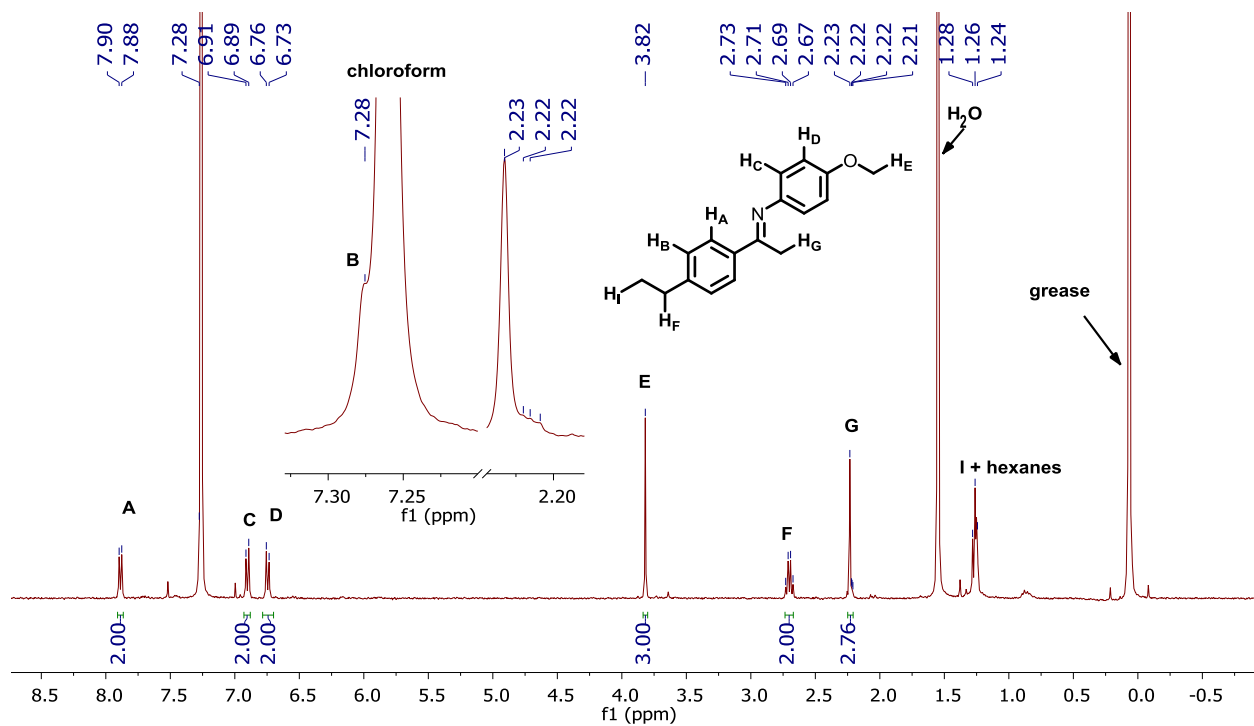
Figure 3.27. ^{1}H NMR spectrum in chloroform-d of the purified organic components resulting from a heated mixture of **1a** and **Co-Li** that was quenched by benzoic acid-d. *Ortho*-H(D) exchange was not observed. Deuterium incorporation into the iminyl -C(N)CH$_3$ position (shoulder of resonance G).

Deuteron-Quench Experiment C: 1a and diphenylacetylene with Co-Li Quenched by C₆H₅COOD

E-2a	E-3a	1a	Z-2a	Z-3a
18%	6%	51%	12%	13%
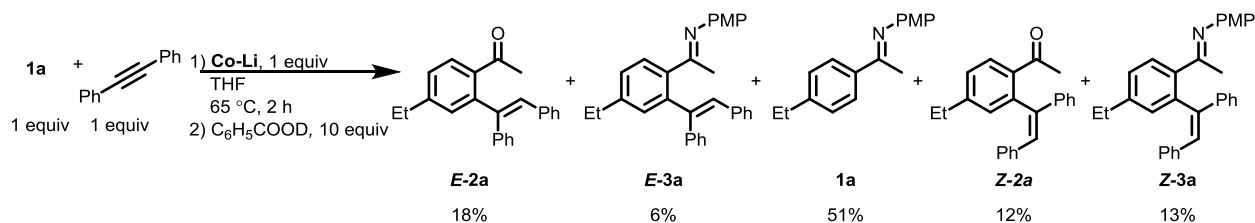
Inside an N_2 glovebox, a solution of **1a** (12 mg, 47 µmol, 1 equiv), diphenylacetylene (8.0 mg, 45 µmol, 1 equiv), and **Co-Li** (50 mg, 46 µmol, 1 equiv) in THF (0.7 mL) was added to a sealed Teflon capped J-Young NMR tube and heated to 65 °C for 2 h. After heating, the reaction mixture was cooled to room temperature. Inside an N_2 glovebox, benzoic acid-d (C₆H₅COOD, 55 mg, 0.45 mmol, 10 equiv) was added to the reaction mixture. A ^{2}H NMR spectrum of the crude reaction mixture was acquired (Figure 3.28), which indicates the presence of H(D) exchange at the iminyl -C(N)CH₃ fragment of **1a**. Under ambient atmosphere, the reaction mixture was passed through a plug of Al_2O_3. The volatile components were removed under reduced pressure to afford a brown oily film. The organic products were further purified by SiO_2 column chromatography (eluting with hexanes then 2% EtOAc/hexanes; Figure 3.29). Deuterium incorporation was determined by relative integrations from a long relaxation-delay ^{1}H NMR spectrum ($d1$ = 60 s).
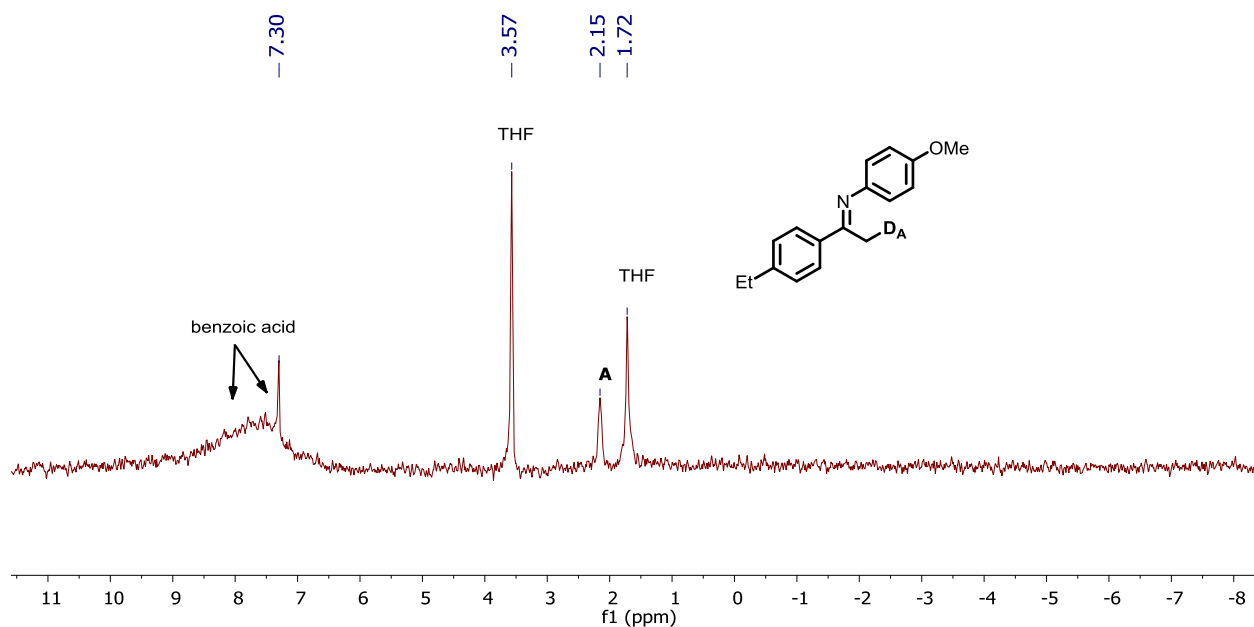
Figure 3.28. ^{2}H NMR spectrum in THF-d_0 of the crude reaction mixture resulting from a heated mixture of **1a**, diphenylacetylene, and **Co-Li** that was quenched by benzoic acid-d. Only iminyl H(D) exchange was observed.
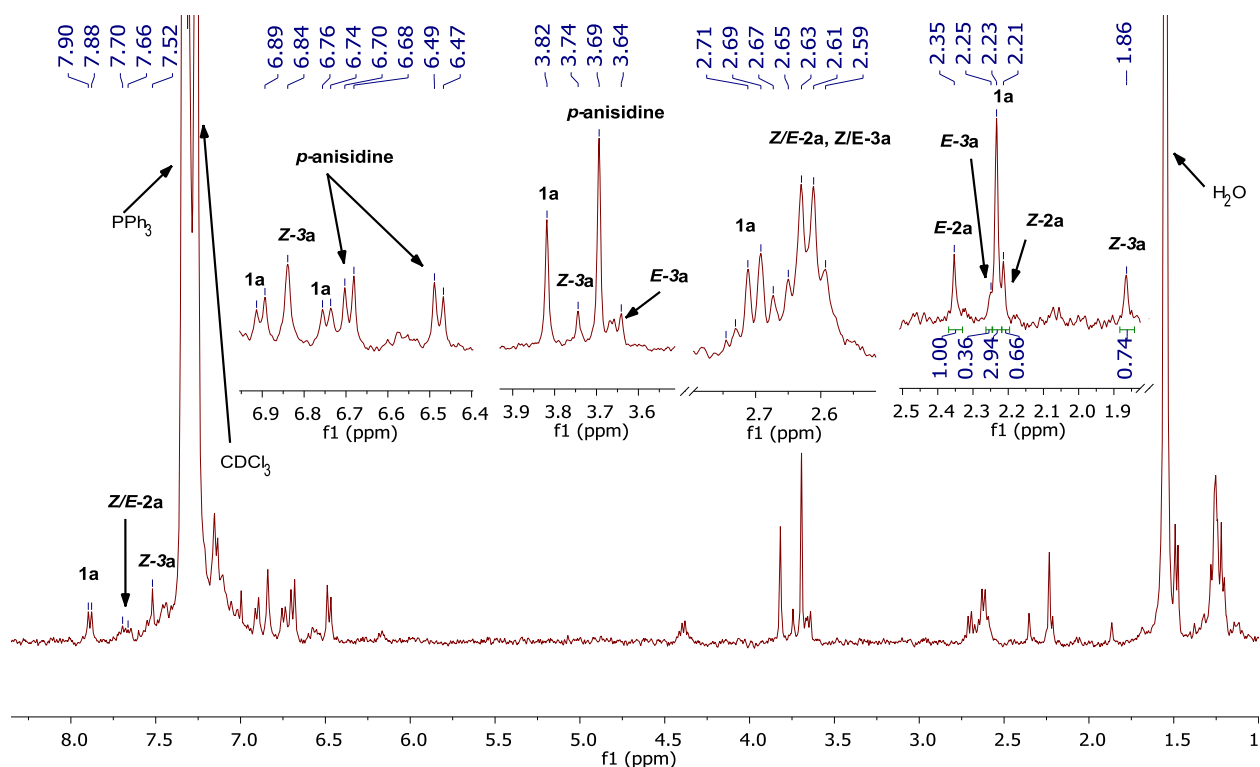
Figure 3.29. ^{1}H NMR spectrum in chloroform-*d* of the purified organic components resulting from a heated mixture of **1a**, diphenylacetylene, and **Co-Li** that was quenched by benzoic acid-*d*. Multiple species resulting from C–H bond activation were observed (**Z/E-2a** and **Z/E-3a**) and are labeled above. Deuterium incorporation from this mixture was determined from the ^{2}H NMR spectrum above in Figure 3.28.

KIE Experiment (A): Independent Rates. Inside an N$_2$ glovebox, a solution of **1a** (12 mg, 72 mM, 47 µmol, 1 equiv), diphenylacetylene (9 mg, 72 mM, 47 µmol, 1 equiv), and **Co-Li** (8 mg, 10 mM, 7 µmol, 14 mol%) in benzene-*d$_6$* (0.7 mL) with Si(SiMe$_3$)$_4$ as an internal standard was prepared and added to a sealed Teflon capped J-Young NMR tube. Prior to injection into a 500 MHz NMR spectrometer, the probe temperature was calibrated to 336 K. Upon injection into the spectrometer, spectra were acquired every 20 seconds (d1 = 5 s, d7 = 20 s, ns = 1, TD = 30). Initial rates were calculated by the decay of **1a** overtime as determined by integration of the acyl-CH$_3$ resonance of **1a** versus internal standard (see Figure 3.7 for representative reaction profile). Error was calculated as the standard deviation of triplicate experiments. A $k_{\text{obs,H}}$ was calculated to be (8.5 ± 0.5) x 10^{-6} M s^{-1}.

An analogous experiment with **1a-*d$_2$*** (12 mg, 72 mM, 47 µmol, 1 equiv) was performed in the same manner as that described above (see Figure 3.14 and Scheme 3.3). A $k_{\text{obs,D}}$ was calculated from triplicate runs to be (4.3 ± 0.3) x 10^{-6} M s^{-1}. The independent rates KIE was calculated to be $k_{\text{obs,H}} / k_{\text{obs,D}} = 2.0 ± 0.3$.

KIE Experiment (B): Intermolecular Competition. In a N$_2$ glovebox, a 100 mL Teflon stoppered Schlenk tube equipped with a stir bar was charged with a solution of **Co-Li** (65 mg, 60 µmol, 5 mol%), diphenylacetylene (192 mg, 1.1 mmol, 0.1 M, 1 equiv), *N*-Aryl imine **1a** (140 mg, 0.6 mmol, 0.05 M, 0.5 equiv), and *N*-Aryl imine **1a-*d$_2$*** (140 mg, 0.6 mmol, 0.05 M, 0.5 equiv) in THF (10 mL). On a Schlenk line, TMEDA (0.5 mL) was added. The reaction mixture was then sealed and allowed to heat at 65 °C for 20 h. Upon completion, the reaction mixture was cooled to ambient temperature and the catalyst was quenched

with 5M HCl (10 mL). After stirring for 1 h, the organic components were extracted with CH_2Cl_2 (2 x 50 mL), washed with H_2O, dried with Na_2SO_4, and filtered. Volatile components were removed under reduced pressure to afford the crude product as an orange oil. Purification by SiO_2 column chromatography (eluting with 1% EtOAc/hexanes) afforded the hydroarylation products as a colorless oil (58 mg, 18%). The products were identified as a mixture of isotopomers and the intramolecular KIE (0.78/0.22 = **3.5**) was determined as the ratio of (Z)-1-(2-(1,2-diphenylvinyl-2-d)phenyl)ethan-1-one (**Z-2a**, 14%) to (Z)-1-(2-(1,2-diphenylvinyl-6-d)phenyl-6-d)ethan-1-one (**Z-2a-d₂**, 4%) by ¹H NMR spectroscopy in chloroform-d (Figure 3.30). Note: trace E-isomer existed as evidenced by the CH_3 resonance at 2.35 ppm.

¹H NMR (chloroform-d, 500.1 MHz): δ 7.65 (d, J = 7.9 Hz, 0.78H, **H_A**), 7.33 – 7.28 (m, 5H), 7.15 – 7.07 (m, 5H), 7.02 (s, 0.78H, **H_B**), 6.95 (d, J = 7.0 Hz, 2H), 2.61 (q, J = 7.6 Hz, 2H), 2.21 (s, 3H), 1.14 (t, J = 7.6 Hz, 3H).
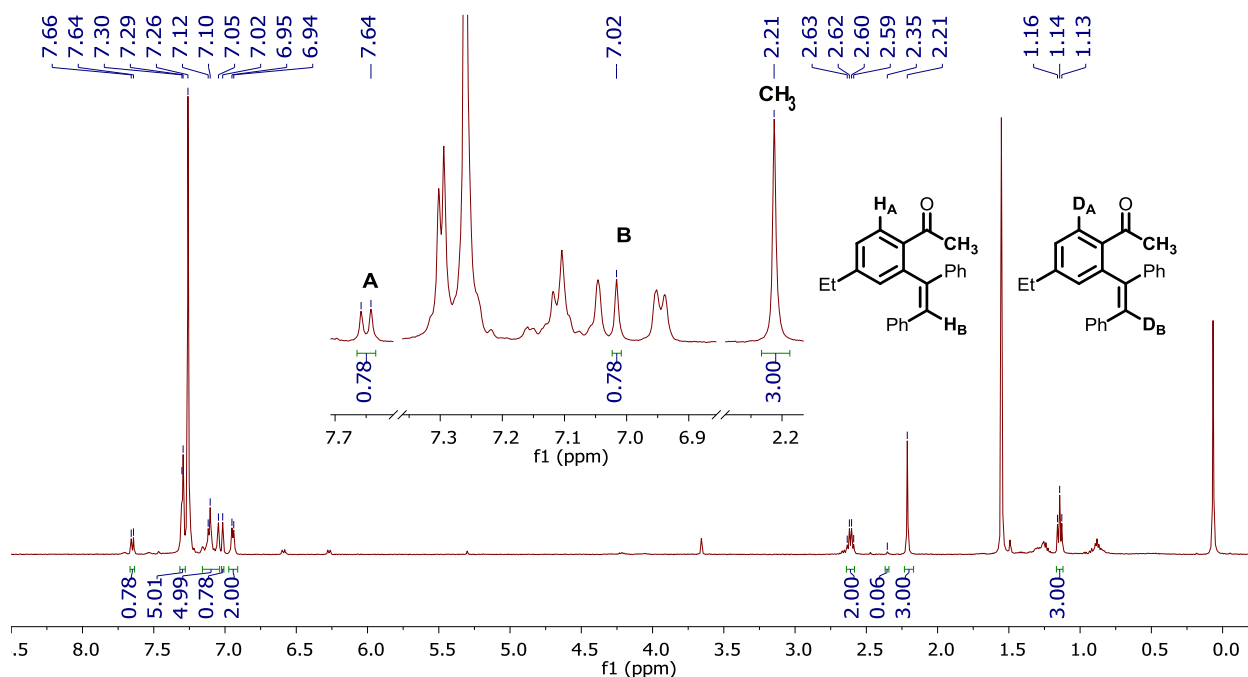
Figure 3.30. ¹H NMR spectrum in chloroform-d of the purified reaction products from the intermolecular competition experiment. Note that on average, 0.78H exist in the hydroarylation products which corresponds to a KIE of 3.5. Also note that H(D) crossover is not observed between the two substrates.

KIE Experiment (C): Intramolecular Competition. In a N_2 glovebox, a 100 mL Teflon stoppered Schlenk tube equipped with a stir bar was charged with a solution of **Co-Li** (0.24 g, 0.22 mmol, 10 mol%), diphenylacetylene (0.39 g, 2.2 mmol, 0.1 M, 1 equiv), and N-Aryl imine **1f-d₁** (0.5 g, 2.2 mmol, 0.1 M, 1 equiv) in THF (21 mL). On a Schlenk line, TMEDA (1.1 mL) was added. The reaction mixture was then sealed and allowed to heat at 65 °C for 20 h. Upon completion, the reaction mixture was cooled to ambient temperature and the catalyst was quenched with 5M HCl (10 mL). After stirring for 1 h, the organic components were extracted with CH_2Cl_2 (2 x 50 mL), washed with H_2O, dried with Na_2SO_4, and filtered. Volatile components were removed under reduced pressure to afford the crude product as an orange solid. A crude ¹H NMR yield was determined in chloroform-d by integration of the acyl CH_3 resonances corresponding to the hydroarylation product (crude ¹H NMR Yield = 42%). Purification by SiO_2 column

chromatography (eluting with 2% EtOAc/hexanes) afforded the hydroarylation products a colorless oil (166 mg, 25%). The products were identified as a mixture of isotopomers and the intramolecular KIE (0.78/0.22 = **3.6**) was determined as the ratio of (Z)-1-(2-(1,2-diphenylvinyl)phenyl-6-d)ethan-1-one to (Z)-1-(2-(1,2-diphenylvinyl-2-d)phenyl)ethan-1-one by ^{1}H NMR spectroscopy in chloroform-d (Figures 3.31 and 3.32).

^{1}H NMR (chloroform-d, 600.1 MHz): δ 7.67 (m, 0.22H, **H_A**), 7.46 (t, J = 7.4 Hz, 1H), 7.44 – 7.38 (m, 1H), 7.32 – 7.27 (m, 4H), 7.26 – 7.22 (m, 2H), 7.16 – 7.09 (m, 3H), 7.03 (s, 0.78H, **H_B**), 6.99 – 6.93 (m, 2H), 2.20 (s, 3H, **acyl-CH_3**).

^{2}H NMR (chloroform-d_0 with added chloroform-d as a reference, 92.1 MHz): δ 7.72 (br s), 7.07 (br s).

HRMS (EI) m/z: [M]$^+$ Calcd for $C_{22}H_{17}DO$ 299.1420; Found 299.1420.
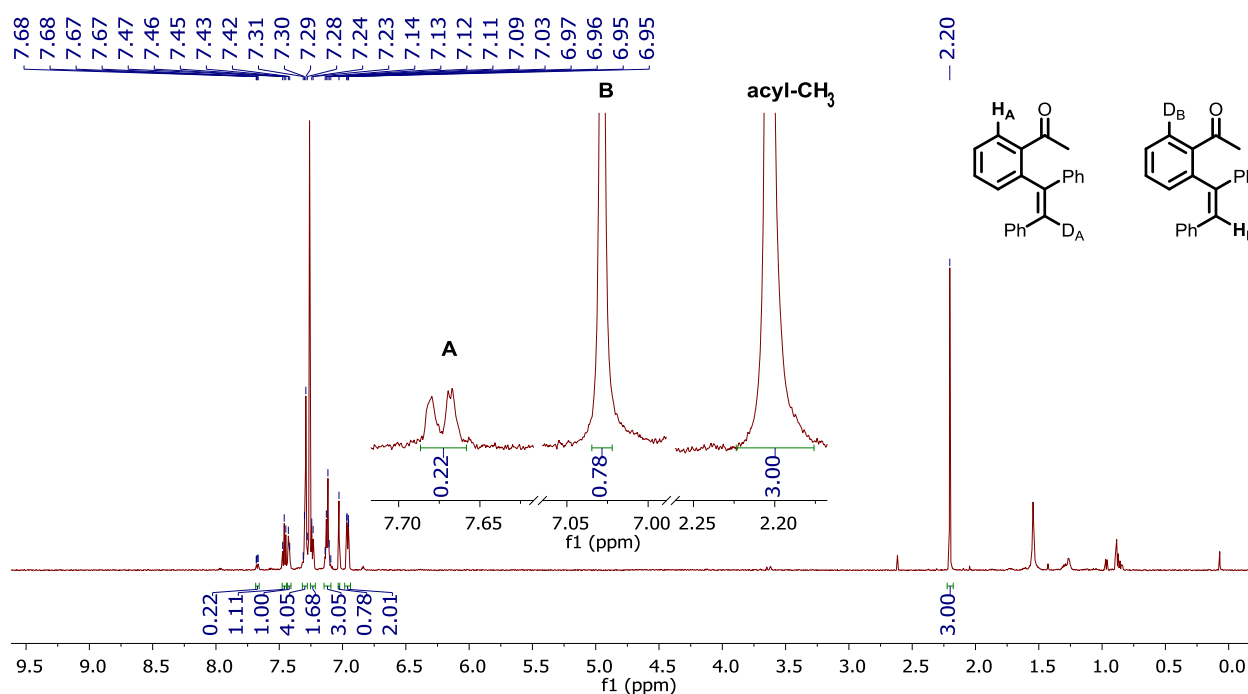
Figure 3.31. ^{1}H NMR spectrum in chloroform-d of the purified reaction products from the intramolecular competition experiment. Note that the ratio of **B:A** corresponds to the isotopological distribution of C–H versus C–D cleavage to give rise to a KIE of 3.6.
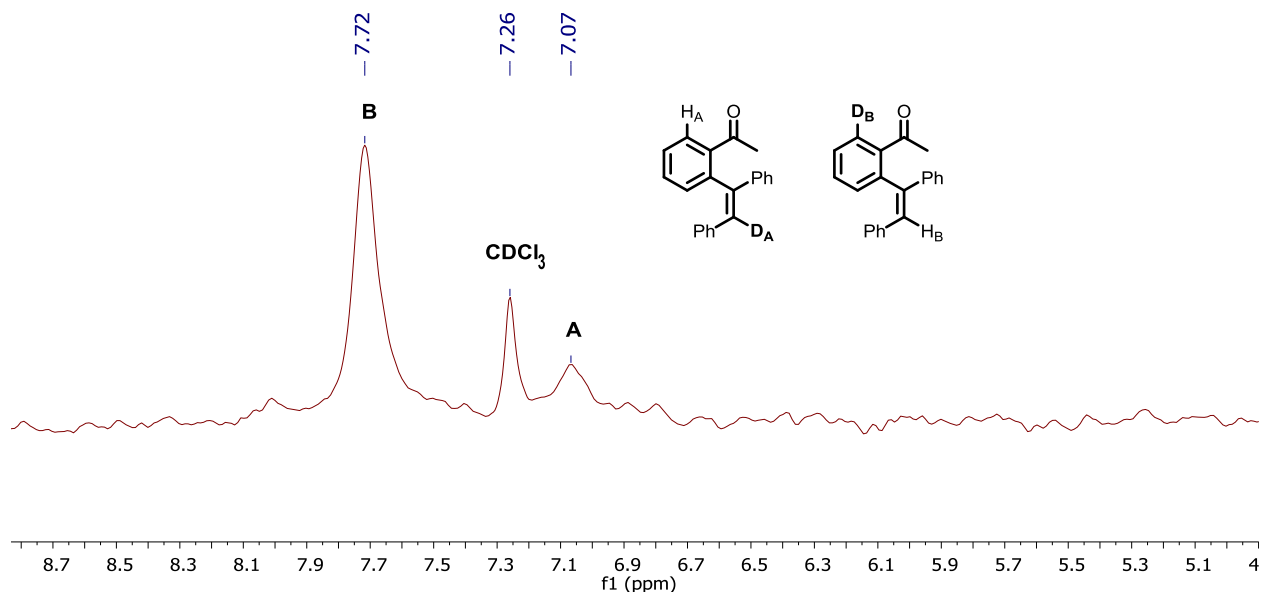
Figure 3.32. ^{2}H NMR spectrum in chloroform-d_0 (with chloroform-d added as an internal reference) of the purified reaction products arising from the intramolecular competition experiment.

Substrate Competition Experiments and Hammett Plots

Substrate Competition (A): Et (1a) vs. CO$_2$Me (1b) Substituted Imines. In a N$_2$ glovebox, a 10 mL Teflon stoppered Schlenk tube equipped with a stir bar was charged with a solution of **Co-Li** (11 mg, 0.01 mmol, 10 mol%), diphenylacetylene (18 mg, 0.1 mmol, 0.05 M, 1 equiv), *N*-Aryl imine **1a** (13 mg, 0.05 mmol, 0.05 M, 0.5 equiv), and *N*-Aryl imine **1b** (14 mg, 0.05 mmol, 0.1 M, 0.5 equiv) in toluene (1 mL). The reaction mixture was then sealed and allowed to heat at 80 °C for 40 h. Upon completion, the reaction mixture was cooled to ambient temperature and the catalyst was quenched with 5M HCl (10 mL). After stirring for 1 h, the organic components were extracted with CH$_2$Cl$_2$ (2 x 50 mL), washed with H$_2$O, dried with Na$_2$SO$_4$, and filtered. Volatile components were removed under reduced pressure to afford the crude product as an orange solid. A crude ^{1}H NMR yield was determined in chloroform-d by integration of the acyl CH$_3$ resonances corresponding to the hydroarylation product (Figure 3.33 Top, below). The product distribution is given above with a preference for the CO$_2$Me derived products of ca. 1.7:1.0.

An analogous experiment was performed with excess imine relative to alkyne as follows. In a N$_2$ glovebox, a 10 mL Teflon stoppered Schlenk tube equipped with a stir bar was charged with a solution of **Co-Li** (11 mg, 0.01 mmol, 10 mol%), diphenylacetylene (18 mg, 0.1 mmol, 0.05 M, 1 equiv), *N*-Aryl imine **1a** (25 mg, 0.1 mmol, 0.05 M, 1 equiv), and *N*-Aryl imine **1b** (28 mg, 0.1 mmol, 0.1 M, 1 equiv) in toluene (1 mL). The reaction mixture was then sealed and allowed to heat at 80 °C for 40 h. Upon completion, the reaction mixture was cooled to ambient temperature and the catalyst was quenched with 5M HCl (10 mL). After stirring for 1 h, the organic components were extracted with CH$_2$Cl$_2$ (2 x 50 mL), washed with H$_2$O, dried with Na$_2$SO$_4$, and filtered. Volatile components were removed under reduced pressure to afford the crude product as an orange solid. A crude ^{1}H NMR yield was determined in chloroform-d by integration of the acyl CH$_3$ resonances corresponding to the hydroarylation product (Figure 3.33 Bottom, Below) with a product distribution favoring CO$_2$Me derived products of ca. 1.4:1.0.
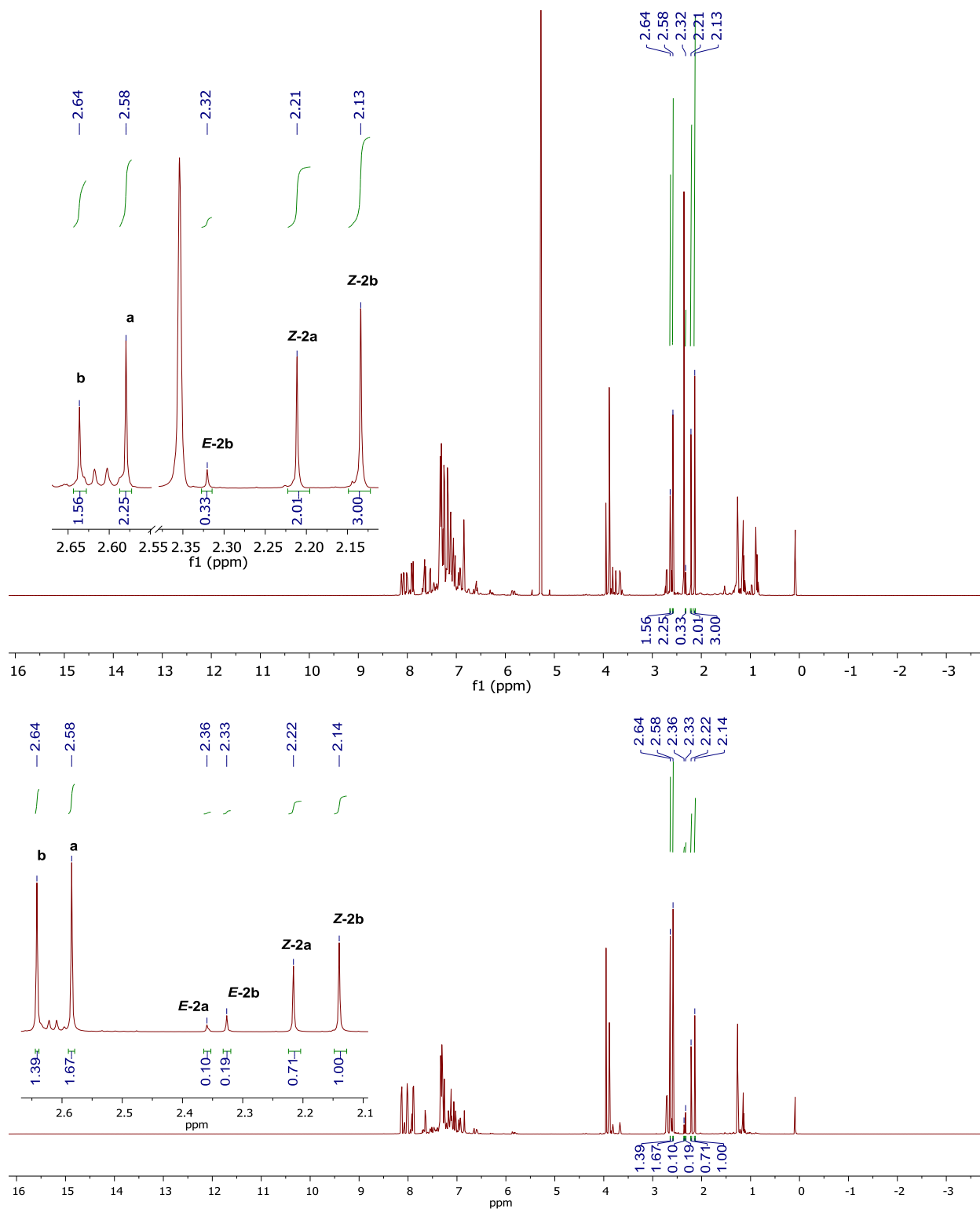
Figure 3.33. ^{1}H NMR spectra in chloroform-*d* of the crude reaction mixture after an acidic workup. **Top:** The imine substrate bearing a CO_2Me substituent (**2b**) is preferred by 1.7:1.0 over the Et imine (**2a**). **Bottom:** The imine substrate bearing a CO_2Me substituent (**2b**) is preferred by 1.4:1.0 over the Et imine (**2a**).

Substrate Competition (B): Et (1a) vs. CF₃ (1d) Substituted Imines. In a N₂ glovebox, a 10 mL Teflon stoppered Schlenk tube equipped with a stir bar was charged with a solution of **Co-Li** (11 mg, 0.01 mmol, 10 mol%), diphenylacetylene (18 mg, 0.1 mmol, 0.1 M, 1 equiv), *N*-Aryl imine **1a** (13 mg, 0.05 mmol, 0.05 M, 0.5 equiv), and *N*-Aryl imine **1d** (15 mg, 0.05 mmol, 0.05 M, 0.5 equiv) in toluene (1 mL). The reaction mixture was then sealed and allowed to heat at 80 °C for 40 h. Upon completion, the reaction mixture was cooled to ambient temperature and the catalyst was quenched with 5M HCl (10 mL). After stirring for 1 h, the organic components were extracted with CH₂Cl₂ (2 x 50 mL), washed with H₂O, dried with Na₂SO₄, and filtered. Volatile components were removed under reduced pressure to afford the crude product as an orange solid. A crude ¹H NMR yield was determined in chloroform-*d* by integration of the acyl CH₃ resonances corresponding to the hydroarylation product (Figure 3.34, below). The product distribution is given above with a preference for the CF₃ derived products of ca. 2.5:1.0.
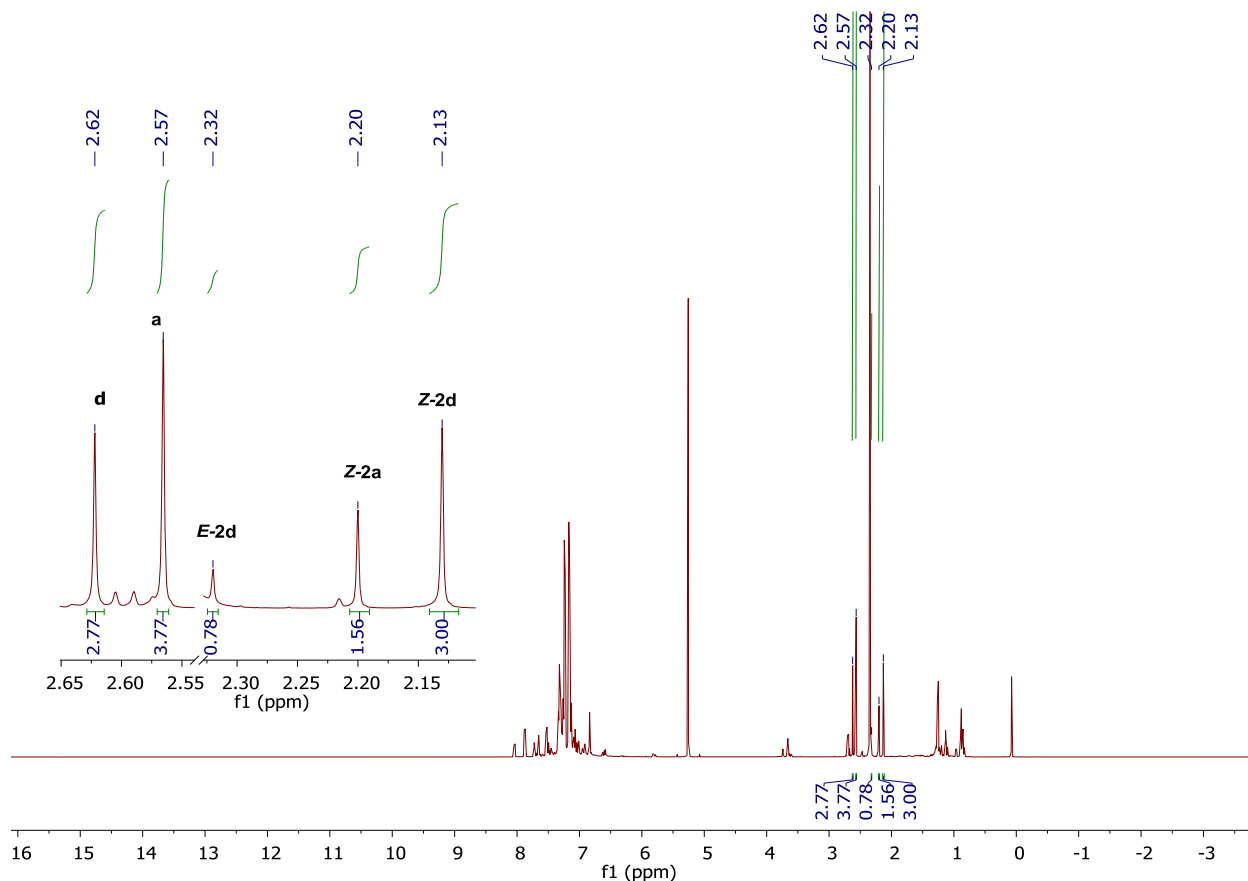
Figure 3.34. ¹H NMR spectrum in chloroform-*d* of the crude reaction mixture after an acidic workup. The imine substrate bearing a CF₃ substituent (**2d**) is preferred by 2.5:1.0 over the Et imine (**2a**).

Substrate Competition (C): CO₂Me (1b) vs. CF₃ (1d) Substituted Imines. In a N_2 glovebox, a 10 mL Teflon stoppered Schlenk tube equipped with a stir bar was charged with a solution of **Co-Li** (11 mg, 0.01 mmol, 10 mol%), diphenylacetylene (18 mg, 0.1 mmol, 0.1 M, 1 equiv), *N*-Aryl imine **1b** (14 mg, 0.05 mmol, 0.05 M, 0.5 equiv), and *N*-Aryl imine **1d** (15 mg, 0.05 mmol, 0.05 M, 0.5 equiv) in toluene (1 mL). The reaction mixture was then sealed and allowed to heat at 80 °C for 40 h. Upon completion, the reaction mixture was cooled to ambient temperature and the catalyst was quenched with 5M HCl (10 mL). After stirring for 1 h, the organic components were extracted with CH_2Cl_2 (2 x 50 mL), washed with H_2O, dried with Na_2SO_4, and filtered. Volatile components were removed under reduced pressure to afford the crude product as an orange solid. A crude ¹H NMR yield was determined in chloroform-*d* by integration of the acyl CH_3 resonances corresponding to the hydroarylation product (Figure 3.35, below). The product distribution is given above with a preference for the CO₂Me derived products of ca. 1.1:1.0.
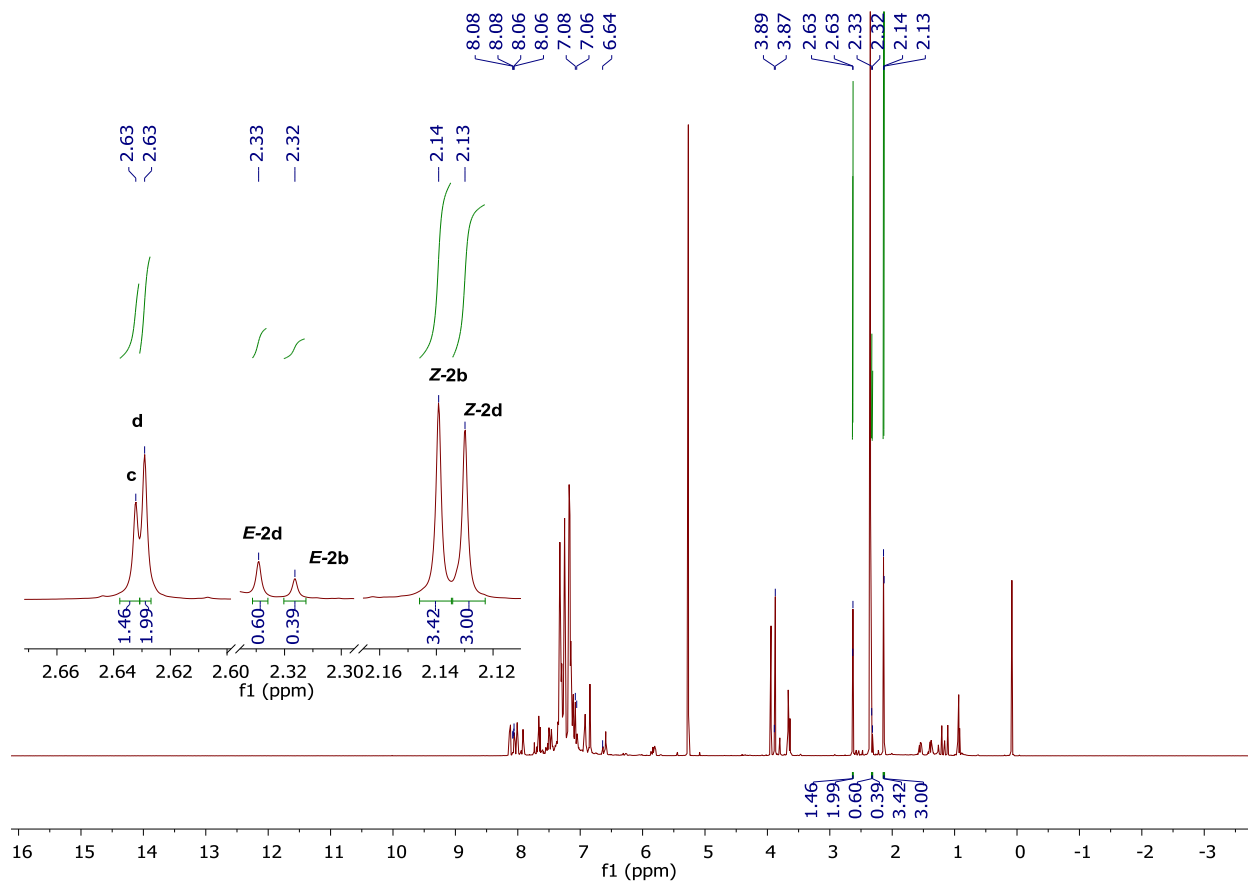
Figure 3.35. ¹H NMR spectrum in chloroform-*d* of the crude reaction mixture after an acidic workup. The imine substrate bearing a CO₂Me substituent (**2b**) is preferred by 1.1:1.0 over the CF₃ imine (**2d**).

Substrate Competition (D): Et (1a) vs. OMe (1e) Substituted Imines. In a N₂ glovebox, a 10 mL Teflon stoppered Schlenk tube equipped with a stir bar was charged with a solution of **Co-Li** (11 mg, 0.01 mmol, 10 mol%), diphenylacetylene (18 mg, 0.1 mmol, 0.1 M, 1 equiv), *N*-Aryl imine **1a** (13 mg, 0.05 mmol, 0.05 M, 0.5 equiv), and *N*-Aryl imine **1e** (13 mg, 0.05 mmol, 0.05 M, 0.5 equiv) in toluene (1 mL). The reaction mixture was then sealed and allowed to heat at 80 °C for 20 h. Upon completion, the reaction mixture was cooled to ambient temperature and the catalyst was quenched with 5M HCl (10 mL). After stirring for 1 h, the organic components were extracted with CH_2Cl_2 (2 x 50 mL), washed with H_2O, dried with Na_2SO_4, and filtered. Volatile components were removed under reduced pressure to afford the crude product as an orange solid. A crude ¹H NMR yield was determined in chloroform-*d* by integration of the acyl CH_3 resonances corresponding to the hydroarylation product (Figure 3.36 Top, below). The product distribution is given above with a preference for the Et derived products of ca. 1.7:1.0.

An analogous experiment was performed with excess imine relative to alkyne as follows. In a N₂ glovebox, a 10 mL Teflon stoppered Schlenk tube equipped with a stir bar was charged with a solution of **Co-Li** (6 mg, 0.005 mmol, 10 mol%), diphenylacetylene (18 mg, 0.05 mmol, 0.1 M, 1 equiv), *N*-Aryl imine **1a** (15 mg, 0.05 mmol, 0.05 M, 1 equiv), and *N*-Aryl imine **1e** (15 mg, 0.05 mmol, 0.05 M, 1 equiv) in toluene (0.5 mL). The reaction mixture was then sealed and allowed to heat at 80 °C for 20 h. Upon completion, the reaction mixture was cooled to ambient temperature and the catalyst was quenched with 5M HCl (10 mL). After stirring for 1 h, the organic components were extracted with CH_2Cl_2 (2 x 50 mL), washed with H_2O, dried with Na_2SO_4, and filtered. Volatile components were removed under reduced pressure to afford the crude product as an orange solid. A crude ¹H NMR yield was determined in chloroform-*d* by integration of the acyl CH_3 resonances corresponding to the hydroarylation product (Figure 3.36 Bottom, below). A crude ¹H NMR yield was determined in chloroform-*d* by integration of the acyl CH_3 resonances corresponding to the hydroarylation product with a product distribution favoring Et derived products of ca. 1.7:1.0.
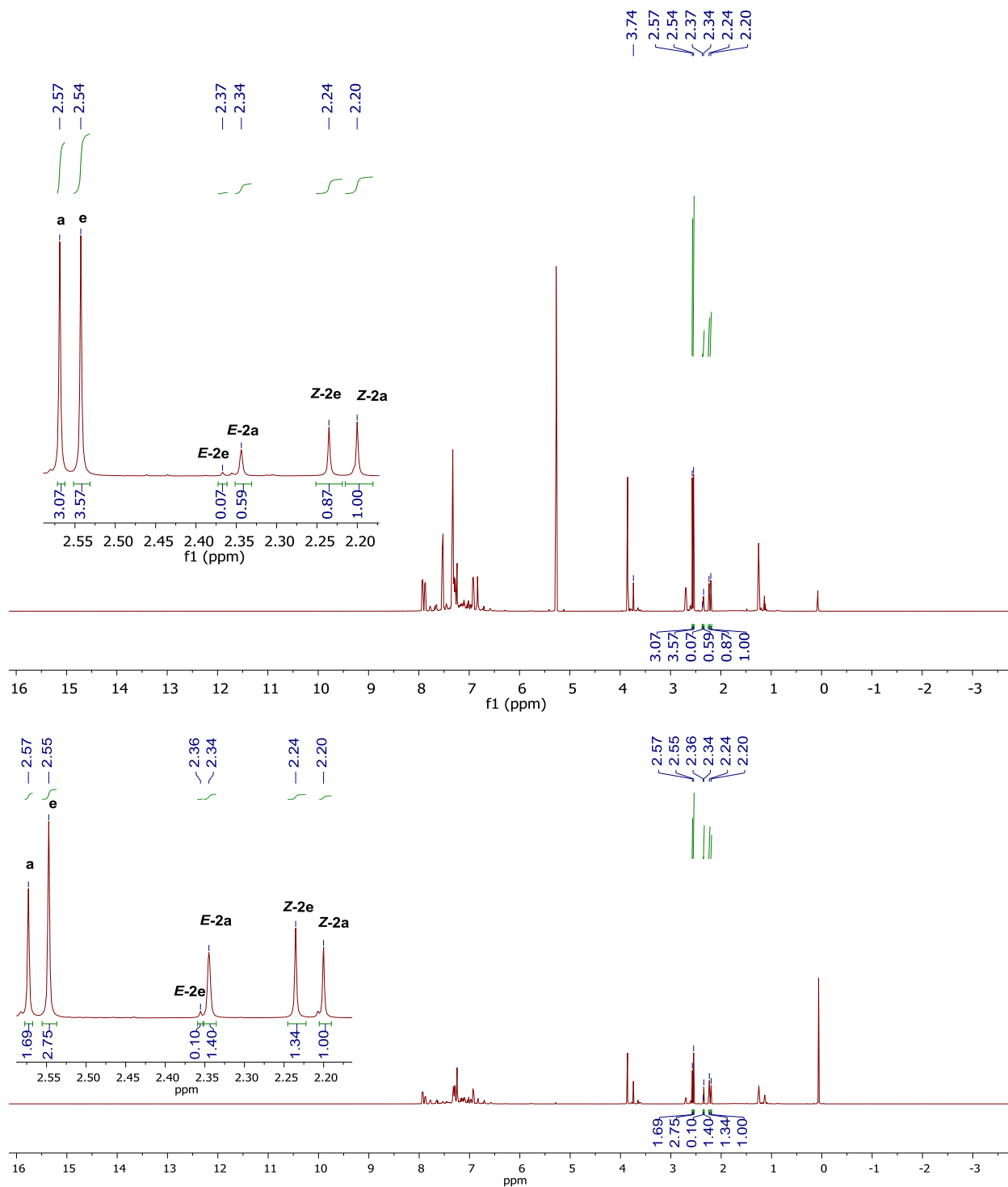
Figure 3.36. ^{1}H NMR spectrum in chloroform-*d* of the crude reaction mixture after an acidic workup. **Top:** The imine substrate bearing an Et substituent (**2a**) is preferred by 1.7:1.0 over the OMe imine (**2e**). **Bottom:** The imine substrate bearing an Et substituent (**2a**) is preferred by 1.7:1.0 over the OMe imine (**2e**).

Hammett Plot Generation: Independent Rate Measurements. Inside an N_2 glovebox, a solution of (*N*-aryl)aryl ethanimine (67 mM, 47 µmol, 1 equiv), diphenylacetylene (8.4 mg, 67 mM, 47 µmol, 1 equiv), and **Co-Li** (8 mg, 10 mM, 7 µmol, 14 mol%) in benzene-d_6 (0.7 mL) with $Si(SiMe_3)_4$ as an internal standard was prepared and added to a sealed Teflon capped J-Young NMR tube. Prior to injection into a 500 MHz NMR spectrometer, the probe temperature was calibrated to 339.5 K. Upon injection into the spectrometer, spectra were acquired every 20 seconds (d1 = 5 s, d7 = 20 s, ns = 1, TD = 90). Initial rates were calculated by the decay of (*N*-aryl)aryl ethanimine over time as determined by integration of the acyl-CH_3 resonance versus internal standard. Errors were calculated as the standard deviation of triplicate experiments. This procedure was duplicated for **1a**, **1b**, **1d**, and **1e** as substrate. The initial rate constants ($k_{initial}$) were compared to the σ_{para} parameter (Table 3.13) to generate Figure 3.15. A normalized Hammett plot (Figure 3.15B) was generated from the data in Table 3.13 below by normalizing the observed rates by the observed rate for **1a** as a substrate.

Table 3.13. Observed rates for the hydroarylations of **1a**, **1b**, **1d**, and **1e** ($[1]_0$ = 67 mM) with diphenylacetylene ($[\text{diphenylacetylene}]_0$ = 67 mM) catalyzed by **Co-Li** ($[\text{Co-Li}]_0$ = 10 mM).
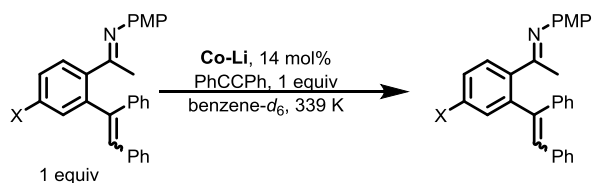
X	Compound #	σ_{para}[98]	$k_{initial}$ X 10^{-5} (M s^{-1}) [a]	k_X/k_{Et}	log(k_X/k_{Et})
CF$_3$	**1d**	0.54	1.65(20)	1.94	0.29
CO$_2$Me	**1b**	0.45	1.26(10)	1.48	0.17
Et	**1a**	-0.07	0.85(5)	1.00	0.00
OMe	**1e**	-0.27	0.78(6)	0.91	-0.04

[a] Initial rates ($k_{initial}$) were determined by ^{1}H NMR spectroscopy in benzene-d_6 vs $Si(SiMe_3)_4$ as an internal standard with the NMR probe temperature calibrated to 339 K. Error bars were determined as the standard deviation of triplicate experiments. The initial rates vs. the σ_{para} parameter generated Figure 3.15A. The initial rates were normalized vs. the rate for **1a**. The log of this ratio vs. the σ_{para} parameter generated the normalized Hammett plot in Figure 3.15B.

Hydroarylation Kinetics Experiments and Michaelis-Menten Analysis

Reaction Order in Co-Li. Inside an N_2 glovebox, a stock solution comprised of **1a** (69 mg, 67 mM, 0.27 mmol, 1 equiv), diphenylacetylene (48 mg, 67 mM, 0.27 mmol, 1 equiv), and benzene-d_6 (4.0 mL) with $Si(SiMe_3)_4$ as an internal standard was prepared. Five separate experiments were performed with 0.7 mL of the stock solution and varied [**Co-Li**] (1.0 mg/1.2 mM, 1.6 mg/2.1 mM, 3.6 mg/4.7 mM, 4.0 mg/5.3 mM, and 7.1 mg/9.3 mM, respectively) inside a sealed Teflon capped J-Young NMR tube. Each catalytic sample was immediately frozen after preparation in a -78 °C bath to prevent background reactivity. Each sample was thawed prior to injection into a 500 MHz NMR spectrometer with a probe temperature calibrated to

338 K. Upon injection into the spectrometer, spectra were acquired every 120 seconds (d1 = 5 s, d7 = 120 s, ns = 1, TD = 30). Initial rates were calculated by the decay of **1a** over time as determined by integration of the acyl-CH$_3$ resonance of **1a** versus internal standard. The results are summarized in Table 3.14 below and in Figure 3.9. Note that the catalysis is first-order in $[\textbf{Co-Li}]_0$ with a measured $k_{obs} = 9.4(19) \times 10^{-4}\,\text{s}^{-1}$.

Table 3.14. Dependence of $[\textbf{Co-Li}]$ on the hydroarylation of **1a** ($[\textbf{1a}]_0 = 67$ mM) with diphenylacetylene ($[\text{diphenylacetylene}]_0 = 67$ mM).
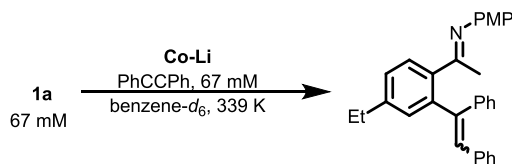
$[\textbf{Co-Li}]_0$ (mM)	$k_{initial} \times 10^{-6}$ (M s^{-1}) [a]
1.2	0.3
2.1	1.9
4.7	2.0
5.3	3.2
9.3	8.5

Initial rates ($k_{initial}$) were determined by ^{1}H NMR spectroscopy in benzene-d_6 vs Si(SiMe$_3$)$_4$ as an internal standard with the NMR probe temperature calibrated to 339 K.

Reaction Order in Co$_2$-Mg. Inside an N$_2$ glovebox, a stock solution comprised of **1a** (131 mg, 67 mM, 0.52 mmol, 1 equiv), diphenylacetylene (92 mg, 67 mM, 0.52 mmol, 1 equiv), and benzene-d_6 (7.7 mL) with Si(SiMe$_3$)$_4$ as an internal standard was prepared. Ten separate experiments were performed with 0.7 mL of the stock solution and varied $[\textbf{Co}_2\textbf{-Mg}]$ (2.4 mg/1.7 mM, 4.8 mg/3.4 mM (in triplicate), 8.9 mg/6.2 mM, 10.2 mg/7.1 mM, 12.7 mg/8.8 mM, 14.2 mg/9.8 mM, 17.0 mg/10 mM, and 20.0 mg/13.9 mM, respectively) inside a sealed Teflon capped J-Young NMR tube. Each catalytic sample was immediately frozen after preparation in a -78 °C bath to prevent background reactivity. Each sample was thawed prior to injection into a 500 MHz NMR spectrometer with a probe temperature calibrated to 338 K. Upon injection into the spectrometer, spectra were acquired every 120 seconds (d1 = 5 s, d7 = 120 s, ns = 1, TD = 30). Initial rates were calculated by the decay of **1a** over time as determined by integration of the acyl-CH$_3$ resonance of **1a** versus internal standard. The results are summarized in Table 3.15 below and in Figure 3.10. Note that the catalysis is first-order in $[\textbf{Co}_2\textbf{-Mg}]_0$ with a measured $k_{obs} = 3.0(3) \times 10^{-5}\,\text{s}^{-1}$.

Table 3.15. Dependence of [**Co₂-Mg**] on the hydroarylation of **1a** ([**1a**]$_0$ = 67 mM) with diphenylacetylene ([diphenylacetylene]$_0$ = 67 mM).
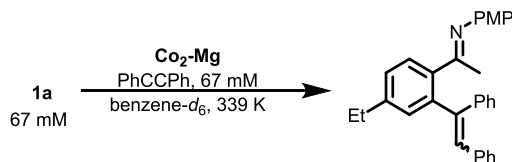
[Co₂-Mg]$_0$ (mM)	$k_{initial}$ x 10^{-8} (M s^{-1}) [a]
1.7	3.9
3.4	8.7
3.4	8.6
3.4	7.7
6.2	16.4
7.1	25.6
8.8	31.5
9.8	27.3
11.8	34.4
13.9	40.6

[a] Initial rates ($k_{initial}$) were determined by ^{1}H NMR spectroscopy in benzene-d_6 vs Si(SiMe₃)₄ as an internal standard with the NMR probe temperature calibrated to 339 K.

Reaction Order in [PhCCPh]. Inside an N₂ glovebox, a stock solution comprised of **1a** (66 mg, 67 mM, 0.26 mmol, 1 equiv), **Co-Li** (29 mg, 7 mM, 26 µmol, 10 mol%), and benzene-d_6 (3.9 mL) with Si(SiMe₃)₄ as an internal standard was prepared. Five separate experiments were performed with 0.7 mL of the stock solution and varied [diphenylacetylene]$_0$ (6.5 mg/52 mM, 11 mg/90 mM, 19 mg/150 mM, 25 mg/200 mM, and 44 mg/355 mM, respectively) inside a sealed Teflon capped J-Young NMR tube. Each catalytic sample was immediately frozen after preparation in a -78 °C bath to prevent background reactivity. Each sample was thawed prior to injection into a 500 MHz NMR spectrometer with a probe temperature calibrated to 339 K. Upon injection into the spectrometer, spectra were acquired every 20 seconds (d1 = 5 s, d7 = 20 s, ns = 1, TD = 30). Initial rates were calculated by the decay of **1a** over time as determined by integration of the acyl-CH₃ resonance of **1a** versus internal standard. The results are summarized in Figure 3.37 and Table 3.16 below. Note that saturation behavior is observed in [PhCCPh]$_0$. Error bars were determined as the standard deviation of triplicate runs.

Table 3.16. Data for the hydroarylation of 1a with varying [diphenylacetylene]$_0$.
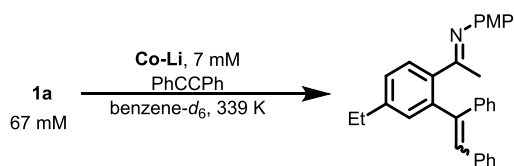
[PhCCPh]$_0$ (M)	$k_{initial}$ x 10^{-6} (M s^{-1}) [a]
52	0.50 ± 0.08
90	0.81 ± 0.14
150	1.3 ± 0.13
200	1.6 ± 0.17
355	1.9 ± 0.19

[a] Initial rates ($k_{initial}$) were determined by ^{1}H NMR spectroscopy in benzene-d_6 vs Si(SiMe$_3$)$_4$ as an internal standard with the NMR probe temperature calibrated to 339 K.
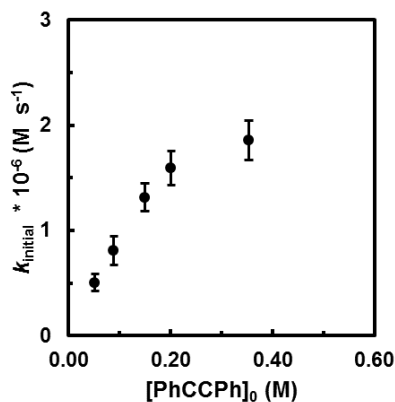
Figure 3.37. Dependence of [diphenylacetylene] on the hydroarylation of **1a** ([**1a**]$_0$ = 67 mM) catalyzed by **Co-Li** ([**Co-Li**]$_0$ = 7 mM). Initial rates ($k_{initial}$) were determined by ^{1}H NMR spectroscopy in benzene-d_6 vs Si(SiMe$_3$)$_4$ as an internal standard with the NMR probe temperature calibrated to 339 K.

Michaelis-Menten Analysis and Secondary Michaelis-Menten Plots. General procedure: Inside an N_2 glovebox, a stock solution comprised of diphenylacetylene (see Table 3.17 below), **Co-Li** (29 mg, 7 mM, 26 µmol), and benzene-d_6 (3.9 mL) with $Si(SiMe_3)_4$ as an internal standard was prepared. Five separate experiments were performed with 0.7 mL of the stock solution and varied $[1a]_0$ (see Table 3.17 below) inside a sealed Teflon capped J-Young NMR tube. Each catalytic sample was immediately frozen after preparation in a -78 °C bath to prevent background reactivity. Each sample was thawed prior to injection into a 500 MHz NMR spectrometer with a probe temperature calibrated to 338 K. Upon injection into the spectrometer, spectra were acquired every 20 seconds (d1 = 5 s, d7 = 20 s, ns = 1, TD = 30). Initial rates were calculated by the decay of **1a** over time as determined by integration of the acyl-CH_3 resonance of **1a** versus internal standard. The Lineweaver-Burke plots (Figure 3.11) were generated from the double reciprocal data described in Table 3.18 below which was generated from the data collected in Table 3.17. The secondary Michaelis-Menten plot (see Figure 3.11, expansion) was generated by plotting the slopes calculated from the main Lineweaver-Burke plot against the [diphenylacetylene]$_0$ as described in Table 3.19 below. Note that a parabolic-like behavior is observed, which indicates a complicated dependency on alkyne.

Table 3.17. Initial rate data for the hydroarylation of diphenylacetylene and **1a** catalyzed by **Co-Li** (7 mM).

$[PhCCPh]_0$ (M)	$[1a]_0$ (M)	$k_{initial}$ x 10^{-7} (M s^{-1}) [a]	$[PhCCPh]_0$ (M)	$[1a]_0$ (M)	$k_{initial}$ x 10^{-7} (M s^{-1}) [a]
0.034	0.075	5.5	0.102	0.049	7.1
0.034	0.143	10.8	0.102	0.128	15.2
0.034	0.199	14.4	0.102	0.174	18.0
0.034	0.288	18.2	0.102	0.252	26.2
0.034	0.383	21.4	0.102	0.399	57.1
0.049	0.083	7.1	0.138	0.073	5.9
0.049	0.123	10.8	0.138	0.131	8.7
0.049	0.199	18.3	0.138	0.198	17.2
0.049	0.340	25.7	0.138	0.243	16.0
0.049	0.461	26.7	0.138	0.357	25.1
0.071	0.080	19.5	0.210	0.085	3.8
0.071	0.139	23.9	0.210	0.139	5.9
0.071	0.195	31.9	0.210	0.196	7.9
0.071	0.265	46.8	0.210	0.269	10.4
0.071	0.323	88.7	0.210	0.388	18.5
			0.280	0.083	3.1
			0.280	0.144	5.2
			0.280	0.205	7.4
			0.280	0.283	9.9
			0.280	0.390	13.4

[a] Initial rates ($k_{initial}$) were determined by ^1H NMR spectroscopy in benzene-d_6 with $Si(SiMe_3)_4$ as an internal standard and with the NMR spectrometer probe calibrated to 338 K.

Table 3.18. Double-reciprocal data (see Figure 3.11) for the hydroarylation of diphenylacetylene and **1a** catalyzed by **Co-Li** (7 mM) which was generated from data in Table 3.17 above.

$[PhCCPh]_0$ (M)	$1/[1a]_0$ (M^{-1})	$1/k_{initial}$ x 10^5 (s M^{-1})	$[PhCCPh]_0$ (M)	$1/[1a]_0$ (M^{-1})	$1/k_{initial}$ x 10^5 (s M^{-1})
0.034	13.4	18.1	0.102	20.6	14.0
0.034	7.0	9.3	0.102	7.8	6.6
0.034	5.0	6.9	0.102	5.7	5.5
0.034	3.5	5.5	0.102	4.0	3.8
0.034	2.6	4.7	0.102	2.5	1.8
0.049	12.0	14.1	0.138	13.6	17.0
0.049	8.1	9.3	0.138	7.6	11.5
0.049	5.0	5.5	0.138	5.1	5.8
0.049	2.9	3.9	0.138	4.1	6.2
0.049	2.2	3.7	0.138	2.8	4.0
0.071	12.5	5.1	0.210	11.7	26
0.071	7.2	4.2	0.210	7.2	17
0.071	5.1	3.1	0.210	5.1	12.7
0.071	3.8	2.1	0.210	3.7	9.6
0.071	3.1	1.1	0.210	2.6	5.4
			0.280	12.0	32.3
			0.280	6.9	19.2
			0.280	4.9	13.5
			0.280	3.5	10.1
			0.280	2.6	7.5

[a] A maximum rate achievable (V_{max}) was calculated to be (1.2 ± 0.2) x 10^{-5} M s^{-1} which was calculated from the y-intercepts of each linear fit of the Michaelis-Menten experiments

Table 3.19. Secondary Michaelis-Menten data for the hydroarylation of **1a** with diphenylacetylene catalyzed by **Co-Li** (7 mM). The Lineweaver-Burke slopes were generated from the linear fits of each data set described in Table 3.18 above.

[PhCCPh]$_0$ (mM)	Lineweaver-Burke Slope ($\Delta[1a]_0 / \Delta k_{initial}$) x 10^4 (s)
34	12.5
49	10.8
71	3.9
102	6.4
138	12.3
210	22.0
280	26.1

Reaction Order in Added PPh$_3$. Inside an N$_2$ glovebox, a stock solution comprised of **1a** (85 mg, 67 mM, 0.34 mmol, 1 equiv), diphenylacetylene (60 mg, 67 mM, 0.34 mmol, 1 equiv), **Co-Li** (37 mg, 7 mM, 34 µmol, 10 mol%), and benzene-d_6 (5.0 mL) with Si(SiMe$_3$)$_4$ as an internal standard was prepared. Seven separate experiments were performed with 0.7 mL of the stock solution and varied quantities of excess PPh$_3$ (none, 4.3 mg/23 mM, 10 mg/56 mM, 19 mg/103 mM, 39 mg/213 mM, 62 mg/365 mM, and 124 mg/692 mM, respectively) inside a sealed Teflon capped J-Young NMR tube. Each catalytic sample was immediately frozen after preparation in a -78 °C bath to prevent background reactivity. Each sample was thawed prior to injection into a 500 MHz NMR spectrometer with a probe temperature calibrated to 339 K. Upon injection into the spectrometer, spectra were acquired every 20 seconds (d1 = 5 s, d7 = 20 s, ns = 1, TD = 90). Initial rates were calculated by the decay of **1a** over time as determined by integration of the acyl-CH$_3$ resonance of **1a** versus internal standard. The results are summarized in Table 3.20 below and in Figure 3.12. Error bars were determined as the standard deviation of triplicate runs except for [PPh$_3$]$_0$ = 692 mM, which was performed in pentaplicate.

Table 3.20. Data for the hydroarylation of **1a** (67 mM) with diphenylacetylene (67 mM) catalyzed by **Co-Li** (7 mM) with added PPh₃.
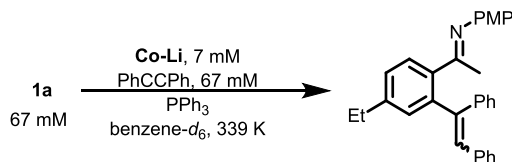
Added [PPh₃] (mM)	$k_{initial}$ x 10^{-6} (M s⁻¹) [a]
0	1.0 ± 0.1
23	4.1 ± 0.6
56	8.0 ± 0.7
103	9.7 ± 0.8
213	10.5 ± 0.8
365	11.0 ± 0.9
692	9.4 ± 1.5

[a] Initial rates ($k_{initial}$) were determined by ¹H NMR spectroscopy in benzene-d_6 with Si(SiMe₃)₄ as an internal standard and with the NMR spectrometer probe calibrated to 339 K.

Reaction Order in Added P(Mes)₃. Inside an N₂ glovebox, a stock solution comprised of **1a** (66 mg, 67 mM, 0.26 mmol, 1 equiv), diphenylacetylene (46.4 mg, 67 mM, 0.26 mmol, 1 equiv), **Co-Li** (28.6 mg, 7 mM, 26 μmol, 10 mol%), and benzene-d_6 (3.9 mL) with Si(SiMe₃)₄ as an internal standard was prepared. Five separate experiments were performed with 0.7 mL of the stock solution and varied quantities of excess P(Mes)₃ (2.9 mg/10.6 mM, 7.0 mg/25.8 mM, 14.3 mg/52.7 mM, 22.3 mg/82.1 mM, and 27.1 mg/99.8 mM, respectively) inside a sealed Teflon capped J-Young NMR tube. Each catalytic sample was immediately frozen after preparation in a -78 °C bath to prevent background reactivity. Each sample was thawed prior to injection into a 500 MHz NMR spectrometer with a probe temperature calibrated to 339 K. Upon injection into the spectrometer, spectra were acquired every 20 seconds (d1 = 5 s, d7 = 20 s, ns = 1, TD = 90). Initial rates were calculated by the decay of **1a** over time as determined by integration of the acyl-CH₃ resonance of **1a** versus internal standard. The results are summarized in Table 3.21 below and in Figure 3.12.

Table 3.21. Data for the hydroarylation of **1a** (67 mM) with diphenylacetylene (67 mM) catalyzed by **Co-Li** (7 mM) with added P(Mes)$_3$.
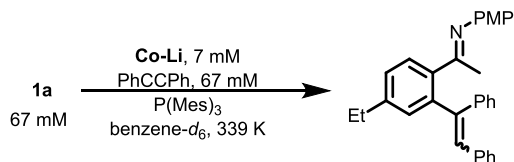
Added [P(Mes)$_3$] (mM)	$k_{initial}$ x 10^{-6} (M s^{-1}) [a]
10.6	4.3
25.8	5.6
52.7	6.3
82.1	6.5
99.8	6.6

[a] Initial rates ($k_{initial}$) were determined by ^{1}H NMR spectroscopy in benzene-d_6 with Si(SiMe$_3$)$_4$ as an internal standard and with the NMR spectrometer probe calibrated to 339 K.

Reaction Order in Added P(C$_6$F$_5$)$_3$. Inside an N$_2$ glovebox, a stock solution comprised of **1a** (66 mg, 67 mM, 0.26 mmol, 1 equiv), diphenylacetylene (46.4 mg, 67 mM, 0.26 mmol, 1 equiv), **Co-Li** (28.6 mg, 7 mM, 26 μmol, 10 mol%), and benzene-d_6 (3.9 mL) with Si(SiMe$_3$)$_4$ as an internal standard was prepared. Five separate experiments were performed with 0.7 mL of the stock solution and varied quantities of excess P(C$_6$F$_5$)$_3$ (7.8 mg/20.9 mM, 14.8 mg/ 39.7 mM, 19.6 mg/ 52.6 mM, 37.8 mg/ 102 mM, and 42.4 mg/ 114 mM, respectively) inside a sealed Teflon capped J-Young NMR tube. Each catalytic sample was immediately frozen after preparation in a -78 °C bath to prevent background reactivity. Each sample was thawed prior to injection into a 500 MHz NMR spectrometer with a probe temperature calibrated to 338 K. Upon injection into the spectrometer, spectra were acquired every 20 seconds (d1 = 5 s, d7 = 20 s, ns = 1, TD = 90). Initial rates were calculated by the decay of **1a** over time as determined by integration of the acyl-CH$_3$ resonance of **1a** versus internal standard. The results are summarized in Table 3.22 below and in Figure 3.12.

Table 3.22. Data for the hydroarylation of **1a** (67 mM) with diphenylacetylene (67 mM) catalyzed by **Co-Li** (7 mM) with added P(C$_6$F$_5$)$_3$.
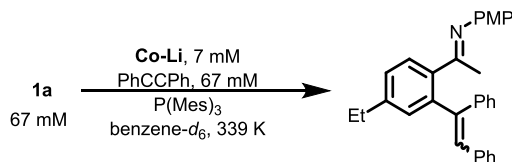
Added [P(Mes)$_3$] (mM)	$k_{initial}$ x 10^{-6} (M s^{-1}) [a]
20.9	4.8
39.7	2.7
52.6	2.0
102	0.8
114	0.7

[a] Initial rates ($k_{initial}$) were determined by ^{1}H NMR spectroscopy in benzene-d_6 with Si(SiMe$_3$)$_4$ as an internal standard and with the NMR spectrometer probe calibrated to 339 K.

Monitored Hydroarylation Catalysis by Time Resolved ^{31}P{^{1}H} NMR Spectroscopy. Inside an N$_2$ glovebox, a solution comprised of **1a** (18 mg, 100 mM, 0.07 mmol, 1 equiv), diphenylacetylene (13 mg, 100 mM, 0.07 mmol, 1 equiv), **Co-Li** (8 mg, 10 mM, 7 μmol, 10 mol%), and benzene-d_6 (0.7 mL) was prepared inside a sealed Teflon capped J-Young NMR tube. The sample was injected into a 600 MHz NMR spectrometer equipped with a liquid N$_2$ cryoprobe broadband channel and the sample probe temperature was calibrated to 339 K. Upon injection into the spectrometer, spectra were acquired every 20 seconds as the average of 8 scans (d1 = 1 s, d20 = 20 s, ns = 8, TD = 90) and the spectra is depicted in Figure 3.13. Two new peaks were observed at 69.27 and 9.90 ppm and grew more intense over time. These peaks were assigned to a new Co-PPh$_3$ species and a phosphonium-ylide-like species, respectively.

Off-Cycle Olefin Isomerizations with Co-Li: Catalytic Methods and Kinetic Experiments

Isomerization of *cis*-Stilbene: Quantitative Conversion at Elevated Temperatures. Inside an N$_2$ glovebox, *cis*-stilbene (20 μL, 0.12 mmol, 1 equiv) and **Co-Li** (7 mg, 7 μmol, 6 mol%) in benzene-d_6 (0.7 mL) were added to a sealed Teflon capped J-Young NMR tube. In a separate control experiment, *cis*-stilbene (20 μL) was dissolved benzene-d_6 (0.7 mL). The catalytic reaction mixture and the control were then heated to 65 °C outside the glovebox for 1 d in the dark after which a ^{1}H NMR spectrum was acquired. Quantitative conversion to *trans*-stilbene was observed after 1 d when **Co-Li** was added. No conversion occurred in the control experiment (Figure 3.16).

Selected ^{1}H NMR resonances for *cis*-stilbene:[99]

^{1}H NMR (benzene-d_6, 500.1 MHz): δ 6.47 (s, vinyl-H).

Selected ^{1}H NMR resonances for *trans*-stilbene:[99]

^{1}H NMR (benzene-d_6, 500.1 MHz): δ 7.02 (s, vinyl-H).

Isomerization of *cis*-β-methylstyrene: Quantitative Conversion at Elevated Temperatures. Inside an N$_2$ glovebox, *cis*-β-methystyrene (20 μL, 0.12 mmol, 1 equiv) and **Co-Li** (7 mg, 7 μmol, 6 mol%) in benzene-d_6 (0.7 mL) were added to a sealed Teflon capped J-Young NMR tube. In a separate control experiment, *cis*-stilbene (20 μL) was dissolved benzene-d_6 (0.7 mL). The catalytic reaction mixture and the control were then heated to 65 °C outside the glovebox for 1 d in the dark after which a ^{1}H NMR spectrum was acquired. Quantitative conversion to *trans*-β-methylstyrene was observed after 1 d when **Co-Li** was added. No conversion occurred in the control experiment (Figure 3.17).

Selected ^{1}H NMR resonances for *cis*-β-methylstyrene:[100]

^{1}H NMR (benzene-d_6, 500.1 MHz): δ 6.52 (dq, J = 11.5, 1.7 Hz, Ph**HC**=CHMe), 5.74 (dq, J = 15.7, 7.1 Hz, PhHC=C**H**Me), 1.81 (dd, J = 6.8, 1.8 Hz, **CH₃**).

Selected ^{1}H NMR resonances for *trans*-β-methylstyrene:[99]

^{1}H NMR (benzene-d_6, 500.1 MHz): δ 6.40 (dq, J = 15.4, 1.7 Hz, Ph**HC**=CHMe), 6.13 (dq, J = 15.3, 7.1 Hz, PhHC=C**H**Me) 1.74 (dd, J = 7.0, 1.7 Hz, **CH₃**).

Attempted Isomerization of *trans*-Stilbene. Inside an N$_2$ glovebox, *trans*-stilbene (20 mg, 0.11 mmol, 1 equiv) and **Co-Li** (3 mg, 3 μmol, 3 mol%) in benzene-d_6 (0.7 mL) were added to a sealed Teflon capped J-Young NMR tube. Outside the glovebox, the reaction mixture was heated to 65 °C in the dark for 1 d. A ^{1}H NMR spectrum was acquired (Figure 3.18) and no observable change from the initial spectrum occurred, which indicated that *trans*- to *cis*- isomerization does not occur with **Co-Li**.

Attempted Isomerization of *cis*-2-Butene with Co-Li. Inside an N$_2$ glovebox, **Co-Li** (7 mg, 7 μmol) was dissolved in benzene-d_6 (0.7 mL) and the solution was added to a sealed Teflon capped J-Young NMR tube. In a separate control experiment, benzene-d_6 (0.7 mL) was added to a Teflon capped J-Young NMR tube. Each sample was degassed on a Schlenk line by 2 freeze/pump/thaw cycles and then *cis*-2-butene (1 atm) was added. The catalytic reaction mixture and the control were then heated to 65 °C for 1 d in the dark after which a ^{1}H NMR spectrum was acquired. No conversion occurred in the presence of **Co-Li** or in the control experiment (Figure 3.19).

Selected ^{1}H NMR resonances for *cis*-2-butene:[99]

^{1}H NMR (benzene-d_6, 500.1 MHz): δ 5.48 (m, vinyl C–H), 1.51 (d, J = 5.0 Hz, CH$_3$).

Selected ^{1}H NMR resonances for *trans*-2-butene:[99]

^{1}H NMR (benzene-d_6, 500.1 MHz): δ 5.38 (m, vinyl C–H), 1.57 (d, J = 5.0 Hz, CH$_3$).

Isomerization of *cis*-2-Butene with Co-Li and Added 9,10-Dihydroanthracene. Inside an N$_2$ glovebox, **Co-Li** (7 mg, 7 μmol) and 9,10-dihydroanthracene (5 mg, 27 μmol) was dissolved in benzene-d_6 (0.7 mL) and the solution was added to a sealed Teflon capped J-Young NMR tube. The solution was degassed on a

Schlenk line by 2 freeze/pump/thaw cycles and then *cis*-2-butene (1 atm) was added. The catalytic reaction mixture was then heated to 65 °C for 10 h in the dark after which a ^{1}H NMR spectrum was acquired. Note that *cis*- to *trans*-isomerization occurs with a half-life of ca. 5 h as evidenced in Figure 3.20.

Selected ^{1}H NMR resonances for 9,10-dihydroanthracene:[101]

^{1}H NMR (500.1 MHz, benzene-d_6): δ 3.62 (s, **9,10-CH$_2$**).

Isomerization of *cis*-Stilbene: Kinetic Analysis. Inside an N$_2$ glovebox, a catalyst stock solution comprised of **Co-Li** (29 mg, 7 mM, 26 μmol) and benzene-d_6 (3.9 mL) with Si(SiMe$_3$)$_4$ as an internal standard was prepared. Five separate experiments were performed with 0.7 mL of the stock solution and varied [*cis*-stilbene]$_0$ (8μL/65 mM , 11 μL/89 mM, 22 μL/180 mM, 35 μL/277 mM, and 62 μL/494 mM, respectively) inside a sealed Teflon capped J-Young NMR tube. Each catalytic sample was immediately frozen after preparation in a -78 °C bath to prevent background reactivity. Each sample was thawed prior to injection into a 500 MHz NMR spectrometer with a probe temperature calibrated to 295 K. Upon injection into the spectrometer, spectra were acquired every 5 min (d1 = 5 s, d7 = 300 s, ns = 1, TD = 20). Initial rates were calculated by the decay of *cis*-stilbene over time as determined by integration of the vinyl C–H resonance versus internal standard. The results are summarized in Table 3.23 below and in the main text, Figure 3.21. Note that the isomerization is first order in [*cis*-stilbene]$_0$ with a k_{obs} = 3.1 x 10^{-6} s^{-1}.

Table 3.23. Kinetics data for the isomerization of *cis*-stilbene catalyzed by **Co-Li** (7 mM).
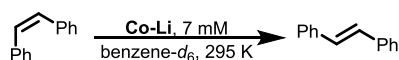
[*cis*-Stilbene]$_0$ (mM)	$k_{initial}$ x 10^{-7} (M s^{-1}) [a]
65	1.1
89	2.0
180	3.3
277	6.7
494	14.7

[a] Initial rates ($k_{initial}$) were determined by ^{1}H NMR spectroscopy in benzene-d_6 with Si(SiMe$_3$)$_4$ as an internal standard and with the NMR spectrometer probe calibrated to 295 K.

Isomerization of *cis*-β-Methylstyrene: Kinetic Analysis. Inside an N$_2$ glovebox, a catalyst stock solution comprised of **Co-Li** (29 mg, 7 mM, 26 μmol) and benzene-d_6 (3.9 mL) with Si(SiMe$_3$)$_4$ as an internal standard was prepared. Five separate experiments were performed with 0.7 mL of the stock solution and varied [*cis*-β-methylstyrene]$_0$ (6 μL/60 mM, 11 μL/118 mM, 14 μL/156 mM, 24 μL/261 mM, 45 μL/489 mM, respectively) inside a sealed Teflon capped J-Young NMR tube. Each catalytic sample was immediately frozen after preparation in a -78 °C bath to prevent background reactivity. Each sample was thawed prior to injection into a 500 MHz NMR spectrometer with a probe temperature calibrated to 295 K. Upon injection into the spectrometer, spectra were acquired every 5 min (d1 = 5 s, d7 = 300 s, ns = 1, TD

= 20). Initial rates were calculated by the decay of *cis*-β-methylstyrene over time as determined by integration of the terminal CH_3 resonance versus internal standard. The results are summarized in Table 3.24 below and in Figure 3.23. Note that the isomerization is inverse first order in [*cis*-β-methylstyrene]$_0$ with a $k_{obs} = 1.3$ x 10^{-7} M^2 s^{-1}.

Table 3.24. Kinetics data for the isomerization of *cis*-β-methylstyrene catalyzed by **Co-Li** (7 mM).
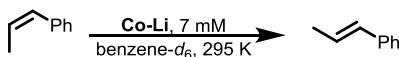
[*cis*-β-methylstyrene]$_0$ (mM)	1/[*cis*-β-methylstyrene]$_0$ (M^{-1})	$k_{initial}$ x 10^{-7} (M s^{-1}) [a]
60	16.7	19.6
118	8.4	10.5
156	6.4	4.5
261	3.8	1.9
489	2.0	2.0

[a] Initial rates ($k_{initial}$) were determined by ^1H NMR spectroscopy in benzene-d_6 with $Si(SiMe_3)_4$ as an internal standard and with the NMR spectrometer probe calibrated to 295 K.

Rate Law Derivation: Assumptions and Model

The following simplified Michaelis-Menten substrate model was used in the Mathematica model of substrate binding to the catalyst center. Intermediates C, AC, ACA, and ACI correspond to substrate-free complex, alkyne-catalyst complex, bis(alkyne)-catalyst complex, and alkyne-imine-catalyst complex, respectively. [Cat]$_0$ corresponds to the initial concentration of added precatalyst:
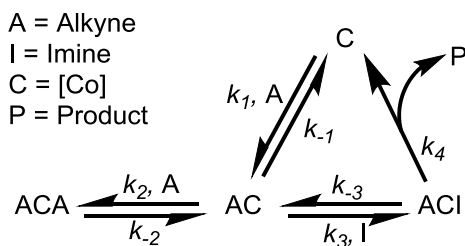
(1) It was assumed that alkyne binds prior to the imine as a simplification.

(2) All ligand coordination steps were assumed to be reversible with an irreversible catalytic step with a catalytic rate constant, k_4.

Given the graphical depiction of the truncated catalytic cycle above, a set of linear equations were derived (eqs 3.19-3.22) following the King-Altman method typically employed with multiple substrate enzymatic systems. See references for detailed methodology in modeling complex enzymatic rate laws.[66,102,103]

Simplified rate expression:

$$(\textbf{3.19})\ d[P]/dt = v = k_4[\text{ACI}]$$

Steady state approximation:

$$(\textbf{3.20})\ d[\text{ACI}]/dt = d[\text{ACA}]/dt = d[\text{AC}]/dt = d[C]/dt = 0$$

Conservation of catalyst:

$$(\textbf{3.21})[C] + [\text{AC}] + [\text{ACA}] + [\text{ACI}] = [\text{Cat}]_0$$

$$(\textbf{3.22a})\ d[C]/dt = k_{-1}[\text{AC}] + k_4[\text{ACI}] - k_1[A][C]$$

$$(\textbf{3.22b})\ d[\text{AC}]/dt = k_1[A][C] + k_{-2}[\text{ACA}] + k_{-3}[\text{ACI}] - [\text{AC}](k_2[A] + k_{-1} + k_3[\text{I}])$$

$$(\textbf{3.22c})\ d[\text{ACA}]/dt = k_2[\text{AC}][A] - k_{-2}[\text{ACA}]$$

$$(\textbf{3.22d})\ d[\text{ACI}]/dt = k_3[I][\text{AC}] - [\text{ACI}](k_4 + k_{-3})$$

The linear equations above were depicted in matrix form to yield eq **3.23**:

$$(\textbf{3.23})\begin{pmatrix} -k_1[A] & k_{-1} & 0 & k_{-1} \\ k_1[A] & -k_{-1} - k_2[A] - k_3[\text{I}] & k_{-2} & k_{-3} \\ 0 & k_2[A] & -k_{-2} & 0 \\ 0 & k_3[\text{I}] & 0 & -k_{-3} - k_4 \end{pmatrix}\begin{pmatrix} [C] \\ [\text{AC}] \\ [\text{ACA}] \\ [\text{ACI}] \end{pmatrix} = \begin{pmatrix} 0 \\ 0 \\ 0 \\ 0 \end{pmatrix}$$

The determinant of the matrix (eq 3.24) above is zero, which indicates that the four linear equations are not mutually independent.

$$(\textbf{3.24})\begin{vmatrix} -k_1[A] & k_{-1} & 0 & k_{-1} \\ k_1[A] & -k_{-1} - k_2[A] - k_3[\text{I}] & k_{-2} & k_{-3} \\ 0 & k_2[A] & -k_{-2} & 0 \\ 0 & k_3[\text{I}] & 0 & -k_{-3} - k_4 \end{vmatrix} = 0$$

Adding the additional constraint from eq 3.21, a full system of equations can be given as the following 5 x 5 square weighted matrix. The 5th column represents the "right side" of the linear equation.

$$(3.25) \begin{pmatrix} -k_1[A] & k_{-1} & 0 & k_4 & 0 \\ k_1[A] & -k_{-1} - k_2[A] - k_3[I] & k_{-2} & k_{-3} & 0 \\ 0 & k_2[A] & -k_{-2} & 0 & 0 \\ 0 & k_3[I] & 0 & -k_{-3} - k_4 & 0 \\ 1 & 1 & 1 & 1 & [Cat]_0 \end{pmatrix}$$

By applying the method of row-reduction, the following reduced matrix was generated (eq 3.26):

$$(3.26) \begin{pmatrix} 1 & 0 & 0 & 0 & \dfrac{[Cat]_0 k_{-2}([I]k_3 k_4 + k_{-1}(k_{-3} + k_4))}{[I]k_{-2}k_3 k_4 + [A]^2 k_1 k_2(k_{-3} + k_4) + k_{-1}k_{-2}(k_{-3} + k_4) + [A]k_1 k_{-2}([I]k_3 + k_{-3} + k_4)} \\ 0 & 1 & 0 & 0 & \dfrac{[A][Cat]_0 k_1 k_{-2}(k_{-3} + k_4)}{[I]k_{-2}k_3 k_4 + [A]^2 k_1 k_2(k_{-3} + k_4) + k_{-1}k_{-2}(k_{-3} + k_4) + [A]k_1 k_{-2}([I]k_3 + k_{-3} + k_4)} \\ 0 & 0 & 1 & 0 & \dfrac{[A]^2[Cat]_0 k_1 k_2(k_{-3} + k_4)}{[I]k_{-2}k_3 k_4 + [A]^2 k_1 k_2(k_{-3} + k_4) + k_{-1}k_{-2}(k_{-3} + k_4) + [A]k_1 k_{-2}([I]k_3 + k_{-3} + k_4)} \\ 0 & 0 & 0 & 1 & \dfrac{[A][Cat]_0[I]k_1 k_{-2}k_3}{[I]k_{-2}k_3 k_4 + [A]^2 k_1 k_2(k_{-3} + k_4) + k_{-1}k_{-2}(k_{-3} + k_4) + [A]k_1 k_{-2}([I]k_3 + k_{-3} + k_4)} \\ 0 & 0 & 0 & 0 & 0 \end{pmatrix}$$

The right most column of the matrix in eq 3.26 corresponds to the concentrations of each of the intermediates (C, AC, ACA, ACI, respectively, with a null fifth row) during the course of the reaction. Given the definition of the observed rate in eq 3.19, the value of [ACI] can be substituted from the above matrix to arrive at the full rate expression for product formation.

$$(3.27)\ v = k_4 \frac{[A][Cat]_0[I]k_1 k_{-2}k_3}{[I]k_{-2}k_3 k_4 + [A]^2 k_1 k_2(k_{-3} + k_4) + k_{-1}k_{-2}(k_{-3} + k_4) + [A]k_1 k_{-2}([I]k_3 + k_{-3} + k_4)}$$

The rate (v) can be described in Michaelis-Menten form to give eq 3.28:

$$(3.28)\ \frac{1}{v} = \frac{[I]k_{-2}k_3 k_4 + [A]^2 k_1 k_2(k_{-3} + k_4) + k_{-1}k_{-2}(k_{-3} + k_4) + [A]k_1 k_{-2}([I]k_3 + k_{-3} + k_4)}{[A][Cat]_0[I]k_1 k_{-2}k_3 k_4}$$

Simplification of eq 3.28 gives eq 3.29:

$$(3.29)\ \frac{1}{v} = \frac{[A]k_1 + k_4}{k_1 k_4 [A][Cat]_0} + \frac{k_1 k_{-2}(k_{-3} + k_4) + [A]k_1 k_2(k_{-3} + k_4) + \frac{k_{-1}k_{-2}(k_{-3} + k_4)}{[A]}}{[Cat]_0 [I] k_1 k_{-2} k_3 k_4}$$

Since the equilibrating rate constants cannot be independently measured, they are redefined into three "binding" terms: K'_I (imine disassociation), K'_A (on cycle alkyne disassociation), and K''_A (off-cycle alkyne association):

$$(3.30)\ \frac{1}{v} = \frac{[A]k_1 + k_4}{k_1 k_4 [A][Cat]_0} + \frac{K'_I + [A]K''_A + \frac{K'_A}{[A]}}{[Cat]_0 [I] k_4}$$

Several key features can be extracted from eq 3.30. First, the "y" intercept is independent of [I], and essentially 0th order in [alkyne] except at exceedingly low concentrations. The maximum rate velocity, v_{max}, is given in eq 3.31:

$$(3.31)\ \frac{1}{v} = \frac{1}{v_{max}} = \frac{[A]k_1 + k_4}{k_1 k_4 [A][Cat]_0} \sim \frac{1}{k_4 [Cat]_0}\ \left(when\ \frac{1}{[I]} = 0\ and\ [A]k_1 \gg k_4\right)$$

From eq 3.31 we can derive a final, simplified rate expression:

$$(3.32)\ \frac{1}{v} = \frac{1}{v_{max}} + \frac{1}{v_{max}[I]}\left(K'_I + [A]K''_A + \frac{K'_A}{[A]}\right)$$

From the Michaelis-Menten analysis (Figure 3.11), the v_{max} was calculated to be (1.2 ± 0.2) x 10^{-5} M s^{-1}. From this, the catalytic rate constant (k_4) can be determined (eqs 3.33 and 3.34):

$(3.33)\ v_{max} \sim k_4 [Cat]_0 = (1.2 \pm 0.2)$ x 10^{-5} M s^{-1} ($[Cat]_0 = 7.1$ mM under the standard catalyst concentration)

$(3.34)\ k_4 = (1.5 \pm 0.2)$ x 10^{-3} s^{-1}

The derivative of equation 3.32 with respect to [imine], has three terms: 1st order in [alkyne], 0th order in [alkyne], and inverse 1st order in [alkyne]. This hyperbolic-like function matches the data presented in the secondary plot of Figure 3.11. This indicates that at low [alkyne], the observed rate is hindered by lack of alkyne substrate. At high [alkyne], the rate is inhibited by competitive over ligation with alkyne to generate a bis(alkyne) complex. Given the simplifications and assumptions above, the specific values of the hyperbolic fit do not correspond to specific disassociation constants.

References

1. Wang, S.; Chen, S. Y.; Yu, X. Q. *Chem. Commun.* **2017**, *53*, 3165-3180.

2. Moselage, M.; Li, J.; Ackermann, L. *ACS Catal.* **2016**, *6*, 498-525.

3. Gao, K.; Yoshikai, N. *Acc. Chem. Res.* **2014**, *47*, 1208-1219.

4. Vastine, B. A.; Hall, M. B. *J. Am. Chem. Soc.* **2007**, *129*, 12068-12069.

5. Pototschnig, G.; Maulide, N.; Schnürch, M. *Chem. Eur. J.* **2017**, *23*, 9206-9232.

6. Balcells, D.; Clot, E.; Eisenstein, O. *Chem. Rev.* **2010**, *110*, 749-823.

7. Lersch, M.; Tilset, M. *Chem. Rev.* **2005**, *105*, 2471-2526.

8. Colby, D. A.; Bergman, R. G.; Ellman, J. A. *Chem. Rev.* **2010**, *110*, 624-655.

9. Suslick, B. A.; Tilley, T. D. In *Catalytic Hydroarylation of Carbon-Carbon Multiple Bonds*; Ackermann, L., Gunnoe, T. B., Habgood, L. G., Eds.; Willey-VCH: Weinheim, 2017, p 107-174.

10. Evano, G.; Theunissen, C. *Angew Chem Int Ed* **2019**, *58*, 7558-7598.

11. Murai, S.; Kakiuchi, F.; Sekine, S.; Tanaka, Y.; Kamatani, A.; Sonoda, M.; Chatani, N. *Nature* **1993**, *366*, 529.

12. Kakiuchi, F.; Murai, S. *Acc. Chem. Res.* **2002**, *35*, 826-834.

13. Thalji, R. K.; Ahrendt, K. A.; Bergman, R. G.; Ellman, J. A. *J. Am. Chem. Soc.* **2001**, *123*, 9692-9693.

14. Ryu, J.; Cho, S. H.; Chang, S. *Angew. Chem. Int. Ed.* **2012**, *51*, 3677-3681.

15. Lim, S.-G.; Ahn, J.-A.; Jun, C.-H. *Org. Lett.* **2004**, *6*, 4687-4690.

16. Jun, C. H.; Hong, J. B.; Kim, Y. H.; Chung, K. Y. *Angew. Chem. Int. Ed.* **2000**, *39*, 3440-3442.

17. Webster-Gardiner, M. S.; Fu, R.; Fortman, G. C.; Nielsen, R. J.; Gunnoe, T. B.; Goddard III, W. A. *Catalysis Science & Technology* **2015**, *5*, 96-100.

18. Yamaguchi, T.; Natsui, S.; Shibata, K.; Yamazaki, K.; Rej, S.; Ano, Y.; Chatani, N. *Chem. Eur. J.* **2019**, *25*, 6915-6919.

19. Sevov, C. S.; Hartwig, J. F. *J. Am. Chem. Soc.* **2013**, *135*, 2116-2119.

20. Ebe, Y.; Nishimura, T. *J. Am. Chem. Soc.* **2015**, *137*, 5899-5902.

21. Crisenza, G. E. M.; McCreanor, N. G.; Bower, J. F. *J. Am. Chem. Soc.* **2014**, *136*, 10258-10261.

22. Podhajsky, S. M.; Iwai, Y.; Cook-Sneathen, A.; Sigman, M. S. *Tetrahedron* **2011**, *67*, 4435-4441.

23. Suslick, B. A.; Liberman-Martin, A. L.; Wambach, T. C.; Tilley, T. D. *ACS Catal.* **2017**, *7*, 4313-4322.

24. McKeown, B. A.; Gonzalez, H. E.; Friedfeld, M. R.; Gunnoe, T. B.; Cundari, T. R.; Sabat, M. *J. Am. Chem. Soc.* **2011**, *133*, 19131-19152.

25. Luedtke, A. T.; Goldberg, K. I. *Angew. Chem. Int. Ed.* **2008**, *47*, 7694-7696.

26. Vaughan, B. A.; Khani, S. K.; Gary, J. B.; Kammert, J. D.; Webster-Gardiner, M. S.; McKeown, B. A.; Davis, R. J.; Cundari, T. R.; Gunnoe, T. B. *J. Am. Chem. Soc.* **2017**, *139*, 1485-1498.

27. Chirik, P.; Morris, R. *Acc. Chem. Res.* **2015**, *48*, 2495-2495.

28. Kimura, N.; Kochi, T.; Kakiuchi, F. *J. Am. Chem. Soc.* **2017**, *139*, 14849-14852.

29. Lee, P.-S.; Fujita, T.; Yoshikai, N. *J. Am. Chem. Soc.* **2011**, *133*, 17283-17295.

30. Bera, S.; Hu, X. *Angew. Chem. Int. Ed.*, *0*.

31. Barber, E. R.; Hynds, H. M.; Stephens, C. P.; Lemons, H. E.; Fredrickson, E. T.; Wilger, D. J. *The Journal of Organic Chemistry* **2019**.

32. Bair, J. S.; Schramm, Y.; Sergeev, A. G.; Clot, E.; Eisenstein, O.; Hartwig, J. F. *J. Am. Chem. Soc.* **2014**, *136*, 13098-13101.

33. Guihaumé, J.; Halbert, S.; Eisenstein, O.; Perutz, R. N. *Organometallics* **2012**, *31*, 1300-1314.

34. Elsby, M. R.; Johnson, S. A. *J. Am. Chem. Soc.* **2017**, *139*, 9401-9407.

35. Hartwig, J. F. *Organotransition Metal Chemistry: From Bonding to Catalysis*; University Science Books: Mill Valley, CA, 2010.

36. Sakata, K.; Eda, M.; Kitaoka, Y.; Yoshino, T.; Matsunaga, S. *J. Org. Chem.* **2017**, *82*, 7379-7387.

37. Ikemoto, H.; Yoshino, T.; Sakata, K.; Matsunaga, S.; Kanai, M. *J. Am. Chem. Soc.* **2014**, *136*, 5424-5431.

38. Hummel, J. R.; Ellman, J. A. *J. Am. Chem. Soc.* **2015**, *137*, 490-498.

39. Gao, K.; Lee, P.-S.; Fujita, T.; Yoshikai, N. *J. Am. Chem. Soc.* **2010**, *132*, 12249-12251.

40. Gao, K.; Yoshikai, N. *J. Am. Chem. Soc.* **2011**, *133*, 400-402.

41. Lee, P. S.; Yoshikai, N. *Angew. Chem. Int. Ed.* **2013**, *52*, 1240-1244.

42. Xu, W.; Yoshikai, N. *Angew. Chem. Int. Ed.* **2016**, *55*, 12731-12735.

43. Ding, Z.; Yoshikai, N. *Angew. Chem. Int. Ed.* **2012**, *51*, 4698-4701.

44. Xu, W.; Pek, J. H.; Yoshikai, N. *Adv. Synth. Catal.* **2016**, *358*, 2564-2568.

45. Gao, K.; Yoshikai, N. *Angew. Chem. Int. Ed.* **2011**, *50*, 6888-6892.

46. Gandeepan, P.; Muller, T.; Zell, D.; Cera, G.; Warratz, S.; Ackermann, L. *Chem Rev* **2019**, *119*, 2192-2452.

47. Sanjosé-Orduna, J.; Gallego, D.; Garcia-Roca, A.; Martin, E.; Benet-Buchholz, J.; Pérez-Temprano, M. H. *Angew. Chem. Int. Ed.* **2017**, *56*, 12137-12141.

48. Sanjosé-Orduna, J.; Benet-Buchholz, J.; Pérez-Temprano, M. H. *Inorg. Chem.* **2019**.

49. Fallon, B. J.; Derat, E.; Amatore, M.; Aubert, C.; Chemla, F.; Ferreira, F.; Perez-Luna, A.; Petit, M. *J. Am. Chem. Soc.* **2015**, *137*, 2448-2451.

50. Wakatsuki, Y.; Yamazaki, H.; Lindner, E.; Bosamle, A. In *Inorg. Synth.*; H. D., K., Ed.; Willey: 1989.

51. Sacco, A.; Rossi, M. *Chem. Commun.* **1967**, 316-316.

52. Yamamoto, A.; Kitazume, S.; Pu, L. S.; Ikeda, S. *J. Am. Chem. Soc.* **1971**, *93*, 371-380.

53. Halbritter, G.; Knoch, F.; Wolski, A.; Kisch, H. *Angew. Chem. Int. Ed.* **1994**, *33*, 1603-1605.

54. Morris, R. H. *J. Am. Chem. Soc.* **2014**, *136*, 1948-1959.

55. Morris, R. H. *Chem. Rev.* **2016**, *116*, 8588-8654.

56. Kosar, W. In *Handbook of Grignard Reagents*; Silverman, G. S., Rakita, P. E., Eds.; Marcel Dekker, Inc.: New York, New York, 1996, p 441-454.

57. Yamamoto, A.; Miura, Y.; Ito, T.; Chen, H. L.; Iri, K.; Ozawa, F.; Miki, K.; Sei, T.; Tanaka, N.; Kasai, N. *Organometallics* **1983**, *2*, 1429-1436.

58. Reich, H. J. *The Journal of Organic Chemistry* **2012**, *77*, 5471-5491.

59. Reich, H. J.; Kulicke, K. J. *J. Am. Chem. Soc.* **1996**, *118*, 273-274.

60. Reich, H. J.; Sikorski, W. H.; Sanders, A. W.; Jones, A. C.; Plessel, K. N. *The Journal of Organic Chemistry* **2009**, *74*, 719-729.

61. Apps, S. L.; Miller, P. W.; Long, N. J. *Chem. Commun.* **2019**, *55*, 6579-6582.

62. Gao, Y.; Li, G.; Deng, L. *J. Am. Chem. Soc.* **2018**, *140*, 2239-2250.

63. Kreyenschmidt, F.; Meurer, S. E.; Koszinowski, K. *Chem. Eur. J.* **2019**, *25*, 5912-5921.

64. Barton, J. S. *J. Chem. Educ.* **2011**, *88*, 1336-1339.

65. Charlotte Pratt, K. C. In *Essential Biochemistry*; 3rd ed.; John Wiley and Sons, Inc: Hoboken, NJ, 2014, p 188-220.

66. G. B. Marin, G. S. Y. *Kinetics of Chemical Reactions*; Wiley-VCH: Weinheim, Germany, 2011.

67. Albright, T. A.; Gordon, M. D.; Freeman, W. J.; Schweizer, E. E. *J. Am. Chem. Soc.* **1976**, *98*, 6249-6252.

68. Chin, C. S.; Park, Y.; Kim, J.; Lee, B. *J. Chem. Soc., Chem. Commun.* **1995**, 1495-1496.

69. Huggins, J. M.; Bergman, R. G. *J. Am. Chem. Soc.* **1981**, *103*, 3002-3011.

70. Yang, K.; Bott, S. G.; Richmond, M. G. *Organometallics* **1994**, *13*, 3767-3769.

71. A. Fairhurst, S.; L. Hughes, D.; Marjani, K.; L. Richards, R. *Journal of the Chemical Society, Dalton Transactions* **1998**, 1899-1904.

72. Hoffman, D. M.; Huffman, J. C.; Lappas, D.; Wierda, D. A. *Organometallics* **1993**, *12*, 4312-4320.

73. Allen, A.; Lin, W. *Organometallics* **1999**, *18*, 2922-2925.

74. Takats, J.; Washington, J.; Santarsiero, B. D. *Organometallics* **1994**, *13*, 1078-1080.

75. Simmons, E. M.; Hartwig, J. F. *Angew. Chem. Int. Ed.* **2012**, *51*, 3066-3072.

76. Wang, L.; Carrow, B. P. *ACS Catal.* **2019**, *9*, 6821-6836.

77. Lam, W. H.; Jia, G.; Lin, Z.; Lau, C. P.; Eisenstein, O. *Chem. Eur. J.* **2003**, *9*, 2775-2782.

78. Lapointe, D.; Fagnou, K. *Chem. Lett.* **2010**, *39*, 1118-1126.

79. Yamazaki, K.; Obata, A.; Sasagawa, A.; Ano, Y.; Chatani, N. *Organometallics* **2018**, *38*, 248-255.

80. Ma, P.; Chen, H. *ACS Catal.* **2019**, *9*, 1962-1972.

81. Schipper, D. J.; Hutchinson, M.; Fagnou, K. *J. Am. Chem. Soc.* **2010**, *132*, 6910-6911.

82. Schmidt, A.; Nödling, A. R.; Hilt, G. *Angew. Chem. Int. Ed.* **2015**, *54*, 801-804.

83. Spees, W. M.; Song, S.-K.; Garbow, J. R.; Neil, J. J.; Ackerman, J. J. H. *Magnetic resonance in medicine* **2012**, *68*, 319-324.

84. Shu, A. Y. L.; Chen, W.; Heys, J. R. *J. Organomet. Chem.* **1996**, *524*, 87-93.

85. Lei, C.; Peng, L.; Ding, K. *Adv. Synth. Catal.* **2018**, *360*, 2952-2958.

86. Yoshikai, N.; Matsumoto, A.; Norinder, J.; Nakamura, E. *Angew. Chem. Int. Ed.* **2009**, *48*, 2925-2928.

87. Liu, W.; Zell, D.; John, M.; Ackermann, L. *Angew. Chem. Int. Ed.* **2015**, *54*, 4092-4096.

88. Pilgrim, B. S.; Gatland, A. E.; McTernan, C. T.; Procopiou, P. A.; Donohoe, T. J. *Org. Lett.* **2013**, *15*, 6190-6193.

89. Park, C. P.; Nagle, A.; Yoon, C. H.; Chen, C.; Jung, K. W. *The Journal of Organic Chemistry* **2009**, *74*, 6231-6236.

90. Tai, C.-C.; Yu, M.-S.; Chen, Y.-L.; Chuang, W.-H.; Lin, T.-H.; Yap, G. P. A.; Ong, T.-G. *Chem. Commun.* **2014**, *50*, 4344-4346.

91. Bauer, H.; Alonso, M.; Fischer, C.; Rösch, B.; Elsen, H.; Harder, S. *Angew. Chem. Int. Ed.* **2018**, *57*, 15177-15182.

92. Fulmer, G. R.; Miller, A. J. M.; Sherden, N. H.; Gottlieb, H. E.; Nudelman, A.; Stoltz, B. M.; Bercaw, J. E.; Goldberg, K. I. *Organometallics* **2010**, *29*, 2176-2179.

93. Elschenbroich, C.; Schneider, J.; Wünsch, M.; Pierre, J.-L.; Baret, P.; Chautemps, P. *Chem. Ber.* **1988**, *121*, 177-183.

94. Calderazzo, F.; Ferri, I.; Pampaloni, G.; Troyanov, S. *J. Organomet. Chem.* **1996**, *518*, 189-196.

95. Luechinger, M.; Pirngruber, G. D.; Prins, R. *The Journal of Physical Chemistry B* **2004**, *108*, 10903-10910.

96. Sadykov, R. A.; Shishlov, N. M. *J. Organomet. Chem.* **1989**, *369*, 1-7.

97. Xu, C.; Du, W.; Zeng, Y.; Dai, B.; Guo, H. *Org. Lett.* **2014**, *16*, 948-951.

98. Hansch, C.; Leo, A.; Taft, R. W. *Chem. Rev.* **1991**, *91*, 165-195.

99. Bailey, G. A.; Foscato, M.; Higman, C. S.; Day, C. S.; Jensen, V. R.; Fogg, D. E. *J. Am. Chem. Soc.* **2018**, *140*, 6931-6944.

100. Hall, J. W.; Unson, D. M. L.; Brunel, P.; Collins, L. R.; Cybulski, M. K.; Mahon, M. F.; Whittlesey, M. K. *Organometallics* **2018**, *37*, 3102-3110.

101. Nied, D.; Köppe, R.; Klopper, W.; Schnöckel, H.; Breher, F. *J. Am. Chem. Soc.* **2010**, *132*, 10264-10265.

102. Halász, Á. M.; Lai, H.; Pryor, M. M.; Radhakrishnan, K.; Edwards, J. S. *IEEE/ACM Transactions on Computational Biology and Bioinformatics* **2013**, *10*, 957-969.

103. Lloyd Wolfinbarger, J. In *Enzyme Regulation in Metabolic Pathways*; John Wiley & Sons, Inc.: 2017, p 117-139.

Chapter Four

Olefin Hydroarylations Catalyzed by

a Single-Component Cobalt(-I) Complex

Recent developments in metal-mediated C–H bond activation chemistry have enabled new catalytic transformations to generate value added products.[1-4] Such late-stage C–H functionalizations present attractive alternatives to common molecular elaboration methods such as cross-coupling, which requires sacrificial and often toxic reagents. In particular, olefin and alkyne hydroarylations have provided atom economical routes to form C–C bonds.[5-7] The Murai group[7,8] described the reactivity of the first hydroarylation precatalyst, $RuH_2(CO)(PPh_3)_3$. Subsequent developments focused on heavy, late-transition metal catalysts (*i.e.,* Rh,[9-12] Ir,[13-17] Pd,[18-20] and Pt[21-25]), and illustrated the synthetic value of hydroarylation as a convenient transformation for C–H bond diversification. Given the low abundance and high cost of late-transition metals,[26] the discovery of highly active first-row analogues is paramount for environmentally benign, industrial-scale applications.

In this context, cobalt catalysts have emerged as a versatile platform for *ortho*-directed C–H elaborations (eq 4.1).[4,27-39] Current Co catalyzed *ortho*-hydroarylation methods involve *in situ* catalyst generation, whereby CoX_2 salts are treated with an excess of a Grignard reagent (*e.g.,* NpMgBr, Me_3SiCH_2MgBr, CyMgCl, etc.) in the presence of a triaryl phosphine ligand.[32-39] As a consequence, the nature of the active species and its mode of action are not well understood.
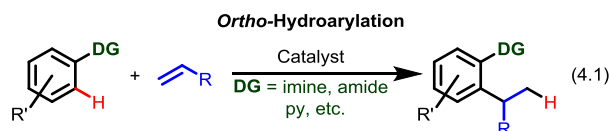
In our efforts to study this mechanism, we developed well defined Co(-I) complexes as single-component hydroarylation catalysts (see Chapter Three). The precatalyst, $[(PPh_3)_3Co(N_2)]Li(THF)_3$ (**Co-Li**), was conveniently prepared by a three step sequence (eq 4.2) starting from $CoCl_2(H_2O)_6$. Phosphine ligation and reduction with $NaBH_4$ affords $(PPh_3)_3CoCl$ in high yields (70%),[40] and treatment of this Co(I) species with CyMgCl under an atmosphere of N_2 afforded the Co-hydride species $(PPh_3)_3Co(N_2)H$.[41] Finally, deprotonation with ^nBuLi generates **Co-Li** as an acid-sensitive dark red-black solid.[42]
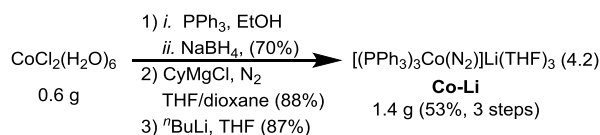
As an alkyne hydroarylation precatalyst, **Co-Li** is converted to an active species *via* displacement of PPh_3 and N_2 ligands by the alkyne and (*N*-aryl)aryl imine substrates. Subsequent CMD-like proton transfer and C–C reductive elimination affords the final hydroarylation products. This complex displays several advantages to systems that require *in situ* catalyst generation. The shelf-life of **Co-Li** in the solid-state under an N_2 atmosphere at ambient temperatures is at least three months without loss of catalytic activity. Freshly prepared ^1H NMR samples of **Co-Li** in benzene-d_6 remain identical over such periods. The solid catalyst can be prepared on a large scale with relatively inexpensive reagents. Perhaps the most important advantage of **Co-Li** is that nucleophilic activators (*i.e.,* RMgX) are no longer required. Many desirable functional groups (*e.g.,* organic carbonyls) react with such reagents and are therefore incompatible with catalysts derived by *in situ* preparation.[32-39] Herein, we describe the use of **Co-Li** as a catalyst for olefin hydroarylations.

The two general catalytic conditions employed in this study were based on initial optimizations described in the alkyne hydroarylation system (see Chapter Three). Catalytic reactions were performed under dilute substrate concentrations (0.1 M) in toluene with 10 mol% catalyst loading at either at 25 or 80

°C. On its own, efficient pre-coordination of acetophenone to the metal center does not occur; competent catalysis requires a better directing group, such as an *N*-coordinating imine. The imine substrates (**1A-1X**, Chart 4.1) were prepared by condensation of the corresponding substituted acetophenone with *para*-anisidine. The acid-sensitivity of **Co-Li** necessitated preparation of the imine substrate prior to catalysis. Treatment of an equimolar mixture of acetophenone and *para*-anisidine with catalytic quantities of **Co-Li** resulted in rapid N–H deprotonation to generate the inactive complex, $(PPh_3)_3Co(N_2)H$, as has been discussed previously in Chapter Three. The identity of the solvent does not affect the catalytic efficacy in this system as determined with alkyne-based substrates (see Chapter Three). The (*N*-aryl)aryl imine scope with styrene derivatives (**2a-2m**) or non-aromatic vinyl compounds (**2n-2r**) elucidated the generality of catalysis with **Co-Li**, as described in Scheme 4.1. A list of olefin coupling partners employed in this study is given in Chart 4.2.

Chart 4.1. Imine Coupling Partners 1A-1X.
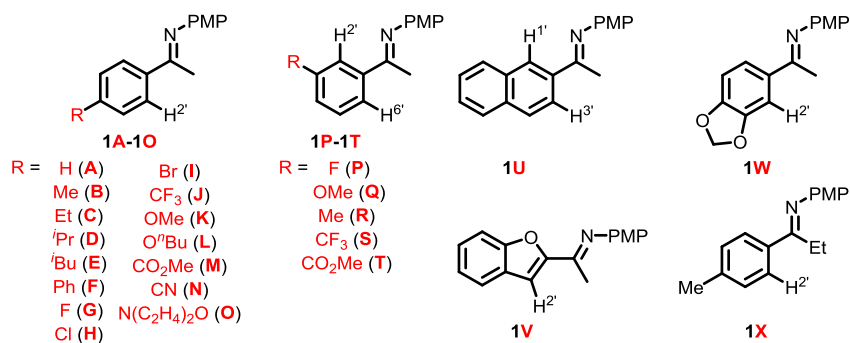
a The catalytically cleavable C–H bonds are labeled with 1', 2', 3', or 6'.

Chart 4.2. Olefin Coupling Partners 2a-2r.
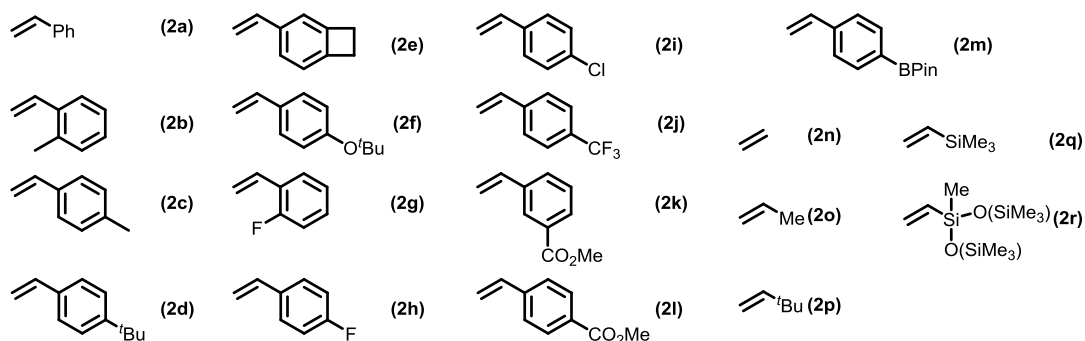
For clarity, branched products (**3**) and linear products (**4**) are encoded with two letters corresponding to the imine (first, upper-case) and olefin (second, lower-case) coupling partners. With **2a** as the olefin coupling partner, only branched products **3Aa-3Xa** were formed except in one case (*vide infra*). Generally, catalysis proceeded in higher yields at ambient temperatures.

Scheme 4.1. Olefin Hydroarylations with (*N*-Aryl)Aryl Imines Catalyzed by Co-Li.

1) **CoLi**, 10 mol%, toluene, 0.1 M, **25** or **80** °C, 20 h
2) H⁺, rt, 1 h

1A-1X + **2a-2r**   PMP = *p*-methoxyphenyl   **3** or **4**

Prod.	R	Yield 25 °C (%)	Yield 80 °C (%)
3Aa	H	83	53 (39)
3Ba	Me	62	46 (35)
3Ca	Et	81	39 (26)
3Da	*i*Pr	72 (55)	29
3Ea	*i*Bu	74 (54)	24
3Fa	Ph	77	83 (66)
3Ga	F	89	72 (55)
3Ha	Cl	40	16 (10)
3Ia	Br	0	0
3Ja	CF₃	50	92 (69)
3Ka	OMe	83	66 (56)
3La	O*ⁿ*Bu	51 (46)	16
3Ma	CO₂Me	quant	92 (77)
3Na	CN	0	12 (8)
3Oa	N(C₂H₄)₂O	19 (12)	7

Prod.	R	Yield 25 °C (%)	Yield 80 °C (%)
3Pa	F	89 [20]ᶜ (67)	38
3Qa	OMe	7	3

Prod.	R	Yield 25 °C (%)	Yield 80 °C (%)
3Ra	Me	30 (15)	10
3Sa	CF₃	36 (14)	33
3Ta	CO₂Me	97 (91)	65

Prod.	R'	Yield 25 °C (%)	Yield 80 °C (%)
3Ma	Ph	quant	92 (77)
3Mb	2-(Me)C₆H₄	33 (31)	-
3Mc	4-(Me)C₆H₄	quant (95)	-
3Md	4-(*t*Bu)C₆H₄	quant (93)	-
3Me	3,4-*cy*(CH₂)₂C₆H₃	quant (97)	-
3Mf	4-(O*t*Bu)C₆H₄	-	65 (46)
3Mg	2-(F)C₆H₄	15 (8)	-
3Mh	4-(F)C₆H₄	80 (67)	-
3Mi	4-(Cl)C₆H₄	21 (17)	-
3Mj	4-(CF₃)C₆H₄	quant (93)	-
3Mk	3-(CO₂Me)C₆H₄	quant (98)	-
3Ml	4-(CO₂Me)C₆H₄	quant (93)	-
3Mm	4-(BPin)C₆H₄	88 (74)	-

Prod.	R'	Yield 25 °C (%)	Yield 80 °C (%)
4Mn	Hᶠ	-	70 (54)
4Mo	Meᶠ	2	13 (8)
4Mp	*t*Bu	-	< 2
4Mq	SiMe₃	-	58 (55)
4Mr	SiMe(OSiMe₃)₂	-	39 (20)

3Ua: 53 [4.8]ᵈ (51) 7

3Va: 24 {9.8}ᵉ (21) 25

3Wa: quant (75) 15

3Xa: 82 (68) 58

ᵃ Reaction conditions: **1** (0.1 M, 1 equiv), **2** (0.1 M, 1 equiv), and **Co-Li** (10 mol%) in toluene at either **25** or **80** °C under N₂. ¹H NMR yields (%) are reported for **25** and **80** °C as the reaction temperatures and given in **blue** and **red**, respectively. ᵇ Isolated yields were determined from catalysis at **25** or **80** °C and are given in parenthesis. ᶜ The ratio of regio-isomers resulting from 2'- or 6'- C–H activation is given in square brackets. ᵈ The ratio of regio-isomers resulting from 1'- or 3'- C–H activation is given in square brackets. ᵉ The ratio of branched (**3Va**) to linear (**4Va**) products is given in curly brackets. ᶠ An excess of ethylene or propylene (1 atm) was added.

Study of (*N*-aryl)aryl imine substrates possessing various *para*-substituents (**1B-1O**) revealed several substitutional effects. Aliphatic or aromatic groups (**1B-1F**) distal to the *N*-coordinating imine did not affect the product yields (by ¹H NMR spectroscopy). The observed yields of products **3Ga-3Ia**, which were derived from substrates bearing halides, decreased as a function of the C–X bond strength (*i.e.*, F > Cl >> Br). Catalyst decomposition may occur with substrates bearing weak C–X bonds by LiX elimination. Indeed, there is precedent for rapid bond activations of this type with anionic metal fragments, as best illustrated by the reactivity of the Fp⁻ anion with alkyl halides.[43] Such competing and non-productive C–X activations irreversibly decompose the catalyst, thereby limiting the halide scope to F or Cl atoms. Both electron rich (**1B-1F**, **1K**, and **1L**) and electron poor (**1G, 1H, 1J,** and **1M**) substrates were tolerated in good to excellent yields. In particular, substrate **1M** illustrated the advantage of this single-component catalyst; **1M** quantitatively converted to the hydroarylation product **3Ma** despite its reactivity with Grignard reagents. Substrates **1M** and **1O** proved problematic due to competitive binding through the *N*-coordinating substituent.

Catalysis with unsymmetrical substrates (**1P-1W**) examined the regioselectivity of C–H cleavage (Chart 4.1 and Scheme 4.1). With **1P-1T**, two distinct C–H bonds *ortho-* to the imine directing group exist (*i.e.*, 2'- or 6'-C–H). The 3'-fluorine containing substrate, **1P**, afforded a mixture of products, which resulted from 2'- and 6'- C–H bond cleavage in a ratio of 20:1. In contrast, hydroarylations with substrates bearing 3'-Me (**1R**), 3'-CF$_3$ (**1S**), or 3'-CO$_2$Me (**1T**) afforded only one regioisomer that has been functionalized at the 6'-position. The worst regioselectivity occurred with naphthyl ethanimine **1U**, which possessed a slight preference for C–H activation at the 1'-site by a ratio of ca. 5:1.

Heterocyclic aryl imines were tolerated, albeit in poor yields. Interestingly, the benzofuran derived species, **1V**, was the only substrate which afforded a mixture of branched and linear products (**3Va** and **4Va**, respectively) in a ratio of 9.8:1.0. Pyridyl and thiophenyl derived substrates were unreactive, likely due to the formation of stable N–E (E = S or N) chelates with the Co metal center. In contrast to the conjugated heterocyclic substrate, **1W** bearing a 3',4'-(methylenedioxy)phenyl skeleton underwent quantitative hydroarylation to form **3Wa**.

Substitutional effects on the styrene coupling partner were explored with substrates **2a-2m** (see Chart 4.2 and Scheme 4.1); most of these olefins provided quantitative yields with the methyl ester containing imine **1M**. Non-quantitative yields occurred only with styrene derivatives bearing *ortho-* (**2b** and **2g**) or halide (**2h** and **2i**) substituents. These examples are likely limited by either sterically congested metal centers or competitive C–X bond activations, respectively.

Other, non-styrene derived olefins underwent catalytic hydroarylations, as evidenced by the formation of products **4Mn-4Mr**. Such olefins exclusively provided linear products, which is observed in other hydrofunctionalization chemistries.[31,33,38] Good yields were observed with ethylene (**2n**) and vinyl silanes **2q** and **2r**. Unfortunately, the olefin scope possesses several limitations. Proximal steric bulk prohibits efficient catalysis by inhibiting olefin coordination, as evidenced with *tert*-butyl ethylene (**2p**). Internal olefins do not undergo catalysis (*e.g., cis*-β-methyl styrene or *cis*-2-butene). Long chain olefins (*e.g.,* 1-octene) undergo rapid isomerization to form internal alkenes, thereby rendering the substrate inert. A comprehensive list of inactive substrates is given below in Chart 4.3.

Chart 4.3. Substrates Unable to Undergo Hydroarylation.
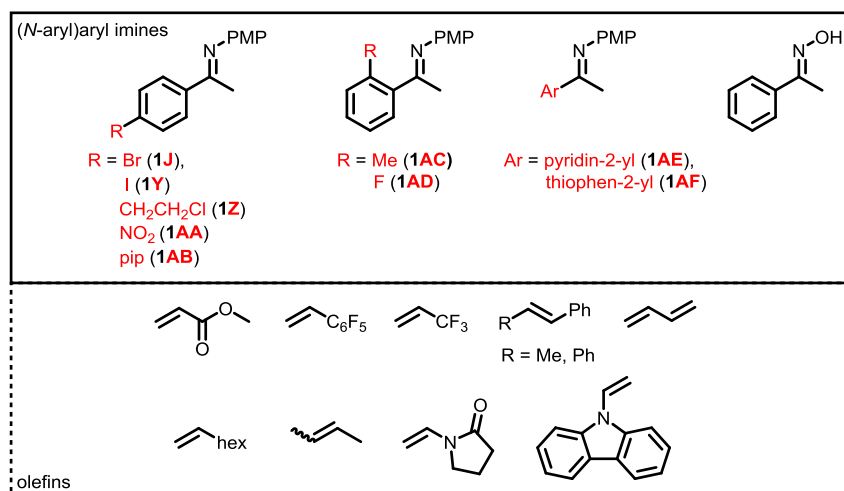
Several key features exist for the imine substrates above (Chart 4.3) that failed to undergo hydroarylation. As mentioned previously, weak C–X bonds (**1J**, **1Y**, and **1Z**) result in competitive C–X activation, which degrades the active catalyst into an unreactive species. Unsurprisingly, reactive NO_2 functionalities rapidly decompose **Co-Li** as evidenced by a rapid color change from dark-red to green upon exposure to **1AA**. *Ortho*-substituted (*N*-aryl)aryl imines (**1AC** and **1AD**) did not react under catalytic conditions, but it is unclear whether this is a result of steric congestion created in a substrate-bound intermediate or C–H bond deactivation by the *meta*-deactivating substituent (Me and F). Strongly donating heterocycles, such as pyridinyl (**1AE**) or thiophenyl (**1AF**), form stable N-Co-E chelates, which outcompetes C–H activation. Acidic species (such as acetophenone oxime) undergo deprotonation by **Co-Li** to generate the catalytically incompetent species, $(PPh_3)_3Co(N_2)H$ (see Chapter Three).

Finally, the identity of the aryl moiety on the *N*-coordinating directing group affected the catalytic yields (Table 4.1). Electron rich *N*-aryl groups led to higher yields than electron deficient directing groups (*i.e.*, **1M** > **5** > **6**). The steric environment proximal to the *N*-coordinating imine dictated coordination to the metal center. *Ortho*-substituted aryl groups (**7** and **8**) provide a sterically inaccessible imine, which precludes catalytic activity. These steric effects are somewhat mitigated if the steric bulk is distal to the N atom (**9**). Overall, *para*-methoxyphenyl (PMP) as the donor group provided the best yields.

Table 4.1. Imine Directing Group Scope.
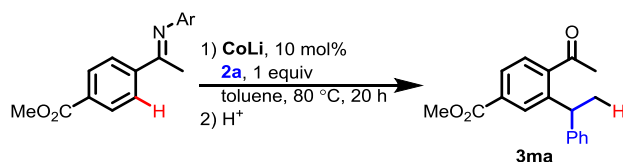
Substrate	Ar	^{1}H NMR Yield (%)
1M	4-(OMe)C₆H₄ (PMP)	92
5	Ph	78
6	4-(CF₃)C₆H₄	63
7	2-(OMe)C₆H₄	17
8	2-(ᵗBu)C₆H₄	0
9	3,5-(ᵗBu₂)C₆H₃	72

Reaction conditions: (*N*-aryl)aryl imine **1M** or **5-9** (0.1 M, 1 equiv), **2a** (0.1 M, 1 equiv), **Co-Li** (10 mol%) in toluene at 80 °C under N₂.

A plausible mechanism for olefin hydroarylations catalyzed by **Co-Li** is given in Scheme 4.2. A mechanism similar to that described for alkyne hydroarylations in Chapter Three is likely operative. Initial coordination of the olefin (**A**) occurs to displace an ancillary PPh₃ ligand (along with N₂). Subsequent coordination of the imine affords **B**, which may undergo a CMD-like proton transfer (**T.S.**^{BC}) to form a species akin to **C**. Reductive elimination from **C** produces the observed hydroarylation product and regenerates the active catalyst. It may be possible that a more classical C–H oxidative addition and subsequent C–H insertion occurs to generate **C**.

Scheme 4.2. Plausible Olefin Hydroarylation Mechanism.
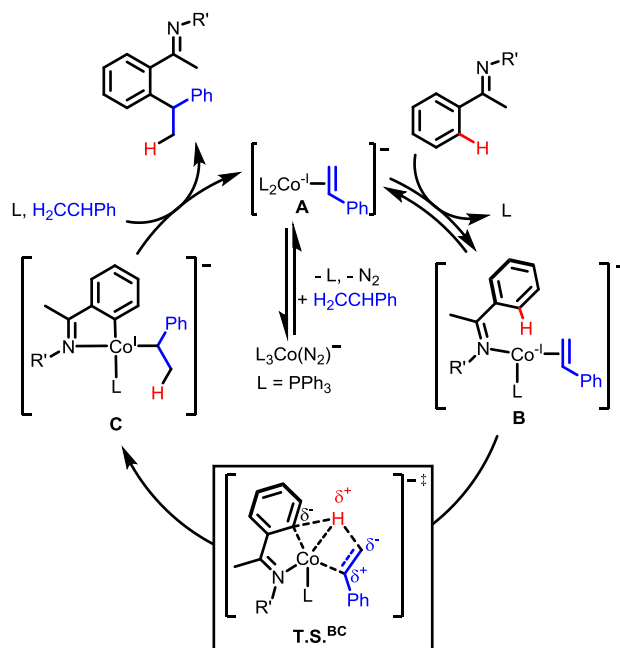
[a] Li counter-ions have been omitted for clarity.

In summary, a single-component Co(-I) catalyst for olefin hydroarylations has been developed and applied to over 40 substrate examples. This storable catalyst provides a new route for C–C bond formations with substrates bearing reactive functional groups which are incompatible with nucleophilic co-reagents. Generally high yields were observed under mild conditions for substrates bearing a variety of electronic and steric environments. Only branched products existed in the catalysis with styrene derived olefins; in contrast, linear products were exclusively observed with vinyl silane substrates. Given the well-defined nature of the Co(-I) catalyst, it may be possible to directly tune the reactivity through modification of the phosphine ligand or the counter cation. One such avenue of interest is the development of an enantioselective catalyst; this may be achieved through the use of *P*-chiral phosphine ligands or by the addition of chiral information to the participatory Li cation in the form of a chiral crowning reagent. Further developments are currently ongoing in this laboratory.

Experimental

General Considerations

All reactions and experiments, unless otherwise noted, were performed using standard Schlenk techniques under N_2 atmosphere or inside a N_2 glovebox. Schlenk glassware was oven dried overnight before use. Solvents were stored over 3 Å molecular sieves after drying with a JC Meyers Phoenix SDS solvent purification system. Solvents for organic syntheses were used without further purification. Deuterated NMR solvents were purchased from Cambridge Isotope Laboratory. Substituted acetophenones, $CoCl_2(H_2O)_6$, $NaBH_4$, PPh_3, diphenylacetylene, substituted anilines, tosylic acid monohydrate, vinyl trimethylsilane, vinyl methyl bis(trimethylsiloxyl)silane, *tert*-butyl ethylene, and styrene derivatives were purchased form commercial sources and used without further purification unless otherwise noted. Ethylene, propylene, trifluoropropylene, and 1,3-butadiene were purchased from Praixair and used without further purification.

All ^{1}H, ^{13}C{^{1}H}, and ^{19}F NMR experiments were carried out using Bruker AV-300, AVB-400, AVQ-400, AV-500, NEO-500, or AV-600 MHz (equipped with a Prodigy liquid N$_2$ broadband/^{1}H dual cryoprobe) spectrometers at ambient temperatures (unless otherwise noted). ^{1}H and ^{13}C{^{1}H} NMR spectra were internally calibrated to residual solvents relative to tetramethylsilane. ^{19}F NMR spectra were calibrated externally to CFCl$_3$.

High resolution mass spectrometry (HRMS) experiments were carried out by the QB3/Chemistry Mass Spectrometry Facility at the University of California, Berkeley. ESIHR experiments were performed on a LTQ-FT instrument (from Thermo-Finnigan) with direct injection using Excalibur software. EIHR experiments were performed on an Autospec Premier instrument (from Waters) using MassLynx software. Elemental analyses were performed at the Microanalytical Laboratory at the University of California, Berkeley using a Perkin Elmer 2400 Series II combustion analyzer equipped for determination of %C, %H and %N.

Synthesis of the Single Component Catalyst

The single component catalyst, [(PPh$_3$)$_3$Co(N$_2$)][Li(THF)$_3$] was prepared according to the procedure reported in Chapter Three. The synthesis described in this chapter, eq 4.2, employed 0.6 g of CoCl$_2$ • 6 H$_2$O to afford **Co-Li** with an overall yield of 1.4 g (53% over three steps).

Synthesis of *N*-Aryl Imine Substrates and Precursors

General Imine Synthesis: Method A

To a round bottom flask equipped with a Dean Stark apparatus and 4 Å molecular sieves (ca. 10 g), a solution of substituted acetophenone (1 equiv), *p*-anisidine (1 equiv), and a catalytic quantity of tosylic acid monohydrate (0.1 equiv) in toluene (40 mL) was heated to reflux for 16 h. Upon completion, the reaction mixture was allowed to cool to ambient temperature and filtered to remove residual solids. Volatile components were removed under reduced pressure to afford an orange oil as the crude product. Purification details are given below for each compound.

General Imine Synthesis: Method B

To a 20 mL scintillation vial equipped with a stir bar, a mixture of substituted acetophenone (1 equiv), *p*-anisidine (1 equiv), and 4Å molecular sieves (ca. 3 g) in toluene (10 mL) was stirred at ambient temperatures for 20 h. Upon completion, the mixture was filtered to remove residual solids. Volatile components were removed under reduced pressure to afford an orange oil as the crude product. Purification details are given below for each compound.
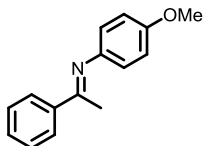
Synthesis of (*E*)-*N*-(4-methoxyphenyl)-1-phenylethan-1-imine (1A)

Method A was employed with acetophenone (1.0 mL, 8.6 mmol), *p*-anisidine (1.1 g, 8.6 mmol), and tosylic acid monohydrate (0.2 g, 0.9 mmol). Crystallization from toluene/pentane at -30 °C afforded the title compound as an orange solid (1.4 g, 75%), with spectroscopic features matching literature reported values.[44,45]
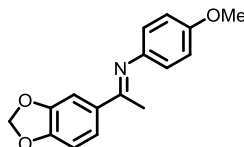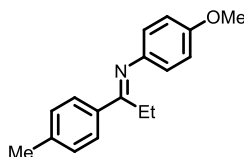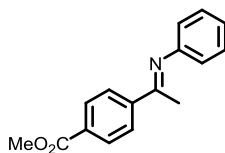
^{1}H NMR (chloroform-*d*, 400.1 MHz): δ 8.00 –7.92 (m, 2H, Ph), 7.50 – 7.40 (m, 3H, Ph), 6.95 – 6.87 (m, 2H, PMP), 6.79 – 6.72 (m, 2H, PMP), 3.82 (s, 3H, OMe), 2.25 (s, 3H, C(NAr)C**H₃**).
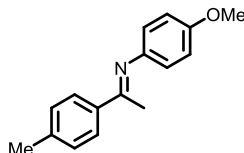
Synthesis of (*E*)-*N*-(4-methoxyphenyl)-1-phenylethan-1-imine (1B)

Method A was employed with 4'methylacetophenone (1.0 mL, 7.5 mmol), *p*-anisidine (0.9 g, 7.5 mmol), and tosylic acid monohydrate (0.2 g, 0.9 mmol). Crystallization from toluene/pentane at -30 °C afforded the title compound as an off-white solid (1.0 g, 57%), with spectroscopic features matching literature reported values.[45,46]

^{1}H NMR (chloroform-*d*, 500.0 MHz): δ 7.90 – 7.79 (m, 2H, Ar), 7.25 – 7. 20 (m, 2H, Ar), 7.00 – 6.88 (m, 2H, PMP), 6.82 – 6.71 (m, 2H, PMP), 3.82 (s, 3H, OMe), 2.41 (s, 3H, Me), 2.23 (s, 3H, C(NAr)C**H₃**).
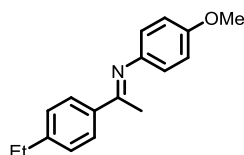
Synthesis of (*E*)-1-(4-ethylphenyl)-*N*-(4-methoxyphenyl)ethan-1-imine (1C)

Method A was employed with 4'-ethylacetophenone (6.1 mL, 41 mmol), *p*-anisidine (5.0 g, 41 mmol), and tosylic acid monohydrate (0.9 g, 4.2 mmol). Crystallization from toluene/pentane at -30 °C afforded the title compound as a yellow solid (6.0 g, 59%).

^{1}H NMR (chloroform-*d*, 400.1 MHz): δ 7.93 (d, *J* = 7.9 Hz, 2H, Ar), 7.28 (d, *J* = 8.3 Hz, 2H, Ar), 6.91 (d, *J* = 8.9 Hz, 2H, PMP), 6.65 (d, *J* = 8.6 Hz, 2H, PMP), 3.82 (s, 3H, OMe), 2.71 (q, *J* = 7.7 Hz, 2H, Et), 2.23 (s, 3H, C(NAr)C**H₃**), 1.27 (t, *J* = 7.6 Hz, 3H, Et).

^{1}H NMR (benzene-*d₆*, 400.1 MHz): δ 8.04 (d, *J* = 8.2 Hz, 2H), 7.09 (d, *J* = 8.2 Hz, 2H), 6.87 – 6.82 (m, 2H), 6.79 – 6.74 (m, 2H), 3.36 (s, 3H), 2.46 (q, *J* = 7.6 Hz, 2H), 1.97 (s, 3H), 1.08 (t, *J* = 7.6 Hz, 3H).

^{13}C{^{1}H} NMR (benzene-*d₆*, 125.6 MHz): δ 164.4, 156.5, 146.8, 145.7, 137.9, 128.3, 127.8, 121.2, 114.6, 55.0, 29.0, 16.7, 15.7.

Anal. Calcd for $C_{17}H_{19}NO$: C, 80.6; H, 7.56; N, 5.53. Found: C, 80.6; H, 7.54; N, 5.54.
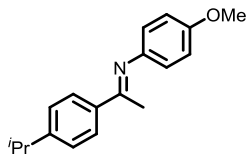
Synthesis of (*E*)-1-(4-isopropylphenyl)-*N*-(4-methoxyphenyl)ethan-1-imine (1D)

Method B was employed with 4'-isopropylacetophenone (0.5 mL, 3.0 mmol) and *p*-anisidine (0.4 g, 3.0 mmol). Crystallization from hexanes at -30 °C afforded the title compound a yellow solid (0.3 g, 35%),

^{1}H NMR (chloroform-*d*, 600.13 MHz): δ 7.90 (d, *J* = 8.3 Hz, 2H, Ar), 7.30 (d, *J* = 8.3 Hz, 2H, Ar), 6.94 – 6.88 (m, 2H, PMP), 6.76 – 6.72 (m, 2H, PMP), 3.82 (s, 3H, OMe), 2.96 (hept, *J* = 6.9 Hz, 1H, ^{i}Pr), 2.23 (s, 3H, C(NAr)C**H₃**), 1.28 (d, *J* = 6.9 Hz, 6H, ^{i}Pr).

^{13}C{^{1}H} NMR (chloroform-*d*, 150.92 MHz): δ 165.6, 155.8, 151.5, 145.0, 137.4, 127.2, 126.4, 120.8, 114.2, 55.5, 34.0, 23.9, 17.2.

HRMS (ESI) *m/z*: [M+H]⁺ Calcd for $C_{18}H_{22}NO^+$ 268.11696. Found 268.1700.
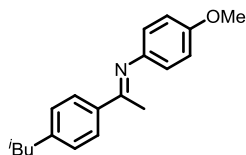
Synthesis of (*E*)-1-(4-isobutylphenyl)-*N*-(4-methoxyphenyl)ethan-1-imine (1E)

Method B was employed with 4'-isobutylacetophenone (1.0 mL, 5.5 mmol) and *p*-anisidine (0.7 g, 5.5 mmol). Crystallization from hexanes at -78 °C afforded the title compound as a fluffy pale-yellow powder (0.9 g, 56%).

^{1}H NMR (chloroform-*d*, 600.13 MHz): δ 7.94 – 7.81 (m, 2H, Ar), 7.25 – 7.19 (m, 2H, Ar), 6.96 (m, 2H, PMP), 6.82 – 6.72 (m, 2H, PMP), 3.82 (s, 3H, OMe), 2.53 (d, *J* = 7.2 Hz, 2H, C**H₂**CH(CH₃)₂), 2.24 (s, 3H, C(NAr)C**H₃**), 1.95 – 1.84 (m, 1H, CH₂C**H**(CH₃)₂), 0.92 (d, *J* = 6.7 Hz, 6H, CH₂CH(C**H₃**)₂).

^{13}C{^{1}H} NMR (chloroform-*d*, 150.92 MHz): δ 155.9, 139.9, 137.2, 129.1, 127.0, 120.9, 116.4, 114.8, 114.2, 55.5, 45.2, 30.2, 22.4, 17.3.

HRMS (ESI) *m/z*: [M+H]⁺ Calcd for $C_{19}H_{24}NO^+$ 282.1852. Found 282.1851.
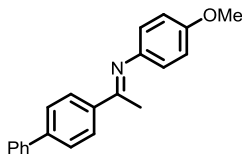
Synthesis of (*E*)-1-([1,1'-biphenyl]-4-yl)-*N*-(4-methoxyphenyl)ethan-1-imine (1F)

Method A was employed with 1-([1,1'-biphenyl]-4-yl)ethan-1-one (1 g, 5.1 mmol), *p*-anisidine (0.6 g, 5.1 mmol), and tosylic acid monohydrate (0.1 g, 0.5 mmol). Crystallization from toluene/hexanes afforded the title compound as a light orange solid (0.7 g, 48%), with spectroscopic features matching literature reported values.[34]

^{1}H NMR (chloroform-*d*, 300.1 MHz): δ 8.10 – 8.00 (m, 2H, biphenyl), 7.75 – 7.61 (m, 4H, biphenyl), 7.53 – 7.43 (m, 2H, biphenyl), 7.44 – 7.34 (m, 1H, biphenyl), 6.96 – 6.87 (m, 2H, PMP), 6.82 – 6.72 (m, 2H, PMP), 3.83 (s, 3H, OMe), 2.30 (s, 3H, C(NAr)C**H₃**).
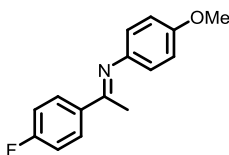
Synthesis of (*E*)-*N*-(4-methoxyphenyl)-1-(4-fluorophenyl)ethan-1-imine (1G)

Method A was employed with 4'-fluoroacetophenone (1.0 mL, 8.3 mmol), *p*-anisidine (1.0 g, 8.3 mmol), and tosylic acid monohydrate (0.2 g, 0.8 mmol). Crystallization from hexanes afforded the title compound as bright yellow crystals (0.7 g, 35%), with spectroscopic features matching literature reported values.[35]

^{1}H NMR (chloroform-*d*, 400.1 MHz): δ 8.02 – 7.92 (m, 2H, Ar), 7.16 – 7.06 (m, 2H, Ar), 6.99 – 6.86 (m, 2H, PMP), 6.80 – 6.70 (m, 2H, PMP), 3.82 (s, 3H, OMe), 2.24 (s, 3H, C(NAr)C**H₃**).

^{19}F{^{1}H} NMR (chloroform-*d*, 376.5 MHz): δ -109.89 (br s).
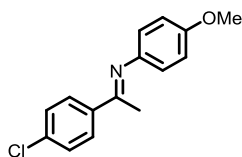
Synthesis of (*E*)-*N*-(4-methoxyphenyl)-1-(4-chlorophenyl)ethan-1-imine (1H)

Method A was employed with 4'-chloroacetophenone (1.0 mL, 7.7 mmol), *p*-anisidine (0.9 g, 7.7 mmol), and tosylic acid monohydrate (0.2 g, 0.8 mmol). Crystallization from toluene/hexanes afforded the title compound as bright yellow crystals (0.8 g, 42%), with spectroscopic features matching literature reported values.[35,46]

^{1}H NMR (chloroform-*d*, 400.1 MHz): δ 7.95 – 7.86 (m, 2H, Ar), 7.44 – 7.34 (m, 2H, Ar), 6.95 – 6.88 (m, 2H, PMP), 6.78 – 6.71 (m, 2H, PMP), 3.82 (s, 3H, OMe), 2.24 (s, 3H, C(NAr)C**H₃**).
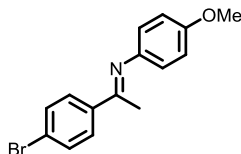
Synthesis of (*E*)-*N*-(4-methoxyphenyl)-1-(4-bromophenyl)ethan-1-imine (1I)

Method A was employed with 4'-bromoacetophenone (1.0 g, 5.0 mmol), *p*-anisidine (0.6 g, 5.0 mmol), and tosylic acid monohydrate (0.1 g, 0.4 mmol). Crystallization from toluene/hexanes afforded the title compound as bright yellow crystals (1.5 g, 98%), with spectroscopic features matching literature reported values.[45]

^{1}H NMR (chloroform-*d*, 400.1 MHz): δ 8.29 (d, *J* = 8.3 Hz, 2H, Ar), 7.57 (d, *J* = 8.3 Hz, 2H, Ar), 6.91 (d, *J* = 8.5 Hz, 2H, PMP), 6.75 (d, *J* = 8.5 Hz, 2H, PMP), 3.82 (s, 3H, OMe), 2.23 (s, 3H, C(NAr)C**H₃**).
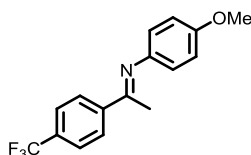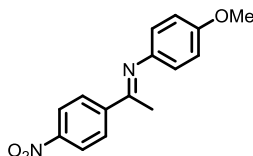

Synthesis of (*E*)-*N*-(4-methoxyphenyl)-1-(4-(trifluoromethyl)phenyl)ethan-1-imine (1J)

Method A was employed with 4'-(trifluoromethyl)acetophenone (1.0 g, 5.3 mmol), *p*-anisidine (0.65 g, 5.3 mmol), and tosylic acid monohydrate (0.13 g, 0.7 mmol). Crystallization from toluene/pentane at -30 °C afforded the title compound as bright-yellow needles (0.86 g, 55%), with spectroscopic features matching literature reported values.[39,47]

^{1}H NMR (chloroform-*d*, 400.1 MHz): δ 8.08 (d, *J* = 8.2 Hz, 2H, Ar), 7.70 (d, *J* = 8.2 Hz, 2H, Ar), 7.07 – 6.87 (m, 2H, PMP), 6.82 – 6.72 (m, 2H, PMP), 3.83 (s, 3H, OMe), 2.29 (s, 3H, C(NAr)C**H₃**).

^{19}F{^{1}H} NMR (chloroform-*d*, 376.5 MHz): δ -61.92.
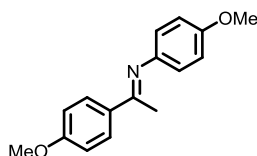
Synthesis of (*E*)-*N*,1-bis(4-methoxyphenyl)ethan-1-imine (1K)

Method A was employed with 4'-methoxyacetophenone (1.0 g, 6.7 mmol), *p*-anisidine (0.82 g, 6.7 mmol,), and tosylic acid monohydrate (0.13 g, 0.7 mmol). Purification of the crude prodcut by SiO₂ column chromatography (toluene) afforded the title compound as a dull-orange powder (0.57 g, 34%), with spectroscopic features matching literature reported values.[39,46,47]

^{1}H NMR (chloroform-*d*, 400.1 MHz): δ 8.01 – 7.84 (m, 2H, Ar), 6.99 – 6.93 (m, 2H, Ar), 6.92 – 6.89 (m, 2H, PMP), 6.83 – 6.71 (m, 2H, PMP), 3.87 (s, 3H, OMe), 3.82 (s, 3H, OMe), 2.23 (s, 3H, C(NAr)C**H₃**).
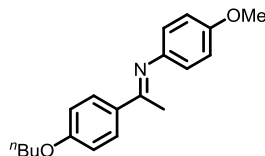
Synthesis of (*E*)-1-(4-*ⁿ*butoxyphenyl)-*N*-(4-methoxyphenyl)ethan-1-imine (1L)

Method B was employed with 4'-*ⁿ*butoxyacetophenone (1.0 mL, 5.2 mmol) and *p*-anisidine (0.6 g, 5.2 mmol). Crystallization from hexanes at -78 °C afforded the title compound as a pale-yellow solid (0.3 g, 21%).

¹H NMR (chloroform-*d*, 600.13 MHz): δ 7.96 – 7.84 (m, 2H, Ar), 6.96 – 6.93 (m, 2H, Ar), 6.92 – 6.87 (m, 2H, PMP), 6.79 – 6.73 (m, 2H, PMP), 4.02 (t, *J* = 6.5 Hz, 2H, O*ⁿ*Bu), 3.82 (s, 3H, OMe), 2.22 (s, 3H, C(NAr)C**H₃**), 1.85 – 1.73 (m, 2H, O*ⁿ*Bu), 1.57 – 1.43 (m, 2H overlapping residual H₂O, O*ⁿ*Bu), 0.99 (t, *J* = 7.4 Hz, 3H, O*ⁿ*Bu).

¹³C{¹H} NMR (chloroform-*d*, 150.92 MHz): δ 165.0, 161.2, 155.9, 145.2, 132.3, 128.8, 121.0, 114.3, 114.2, 67.9, 55.6, 31.4, 19.4, 17.2, 14.0.

HRMS (ESI) *m/z*: [M+H]⁺ Calcd for C₁₉H₂₄NO₂⁺ 298.1802. Found 298.1801.
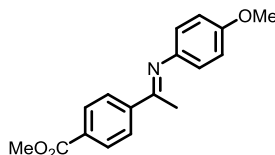
Synthesis of Methyl (*E*)-4-(1-((4-methoxyphenyl)imino)ethyl)benzoate (1M)

Method A was employed with methyl 4-acetylbenzoate (2.0 g, 11 mmol), *p*-anisidine (1.4 g, 11 mmol), and tosylic acid monohydrate (0.2 g, 1.1 mmol). Crystallization from petroleum ether/toluene at -30 °C afforded the title compound as yellow needles (2.3 g, 72%), with spectroscopic features matching literature reported values.[48]

¹H NMR (chloroform-*d*, 400.1 MHz): δ 8.10 (d, *J* = 8.5 Hz, 2H, Ar), 8.02 (d, *J* = 8.5 Hz, 2H, Ar), 6.92 (d, *J* = 8.8 Hz, 2H, PMP), 6.77 (d, *J* = 8.9 Hz, 2H, PMP), 3.94 (s, 3H, CO₂C**H₃**), 3.82 (s, 3H, OMe), 2.28 (s, 3H C(NAr)C**H₃**).
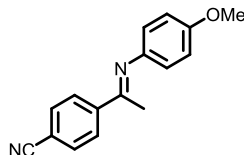
Synthesis of (*E*)-4-(1-((4-methoxyphenyl)imino)ethyl)benzonitrile (1N)

Method A was employed with 4-acetylbenzonitrile (1 g, 6.9 mmol), *p*-anisidine (0.9 g, 6.9 mmol), and tosylic acid monohydrate (0.13 g, 0.7 mmol). Crystallization from hexane/toluene at -30 °C afforded the title compound as a bright yellow powder (1.5 g, 88%), with spectroscopic features matching literature reported values.[47]

^{1}H NMR (chloroform-d, 300.1 MHz): δ 8.12 – 8.01 (m, 2H, Ar), 7.78 – 7.70 (m, 2H, Ar), 6.98 – 6.89 (m, 2H, PMP), 6.80 – 6.72 (m, 2H, PMP), 3.83 (s, 3H, OMe), 2.29 (s, 3H, C(NAr)C**H$_3$**).
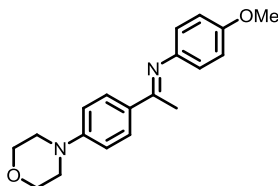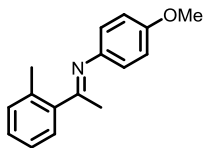

Synthesis of (*E*)-*N*-(4-methoxyphenyl)-1-(4-morpholinophenyl)ethan-1-imine (1O)

Method B was employed with 4'-morpholinoacetophenone (0.5 g, 2.4 mmol) and *p*-anisidine (0.3 g, 2.4 mmol). Crystallization from hexanes at -30 °C afforded the title compound as a pale-yellow solid (0.15 g, 21%).

^{1}H NMR (chloroform-d, 600.13 MHz): δ 7.91 (d, J = 8.9 Hz, 2H, Ar), 6.92 (d, J = 8.9 Hz, 2H, Ar), 6.89 (d, J = 8.7 Hz, 2H, PMP), 6.74 (d, J = 8.7 Hz, 2H, PMP), 3.92 – 3.84 (m, 4H, morph), 3.81 (s, 3H, OMe), 3.30 – 3.20 (m, 4H, morph), 2.20 (s, 3H, C(NAr)C**H$_3$**).

^{13}C{^{1}H} NMR (chloroform-d, 150.92 MHz): δ 165.0, 155.9, 152.8, 130.5, 128.6, 121.1, 114.4, 114.3, 113.4, 66.9, 55.6, 48.6, 17.1.

HRMS (ESI) *m/z*: [M+H]$^+$ Calcd for C$_{19}$H$_{23}$N$_2$O$_2$$^+$ 311.1754. Found 311.1753.

Synthesis of (*E*)-1-(3-fluorophenyl)-*N*-(4-methoxyphenyl)ethan-1-imine (1P)

Method B was employed with 3'-fluoroacetophenone (0.5 mL, 4.1 mmol) and *p*-anisidine (0.5 g, 4.1 mmol). Crystallization from hexanes at -78 °C afforded the title compound as an orange solid (0.6 g, 60%), with spectroscopic features matching literature reported values.[35]

^{1}H NMR (chloroform-d, 500.1 MHz): δ 7.75 – 7.66 (m, 2H, Ar), 7.43 – 7.37 (m, 1H, Ar), 7.18 – 7.12 (m, 1H, Ar), 6.96 – 6.87 (m, 2H, PMP), 6.79 – 6.72 (m, 2H, PMP), 3.82 (s, 3H, OMe), 2.24 (s, C(NAr)C**H$_3$**).

Synthesis of (*E*)-1-(3-fluorophenyl)-*N*-(4-methoxyphenyl)ethan-1-imine (1Q)

Method B was employed with 3'-methoxyacetophenone (1.0 mL, 7.3 mmol) and *p*-anisidine (0.9 g, 7.3 mmol). Crystallization from hexanes at -78 °C afforded the title compound as a pale-yellow solid (1.5 g, 81%), with spectroscopic features matching literature reported values.[46]

^{1}H NMR (chloroform-*d*, 500.1 MHz): δ 7.57 (dd, *J* = 2.6, 1.6 Hz, 1H, 2'-Ar**H**), 7.50 (ddd, *J* = 7.7, 1.7, 0.9 Hz, 1H, 6'-Ar**H**), 7.35 (t, *J* = 7.9 Hz, 1H, 5'-Ar**H**), 7.01 (ddd, *J* = 8.2, 2.6, 0.9 Hz, 1H, 4-Ar**H**), 6.96 – 6.86 (m, 2H, PMP), 6.78 – 6.72 (m, 2H, PMP), 3.88 (s, 3H, OMe), 3.82 (s, 3H, OMe), 2.24 (s, 3H, C(NAr)C**H₃**).

Synthesis of (*E*)-*N*-(4-methoxyphenyl)-1-(*m*-tolyl)ethan-1-imine (1R)

Method B was employed with 3'-methylacetophenone (0.5 mL, 3.7 mmol) and *p*-anisidine (0.5 g, 3.7 mmol). Crystallization from hexanes at -78 °C afforded the title compound as a yellow solid (0.5 g, 57%), with spectroscopic features matching literature reported values.[46]

^{1}H NMR (chloroform-*d*, 500.1 MHz): δ 7.82 (t, *J* = 1.8 Hz, 1H, 2'-Ar**H**), 7.72 (dt, *J* = 7.8, 1.3 Hz, 1H, 6'-Ar**H**), 7.33 (t, *J* = 7.6 Hz, 1H, 5'-Ar**H**), 7.27 (dt, *J* = 7.7, 1.4 Hz, 1H overlapping with residual CHCl₃, 4'-Ar**H**), 6.93 – 6.87 (m, 2H, PMP), 6.78 – 6.72 (m, 2H, PMP), 3.82 (s, OMe), 2.42 (3H, Me), 2.24 (s, 3H, C(NAr)C**H₃**).

Synthesis of (*E*)-*N*-(4-methoxyphenyl)-1-(3-(trifluoromethyl)phenyl)ethan-1-imine (1S)

Method B was employed with 3'-(trifluoromethyl)acetophenone (1.0 mL, 6.6 mmol) and *p*-anisidine (0.8 g, 6.6 mmol). Crystallization from hexanes at -78 °C afforded the title compound as a yellow solid (0.4 g, 22%), with spectroscopic features matching literature reported values.[33]

^{1}H NMR (chloroform-*d*, 500.1 MHz): δ 8.24 (br s, 1H, 2'-Ar**H**), 8.14 (d, *J* = 7.9 Hz, 1H, 6'-Ar**H**), 7.71 (d, *J* = 7.8 Hz, 1H, 4'-Ar**H**), 7.57 (t, *J* = 7.8 Hz, 1H, 5'-Ar**H**), 6.98 – 6.84 (m, 2H, PMP), 6.81 – 6.69 (m, 2H, PMP), 3.83 (s, 3H, OMe), 2.29 (s, 3H, C(NAr)C**H₃**).

^{19}F NMR (chloroform-*d*, 470.1 MHz): δ -62.59 (s).

Synthesis of methyl 3-acetylbenzoate

A solution of 3-acetylbenzoic acid (0.5 g, 3.1 mmol, 1 equiv) in MeOH (20 mL) with a catalytic quantity of concentrated H_2SO_4 was heated to reflux for 20 h. After completion, the mixture was cooled to room temperature and the volatile components were removed under reduced pressure. The resultant oil was diluted in dichloromethane (20 mL) and then washed thoroughly with saturated, aqueous $NaHCO_3$ (2 x 10 mL) and then with distilled H_2O (10 mL). The organic layer was dried with Na_2SO_4 and filtered. Volatile components were removed under reduced pressure to afford an off-yellow oil which solidified upon standing (0.3 g, 58%). Spectroscopic features matched literature reported values.[49]

^{1}H NMR (chloroform-d, 500.1 MHz): δ 8.60 (td, J = 1.8, 0.6 Hz, 1H, 2-Ar**H**), 8.24 (dt, J = 7.8, 1.5 Hz, 1H, 4-Ar**H**), 8.16 (ddd, J = 7.8, 1.8, 1.2 Hz, 1H, 6-Ar**H**)), 7.57 (td, J = 7.8, 0.6 Hz, 1H, 5-Ar**H**), 3.96 (s, 3H, CO$_2$Me), 2.66 (s, 3H, COC**H$_3$**).

Synthesis of methyl (*E*)-3-(1-((4-methoxyphenyl)imino)ethyl)benzoate (1T)

Method B was employed with methyl 3-acetylbenzoate (0.3 g, 1.8 mmol) and *p*-anisidine (0.2 g, 1.8 mmol). Crystallization from toluene/hexanes at -30 °C afforded the title compound as bright yellow crystals (0.3 g, 53%).

^{1}H NMR (chloroform-d, 600.13 MHz): δ 8.58 (t, J = 1.4 Hz, 1H, 2'-Ar**H**), 8.21 (ddd, J = 7.9, 1.9, 1.3 Hz, 1H, 4'-Ar**H**), 8.13 (ddd, J = 7.7, 1.9, 1.4 Hz, 1H, 6'-Ar**H**), 7.52 (dd, J = 7.9, 7.4 Hz, 1H, 5'-Ar**H**), 6.95 – 6.87 (m, 2H, PMP), 6.80 – 6.71 (m, 2H, PMP), 3.95 (s, 3H, CO$_2$Me), 3.82 (s, 3H, OMe), 2.29 (s, 3H, C(NAr)C**H$_3$**).

^{13}C{^{1}H} NMR (chloroform-d, 150.92 MHz): δ 167.0, 164.9, 156.3, 144.5, 140.2, 131.6, 131.4, 130.5, 128.6, 128.4, 120.9, 114.4, 55.6, 52.4, 17.5.

HRMS (ESI) *m/z*: [M+H]$^+$ Calcd for $C_{17}H_{18}NO_3^+$ 284.1281. Found 284.1279.

Synthesis of (*E*)-*N*-(4-methoxyphenyl)-1-(naphthalen-2-yl)ethan-1-imine (1U)

Method B was employed with 2-acetonaphthone (1.0 g, 5.9 mmol) and *p*-anisidine (0.7 g, 5.9 mmol). Crystallization from toluene/hexanes at -78 °C afforded the title compound as a pale-yellow solid (0.5 g, 31%), with spectroscopic features matching literature reported values.[46]

^{1}H NMR (chloroform-d, 500.1 MHz): δ 8.34 (s, 1H, naph), 8.22 (dd, J = 8.7, 1.8 Hz, 1H, naph), 7.96 – 7.84 (m, 3H, naph), 7.59 – 7.48 (m, 2H, naph), 6.98 – 6.89 (m, 2H, PMP), 6.84 – 6.77 (m, 2H, PMP), 3.84 (s, 3H, OMe), 2.39 (s, 3H, C(NAr)C**H₃**).

Synthesis of (*E*)-*N*-(4-methoxyphenyl)-1-(naphthalen-2-yl)ethan-1-imine (1V)

Method B was employed with 1-(benzofuran-2-yl)ethan-1-one (0.8 g, 5.1 mmol) and *p*-anisidine (0.6 g, 5.1 mmol). Crystallization from toluene/hexanes at -78 °C afforded the title compound as a pale-yellow solid (0.2 g, 16%), with spectroscopic features matching literature reported values.[50]

^{1}H NMR (chloroform-d, 300.1 MHz): δ 7.66 (d, J = 7.7 Hz, 1H, Ar), 7.61 (dd, J = 8.3, 1.0 Hz, 1H, Ar), 7.39 (td, J = 8.3, 1.3 Hz, 1H, Ar), 7.32 – 7.25 (m, 2H overlapping residual CHCl₃), 6.96 – 6.90 (m, 2H, PMP), 6.89 – 6.81 (m, 2H, PMP), 3.83 (s, 3H, OMe), 2.30 (s, 3H, C(NAr)C**H₃**).

Synthesis of (*E*)-1-(benzo[*d*][1,3]dioxol-5-yl)-*N*-(4-methoxyphenyl)ethan-1-imine (1W)

Method B was employed with 3',4'-(methylenedioxy)acetophenone (0.5 g, 3.1 mmol) and *p*-anisidine (0.4 g, 3.1 mmol). Crystallization from hexanes at -30 °C afforded the title compound as a dull-yellow solid (0.2 g, 23%), with spectroscopic features matching literature reported values.[51]

^{1}H NMR (chloroform-d, 500.1 MHz): δ 7.57 (s, 1H, Ar), 7.49 – 7.40 (m, 1H, Ar), 6.93 – 6.88 (m, 2H, PMP), 6.85 (d, J = 8.2 Hz, 1H, Ar), 6.77 – 6.67 (m, 2H, PMP), 6.02 (s, 2H, OC**H₂**O), 3.82 (s, 3H, OMe), 2.20 (s, 3H, C(NAr)C**H₃**).

Synthesis of (*E*)-*N*-(4-methoxyphenyl)-1-(*p*-tolyl)propan-1-imine (1X)

Method B was employed with 4'-methylpropiophenone (1.0 mL, 6.8 mmol) and *p*-anisidine (0.8 g, 6.8 mmol) and with the following modifications; the reaction was stirred at ambient temperatures for 1 week under a slow bubble of N₂ gas. Crystallization from hexanes at -30 °C afforded the title compound as orange crystals (0.3 g, 16%), with spectroscopic features matching literature reported values.[52]

^{1}H NMR (chloroform-d, 300.1 MHz): δ 7.86 – 7.77 (m, 2H, Ar), 7.27 – 7.24 (m, 2H overlapping residual CHCl₃, Ar), 6.98 – 6.84 (m, 2H, PMP), 6.81 – 6.73 (m, 2H, PMP), 3.83 (s, 3H, OMe), 2.68 (q, J = 7.6 Hz, 2H, C(NAr)C**H₂**CH₃), 2.41 (s, 3H, Me), 1.09 (t, J = 7.6 Hz, 3H, C(NAr)CH₂C**H₃**).

Synthesis of methyl (*E*)-4-(1-(phenylimino)ethyl)benzoate (5)

Method B was employed with methyl 4-acetylbenzoate (0.5 g, 2.8 mmol) and aniline (0.26 mL, 2.8 mmol). Crystallization from hexanes at -30 °C afforded the title compound as a fluffy yellow solid (0.5 g, 64%).

^{1}H NMR (chloroform-*d*, 600.13 MHz): δ 8.14 – 8.09 (m, 2H, Ar), 8.06 – 8.01 (m, 2H, Ar), 7.40 – 7.33 (m, 2H, Ph), 7.13 – 7.07 (m, 1H, Ph), 6.84 – 6.76 (m, 2H, Ph), 3.95 (s, 3H, CO$_2$Me), 2.26 (s, 3H, C(NAr)C**H$_3$**).

^{13}C{^{1}H} NMR (chloroform-*d*, 150.92 MHz): δ 166.8, 164.9, 151.4, 143.5, 131.8, 129.7, 129.1, 127.3, 123.7, 119.3, 52.4, 17.6.

HRMS (ESI) *m/z*: [M+H]$^+$ Calcd for C$_{16}$H$_{16}$NO$_2$$^+$ 254.1176. Found 254.1175.
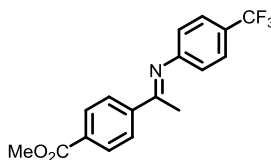
Synthesis of methyl (*E*)-4-(1-((4-(trifluoromethyl)phenyl)imino)ethyl)benzoate (6)

Method B was employed with methyl 4-acetylbenzoate (0.5 g, 2.8 mmol) and 4-(trifluoromethyl)aniline HCl salt (0.55 g, 2.8 mmol). Purification by SiO$_2$ column chromatography (10% EtOAc/hexanes) afforded the title compound as a white solid (0.1 g, 10%).

^{1}H NMR (chloroform-*d*, 600.13 MHz): δ 8.15 – 8.10 (m, 2H), 8.07 – 8.02 (m, 2H), 7.65 – 7.59 (m, 2H), 6.91 – 6.85 (m, 2H), 3.96 (s, 3H, CO$_2$Me), 2.26 (s, 3H, C(NAr)C**H$_3$**).

^{13}C{^{1}H} NMR (chloroform-*d*, 150.92 MHz): δ 166.7, 165.7, 154.5, 142.8, 132.2, 129.8, 127.4, 126.5 (q, $^3J_{CF}$ = 3.8 Hz), 125.9 (q, $^2J_{CF}$ = 32.7 Hz), 123.7 (q, $^1J_{CF}$ = 272.7 Hz), 119.4, 52.5, 17.9.

^{19}F NMR (chloroform-*d*, 470.1 MHz): δ -61.87 (s).

HRMS (ESI) *m/z*: [M+H]$^+$ Calcd for C$_{17}$H$_{15}$F$_3$NO$_2$$^+$ 322.1049. Found 322.1408.

Synthesis of methyl (*E*)-4-(1-(phenylimino)ethyl)benzoate (7)

Method B was employed with methyl 4-acetylbenzoate (0.5 g, 2.8 mmol) and *o*-anisidine (0.35 g, 2.8 mmol). Crystallization from hexanes at -30 °C afforded the title compound as a fluffy yellow solid (0.2 g, 23%) with ca. 30% residual methyl 4-acetylbenzoate. Column chromatography (SiO$_2$, gradient from 4% to 10% EtOAc/hexanes) was unable to resolve the product from the residual starting material. It was used without additional purification.

^{1}H NMR (chloroform-*d*, 600.13 MHz): δ 8.14 (d, *J* = 8.6 Hz, 0.9H, methyl 4-acetylbenzoate), 8.13 – 8.11 (m, 2H, Ar, **6**), 8.10 – 8.06 (m, 2H, Ar, **6**), 7.11 (td, *J* = 7.8, 1.7 Hz, 1H, OMP, **6**), 6.99 (td, *J* = 7.6, 1.2 Hz, 1H, OMP, **6**), 6.96 (dd, *J* = 8.2, 1.0 Hz, 1H, OMP, **6**), 6.79 (dd, *J* = 7.6, 1.6 Hz, 1H, OMP, **6**), 3.97 (s, 1.5H, methyl 4-acetylbenzoate), 3.96 (s, 3H, CO$_2$Me, **6**), 3.81 (s, 3H, OMe, **6**), 2.66 (s, 1.4H, methyl 4-acetylbenzoate), 2.21 (s, 3H, C(NAr)C**H$_3$**, **6**).

^{13}C{^{1}H} NMR (chloroform-*d*, 150.92 MHz, **6**): δ 166.8, 166.4, 148.7, 143.3, 129.8, 129.5, 128.2, 127.3, 124.5, 120.9, 120.4, 111.6, 55.6, 52.2, 17.9.

HRMS (ESI) *m/z*: [M+H]$^{+}$ Calcd for C$_{17}$H$_{18}$NO$_3$$^{+}$ 284.1281. Found 284.1285.
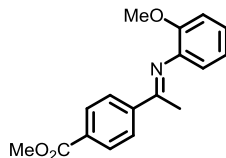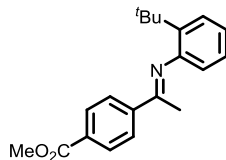
Synthesis of methyl (*E*)-4-(1-((2-*tert*-butylphenyl)imino)ethyl)benzoate (8)

Method A was employed with methyl 4-acetylbenzoate (0.5 g, 2.8 mmol), 2-*tert*-butylaniline (0.44 mL, 2.8 mmol), and tosylic acid monohydrate (0.1 g, 0.3 mmol). Crystallization from hexanes at -30 °C afforded the title compound as pale-yellow needles (0.6 g, 69%).

^{1}H NMR (chloroform-*d*, 600.13 MHz): δ 8.15 – 8.12 (m, 2H), 8.10 – 8.06 (m, 2H), 7.42 (dd, *J* = 7.9, 1.4 Hz, 1H), 7.18 (td, *J* = 7.5, 1.4 Hz, 1H0, 7.07 (td, *J* = 7.6, 1.5 Hz, 1H), 6.48 (dd, *J* = 7.7, 1.4 Hz, 1H), 3.96 (s, 3H, CO$_2$Me), 2.25 (s, 3H, C(NAr)C**H$_3$**), 1.34 (s, 9H, *t*Bu).

^{13}C{^{1}H} NMR (chloroform-*d*, 150.92 MHz): δ 166.9, 162.6, 149.8, 143.5, 139.9, 131.7, 129.8, 127.3, 126.5, 126.5, 123.9, 119.8, 52.4, 35.3, 29.7, 18.2.

HRMS (ESI) *m/z*: [M+H]$^{+}$ Calcd for C$_{20}$H$_{24}$NO$_2$$^{+}$ 310.1802. Found 310.1799.
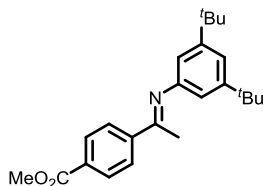
Synthesis of methyl (*E*)-4-(1-((3,5-di-*tert*-butylphenyl)imino)ethyl)benzoate (9)

Method A was employed with methyl 4-acetylbenzoate (0.2 g, 1.2 mmol), 3,5-di-*tert*-butylaniline (0.3 g, 1.2 mmol), and tosylic acid monohydrate (0.1 g, 0.3 mmol). Crystallization from hexanes at -30 °C afforded the title compound as a yellow powder (0.2 g, 48%).

^{1}H NMR (chloroform-*d*, 600.13 MHz): δ 8.16 – 8.11 (m, 2H), 8.09 – 8.05 (m, 2H), 7.18 (t, *J* = 1.8 Hz, 1H), 6.66 (d, *J* = 1.7 Hz, 2H), 3.98 (s, 3H, CO$_2$Me), 2.31 (s, 3H, C(NAr)C**H$_3$**), 1.36 (s, 18H, ^{t}Bu).

^{13}C{^{1}H} NMR (chloroform-*d*, 150.92 MHz): δ 166.8, 151.6, 143.7, 131.5, 129.8, 129.6, 128.2, 127.1, 117.5, 113.6, 52.2, 34.9, 31.5, 17.5.

HRMS (ESI) *m/z*: [M+H]$^+$ Calcd for C$_{24}$H$_{32}$NO$_2^+$ 366.2428. Found 366.2426.
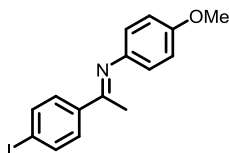
Synthesis of (*E*)-1-(4-iodophenyl)-*N*-(4-methoxyphenyl)ethan-1-imine (1Y)

Method A was employed with 4'-iodoacetophenone (1.0 g, 4.1 mmol), *p*-anisidine (0.5 g, 4.1 mmol), and tosylic acid monohydrate (0.1 g, 0.5 mmol). Crystallization from hexanes at -30 °C afforded the title compound as a yellow-orange powder (1.3 g, 89%), with spectroscopic features matching literature reported values.[47]

^{1}H NMR (chloroform-*d*, 300.1 MHz): δ 7.85 – 7.75 (m, 2H, Ar), 7.74 – 7.66 (m, 2H, Ar), 6.97 – 6.88 (m, 2H, PMP), 6.80 – 6.68 (m, 2H, PMP), 3.82 (s, 3H, OMe), 2.23 (s, 3H, C(NAr)C**H$_3$**).
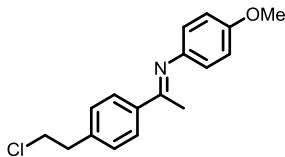
Synthesis of (*E*)-1-(4-(2-chloroethyl)phenyl)-*N*-(4-methoxyphenyl)ethan-1-imine (1Z)

Method A was employed with 4'-(2-chloroethyl)acetophenone (1.0 mL, 6.3 mmol), *p*-anisidine (0.8 g, 6.3 mmol), and tosylic acid monohydrate (0.12 g, 0.6 mmol). Crystallization from hexanes at -30 °C afforded the title compound as a fluffy yellow powder (0.7 g, 38%).

¹H NMR (chloroform-*d*, 600.13 MHz): δ 7.98 – 7.91 (m, 2H, Ar), 7.34 – 7.29 (m, 2H, Ar), 6.97 – 6.89 (m, 2H, PMP), 6.81 – 6.72 (m, 2H, PMP), 3.85 (s, 3H, OMe), 3.77 (t, *J* = 7.3 Hz, 2H, ArCH$_2$C**H$_2$**Cl), 3.15 (t, *J* = 7.3 Hz, 2H, ArC**H$_2$**CH$_2$Cl), 2.27 (s, 3H, C(NAr)C**H$_3$**).

¹³C{¹H} NMR (chloroform-*d*, 150.92 MHz): δ 156.0, 140.5, 138.4, 128.8, 127.4, 120.8, 116.4, 114.8, 114.3, 55.5, 44.7, 38.9, 17.3.

HRMS (ESI) *m/z*: [M+H]⁺ Calcd for C$_{17}$H$_{19}$ClNO⁺ 288.1150. Found 288.1149.

Synthesis of (*E*)-*N*-(4-methoxyphenyl)-1-(4-nitrophenyl)ethan-1-imine (1AA)

Method A was employed with 4'-nitroacetophenone (1.2 g, 7.4 mmol), *p*-anisidine (0.9 g, 7.4 mmol), and tosylic acid monohydrate (0.14 g, 0.7 mmol). Crystallization from toluene/hexanes at -30 °C afforded the title compound as a yellow-orange powder (1.3 g, 64%), with spectroscopic features matching literature reported values.[53]

¹H NMR (chloroform-*d*, 400.1 MHz): δ 8.34 – 8.23 (m, 2H, Ar), 8.18 – 8.10 (m, 2H, Ar), 6.99 – 6.90 (m, 2H, PMP), 6.83 – 6.75 (m, 2H, PMP), 3.83 (s, 3H, OMe), 2.33 (s, 3H, C(NAr)C**H$_3$**).
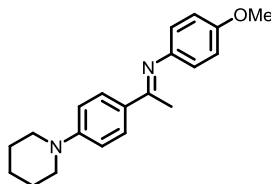
Synthesis of (*E*)-*N*-(4-methoxyphenyl)-1-(4-(piperidin-1-yl)phenyl)ethan-1-imine (1AB)

Method A was employed with 4'-(piperidin-1-yl)acetophenone (1.0 g, 4.9 mmol), *p*-anisidine (0.6 g, 4.9 mmol), and tosylic acid monohydrate (0.1 g, 0.5 mmol). Crystallization from toluene/hexanes at -30 °C afforded the title compound as dull-yellow crystals (1.0 g, 68%).

¹H NMR (chloroform-*d*, 600.13 MHz): δ 7.98 – 7.77 (m, 2H, Ar), 6.96 – 6.91 (m, 2H), 6.91 – 6.84 (m, 2H), 6.76 – 6.66 (m, 2H), 3.81 (s, 3H, OMe), 3.32 – 3.26 (m, 4H, pip), 2.19 (s, 3H, C(NAr)C**H$_3$**), 1.74 – 1.66 (m, 4H, pip), 1.65 – 1.59 (m, 2H, pip).

¹³C{¹H} NMR (chloroform-*d*, 150.92 MHz): δ 167.4, 165.0, 155.7, 153.4, 137.7, 128.5, 121.2, 114.8, 114.3, 55.6, 49.7, 25.6, 24.5, 17.0.

HRMS (ESI) *m/z*: [M+H]⁺ Calcd for C$_{20}$H$_{25}$N$_2$O⁺ 309.1691. Found 309.1964.

Synthesis of (*E*)-*N*-(4-methoxyphenyl)-1-(*o*-tolyl)ethan-1-imine (1AC)

Method A was employed with 2'-methylacetophenone (0.7 mL, 5.4 mmol), *p*-anisidine (0.9 g, 7.7 mmol), and tosylic acid monohydrate (0.15 g, 0.8 mmol). Purification by SiO_2 column chromatography (10% EtOAc/hexanes) afforded the title compound as a yellow oil (1.0 g, 68%), with spectroscopic features matching literature reported values.[46] The product contains a mixture of *E*- and *Z*-isomers (ca. 1.4:1.0) which is consistent with the literature report.[46]

^{1}H NMR (chloroform-*d*, 300.1 MHz): δ 7.40 – 7.35 (m, 1H), 7.30 – 7.20 (m, 2H overlapping CHCl₃), 7.16 – 7.00 (m, 3H), 6.95 – 6.90 (m, 2H, PMP), 6.84 – 6.76 (m, 2H, PMP), 6.65 – 6.59 (m, 3H), 3.82 (s, 3H, OMe, *E*-isomer), 3.69 (s, 2.1H, OMe, *Z*-isomer), 2.48 (s, 3H, C(NAr)**CH₃**, *E*-isomer), 2.46 (s, 3H, C(NAr)**CH₃**, *Z*-isomer), 2.17 (s, 3H, Me, *E*-isomer), 2.05 (s, 3H, Me, *Z*-isomer).
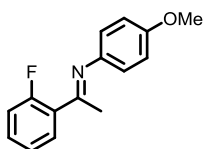
Synthesis of (*E*)-1-(2-fluorophenyl)-*N*-(4-methoxyphenyl)ethan-1-imine (1AD)

Method B was employed with 2'-fluoroacetophenone (0.5 mL, 4.1 mmol) and *p*-anisidine (0.51 g, 4.1 mmol). Crystallization of impurities from toluene/hexanes at -30 °C afforded the title compound as an orange oil (0.24 g, 24%), with spectroscopic features matching literature reported values.[54]

^{1}H NMR (chloroform-*d*, 500.1 MHz): δ 7.82 (td, *J* = 7.7, 1.8 Hz, 1H), 7.40 (tdd, *J* = 7.5, 5.0, 1.8 Hz, 1H), 7.21 (td, *J* = 7.5, 1.1 Hz, 1H), 7.14 –7.08 (m, 1H), 6.95 – 6.89 (m, 2H, PMP), 6.83 – 6.78 (m, 2H, PMP), 3.82 (s, 3H, OMe), 2.27 (d, J_{HF} = 3.5 Hz, 3H, C(NAr)**CH₃**).

^{19}F NMR (chloroform-*d*, 470.1 MHz): δ -113.51 (m).
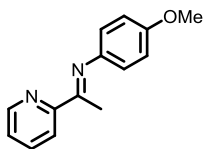
Synthesis of (*E*)-*N*-(4-methoxyphenyl)-1-(pyridine-2-yl)ethan-1-imine (1AE)

Method B was employed with 2-acetylpyridine (0.5 mL, 4.5 mmol) and *p*-anisidine (0.55 g, 4.5 mmol). Crystallization of impurities from toluene/hexanes at -30 °C afforded the title compound as an orange oil (0.6 g, 60%), with spectroscopic features matching literature reported values.[50]

^{1}H NMR (chloroform-d, 500.1 MHz): δ 8.66 (ddd, J = 4.8, 1.9, 1.0 Hz, 1H, py), 8.26 (dt, J = 7.9, 1.1 Hz, 1H, py), 7.77 (ddd, J = 8.1, 7.5, 1.8 Hz, 1H, py), 7.45 (ddd, J = 7.5, 4.8, 1.2 Hz, 1H, py), 6.96 – 6.88 (m, 2H, PMP), 6.86 – 6.77 (m, 2H, PMP), 3.83 (s, 3H, OMe), 2.38 (s, 3H, C(NAr)C**H₃**).
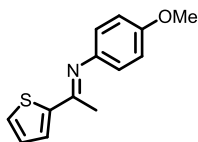
Synthesis of (E)-N-(4-methoxyphenyl)-1-(thiophen-2-yl)ethan-1-imine (1AF)

Method B was employed with 2-acetylpyridine (0.5 mL, 4.5 mmol) and p-anisidine (0.55 g, 4.5 mmol). Crystallization of impurities from toluene/hexanes at -30 °C afforded the title compound as an orange oil (0.6 g, 60%), with spectroscopic features matching literature reported values.[50] The product contains a mixture of E- and Z-isomers (ca. 1.0:0.6) which is consistent with the literature report.[50]

^{1}H NMR (chloroform-d, 500.1 MHz): δ 7.70 (dd, J = 3.8, 1.1 Hz, 0.6H, thiophenyl, Z-isomer), 7.64 (dd, J = 5.0, 1.1 Hz, 0.6H, thiophenyl, Z-isomer), 7.46 (dd, J = 3.7, 1.2 Hz, 1H, thiophenyl, E-isomer), 7.44 (dd, J = 5.1, 1.1 Hz, 1H, thiophenyl, E-isomer), 7.13 (dd, J = 5.0, 3.7 Hz, 0.6H, thiophenyl, Z-isomer), 7.08 (dd, J = 5.1, 3.7 Hz, 1H, thiophenyl, E-isomer), 6.93 – 6.87 (m, 2H, PMP, E-isomer), 6.79 – 6.76 (m, 2H, PMP, E-isomer), 6.76 – 6.72 (m, 1.6H, PMP, Z-isomer), 6.67 – 6.63 (m, 1.6H, PMP, Z-isomer), 3.81 (s, 3H, OMe, E-isomer), 3.74 (s, 3H, OMe, Z-isomer), 2.57 (s, 2H, C(NAr)C**H₃**, Z-isomer), 2.26 (s, 3H, C(NAr)C**H₃**, E-isomer).

Synthesis of Substituted Styrene Substrates
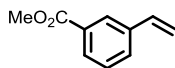
Synthesis of methyl 3-vinylbenzoate (2k)

A solution of 3-vinylbenzoic acid (1.0 g, 6.8 mmol, 1 equiv) in MeOH (20 mL) with a catalytic quantity of tosylic acid monohydrate was heated to reflux for 20 h. After completion, the mixture was cooled to room temperature and the volatile components were removed under reduced pressure. The resultant oil was diluted in dichloromethane (20 mL) and then washed thoroughly with saturated, aqueous $NaHCO_3$ (2 x 10 mL) and then with distilled H_2O (10 mL). The organic layer was dried with Na_2SO_4 and filtered. Volatile components were removed under reduced pressure to afford a pale-yellow oil (0.6 g, 55%), with spectroscopic features matching literature reported values.[55]

^{1}H NMR (chloroform-*d*, 600.13 MHz): δ 8.08 (t, *J* = 1.8 Hz, 1H, 2-Ar**H**), 7.92 (dt, *J* = 7.8, 1.4 Hz, 1H, 4-Ar**H**), 7.59 (dt, *J* = 7.7, 1.4 Hz, 1H, 6-Ar**H**), 7.40 (t, *J* = 7.7 Hz, 1H, 5-Ar**H**), 6.75 (dd, *J* = 17.6, 10.9 Hz, 1H, ArC**H**=CH$_2$), 5.83 (dd, *J* = 17.6, 0.8 Hz, 1H, ArCH=C**H$_2$**), 5.33 (dd, *J* = 10.9, 0.7 Hz, 1H, ArCH=C**H$_2$**), 3.93 (s, 3H, CO$_2$Me).
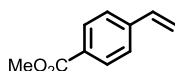
Synthesis of methyl 4-vinylbenzoate (2l)

A solution of 4-vinylbenzoic acid (0.5 g, 3.4 mmol, 1 equiv) in MeOH (20 mL) with a catalytic quantity of tosylic acid monohydrate was heated to reflux for 20 h. After completion, the mixture was cooled to room temperature and the volatile components were removed under reduced pressure. The resultant oil was diluted in dichloromethane (20 mL) and then washed thoroughly with saturated, aqueous $NaHCO_3$ (2 x 10 mL) and then with distilled H_2O (10 mL). The organic layer was dried with Na_2SO_4 and filtered. Volatile components were removed under reduced pressure to afford an off-white solid (0.3 g, 61%), with spectroscopic features matching literature reported values.[56]

^{1}H NMR (chloroform-*d*, 400.1 MHz): δ 8.00 (d, *J* = 8.4 Hz, 2H, Ar), 7.46 (d, *J* = 8.3 Hz, 2H, Ar), 6.75 (dd, *J* = 17.6, 10.9 Hz, 1H, ArC**H**=CH$_2$), 5.87 (d, *J* = 17.6 Hz, 1H, ArCH=C**H$_2$**), 5.38 (d, *J* = 10.9 Hz, 1H, ArCH=C**H$_2$**), 3.91 (s, 3H, CO$_2$Me).
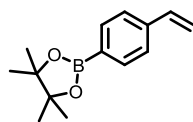
Synthesis of 4,4,5,5-tetramethyl-2-(4-vinylphenyl)-1,3,2-dioxoaborolane (2m)

A solution of 4-vinylphenylboronic acid (0.5 g, 3.4 mmol, 1 equiv) and pinacol (0.4 g, 3.5 mmol, 1.1 equiv) in dichloromethane (10 mL) was stirred at ambient temperatures over 4 Å molecular sieves for 20 h. After completion, the reaction mixture was filtered to remove residual solids. Volatile components were removed

under reduced pressure to afford a colorless oil (0.6 g, 75%), which was pure by ^{1}H NMR and matched literature reported spectroscopic features.[57] No further purifications were performed.

^{1}H NMR (chloroform-*d*, 600.13 MHz): δ 7.83 – 7.74 (m, 2H, Ar), 7.45 – 7.37 (m, 2H, Ar), 6.73 (dd, *J* = 17.6, 10.9 Hz, 1H, ArC**H**=CH$_2$), 5.81 (dd, *J* = 17.6, 0.9 Hz, 1H, ArCH=C**H$_2$**), 5.29 (dd, *J* = 10.9, 0.9 Hz, 1H overlapping residual dichloromethane, ArCH=C**H$_2$**), 1.35 (s, 12H, BPin).

General ^{1}H NMR Scale Hydroarylation Catalysis at Ambient Temperatures: Method C

Inside an N$_2$ glovebox, a mixture of substituted (*N*-aryl)aryl imine (0.1 mmol, 1 equiv, 0.1 M), olefin (0.1 mmol, 1 equiv, 0.1 M), and **Co-Li** (11 mg, 0.01 mmol, 10 mol%, 0.01 M) in toluene (1 mL) was stirred at ambient temperatures for 20 h in a 20 mL scintillation vial equipped with a stir bar. Upon completion, the catalytic mixture was quenched with 5M HCl (ca. 2 mL) under ambient atmosphere for 1 h. The organic components were extracted with dichloromethane (2 x 25 mL), and the organic layers were washed with H$_2$O, dried with Na$_2$SO$_4$, and filtered. Volatile components were removed under reduced pressure to afford the crude product as a brown oily solid. Crude ^{1}H NMR yields were determined by ^{1}H NMR spectroscopy of the resultant mixed oily products as the ratio of hydroarylation products to unreacted, hydrolyzed starting material.

General ^{1}H NMR Scale Hydroarylation Catalysis at 80 °C: Method D

Inside an N$_2$ glovebox, a mixture of substituted (*N*-aryl)aryl imine (0.1 mmol, 1 equiv, 0.1 M), olefin (0.1 mmol, 1 equiv, 0.1 M), and **Co-Li** (11 mg, 0.01 mmol, 10 mol%, 0.01 M) in toluene (1 mL) was added to a 25 mL Teflon stoppered Schlenk flask equipped with a stir bar. The flask was sealed, removed from the glovebox, and heated in an 80 °C oil bath for 20 h. Upon completion, the catalytic mixture was cooled to ambient temperatures and then quenched with 5M HCl (ca. 2 mL) under ambient atmosphere for 1 h. The organic components were extracted with dichloromethane (2 x 25 mL), and the organic layers were washed with H$_2$O, dried with Na$_2$SO$_4$, and filtered. Volatile components were removed under reduced pressure to afford the crude product as a brown oily solid. Crude ^{1}H NMR yields were determined by ^{1}H NMR spectroscopy of the resultant mixed oily products as the ratio of hydroarylation products to unreacted, hydrolyzed starting material.

General Large Scale Hydroarylation Catalysis at Ambient Temperatures: Method E

Inside an N$_2$ glovebox, a mixture of substituted (*N*-aryl)aryl imine (0.4 mmol, 1 equiv, 0.1 M), olefin (0.4 mmol, 1 equiv, 0.1 M), and **Co-Li** (43 mg, 0.04 mmol, 0.01 M, 10 mol%) in toluene (4 mL) was stirred at ambient temperatures for 20 h in a 20 mL scintillation vial equipped with a stir bar. Upon completion, the catalytic mixture was quenched with 5M HCl (ca. 10 mL) under ambient atmosphere for 1 h. The organic components were extracted with dichloromethane (2 x 50 mL), and the organic layers were washed with H$_2$O, dried with Na$_2$SO$_4$, and filtered. Volatile components were removed under reduced pressure to afford the crude product as a brown oily solid. Crude ^{1}H NMR yields were determined by ^{1}H NMR spectroscopy of the resultant mixed oily products as the ratio of hydroarylation products to unreacted, hydrolyzed starting material. Purification details are given below for each compound.

General Large Scale Hydroarylation Catalysis at 80 °C: Method F

Inside an N$_2$ glovebox, a mixture of substituted (*N*-aryl)aryl imine (0.4 mmol, 1 equiv, 0.1 M), olefin (0.04 mmol, 1 equiv, 0.1 M), and **Co-Li** (43 mg, 0.04 mmol, 0.01 M, 10 mol%) in toluene (4 mL) was added to a 100 mL Teflon stoppered Schlenk flask equipped with a stir bar. The flask was sealed, removed from the

glovebox, and heated in an 80 °C oil bath for 20 h. Upon completion, the catalytic mixture was cooled to ambient temperatures and then quenched with 5M HCl (ca. 10 mL) under ambient atmosphere for 1 h. The organic components were extracted with dichloromethane (2 x 50 mL), and the organic layers were washed with H_2O, dried with Na_2SO_4, and filtered. Volatile components were removed under reduced pressure to afford the crude product as a brown oily solid. Crude ^{1}H NMR yields were determined by ^{1}H NMR spectroscopy of the resultant mixed oily products as the ratio of hydroarylation products to unreacted, hydrolyzed starting material. Purification details are given below for each compound.

Characterization Data for Hydroarylation Products 3 and 4
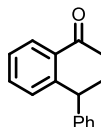
Synthesis of 1-(2-(1-phenylethyl)phenyl)ethan-1-one (3Aa)

For small-scale catalysis, **Method C** (25 °C) was employed with imine **1A** (23 mg) and styrene (12 µL) to afford a ^{1}H NMR yield of 83%.
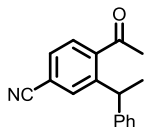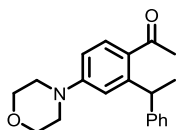
For large-scale catalysis, **Method F** (80 °C) was employed with imine **1A** (90 mg) and styrene (45 µL). Purified by SiO_2 column chromatography (2% EtOAc/hexanes) to afford the title compound as a yellow oil (53% ^{1}H NMR yield, 35 mg isolated, 39% isolated yield).

^{1}H NMR (chloroform-d, 600.13 MHz): δ 7.47 (dd, J = 7.7, 1.0 Hz, 1H), 7.39 (obs td, J = 7.5, 0.7 Hz, 1H), 7.34 (obs dt, J = 7.5, 0.7 Hz, 1H), 7.29 – 7.22 (m, 3H overlapping residual CHCl₃), 7.20 – 7.12 (m, 3H), 4.87 (q, J = 7.1 Hz, 1H, **CH**Ar₂CH₃), 2.36 (s, 3H, COCH₃), 1.61 (d, J = 7.2 Hz, 3H, CHAr₂CH₃).

¹³C{¹H} NMR (chloroform-d, 150.92 MHz): δ 204.0, 146.3, 145.3, 139.5, 131.0, 128.5, 128.4, 128.2, 127.8, 126.0, 125.8, 39.7, 30.5, 22.1.

HRMS (EI) *m/z*: [M]⁺ Calcd for $C_{16}H_{16}O$ 224.1201. Found 224.1199.
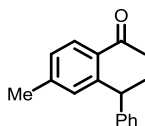
Synthesis of 1-(4-methyl-2-(1-phenylethyl)phenyl)ethan-1-one (3Ba)

For small-scale catalysis, **Method C** (25 °C) was employed with imine **1B** (24 mg) and styrene (12 µL) to afford a ^{1}H NMR yield of 62%.

For large-scale catalysis, **Method F** (80 °C) was employed with imine **1B** (96 mg) and styrene (45 µL). Purified by SiO_2 column chromatography (2.5% EtOAc/hexanes) to afford the title compound as a colorless oil (46% ^{1}H NMR yield, 33 mg isolated, 35% isolated yield).

^{1}H NMR (chloroform-*d*, 600.13 MHz): δ 7.44 (d, *J* = 7.9 Hz, 1H, 6-Ar**H**), 7.28 – 7.22 (m, 2H overlapping residual CHCl$_3$, Ph), 7.20 – 7.13 (m, 3H, Ph), 7.12 (d, *J* = 0.9 Hz, 1H, 3-Ar**H**), 7.05 (dd, *J* = 7.9, 0.9 Hz, 1H, 5-Ar**H**), 4.96 (q, *J* = 7.2 Hz, 1H, C**H**Ar$_2$CH$_3$), 2.39 (s, 3H, COC**H$_3$**), 1.59 (d, *J* = 7.2 Hz, 3H, CHAr$_2$C**H$_3$**).

^{13}C{^{1}H} NMR (chloroform-*d*, 150.92 MHz): δ 203.2, 146.5, 145.9, 141.5, 136.3, 129.4, 128.6, 128.3, 128.2, 126.5, 125.9, 39.4, 30.3, 22.1, 21.8.

HRMS (EI) *m/z*: [M]$^+$ Calcd for C$_{17}$H$_{18}$O 238.1358. Found 238.1360.
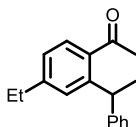
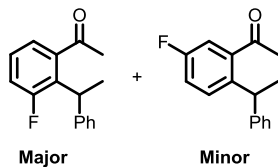### Synthesis of 1-(4-ethyl-2-(1-phenylethyl)phenyl)ethan-1-one (3Ca)

For small-scale catalysis, **Method C** (25 °C) was employed with imine **1C** (25 mg) and styrene (12 µL) to afford a ^{1}H NMR yield of 81%.

For large-scale catalysis, **Method F** (80 °C) was employed with imine **1C** (100 mg) and styrene (45 µL). Purified by SiO$_2$ column chromatography (gradient from 1% to 2.5% EtOAc/hexanes) to afford the title compound as a colorless oil (39% ^{1}H NMR yield, 26 mg isolated, 26% isolated yield).

^{1}H NMR (chloroform-*d*, 600.13 MHz): δ 7.45 (d, *J* = 7.9 Hz, 1H, 6-Ar**H**), 7.27 – 7.21 (m, 2H, overlapping residual CHCl$_3$, Ph), 7.21 – 7.11 (m, 4H), 7.07 (d, *J* = 7.9 Hz, 1H, 5-Ar**H**), 4.96 (q, *J* = 7.1, 1H, C**H**Ar$_2$CH$_3$), 2.62 (q, *J* = 7.6 Hz, 2H, C**H$_2$**CH$_3$), 2.37 (s, 3H, COC**H$_3$**), 1.60 (d, *J* = 7.2 Hz, 3H, CHAr$_2$C**H$_3$**), 1.20 (t, *J* = 7.6 Hz, 3H, CH$_2$C**H$_3$**).

^{13}C{^{1}H} NMR (chloroform-*d*, 150.92 MHz): 203.3, 147.7, 146.5, 145.8, 136.6, 128.6, 128.3, 128.2, 128.2, 125.9, 125.2, 39.5, 30.3, 29.0, 22.2, 15.4.

HRMS (EI) *m/z*: [M]$^+$ Calcd for C$_{18}$H$_{20}$O 252.1514. Found 252.1516.
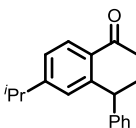
Synthesis of 1-(4-isopropyl-2-(1-phenylethyl)phenyl)ethan-1-one (3Da)

For small-scale catalysis, **Method D** (80 °C) was employed with imine **1D** (27 mg) and styrene (12 µL) to afford a ^{1}H NMR yield of 29%.
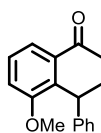
For large-scale catalysis, **Method E** (25 °C) was employed with imine **1D** (107 mg) and styrene (45 µL). Purified by SiO$_2$ column chromatography (2% EtOAc/hexanes) to afford the title compound as a colorless oil (72% ^{1}H NMR yield, 58 mg isolated, 55% isolated yield).

^{1}H NMR (chloroform-*d*, 600.13 MHz): δ 7.47 (d, *J* = 7.9 Hz, 1H, 6-Ar**H**), 7.28 – 7.23 (m, 2H overlapping residual CHCl₃, Ph), 7.19 (d, *J* = 1.6 Hz, 1H, 3-Ar**H**), 7.18 – 7.13 (m, 3H, Ph), 7.11 (dd, *J* = 8.0, 1.7 Hz, 1H, 5-Ar**H**), 4.96 (q, *J* = 7.2 Hz, 1H, C**H**Ar₂CH₃), 2.89 (hept, *J* = 6.9 Hz, 1H, ^{i}Pr), 2.37 (s, 3H, COC**H₃**), 1.61 (d, *J* = 7.2 Hz, 3H, CHAr₂C**H₃**), 1.23 (d, *J* = 6.9 Hz, 3H, ^{i}Pr), 1.22 (d, *J* = 6.8 Hz, 3H, ^{i}Pr).

^{13}C{^{1}H} NMR (chloroform-*d*, 150.92 MHz): δ 203.1, 152.1, 146.4, 145.6, 136.6, 128.5, 128.1, 128.0, 126.8, 125.8, 123.4, 39.5, 34.2, 30.2, 23.8, 23.7, 22.1.

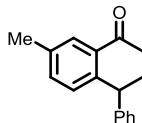HRMS (EI) *m/z*: [M]⁺ Calcd for C₁₉H₂₂O 266.1671. Found 266.1672.
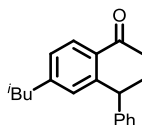
Synthesis of 1-(4-isobutyl-2-(1-phenylethyl)phenyl)ethan-1-one (3Ea)

For small-scale catalysis, **Method D** (80 °C) was employed with imine **1E** (28 mg) and styrene (12 µL) to afford a ^{1}H NMR yield of 24%.

For large-scale catalysis, **Method E** (25 °C) was employed with imine **1E** (112 mg) and styrene (45 µL). Purified by SiO₂ column chromatography (1.5% EtOAc/hexanes) to afford the title compound as a pale-yellow oil (74% ^{1}H NMR yield, 60 mg isolated, 54% isolated yield).

^{1}H NMR (chloroform-*d*, 600.13 MHz): δ 7.45 (d, *J* = 7.8 Hz, 1H, 6-Ar**H**), 7.26 – 7.22 (m, 2H, Ph), 7.19 – 7.12 (m, 3H, Ph), 7.10 (d, *J* = 1.4 Hz, 1H, 3-Ar**H**), 7.02 (dd, *J* = 7.9, 1.6 Hz, 1H, 5-Ar**H**), 4.96 (q, *J* = 7.1 Hz, 1H, C**H**Ar₂CH₃), 2.52 – 2.41 (m, 2H, ^{i}Bu), 2.38 (s, 3H, COC**H₃**), 1.89 – 1.77 (m, 1H, ^{i}Bu), 1.60 (d, *J* = 7.2 Hz, 3H, CHAr₂C**H₃**), 0.88 (d, *J* = 6.6 Hz, 3H, ^{i}Bu), 0.86 (d, *J* = 6.6 Hz, 3H, ^{i}Bu).

^{13}C{^{1}H} NMR (chloroform-*d*, 150.92 MHz): δ 203.3, 146.6, 145.6, 145.2, 136.6, 129.5, 128.4, 128.3, 128.1, 126.5, 125.9, 45.5, 39.5, 30.3, 30.2, 22.5, 22.4, 22.2.

HRMS (EI) *m/z*: [M]⁺ Calcd for C₂₀H₂₄O 280.1827. Found 280.1831.
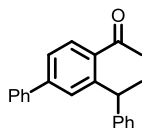
Synthesis of 1-(3-(1-phenylethyl)-[1,1'-biphenyl]-4-yl)ethan-1-one (3Fa)
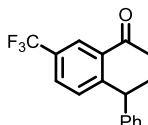
For small-scale catalysis, **Method C** (25 °C) was employed with imine **1F** (30 mg) and styrene (12 µL) to afford a ^{1}H NMR yield of 77%.

For large-scale catalysis, **Method F** (80 °C) was employed with imine **1F** (120 mg) and styrene (45 µL).

Purified by SiO₂ column chromatography (gradient from 1% to 2% EtOAc/hexanes) to afford the title compound as a pale-yellow oil (83% ^{1}H NMR yield, 79 mg isolated, 66% isolated yield).

^{1}H NMR (chloroform-*d*, 600.13 MHz): δ 7.59 (d, *J* = 8.0 Hz, 1H, 6-Ar**H**), 7.56 (d, *J* = 1.6 Hz, 1H, 3-Ar**H**), 7.55 – 7.52 (m, 2H, Ph), 7.47 (dd, *J* = 8.0, 1.7 Hz, 1H, 5-Ar**H**), 7.46 – 7.42 (m, 2H, Ph), 7.40 – 7. 35 (m, 1H, Ph), 7.28 – 7.24 (m, 2H overlapping residual CHCl$_3$, Ph), 7.23 – 7.20 (m, 2H, Ph), 7.19 – 7.13 (m, 1H, Ph), 5.00 (q, *J* = 7.1 Hz, 1H, C**H**Ar$_2$CH$_3$), 2.42 (s, 3H, COC**H$_3$**), 1.67 (d, *J* = 7.2 Hz, 3H, CHAr$_2$C**H$_3$**).

^{13}C{^{1}H} NMR (chloroform-*d*, 150.92 MHz): δ 203.3, 146.3, 146.2, 143.8, 140.5, 137.9, 129.0, 128.8, 128.4, 128.2, 128.1, 127.4, 127.4, 126.1, 124.5, 39.7, 30.4, 22.2.

HRMS (EI) *m/z*: [M]$^+$ Calcd for C$_{22}$H$_{20}$O 300.1514. Found 300.1511.
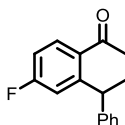
Synthesis of 1-(4-fluoro-2-(1-phenylethyl)phenyl)ethan-1-one (3Ga)

For small-scale catalysis, **Method C** (25 °C) was employed with imine **1G** (24 mg) and styrene (12 µL) to afford a ^{1}H NMR yield of 89%.

For large-scale catalysis, **Method F** (80 °C) was employed with imine **1G** (97 mg) and styrene (45 µL).

Purified by SiO$_2$ column chromatography (gradient from 2% to 3% EtOAc/hexanes) to afford the title compound as a pale-yellow oil (72% ^{1}H NMR yield, 53 mg isolated, 55% isolated yield).

^{1}H NMR (chloroform-*d*, 600.13 MHz): δ 7.55 (dd, *J*$_{HF}$ = 5.9 Hz, *J*$_{HH}$ = 8.4 Hz, 1H, 6-Ar**H**), 7.31 – 7.24 (m, 2H overlapping residual CHCl$_3$, Ph), 7.20 – 7.14 (m, 3H, Ph), 7.02 (dd, *J*$_{HF}$ = 10.2 Hz, *J*$_{HH}$ = 2.4 Hz, 1H, 3-Ar**H**), 6.93 (ddd, *J*$_{HF}$ = 7.8 Hz, *J*$_{HH}$ = 8.2, 2.5 Hz, 1H, 5-Ar**H**), 4.99 (q, *J*$_{HH}$ = 7.2 Hz, 1H, C**H**Ar$_2$CH$_3$), 2.39 (s, 3H, COC**H$_3$**), 1.59 (d, *J*$_{HH}$ = 7.1 Hz, 3H, CHAr$_2$C**H$_3$**).

^{13}C{^{1}H} NMR (chloroform-*d*, 150.92 MHz): δ 201.9, 164.1 (d, $^1J_{CF}$ = 251.8 Hz), 149.5 (d, $^3J_{CF}$ = 7.4 Hz), 145.4, 135.0 (d, $^4J_{CF}$ = 3.2 Hz), 130.5 (d, $^3J_{CF}$ = 9.1 Hz), 128.4, 128.0, 125.2, 115.7 (d, $^2J_{CF}$ = 22.0 Hz), 112.6 (d, $^2J_{CF}$ = 21.6 Hz), 39.5, 30.2, 21.8.

^{19}F NMR (chloroform-*d*, 564.63 MHz): δ -107.73 (m).

HRMS (EI) *m/z*: [M]$^+$ Calcd for C$_{16}$H$_{15}$FO 242.1107. Found 242.1105.
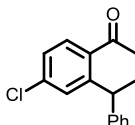
Synthesis of 1-(4-chloro-2-(1-phenylethyl)phenyl)ethan-1-one (3Ha)

For small-scale catalysis, **Method C** (25 °C) was employed with imine **1H** (26 mg) and styrene (12 µL) to afford a ^{1}H NMR yield of 40%.

For large-scale catalysis, **Method F** (80 °C) was employed with imine **1H** (104 mg) and styrene (45 µL).

Purified by SiO$_2$ column chromatography (gradient from 1% to 2% EtOAc/hexanes) to afford the title compound as a colorless oil (16% ^{1}H NMR yield, 10 mg isolated, 10% isolated yield).

^{1}H NMR (chloroform-d, 600.13 MHz): δ 7.43 (d, J = 8.3 Hz, 1H, 6-Ar**H**), 7.31 (d, J = 1.9 Hz, 1H, 3-Ar**H**), 7.29 – 7.25 (m, 2H overlapping residual CHCl$_3$, Ph), 7.23 (dd, J =8.2, 1.9 Hz, 1H, 5-Ar**H**) 7.19 – 7.16 (m, 1H, Ph), 7.15 – 7.12 (m, 2H, Ph), 4.88 (d, J = 7.2 Hz, 1H, C**H**Ar$_2$CH$_3$), 2.33 (s, 3H, COC**H$_3$**), 1.59 (d, J = 7.2 Hz, 3H, CHAr$_2$C**H$_3$**).

^{13}C{^{1}H} NMR (chloroform-d, 150.92 MHz): δ 202.6, 147.8, 145.5, 137.6, 137.2, 129.4, 128.8, 128.5, 128.2, 126.4, 126.1, 39.6, 30.4, 22.0.

HRMS (EI) m/z: [M]$^+$ Calcd for C$_{16}$H$_{15}$ClO 258.0811. Found 258.0808.
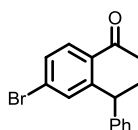
Attempted Synthesis of 1-(4-bromo-2-(1-phenylethyl)phenyl)ethan-1-one (3Ia)

For small-scale catalysis, **Method C** (25 °C) was employed with imine **1I** (30 mg) and styrene (12 µL) to afford a ^{1}H NMR yield of 0%.

For large-scale catalysis, **Method F** (80 °C) was employed with imine **1I** (121 mg) and styrene (45 µL). By ^{1}H NMR spectroscopy of the crude mixture after acidic work up, resonances corresponding to the methine and methyl of the phenylethyl fragment were not observed (0% ^{1}H NMR yield).
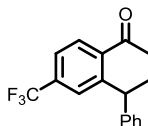
Synthesis of 1-(2-(1-phenylethyl)-4-(trifluoromethyl)phenyl)ethan-1-one (3Ja)

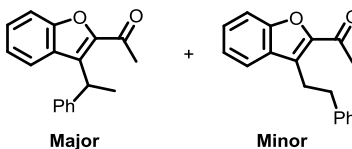For small-scale catalysis, **Method C** (25 °C) was employed with imine **1J** (29 mg) and styrene (12 µL) to afford a ^{1}H NMR yield of 50%.

For large-scale catalysis, **Method F** (80 °C) was employed with imine **1J** (117 mg) and styrene (45 µL).

Purified by SiO$_2$ column chromatography (2% EtOAc/hexanes) to afford the title compound as a colorless oil (92% ^{1}H NMR yield, 80 mg isolated, 69% isolated yield).

^{1}H NMR (chloroform-d, 600.13 MHz): δ 7.62 (s, 1H), 7.54 – 7.45 (m, 2H), 7.30 – 7.24 (m, 2H overlapping residual CHCl$_3$), 7.21 – 7.15 (m, 1H), 7.13 – 7.07 (m, 2H), 4.78 (q, J_{HH} = 7.2 Hz, 1H, C**H**Ar$_2$CH$_3$), 2.26 (s, 3H, COC**H$_3$**), 1.64 (d, J_{HH} = 7.2 Hz, 3H, CHAr$_2$C**H$_3$**).

^{13}C{^{1}H} NMR (chloroform-d, 150.92 MHz): δ 203.5, 145.6, 145.3, 143.3, 132.4 (q, $^{2}J_{CF}$ = 32.4 Hz), 128.6, 128.2, 127.4, 126.5, 125.0 (q, $^{3}J_{CF}$ = 3.7 Hz), 124.4 (q, $^{1}J_{CF}$ = 269.0 Hz), 123.0 (q, $^{3}J_{CF}$ = 3.7 Hz), 40.0, 30.5, 22.0.

^{19}F NMR (chloroform-d, 564.63 MHz): δ -62.92 (s).

HRMS (EI) m/z: [M]$^{+}$ Calcd for C$_{18}$H$_{20}$F$_{3}$O 292.1075. Found 292.1073.
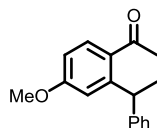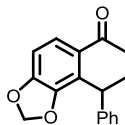

Synthesis of 1-(4-methoxy-2-(1-phenylethyl)phenyl)ethan-1-one (3Ka)

For small-scale catalysis, **Method C** (25 °C) was employed with imine **1K** (26 mg) and styrene (12 µL) to afford a ^{1}H NMR yield of 83%.

For large-scale catalysis, **Method F** (80 °C) was employed with imine **1K** (100 mg) and styrene (45 µL).

Purified by SiO$_{2}$ column chromatography (gradient from 2% to 5% EtOAc/hexanes) to afford the title compound as a pale-yellow oil (66% ^{1}H NMR yield, 52 mg isolated, 56% isolated yield).

^{1}H NMR (chloroform-d, 600.13 MHz): δ 7.63 (d, J = 8.6 Hz, 1H, 6-Ar**H**), 7.31 – 7.22 (m, 2H overlapping residual CHCl$_{3}$, Ph), 7.22 – 7.19 (m, 2H, Ph), 7.18 – 7.11 (m, 1H, Ph), 6.83 (d, J = 2.5 Hz, 1H, 3-Ar**H**), 6.74 (dd, J = 8.6, 2.6 Hz, 1H, 5-Ar**H**), 5.17 (q, J = 7.1 Hz, 1H, C**H**Ar$_{2}$CH$_{3}$), 3.79 (s, 3H, OC**H$_{3}$**), 2.44 (s, 3H, COC**H$_{3}$**), 1.59 (d, J = 7.1 Hz, 3H, CHAr$_{2}$C**H$_{3}$**).

^{13}C{^{1}H} NMR (chloroform-d, 150.92 MHz): δ 201.3, 161.9, 149.5, 146.3, 131.6, 130.9, 128.3, 128.1, 126.0, 115.3, 110.0, 55.4, 39.5, 30.0, 22.1.

HRMS (EI) m/z: [M]$^{+}$ Calcd for C$_{17}$H$_{18}$O$_{2}$ 254.1307. Found 254.1305.
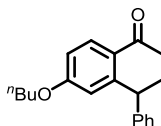
Synthesis of 1-(4-n-butoxy-2-(1-phenylethyl)phenyl)ethan-1-one (3La)

For small-scale catalysis, **Method D** (80 °C) was employed with imine **1L** (30 mg) and styrene (12 µL) to afford a ^{1}H NMR yield of 16%.

For large-scale catalysis, **Method E** (25 °C) was employed with imine **1L** (119 mg) and styrene (45 µL). Purified by SiO$_{2}$ column chromatography (4% EtOAc/hexanes) to afford the title compound as a pale-yellow oil (51% ^{1}H NMR yield, 55 mg isolated, 46% isolated yield).

^{1}H NMR (chloroform-d, 600.13 MHz): δ 7.61 (d, J = 8.6 Hz, 1H, 6-Ar**H**), 7.26 – 7.23 (m, 2H overlapping residual CHCl$_3$, Ph), 7.22 – 7.18 (m, 2H, Ph), 7.17 – 7.13 (m, 1H, Ph), 6.81 (d, J = 2.6 Hz, 1H, 3-Ar**H**), 6.72 (dd, J = 8.6, 2.6 Hz, 1H, 5-Ar**H**), 5.17 (q, J = 7.1 Hz, 1H, C**H**Ar$_2$CH$_3$), 3.98 – 3.89 (m, 2H, ^{n}BuO), 2.43 (s, 3H, COC**H$_3$**), 1.81 – 1.67 (m, 2H, ^{n}BuO), 1.58 (d, J = 7.1 Hz, 3H, CHAr$_2$C**H$_3$**), 1.51 – 1.42 (m, 2H, ^{n}BuO), 0.96 (t, J = 7.4 Hz, 3H ^{n}BuO).

^{13}C{^{1}H} NMR (chloroform-d, 150.92 MHz): δ 200.0, 160.4, 148.3, 145.2, 130.5, 129.5, 127.1, 127.0, 124.8, 114.5, 109.4, 66.7, 38.3, 30.1, 28.8, 20.9, 18.2, 12.8.

HRMS (EI) m/z: [M]$^+$ Calcd for C$_{20}$H$_{24}$O$_2$ 296.1776. Found 296.1778.
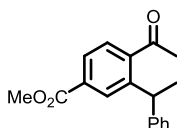
Synthesis of methyl 4-acetyl-3-(1-phenylethyl)benzoate (3Ma)

For small-scale catalysis, **Method C** (25 °C) was employed with imine **1M** (28 mg) and styrene (12 μL) to afford a quantitative ^{1}H NMR yield.

For large-scale catalysis, **Method F** (80 °C) was employed with imine **1M** (113 mg) and styrene (45 μL).

Purified by SiO$_2$ column chromatography (gradient from 5% to 7.5% EtOAc/hexanes) to afford the title compound as a colorless oil (92% ^{1}H NMR yield, 87 mg isolated, 77% isolated yield).

^{1}H NMR (chloroform-d, 600.13 MHz): δ 8.08 (d, J = 1.3 Hz, 1H, 2-Ar**H**), 7.92 (dd, J = 8.0, 1.6 Hz, 1H, 6-Ar**H**), 7.44 (d, J = 8.0, 1H, 5-Ar**H**), 7.28 – 7.23 (m, 2H overlapping residual CHCl$_3$, Ph), 7.18 – 7.15 (m, 1H, Ph), 7.14 – 7.09 (m, 2H, Ph), 4.75 (d, J = 7.2 Hz, 1H, C**H**Ar$_2$CH$_3$), 3.93 (s, 3H, CO$_2$C**H$_3$**), 2.25 (s, 3H, COC**H$_3$**), 1.65 (d, J = 7.2 Hz, 3H, CHAr$_2$C**H$_3$**).

^{13}C{^{1}H} NMR (chloroform-d, 150.92 MHz): δ 204.1, 166.6, 145.7, 144.8, 144.1, 131.9, 129.3, 128.5, 128.2, 127.3, 127.0, 126.3, 52.5, 40.0, 30.6, 22.1.

HRMS (EI) m/z: [M]$^+$ Calcd for C$_{18}$H$_{18}$O$_3$ 282.1256. Found 282.1253.

Synthesis of 4-acetyl-3-(1-phenylethyl)benzonitrile (3Na)

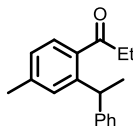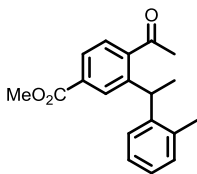For small-scale catalysis, **Method C** (25 °C) was employed with imine **1N** (25 mg) and styrene (12 μL) to afford a ^{1}H NMR yield of 0%.

For large-scale catalysis, **Method F** (80 °C) was employed with imine **1N** (100 mg) and styrene (45 μL).

Purified by SiO$_2$ column chromatography (gradient from 2% to 6% to 10% EtOAc/hexanes) to afford the title compound as a colorless oil (12% ^{1}H NMR yield, 8 mg isolated, 8% isolated yield).

^{1}H NMR (chloroform-d, 600.13 MHz): δ 7.63 (d, J = 1.2 Hz, 1H, 2-Ar**H**), 7.56 (dd, J = 7.9, 1.3 Hz, 1H, 6-Ar**H**), 7.46 (d, J = 7.9 Hz, 1H, 5-Ar**H**), 7.31 – 7.27 (m, 2H, Ph), 7.24 – 7.16 (m, 1H, Ph), 7.13 – 7.05 (m, 2H, Ph), 4.73 (q, J = 7.2 Hz, 1H, C**H**Ar$_2$CH$_3$), 2.27 (s, 3H, COC**H$_3$**), 1.62 (d, J = 7.2 Hz, 3H, CHAr$_2$C**H$_3$**).

^{13}C{^{1}H} NMR (chloroform-d, 150.92 MHz): δ 202.8, 146.0, 144.6, 143.7, 131.9, 129.6, 128.6, 128.1, 127.3, 126.6, 118.3, 114.2, 39.7, 30.3, 21.7.

HRMS (EI) m/z: [M]$^+$ Calcd for C$_{17}$H$_{15}$NO 249.1154. Found 249.1154.

Synthesis of 1-(4-morpholino-2-(1-phenylethyl)phenyl)ethan-1-one (3Oa)

For small-scale catalysis, **Method D** (80 °C) was employed with imine **1O** (31 mg) and styrene (12 µL) to afford a ^{1}H NMR yield of 7%.

For large-scale catalysis, **Method E** (25 °C) was employed with imine **1O** (124 mg) and styrene (45 µL). Purified by SiO$_2$ column chromatography (gradient from 10% to 20% EtOAc/hexanes) to afford the title compound as a colorless oil (19% ^{1}H NMR yield, 15 mg isolated, 12% isolated yield).

^{1}H NMR (chloroform-d, 600.13 MHz): δ 7.64 (d, J = 8.7 Hz, 1H, 6'-Ar**H**), 7.28 – 7.23 (m, 2H overlapping residual CHCl$_3$, Ph), 7.21 – 7.19 (m, 2H, Ph), 7.17 – 7.11 (m, 1H, Ph), 6.72 (dd, J = 8.7, 2.5 Hz, 1H, 5'-Ar**H**), 6.72 (d, J = 2.4 Hz, 1H, 3'-Ar**H**), 5.28 (q, J = 7.2 Hz, 1H, C**H**Ar$_2$CH$_3$), 3.89 – 3.70 (m, 4H, morph), 3.22 – 3.12 (m, 4H, morph), 2.46 (s, 3H, COC**H$_3$**), 1.58 (d, J = 7.1 Hz, 3H, CHAr$_2$C**H$_3$**).

^{13}C{^{1}H} NMR (chloroform-d, 150.92 MHz): δ 200.4, 153.1, 149.5, 146.5, 132.0, 128.4, 128.3, 128.1, 125.9, 114.8, 110.9, 66.7, 47.8, 39.6, 29.7, 22.1.

HRMS (EI) m/z: [M]$^+$ Calcd for C$_{20}$H$_{23}$NO$_2$ 309.1729. Found 309.1728.

Major   Minor

Synthesis of 1-(3-fluoro-2-(1-phenylethyl)phenyl)ethan-1-one (3Pa, major) and 1-(5-fluoro-2-(1-phenylethyl)phenyl)ethan-1-one (3Pa', minor)

For small-scale catalysis, **Method D** (80 °C) was employed with imine **1P** (24 mg) and styrene (12 µL) to afford a ^{1}H NMR yield of 38%.

For large-scale catalysis, **Method E** (25 °C) was employed with imine **1P** (97 mg) and styrene (45 µL). Purified by SiO$_2$ column chromatography (5% EtOAc/hexanes) to afford the title compounds as a colorless oil (89% ^{1}H NMR yield, 65 mg isolated, 67% isolated yield) in a ratio of ~20:1. The two isomers were inseparable by SiO$_2$ column chromatography.

^{1}H NMR (chloroform-*d*, 600.13 MHz): δ 7.30 − 7.15 (m, 7H overlapping residual CHCl$_3$, **major** and **minor**), 7.06 (ddd, $^2J_{HF}$ = 11.1 Hz, J_{HH} = 8.0, 1.5 Hz, 1H, 4'-Ar**H, major**), 4.79 (q, J_{HH} = 7.2 Hz, 0.05H, C**H**Ar$_2$CH$_3$, **minor**), 4.69 (br q, J_{HH} = 7.2 Hz, 1H, C**H**Ar$_2$CH$_3$, **major**), 2.38 (s, 3H, COC**H$_3$**, **major**), 2.33 (s, 0.13H, COC**H$_3$**, **minor**), 1.74 (dd, J_{HH} = 7.2 Hz, J_{HF} = 1.3 Hz, 3H, CHAr$_2$C**H$_3$**, **major**), 1.59 (d, J_{HH} = 7.2 Hz, 0.17H, CHAr$_2$C**H$_3$**, **minor**).

^{13}C{^{1}H} NMR (chloroform-*d*, 150.92 MHz, **major**): δ 203.3 (d, $^4J_{CF}$ = 2.6 Hz), 161.9 (d, $^1J_{CF}$ = 249.7 Hz), 143.9, 142.5 (d, $^3J_{CF}$ = 4.2 Hz), 132.1 (d, $^2J_{CF}$ = 13.6 Hz), 128.0, 127.6 (d, $^3J_{CF}$ = 9.0 Hz) 127.6 (d, $^4J_{CF}$ = 1.6 Hz), 125.9, 122.7 (d, $^4J_{CF}$ = 3.4 Hz), 118.3 (d, $^2J_{CF}$ = 23.6 Hz), 36.6 (d, $^4J_{CF}$ = 1.1 Hz), 30.8, 18.6 (d, $^3J_{CF}$ = 3.8 Hz).

^{19}F NMR (chloroform-*d*, 564.63 MHz): δ -111.01 − -111.18 (m, 19.7F, **major**), -111.90 − -112.00 (m, 1F, **minor**).

HRMS (EI) *m/z*: [M]$^+$ Calcd for C$_{16}$H$_{15}$FO 242.1107. Found 242.1109.

Synthesis of 1-(3-methoxy-2-(1-phenylethyl)phenyl)ethan-1-one (3Qa)

For small-scale catalysis, **Method D** (80 °C) was employed with imine **1Q** (26 mg) and styrene (12 µL) to afford a ^{1}H NMR yield of 3%.

For large-scale catalysis, **Method E** (25 °C) was employed with imine **1Q** (102 mg) and styrene (45 µL). Purified by SiO$_2$ column chromatography (5% EtOAc/hexanes) to afford the title compound as a colorless oil (7% ^{1}H NMR yield, 4 mg isolated, 4% isolated yield). The acquired ^{1}H NMR spectra is consistent with previously reported spectral data. Given the low yield of the reaction, ^{13}C NMR spectra nor HRMS were acquired.

¹H NMR (chloroform-*d*, 600.13 MHz): δ 7.25 – 7.18 (m, 5H, Ph), 7.14 – 7. 10 (m, 1H), 6.94 – 6.89 (m, 2H), 4.64 (q, *J* = 7.2 Hz, 1H, C**H**Ar₂CH₃), 3.64 (s, 3H, OMe), 2.21 (s, 3H, COC**H₃**), 1.70 (d, *J* = 7.1 Hz, 3H), CHAr₂C**H₃**).

Synthesis of 1-(5-methyl-2-(1-phenylethyl)phenyl)ethan-1-one (3Ra)

For small-scale catalysis, **Method D** (80 °C) was employed with imine **1R** (24 mg) and styrene (12 μL) to afford a ¹H NMR yield of 10%.

For large-scale catalysis, **Method E** (25 °C) was employed with imine **1R** (96 mg) and styrene (45 μL). Purified by SiO₂ column chromatography (5% EtOAc/hexanes) to afford the title compound as a colorless oil (30% ¹H NMR yield, 12 mg isolated, 13% isolated yield).

¹H NMR (chloroform-*d*, 600.13 MHz): δ 7.28 – 7.25 (m, 1H overlapping residual CHCl₃), 7.24 – 7.18 (m, 4H), 7.17 – 7.12 (m, 3H), 4.80 (q, *J* = 7.2 Hz, 1H, C**H**Ar₂CH₃), 2.35 (s, 3H), 2.34 (s, 3H), 1.59 (d, *J* = 7.2 Hz, 3H, CHAr₂C**H₃**).

¹³C{¹H} NMR (chloroform-*d*, 150.92 MHz): δ 204.1, 146.6, 142.2, 139.5, 135.4, 131.7, 128.4, 128.4, 128.3, 128.1, 126.0, 39.4, 30.5, 22.2, 21.1.

HRMS (EI) *m/z*: [M]⁺ Calcd for C₁₇H₁₈O 238.1358. Found 238.1360.

Synthesis of 1-(2-(1-phenylethyl)-5-(trifluoromethyl)phenyl)ethan-1-one (3Sa)

For small-scale catalysis, **Method D** (80 °C) was employed with imine **1S** (29 mg) and styrene (12 μL) to afford a ¹H NMR yield of 33%.

For large-scale catalysis, **Method E** (25 °C) was employed with imine **1S** (117 mg) and styrene (45 μL). Purified by SiO₂ column chromatography (2% EtOAc/hexanes) to afford the title compound as a colorless oil (36% ¹H NMR yield, 16 mg isolated, 14% isolated yield).

¹H NMR (chloroform-*d*, 600.13 MHz): δ 7.70 (d, *J*$_{HH}$ = 1.6 Hz, 1H, 6'-Ar**H**), 7.65 (dd, *J*$_{HH}$ = 8.2, 1.7 Hz, 1H, 4'-Ar**H**), 7.49 (d, *J*$_{HH}$ = 8.2 Hz, 1H, 3'-Ar**H**), 7.32 – 7.27 (m, 2H overlapping residual CHCl₃, Ph), 7.24 – 7.19 (m, 1H, Ph), 7.18 – 7.12 (m, 2H, Ph), 4.89 (q, *J*$_{HH}$ = 7.2 Hz, 1H, C**H**Ar₂CH₃), 2.40 (s, 3H, COC**H₃**), 1.65 (d, *J*$_{HH}$ = 7.2 Hz, 3H, CHAr₂C**H₃**).

$^{13}C\{^1H\}$ NMR (chloroform-*d*, 150.92 MHz): 202.6, 149.3, 145.2, 140.1, 129.2, 128.6, 128.5 (q, $^2J_{CF}$ = 33.9 Hz), 128.2, 127.5 (q, $^3J_{CF}$ = 3.6 Hz), 126.5, 124.3 (q, $^3J_{CF}$ = 3.7 Hz), 122.1 (q, $^1J_{CF}$ = 272.1 Hz), 39.9, 30.4, 21.9.

^{19}F NMR (chloroform-*d*, 564.63 MHz): δ -62.61 (s).

HRMS (EI) *m/z*: [M]$^+$ Calcd for $C_{17}H_{15}F_3O$ 292.1075. Found 292.1075.
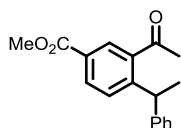
Synthesis of methyl 3-acetyl-4-(1-phenylethyl)benzoate (3Ta)

For small-scale catalysis, **Method D** (80 °C) was employed with imine **1T** (28 mg) and styrene (12 µL) to afford a ^1H NMR yield of 65%.

For large-scale catalysis, **Method E** (25 °C) was employed with imine **1T** (113 mg) and styrene (45 µL). Purified by SiO_2 column chromatography (6% EtOAc/hexanes) to afford the title compound as a colorless oil (97% ^1H NMR yield, 103 mg isolated, 91% isolated yield).

^1H NMR (chloroform-*d*, 600.13 MHz): δ 8.14 (d, *J* = 1.8 Hz, 1H, 2-Ar**H**), 8.03 (dd, *J* = 8.2, 1.9 Hz, 1H, 6-Ar**H**), 7.42 (d, *J* = 8.2 Hz, 1H, 5-Ar**H**), 7.30 – 7.24 (m, 2H, overlapping residual CHCl₃), 7.19 – 7.16 (m, 1H), 7.15 – 7.12 (m, 2H), 4.91 (q, *J* = 7.1 Hz, 1H, C**H**Ar₂CH₃), 3.92 (s, 3H, CO₂C**H₃**), 2.39 (s, 3H, COC**H₃**), 1.62 (d, *J* = 7.1 Hz, 3H, CHAr₂C**H₃**).

$^{13}C\{^1H\}$ NMR (chloroform-*d*, 150.92 MHz): δ 203.0, 166.4, 150.6, 145.5, 139.6, 131.8, 128.9, 128.8, 128.5, 128.2, 127.9, 126.4, 52.4, 39.9, 30.4, 21.9.

HRMS (EI) *m/z*: [M]$^+$ Calcd for $C_{18}H_{18}O_3$ 282.1256. Found 282.1257.
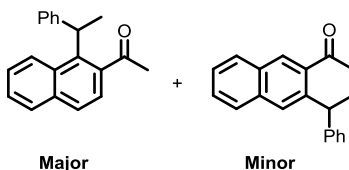
Synthesis of 1-(1-(1-phenylethyl)naphthalen-2-yl)ethan-1-one (3Ua, major) and 1-(3-(1-phenylethyl)naphthalen-2-yl)ethan-1-one (3Ua', minor)

For small-scale catalysis, **Method D** (80 °C) was employed with imine **1U** (28 mg) and styrene (12 µL) to afford a ^1H NMR yield of 7%.
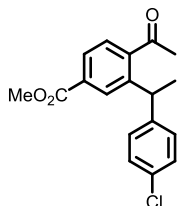
For large-scale catalysis, **Method E** (25 °C) was employed with imine **1U** (110 mg) and styrene (45 µL). Purified by SiO_2 column chromatography (2% EtOAc/hexanes) to afford the title compounds as a colorless

oil (53% ^{1}H NMR yield, 56 mg isolated, 51% isolated yield) in a ratio of ~4.8:1.0. The two isomers were inseparable by SiO_2 column chromatography.

^{1}H NMR (chloroform-d, 600.13 MHz): δ 7.94 − 7.89 (m, 1.2H, **major** and **minor** overlapping), 7.85 − 7.80 (m, 1.6H, **major** and **minor** overlapping), 7.78 (d, J = 8.5 Hz, 1H, naph, **major**), 7.58 − 7.46 (m, 0.5H, **minor**), 7.43 (t, J = 7.5 Hz, 1H, naph, **major**), 7.37 (d, J = 8.5 Hz, 1H, naph, **major**), 7.33 (t, J = 7.8 Hz, 1H, naph, **major**), 7.28 − 7.24 (m, 4H overlapping $CHCl_3$, **major** and **minor** overlapping), 7.23 − 7.08 (m, 2H, **major** and **minor** overlapping), 5.03 (q, J = 7.1 Hz, 1.2H, C**H**Ar$_2$CH$_3$, **major** and **minor** overlapping), 2.36 (s, 3H, COC**H$_3$**, **major**), 2.27 (s, 3H, COC**H$_3$**, **minor**) 1.91 (d, J = 7.3 Hz, 3H, CHAr$_2$C**H$_3$**, **major**), 1.70 (d, J = 7.2 Hz, 0.6H, CHAr$_2$C**H$_3$**, **minor**).

^{13}C{^{1}H} NMR (chloroform-d, 150.92 MHz, **major**): δ 206.4, 144.9, 140.1, 139.9, 134.9, 131.5, 129.0, 128.4, 127.8, 127.5, 126.6, 126.4, 126.3, 125.9, 123.0, 39.2, 31.2, 19.5. ^{13}C{^{1}H} NMR (chloroform-d, 150.92 MHz, **minor**): δ 203.9, 146.7, 141.6, 138.7, 134.3, 131.0, 128.6, 128.3, 128.2, 127.9, 127.8, 126.7, 126.6, 126.5, 126.0, 40.1, 30.2, 22.4.

HRMS (EI) m/z: [M]$^+$ Calcd for $C_{20}H_{18}O$ 274.1358. Found 274.1360.

Major   Minor

Synthesis of 1-(3-(1-phenylethyl)benzofuran-2-yl)ethan-1-one (3Va, major) and 1-(3-phenylethylbenzofuran-2-yl)ethan-1-one (4Va, minor)

For small-scale catalysis, **Method D** (80 °C) was employed with imine **1V** (27 mg) and styrene (12 μL) to afford a ^{1}H NMR yield of 25%.
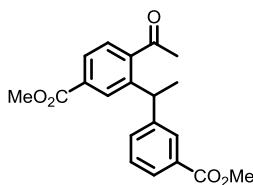
For large-scale catalysis, **Method E** (25 °C) was employed with imine **1V** (106 mg) and styrene (45 μL). Purified by SiO_2 column chromatography (2% EtOAc/hexanes) to afford the title compounds as a colorless oil (24% ^{1}H NMR yield, 22 mg isolated, 21% isolated yield) in a ratio of ~9.8:1.0. The two isomers were inseparable by SiO_2 column chromatography.

^{1}H NMR (chloroform-d, 600.13 MHz): δ 7.50 (dt, J = 8.3, 0.9 Hz, 1H, benzofuranyl, **major**), 7.41 − 7.38 (m, 3H, Ph, **major**), 7.36 (dt, J = 8.1, 1.0 Hz, 1H, benzofuranyl, **major**), 7.31 − 7.27 (m, 2H, Ph, **major**), 7.20 (dt, J = 8.1, 1.0 Hz, 1H, benzofuranyl, **major**), 7.11 (ddd, J = 8.2, 7.1, 1.0 Hz, 1H, benzofuranyl, **major**), 5.49 (q, J = 7.3 Hz, 1H, C**H**Ar$_2$CH$_3$, **major**), 3.41 − 3.35 (m, 0.21H, ArC**H$_2$**CH$_2$Ph, **minor**), 2.98 − 2.92 (m, 0.21H, ArCH$_2$C**H$_2$**Ph, **minor**), 2.68 (s, 3H, COC**H$_3$**, **major**), 2.62 (s, 0.31H, COC**H$_3$**, **minor**), 1.79 (d, J = 7.4 Hz, 3H, CHAr$_2$C**H$_3$**, **major**).

^{13}C{^{1}H} NMR (chloroform-d, 150.92 MHz, **major**): δ 192.0, 154.5, 147.2, 143.6, 132.3, 128.4, 127.8, 127.6, 127.3, 126.4, 123.7, 123.2, 112.4, 34.2, 28.4, 19.2.

HRMS (EI) m/z: [M]$^+$ Calcd for $C_{18}H_{16}O_2$ 264.1150. Found 264.1153.

Synthesis of 1-(4-(1-phenylethyl)benzo[*d*][1,3]dioxol-5-yl)ethan-1-one (3Wa)

For small-scale catalysis, **Method D** (80 °C) was employed with imine **1W** (27 mg) and styrene (12 μL) to afford a ^{1}H NMR yield of 15%.
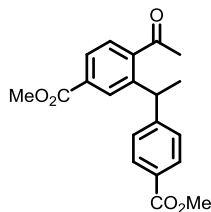
For large-scale catalysis, **Method E** (25 °C) was employed with imine **1W** (108 mg) and styrene (45 μL). Purified by SiO$_2$ column chromatography (6% EtOAc/hexanes) to afford the title compound as a colorless oil (quantitative ^{1}H NMR yield, 82 mg isolated, 75% isolated yield).

^{1}H NMR (chloroform-*d*, 600.13 MHz): δ 7.31 (m, 2H, Ph), 7.28 – 7.23 (m, 2H overlapping CHCl$_3$, Ph), 7.20 (d, *J* = 8.2 Hz, 1H, 6-Ar**H**), 7.18 – 7. 11 (m, 1H, Ph), 6.71 (d, *J* = 8.2 Hz, 1H, 5-Ar**H**), 5.95 (d, *J* = 1.4 Hz, 1H, OC**H**HO), 5.87 (d, *J* = 1.4 Hz, 1H, OCH**H**O), 4.97 (q, *J* = 7.3 Hz, 1 H, C**H**Ar$_2$CH$_3$), 2.47 (s, 3H, COC**H$_3$**), 1.70 (d, *J* = 7.3 Hz, 3H, CHAr$_2$C**H$_3$**).

^{13}C{^{1}H} NMR (chloroform-*d*, 150.92 MHz): δ 201.5, 150.2, 147.0, 144.8, 133.5, 128.4, 128.1, 127.7, 125.9, 124.4, 105.9, 101.3, 36.7, 30.4, 18.6.

HRMS (EI) *m/z*: [M]$^+$ Calcd for C$_{17}$H$_{16}$O$_3$ 268.1099. Found 268.1100.

Synthesis of 1-(4-methyl-2-(1-phenylethyl)phenyl)propan-1-one (3Xa)

For small-scale catalysis, **Method D** (80 °C) was employed with imine **1X** (25 mg) and styrene (12 μL) to afford a ^{1}H NMR yield of 58%.

For large-scale catalysis, **Method E** (25 °C) was employed with imine **1X** (101 mg) and styrene (45 μL). Purified by SiO$_2$ column chromatography (gradient from 1% to 2% EtOAc/hexanes) to afford the title compound as a colorless oil (82% ^{1}H NMR yield, 68 mg isolated, 68% isolated yield).

^{1}H NMR (chloroform-*d*, 600.13 MHz): δ 7.34 (d, *J* = 7.8 Hz, 1H, 6-Ar**H**), 7.29 – 7.22 (m, 2H overlapping residual CHCl$_3$, Ph), 7.18 (s, 1H, 3-Ar**H**), 7.17 – 7.14 (m, 3H), 7.05 (d, *J* = 7.7 Hz, 1H, 5-Ar**H**), 4.81 (q, *J* = 7.1 Hz, 1H, C**H**Ar$_2$CH$_3$), 2.76 (dq, *J* = 17.7, 7.2 Hz, 1H, COC**H$_2$**CH$_3$), 2.51 (dq, *J* = 17.8, 7.3 Hz, 1H, COC**H$_2$**CH$_3$), 2.35 (s, 3H, Me), 1.61 (d, *J* = 7.2 Hz, 3H, CHAr$_2$C**H$_3$**), 1.03 (t, *J* = 7.2 Hz, 3H, COCH$_2$C**H$_3$**).

^{13}C{^{1}H} NMR (chloroform-*d*, 150.92 MHz): δ 206.8, 146.3, 145.1, 140.7, 136.9, 128.9, 128.2, 128.0, 127.3, 126.3, 125.8, 39.5, 35.7, 22.0, 21.6, 8.2.

HRMS (EI) *m/z*: [M]$^+$ Calcd for C$_{18}$H$_{20}$O 252.1514. Found 252.1517.

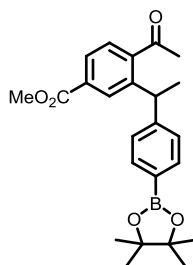**Synthesis of methyl 4-acetyl-3-(1-(*o*-tolyl)ethyl)benzoate (3Mb)**

For large-scale catalysis, **Method E** (25 °C) was employed with imine **1M** (113 mg) and 2-methylstyrene (52 μL). Purified by SiO$_2$ column chromatography (5% EtOAc/hexanes) to afford the title compound as a colorless oil (33% ^{1}H NMR yield, 37 mg isolated, 31% isolated yield).

^{1}H NMR (chloroform-*d*, 600.13 MHz): δ 8.02 (d, *J* = 1.3 Hz, 1H, 2-Ar**H**), 7.92 (dd, *J* = 7.7, 1.2 Hz, 1H, 6-Ar**H**), 7.43 (d, *J* = 7.9 Hz, 1H, 5-Ar**H**), 7.13 – 7.07 (m, 3H), 6.97 – 6.91 (m, 1H), 4.87 (q, *J* = 7.1 Hz, 1H, C**H**Ar$_2$CH$_3$), 3.92 (s, 3H, CO$_2$C**H**$_3$), 2.22 (s, 3H), 2.12 (s, 3H), 1.60 (d, *J* = 7.1 Hz, 3H, CHAr$_2$C**H**$_3$).

^{13}C{^{1}H} NMR (chloroform-*d*, 150.92 MHz): δ 203.8, 166.6, 145.0, 144.3, 144.1, 136.4, 131.7, 130.5, 129.0, 127.5, 127.2, 126.9, 126.5, 126.3, 52.5, 36.7, 29.9, 21.2, 19.5.

HRMS (EI) *m/z*: [M]$^+$ Calcd for C$_{19}$H$_{20}$O$_3$ 296.1412. Found 296.1411.
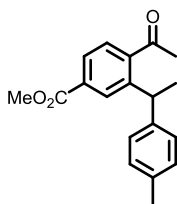
Synthesis of methyl 4-acetyl-3-(1-(*p*-tolyl)ethyl)benzoate (3Mc)

For large-scale catalysis, **Method E** (25 °C) was employed with imine **1M** (113 mg) and 4-methylstyrene (53 μL). Purified by SiO$_2$ column chromatography (6% EtOAc/hexanes) to afford the title compound as a pale yellow oil (quantitative ^{1}H NMR yield, 112 mg isolated, 95% isolated yield).

^{1}H NMR (chloroform-*d*, 600.13 MHz): δ 8.06 (d, *J* = 1.7 Hz, 1H, 2-Ar**H**), 7.91 (dd, *J* = 7.9, 1.7 Hz, 1H, 6-Ar**H**), 7.42 (d, *J* = 7.9 Hz, 1H, 5-Ar**H**), 7.07 – 7.04 (m, 2H), 7.02 – 6.99 (m, 2H), 4.69 (q, *J* = 7.2 Hz, 1H, C**H**Ar$_2$CH$_3$), 3.92 (s, 3H, CO$_2$C**H**$_3$), 2.29 (s, 3H), 2.27 (s, 3H), 1.63 (d, *J* = 7.2 Hz, 3H, CHAr$_2$C**H**$_3$).

^{13}C{^{1}H} NMR (chloroform-*d*, 150.92 MHz): δ 204.1, 166.6, 145.0, 144.1, 142.7, 135.8, 131.8, 129.2, 129.2, 128.1, 127.2, 127.0, 52.5, 39.6, 30.7, 22.1, 21.1.

HRMS (EI) *m/z*: [M]$^+$ Calcd for C$_{19}$H$_{20}$O$_3$ 296.1412. Found 296.1409.
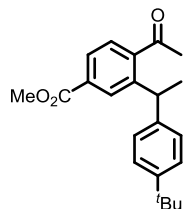
Synthesis of methyl 4-acetyl-3-(1-(4-*tert*-butylphenyl)ethyl)benzoate (3Md)

For large-scale catalysis, **Method E** (25 °C) was employed with imine **1M** (113 mg) and 4-tert-butylstyrene (73 µL). Purified by SiO$_2$ column chromatography (6% EtOAc/hexanes) to afford the title compound as a colorless oil (quantitative ^{1}H NMR yield, 126 mg isolated, 95% isolated yield).

^{1}H NMR (chloroform-*d*, 600.13 MHz): δ 8.08 (d, *J* = 1.3 Hz, 1H, 2-Ar**H**), 7.90 (dd, *J* = 8.0, 1.6 Hz, 1H, 6-Ar**H**), 7.41 (d, *J* = 8.0 Hz, 1H, 5-Ar**H**), 7.29 −7.25 (m, 2H overlapping residual CHCl$_3$), 7.11 − 6.95 (m, 2H), 4.68 (q, *J* = 7.1 Hz, 1H, C**H**Ar$_2$CH$_3$), 3.93 (s, 3H, CO$_2$C**H$_3$**), 2.23 (s, 3H, COC**H$_3$**), 1.64 (d, *J* = 7.2 Hz, 3H, CHAr$_2$C**H$_3$**), 1.28 (s, 9H, ^{t}Bu).

^{13}C{^{1}H} NMR (chloroform-*d*, 150.92 MHz): δ 204.3, 166.6, 149.1, 145.0, 144.3, 142.6, 131.8, 129.3, 127.9, 127.2, 126.8, 125.4, 52.5, 39.5, 34.5, 31.5, 30.6, 22.0.

HRMS (EI) *m/z*: [M]$^+$ Calcd for C$_{22}$H$_{26}$O$_3$ 338.1882. Found 338.1879.
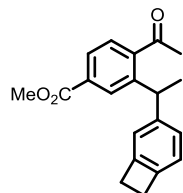
Synthesis of methyl 4-acetyl-3-(1-(bicyclo[4.2.0]octa-1(6),2,4-trien-3-yl)ethyl)benzoate (3Me)

For large-scale catalysis, **Method E** (25 °C) was employed with imine **1M** (113 mg) and 4-vinylbenzocyclobutene (54 µL). Purified by SiO$_2$ column chromatography (gradient from 5% to 10% EtOAc/hexanes) to afford the title compound as a colorless oil (quantitative ^{1}H NMR yield, 119 mg isolated, 97% isolated yield).

^{1}H NMR (chloroform-*d*, 600.13 MHz): δ 8.08 (d, *J* = 1.5 Hz, 1H, 2-Ar**H**), 7.90 (dd, *J* = 8.0, 1.6 Hz, 1H, 6-Ar**H**), 7.42 (d, *J* = 8.0 Hz, 1H, 5-Ar**H**), 7.01 − 6.87 (m, 2H), 6.83 (s, 1H), 4.69 (q, *J* = 7.1 Hz, 1H, C**H**Ar$_2$CH$_3$), 3.93 (s, 3H, CO$_2$C**H$_3$**), 3.10 (s, 4H, ArC$_2$**H$_4$**Ar), 2.27 (s, 3H, COC**H$_3$**), 1.63 (d, *J* = 7.2 Hz, 3H, CHAr$_2$C**H$_3$**).

^{13}C{^{1}H} NMR (chloroform-*d*, 150.92 MHz): δ 204.2, 166.6, 146.0, 145.1, 144.5, 144.2, 143.7, 131.8, 129.2, 127.1, 126.9, 126.9, 122.6, 122.4, 52.5, 40.4, 30.7, 29.5, 29.4, 22.5.

HRMS (EI) *m/z*: [M]$^+$ Calcd for C$_{20}$H$_{20}$O$_3$ 308.1412. Found 308.1410.
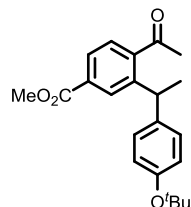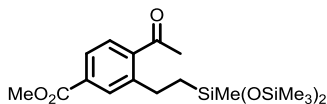
Synthesis of methyl 4-acetyl-3-(1-(4-*tert*-butoxyphenyl)ethyl)benzoate (3Mf)

For large-scale catalysis, **Method F** (80 °C) was employed with imine **1M** (113 mg) and 4-*tert*-butoxystyrene (75 µL). Purified by SiO$_2$ column chromatography (gradient from 2% to 5% to 10% EtOAc/hexanes) to afford the title compound as a colorless oil (65% ^{1}H NMR yield, 64 mg isolated, 46% isolated yield).

^{1}H NMR (chloroform-*d*, 600.13 MHz): δ 8.05 (d, *J* = 1.6 Hz, 1H, 2-Ar**H**), 7.91 (dd, *J* = 7.9, 1.7 Hz, 1H, 6-Ar**H**), 7.39 (d, *J* = 7.9 Hz, 1H, 5-Ar**H**) 7.04 − 6.94 (m, 2H), 6.92 − 6.84 (m, 2H), 4.68 (q, *J* = 7.2 Hz, 1H, C**H**Ar$_2$CH$_3$), 3.92 (s, 3H, CO$_2$C**H$_3$**) 2.18 (s, 3H, COC**H$_3$**), 1.62 (d, *J* = 7.2 Hz, 3H, CHAr$_2$C**H$_3$**), 1.30 (s, 9H, O^t**Bu**).^{13}C{^{1}H} NMR (chloroform-*d*, 150.92 MHz): δ 204.3, 166.6, 153.7, 144.9, 144.4, 140.7, 131.7, 130.0, 129.0, 128.8, 128.3, 127.2, 126.8, 124.2, 78.4, 52.5, 39.4, 30.6, 29.0, 22.1.

HRMS (EI) *m/z*: [M]$^+$ Calcd for C$_{22}$H$_{26}$O$_4$ 354.1831. Found 354.1831.
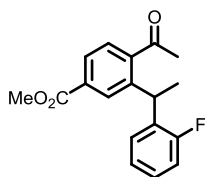
Synthesis of methyl 4-acetyl-3-(1-(2-fluorophenyl)ethyl)benzoate (3Mg)

For large-scale catalysis, **Method E** (25 °C) was employed with imine **1M** (70 mg, 0.25 mmol, 0.1 M, 1 equiv) and 2-fluorostyrene (29 µL, 0.25 mmol, 0.1 M, 1 equiv) in toluene (2.5 mL). Purified by SiO$_2$ column chromatography (5% EtOAc/hexanes) to afford the title compound as a colorless oil (15% ^{1}H NMR yield, 10 mg isolated, 8% isolated yield).

^{1}H NMR (chloroform-*d*, 600.13 MHz): δ 7.99 (d, *J*$_{HH}$ = 1.6 Hz, 1H, 2-Ar**H**), 7.94 (dd, *J*$_{HH}$ = 8.0, 1.6, 1H, 6-Ar**H**), 7.51 (d, *J*$_{HH}$ = 8.0 Hz, 1H, 5-Ar**H**), 7.24 (td, *J* = 7.8, 1.8 Hz, 1H), 7.20 (ddd, *J* = 7.4, 5.4, 1.9 Hz, 1H), 7.12 (td, *J* = 7.5, 1.3 Hz, 1H), 6.96 (ddd, *J* = 10.5, 8.1, 1.3, 1H), 4.95 (q, *J*$_{HH}$ = 7.1 Hz, 1H, C**H**Ar$_2$CH$_3$), 3.93 (s, 3H, CO$_2$C**H$_3$**), 2.43 (s, 3H, COC**H$_3$**), 1.68 (d, *J*$_{HH}$ = 7.2 Hz, 1H, CHAr$_2$C**H$_3$**).

^{13}C{^{1}H} NMR (chloroform-*d*, 150.92 MHz): δ 203.6, 166.5, 160.8 (d, ^{1}*J*$_{CF}$ = 246.3 Hz), 144.0, 143.6, 132.7 (d, ^{3}*J*$_{CF}$ = 14.3 Hz), 132.0, 129.9, 129.5, 128.6 (d, ^{4}*J*$_{CF}$ = 4.3 Hz), 128.2 (d, ^{3}*J*$_{CF}$ = 8.3 Hz), 127.3 (d, ^{2}*J*$_{CF}$ = 21.6 Hz), 124.3 (d, ^{4}*J*$_{CF}$ = 3.5 Hz), 115.4 (d, ^{2}*J*$_{CF}$ = 22.1 Hz), 52.5, 33.8 (d, ^{3}*J*$_{CF}$ = 2.7 Hz), 30.3, 20.8.

^{19}F NMR (chloroform-*d*, 564.63 MHz): δ -116.83 (m).

HRMS (EI) *m/z*: [M]$^+$ Calcd for C$_{18}$H$_{17}$FO$_3$ 300.1162. Found 300.1165.
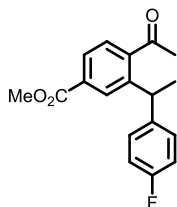
Synthesis of methyl 4-acetyl-3-(1-(4-fluorophenyl)ethyl)benzoate (3Mh)

For large-scale catalysis, **Method E** (25 °C) was employed with imine **1M** (113 mg) and 4-fluorostyrene (48 µL). Purified by SiO$_2$ column chromatography (gradient from 3% to 7% EtOAc/hexanes) to afford the title compound as a pale-yellow oil (80% ^{1}H NMR yield, 80 mg isolated, 67% isolated yield).

^{1}H NMR (chloroform-d, 600.13 MHz): δ 8.03 (d, J_{HH} = 1.5 Hz, 1H, 2-Ar**H**), 7.93 (dd, J_{HH} = 8.0, 1.6 Hz, 1H, 6-Ar**H**), 7.47 (d, J_{HH} = 8.0 Hz, 1H, 5-Ar**H**), 7.11 − 7.06 (m, 2H), 6.97 − 6.91 (m, 2H), 4.76 (q, J_{HH} = 7.6 Hz, 1H, C**H**Ar$_2$CH$_3$), 3.93 (s, 3H, CO$_2$C**H$_3$**), 2.30 (s, 3H, COC**H$_3$**), 1.62 (d, J_{HH} = 7.2 Hz, 3H, CHAr$_2$C**H$_3$**).

^{13}C{^{1}H} NMR (chloroform-d, 150.92 MHz): δ 203.8, 166.5, 161.4 (d, $^1J_{CF}$ = 244.7 Hz), 144.8, 143.7, 141.5 (d, $^4J_{CF}$ = 3.2 Hz), 132.1, 129.7, 129.6, 129.2, 127.4 (d, $^3J_{CF}$ = 7.3 Hz), 115.3 (d, $^2J_{CF}$ = 21.2 Hz), 52.5, 39.2, 30.6, 22.2.

^{19}F NMR (chloroform-d, 564.63 MHz): δ -116.93 (tt, J_{HF} = 8.6, 5.4 Hz).

HRMS (EI) *m/z*: [M]$^+$ Calcd for C$_{18}$H$_{17}$FO$_3$ 300.1162. Found 300.1162.

Synthesis of methyl 4-acetyl-3-(1-(4-chlorophenyl)ethyl)benzoate (3Mi)

For large-scale catalysis, **Method E** (25 °C) was employed with imine **1M** (113 mg) and styrene (47 µL). Purified by SiO$_2$ column (gradient from 2% to 4% to 6% EtOAc/hexanes) to afford the title compound as a pale-yellow oil (21% ^{1}H NMR yield, 21 mg isolated, 17% isolated yield).

^{1}H NMR (chloroform-d, 600.13 MHz): δ 8.05 (d, J = 1.2 Hz, 1H, 2-Ar**H**), 7.96 (dd, J = 8.0, 1.5 Hz, 1H, 6-Ar**H**), 7.52 (d, J = 8.0 Hz, 1H, 5-Ar**H**), 7.27 − 7.22 (m, 2H overlapping with residual CHCl$_3$), 7.12 − 7.08 (m, 2H), 4.79 (q, J = 7.1 Hz, 1H, C**H**Ar$_2$CH$_3$), 3.95 (s, 3H, CO$_2$C**H$_3$**), 2.36 (s, 3H, COC**H$_3$**), 1.65 (d, J = 7.2 Hz, 3H, CHAr$_2$C**H$_3$**).

^{13}C{^{1}H} NMR (chloroform-d, 150.92 MHz): δ 203.6, 166.4, 144.5, 144.3, 143.5, 132.2, 132.1, 129.5, 129.3, 128.7, 127.5, 127.5, 52.6, 39.3, 30.6, 22.1.

HRMS (EI) *m/z*: [M]$^+$ Calcd for C$_{18}$H$_{17}$O$_3$Cl 316.0866. Found 316.0872.
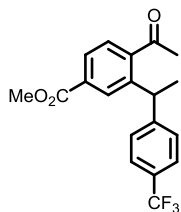
Synthesis of methyl 4-acetyl-3-(1-(4-(trifluoromethyl)phenyl)ethyl)benzoate (3Mj)

For large-scale catalysis, **Method E** (25 °C) was employed with imine **1M** (113 mg) and 4-(trifluoromethyl)styrene (60 µL). Purified by SiO_2 column chromatography (gradient from 5% to 10% EtOAc/hexanes) to afford the title compound as a pale-yellow oil (quantitative ^{1}H NMR yield, 130 mg isolated, 93% isolated yield).

^{1}H NMR (chloroform-*d*, 600.13 MHz): δ 8.04 (d, J_{HH} = 1.6 Hz, 1H, 2-Ar**H**), 7.95 (dd, J_{HH} = 8.0, 1.7 Hz, 1H, 6-Ar**H**), 7.54 (d, J_{HH} = 8.0 Hz, 1H, 5-Ar**H**), 7.52 − 7.48 (m, 2H), 7.29 − 7.23 (m, 2H overlapping residual CHCl₃) 4.88 (q, J_{HH} = 7.2 Hz, 1H, C**H**Ar₂CH₃), 3.93 (s, 3H, CO₂C**H₃**), 2.35 (s, 3H, COC**H₃**), 1.66 (d, J_{HH} = 7.2 Hz, 3H, CHAr₂C**H₃**).

^{13}C{^{1}H} NMR (chloroform-*d*, 150.92 MHz): δ 203.3, 166.4, 149.8, 144.2, 143.2, 132.3, 129.4, 128.6 (q, $^2J_{CF}$ = 32.5 Hz), 128.4, 127.8, 127.6, 125.5 (q, $^3J_{CF}$ = 3.7 Hz), 124.3 (q, $^1J_{CF}$ = 271.9 Hz), 52.6, 39.7, 30.5, 22.0.

^{19}F NMR (chloroform-*d*, 564.63 MHz): δ -62.41.

HRMS (EI) *m/z*: [M]$^+$ Calcd for $C_{19}H_{17}F_3O_3$ 350.1130. Found 350.1130.

Synthesis of methyl 4-acetyl-3-(1-(3-(methoxycarbonyl)phenyl)ethyl)benzoate (3Mk)

For large-scale catalysis, **Method E** (25 °C) was employed with imine **1M** (113 mg) and methyl 3-vinylbenzoate (65 mg). Purified by SiO_2 column chromatography (gradient from 10% to 15% EtOAc/hexanes) to afford the title compound as a pale-yellow oil (quantitative ^{1}H NMR yield, 134 mg isolated, 98% isolated yield).

^{1}H NMR (chloroform-*d*, 600.13 MHz): δ 8.01 (d, *J* = 1.6 Hz, 1H, 2'-Ar**H**), 7.94 (dd, *J* = 8.0, 1.6 Hz, 1H, 6'-Ar**H**), 7.87 − 7.84 (m, 1H), 7.82 (br s, 1H), 7.50 (d, *J* = 8.0 Hz, 1H, 5'-Ar**H**), 7.37 − 7.31 (m, 2H), 4.85 (q, *J* = 7.2 Hz, 1H, C**H**Ar₂CH₃), 3.92 (s, 3H, CO₂C**H₃**), 3.89 (s, 3H, CO₂C**H₃**), 2.33 (s, 3H, COC**H₃**), 1.67 (d, *J* = 7.2 Hz, 3H, CHAr₂C**H₃**).

^{13}C{^{1}H} NMR (chloroform-*d*, 150.92 MHz): δ 203.5, 167.2, 166.4, 146.1, 144.5, 143.5, 133.0, 132.2, 130.5, 129.5, 129.0, 128.6, 127.7, 127.5, 127.5, 52.5, 52.3, 39.7, 30.6, 22.0.

HRMS (EI) *m/z*: [M]$^+$ Calcd for $C_{20}H_{20}O_5$ 340.1311. Found 340.1310.

Synthesis of methyl 4-acetyl-3-(-1-(4-(methoxycarbonyl)phenyl)ethyl)benzoate (3Ml)

For large-scale catalysis, **Method E** (25 °C) was employed with imine **1m** (113 mg) and methyl 4-vinylbenzoate (65 mg). Purified by SiO$_2$ column chromatography (10% EtOAc/hexanes) to afford the title compound as a pale-yellow oil (quantitative ^{1}H NMR yield, 126 mg isolated, 93% isolated yield).

^{1}H NMR (chloroform-*d*, 600.13 MHz): δ 8.03 (d, *J* = 1.6 Hz, 1H, 2-Ar**H**), 7.96 – 7.91 (m, 3H), 7.51 (d, *J* = 8.0 Hz, 1H, 5-Ar**H**), 7.24 – 7.15 (m, 2H), 4.86 (q, *J* = 7.2 Hz, 1H, C**H**Ar$_2$CH$_3$), 3.93 (s, 3H, CO$_2$C**H$_3$**), 3.89 (s, 3H, CO$_2$C**H$_3$**), 2.31 (s, 3H, COC**H$_3$**), 1.66 (d, *J* = 7.2 Hz, 3H, CHAr$_2$C**H$_3$**).

^{13}C{^{1}H} NMR (chloroform-*d*, 150.92 MHz): δ 203.5, 167.1, 166.4, 151.1, 144.2, 143.5, 132.2, 129.9, 129.4, 128.3, 128.2, 127.6, 127.6, 52.6, 52.2, 39.9, 30.6, 21.9.

HRMS (EI) *m/z*: [M]$^+$ Calcd for C$_{20}$H$_{20}$O$_5$ 340.1311. Found 340.1312.

Synthesis of methyl 4-acetyl-3-(1-(4-(4,4,5,5-tetramethyl-1,3,2-dioxyborolan-2-yl)phenyl)ethyl)benzoate (3Mm)

For large-scale catalysis, **Method E** (25 °C) was employed with imine **1M** (113 mg) and **2m** (92 mg). Purified by SiO$_2$ column chromatography (gradient from 5% to 10% EtOAc/hexanes) to afford the title compound as a colorless oil which solidified upon standing (88% ^{1}H NMR yield, 120 mg isolated, 74% isolated yield).

^{1}H NMR (chloroform-*d*, 600.13 MHz): δ 8.05 (d, *J* = 1.5 Hz, 1H, 2-Ar**H**), 7.92 (dd, *J* = 7.9, 1.6 Hz, 1H, 6-Ar**H**), 7.69 (d, *J* = 7.7 Hz, 2H), 7.44 (d, *J* = 7.9 Hz, 1H, 5-Ar**H**), 7.12 (d, *J* = 7.8 Hz, 2H), 4.77 (q, *J* = 7.1 Hz, 1H, C**H**Ar$_2$CH$_3$), 3.92 (s, 3H, CO$_2$C**H$_3$**), 2.26 (s, 3H, COC**H$_3$**), 1.64 (d, *J* = 7.2 Hz, 3H, CHAr$_2$C**H$_3$**), 1.32 (s, 12H, BPin).

^{13}C{^{1}H} NMR (chloroform-*d*, 150.92 MHz): δ 204.1, 166.6, 149.0, 144.5, 143.9, 135.1, 133.3, 131.9, 129.2, 127.6, 127.3, 127.1, 83.9, 52.5, 40.0, 30.7, 25.0, 21.9.

HRMS (EI) *m/z*: [M]$^+$ Calcd for C$_{24}$H$_{29}$BO$_5$ 408.2108. Found 408.2113.
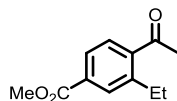
Synthesis of methyl 4-acetyl-3-ethylbenzoate (4Mn)

For large-scale catalysis, **Method F** (80 °C) was employed with imine **1M** (113 mg) and ethylene (1 atm added after 3 freeze/pump/thaw cycles in 1 500 mL Teflon-stoppered flask). Purified by SiO_2 column chromatography (gradient from 2% to 5% to 10% EtOAc/hexanes) to afford the title compound as a colorless oil (70% ^{1}H NMR yield, 44 mg isolated, 54% isolated yield).

^{1}H NMR (chloroform-d, 600.13 MHz): δ 7.95 (d, J = 1.6 Hz, 1H, 2-Ar**H**), 7.90 (dd, J = 8.0, 1.7 Hz, 1H, 6-Ar**H**), 7.60 (d, J = 8.0 Hz, 1H, 5-Ar**H**), 3.93 (s, 3H, CO$_2$C**H$_3$**), 2.86 (q, J = 7.5 Hz, 2H, ArC**H$_2$**CH$_3$), 2.59 (s, 3H, COC**H$_3$**), 1.23 (t, J = 7.5 Hz, 3H, ArCH$_2$C**H$_3$**).

^{13}C{^{1}H} NMR (chloroform-d, 150.92 MHz): δ 202.4, 166.6, 143.9, 142.2, 132.3, 131.5, 128.4, 127.0, 52.5, 30.4, 26.9, 15.9.

HRMS (EI) m/z: [M]$^+$ Calcd for $C_{12}H_{14}O_3$ 206.0943. Found 206.0942.
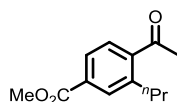
Synthesis of methyl 4-acetyl-3-propylbenzoate (4Mo)

For large-scale catalysis, **Method F** (80 °C) was employed with imine **1M** (113 mg) and propylene (1 atm added after 3 freeze/pump/thaw cycles in a 500 mL Teflon-stoppered flask). Purified by SiO_2 column chromatography (gradient from 2% to 5% EtOAc/hexanes) to afford the title compound as a colorless oil (13% ^{1}H NMR yield, 7 mg isolated, 8% isolated yield).

^{1}H NMR (chloroform-d, 600.13 MHz): δ 7.93 (d, J = 1.3 Hz, 1H, 2-Ar**H**), 7.91 (dd, J = 8.0, 1.6 Hz, 1H, 6-Ar**H**), 7.60 (d, J = 8.0 Hz, 1H, 5-Ar**H**), 3.94 (s, 3H, CO$_2$C**H$_3$**), 2.85 − 2.78 (m, 2H, ArC**H$_2$**CH$_2$CH$_3$), 2.59 (s, 3H, COC**H$_3$**), 1.66 − 1.58 (m, 2H, ArCH$_2$C**H$_2$**CH$_3$), 0.96 (t, J = 7.3 Hz, 3H, ArCH$_2$CH$_2$C**H$_3$**).

^{13}C{^{1}H} NMR (chloroform-d, 150.92 MHz): δ 202.5, 166.6, 142.5, 142.3, 132.2, 132.1, 128.3, 127.0, 52.5, 35.7, 30.4, 25.0, 14.2.

HRMS (EI) m/z: [M]$^+$ Calcd for $C_{13}H_{16}O_2$ 220.1099. Found 220.1096.
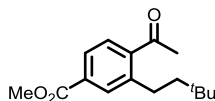
Attempted Synthesis of methyl 4-acetyl-3-(3,3-dimethylbutyl)benzoate (4Mp)

For large-scale catalysis, **Method F** (80 °C) was employed with imine **1M** (113 mg) and *tert*-butylethylene (52 μL). Isolation and complete characterization of the title compound were prohibited by the exceedingly low yield (< 2%). However, diagnostic resonances corresponding to the hydroarylation product (see Appendix C, Figure C141) suggest that the title compound exists to a detectable degree.

Selected ^{1}H NMR resonances corresponding to the title compound: ^{1}H NMR (chloroform-*d*, 600.13 MHz): δ 3.94 (s, 3H CO₂C**H₃**), 2.85 – 2.78 (m, 2H, **CH₂**CH₂^{t}Bu), 1.48 – 1.44 (m, 2H, CH₂**CH₂**^{t}Bu), 0.98 (s, 9H, ^{t}Bu).
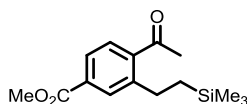
Synthesis of methyl 4-acetyl-3-(2-(trimethylsilyl)ethyl)benzoate (4Mq)

For large-scale catalysis, **Method F** (80 °C) was employed with imine **1M** (113 mg) and vinyltrimethylsilane (59 μL). Purified by SiO₂ column chromatography (gradient from 2% to 5% to 10% EtOAc/hexanes) to afford the title compound as a colorless oil, which solidified to a white solid over time (58% ^{1}H NMR yield, 61 mg isolated, 55% isolated yield).

^{1}H NMR (chloroform-*d*, 600.13 MHz): δ 7.94 (d, *J* = 1.2 Hz, 1H, 2-Ar**H**), 7.89 (dd, *J* = 8.0, 1.5 Hz, 1H, 6--Ar**H**), 7.61 (d, *J* = 8.0 Hz, 1H, 5-Ar**H**), 3.94 (s, 3H, CO₂C**H₃**), 2.88 – 2.78 (m, 2H, ArC**H₂**R), 2.59 (s, 3H, COC**H₃**), 0.84 – 0.80 (m, 2H, RC**H₂**SiMe₃), 0.05 (s, 9H, RSi(C**H₃**)₃).

^{13}C{^{1}H} NMR (chloroform-*d*, 150.92 MHz): δ 202.3, 166.6, 145.6, 141.7, 132.3, 131.6, 128.6, 126.8, 52.5, 30.3, 28.2, 19.6, -1.7.

HRMS (EI) *m/z*: [M]⁺ Calcd for C₁₅H₂₂O₃Si 278.1338. Found 278.1335.

Synthesis of methyl 4-acetyl-3-(2-(1,1,1,3,5,5,5-heptamethyltrisiloxan-3-yl)ethyl)benzoate (4Mr)

For large-scale catalysis, **Method F** (80 °C) was employed with imine **1M** (113 mg) and methylbis(trimethylsilyloxy)vinylsilane (116 μL). Purified by SiO₂ column chromatography (gradient from 2% to 5% to 7.5% EtOAc/hexanes) to afford the title compound as a colorless oil (39% ^{1}H NMR yield, 34 mg isolated, 20% isolated yield).

^{1}H NMR (chloroform-d, 600.13 MHz): δ 7.94 (d, J = 1.4 Hz, 1H, 2-Ar**H**), 7.89 (dd, J = 8.0, 1.6 Hz, 1H, 6-Ar**H**), 7.57 (d, J = 8.0 Hz, 1H, 5-Ar**H**), 3.94 (s, 3H, CO$_2$C**H$_3$**), 2.95 – 2.73 (m, 2H, ArC**H$_2$**R), 2.58 (s, 3H, COC**H$_3$**), 0.89 – 0.64 (m, 2H, RC**H$_2$**SiMe(OSiMe$_3$)$_2$), 0.11 (s, 18H, R$_3$Si(OSi(C**H$_3$**)$_3$)$_2$), 0.06 (s, 3H, R$_3$SiC**H$_3$**).

^{13}C{^{1}H} NMR (chloroform-d, 150.92 MHz): δ 202.4, 166.6, 145.0, 142.2, 132.2, 131.5, 128.3, 126.8, 52.5, 30.4, 27.3, 20.2, 2.0, -0.2.

HRMS (EI) m/z: [M]$^+$ Calcd for C$_{19}$H$_{34}$O$_5$Si$_3$ 426.1714. Found 426.1713.

Hydroarylations with Substrates Bearing Varied *N*-Aryl Directing Groups (Table 4.1)

Catalysis with Substrate 5 (Ar = Ph).

For small-scale catalysis, **Method D** (80 °C) was employed with imine **5** (25 mg) and styrene (12 μL) to afford a ^{1}H NMR yield of 78%.

Catalysis with Substrate 6 (Ar = 4-(CF$_3$)C$_6$H$_4$).

For small-scale catalysis, **Method D** (80 °C) was employed with imine **6** (32 mg) and styrene (12 μL) to afford a ^{1}H NMR yield of 63%.

Catalysis with Substrate 7 (Ar = 2-(OMe)C$_6$H$_4$).

For small-scale catalysis, **Method D** (80 °C) was employed with imine **7** (28 mg) and styrene (12 μL) to afford a ^{1}H NMR yield of 17%.

Catalysis with Substrate 8 (Ar = 2-^{t}BuC$_6$H$_4$).

For small-scale catalysis, **Method D** (80 °C) was employed with imine **8** (31 mg) and styrene (12 μL) to afford a ^{1}H NMR yield of 0%.

Catalysis with Substrate 9 (Ar = 3,5-(^{t}Bu)$_2$C$_6$H$_3$).

For small-scale catalysis, **Method D** (80 °C) was employed with imine **9** (33 mg) and styrene (12 μL) to afford a ^{1}H NMR yield of 72%.

Substrates Which Failed to Undergo Hydroarylation

For the (*N*-aryl)aryl imine substrates listed above in Chart 4.3, **Method E** (25 °C) and **Method F** (80 °C) were employed with styrene (45 μL) and the imines above (0.4 mmol). Hydroarylation products were not observed by ^{1}H NMR spectroscopy of the crude reaction mixtures.

For the olefin substrates listed above in Chart 4.3, **Method E** (25 °C) and **Method F** (80 °C) were employed with imine **1M** (113 mg) and the olefin (0.4 mmol). For trifluoropropylene, 1,3-butadiene, and *cis/trans*-2-butene, 1 atm of olefin was used. Hydroarylation products were not observed by ^{1}H NMR spectroscopy of the crude reaction mixtures.

References

1.   Evano, G.; Theunissen, C. *Angew. Chem. Int. Ed.* **2019**, *58*.

2.   Goldman, A. S.; Goldberg, K. I. In *Activation and Functionalization of C—H Bonds*; American Chemical Society: 2004; Vol. 885, p 1-43.

3.   Gandeepan, P.; Muller, T.; Zell, D.; Cera, G.; Warratz, S.; Ackermann, L. *Chem Rev* **2019**, *119*, 2192-2452.

4.   Pototschnig, G.; Maulide, N.; Schnürch, M. *Chem. Eur. J.* **2017**, *23*, 9206-9232.

5.   Suslick, B. A.; Tilley, T. D. In *Catalytic Hydroarylation of Carbon‑Carbon Multiple Bonds*; Ackermann, L., Gunnoe, T. B., Habgood, L. G., Eds.; Willey-VCH: Weinheim, 2017, p 107-174.

6.   Colby, D. A.; Bergman, R. G.; Ellman, J. A. *Chem. Rev.* **2010**, *110*, 624-655.

7.   Kakiuchi, F.; Murai, S. *Acc. Chem. Res.* **2002**, *35*, 826-834.

8.   Murai, S.; Kakiuchi, F.; Sekine, S.; Tanaka, Y.; Kamatani, A.; Sonoda, M.; Chatani, N. *Nature* **1993**, *366*, 529.

9.   Vaughan, B. A.; Webster-Gardiner, M. S.; Cundari, T. R.; Gunnoe, T. B. *Science* **2015**, *348*, 421-424.

10.   Filloux, C. M.; Rovis, T. *J. Am. Chem. Soc.* **2015**, *137*, 508-517.

11.   Jun, C. H.; Hong, J. B.; Kim, Y. H.; Chung, K. Y. *Angew. Chem. Int. Ed.* **2000**, *39*, 3440-3442.

12.   Thalji, R. K.; Ahrendt, K. A.; Bergman, R. G.; Ellman, J. A. *J. Am. Chem. Soc.* **2001**, *123*, 9692-9693.

13.   Crisenza, G. E. M.; McCreanor, N. G.; Bower, J. F. *J. Am. Chem. Soc.* **2014**, *136*, 10258-10261.

14.   Oxgaard, J.; Muller, R. P.; Goddard, W. A.; Periana, R. A. *J. Am. Chem. Soc.* **2004**, *126*, 352-363.

15.   Oxgaard, J.; Periana, R. A.; Goddard, W. A. *J. Am. Chem. Soc.* **2004**, *126*, 11658-11665.

16.   Sevov, C. S.; Hartwig, J. F. *J. Am. Chem. Soc.* **2013**, *135*, 2116-2119.

17.   Xing, D.; Qi, X.; Marchant, D.; Liu, P.; Dong, G. *Angew. Chem. Int. Ed.* **2019**, *58*, 4366-4370.

18.   Podhajsky, S. M.; Iwai, Y.; Cook-Sneathen, A.; Sigman, M. S. *Tetrahedron* **2011**, *67*, 4435-4441.

19.   Gligorich, K. M.; Cummings, S. A.; Sigman, M. S. *J. Am. Chem. Soc.* **2007**, *129*, 14193-14195.

20.   Cacchi, S. *Pure Appl. Chem.* **1990**, *62*, 713-722.

21.   Bowring, M. A.; Bergman, R. G.; Tilley, T. D. *J. Am. Chem. Soc.* **2013**, *135*, 13121-13128.

22.   Luedtke, A. T.; Goldberg, K. I. *Angew. Chem. Int. Ed.* **2008**, *47*, 7694-7696.

23.   McKeown, B. A.; Gonzalez, H. E.; Friedfeld, M. R.; Gunnoe, T. B.; Cundari, T. R.; Sabat, M. *J. Am. Chem. Soc.* **2011**, *133*, 19131-19152.

24.   Karshtedt, D.; Bell, A. T.; Tilley, T. D. *Organometallics* **2004**, *23*, 4169-4171.

25.   Suslick, B. A.; Liberman-Martin, A. L.; Wambach, T. C.; Tilley, T. D. *ACS Catal.* **2017**, *7*, 4313-4322.

26.   Chirik, P.; Morris, R. *Acc. Chem. Res.* **2015**, *48*, 2495-2495.

27.   Moselage, M.; Li, J.; Ackermann, L. *ACS Catal.* **2016**, *6*, 498-525.

28.   Gao, K.; Yoshikai, N. *Acc. Chem. Res.* **2014**, *47*, 1208-1219.

29.   Wang, S.; Chen, S. Y.; Yu, X. Q. *Chem. Commun.* **2017**, *53*, 3165-3180.

30.   Schroeter, F.; Lerch, S.; Kaliner, M.; Strassner, T. *Org. Lett.* **2018**.

31.   Ilies, L.; Chen, Q.; Zeng, X.; Nakamura, E. *J. Am. Chem. Soc.* **2011**, *133*, 5221-5223.

32.   Gao, K.; Lee, P.-S.; Fujita, T.; Yoshikai, N. *J. Am. Chem. Soc.* **2010**, *132*, 12249-12251.

33.   Gao, K.; Yoshikai, N. *Angew. Chem. Int. Ed.* **2011**, *50*, 6888-6892.

34.   Gao, K.; Yoshikai, N. *J. Am. Chem. Soc.* **2011**, *133*, 400-402.

35.   Dong, J.; Lee, P.-S.; Yoshikai, N. *Chem. Lett.* **2013**, *42*, 1140-1142.

36.   Lee, P. S.; Yoshikai, N. *Angew. Chem. Int. Ed.* **2013**, *52*, 1240-1244.

37.   Xu, W.; Pek, J. H.; Yoshikai, N. *Adv. Synth. Catal.* **2016**, *358*, 2564-2568.

38.   Xu, W.; Yoshikai, N. *Angew. Chem. Int. Ed.* **2016**, *55*, 12731-12735.

39.   Lee, P.-S.; Fujita, T.; Yoshikai, N. *J. Am. Chem. Soc.* **2011**, *133*, 17283-17295.

40.   Wakatsuki, Y.; Yamazaki, H.; Lindner, E.; Bosamle, A. In *Inorg. Synth.*; H. D., K., Ed.; Willey: 1989.

41.   Sacco, A.; Rossi, M. *Chem. Commun.* **1967**, 316-316.

42.   Yamamoto, A.; Miura, Y.; Ito, T.; Chen, H. L.; Iri, K.; Ozawa, F.; Miki, K.; Sei, T.; Tanaka, N.; Kasai, N. *Organometallics* **1983**, *2*, 1429-1436.

43.   Collman, J. P.; Finke, R. G.; Cawse, J. N.; Brauman, J. I. *J. Am. Chem. Soc.* **1977**, *99*, 2515-2526.

44.   Hamachi, Y.; Katano, M.; Ogiwara, Y.; Sakai, N. *Org. Lett.* **2016**, *18*, 1634-1637.

45.   Chen, F.; Ding, Z.; He, Y.; Qin, J.; Wang, T.; Fan, Q.-H. *Tetrahedron* **2012**, *68*, 5248-5257.

46.   Moessner, C.; Bolm, C. *Angew. Chem. Int. Ed.* **2005**, *44*, 7564-7567.

47.   Yoshikai, N.; Matsumoto, A.; Norinder, J.; Nakamura, E. *Angew. Chem. Int. Ed.* **2009**, *48*, 2925-2928.

48.   Lei, C.; Peng, L.; Ding, K. *Adv. Synth. Catal.* **2018**, *360*, 2952-2958.

49.   Shimomaki, K.; Murata, K.; Martin, R.; Iwasawa, N. *J. Am. Chem. Soc.* **2017**, *139*, 9467-9470.

50.   Malkov, A. V.; Vranková, K.; Stončius, S.; Kočovský, P. *The Journal of Organic Chemistry* **2009**, *74*, 5839-5849.

51.   Wu, J.; Barnard, J. H.; Zhang, Y.; Talwar, D.; Robertson, C. M.; Xiao, J. *Chem. Commun.* **2013**, *49*, 7052-7054.

52.   Saito, K.; Horiguchi, K.; Shibata, Y.; Yamanaka, M.; Akiyama, T. *Chem. Eur. J.* **2014**, *20*, 7616-7620.

53.   Kanemitsu, T.; Umehara, A.; Haneji, R.; Nagata, K.; Itoh, T. *Tetrahedron* **2012**, *68*, 3893-3898.

54.   Lu, B.; Wu, J.; Yoshikai, N. *J. Am. Chem. Soc.* **2014**, *136*, 11598-11601.

55.   Tomita, R.; Yasu, Y.; Koike, T.; Akita, M. *Angew. Chem. Int. Ed.* **2014**, *53*, 7144-7148.

56.   Xu, T.; Sha, F.; Alper, H. *J. Am. Chem. Soc.* **2016**, *138*, 6629-6635.

57.   Cambre, J. N.; Roy, D.; Gondi, S. R.; Sumerlin, B. S. *J. Am. Chem. Soc.* **2007**, *129*, 10348-10349.

Appendix A

NMR Spectral Data

and

Tables of XRD Determined Bond Lengths/Angles

from

Chapter Two:

Olefin Hydroarylation Catalyzed by (Pyridyl-Indolate)Pt(II) Complexes:
Catalytic Efficiencies and Mechanistic Aspects

NMR Spectral Data
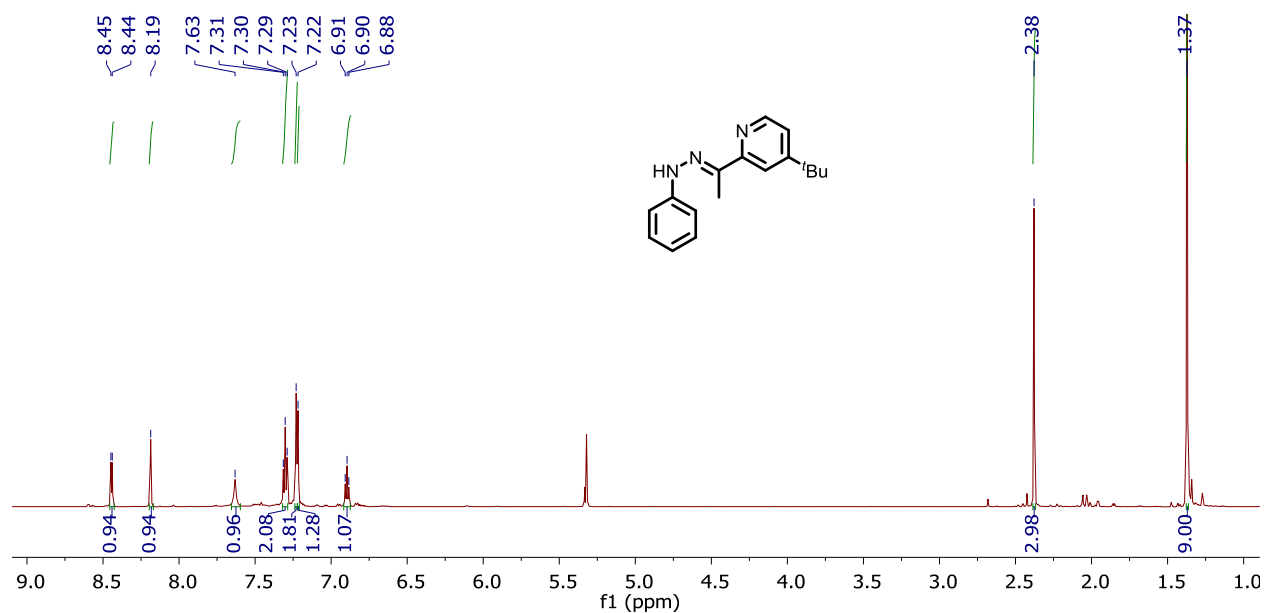
Figure A1a. ^{1}H NMR spectrum of **3a** in dichloromethane-d_2.
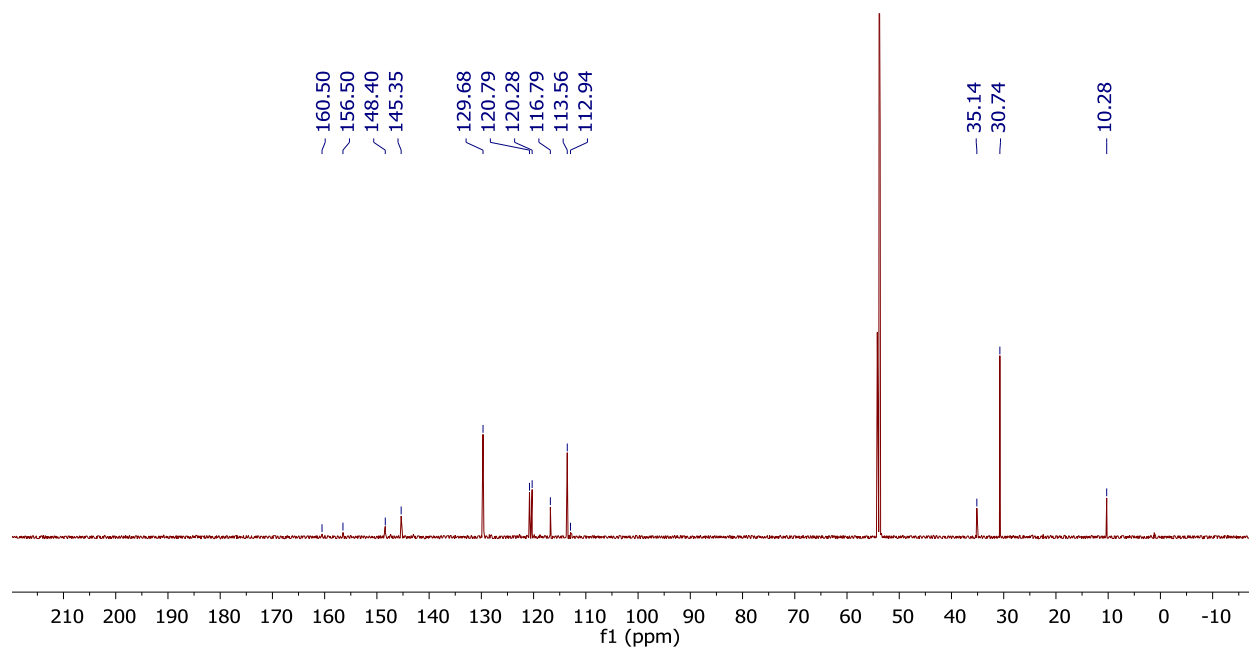
Figure A1b. ^{13}C{^{1}H} NMR spectrum of **3a** in dichloromethane-d_2.
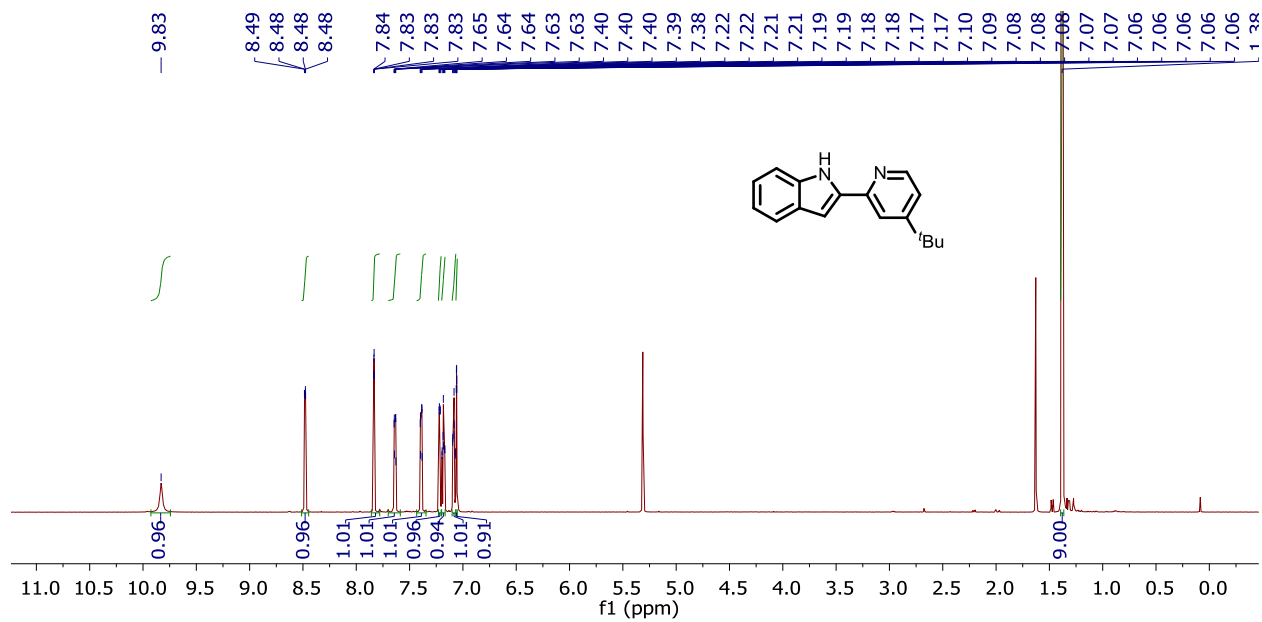
Figure A2a. ^{1}H NMR spectrum of **4a** in dichloromethane-d_2.
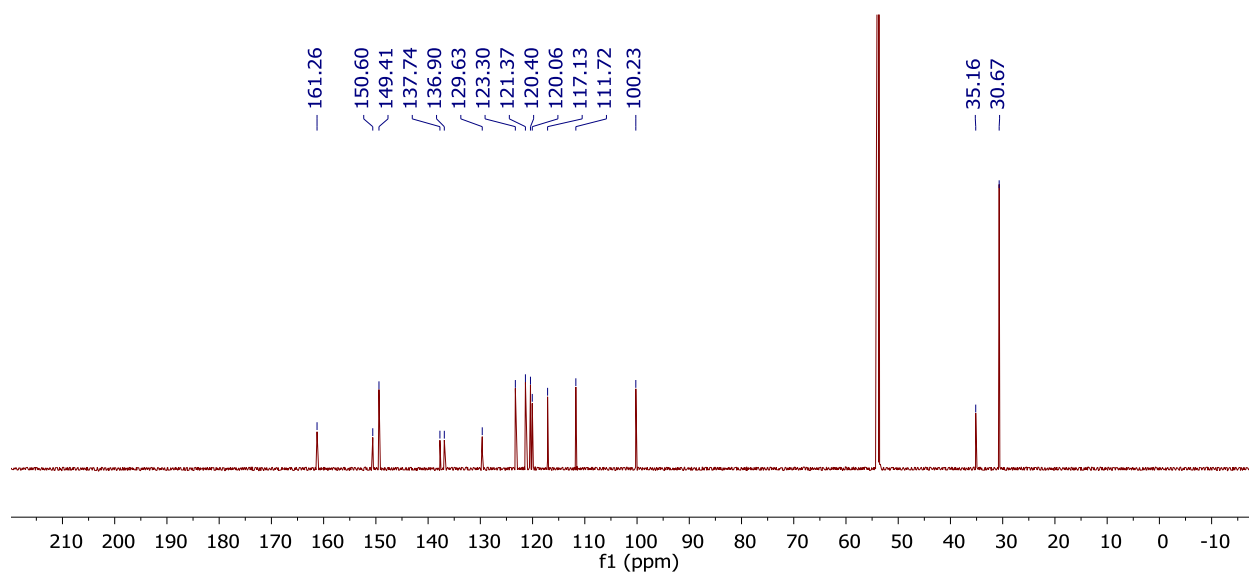
Figure A2b. ^{13}C{^{1}H} NMR spectrum of **4a** in dichloromethane-d_2.
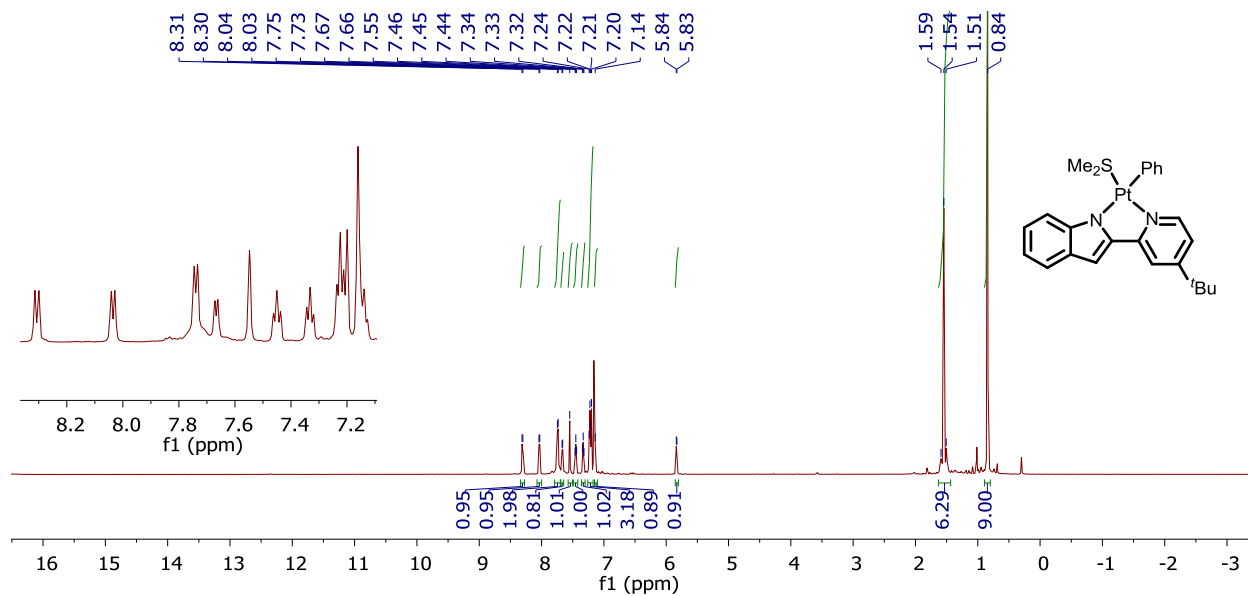
Figure A3a. ^{1}H NMR spectrum of **5a** in benzene-d_6.
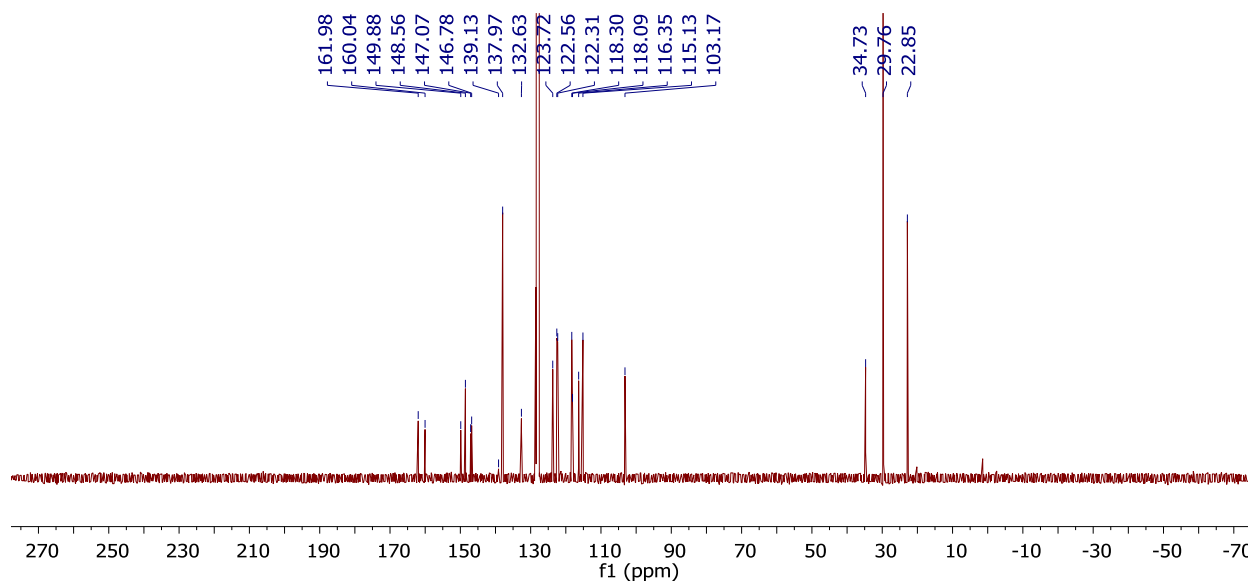
Figure A3b. ^{13}C{^{1}H} NMR spectrum of **5a** in benzene-d_6.

Figure A4a. ^{1}H NMR spectrum of **3b** in dichloromethane-d_2.

Figure A4b. ^{13}C{^{1}H} NMR spectrum of **3b** in dichloromethane-d_2.

Figure A4c. ^{19}F NMR spectrum of **3b** in dichloromethane-d_2.

Figure A5a. ^{1}H NMR spectrum of **4b** in dichloromethane-d_2.

Figure A5b. ^{13}C{^{1}H} NMR spectrum of **4b** in dichloromethane-d_2.

Figure A5c. ^{19}F NMR spectrum of **4b** in dichloromethane-d_2.
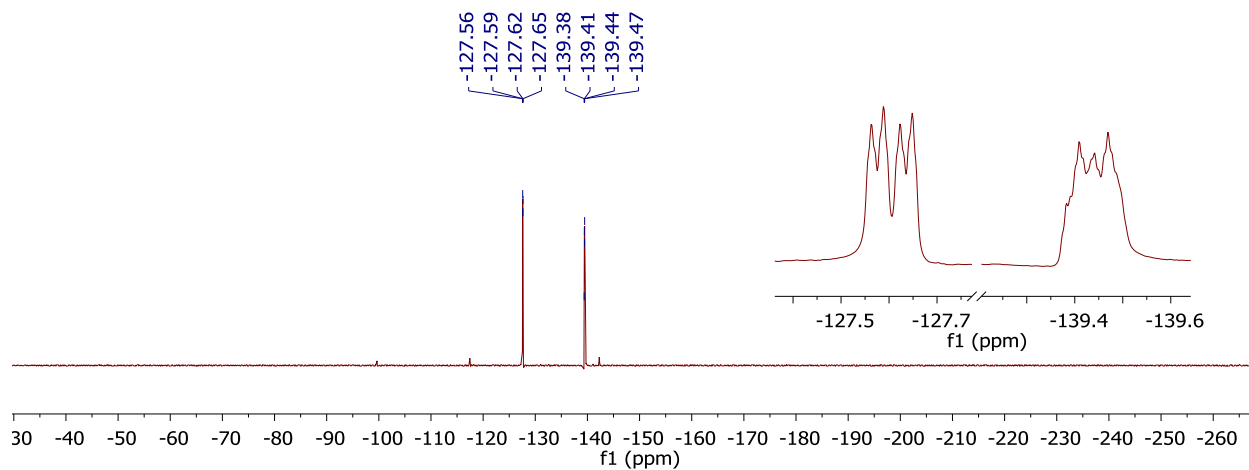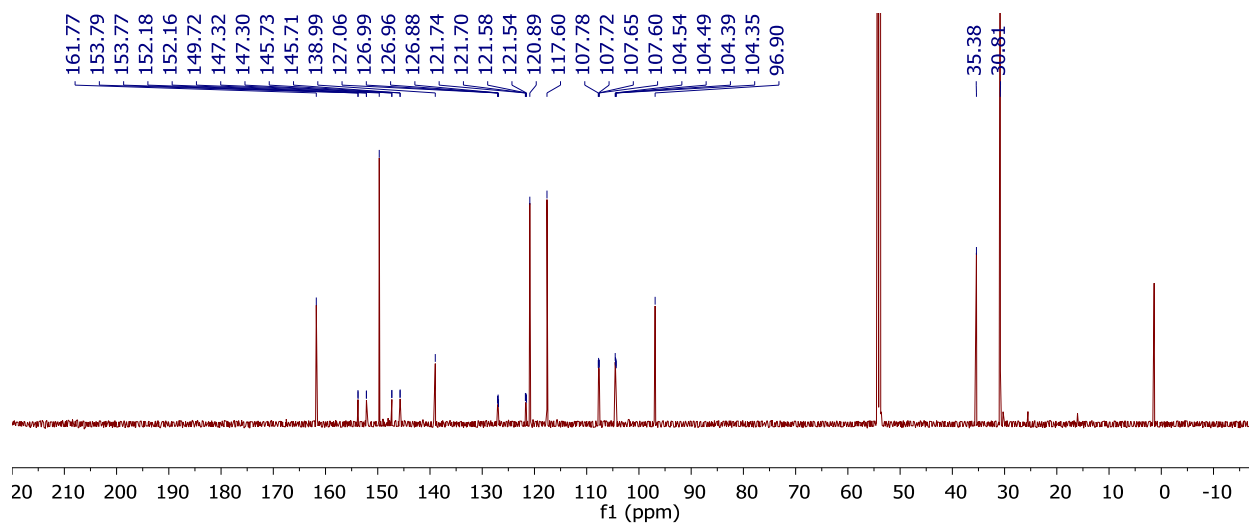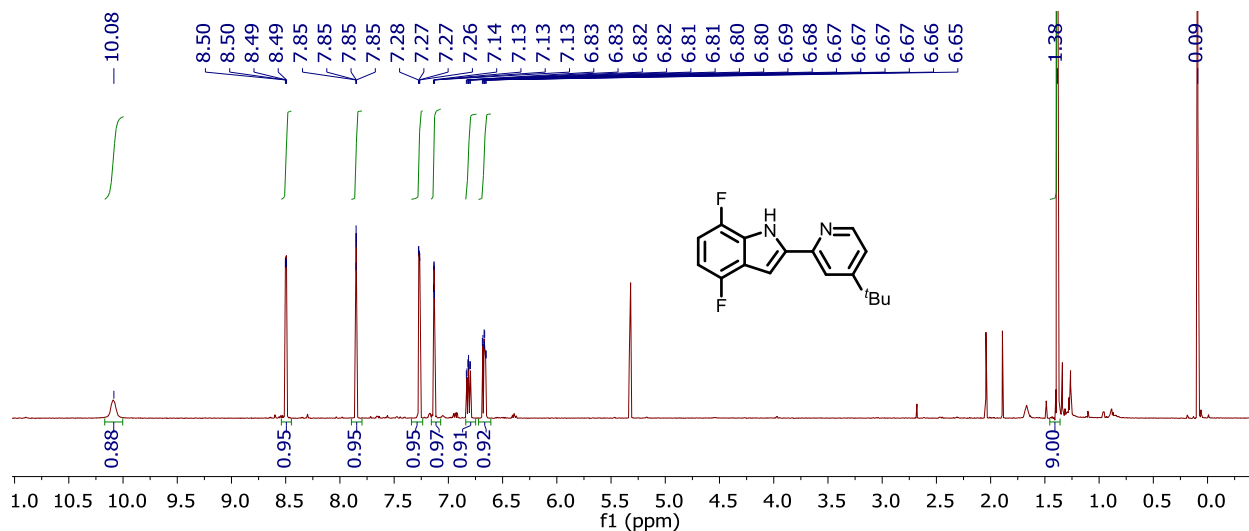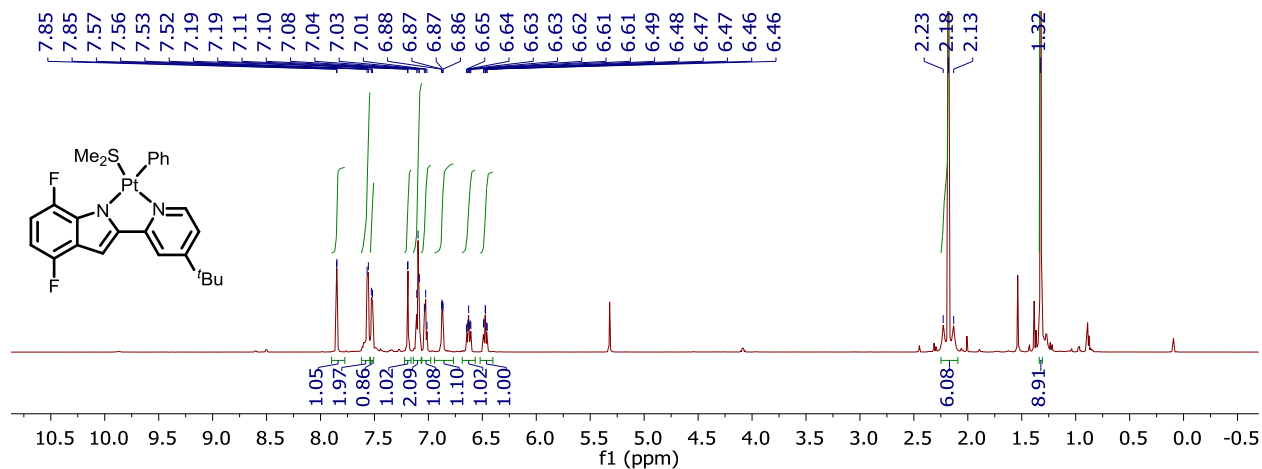
Figure A6a. ¹H NMR spectrum of **5b** in dichloromethane-d_2.
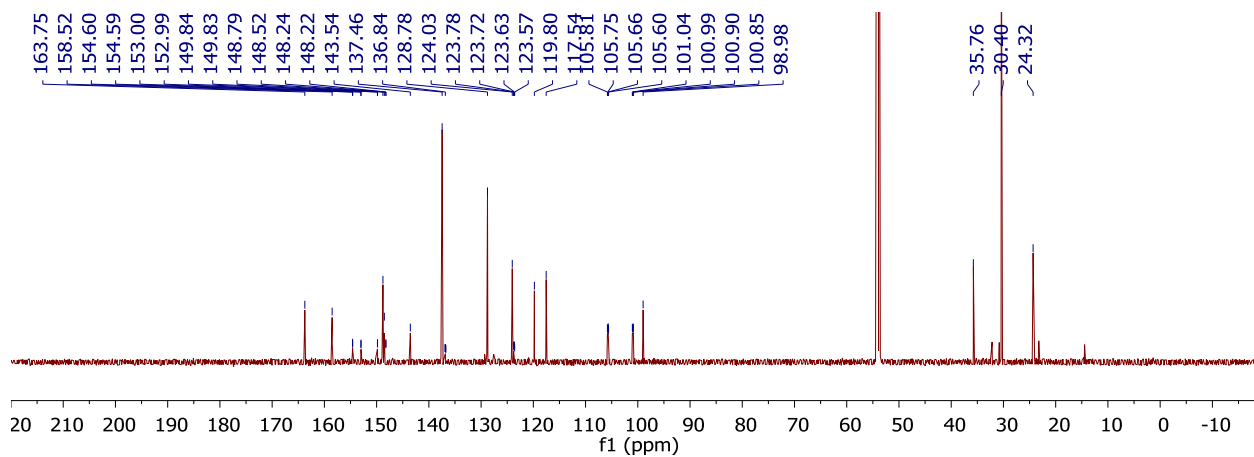
Figure A6b. ¹³C{¹H} NMR spectrum of **5b** in dichloromethane-d_2.
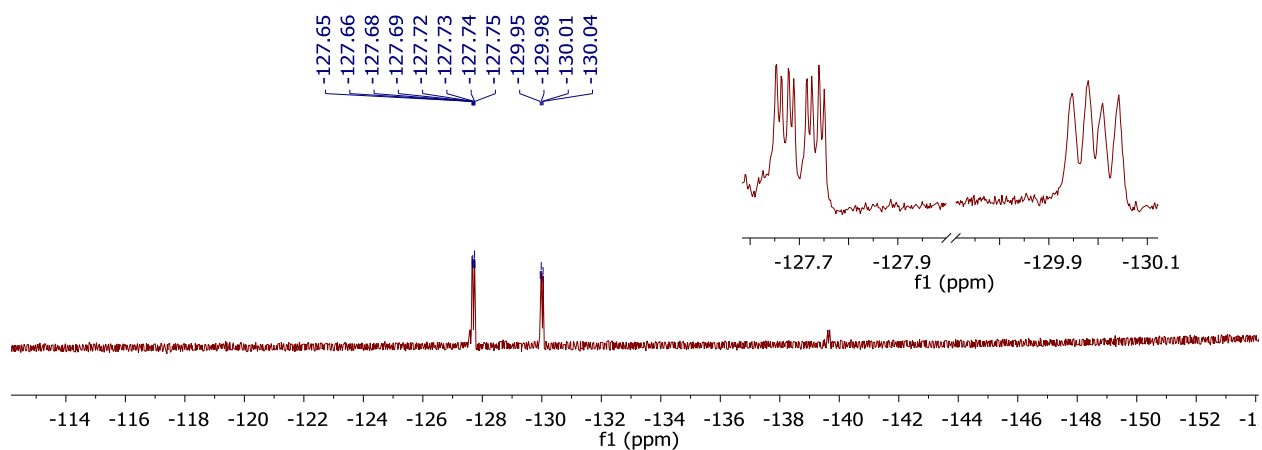
Figure A6c. ¹⁹F NMR spectrum of **5b** in dichloromethane-d_2.
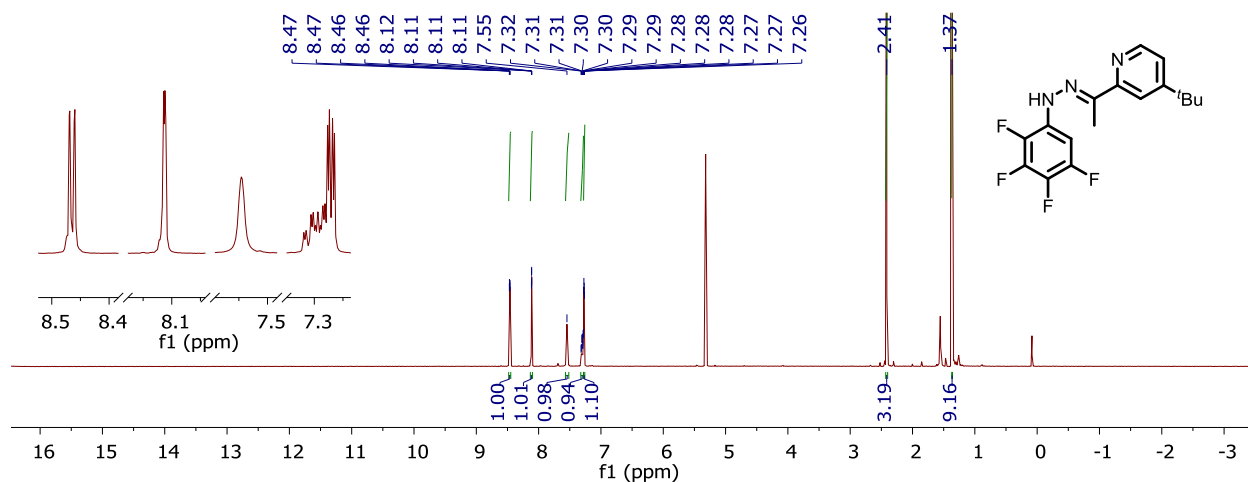
Figure A7a. ¹H NMR spectrum of **3c** in dichloromethane-d_2.
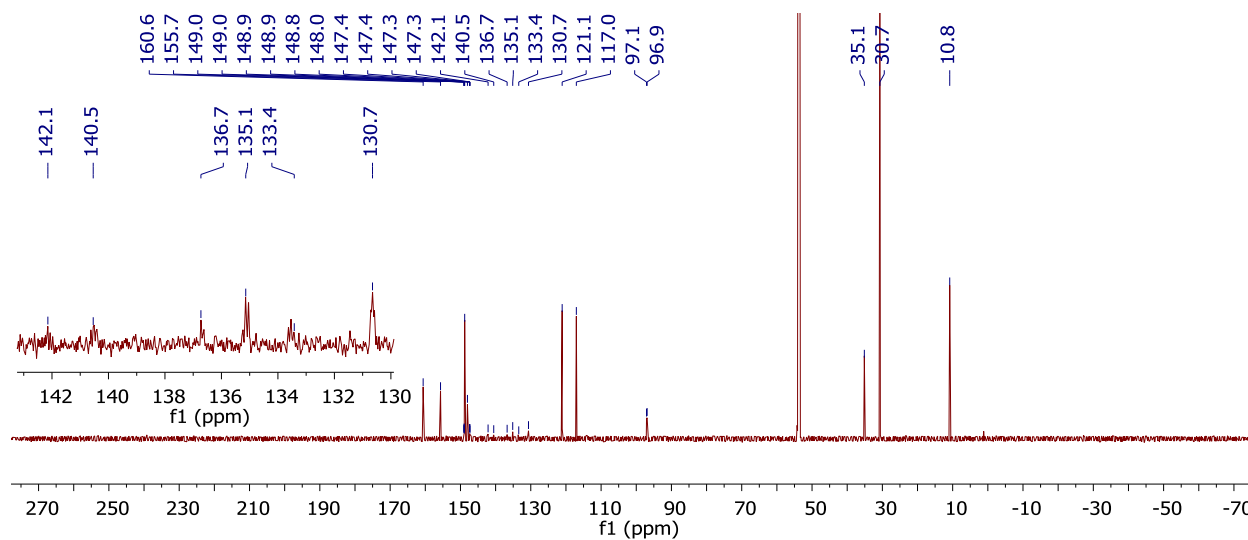
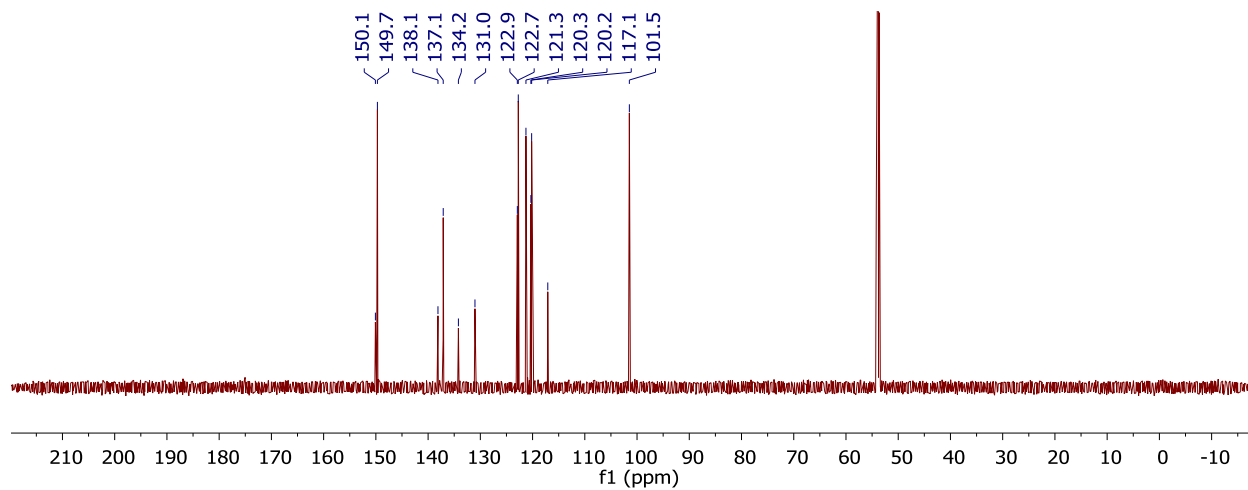**Figure A7b.** ¹³C{¹H} NMR spectrum of **3c** in dichloromethane-d_2.
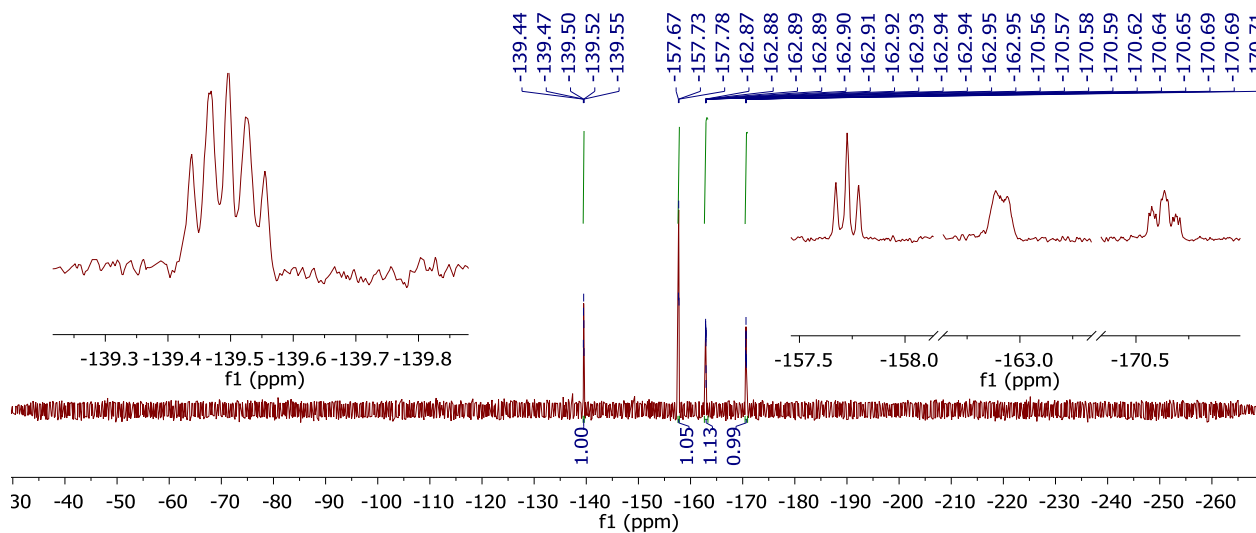
Figure A7c. ¹⁹F NMR spectrum of **3c** in dichloromethane-d_2.
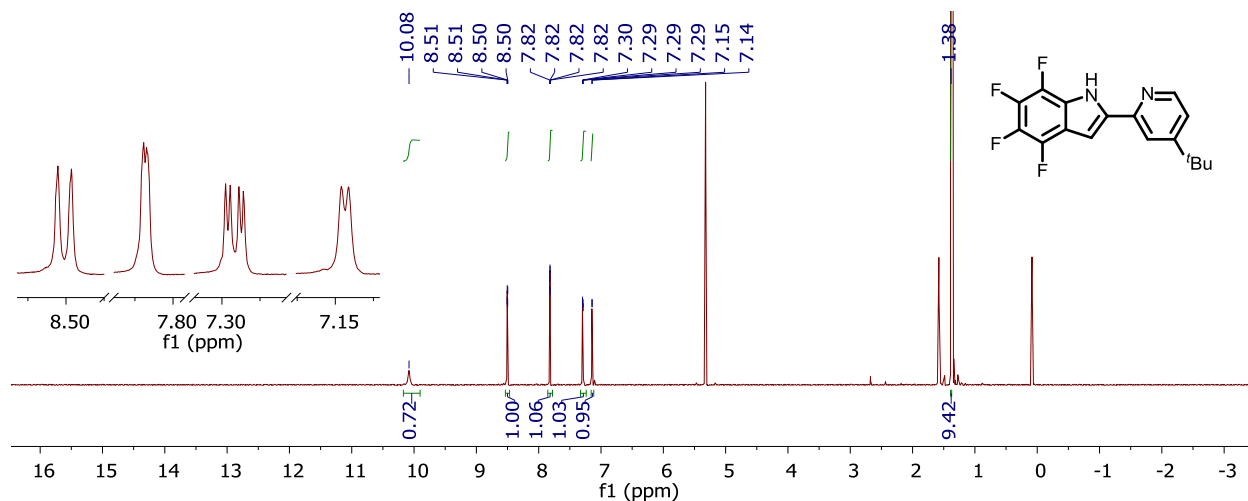
Figure A8a. ^{1}H NMR spectrum of **4c** in dichloromethane-d_2
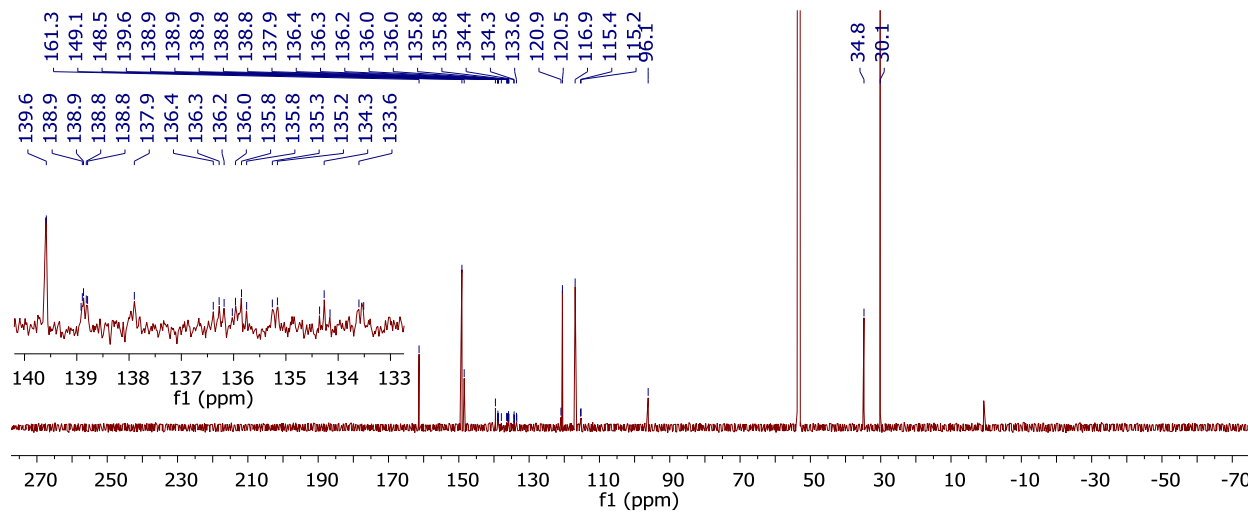
Figure A8b. ^{13}C{^{1}H} NMR spectrum of **4c** in dichloromethane-d_2.
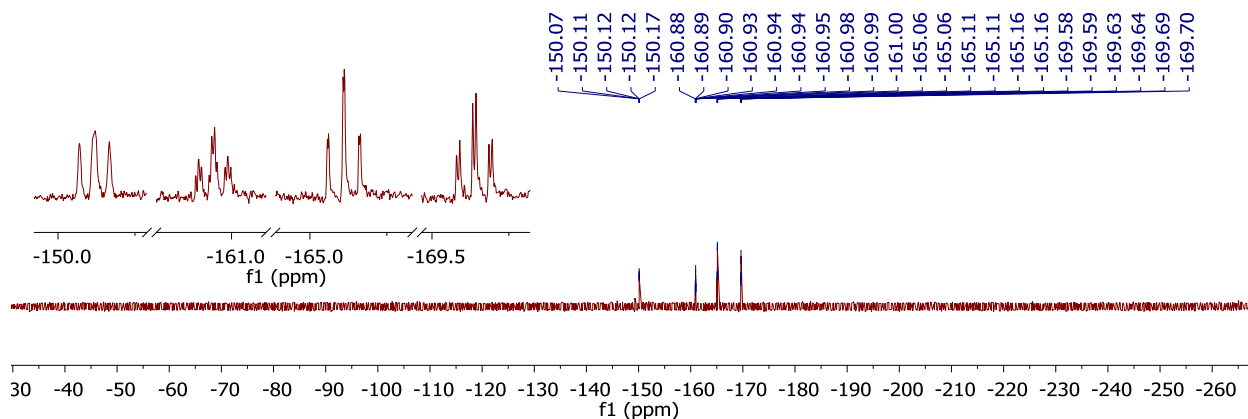
Figure A8c. ^{19}F NMR spectrum of **4c** in dichloromethane-d_2.
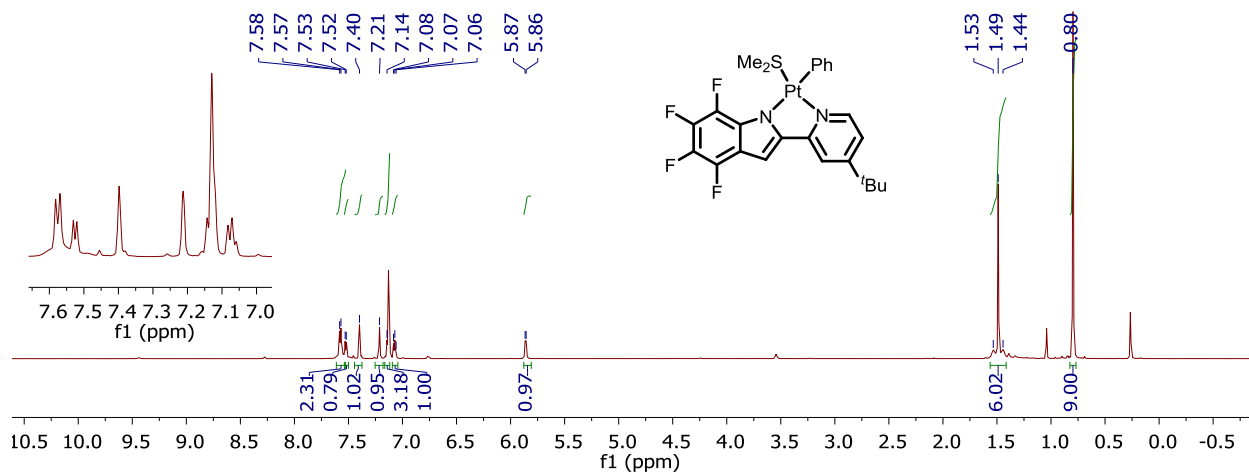
Figure A9a. ¹H NMR spectrum of **5c** in benzene-d_6.
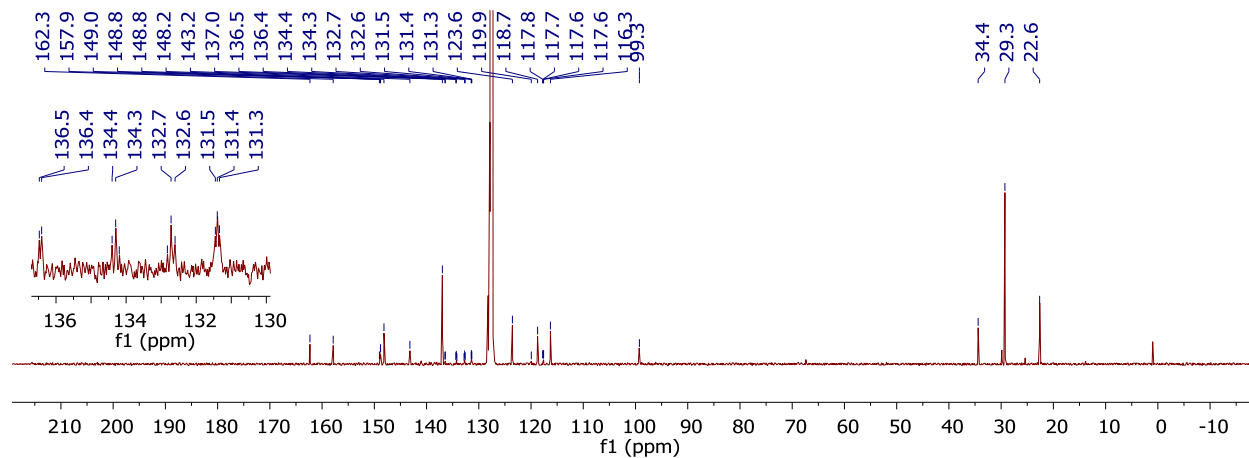
Figure A9b. ¹³C{¹H} NMR spectrum of **5c** in benzene-d_6.
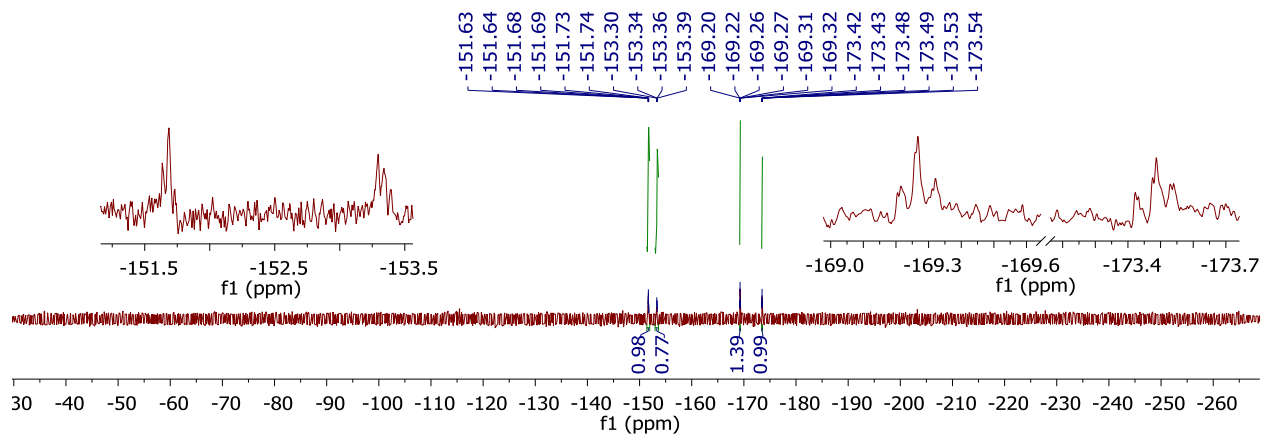
Figure A9c. ¹⁹F NMR spectrum of **5c** in benzene-d_6.
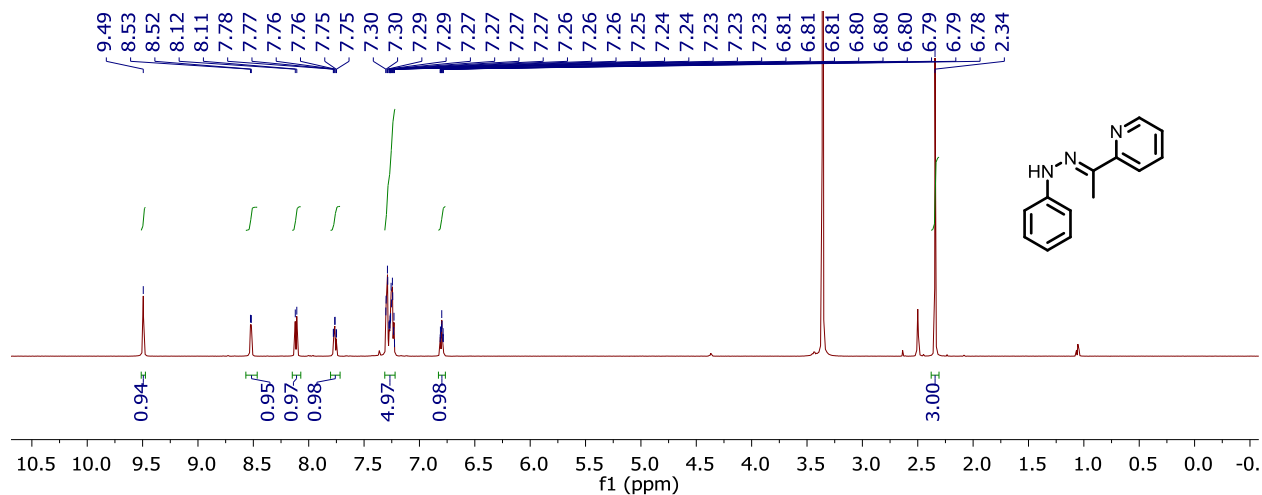
Figure A10a. ^{1}H NMR spectrum of **3d** in dimethylsulfoxide-d_6.
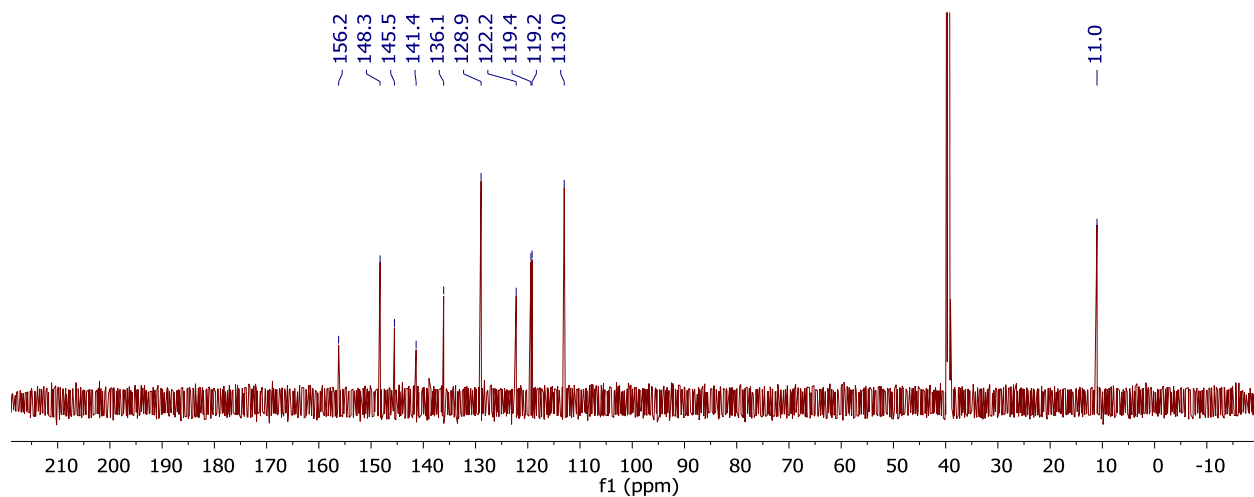
**Figure A10b.** ^{13}C{^{1}H} NMR spectrum of **3d** in dimethylsulfoxide-d_6
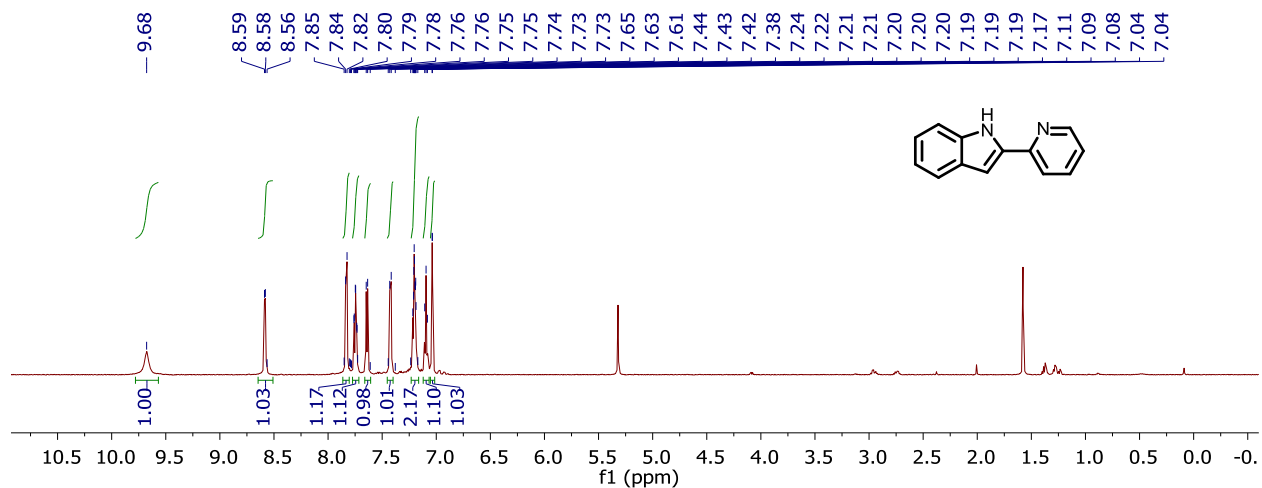
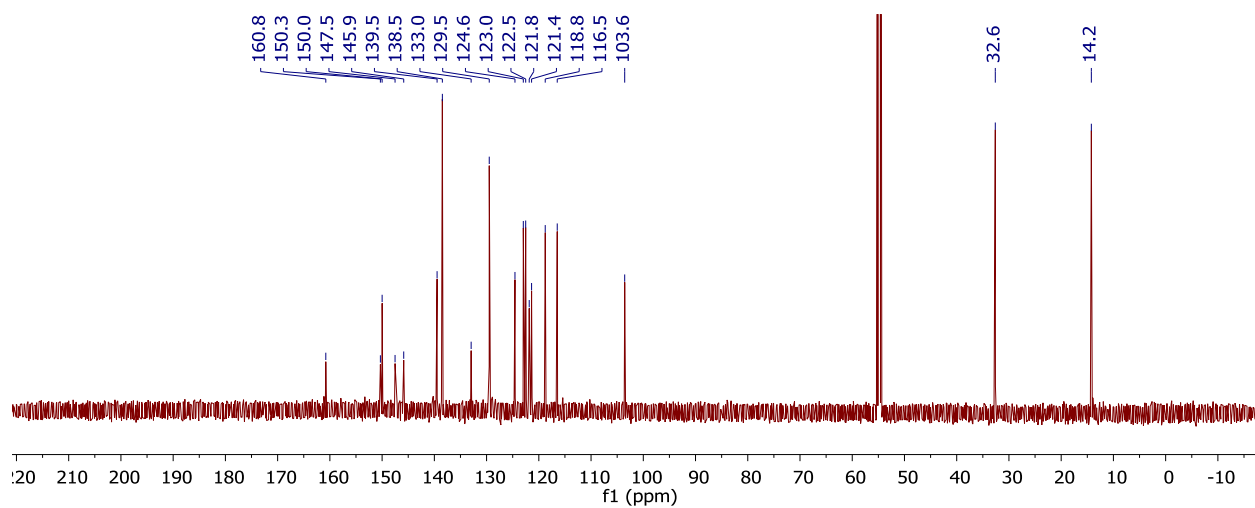**Figure A11a.** ^{1}H NMR spectrum of **4d** in dichloromethane-d_2.
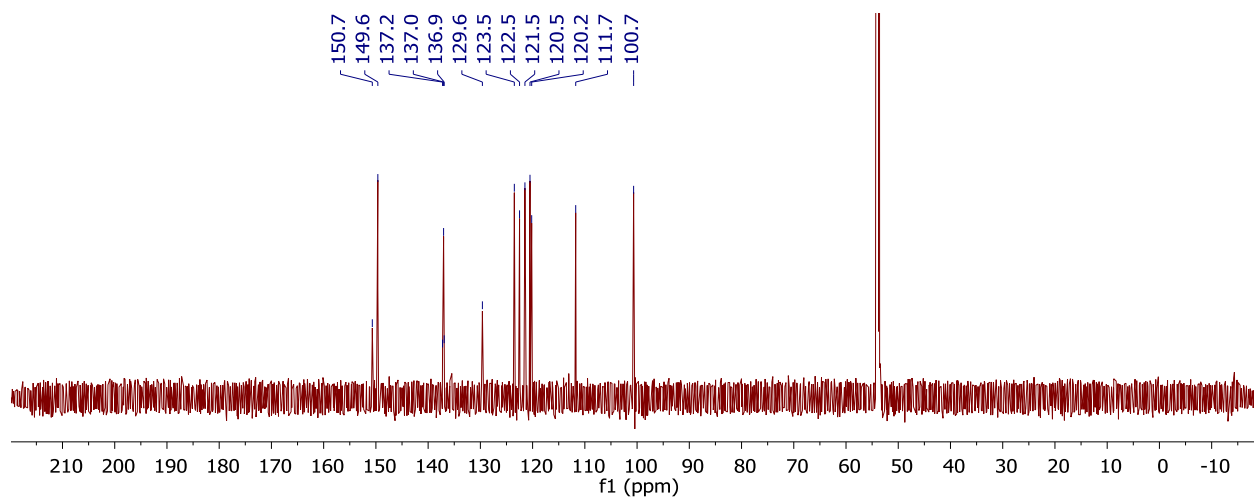
Figure A11b. ^{13}C{^{1}H} NMR spectrum of **4d** in dichloromethane-d_2.
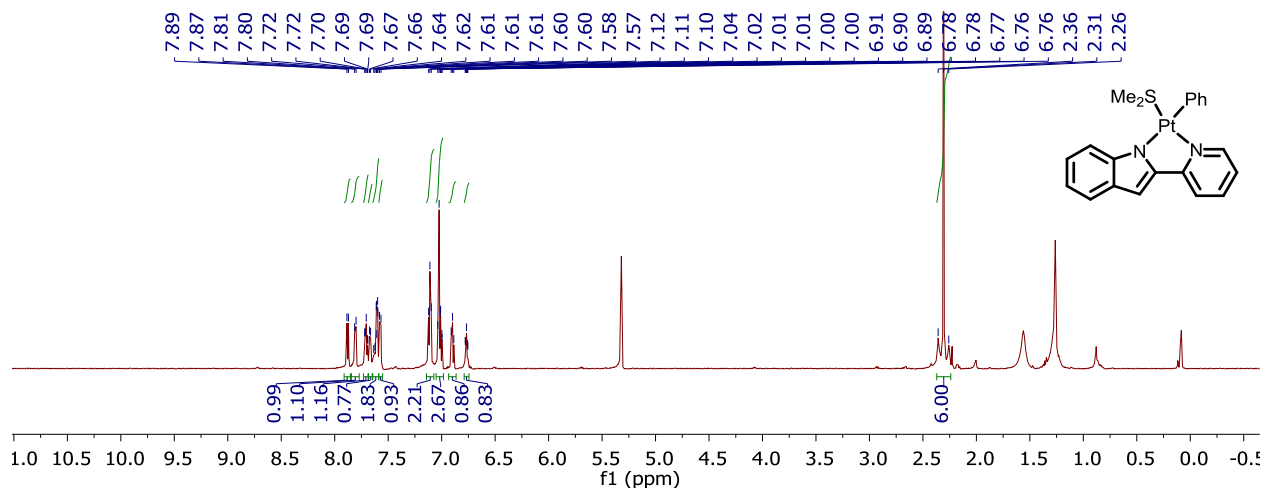
Figure A12a. ^{1}H NMR spectrum of **5d** in dichloromethane-d_2.
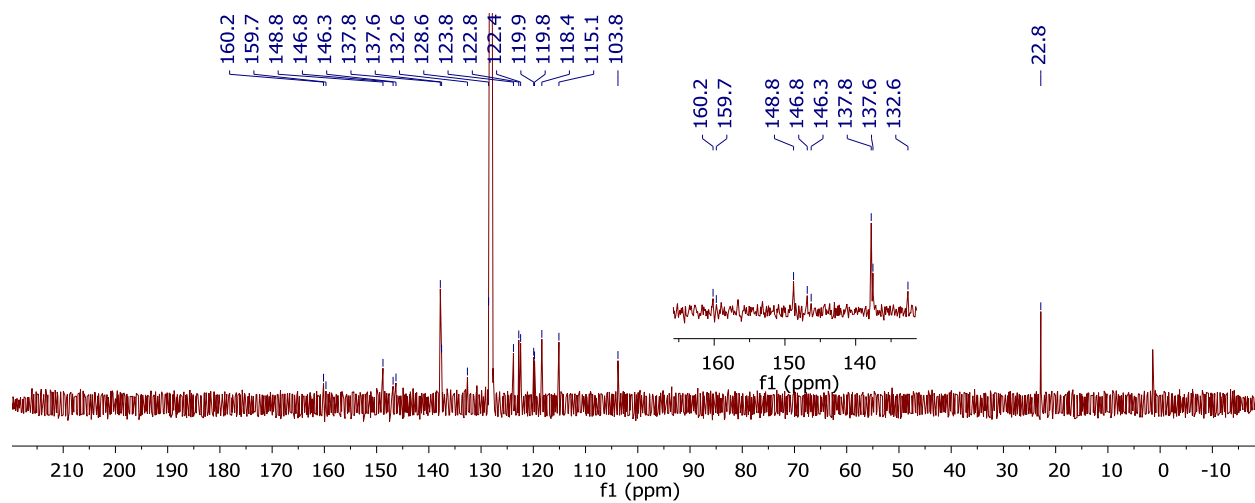
Figure A12b. ^{13}C{^{1}H} NMR spectrum of **5d** in dichloromethane-d_2.
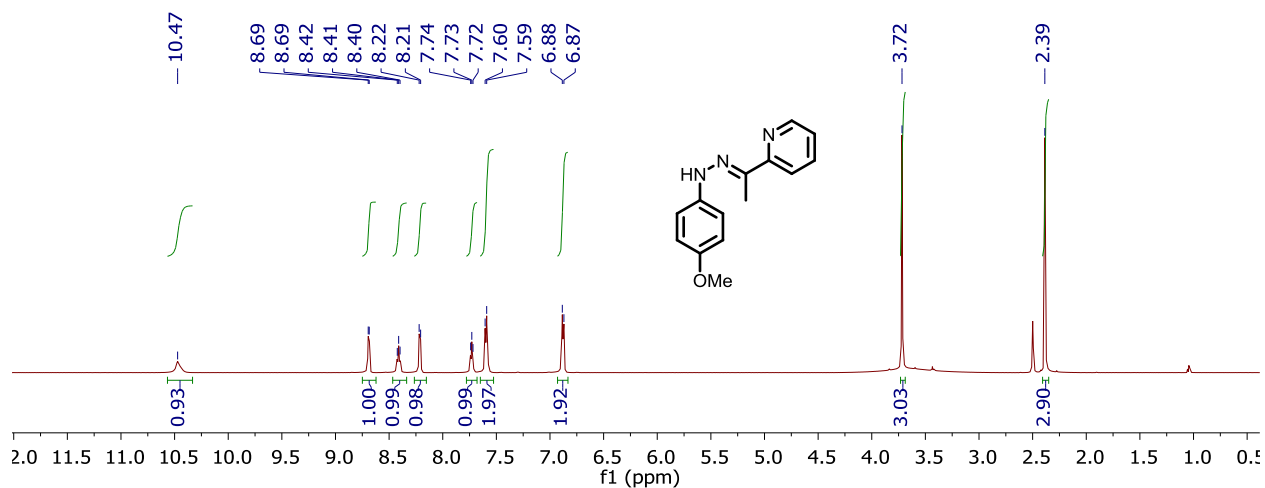
**Figure A13a.** ^{1}H NMR spectrum of **3e** in dimethylsulfoxide-d_6.
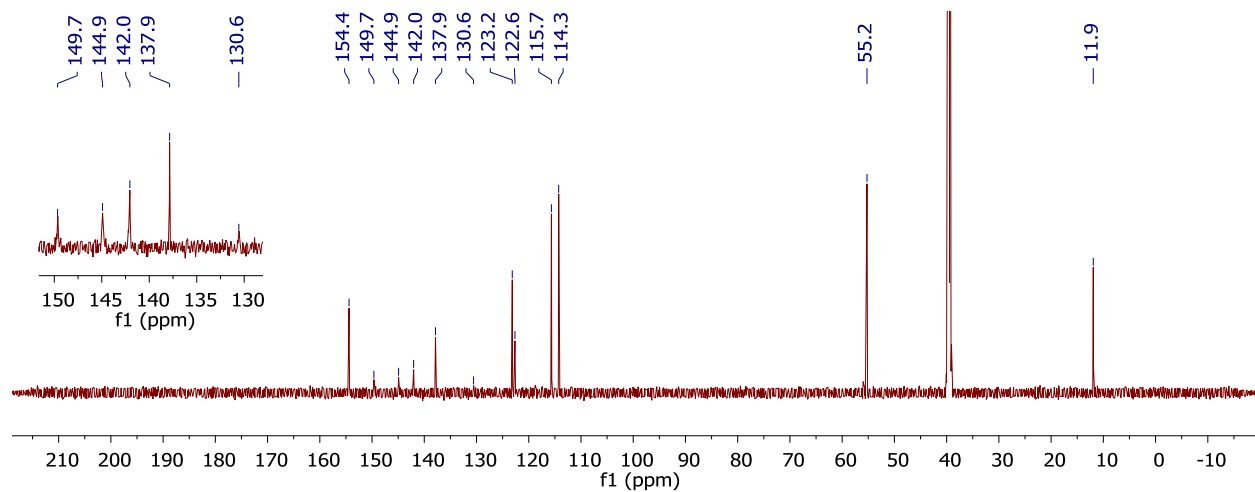
Figure A13b. ^{13}C{^{1}H} NMR spectrum of **3e** in dimethylsulfoxide-d_6.
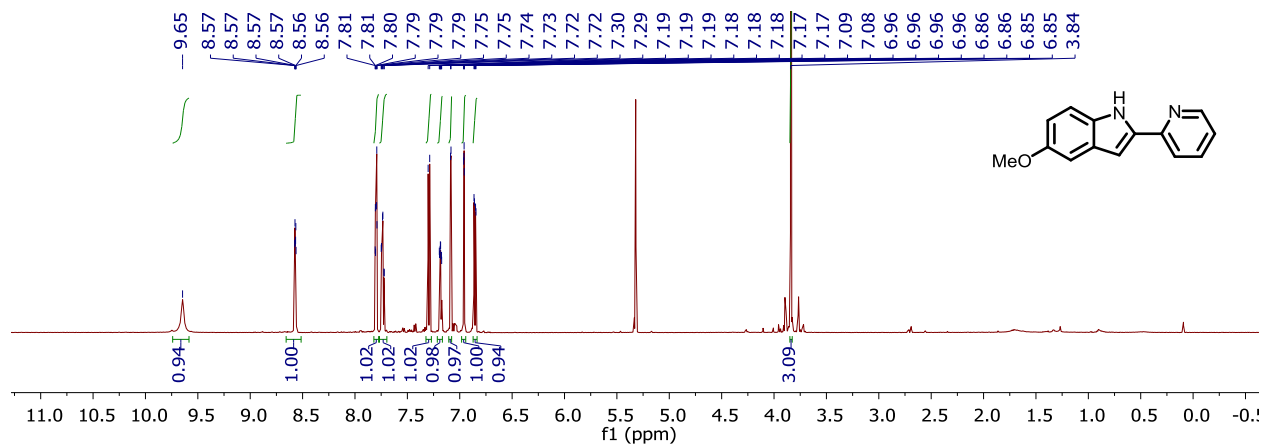
Figure A14a. ^{1}H NMR spectrum of **4e** in dichloromethane-d_2.
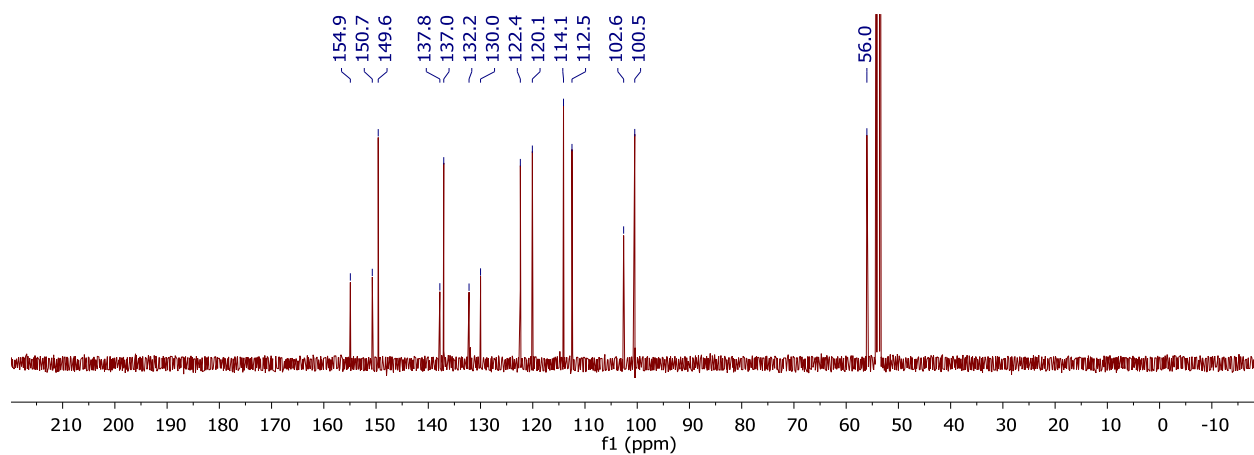
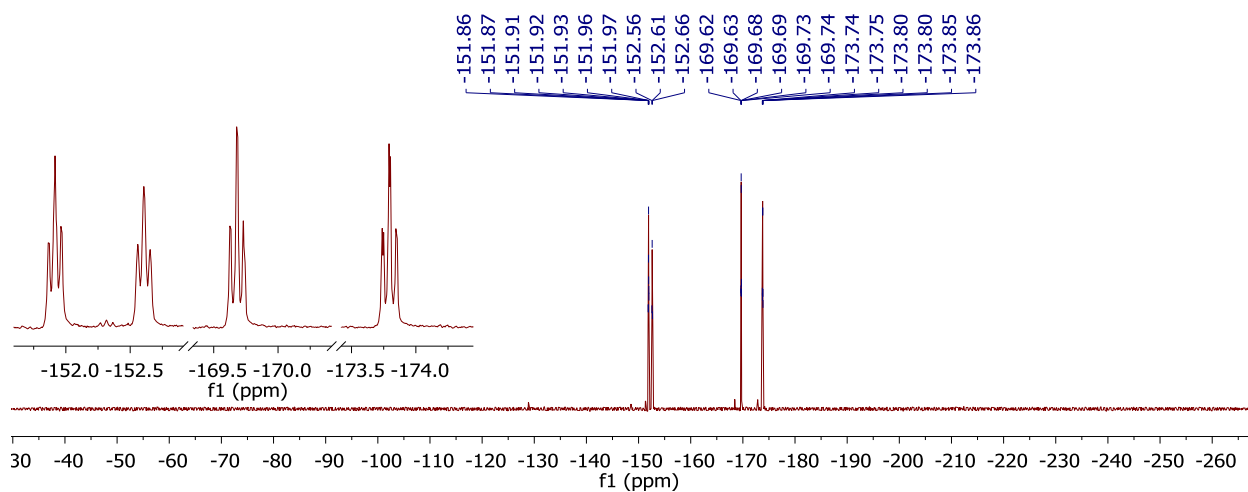**Figure A14b.** ^{13}C{^{1}H} NMR spectrum of **4e** in dichloromethane-d_2.
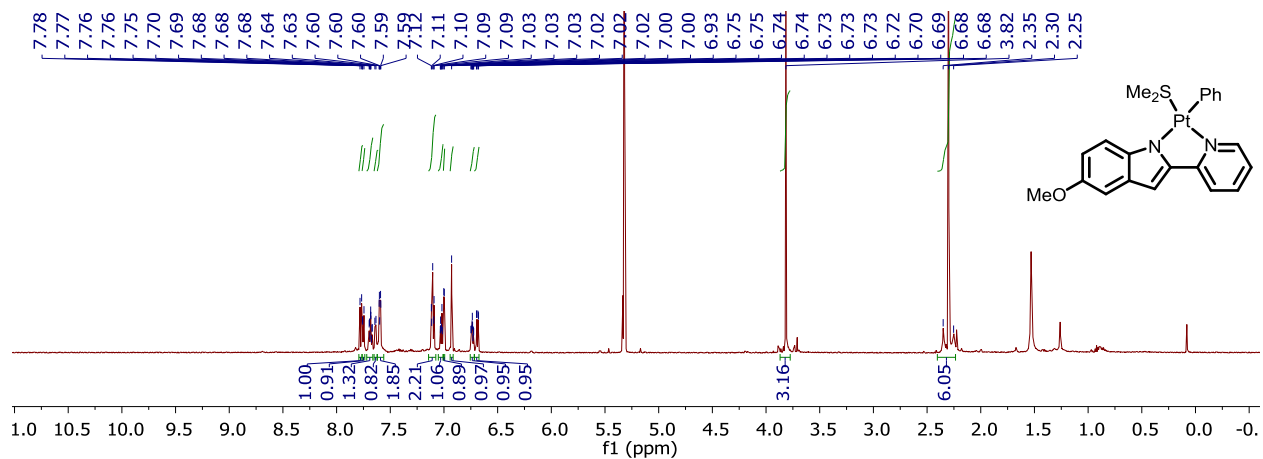
Figure A15a. ^{1}H NMR spectrum of **5e** in dichloromethane-d_2.
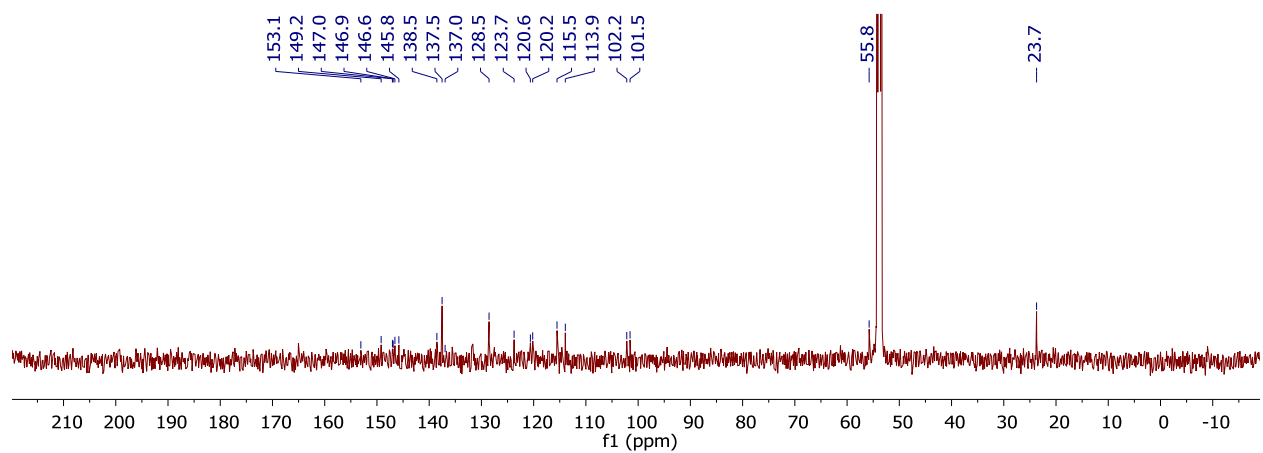
Figure A15b. ^{13}C{^{1}H} NMR spectrum of **5e** in dichloromethane-d_2.
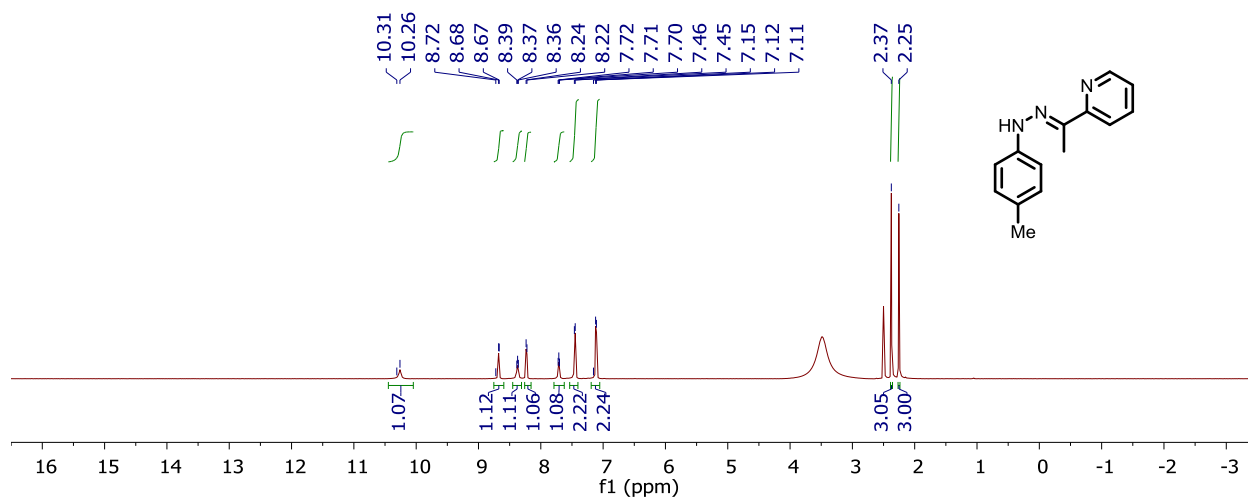
**Figure A16a.** ^{1}H NMR spectrum of **3f** in dimethylsulfoxide-d_6.
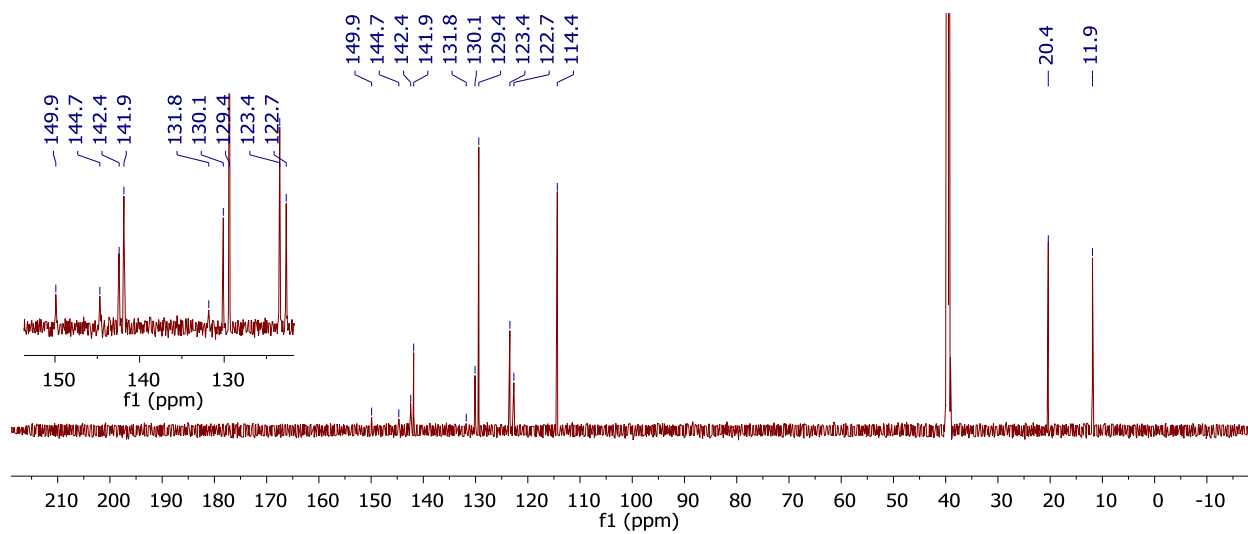
Figure A16b. ^{13}C{^{1}H} NMR spectrum of **3f** in dimethylsulfoxide-d_6.
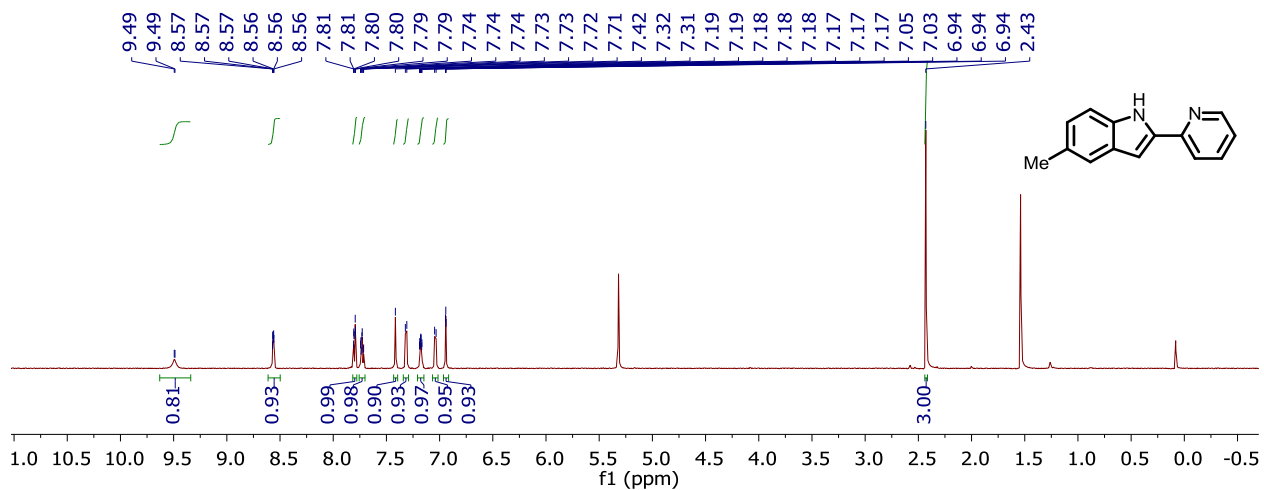
Figure A17a. ^{1}H NMR spectrum of **4f** in dichloromethane-d_2.
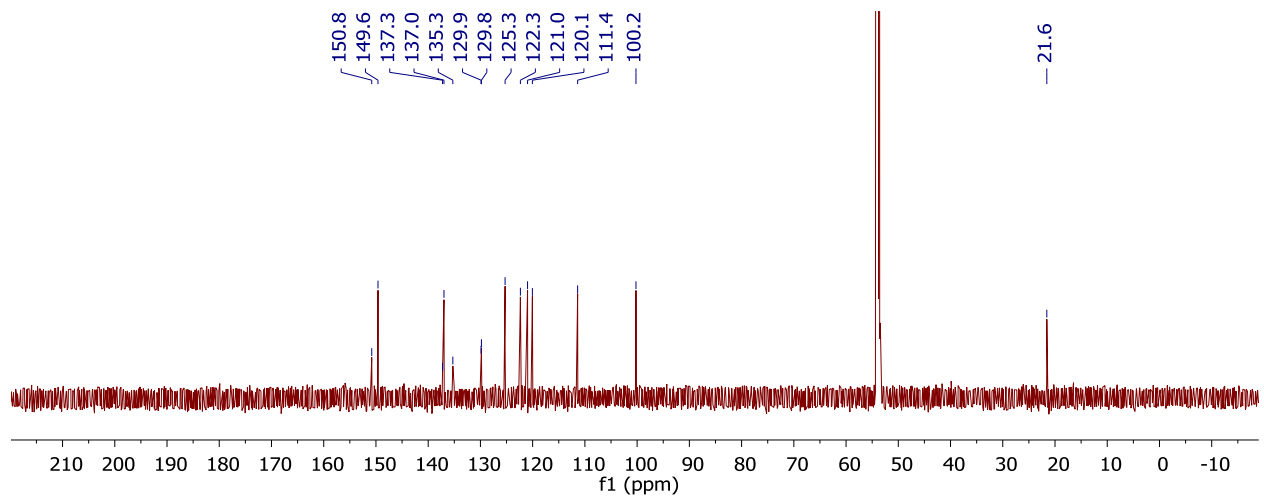
Figure A17b. ^{13}C{^{1}H} NMR spectrum of **4f** in dichloromethane-d_2.
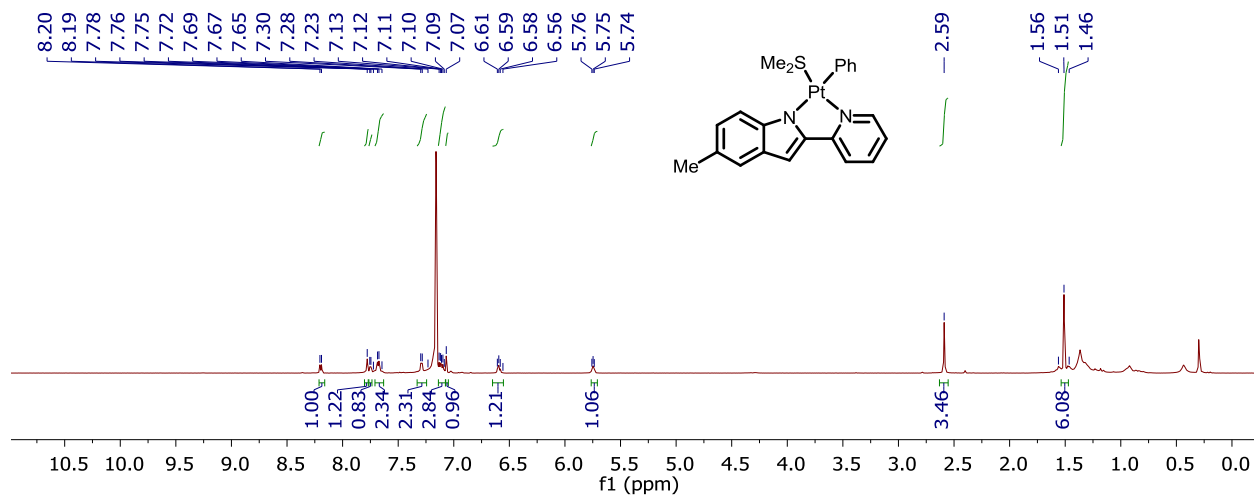
Figure A18a. ^{1}H NMR spectrum of **5f** in dichloromethane-d_2.
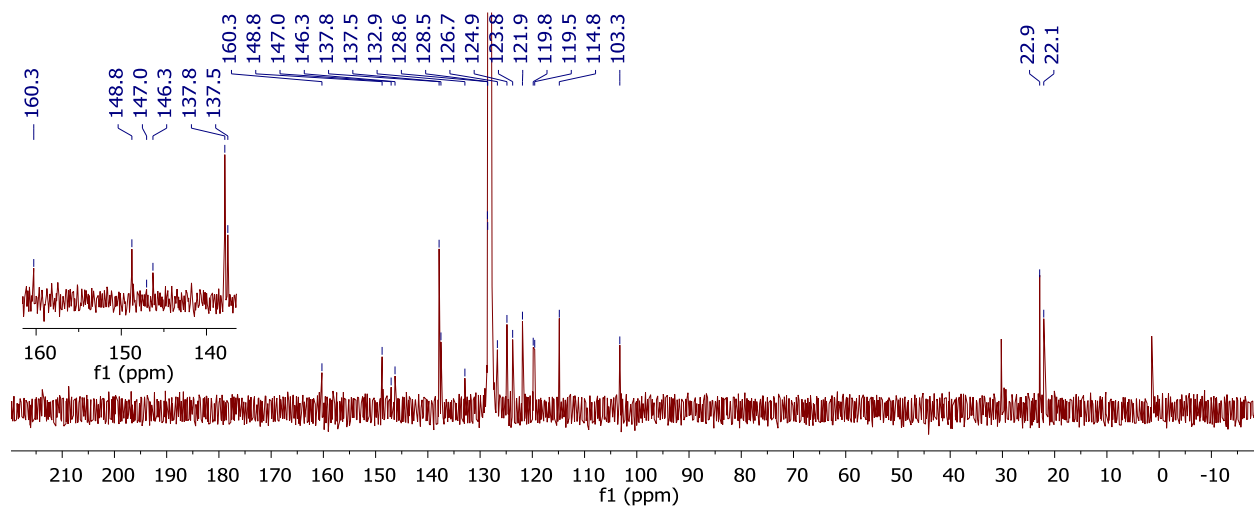
Figure A18b. ^{13}C{^{1}H} NMR spectrum of **5f** in dichloromethane-d_2.
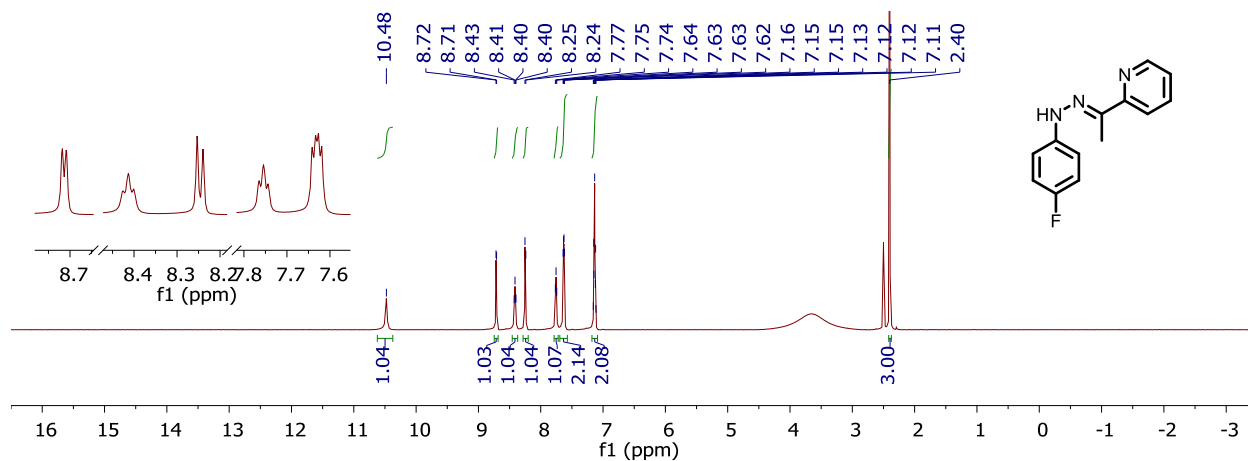
Figure A19a. ^{1}H NMR spectrum of **3g** in dimethylsulfoxide-d_6.
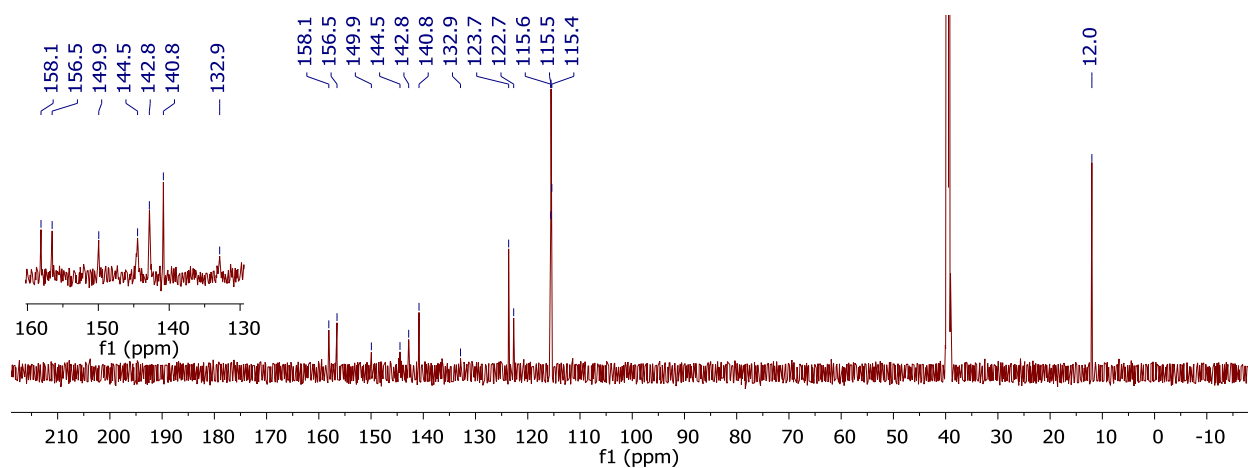
Figure A19b. ^{13}C{^{1}H} NMR spectrum of **3g** in dimethylsulfoxide-d_6.
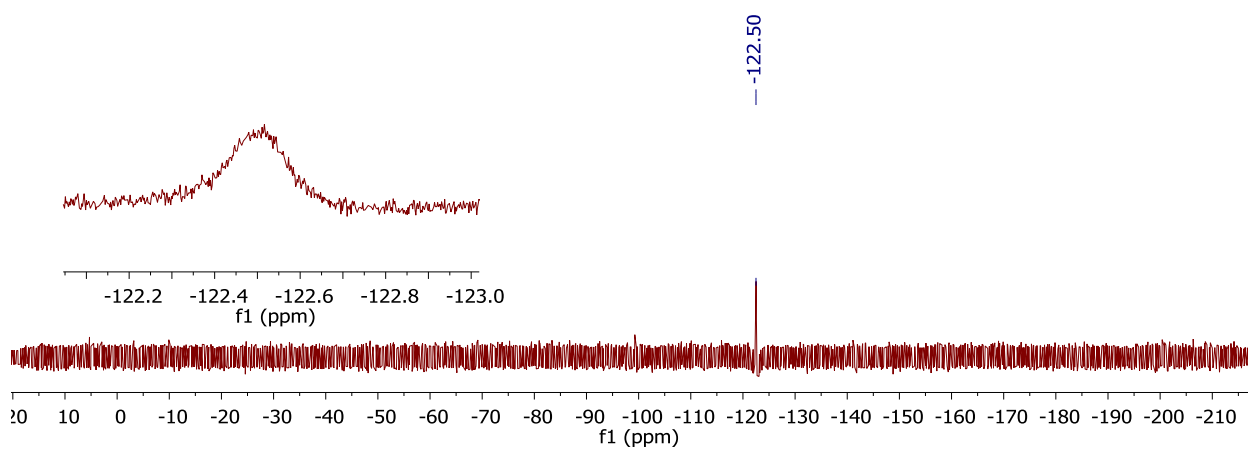
Figure A19c. ^{19}F NMR spectrum of **3g** in dimethylsulfoxide-d_6.
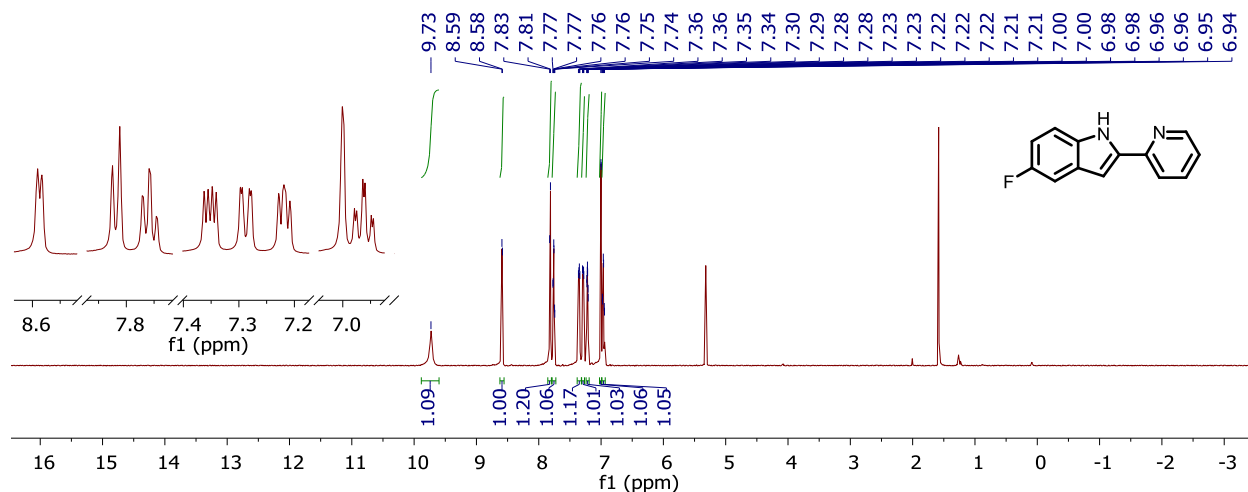
Figure A20a. ^{1}H NMR spectrum of **4g** in dichloromethane-d_2.
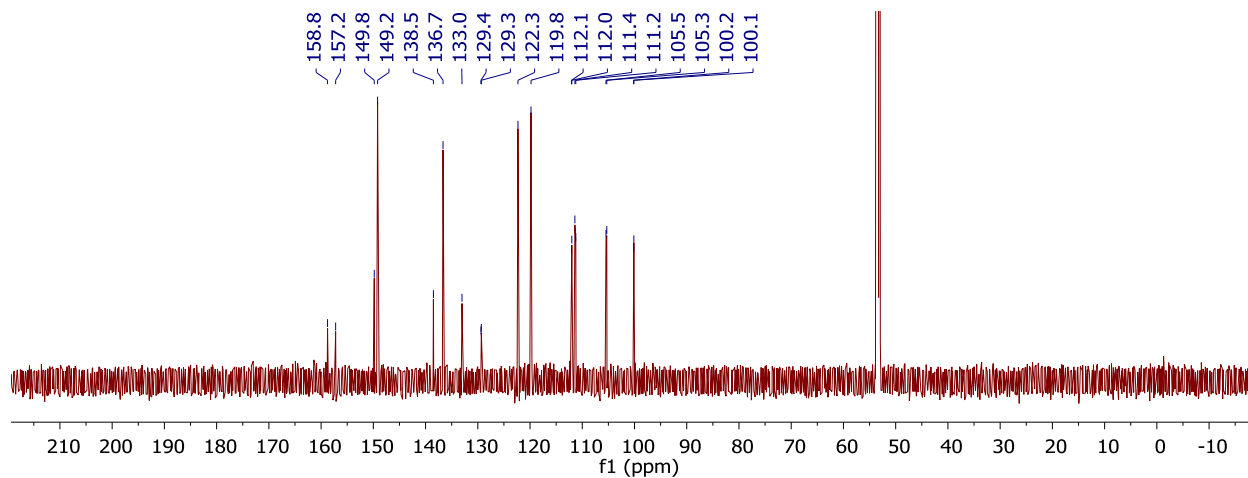
Figure A20b. ^{13}C{^{1}H} NMR spectrum of **4g** in dichloromethane-d_2.
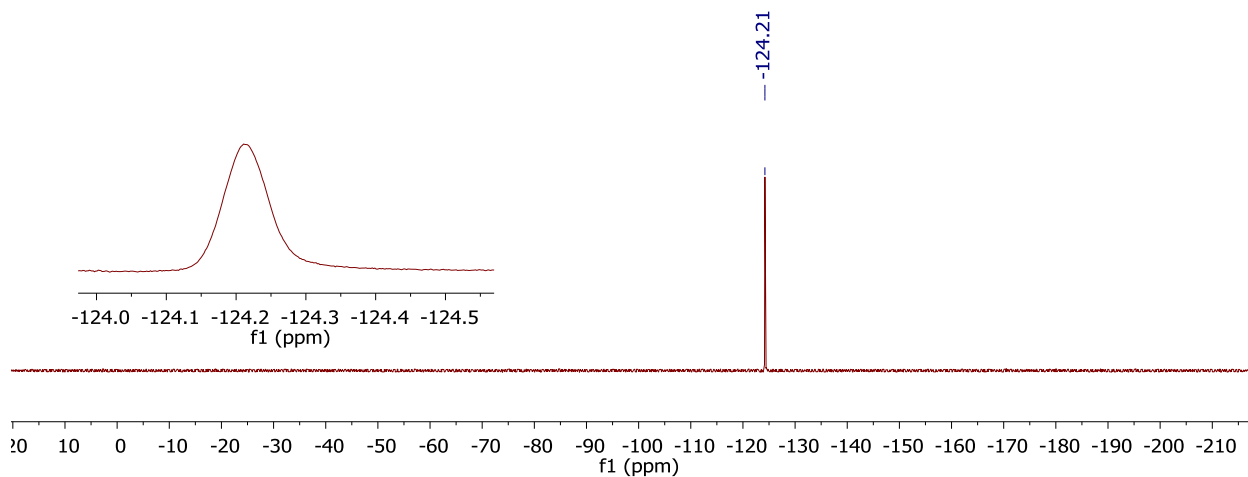
Figure A20c. ^{19}F NMR spectrum of **4g** in dichloromethane-d_2.
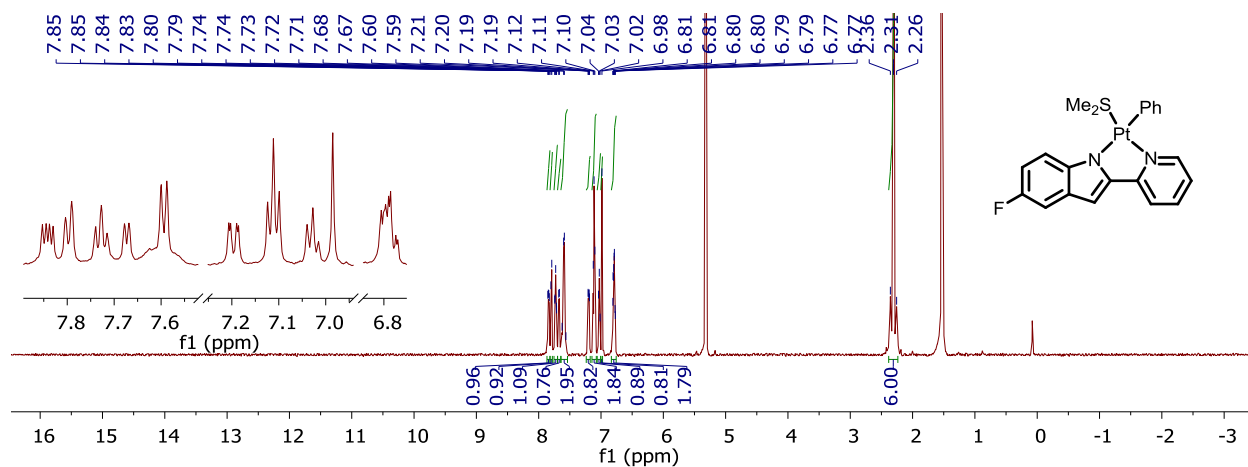
Figure A21a. ^{1}H NMR spectrum of **5g** in dichloromethane-d_2.
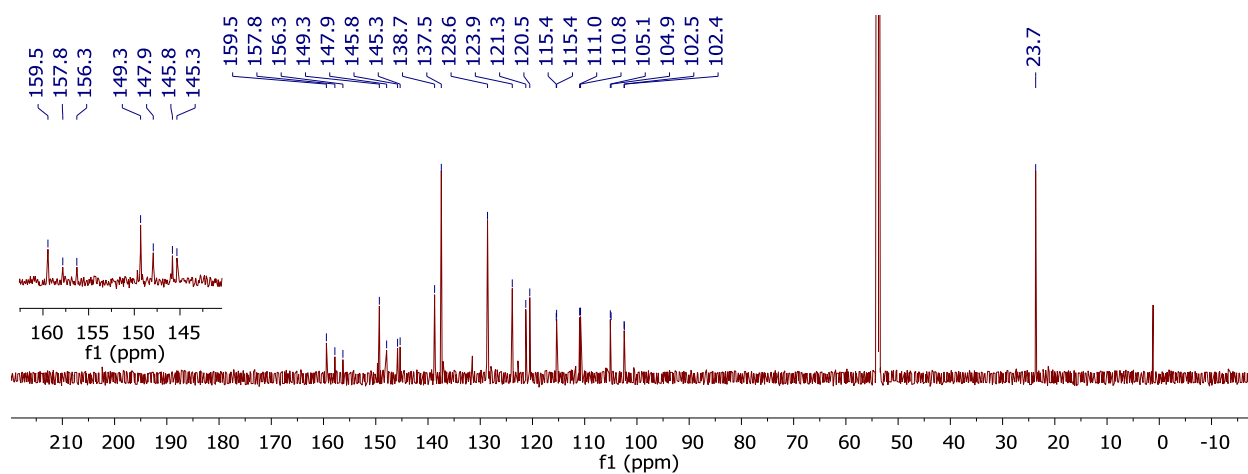
Figure A21b. ^{13}C{^{1}H} NMR spectrum of **5g** in dichloromethane-d_2.
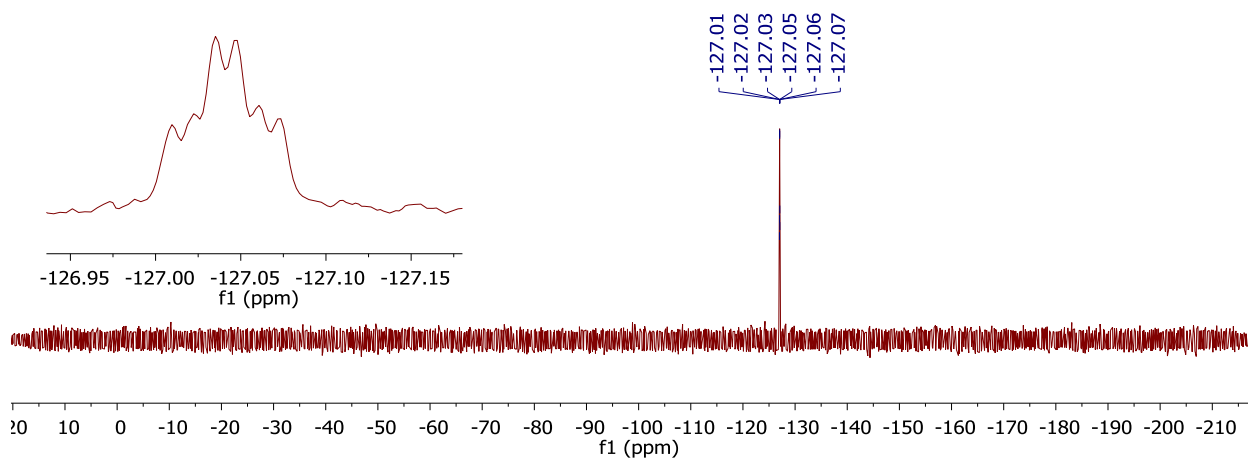
Figure A21c. ^{19}F NMR spectrum of **5g** in dichloromethane-d_2.
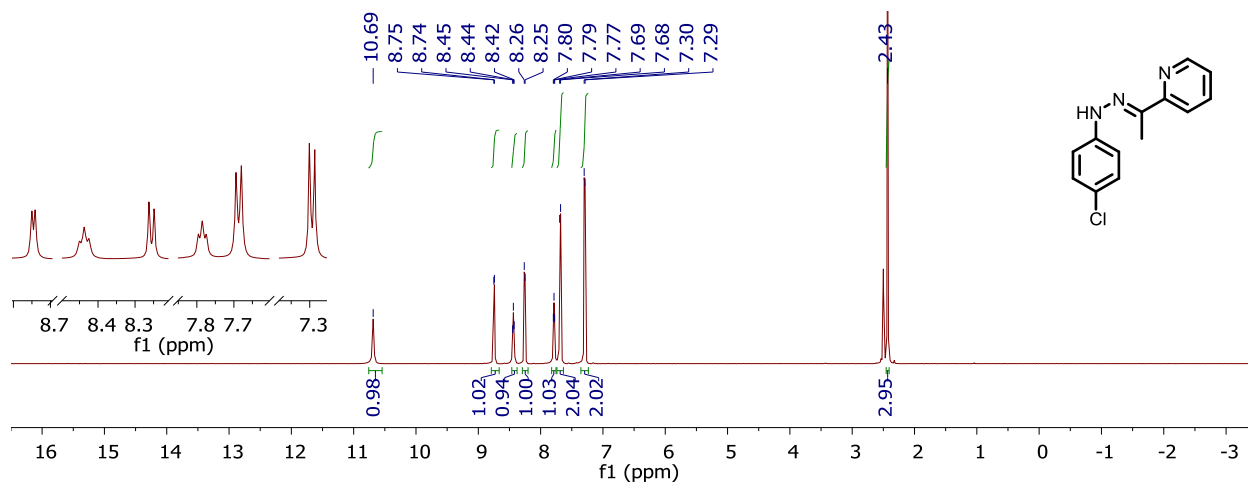
Figure A22a. ^{1}H NMR spectrum of **3h** in dimethylsulfoxide-d_6.
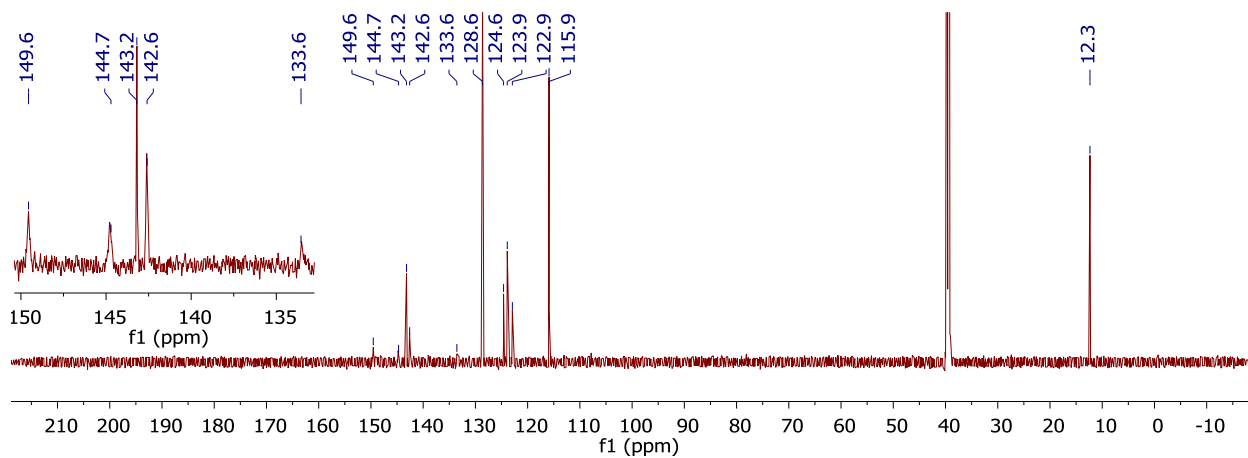
Figure A22b. ^{13}C{^{1}H} NMR spectrum of **3h** in dimethylsulfoxide-d_6.
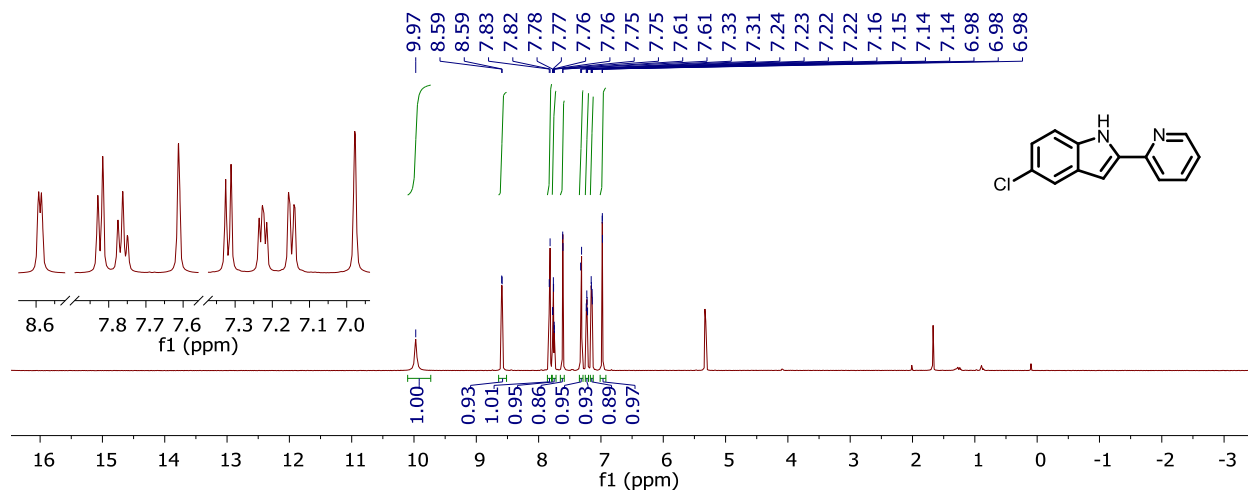
Figure A23a. ^{1}H NMR spectrum of **4h** in dichloromethane-d_2.
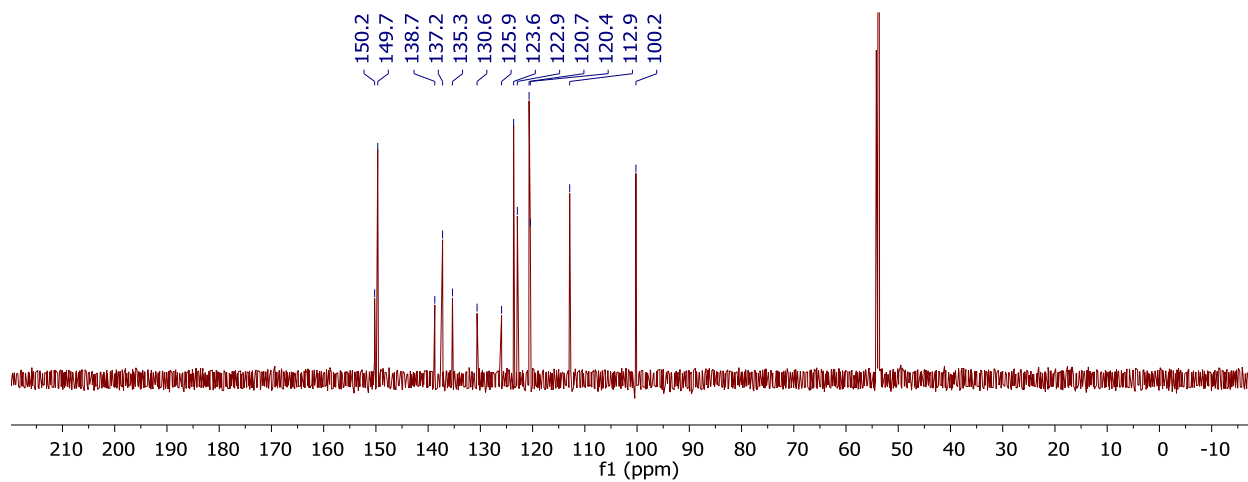
Figure A23b. ^{13}C{^{1}H} NMR spectrum of **4h** in dichloromethane-d_2.
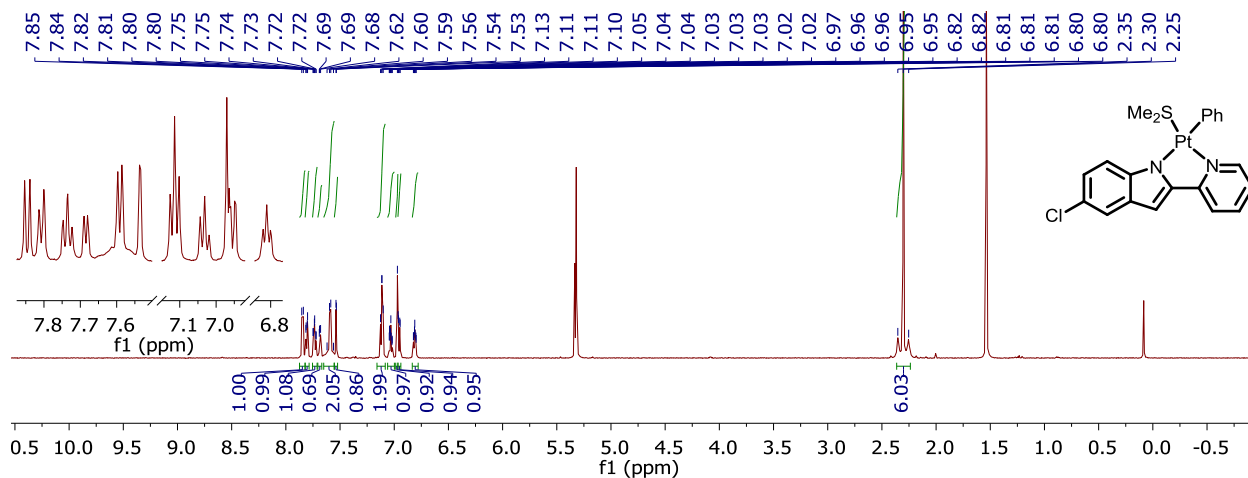
Figure A24a. ^{1}H NMR spectrum of **5h** in dichloromethane-d_2.
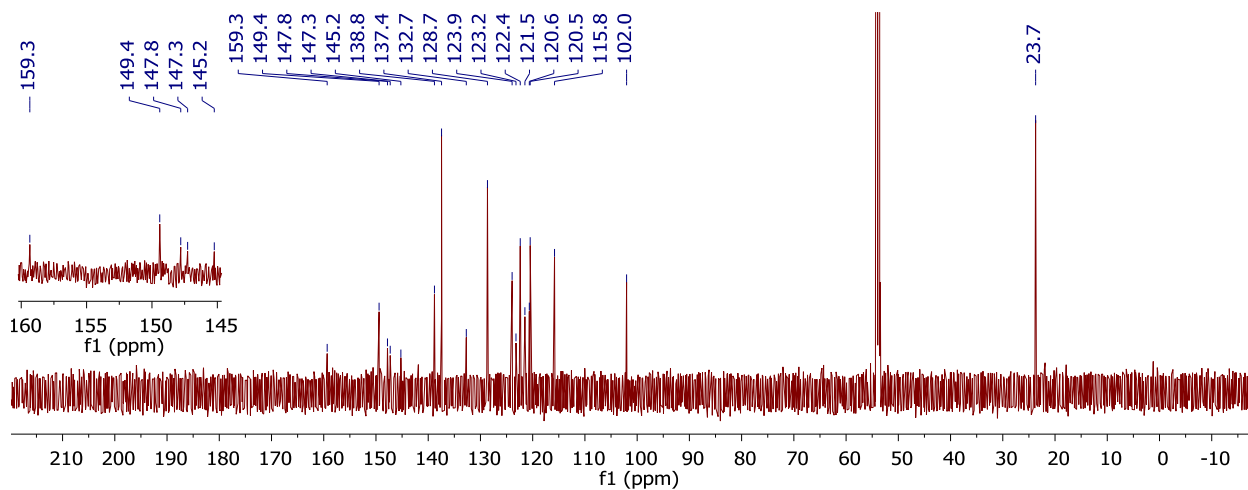
Figure A24b. ^{13}C{^{1}H} NMR spectrum of **5h** in dichloromethane-d_2.
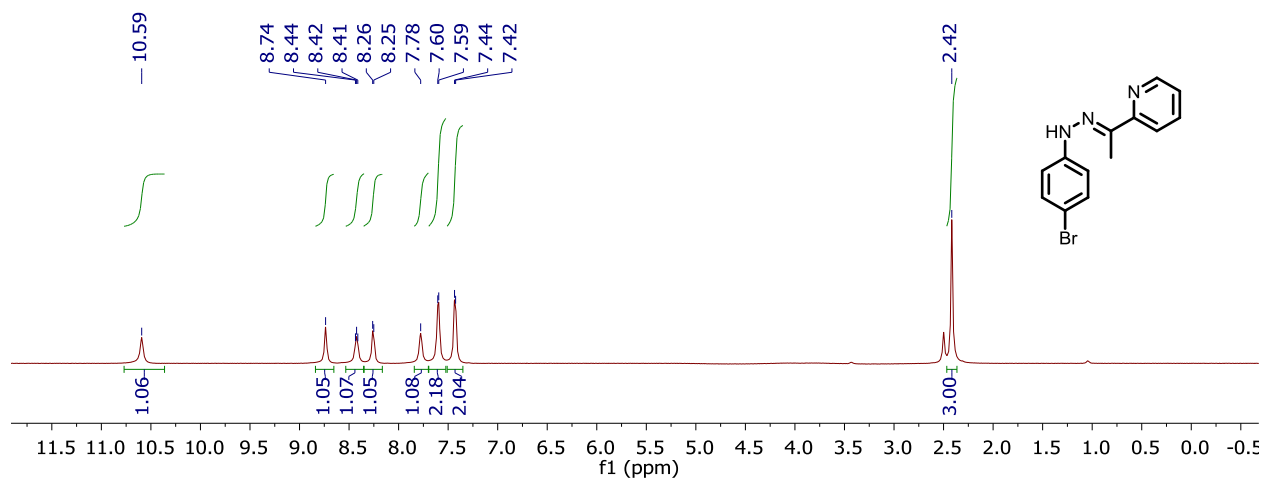
Figure A25a. ^{1}H NMR spectrum of **3i** in dimethylsulfoxide-d_6.
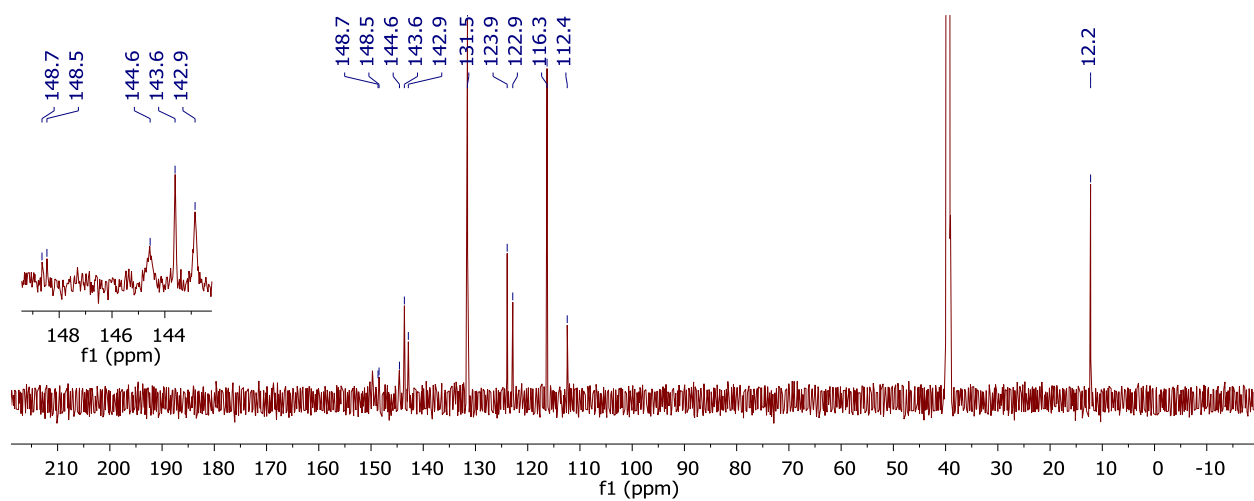
Figure A25b. ^{13}C{^{1}H} NMR spectrum of **3i** in dimethylsulfoxide-d_6.
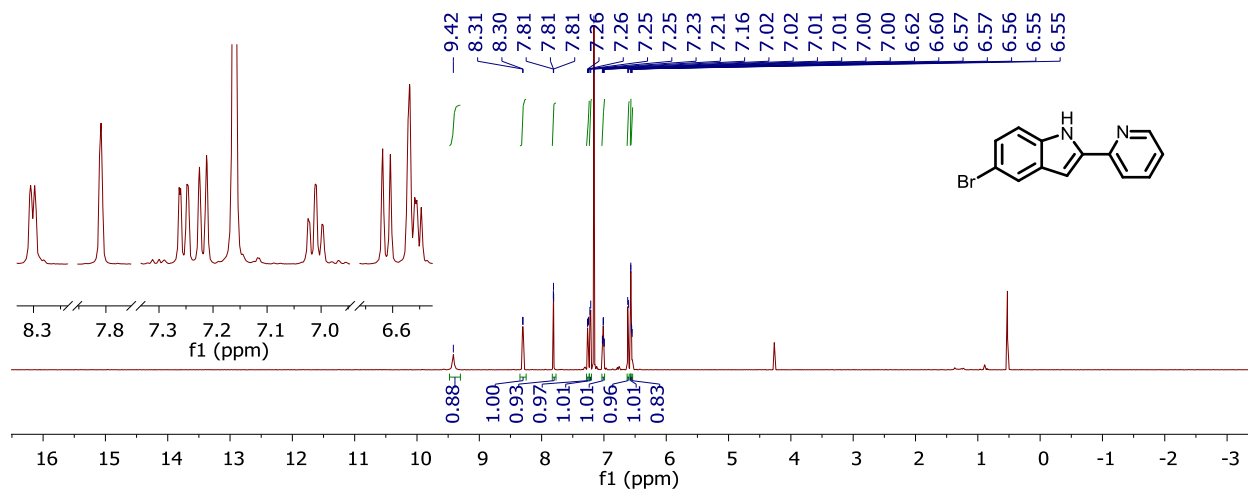
Figure A26a. ^{1}H NMR spectrum of **4i** in benzene-d_6.
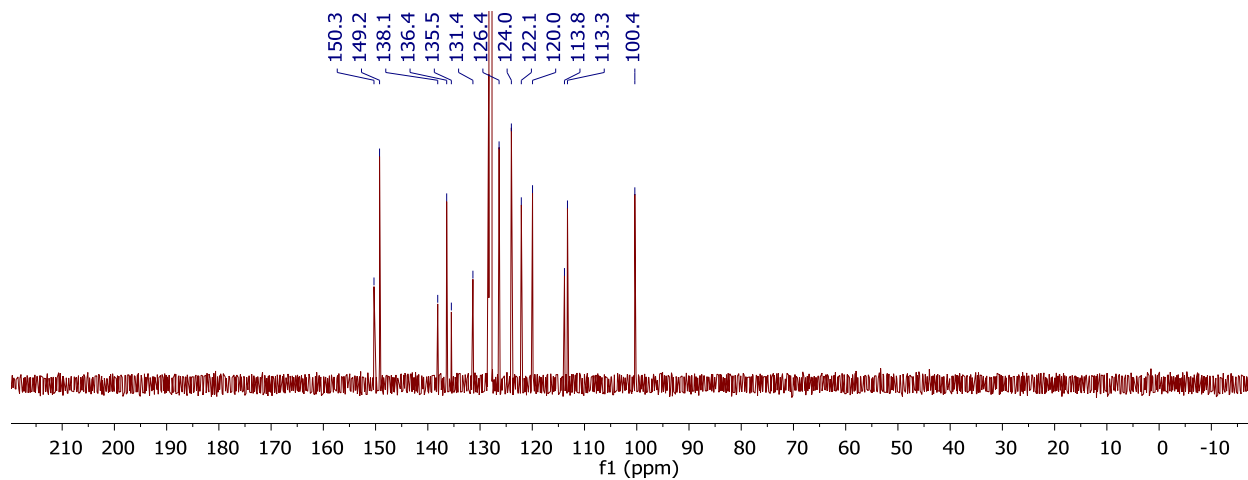
Figure A26b. ^{13}C{^{1}H} NMR spectrum of **4i** in benzene-d_6.
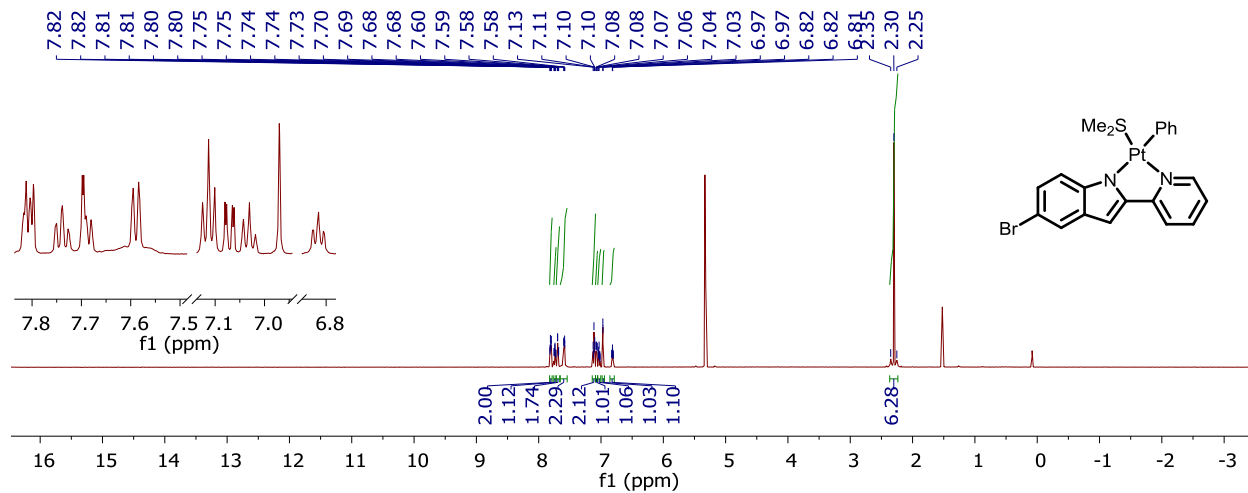
Figure A27a. ^{1}H NMR spectrum of **5i** in dichloromethane-d_2.
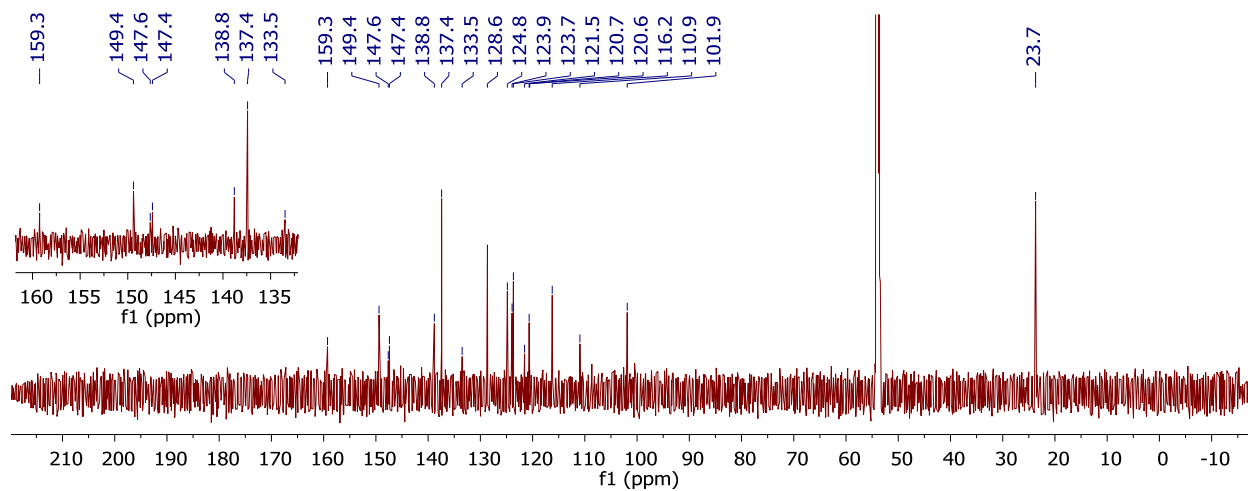
Figure A27b. ^{13}C{^{1}H} NMR spectrum of **5i** in dichloromethane-d_2.
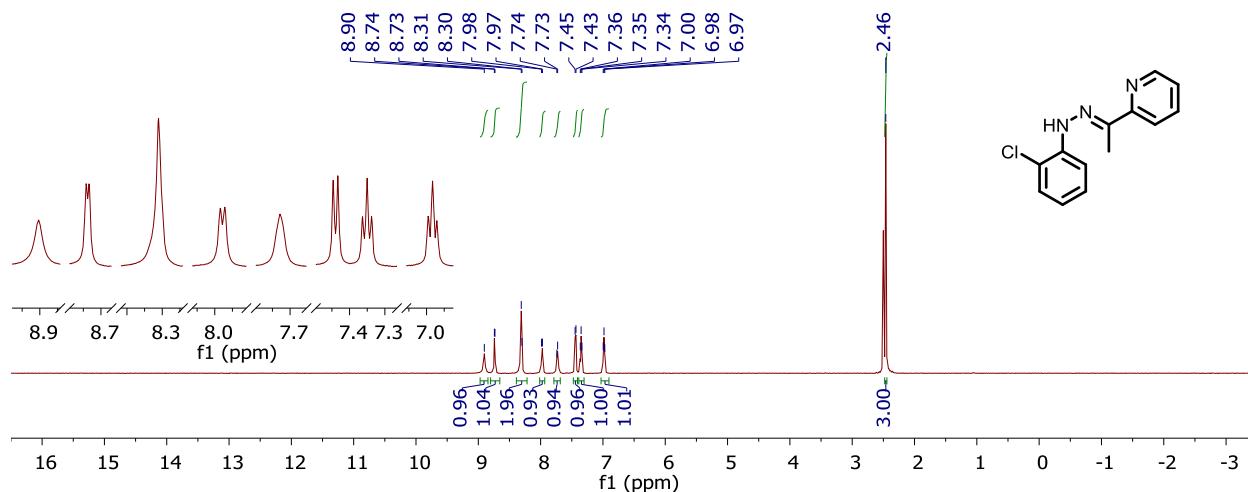
Figure A28a. ^{1}H NMR spectrum of **3j** in dimethylsulfoxide-d_6.
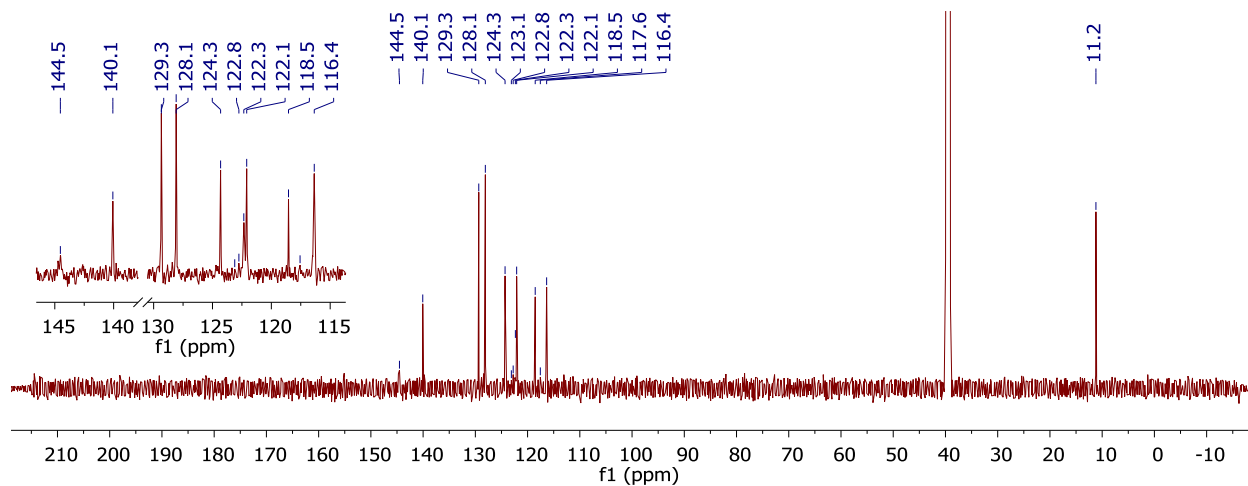
Figure A28b. ^{13}C{^{1}H} NMR spectrum of **3j** in dimethylsulfoxide-d_6.
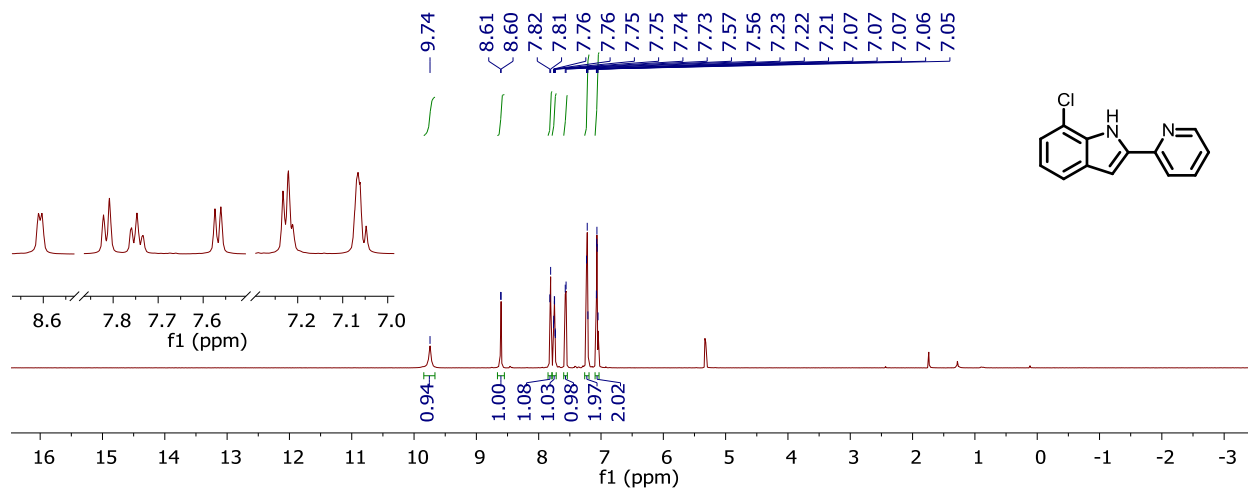
Figure A29a. ^{1}H NMR spectrum of **4j** in dichloromethane-d_2.

Figure A29b. ^{13}C{^{1}H} NMR spectrum of **4j** in dichloromethane-d_2.

Figure A30a. ^{1}H NMR spectrum of **5j** in dichloromethane-d_2.

Figure A30b. ^{13}C{^{1}H} NMR spectrum of **5j** in dichloromethane-d_2.
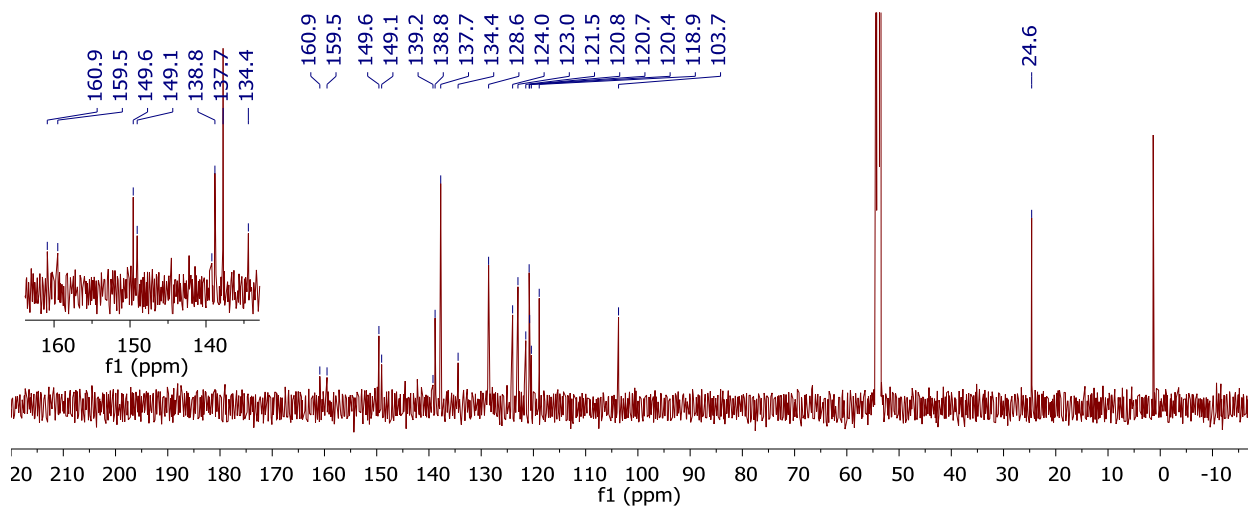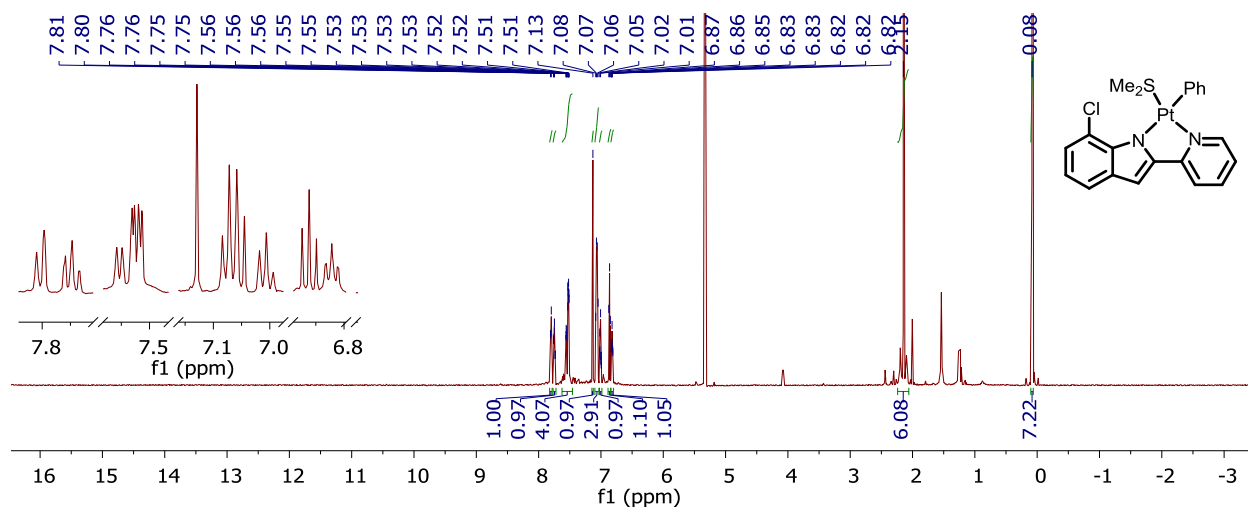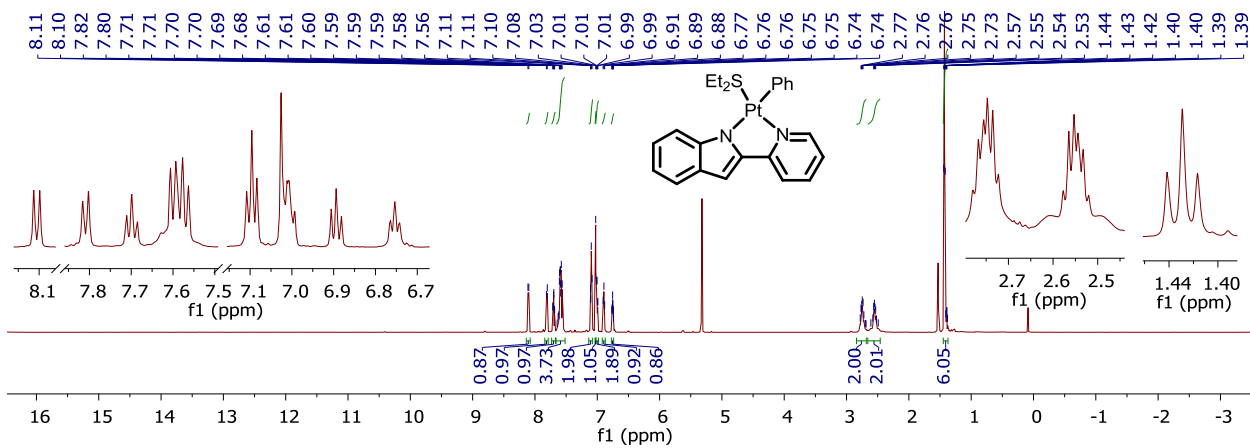
Figure A31a. ^{1}H NMR spectrum of **5k** in dichloromethane-d_2.

Figure A31b. ^{13}C{^{1}H} NMR spectrum of **5k** in dichloromethane-d_2.
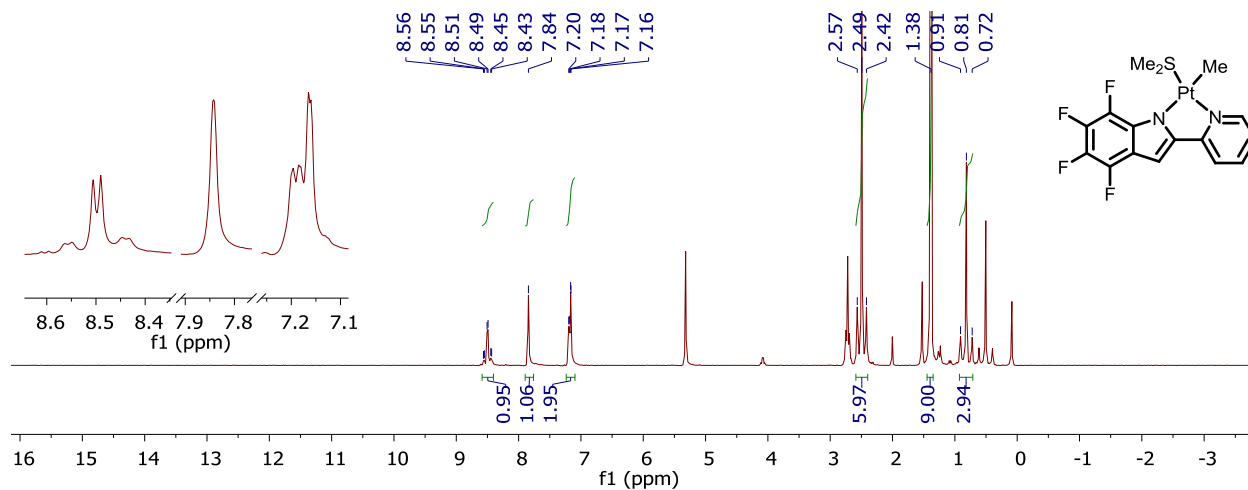
Figure A32a. ^{1}H NMR spectrum of **5l** in dichloromethane-d_2.

Figure A32b. ^{19}F NMR spectrum of **5l** in dichloromethane-d_2.
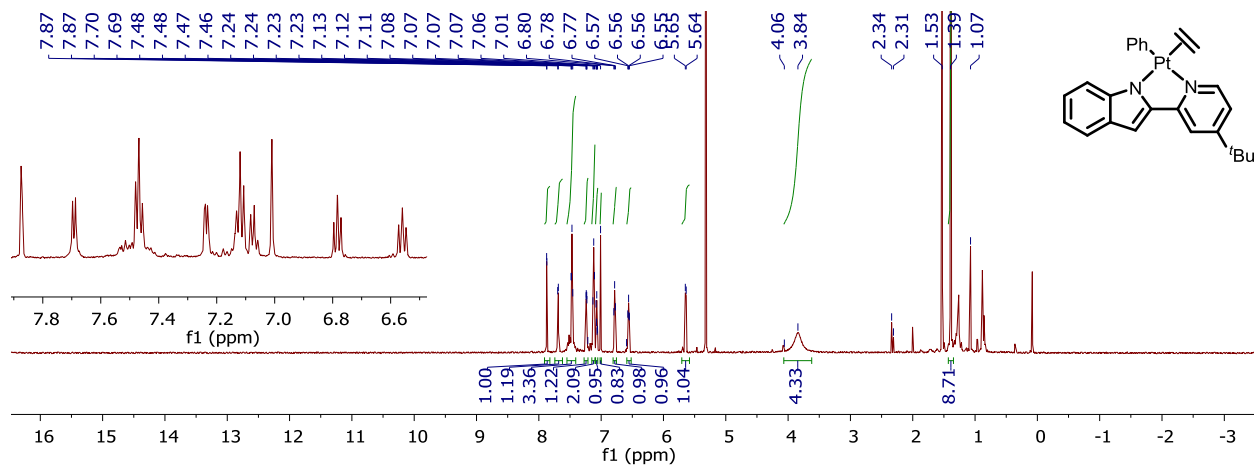
Figure A33a. ^{1}H NMR spectrum of **6** in dichloromethane-d_2.
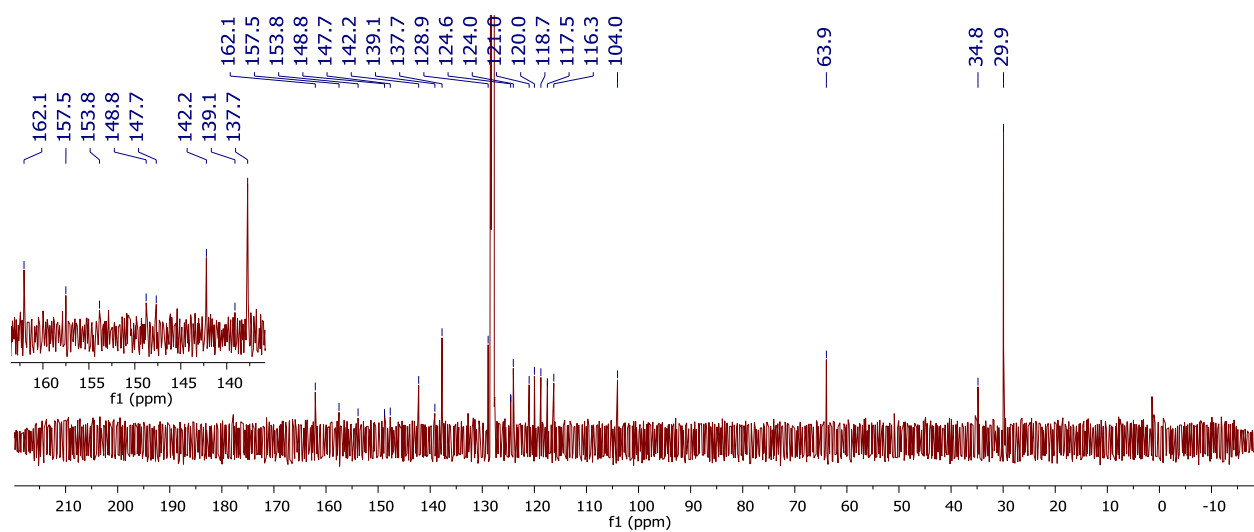
Figure A33b. ^{13}C{^{1}H} NMR spectrum of **6** in benzene-d_6.
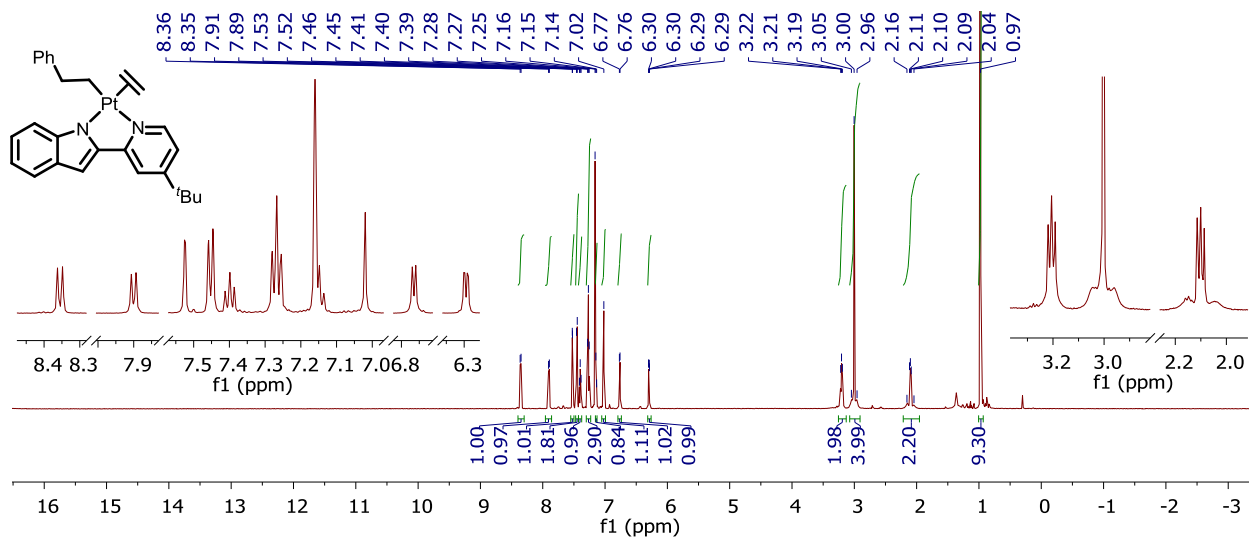
Figure A34a. ^{1}H NMR spectrum of **7** in benzene-d_6.
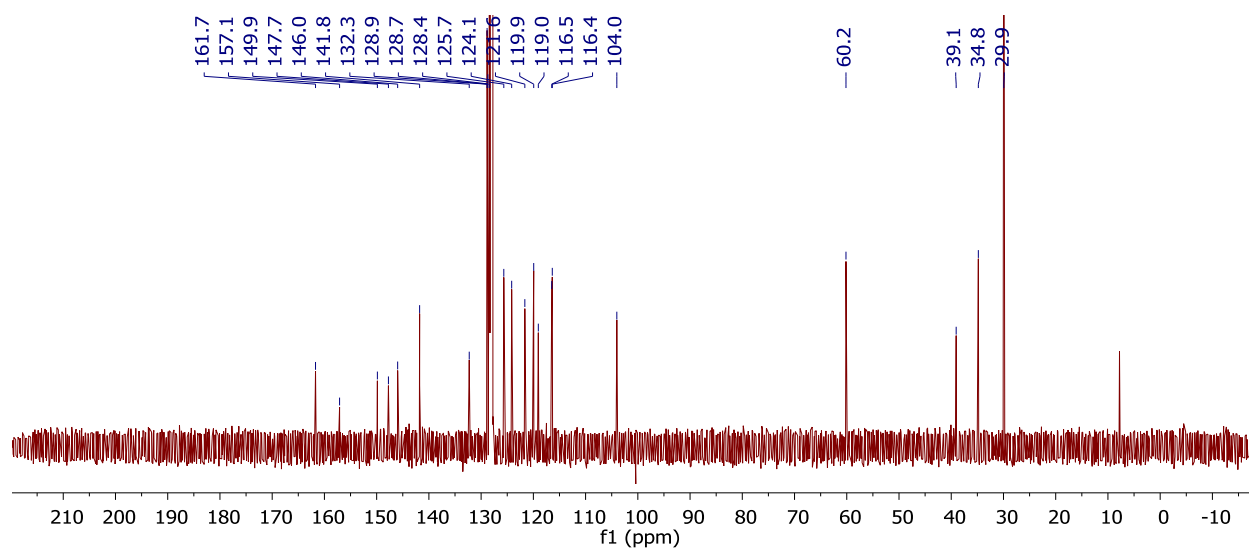
Figure A34b. ^{13}C{^{1}H} NMR spectrum of **7** in dichloromethane-d_2.

Crystallographic Data

Crystallographic Data for Complex **5a**

Table A1. Atomic coordinates (x 10^4) and equivalent isotropic displacement parameters (Å^2 x 10^3) for **5a**. U(eq) is defined as one third of the trace of the orthogonalized U^{ij} tensor.

Atom	x	y	z	U(eq)
C(1)	9544(1)	2562(2)	9718(1)	14(1)
C(2)	9204(1)	1869(2)	9964(1)	17(1)
C(3)	8710(1)	2287(2)	10006(1)	21(1)
C(4)	8543(1)	3422(2)	9808(1)	22(1)
C(5)	8876(1)	4129(2)	9580(1)	22(1)
C(6)	9366(1)	3708(2)	9534(1)	19(1)
C(7)	9356(1)	-108(2)	8677(1)	28(1)
C(8)	9041(1)	1976(2)	7915(1)	22(1)
C(9)	11278(1)	796(2)	9277(1)	14(1)
C(10)	11016(1)	-6(2)	8663(1)	18(1)
C(11)	11363(1)	-613(2)	8408(1)	21(1)
C(12)	11965(1)	-419(2)	8725(1)	21(1)
C(13)	12229(1)	371(2)	9320(1)	19(1)
C(14)	11893(1)	970(2)	9617(1)	15(1)
C(15)	12029(1)	1738(2)	10259(1)	15(1)
C(16)	11509(1)	1981(2)	10280(1)	13(1)
C(17)	11386(1)	2638(2)	10846(1)	13(1)
C(18)	11813(1)	3118(2)	11536(1)	15(1)
C(19)	11666(1)	3704(2)	12066(1)	14(1)
C(20)	11075(1)	3787(2)	11867(1)	16(1)
C(21)	10670(1)	3301(2)	11180(1)	16(1)
C(22)	12109(1)	4287(2)	12816(1)	17(1)
C(23)	12010(1)	3938(2)	13536(1)	25(1)
C(24)	12027(1)	5591(2)	12686(2)	28(1)
C(25)	12731(1)	3985(2)	12987(1)	25(1)
N(1)	10814(1)	2729(2)	10670(1)	13(1)
N(2)	11048(1)	1437(2)	9682(1)	14(1)
S(1)	9684(1)	1127(1)	8459(1)	16(1)
Pt(1)	10249(1)	1959(1)	9634(1)	12(1)

Table A2. Bond lengths [Å] for **5a**.

Bond	Length	Bond	Length
C(1)-C(6)	1.404(3)	C(14)-C(15)	1.414(3)
C(1)-C(2)	1.406(3)	C(15)-C(16)	1.384(3)
C(1)-Pt(1)	2.014(2)	C(15)-H(30)	0.9500
C(2)-C(3)	1.394(3)	C(16)-N(2)	1.376(3)
C(2)-H(6)	0.9500	C(16)-C(17)	1.451(3)
C(3)-C(4)	1.389(3)	C(17)-N(1)	1.362(3)
C(3)-H(24)	0.9500	C(17)-C(18)	1.395(3)
C(4)-C(5)	1.382(3)	C(18)-C(19)	1.388(3)
C(4)-H(35)	0.9500	C(18)-H(14)	0.9500
C(5)-C(6)	1.389(3)	C(19)-C(20)	1.398(3)
C(5)-H(36)	0.9500	C(19)-C(22)	1.526(3)
C(6)-H(100)	0.9500	C(20)-C(21)	1.374(3)
C(7)-S(1)	1.802(2)	C(20)-H(105)	0.9500
C(7)-H(33A)	0.9800	C(21)-N(1)	1.343(3)
C(7)-H(33B)	0.9800	C(21)-H(28)	0.9500
C(7)-H(33C)	0.9800	C(22)-C(25)	1.527(3)
C(8)-S(1)	1.806(2)	C(22)-C(23)	1.535(3)
C(8)-H(12A)	0.9800	C(22)-C(24)	1.538(3)
C(8)-H(12B)	0.9800	C(23)-H(16A)	0.9800
C(8)-H(12C)	0.9800	C(23)-H(16B)	0.9800
C(9)-N(2)	1.370(3)	C(23)-H(16C)	0.9800
C(9)-C(10)	1.404(3)	C(24)-H(8A)	0.9800
C(9)-C(14)	1.434(3)	C(24)-H(8B)	0.9800
C(10)-C(11)	1.377(3)	C(24)-H(8C)	0.9800
C(10)-H(11)	0.9500	C(25)-H(25A)	0.9800
C(11)-C(12)	1.410(3)	C(25)-H(25B)	0.9800
C(11)-H(15)	0.9500	C(25)-H(25C)	0.9800
C(12)-C(13)	1.374(3)	N(1)-Pt(1)	2.0529(18)
C(12)-H(9)	0.9500	N(2)-Pt(1)	2.1030(17)
C(13)-C(14)	1.403(3)	S(1)-Pt(1)	2.2580(5)
C(13)-H(26)	0.9500		

Table A3.   Bond angles [°] for **5a**.

Bond	Angle	Bond	Angle
C(6)-C(1)-C(2)	116.3(2)	N(1)-C(17)-C(18)	121.20(19)
C(6)-C(1)-Pt(1)	121.28(16)	N(1)-C(17)-C(16)	114.88(18)
C(2)-C(1)-Pt(1)	122.38(16)	C(18)-C(17)-C(16)	123.88(19)
C(3)-C(2)-C(1)	122.0(2)	C(19)-C(18)-C(17)	120.9(2)
C(3)-C(2)-H(6)	119.0	C(19)-C(18)-H(14)	119.6
C(1)-C(2)-H(6)	119.0	C(17)-C(18)-H(14)	119.6
C(4)-C(3)-C(2)	119.9(2)	C(18)-C(19)-C(20)	116.6(2)
C(4)-C(3)-H(24)	120.0	C(18)-C(19)-C(22)	123.45(19)
C(2)-C(3)-H(24)	120.0	C(20)-C(19)-C(22)	119.94(19)
C(5)-C(4)-C(3)	119.3(2)	C(21)-C(20)-C(19)	120.5(2)
C(5)-C(4)-H(35)	120.4	C(21)-C(20)-H(105)	119.7
C(3)-C(4)-H(35)	120.4	C(19)-C(20)-H(105)	119.7
C(4)-C(5)-C(6)	120.6(2)	N(1)-C(21)-C(20)	122.8(2)
C(4)-C(5)-H(36)	119.7	N(1)-C(21)-H(28)	118.6
C(6)-C(5)-H(36)	119.7	C(20)-C(21)-H(28)	118.6
C(5)-C(6)-C(1)	121.8(2)	C(25)-C(22)-C(19)	112.38(18)
C(5)-C(6)-H(100)	119.1	C(25)-C(22)-C(23)	108.37(19)
C(1)-C(6)-H(100)	119.1	C(19)-C(22)-C(23)	110.43(18)
S(1)-C(7)-H(33A)	109.5	C(25)-C(22)-C(24)	108.6(2)
S(1)-C(7)-H(33B)	109.5	C(19)-C(22)-C(24)	107.37(18)
H(33A)-C(7)-H(33B)	109.5	C(23)-C(22)-C(24)	109.7(2)
S(1)-C(7)-H(33C)	109.5	C(22)-C(23)-H(16A)	109.5
H(33A)-C(7)-H(33C)	109.5	C(22)-C(23)-H(16B)	109.5
H(33B)-C(7)-H(33C)	109.5	H(16A)-C(23)-H(16B)	109.5
S(1)-C(8)-H(12A)	109.5	C(22)-C(23)-H(16C)	109.5
S(1)-C(8)-H(12B)	109.5	H(16A)-C(23)-H(16C)	109.5
H(12A)-C(8)-H(12B)	109.5	H(16B)-C(23)-H(16C)	109.5
S(1)-C(8)-H(12C)	109.5	C(22)-C(24)-H(8A)	109.5
H(12A)-C(8)-H(12C)	109.5	C(22)-C(24)-H(8B)	109.5
H(12B)-C(8)-H(12C)	109.5	H(8A)-C(24)-H(8B)	109.5
N(2)-C(9)-C(10)	130.4(2)	C(22)-C(24)-H(8C)	109.5
N(2)-C(9)-C(14)	109.52(19)	H(8A)-C(24)-H(8C)	109.5
C(10)-C(9)-C(14)	119.86(19)	H(8B)-C(24)-H(8C)	109.5
C(11)-C(10)-C(9)	118.4(2)	C(22)-C(25)-H(25A)	109.5
C(11)-C(10)-H(11)	120.8	C(22)-C(25)-H(25B)	109.5
C(9)-C(10)-H(11)	120.8	H(25A)-C(25)-H(25B)	109.5
C(10)-C(11)-C(12)	121.9(2)	C(22)-C(25)-H(25C)	109.5
C(10)-C(11)-H(15)	119.1	H(25A)-C(25)-H(25C)	109.5
C(12)-C(11)-H(15)	119.1	H(25B)-C(25)-H(25C)	109.5
C(13)-C(12)-C(11)	120.7(2)	C(21)-N(1)-C(17)	118.07(18)
C(13)-C(12)-H(9)	119.7	C(21)-N(1)-Pt(1)	126.18(14)
C(11)-C(12)-H(9)	119.7	C(17)-N(1)-Pt(1)	115.75(14)
C(12)-C(13)-C(14)	119.0(2)	C(9)-N(2)-C(16)	106.06(17)
C(12)-C(13)-H(26)	120.5	C(9)-N(2)-Pt(1)	141.56(15)
C(14)-C(13)-H(26)	120.5	C(16)-N(2)-Pt(1)	112.09(13)
C(13)-C(14)-C(15)	133.4(2)	C(7)-S(1)-C(8)	99.39(12)
C(13)-C(14)-C(9)	120.1(2)	C(7)-S(1)-Pt(1)	106.58(8)
C(15)-C(14)-C(9)	106.41(18)	C(8)-S(1)-Pt(1)	110.77(8)
C(16)-C(15)-C(14)	105.69(19)	C(1)-Pt(1)-N(1)	93.41(8)
C(16)-C(15)-H(30)	127.2	C(1)-Pt(1)-N(2)	172.73(8)
C(14)-C(15)-H(30)	127.2	N(1)-Pt(1)-N(2)	79.32(7)
N(2)-C(16)-C(15)	112.29(19)	C(1)-Pt(1)-S(1)	90.57(6)
N(2)-C(16)-C(17)	117.02(18)	N(1)-Pt(1)-S(1)	175.43(5)
C(15)-C(16)-C(17)	130.6(2)	N(2)-Pt(1)-S(1)	96.70(5)

Table A4. Anisotropic displacement parameters (Å^2 x 10^3) for **5a**. The anisotropic displacement factor exponent takes the form: -2π^2[h^{2}a^{2}U^{11} + ... + 2hk(abU^{12})].

Atom	U^{11}	U^{22}	U^{33}	U^{23}	U^{13}	U^{12}
C(1)	11(1)	17(1)	13(1)	-1(1)	3(1)	1(1)
C(2)	15(1)	18(1)	18(1)	3(1)	5(1)	2(1)
C(3)	13(1)	29(1)	20(1)	5(1)	7(1)	0(1)
C(4)	15(1)	32(1)	19(1)	2(1)	7(1)	9(1)
C(5)	24(1)	21(1)	19(1)	4(1)	9(1)	8(1)
C(6)	19(1)	18(1)	21(1)	3(1)	9(1)	2(1)
C(7)	35(1)	18(1)	21(1)	2(1)	4(1)	-7(1)
C(8)	18(1)	20(1)	21(1)	3(1)	3(1)	2(1)
C(9)	19(1)	12(1)	15(1)	4(1)	10(1)	3(1)
C(10)	21(1)	18(1)	17(1)	2(1)	9(1)	1(1)
C(11)	32(1)	16(1)	15(1)	0(1)	12(1)	4(1)
C(12)	30(1)	20(1)	21(1)	2(1)	17(1)	8(1)
C(13)	21(1)	20(1)	22(1)	5(1)	14(1)	5(1)
C(14)	15(1)	15(1)	16(1)	5(1)	8(1)	3(1)
C(15)	12(1)	16(1)	16(1)	2(1)	6(1)	2(1)
C(16)	14(1)	12(1)	14(1)	2(1)	7(1)	1(1)
C(17)	13(1)	10(1)	16(1)	3(1)	7(1)	2(1)
C(18)	13(1)	15(1)	17(1)	3(1)	7(1)	1(1)
C(19)	16(1)	12(1)	15(1)	3(1)	7(1)	1(1)
C(20)	16(1)	18(1)	16(1)	-2(1)	10(1)	1(1)
C(21)	14(1)	18(1)	20(1)	2(1)	10(1)	2(1)
C(22)	16(1)	18(1)	16(1)	-1(1)	5(1)	0(1)
C(23)	22(1)	33(1)	18(1)	-2(1)	8(1)	-3(1)
C(24)	29(1)	19(1)	25(1)	-4(1)	3(1)	-4(1)
C(25)	16(1)	37(1)	19(1)	-5(1)	4(1)	-2(1)
N(1)	12(1)	12(1)	15(1)	1(1)	6(1)	0(1)
N(2)	14(1)	12(1)	16(1)	0(1)	8(1)	1(1)
S(1)	15(1)	16(1)	14(1)	0(1)	4(1)	1(1)
Pt(1)	10(1)	12(1)	13(1)	1(1)	5(1)	1(1)

Table A5. Hydrogen coordinates (x 10^4) and isotropic displacement parameters ($\mathring{A}^2$ x 10^3) for **5a**.

Atom	x	y	z	U(eq)
H(6)	9315	1093	10106	21
H(24)	8487	1796	10169	25
H(35)	8204	3710	9829	27
H(36)	8768	4911	9454	26
H(100)	9587	4209	9374	23
H(33A)	9153	130	8990	41
H(33B)	9657	-668	8980	41
H(33C)	9079	-460	8181	41
H(12A)	8800	1597	7410	33
H(12B)	9153	2740	7812	33
H(12C)	8822	2051	8228	33
H(11)	10609	-127	8430	22
H(15)	11192	-1179	8007	25
H(9)	12189	-840	8526	26
H(26)	12633	510	9526	23
H(30)	12401	2027	10604	18
H(14)	12209	3042	11645	17
H(105)	10952	4183	12210	19
H(28)	10272	3372	11060	19
H(16A)	11621	4174	13452	37
H(16B)	12299	4314	14013	37
H(16C)	12047	3103	13604	37
H(8A)	12071	5805	12210	41
H(8B)	12319	5993	13147	41
H(8C)	11639	5806	12619	41
H(25A)	12786	3152	13056	37
H(25B)	12999	4374	13473	37
H(25C)	12807	4234	12543	37

Crystallographic Data for Complex **5b**

Table A6. Atomic coordinates (x 10^4) and equivalent isotropic displacement parameters ($\mathring{A}^2$ x 10^3) for **5b**. U(eq) is defined as one third of the trace of the orthogonalized U^{ij} tensor.

Atom	x	y	z	U(eq)
C(1)	1114(3)	2678(3)	5650(2)	24(1)
C(2)	2122(3)	5223(3)	5385(2)	22(1)
C(3)	2601(3)	4048(3)	3427(2)	16(1)
C(4)	3022(3)	5334(3)	3174(2)	20(1)
C(5)	2088(4)	6073(3)	2627(2)	24(1)
C(6)	696(3)	5540(3)	2296(2)	24(1)
C(7)	256(3)	4274(3)	2527(2)	24(1)
C(8)	1192(3)	3535(3)	3082(2)	19(1)
C(9)	5903(3)	1344(3)	5822(2)	13(1)
C(10)	5209(3)	1245(3)	6700(2)	15(1)
C(11)	5882(3)	729(3)	7486(2)	17(1)
C(12)	7307(3)	255(3)	7439(2)	19(1)
C(13)	7976(3)	306(3)	6589(2)	15(1)
C(14)	7326(3)	822(3)	5766(2)	14(1)
C(15)	7728(3)	938(3)	4806(2)	13(1)
C(16)	6572(3)	1517(3)	4343(2)	12(1)
C(17)	6347(3)	1817(3)	3337(2)	13(1)
C(18)	7280(3)	1439(3)	2635(2)	14(1)
C(19)	6964(3)	1668(3)	1676(2)	17(1)
C(20)	5675(3)	2314(3)	1460(2)	20(1)
C(21)	4799(3)	2683(3)	2181(2)	19(1)
C(22)	7919(3)	1196(3)	886(2)	21(1)
C(23)	7032(6)	120(6)	345(4)	76(2)
C(24)	8254(8)	2281(6)	172(4)	101(3)
C(25)	9375(5)	776(6)	1267(3)	68(2)
N(1)	5111(3)	2446(2)	3112(2)	15(1)
N(2)	5463(2)	1797(2)	4942(2)	13(1)
F(1)	9348(2)	-174(2)	6513(1)	21(1)
F(2)	3806(2)	1633(2)	6775(1)	22(1)

Table A7. Bond lengths [Å] for **5b**.

Bond	Length	Bond	Length
C(1)-S(1)	1.804(3)	C(14)-C(15)	1.410(4)
C(1)-H(26A)	0.9800	C(15)-C(16)	1.379(4)
C(1)-H(26B)	0.9800	C(15)-H(17)	0.9500
C(1)-H(26C)	0.9800	C(16)-N(2)	1.378(3)
C(2)-S(1)	1.799(3)	C(16)-C(17)	1.451(4)
C(2)-H(16A)	0.9800	C(17)-N(1)	1.357(3)
C(2)-H(16B)	0.9800	C(17)-C(18)	1.393(4)
C(2)-H(16C)	0.9800	C(18)-C(19)	1.386(4)
C(3)-C(4)	1.403(4)	C(18)-H(28)	0.9500
C(3)-C(8)	1.403(4)	C(19)-C(20)	1.404(4)
C(3)-Pt(1)	2.009(3)	C(19)-C(22)	1.529(4)
C(4)-C(5)	1.386(4)	C(20)-C(21)	1.378(4)
C(4)-H(10)	0.9500	C(20)-H(25)	0.9500
C(5)-C(6)	1.391(5)	C(21)-N(1)	1.348(4)
C(5)-H(27)	0.9500	C(21)-H(15)	0.9500
C(6)-C(7)	1.379(5)	C(22)-C(25)	1.491(5)
C(6)-H(23)	0.9500	C(22)-C(23)	1.501(6)
C(7)-C(8)	1.393(4)	C(22)-C(24)	1.524(6)
C(7)-H(24)	0.9500	C(23)-H(39A)	0.9800
C(8)-H(20)	0.9500	C(23)-H(39B)	0.9800
C(9)-N(2)	1.373(3)	C(23)-H(39C)	0.9800
C(9)-C(10)	1.402(4)	C(24)-H(10A)	0.9800
C(9)-C(14)	1.432(4)	C(24)-H(10B)	0.9800
C(10)-C(11)	1.362(4)	C(24)-H(10C)	0.9800
C(10)-F(2)	1.363(3)	C(25)-H(33A)	0.9800
C(11)-C(12)	1.412(4)	C(25)-H(33B)	0.9800
C(11)-H(12)	0.9500	C(25)-H(33C)	0.9800
C(12)-C(13)	1.355(4)	N(1)-Pt(1)	2.049(2)
C(12)-H(13)	0.9500	N(2)-Pt(1)	2.125(2)
C(13)-F(1)	1.374(3)	S(1)-Pt(1)	2.2611(7)
C(13)-C(14)	1.395(4)		

Table A8. Bond angles [°] for **5b**.

Bond	Angle	Bond	Angle
S(1)-C(1)-H(26A)	109.5	N(1)-C(17)-C(18)	121.5(2)
S(1)-C(1)-H(26B)	109.5	N(1)-C(17)-C(16)	115.3(2)
H(26A)-C(1)-H(26B)	109.5	C(18)-C(17)-C(16)	123.2(2)
S(1)-C(1)-H(26C)	109.5	C(19)-C(18)-C(17)	121.1(3)
H(26A)-C(1)-H(26C)	109.5	C(19)-C(18)-H(28)	119.4
H(26B)-C(1)-H(26C)	109.5	C(17)-C(18)-H(28)	119.4
S(1)-C(2)-H(16A)	109.5	C(18)-C(19)-C(20)	116.3(3)
S(1)-C(2)-H(16B)	109.5	C(18)-C(19)-C(22)	122.3(3)
H(16A)-C(2)-H(16B)	109.5	C(20)-C(19)-C(22)	121.4(3)
S(1)-C(2)-H(16C)	109.5	C(21)-C(20)-C(19)	120.3(3)
H(16A)-C(2)-H(16C)	109.5	C(21)-C(20)-H(25)	119.8
H(16B)-C(2)-H(16C)	109.5	C(19)-C(20)-H(25)	119.8
C(4)-C(3)-C(8)	116.5(3)	N(1)-C(21)-C(20)	122.9(3)
C(4)-C(3)-Pt(1)	122.2(2)	N(1)-C(21)-H(15)	118.6
C(8)-C(3)-Pt(1)	121.3(2)	C(20)-C(21)-H(15)	118.6
C(5)-C(4)-C(3)	122.0(3)	C(25)-C(22)-C(23)	111.6(4)
C(5)-C(4)-H(10)	119.0	C(25)-C(22)-C(24)	107.4(4)
C(3)-C(4)-H(10)	119.0	C(23)-C(22)-C(24)	106.7(4)
C(4)-C(5)-C(6)	120.3(3)	C(25)-C(22)-C(19)	112.4(3)
C(4)-C(5)-H(27)	119.9	C(23)-C(22)-C(19)	108.3(3)
C(6)-C(5)-H(27)	119.9	C(24)-C(22)-C(19)	110.3(3)
C(7)-C(6)-C(5)	119.0(3)	C(22)-C(23)-H(39A)	109.5
C(7)-C(6)-H(23)	120.5	C(22)-C(23)-H(39B)	109.5
C(5)-C(6)-H(23)	120.5	H(39A)-C(23)-H(39B)	109.5
C(6)-C(7)-C(8)	120.6(3)	C(22)-C(23)-H(39C)	109.5
C(6)-C(7)-H(24)	119.7	H(39A)-C(23)-H(39C)	109.5
C(8)-C(7)-H(24)	119.7	H(39B)-C(23)-H(39C)	109.5
C(7)-C(8)-C(3)	121.5(3)	C(22)-C(24)-H(10A)	109.5
C(7)-C(8)-H(20)	119.2	C(22)-C(24)-H(10B)	109.5
C(3)-C(8)-H(20)	119.2	H(10A)-C(24)-H(10B)	109.5
N(2)-C(9)-C(10)	132.8(2)	C(22)-C(24)-H(10C)	109.5
N(2)-C(9)-C(14)	109.7(2)	H(10A)-C(24)-H(10C)	109.5
C(10)-C(9)-C(14)	117.4(2)	H(10B)-C(24)-H(10C)	109.5
C(11)-C(10)-F(2)	118.3(2)	C(22)-C(25)-H(33A)	109.5
C(11)-C(10)-C(9)	121.8(3)	C(22)-C(25)-H(33B)	109.5
F(2)-C(10)-C(9)	119.9(2)	H(33A)-C(25)-H(33B)	109.5
C(10)-C(11)-C(12)	120.8(3)	C(22)-C(25)-H(33C)	109.5
C(10)-C(11)-H(12)	119.6	H(33A)-C(25)-H(33C)	109.5
C(12)-C(11)-H(12)	119.6	H(33B)-C(25)-H(33C)	109.5
C(13)-C(12)-C(11)	118.3(3)	C(21)-N(1)-C(17)	117.8(2)
C(13)-C(12)-H(13)	120.8	C(21)-N(1)-Pt(1)	126.43(19)
C(11)-C(12)-H(13)	120.8	C(17)-N(1)-Pt(1)	115.71(18)
C(12)-C(13)-F(1)	119.8(2)	C(9)-N(2)-C(16)	105.2(2)
C(12)-C(13)-C(14)	122.8(3)	C(9)-N(2)-Pt(1)	142.82(18)
F(1)-C(13)-C(14)	117.3(2)	C(16)-N(2)-Pt(1)	111.02(17)
C(13)-C(14)-C(15)	134.4(3)	C(2)-S(1)-C(1)	99.21(14)
C(13)-C(14)-C(9)	118.8(2)	C(2)-S(1)-Pt(1)	111.18(10)
C(15)-C(14)-C(9)	106.7(2)	C(1)-S(1)-Pt(1)	106.46(11)
C(16)-C(15)-C(14)	105.2(2)	C(3)-Pt(1)-N(1)	93.16(10)
C(16)-C(15)-H(17)	127.4	C(3)-Pt(1)-N(2)	172.34(9)
C(14)-C(15)-H(17)	127.4	N(1)-Pt(1)-N(2)	79.19(9)
N(2)-C(16)-C(15)	113.2(2)	C(3)-Pt(1)-S(1)	90.10(8)
N(2)-C(16)-C(17)	117.1(2)	N(1)-Pt(1)-S(1)	174.15(7)
C(15)-C(16)-C(17)	129.7(2)	N(2)-Pt(1)-S(1)	97.56(6)

Table A9. Anisotropic displacement parameters (Å^2 x 10^3) for **5b**. The anisotropic displacement factor exponent takes the form: $-2\pi^2[h^2a^2U^{11} + ... + 2hk(abU^{12})]$.

Atom	U^{11}	U^{22}	U^{33}	U^{23}	U^{13}	U^{12}
C(1)	18(2)	22(2)	34(2)	0(1)	9(1)	0(1)
C(2)	20(2)	14(2)	31(2)	-5(1)	6(1)	3(1)
C(3)	14(1)	15(1)	19(1)	-3(1)	3(1)	6(1)
C(4)	16(1)	18(2)	25(2)	0(1)	0(1)	1(1)
C(5)	26(2)	18(2)	30(2)	3(1)	2(1)	4(1)
C(6)	21(2)	28(2)	26(2)	4(1)	-2(1)	11(1)
C(7)	16(2)	25(2)	30(2)	-2(1)	-3(1)	0(1)
C(8)	17(1)	17(2)	22(2)	-2(1)	-1(1)	-1(1)
C(9)	12(1)	9(1)	17(1)	-2(1)	1(1)	-1(1)
C(10)	12(1)	14(1)	21(1)	-2(1)	4(1)	1(1)
C(11)	18(1)	17(2)	17(1)	-1(1)	6(1)	-1(1)
C(12)	20(2)	18(2)	18(1)	5(1)	0(1)	2(1)
C(13)	12(1)	14(1)	21(1)	1(1)	1(1)	4(1)
C(14)	13(1)	10(1)	18(1)	-1(1)	2(1)	0(1)
C(15)	12(1)	12(1)	16(1)	-1(1)	4(1)	2(1)
C(16)	13(1)	9(1)	15(1)	-2(1)	3(1)	0(1)
C(17)	12(1)	10(1)	17(1)	0(1)	1(1)	-1(1)
C(18)	13(1)	13(1)	17(1)	-1(1)	2(1)	2(1)
C(19)	16(1)	16(2)	18(1)	0(1)	2(1)	0(1)
C(20)	23(2)	24(2)	15(1)	3(1)	1(1)	7(1)
C(21)	18(1)	22(2)	18(1)	3(1)	1(1)	8(1)
C(22)	20(2)	30(2)	15(1)	-2(1)	4(1)	7(1)
C(23)	56(3)	97(4)	73(3)	-50(3)	22(3)	-7(3)
C(24)	133(5)	122(5)	66(3)	55(4)	71(4)	91(5)
C(25)	41(2)	140(5)	28(2)	-27(3)	0(2)	38(3)
N(1)	14(1)	13(1)	18(1)	1(1)	0(1)	3(1)
N(2)	10(1)	13(1)	15(1)	-1(1)	2(1)	2(1)
F(1)	16(1)	27(1)	22(1)	6(1)	5(1)	10(1)
F(2)	16(1)	29(1)	22(1)	3(1)	8(1)	9(1)
S(1)	12(1)	16(1)	21(1)	-4(1)	3(1)	3(1)
Pt(1)	9(1)	11(1)	16(1)	-1(1)	1(1)	3(1)

Table A10. Hydrogen coordinates (x 10^4) and isotropic displacement parameters ($Å^2$ x 10^3) for **5b**.

Atom	x	y	z	U(eq)
H(26A)	579	2965	6198	36
H(26B)	1320	1765	5733	36
H(26C)	501	2769	5062	36
H(16A)	1380	5165	4851	32
H(16B)	2937	5866	5237	32
H(16C)	1654	5490	5966	32
H(10)	3975	5711	3385	24
H(27)	2400	6947	2479	29
H(23)	57	6041	1915	29
H(24)	-695	3902	2306	29
H(20)	868	2663	3230	23
H(12)	5387	688	8072	21
H(13)	7785	-90	7989	22
H(17)	8608	673	4535	16
H(28)	8148	1016	2818	17
H(25)	5405	2496	813	24
H(15)	3937	3124	2015	23
H(39A)	7568	-112	-218	113
H(39B)	6058	410	141	113
H(39C)	6892	-640	759	113
H(10A)	8645	3071	516	151
H(10B)	7336	2452	-192	151
H(10C)	8995	2018	-268	151
H(33A)	9198	70	1726	102
H(33B)	9945	1511	1588	102
H(33C)	9939	470	739	102

Crystallographic Data for Complex **5c**

Table A11. Atomic coordinates (x 10^4) and equivalent isotropic displacement parameters (Å^2 x 10^3) for **5c**. U(eq) is defined as one third of the trace of the orthogonalized U^{ij} tensor.

Atom	x	y	z	U(eq)
C(1)	2899(2)	-351(2)	10148(2)	16(1)
C(2)	3850(2)	2259(2)	10732(2)	18(1)
C(3)	2435(2)	886(2)	8399(1)	13(1)
C(4)	3907(2)	1366(2)	8220(2)	17(1)
C(5)	4855(2)	610(2)	7670(2)	20(1)
C(6)	4372(3)	-665(2)	7272(2)	22(1)
C(7)	2924(3)	-1160(2)	7428(2)	23(1)
C(8)	1973(2)	-397(2)	7981(2)	18(1)
C(9)	-901(2)	3652(2)	10801(1)	11(1)
C(10)	-220(2)	3682(2)	11660(1)	13(1)
C(11)	-919(2)	4190(2)	12431(1)	14(1)
C(12)	-2316(2)	4734(2)	12382(1)	14(1)
C(13)	-2995(2)	4735(2)	11551(2)	13(1)
C(14)	-2327(2)	4213(2)	10748(1)	11(1)
C(15)	-2722(2)	4115(2)	9816(1)	12(1)
C(16)	-1563(2)	3514(2)	9357(1)	11(1)
C(17)	-1332(2)	3223(2)	8381(1)	12(1)
C(18)	-2265(2)	3601(2)	7716(1)	14(1)
C(19)	-1940(2)	3382(2)	6793(1)	15(1)
C(20)	-637(2)	2723(2)	6580(2)	19(1)
C(21)	245(2)	2344(2)	7260(2)	18(1)
C(22)	-2967(2)	3819(2)	6066(2)	18(1)
C(23)	-3440(2)	5224(2)	6362(2)	22(1)
C(24)	-4376(3)	2838(3)	5945(2)	30(1)
C(25)	-2192(3)	3818(3)	5146(2)	31(1)
N(1)	-449(2)	3208(2)	9939(1)	11(1)
N(2)	-73(2)	2578(2)	8154(1)	13(1)
F(1)	1161(1)	3234(1)	11771(1)	18(1)
F(2)	-291(1)	4157(1)	13264(1)	19(1)
F(3)	-2952(1)	5251(1)	13170(1)	22(1)
F(4)	-4355(1)	5258(1)	11504(1)	17(1)
S(1)	2129(1)	1234(1)	10450(1)	13(1)
Pt(1)	1093(1)	1982(1)	9222(1)	10(1)

Table A12. Bond lengths [Å] for **5c**.

Bond	Length	Bond	Length
C(1)-S(1)	1.799(2)	C(14)-C(15)	1.404(3)
C(1)-H(1A)	0.9800	C(15)-C(16)	1.380(3)
C(1)-H(1B)	0.9800	C(15)-H(15)	0.9500
C(1)-H(1C)	0.9800	C(16)-N(1)	1.382(3)
C(2)-S(1)	1.804(2)	C(16)-C(17)	1.453(3)
C(2)-H(2A)	0.9800	C(17)-N(2)	1.364(2)
C(2)-H(2B)	0.9800	C(17)-C(18)	1.386(3)
C(2)-H(2C)	0.9800	C(18)-C(19)	1.391(3)
C(3)-C(8)	1.398(3)	C(18)-H(18)	0.9500
C(3)-C(4)	1.408(3)	C(19)-C(20)	1.402(3)
C(3)-Pt(1)	2.008(2)	C(19)-C(22)	1.528(3)
C(4)-C(5)	1.385(3)	C(20)-C(21)	1.376(3)
C(4)-H(4)	0.9500	C(20)-H(20)	0.9500
C(5)-C(6)	1.386(3)	C(21)-N(2)	1.348(3)
C(5)-H(5)	0.9500	C(21)-H(21)	0.9500
C(6)-C(7)	1.384(3)	C(22)-C(23)	1.527(3)
C(6)-H(6)	0.9500	C(22)-C(25)	1.533(3)
C(7)-C(8)	1.393(3)	C(22)-C(24)	1.540(3)
C(7)-H(7)	0.9500	C(23)-H(23A)	0.9800
C(8)-H(8)	0.9500	C(23)-H(23B)	0.9800
C(9)-N(1)	1.371(3)	C(23)-H(23C)	0.9800
C(9)-C(10)	1.394(3)	C(24)-H(24A)	0.9800
C(9)-C(14)	1.436(3)	C(24)-H(24B)	0.9800
C(10)-F(1)	1.358(2)	C(24)-H(24C)	0.9800
C(10)-C(11)	1.367(3)	C(25)-H(25A)	0.9800
C(11)-F(2)	1.348(2)	C(25)-H(25B)	0.9800
C(11)-C(12)	1.403(3)	C(25)-H(25C)	0.9800
C(12)-C(13)	1.360(3)	N(1)-Pt(1)	2.1244(16)
C(12)-F(3)	1.363(2)	N(2)-Pt(1)	2.0522(17)
C(13)-F(4)	1.363(2)	S(1)-Pt(1)	2.2619(5)
C(13)-C(14)	1.395(3)		

Table A13. Bond angles [°] for **5c**.

Bond	Angle	Bond	Angle
S(1)-C(1)-H(1A)	109.5	N(2)-C(17)-C(18)	121.25(19)
S(1)-C(1)-H(1B)	109.5	N(2)-C(17)-C(16)	114.85(17)
H(1A)-C(1)-H(1B)	109.5	C(18)-C(17)-C(16)	123.86(18)
S(1)-C(1)-H(1C)	109.5	C(17)-C(18)-C(19)	121.75(18)
H(1A)-C(1)-H(1C)	109.5	C(17)-C(18)-H(18)	119.1
H(1B)-C(1)-H(1C)	109.5	C(19)-C(18)-H(18)	119.1
S(1)-C(2)-H(2A)	109.5	C(18)-C(19)-C(20)	115.74(19)
S(1)-C(2)-H(2B)	109.5	C(18)-C(19)-C(22)	121.31(18)
H(2A)-C(2)-H(2B)	109.5	C(20)-C(19)-C(22)	122.94(19)
S(1)-C(2)-H(2C)	109.5	C(21)-C(20)-C(19)	120.6(2)
H(2A)-C(2)-H(2C)	109.5	C(21)-C(20)-H(20)	119.7
H(2B)-C(2)-H(2C)	109.5	C(19)-C(20)-H(20)	119.7
C(8)-C(3)-C(4)	116.21(19)	N(2)-C(21)-C(20)	123.03(19)
C(8)-C(3)-Pt(1)	122.24(15)	N(2)-C(21)-H(21)	118.5
C(4)-C(3)-Pt(1)	121.54(15)	C(20)-C(21)-H(21)	118.5
C(5)-C(4)-C(3)	122.1(2)	C(23)-C(22)-C(19)	110.74(18)
C(5)-C(4)-H(4)	118.9	C(23)-C(22)-C(25)	108.04(19)
C(3)-C(4)-H(4)	118.9	C(19)-C(22)-C(25)	111.78(17)
C(4)-C(5)-C(6)	120.4(2)	C(23)-C(22)-C(24)	109.16(18)
C(4)-C(5)-H(5)	119.8	C(19)-C(22)-C(24)	108.12(18)
C(6)-C(5)-H(5)	119.8	C(25)-C(22)-C(24)	109.0(2)
C(7)-C(6)-C(5)	118.8(2)	C(22)-C(23)-H(23A)	109.5
C(7)-C(6)-H(6)	120.6	C(22)-C(23)-H(23B)	109.5
C(5)-C(6)-H(6)	120.6	H(23A)-C(23)-H(23B)	109.5
C(6)-C(7)-C(8)	120.7(2)	C(22)-C(23)-H(23C)	109.5
C(6)-C(7)-H(7)	119.7	H(23A)-C(23)-H(23C)	109.5
C(8)-C(7)-H(7)	119.7	H(23B)-C(23)-H(23C)	109.5
C(7)-C(8)-C(3)	121.8(2)	C(22)-C(24)-H(24A)	109.5
C(7)-C(8)-H(8)	119.1	C(22)-C(24)-H(24B)	109.5
C(3)-C(8)-H(8)	119.1	H(24A)-C(24)-H(24B)	109.5
N(1)-C(9)-C(10)	132.16(18)	C(22)-C(24)-H(24C)	109.5
N(1)-C(9)-C(14)	109.67(17)	H(24A)-C(24)-H(24C)	109.5
C(10)-C(9)-C(14)	118.14(18)	H(24B)-C(24)-H(24C)	109.5
F(1)-C(10)-C(11)	117.15(18)	C(22)-C(25)-H(25A)	109.5
F(1)-C(10)-C(9)	122.14(17)	C(22)-C(25)-H(25B)	109.5
C(11)-C(10)-C(9)	120.71(18)	H(25A)-C(25)-H(25B)	109.5
F(2)-C(11)-C(10)	120.48(17)	C(22)-C(25)-H(25C)	109.5
F(2)-C(11)-C(12)	118.28(18)	H(25A)-C(25)-H(25C)	109.5
C(10)-C(11)-C(12)	121.22(19)	H(25B)-C(25)-H(25C)	109.5
C(13)-C(12)-F(3)	121.84(17)	C(9)-N(1)-C(16)	105.28(15)
C(13)-C(12)-C(11)	119.25(18)	C(9)-N(1)-Pt(1)	142.54(13)
F(3)-C(12)-C(11)	118.91(18)	C(16)-N(1)-Pt(1)	111.08(12)
C(12)-C(13)-F(4)	119.17(17)	C(21)-N(2)-C(17)	117.60(17)
C(12)-C(13)-C(14)	121.34(18)	C(21)-N(2)-Pt(1)	126.55(14)
F(4)-C(13)-C(14)	119.49(18)	C(17)-N(2)-Pt(1)	115.78(13)
C(13)-C(14)-C(15)	134.07(18)	C(1)-S(1)-C(2)	99.30(10)
C(13)-C(14)-C(9)	119.30(18)	C(1)-S(1)-Pt(1)	111.65(8)
C(15)-C(14)-C(9)	106.61(17)	C(2)-S(1)-Pt(1)	106.49(8)
C(16)-C(15)-C(14)	105.69(17)	C(3)-Pt(1)-N(2)	93.64(7)
C(16)-C(15)-H(15)	127.2	C(3)-Pt(1)-N(1)	172.79(7)
C(14)-C(15)-H(15)	127.2	N(2)-Pt(1)-N(1)	79.16(6)
C(15)-C(16)-N(1)	112.74(18)	C(3)-Pt(1)-S(1)	89.83(6)
C(15)-C(16)-C(17)	129.93(18)	N(2)-Pt(1)-S(1)	173.64(5)
N(1)-C(16)-C(17)	117.27(17)	N(1)-Pt(1)-S(1)	97.36(5)

Table A14. Anisotropic displacement parameters ($Å^2$ x 10^3) for **5c**. The anisotropic displacement factor exponent takes the form: $-2\pi^2[h^2a^2U^{11} + ... + 2hk(abU^{12})]$.

Atom	U^{11}	U^{22}	U^{33}	U^{23}	U^{13}	U^{12}
C(1)	15(1)	12(1)	24(1)	5(1)	-2(1)	3(1)
C(2)	13(1)	17(1)	24(1)	2(1)	-6(1)	0(1)
C(3)	14(1)	13(1)	14(1)	6(1)	-1(1)	6(1)
C(4)	18(1)	15(1)	19(1)	7(1)	-1(1)	2(1)
C(5)	17(1)	24(1)	21(1)	9(1)	5(1)	6(1)
C(6)	28(1)	21(1)	20(1)	6(1)	8(1)	11(1)
C(7)	29(1)	16(1)	23(1)	1(1)	2(1)	4(1)
C(8)	17(1)	18(1)	19(1)	3(1)	1(1)	2(1)
C(9)	10(1)	8(1)	14(1)	3(1)	-1(1)	-1(1)
C(10)	8(1)	12(1)	19(1)	5(1)	-1(1)	3(1)
C(11)	13(1)	18(1)	10(1)	5(1)	-5(1)	-1(1)
C(12)	12(1)	18(1)	12(1)	2(1)	4(1)	1(1)
C(13)	9(1)	12(1)	19(1)	4(1)	1(1)	2(1)
C(14)	10(1)	9(1)	14(1)	3(1)	-2(1)	-1(1)
C(15)	9(1)	12(1)	14(1)	5(1)	-2(1)	0(1)
C(16)	11(1)	9(1)	13(1)	5(1)	-2(1)	-1(1)
C(17)	11(1)	9(1)	17(1)	4(1)	-1(1)	-2(1)
C(18)	11(1)	15(1)	15(1)	4(1)	-1(1)	1(1)
C(19)	15(1)	15(1)	15(1)	4(1)	-2(1)	-1(1)
C(20)	23(1)	24(1)	12(1)	2(1)	2(1)	6(1)
C(21)	20(1)	19(1)	15(1)	1(1)	1(1)	6(1)
C(22)	19(1)	24(1)	13(1)	6(1)	-2(1)	3(1)
C(23)	18(1)	28(1)	22(1)	12(1)	-3(1)	4(1)
C(24)	30(1)	31(1)	30(2)	10(1)	-16(1)	-4(1)
C(25)	33(1)	47(2)	16(1)	10(1)	0(1)	15(1)
N(1)	11(1)	9(1)	12(1)	4(1)	-2(1)	1(1)
N(2)	14(1)	11(1)	14(1)	1(1)	-1(1)	3(1)
F(1)	12(1)	26(1)	17(1)	1(1)	-4(1)	9(1)
F(2)	16(1)	31(1)	11(1)	5(1)	-3(1)	6(1)
F(3)	14(1)	42(1)	13(1)	6(1)	3(1)	8(1)
F(4)	11(1)	24(1)	18(1)	3(1)	0(1)	7(1)
S(1)	10(1)	13(1)	16(1)	4(1)	-1(1)	3(1)
Pt(1)	9(1)	10(1)	13(1)	3(1)	-1(1)	2(1)

Table A15. Hydrogen coordinates (x 10^4) and isotropic displacement parameters (Å^2 x 10^3) for **5c**.

Atom	x	y	z	U(eq)
H(1A)	3639	-273	9669	25
H(1B)	2089	-1022	9922	25
H(1C)	3388	-620	10687	25
H(2A)	4359	1951	11251	27
H(2B)	3620	3189	10895	27
H(2C)	4507	2194	10204	27
H(4)	4261	2238	8485	20
H(5)	5843	967	7565	24
H(6)	5022	-1189	6899	27
H(7)	2576	-2029	7154	27
H(8)	983	-758	8077	22
H(15)	-3603	4401	9556	14
H(18)	-3151	4022	7896	16
H(20)	-361	2536	5960	23
H(21)	1119	1897	7093	21
H(23A)	-3968	5241	6940	33
H(23B)	-4109	5481	5892	33
H(23C)	-2546	5852	6443	33
H(24A)	-4079	1936	5749	45
H(24B)	-5052	3101	5482	45
H(24C)	-4894	2852	6527	45
H(25A)	-1245	4377	5229	46
H(25B)	-2851	4173	4713	46
H(25C)	-1987	2904	4907	46

Crystallographic Data for Complex **5l**

Table A16. Atomic coordinates (x 10^4) and equivalent isotropic displacement parameters (Å^2 x 10^3) for **5l**. U(eq) is defined as one third of the trace of the orthogonalized U^{ij} tensor.

Atom	x	y	z	U(eq)
C(1)	6439(4)	-1082(3)	3521(6)	36(1)
C(2)	9305(4)	-1738(3)	4658(6)	34(1)
C(3)	8176(4)	-952(3)	6413(6)	32(1)
C(4)	7618(4)	-3903(2)	4952(5)	19(1)
C(5)	8706(4)	-3908(3)	5662(5)	22(1)
C(6)	9175(4)	-4547(3)	6273(5)	24(1)
C(7)	8610(4)	-5216(3)	6207(5)	24(1)
C(8)	7562(4)	-5232(3)	5521(5)	22(1)
C(9)	7058(4)	-4593(2)	4858(5)	19(1)
C(10)	6048(4)	-4455(2)	3948(5)	20(1)
C(11)	6058(4)	-3714(2)	3538(5)	19(1)
C(12)	5297(4)	-3292(2)	2458(5)	18(1)
C(13)	4415(3)	-3608(2)	1540(5)	19(1)
C(14)	3749(3)	-3191(2)	416(5)	18(1)
C(15)	4044(4)	-2458(3)	275(5)	23(1)
C(16)	4916(4)	-2168(3)	1221(5)	22(1)
C(17)	2785(4)	-3552(3)	-588(5)	22(1)
C(18)	3181(4)	-4140(3)	-1609(6)	28(1)
C(19)	2102(4)	-3925(3)	439(6)	26(1)
C(20)	2096(4)	-2980(3)	-1608(6)	35(1)
N(1)	7003(3)	-3364(2)	4182(4)	20(1)
N(2)	5539(3)	-2558(2)	2326(4)	18(1)
F(1)	9320(2)	-3291(2)	5709(3)	32(1)
F(2)	10221(2)	-4547(2)	6928(3)	32(1)
F(3)	9137(2)	-5840(2)	6794(3)	34(1)
F(4)	7018(2)	-5882(1)	5453(3)	30(1)
S(1)	8234(1)	-1882(1)	5686(1)	22(1)
Pt(1)	6817(1)	-2184(1)	3879(1)	15(1)
Pt(1A)	7425(6)	-2402(3)	4285(6)	27(2)

Table A17. Bond lengths [Å] for **5l**.

Bond	Length	Bond	Length
C(1)-Pt(1)	2.053(5)	C(12)-N(2)	1.367(5)
C(1)-H(1A)	0.9800	C(12)-C(13)	1.383(6)
C(1)-H(1B)	0.9800	C(13)-C(14)	1.403(6)
C(1)-H(1C)	0.9800	C(13)-H(13)	0.9500
C(2)-S(1)	1.801(5)	C(14)-C(15)	1.385(6)
C(2)-H(2A)	0.9800	C(14)-C(17)	1.524(6)
C(2)-H(2B)	0.9800	C(15)-C(16)	1.366(6)
C(2)-H(2C)	0.9800	C(15)-H(15)	0.9500
C(3)-S(1)	1.802(5)	C(16)-N(2)	1.341(6)
C(3)-H(3A)	0.9800	C(16)-H(16)	0.9500
C(3)-H(3B)	0.9800	C(17)-C(19)	1.532(7)
C(3)-H(3C)	0.9800	C(17)-C(20)	1.536(7)
C(4)-N(1)	1.351(6)	C(17)-C(18)	1.540(7)
C(4)-C(5)	1.414(6)	C(18)-H(18A)	0.9800
C(4)-C(9)	1.428(6)	C(18)-H(18B)	0.9800
C(5)-F(1)	1.356(5)	C(18)-H(18C)	0.9800
C(5)-C(6)	1.362(7)	C(19)-H(19A)	0.9800
C(6)-F(2)	1.352(5)	C(19)-H(19B)	0.9800
C(6)-C(7)	1.399(7)	C(19)-H(19C)	0.9800
C(7)-C(8)	1.362(7)	C(20)-H(20A)	0.9800
C(7)-F(3)	1.363(5)	C(20)-H(20B)	0.9800
C(8)-F(4)	1.357(5)	C(20)-H(20C)	0.9800
C(8)-C(9)	1.394(6)	N(1)-Pt(1A)	1.811(5)
C(9)-C(10)	1.410(6)	N(1)-Pt(1)	2.149(4)
C(10)-C(11)	1.385(6)	N(2)-Pt(1)	2.044(4)
C(10)-H(10)	0.9500	S(1)-Pt(1A)	1.736(5)
C(11)-N(1)	1.386(6)	S(1)-Pt(1)	2.2482(12)
C(11)-C(12)	1.446(6)		

Table A18. Bond angles [°] for **5l**.

Bond	Angle	Bond	Angle
S(1)-C(2)-H(2A)	109.5	N(2)-C(16)-H(16)	118.3
S(1)-C(2)-H(2B)	109.5	C(15)-C(16)-H(16)	118.3
H(2A)-C(2)-H(2B)	109.5	C(14)-C(17)-C(19)	109.0(4)
S(1)-C(2)-H(2C)	109.5	C(14)-C(17)-C(20)	111.6(4)
H(2A)-C(2)-H(2C)	109.5	C(19)-C(17)-C(20)	108.7(4)
H(2B)-C(2)-H(2C)	109.5	C(14)-C(17)-C(18)	108.8(4)
S(1)-C(3)-H(3A)	109.5	C(19)-C(17)-C(18)	109.6(4)
S(1)-C(3)-H(3B)	109.5	C(20)-C(17)-C(18)	109.2(4)
H(3A)-C(3)-H(3B)	109.5	C(17)-C(18)-H(18A)	109.5
S(1)-C(3)-H(3C)	109.5	C(17)-C(18)-H(18B)	109.5
H(3A)-C(3)-H(3C)	109.5	H(18A)-C(18)-H(18B)	109.5
H(3B)-C(3)-H(3C)	109.5	C(17)-C(18)-H(18C)	109.5
N(1)-C(4)-C(5)	131.3(4)	H(18A)-C(18)-H(18C)	109.5
N(1)-C(4)-C(9)	111.1(4)	H(18B)-C(18)-H(18C)	109.5
C(5)-C(4)-C(9)	117.3(4)	C(17)-C(19)-H(19A)	109.5
F(1)-C(5)-C(6)	118.1(4)	C(17)-C(19)-H(19B)	109.5
F(1)-C(5)-C(4)	121.5(4)	H(19A)-C(19)-H(19B)	109.5
C(6)-C(5)-C(4)	120.3(4)	C(17)-C(19)-H(19C)	109.5
F(2)-C(6)-C(5)	119.7(4)	H(19A)-C(19)-H(19C)	109.5
F(2)-C(6)-C(7)	118.5(4)	H(19B)-C(19)-H(19C)	109.5
C(5)-C(6)-C(7)	121.7(4)	C(17)-C(20)-H(20A)	109.5
C(8)-C(7)-F(3)	121.8(4)	C(17)-C(20)-H(20B)	109.5
C(8)-C(7)-C(6)	119.5(4)	H(20A)-C(20)-H(20B)	109.5
F(3)-C(7)-C(6)	118.7(4)	C(17)-C(20)-H(20C)	109.5
F(4)-C(8)-C(7)	119.3(4)	H(20A)-C(20)-H(20C)	109.5
F(4)-C(8)-C(9)	120.2(4)	H(20B)-C(20)-H(20C)	109.5
C(7)-C(8)-C(9)	120.5(4)	C(4)-N(1)-C(11)	105.1(4)
C(8)-C(9)-C(10)	133.4(4)	C(4)-N(1)-Pt(1A)	121.5(4)
C(8)-C(9)-C(4)	120.5(4)	C(11)-N(1)-Pt(1A)	133.1(4)
C(10)-C(9)-C(4)	105.9(4)	C(4)-N(1)-Pt(1)	144.5(3)
C(11)-C(10)-C(9)	105.6(4)	C(11)-N(1)-Pt(1)	109.4(3)
C(11)-C(10)-H(10)	127.2	Pt(1A)-N(1)-Pt(1)	23.9(3)
C(9)-C(10)-H(10)	127.2	C(16)-N(2)-C(12)	117.3(4)
C(10)-C(11)-N(1)	112.4(4)	C(16)-N(2)-Pt(1)	127.6(3)
C(10)-C(11)-C(12)	130.0(4)	C(12)-N(2)-Pt(1)	115.2(3)
N(1)-C(11)-C(12)	117.3(4)	Pt(1A)-S(1)-C(3)	134.5(3)
N(2)-C(12)-C(13)	121.3(4)	Pt(1A)-S(1)-C(2)	96.8(2)
N(2)-C(12)-C(11)	115.5(4)	C(3)-S(1)-C(2)	97.7(3)
C(13)-C(12)-C(11)	123.0(4)	Pt(1A)-S(1)-Pt(1)	21.0(3)
C(12)-C(13)-C(14)	121.1(4)	C(3)-S(1)-Pt(1)	113.58(18)
C(12)-C(13)-H(13)	119.5	C(2)-S(1)-Pt(1)	104.88(18)
C(14)-C(13)-H(13)	119.5	N(2)-Pt(1)-C(1)	94.57(18)
C(15)-C(14)-C(13)	115.9(4)	N(2)-Pt(1)-N(1)	79.25(14)
C(15)-C(14)-C(17)	123.9(4)	C(1)-Pt(1)-N(1)	172.83(18)
C(13)-C(14)-C(17)	120.2(4)	N(2)-Pt(1)-S(1)	174.50(11)
C(16)-C(15)-C(14)	120.9(4)	C(1)-Pt(1)-S(1)	90.62(15)
C(16)-C(15)-H(15)	119.6	N(1)-Pt(1)-S(1)	95.46(10)
C(14)-C(15)-H(15)	119.6	S(1)-Pt(1A)-N(1)	133.1(5)
N(2)-C(16)-C(15)	123.5(4)		

Table A19. Anisotropic displacement parameters (Å^2 x 10^3) for **5l**. The anisotropic displacement factor exponent takes the form: $-2\pi^2[h^2a^2U^{11} + ... + 2hk(abU^{12})]$.

Atom	U^{11}	U^{22}	U^{33}	U^{23}	U^{13}	U^{12}
C(1)	42(3)	20(3)	40(3)	-3(2)	-8(3)	0(2)
C(2)	25(3)	40(3)	36(3)	2(3)	5(2)	-7(2)
C(3)	41(3)	25(3)	27(3)	-9(2)	2(2)	-4(2)
C(4)	23(2)	18(2)	15(2)	-7(2)	5(2)	-5(2)
C(5)	26(3)	19(2)	21(3)	0(2)	4(2)	-7(2)
C(6)	24(3)	31(3)	18(3)	-2(2)	2(2)	-4(2)
C(7)	33(3)	21(3)	17(3)	4(2)	0(2)	6(2)
C(8)	32(3)	20(2)	14(3)	-3(2)	2(2)	-9(2)
C(9)	24(3)	21(2)	9(2)	-3(2)	0(2)	-6(2)
C(10)	23(2)	17(2)	18(3)	-2(2)	0(2)	-6(2)
C(11)	23(2)	17(2)	18(3)	-6(2)	5(2)	-5(2)
C(12)	23(2)	13(2)	21(3)	-2(2)	11(2)	0(2)
C(13)	21(2)	17(2)	21(3)	-1(2)	7(2)	-5(2)
C(14)	20(2)	21(2)	17(2)	-2(2)	11(2)	4(2)
C(15)	23(3)	23(2)	23(3)	4(2)	6(2)	5(2)
C(16)	27(2)	14(2)	27(3)	2(2)	13(2)	2(2)
C(17)	22(2)	21(2)	21(3)	4(2)	2(2)	6(2)
C(18)	29(3)	32(3)	23(3)	-3(2)	5(2)	-3(2)
C(19)	20(2)	32(3)	27(3)	-3(2)	7(2)	-1(2)
C(20)	31(3)	36(3)	35(3)	3(2)	-3(2)	-2(2)
N(1)	23(2)	21(2)	18(2)	1(2)	7(2)	-2(2)
N(2)	22(2)	14(2)	20(2)	-3(2)	10(2)	-2(2)
F(1)	25(2)	23(2)	44(2)	2(1)	-1(1)	-8(1)
F(2)	22(2)	35(2)	37(2)	4(1)	-3(1)	1(1)
F(3)	33(2)	34(2)	30(2)	11(1)	-4(1)	0(1)
F(4)	38(2)	19(1)	29(2)	5(1)	-2(1)	-9(1)
S(1)	22(1)	19(1)	24(1)	-1(1)	5(1)	-5(1)
Pt(1)	14(1)	12(1)	19(1)	-1(1)	3(1)	-2(1)
Pt(1A)	29(4)	27(3)	27(3)	-4(2)	11(3)	-3(3)

Table A20. Hydrogen coordinates (x 10^4) and isotropic displacement parameters (Å^2 x 10^3) for **5l**.

Atom	x	y	z	U(eq)
H(1A)	7072	-809	3358	54
H(1B)	6193	-881	4417	54
H(1C)	5873	-1032	2615	54
H(2A)	9378	-2177	4034	51
H(2B)	9972	-1656	5388	51
H(2C)	9148	-1303	3992	51
H(3A)	8169	-595	5579	48
H(3B)	8802	-862	7217	48
H(3C)	7526	-893	6838	48
H(10)	5479	-4798	3674	24
H(13)	4258	-4117	1673	23
H(15)	3635	-2153	-489	27
H(16)	5090	-1662	1089	26
H(18A)	3624	-3901	-2257	42
H(18B)	2567	-4379	-2257	42
H(18C)	3603	-4515	-963	42
H(19A)	2519	-4315	1048	39
H(19B)	1468	-4145	-198	39
H(19C)	1883	-3555	1125	39
H(20A)	1876	-2589	-966	53
H(20B)	1462	-3225	-2191	53
H(20C)	2510	-2760	-2318	53

Crystallographic Data for Complex **6**

Table A21. Atomic coordinates (x 10^4) and equivalent isotropic displacement parameters ($Å^2$ x 10^3) for **6**. U(eq) is defined as one third of the trace of the orthogonalized U^{ij} tensor.

Atom	x	y	z	U(eq)
C(1)	1690(2)	678(4)	1570(4)	23(1)
C(2)	1577(2)	1426(4)	2235(4)	21(1)
C(3)	1244(2)	2478(3)	228(3)	17(1)
C(4)	1009(2)	1795(4)	-581(3)	27(1)
C(5)	570(2)	2012(4)	-1212(4)	29(1)
C(6)	350(2)	2935(4)	-1053(4)	32(1)
C(7)	569(2)	3638(4)	-254(3)	27(1)
C(8)	1007(2)	3406(4)	378(3)	21(1)
C(9)	2727(1)	1476(3)	3033(3)	16(1)
C(10)	3155(1)	1576(3)	3734(3)	19(1)
C(11)	3455(2)	2369(3)	3576(3)	17(1)
C(12)	3292(1)	3015(3)	2687(3)	13(1)
C(13)	2852(1)	2888(3)	2020(3)	14(1)
C(14)	3927(2)	2517(3)	4371(3)	20(1)
C(15)	4180(2)	1433(3)	4562(4)	30(1)
C(16)	4226(2)	3327(4)	3997(4)	27(1)
C(17)	3850(2)	2911(4)	5422(3)	29(1)
C(18)	2649(1)	3591(3)	1126(3)	12(1)
C(19)	2823(1)	4461(3)	732(3)	14(1)
C(20)	2462(1)	4852(3)	-132(3)	15(1)
C(21)	2419(2)	5723(3)	-830(3)	19(1)
C(22)	2013(2)	5862(4)	-1604(3)	23(1)
C(23)	1642(2)	5162(4)	-1704(3)	24(1)
C(24)	1668(2)	4309(3)	-1035(3)	19(1)
C(25)	2075(1)	4155(3)	-228(3)	13(1)
N(1)	2564(1)	2119(3)	2192(3)	14(1)
N(2)	2195(1)	3389(3)	558(2)	12(1)
Pt(1)	1885(1)	2210(1)	1164(1)	13(1)

Table A22.   Bond lengths [Å] for **6**.

Bond	Length	Bond	Length
C(1)-C(2)	1.386(6)	C(14)-C(16)	1.526(6)
C(1)-Pt(1)	2.115(4)	C(14)-C(15)	1.543(6)
C(1)-H(100)	0.94(2)	C(14)-C(17)	1.543(6)
C(1)-H(101)	0.94(2)	C(15)-H(15A)	0.9800
C(2)-Pt(1)	2.130(4)	C(15)-H(15B)	0.9800
C(2)-H(102)	0.95(2)	C(15)-H(15C)	0.9800
C(2)-H(103)	0.96(2)	C(16)-H(16A)	0.9800
C(3)-C(4)	1.394(6)	C(16)-H(16B)	0.9800
C(3)-C(8)	1.406(6)	C(16)-H(16C)	0.9800
C(3)-Pt(1)	2.013(4)	C(17)-H(17A)	0.9800
C(4)-C(5)	1.381(6)	C(17)-H(17B)	0.9800
C(4)-H(4)	0.9500	C(17)-H(17C)	0.9800
C(5)-C(6)	1.375(6)	C(18)-C(19)	1.370(5)
C(5)-H(5)	0.9500	C(18)-N(2)	1.391(5)
C(6)-C(7)	1.386(6)	C(19)-C(20)	1.423(5)
C(6)-H(6)	0.9500	C(19)-H(19)	0.9500
C(7)-C(8)	1.383(6)	C(20)-C(21)	1.406(5)
C(7)-H(7)	0.9500	C(20)-C(25)	1.435(5)
C(8)-H(8)	0.9500	C(21)-C(22)	1.371(6)
C(9)-N(1)	1.343(5)	C(21)-H(21)	0.9500
C(9)-C(10)	1.370(5)	C(22)-C(23)	1.400(6)
C(9)-H(9)	0.9500	C(22)-H(22)	0.9500
C(10)-C(11)	1.396(6)	C(23)-C(24)	1.370(6)
C(10)-H(10)	0.9500	C(23)-H(23)	0.9500
C(11)-C(12)	1.391(6)	C(24)-C(25)	1.397(5)
C(11)-C(14)	1.527(6)	C(24)-H(24)	0.9500
C(12)-C(13)	1.384(5)	C(25)-N(2)	1.380(5)
C(12)-H(12)	0.9500	N(1)-Pt(1)	2.121(3)
C(13)-N(1)	1.357(5)	N(2)-Pt(1)	2.023(3)
C(13)-C(18)	1.458(5)		

Table A23. Bond angles [°] for **6**.

Bond	Angle	Bond	Angle
C(2)-C(1)-Pt(1)	71.5(3)	H(15A)-C(15)-H(15C)	109.5
C(2)-C(1)-H(100)	121(3)	H(15B)-C(15)-H(15C)	109.5
Pt(1)-C(1)-H(100)	107(3)	C(14)-C(16)-H(16A)	109.5
C(2)-C(1)-H(101)	117(3)	C(14)-C(16)-H(16B)	109.5
Pt(1)-C(1)-H(101)	109(3)	H(16A)-C(16)-H(16B)	109.5
H(100)-C(1)-H(101)	118(4)	C(14)-C(16)-H(16C)	109.5
C(1)-C(2)-Pt(1)	70.3(3)	H(16A)-C(16)-H(16C)	109.5
C(1)-C(2)-H(102)	120(3)	H(16B)-C(16)-H(16C)	109.5
Pt(1)-C(2)-H(102)	108(3)	C(14)-C(17)-H(17A)	109.5
C(1)-C(2)-H(103)	122(2)	C(14)-C(17)-H(17B)	109.5
Pt(1)-C(2)-H(103)	112(2)	H(17A)-C(17)-H(17B)	109.5
H(102)-C(2)-H(103)	114(4)	C(14)-C(17)-H(17C)	109.5
C(4)-C(3)-C(8)	116.0(4)	H(17A)-C(17)-H(17C)	109.5
C(4)-C(3)-Pt(1)	124.4(3)	H(17B)-C(17)-H(17C)	109.5
C(8)-C(3)-Pt(1)	119.6(3)	C(19)-C(18)-N(2)	111.6(3)
C(5)-C(4)-C(3)	122.6(4)	C(19)-C(18)-C(13)	131.5(4)
C(5)-C(4)-H(4)	118.7	N(2)-C(18)-C(13)	116.9(3)
C(3)-C(4)-H(4)	118.7	C(18)-C(19)-C(20)	106.4(4)
C(6)-C(5)-C(4)	119.8(4)	C(18)-C(19)-H(19)	126.8
C(6)-C(5)-H(5)	120.1	C(20)-C(19)-H(19)	126.8
C(4)-C(5)-H(5)	120.1	C(21)-C(20)-C(19)	134.1(4)
C(5)-C(6)-C(7)	119.9(5)	C(21)-C(20)-C(25)	119.2(4)
C(5)-C(6)-H(6)	120.1	C(19)-C(20)-C(25)	106.7(4)
C(7)-C(6)-H(6)	120.1	C(22)-C(21)-C(20)	118.8(4)
C(8)-C(7)-C(6)	119.7(5)	C(22)-C(21)-H(21)	120.6
C(8)-C(7)-H(7)	120.1	C(20)-C(21)-H(21)	120.6
C(6)-C(7)-H(7)	120.1	C(21)-C(22)-C(23)	121.4(4)
C(7)-C(8)-C(3)	122.0(4)	C(21)-C(22)-H(22)	119.3
C(7)-C(8)-H(8)	119.0	C(23)-C(22)-H(22)	119.3
C(3)-C(8)-H(8)	119.0	C(24)-C(23)-C(22)	121.6(4)
N(1)-C(9)-C(10)	124.1(4)	C(24)-C(23)-H(23)	119.2
N(1)-C(9)-H(9)	118.0	C(22)-C(23)-H(23)	119.2
C(10)-C(9)-H(9)	118.0	C(23)-C(24)-C(25)	118.3(4)
C(9)-C(10)-C(11)	119.7(4)	C(23)-C(24)-H(24)	120.8
C(9)-C(10)-H(10)	120.1	C(25)-C(24)-H(24)	120.8
C(11)-C(10)-H(10)	120.1	N(2)-C(25)-C(24)	130.9(4)
C(12)-C(11)-C(10)	116.4(4)	N(2)-C(25)-C(20)	108.6(3)
C(12)-C(11)-C(14)	123.2(4)	C(24)-C(25)-C(20)	120.6(4)
C(10)-C(11)-C(14)	120.4(4)	C(9)-N(1)-C(13)	117.0(4)
C(13)-C(12)-C(11)	121.2(4)	C(9)-N(1)-Pt(1)	128.6(3)
C(13)-C(12)-H(12)	119.4	C(13)-N(1)-Pt(1)	114.0(3)
C(11)-C(12)-H(12)	119.4	C(25)-N(2)-C(18)	106.7(3)
N(1)-C(13)-C(12)	121.7(4)	C(25)-N(2)-Pt(1)	138.2(3)
N(1)-C(13)-C(18)	114.6(4)	C(18)-N(2)-Pt(1)	114.7(2)
C(12)-C(13)-C(18)	123.7(4)	C(3)-Pt(1)-N(2)	96.37(14)
C(16)-C(14)-C(11)	112.7(3)	C(3)-Pt(1)-C(1)	90.91(18)
C(16)-C(14)-C(15)	108.8(4)	N(2)-Pt(1)-C(1)	161.83(16)
C(11)-C(14)-C(15)	109.4(3)	C(3)-Pt(1)-N(1)	173.40(15)
C(16)-C(14)-C(17)	109.1(4)	N(2)-Pt(1)-N(1)	79.52(12)
C(11)-C(14)-C(17)	107.7(4)	C(1)-Pt(1)-N(1)	94.52(16)
C(15)-C(14)-C(17)	109.1(4)	C(3)-Pt(1)-C(2)	87.46(17)
C(14)-C(15)-H(15A)	109.5	N(2)-Pt(1)-C(2)	158.43(16)
C(14)-C(15)-H(15B)	109.5	C(1)-Pt(1)-C(2)	38.12(17)
H(15A)-C(15)-H(15B)	109.5	N(1)-Pt(1)-C(2)	94.51(15)
C(14)-C(15)-H(15C)	109.5		

Table A24. Anisotropic displacement parameters (Å^2 x 10^3) for **6**. The anisotropic displacement factor exponent takes the form: $-2\pi^2[h^2a^2U^{11} + ... + 2hk(abU^{12})]$.

Atom	U^{11}	U^{22}	U^{33}	U^{23}	U^{13}	U^{12}
C(1)	23(3)	19(3)	27(3)	3(2)	7(2)	-7(2)
C(2)	17(3)	24(3)	25(3)	8(2)	10(2)	-3(2)
C(3)	16(3)	20(3)	15(2)	4(2)	6(2)	-6(2)
C(4)	29(3)	32(3)	23(3)	-10(2)	10(2)	-4(2)
C(5)	29(3)	40(3)	18(3)	-10(2)	5(2)	-9(2)
C(6)	20(3)	54(4)	21(3)	9(2)	3(2)	-5(3)
C(7)	21(3)	30(3)	29(3)	5(2)	6(2)	-2(2)
C(8)	19(3)	23(3)	18(2)	-2(2)	-1(2)	-3(2)
C(9)	17(3)	15(2)	18(2)	1(2)	8(2)	0(2)
C(10)	25(3)	16(2)	19(2)	9(2)	9(2)	4(2)
C(11)	17(3)	14(2)	22(2)	1(2)	8(2)	7(2)
C(12)	16(3)	9(2)	15(2)	-1(2)	6(2)	-2(2)
C(13)	17(3)	14(2)	14(2)	-1(2)	9(2)	1(2)
C(14)	15(3)	18(3)	23(2)	2(2)	1(2)	2(2)
C(15)	19(3)	30(3)	39(3)	4(2)	2(2)	5(2)
C(16)	19(3)	30(3)	30(3)	3(2)	1(2)	3(2)
C(17)	23(3)	36(3)	25(3)	-1(2)	1(2)	-3(2)
C(18)	14(2)	12(2)	10(2)	-3(2)	4(2)	0(2)
C(19)	15(3)	9(2)	19(2)	-5(2)	5(2)	0(2)
C(20)	20(3)	13(2)	17(2)	-3(2)	10(2)	1(2)
C(21)	24(3)	16(2)	20(2)	-2(2)	12(2)	-1(2)
C(22)	28(3)	24(3)	18(2)	7(2)	9(2)	5(2)
C(23)	18(3)	33(3)	17(2)	4(2)	1(2)	1(2)
C(24)	19(3)	27(3)	12(2)	-2(2)	6(2)	-8(2)
C(25)	17(3)	10(2)	12(2)	-4(2)	7(2)	0(2)
N(1)	17(2)	11(2)	16(2)	0(2)	10(2)	1(2)
N(2)	19(2)	10(2)	9(2)	3(2)	6(2)	-4(2)
Pt(1)	14(1)	12(1)	14(1)	-1(1)	4(1)	-3(1)

Table A25. Hydrogen coordinates (x 10^4) and isotropic displacement parameters ($\mathring{A}^2$ x 10^3) for **6**.

Atom	x	y	z	U(eq)
H(4)	1155	1155	-703	33
H(5)	420	1524	-1754	35
H(6)	50	3091	-1490	38
H(7)	419	4277	-141	32
H(8)	1152	3888	930	25
H(9)	2534	918	3149	19
H(10)	3248	1108	4326	23
H(12)	3486	3553	2535	16
H(15A)	4210	1152	3886	46
H(15B)	4005	926	4866	46
H(15C)	4487	1531	5054	46
H(16A)	4259	3106	3306	41
H(16B)	4531	3360	4513	41
H(16C)	4081	4034	3934	41
H(17A)	4148	2996	5954	43
H(17B)	3664	2386	5674	43
H(17C)	3689	3600	5306	43
H(19)	3125	4748	986	17
H(21)	2668	6207	-766	23
H(22)	1982	6446	-2083	28
H(23)	1365	5281	-2251	28
H(24)	1415	3834	-1117	23
H(100)	1960(10)	270(30)	1790(30)	31(14)
H(101)	1450(11)	410(30)	1000(30)	30(13)
H(102)	1772(14)	1530(40)	2930(20)	44(15)
H(103)	1265(9)	1660(30)	2140(30)	20(12)

Crystallographic Data for Complex **7**

Table A26. Atomic coordinates (x 10^4) and equivalent isotropic displacement parameters (Å^2 x 10^3) for **7**. U(eq) is defined as one third of the trace of the orthogonalized U^{ij} tensor.

Atom	x	y	z	U(eq)
C(1)	3141(5)	-681(2)	-2679(4)	25(1)
C(2)	1777(5)	-938(2)	-2609(4)	22(1)
C(3)	3285(4)	-1025(2)	-97(4)	18(1)
C(4)	4949(4)	-933(2)	270(4)	22(1)
C(5)	5589(4)	-1432(2)	1085(4)	23(1)
C(6)	5622(5)	-2009(2)	622(4)	32(1)
C(7)	6153(5)	-2482(2)	1378(5)	38(1)
C(8)	6648(5)	-2384(2)	2600(5)	38(1)
C(9)	6635(5)	-1817(2)	3081(4)	35(1)
C(10)	6105(4)	-1342(2)	2330(4)	26(1)
C(11)	2380(4)	242(2)	1618(3)	17(1)
C(12)	3126(4)	-159(2)	2443(4)	20(1)
C(13)	3423(4)	4(2)	3677(4)	25(1)
C(14)	3002(4)	561(2)	4111(4)	23(1)
C(15)	2249(4)	957(2)	3309(4)	23(1)
C(16)	1937(4)	806(2)	2044(4)	19(1)
C(17)	1209(4)	1102(2)	1000(4)	20(1)
C(18)	1240(4)	724(2)	10(3)	16(1)
C(19)	709(4)	811(2)	-1294(3)	15(1)
C(20)	-115(4)	1298(2)	-1746(4)	20(1)
C(21)	-593(4)	1355(2)	-3005(4)	20(1)
C(22)	-160(5)	900(2)	-3769(4)	23(1)
C(23)	641(4)	426(2)	-3276(4)	20(1)
C(24)	-1524(5)	1878(2)	-3553(4)	24(1)
C(25)	-2050(6)	2280(2)	-2555(4)	43(1)
C(26)	-567(5)	2238(2)	-4356(5)	48(2)
C(27)	-2887(5)	1652(2)	-4363(5)	36(1)
N(1)	1961(3)	197(1)	353(3)	15(1)
N(2)	1061(3)	366(1)	-2056(3)	17(1)
Pt(1)	2227(1)	-350(1)	-1106(1)	17(1)

Table A27. Bond lengths [Å] for **7**.

Bond	Length	Bond	Length
C(1)-C(2)	1.375(6)	C(14)-H(14)	0.9500
C(1)-Pt(1)	2.108(4)	C(15)-C(16)	1.409(5)
C(1)-H(100)	0.95(4)	C(15)-H(15)	0.9500
C(1)-H(101)	0.88(4)	C(16)-C(17)	1.414(5)
C(2)-Pt(1)	2.104(4)	C(17)-C(18)	1.371(5)
C(2)-H(102)	0.86(4)	C(17)-H(17)	0.9500
C(2)-H(103)	0.99(4)	C(18)-N(1)	1.388(5)
C(3)-C(4)	1.533(5)	C(18)-C(19)	1.455(5)
C(3)-Pt(1)	2.051(4)	C(19)-N(2)	1.358(5)
C(3)-H(3A)	0.9900	C(19)-C(20)	1.390(5)
C(3)-H(3B)	0.9900	C(20)-C(21)	1.389(5)
C(4)-C(5)	1.506(6)	C(20)-H(20)	0.9500
C(4)-H(4A)	0.9900	C(21)-C(22)	1.400(6)
C(4)-H(4B)	0.9900	C(21)-C(24)	1.532(6)
C(5)-C(10)	1.393(6)	C(22)-C(23)	1.368(6)
C(5)-C(6)	1.396(6)	C(22)-H(22)	0.9500
C(6)-C(7)	1.398(6)	C(23)-N(2)	1.340(5)
C(6)-H(6)	0.9500	C(23)-H(23)	0.9500
C(7)-C(8)	1.368(7)	C(24)-C(27)	1.524(6)
C(7)-H(7)	0.9500	C(24)-C(25)	1.525(6)
C(8)-C(9)	1.382(7)	C(24)-C(26)	1.527(6)
C(8)-H(8)	0.9500	C(25)-H(25A)	0.9800
C(9)-C(10)	1.400(6)	C(25)-H(25B)	0.9800
C(9)-H(9)	0.9500	C(25)-H(25C)	0.9800
C(10)-H(10)	0.9500	C(26)-H(26A)	0.9800
C(11)-N(1)	1.385(5)	C(26)-H(26B)	0.9800
C(11)-C(12)	1.394(5)	C(26)-H(26C)	0.9800
C(11)-C(16)	1.424(5)	C(27)-H(27A)	0.9800
C(12)-C(13)	1.383(6)	C(27)-H(27B)	0.9800
C(12)-H(12)	0.9500	C(27)-H(27C)	0.9800
C(13)-C(14)	1.409(6)	N(1)-Pt(1)	2.038(3)
C(13)-H(13)	0.9500	N(2)-Pt(1)	2.134(3)
C(14)-C(15)	1.374(6)		

Table A28. Bond angles [°] for **7**.

Bond	Angle	Bond	Angle
C(2)-C(1)-Pt(1)	70.8(2)	C(18)-C(17)-H(17)	126.8
C(2)-C(1)-H(100)	123(2)	C(16)-C(17)-H(17)	126.8
Pt(1)-C(1)-H(100)	110(2)	C(17)-C(18)-N(1)	111.9(3)
C(2)-C(1)-H(101)	119(3)	C(17)-C(18)-C(19)	129.9(4)
Pt(1)-C(1)-H(101)	105(3)	N(1)-C(18)-C(19)	118.1(3)
H(100)-C(1)-H(101)	115(4)	N(2)-C(19)-C(20)	121.6(3)
C(1)-C(2)-Pt(1)	71.1(2)	N(2)-C(19)-C(18)	114.5(3)
C(1)-C(2)-H(102)	117(3)	C(20)-C(19)-C(18)	123.9(3)
Pt(1)-C(2)-H(102)	108(3)	C(21)-C(20)-C(19)	121.1(4)
C(1)-C(2)-H(103)	123(3)	C(21)-C(20)-H(20)	119.4
Pt(1)-C(2)-H(103)	109(3)	C(19)-C(20)-H(20)	119.4
H(102)-C(2)-H(103)	116(4)	C(20)-C(21)-C(22)	115.7(4)
C(4)-C(3)-Pt(1)	115.5(3)	C(20)-C(21)-C(24)	123.5(4)
C(4)-C(3)-H(3A)	108.4	C(22)-C(21)-C(24)	120.8(3)
Pt(1)-C(3)-H(3A)	108.4	C(23)-C(22)-C(21)	120.9(4)
C(4)-C(3)-H(3B)	108.4	C(23)-C(22)-H(22)	119.6
Pt(1)-C(3)-H(3B)	108.4	C(21)-C(22)-H(22)	119.6
H(3A)-C(3)-H(3B)	107.5	N(2)-C(23)-C(22)	123.1(4)
C(5)-C(4)-C(3)	111.0(3)	N(2)-C(23)-H(23)	118.5
C(5)-C(4)-H(4A)	109.4	C(22)-C(23)-H(23)	118.5
C(3)-C(4)-H(4A)	109.4	C(27)-C(24)-C(25)	108.0(4)
C(5)-C(4)-H(4B)	109.4	C(27)-C(24)-C(26)	109.0(4)
C(3)-C(4)-H(4B)	109.4	C(25)-C(24)-C(26)	109.0(4)
H(4A)-C(4)-H(4B)	108.0	C(27)-C(24)-C(21)	110.2(3)
C(10)-C(5)-C(6)	117.7(4)	C(25)-C(24)-C(21)	112.6(3)
C(10)-C(5)-C(4)	121.7(4)	C(26)-C(24)-C(21)	107.9(4)
C(6)-C(5)-C(4)	120.6(4)	C(24)-C(25)-H(25A)	109.5
C(5)-C(6)-C(7)	121.4(4)	C(24)-C(25)-H(25B)	109.5
C(5)-C(6)-H(6)	119.3	H(25A)-C(25)-H(25B)	109.5
C(7)-C(6)-H(6)	119.3	C(24)-C(25)-H(25C)	109.5
C(8)-C(7)-C(6)	120.0(5)	H(25A)-C(25)-H(25C)	109.5
C(8)-C(7)-H(7)	120.0	H(25B)-C(25)-H(25C)	109.5
C(6)-C(7)-H(7)	120.0	C(24)-C(26)-H(26A)	109.5
C(7)-C(8)-C(9)	119.9(4)	C(24)-C(26)-H(26B)	109.5
C(7)-C(8)-H(8)	120.1	H(26A)-C(26)-H(26B)	109.5
C(9)-C(8)-H(8)	120.1	C(24)-C(26)-H(26C)	109.5
C(8)-C(9)-C(10)	120.4(4)	H(26A)-C(26)-H(26C)	109.5
C(8)-C(9)-H(9)	119.8	H(26B)-C(26)-H(26C)	109.5
C(10)-C(9)-H(9)	119.8	C(24)-C(27)-H(27A)	109.5
C(5)-C(10)-C(9)	120.6(4)	C(24)-C(27)-H(27B)	109.5
C(5)-C(10)-H(10)	119.7	H(27A)-C(27)-H(27B)	109.5
C(9)-C(10)-H(10)	119.7	C(24)-C(27)-H(27C)	109.5
N(1)-C(11)-C(12)	130.3(4)	H(27A)-C(27)-H(27C)	109.5
N(1)-C(11)-C(16)	109.2(3)	H(27B)-C(27)-H(27C)	109.5
C(12)-C(11)-C(16)	120.5(4)	C(11)-N(1)-C(18)	105.8(3)
C(13)-C(12)-C(11)	118.4(4)	C(11)-N(1)-Pt(1)	140.1(3)
C(13)-C(12)-H(12)	120.8	C(18)-N(1)-Pt(1)	113.8(2)
C(11)-C(12)-H(12)	120.8	C(23)-N(2)-C(19)	117.6(3)
C(12)-C(13)-C(14)	121.8(4)	C(23)-N(2)-Pt(1)	128.7(3)
C(12)-C(13)-H(13)	119.1	C(19)-N(2)-Pt(1)	113.8(2)
C(14)-C(13)-H(13)	119.1	N(1)-Pt(1)-C(3)	97.17(14)
C(15)-C(14)-C(13)	120.2(4)	N(1)-Pt(1)-C(2)	161.97(15)
C(15)-C(14)-H(14)	119.9	C(3)-Pt(1)-C(2)	89.11(17)
C(13)-C(14)-H(14)	119.9	N(1)-Pt(1)-C(1)	158.30(16)
C(14)-C(15)-C(16)	119.4(4)	C(3)-Pt(1)-C(1)	87.95(18)
C(14)-C(15)-H(15)	120.3	C(2)-Pt(1)-C(1)	38.12(17)
C(16)-C(15)-H(15)	120.3	N(1)-Pt(1)-N(2)	79.69(12)
C(15)-C(16)-C(17)	133.6(4)	C(3)-Pt(1)-N(2)	176.47(14)
C(15)-C(16)-C(11)	119.7(4)	C(2)-Pt(1)-N(2)	93.42(15)

| C(17)-C(16)-C(11) | 106.7(3) | C(1)-Pt(1)-N(2) | 95.57(16) |
| C(18)-C(17)-C(16) | 106.5(4) | | |

Table A29.   Anisotropic displacement parameters ($\mathring{A}^2$ x 10^3) for **7**. The anisotropic displacement factor exponent takes the form: $-2\pi^2[h^2a^2U^{11} + ... + 2hk(abU^{12})]$.

Atom	U^{11}	U^{22}	U^{33}	U^{23}	U^{13}	U^{12}
C(1)	31(3)	30(3)	15(2)	-5(2)	5(2)	5(2)
C(2)	34(3)	17(2)	15(2)	-5(2)	2(2)	0(2)
C(3)	16(2)	21(2)	17(2)	0(2)	1(2)	-1(2)
C(4)	21(2)	23(2)	23(2)	-1(2)	6(2)	-3(2)
C(5)	13(2)	29(2)	27(2)	-2(2)	4(2)	-1(2)
C(6)	28(2)	34(3)	31(3)	-4(2)	-5(2)	7(2)
C(7)	32(3)	28(3)	51(3)	-6(2)	-2(2)	11(2)
C(8)	27(3)	43(3)	42(3)	13(2)	-3(2)	10(2)
C(9)	29(3)	49(3)	25(3)	1(2)	-3(2)	5(2)
C(10)	19(2)	29(3)	30(3)	-4(2)	2(2)	-1(2)
C(11)	15(2)	23(2)	14(2)	-2(2)	2(2)	-6(2)
C(12)	20(2)	22(2)	18(2)	1(2)	1(2)	0(2)
C(13)	19(2)	36(3)	18(2)	11(2)	-1(2)	-3(2)
C(14)	24(2)	32(2)	14(2)	-4(2)	2(2)	-6(2)
C(15)	26(2)	22(2)	21(2)	-4(2)	7(2)	-4(2)
C(16)	18(2)	18(2)	19(2)	-4(2)	4(2)	-3(2)
C(17)	24(2)	19(2)	18(2)	-2(2)	3(2)	-1(2)
C(18)	18(2)	15(2)	16(2)	-1(2)	4(2)	-4(2)
C(19)	15(2)	16(2)	14(2)	-3(2)	3(2)	-4(2)
C(20)	28(2)	15(2)	16(2)	-2(2)	4(2)	-3(2)
C(21)	23(2)	20(2)	16(2)	1(2)	2(2)	-4(2)
C(22)	31(2)	26(2)	11(2)	2(2)	2(2)	-4(2)
C(23)	24(2)	23(2)	15(2)	-6(2)	4(2)	-3(2)
C(24)	33(2)	19(2)	20(2)	3(2)	-1(2)	2(2)
C(25)	78(4)	23(3)	27(3)	0(2)	-4(3)	16(3)
C(26)	35(3)	47(3)	59(4)	36(3)	0(3)	2(2)
C(27)	33(3)	33(3)	40(3)	-9(2)	-8(2)	7(2)
N(1)	19(2)	18(2)	9(2)	-3(1)	2(1)	-2(1)
N(2)	18(2)	18(2)	14(2)	1(1)	0(1)	-3(1)
Pt(1)	19(1)	18(1)	14(1)	-2(1)	2(1)	-1(1)

Table A30. Hydrogen coordinates (x 10^4) and isotropic displacement parameters (Å^2 x 10^3) for **7**.

Atom	x	y	z	U(eq)
H(3A)	2798	-1081	670	21
H(3B)	3148	-1395	-588	21
H(4A)	5467	-913	-489	27
H(4B)	5110	-553	720	27
H(6)	5277	-2082	-224	38
H(7)	6171	-2870	1043	45
H(8)	7000	-2706	3117	45
H(9)	6989	-1749	3928	42
H(10)	6096	-954	2672	31
H(12)	3422	-535	2164	24
H(13)	3925	-267	4247	29
H(14)	3240	664	4960	28
H(15)	1941	1328	3605	27
H(17)	783	1487	986	24
H(20)	-356	1598	-1186	24
H(22)	-426	921	-4641	27
H(23)	912	126	-3823	24
H(25A)	-2613	2046	-2004	65
H(25B)	-2685	2592	-2951	65
H(25C)	-1189	2459	-2070	65
H(26A)	313	2384	-3841	71
H(26B)	-1141	2575	-4721	71
H(26C)	-260	1987	-5022	71
H(27A)	-2574	1412	-5043	55
H(27B)	-3473	1990	-4708	55
H(27C)	-3491	1410	-3859	55
H(100)	4050(40)	-879(17)	-2430(30)	15(10)
H(101)	3200(40)	-373(19)	-3170(40)	18(11)
H(102)	1760(40)	-1294(18)	-2320(30)	9(10)
H(103)	870(50)	-810(20)	-3130(40)	32(13)

Appendix B
NMR
and
IR Spectral Data

from

Chapter Three:
Mechanistic Interrogation of Hydroarylations Catalyzed by Single-Component Co(-1) Complexes

NMR Spectral Data
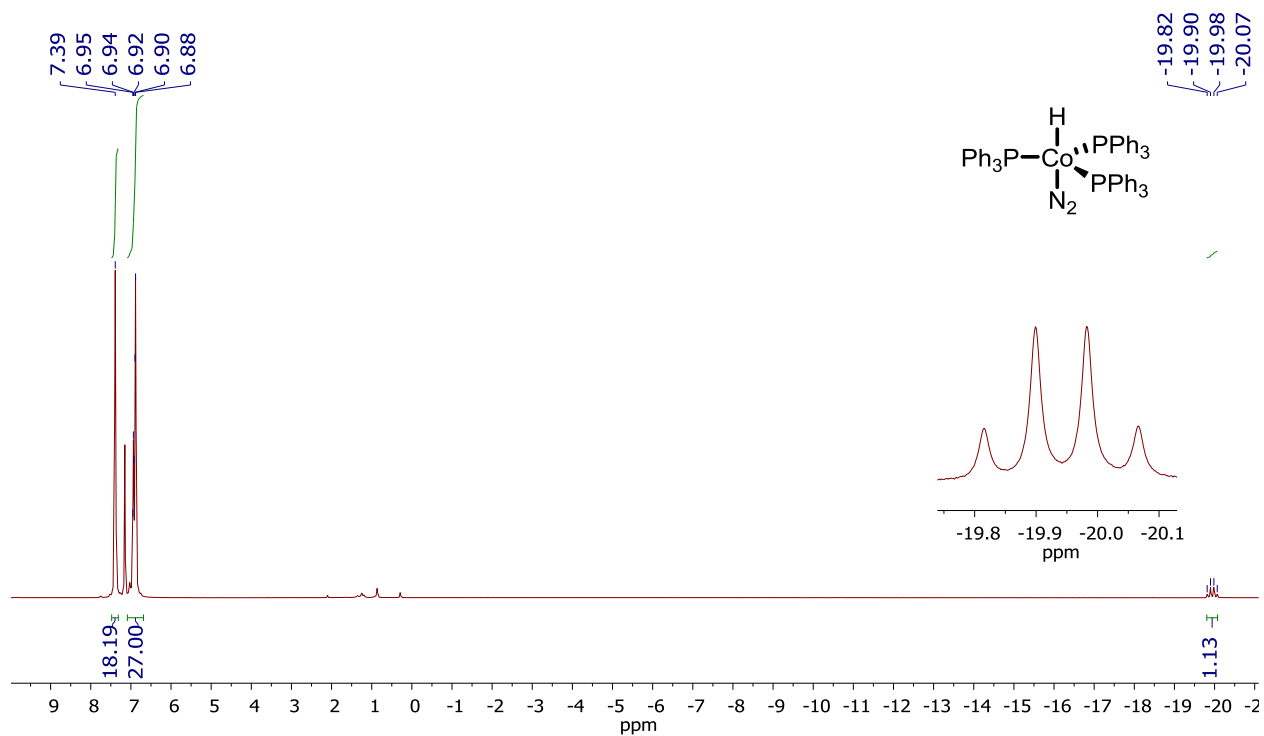
Figure B1a. ^{1}H NMR spectrum of **Co-H** in benzene-d_6.
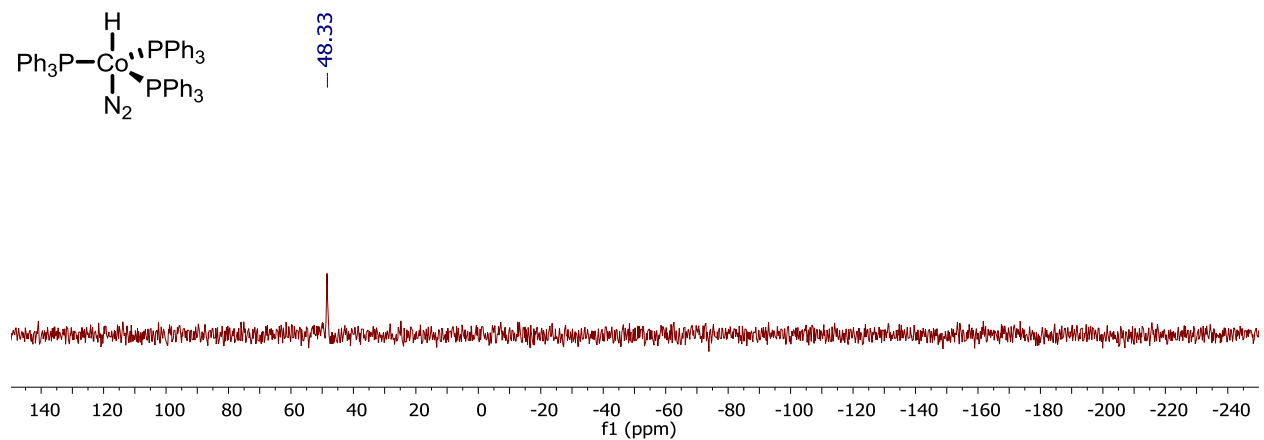
Figure B1b. ^{31}P{^{1}H} NMR spectrum of **Co-H** in benzene-d_6.
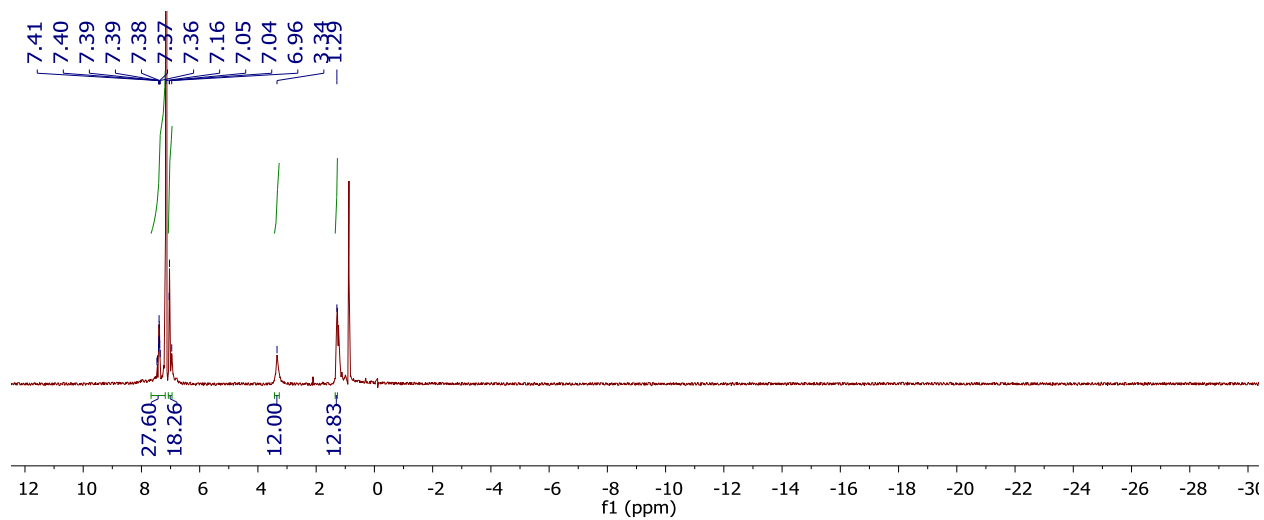
Figure Ba2. ^{1}H NMR spectrum of **Co-Li** in benzene-d_6.
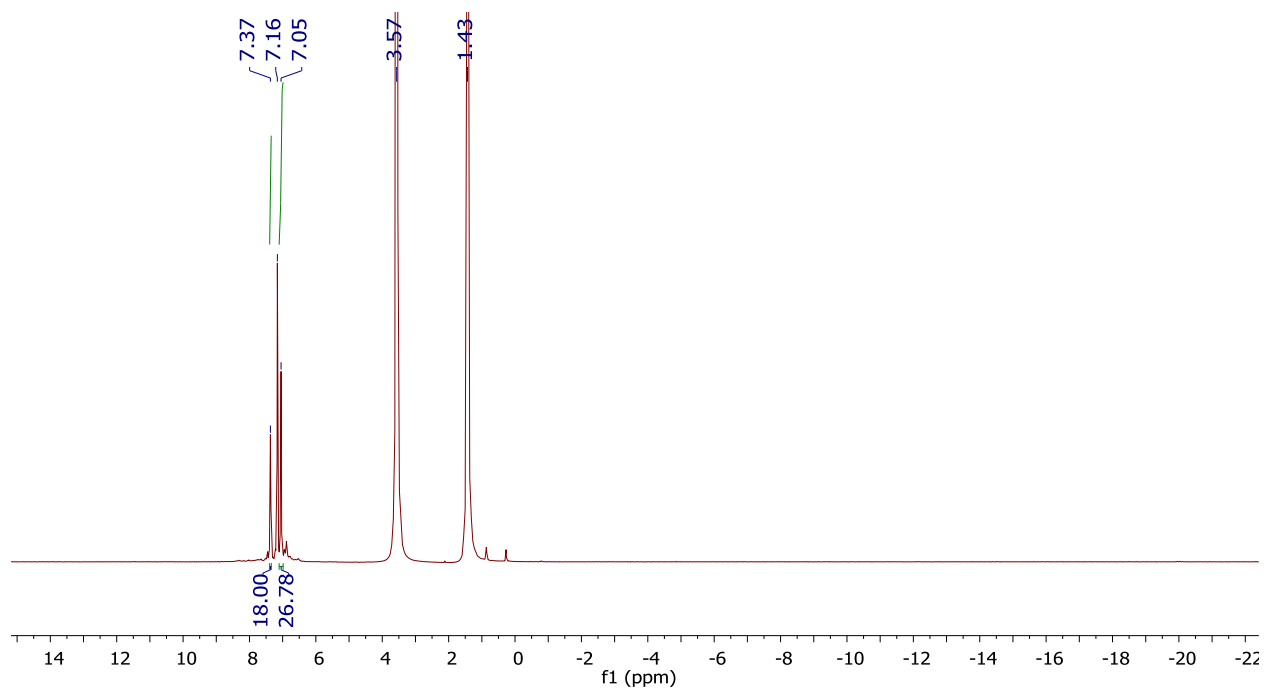
Figure B2b. ^{1}H NMR spectrum of **Co-Li** in tetrahydrofuran-d_0 with added benzene-d_6 as an internal reference.
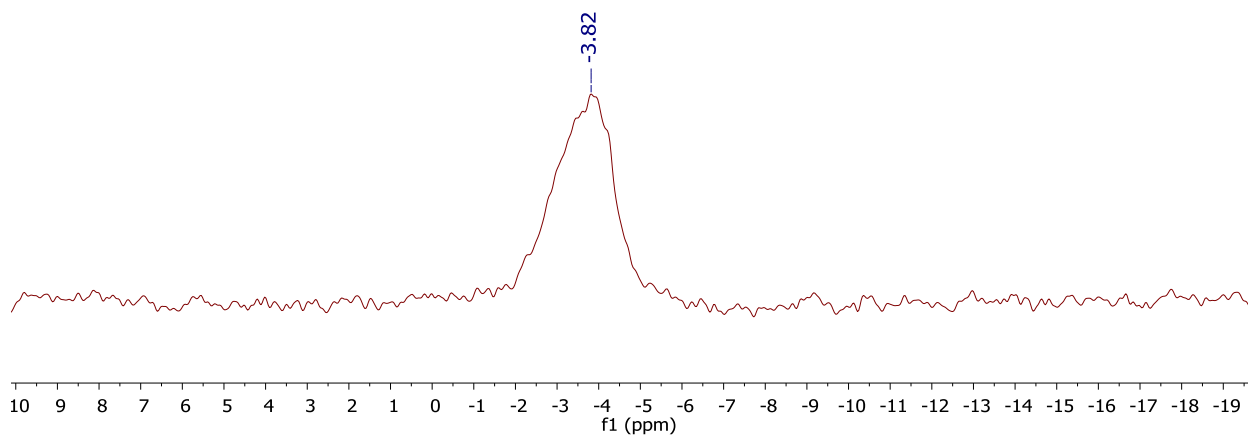
Figure B2c. ^{7}Li{^{1}H} NMR spectrum of **Co-Li** tetrahydrofuran-d_0 with added benzene-d_6 as an internal reference.
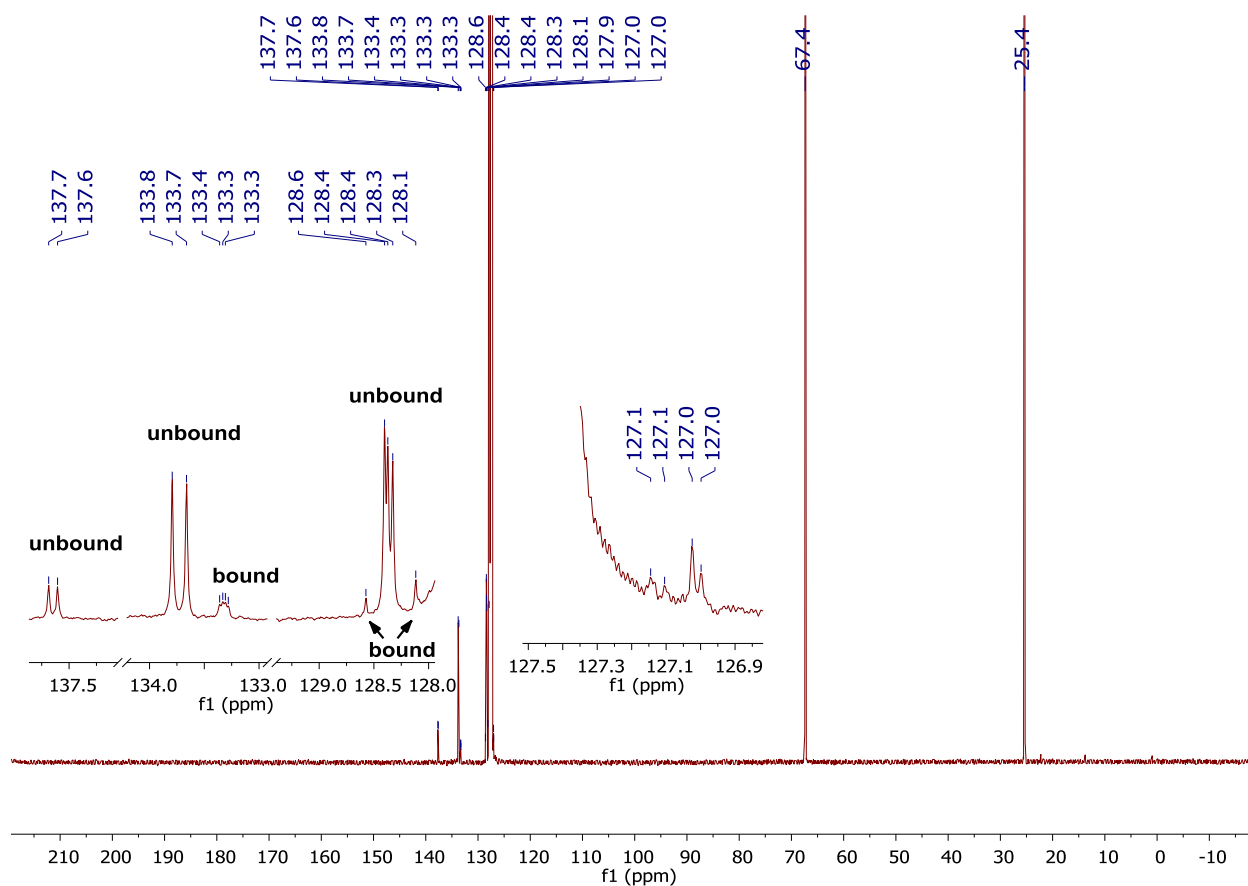
Figure B2d. ^{13}C{^{1}H} NMR spectrum of **Co-Li** tetrahydrofuran-d_0 with added benzene-d_6 as an internal reference.
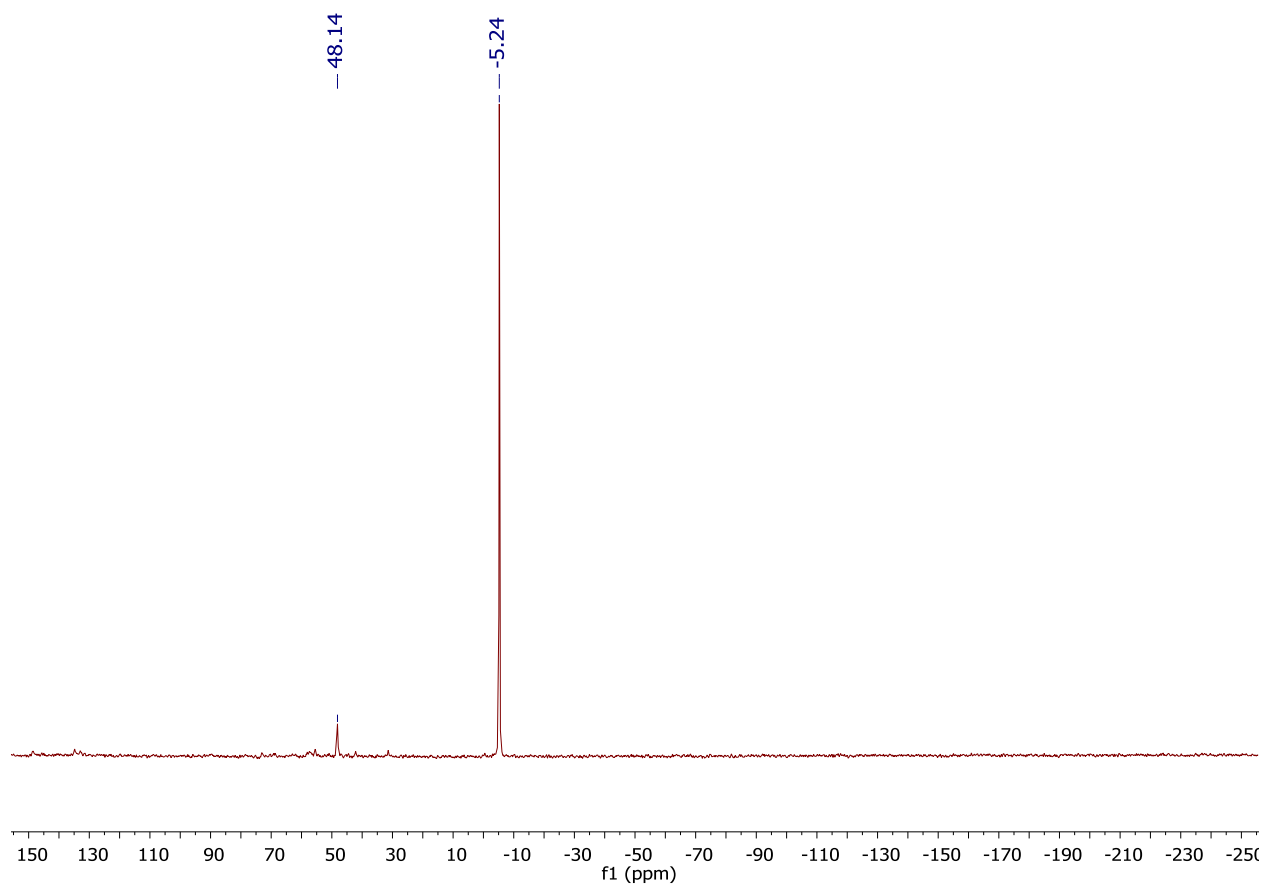
Figure B2e. $^{31}P\{^1H\}$ NMR spectrum of **Co-Li** in tetrahydrofuran-d_0 with added benzene-d_6 as an internal reference.
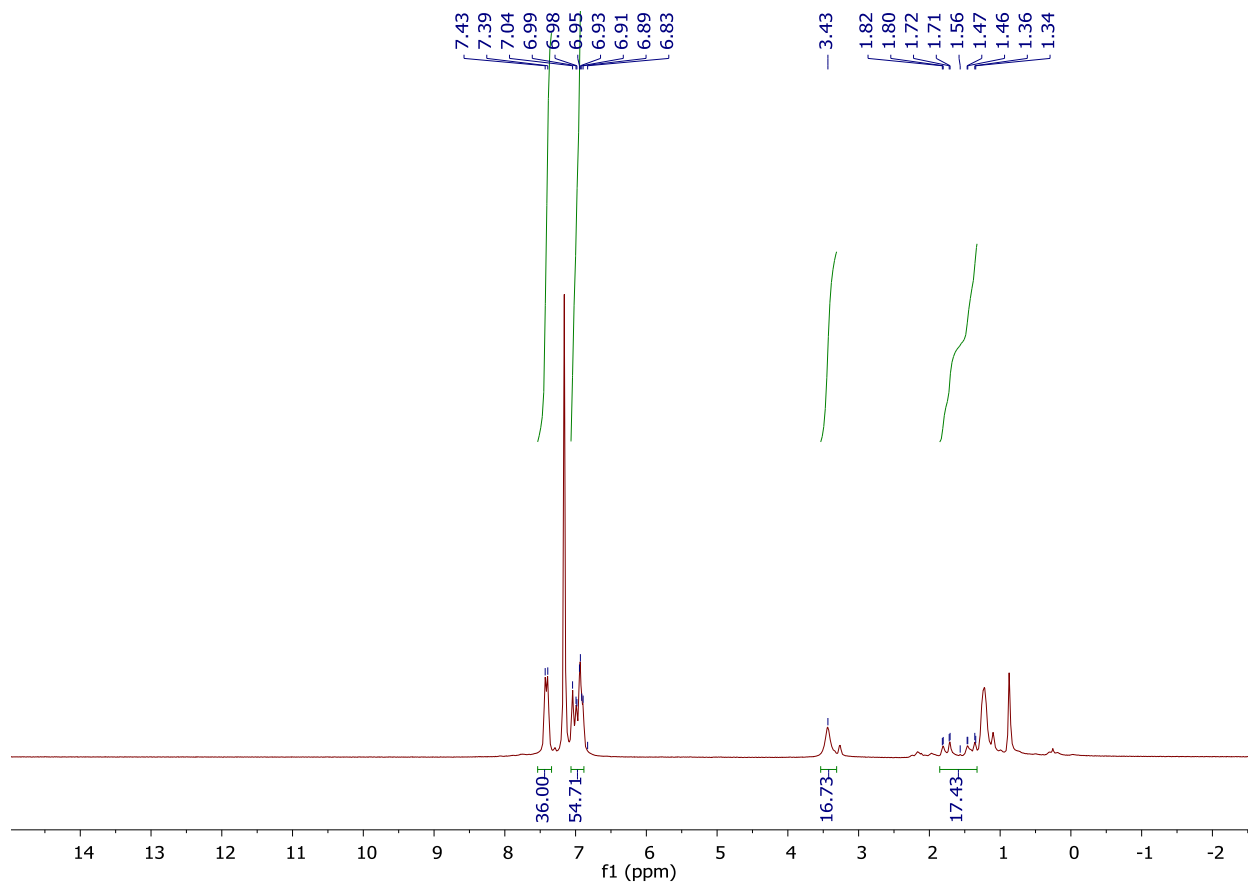
Figure B3a. ^{1}H NMR spectrum of **Co$_2$-Mg** in benzene-d_6. Note that residual pentane exists in the NMR spectrum.
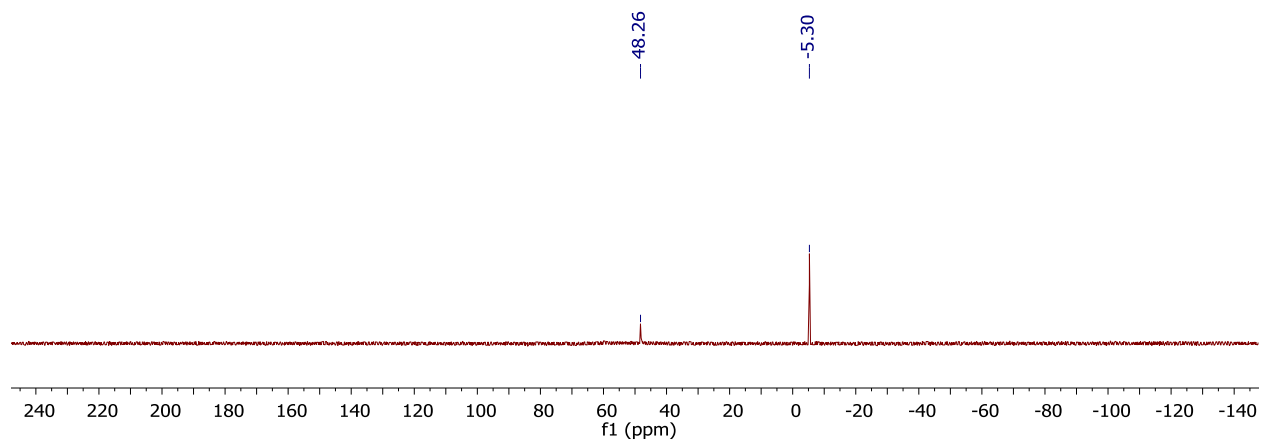
Figure B3b. ^{31}P{^{1}H} NMR spectrum of **Co$_2$-Mg** in benzene-d_6. Note that both free PPh$_3$ and bound PPh$_3$ are observed in the NMR spectrum likely due to rapid ligand exchange dynamics in solution.
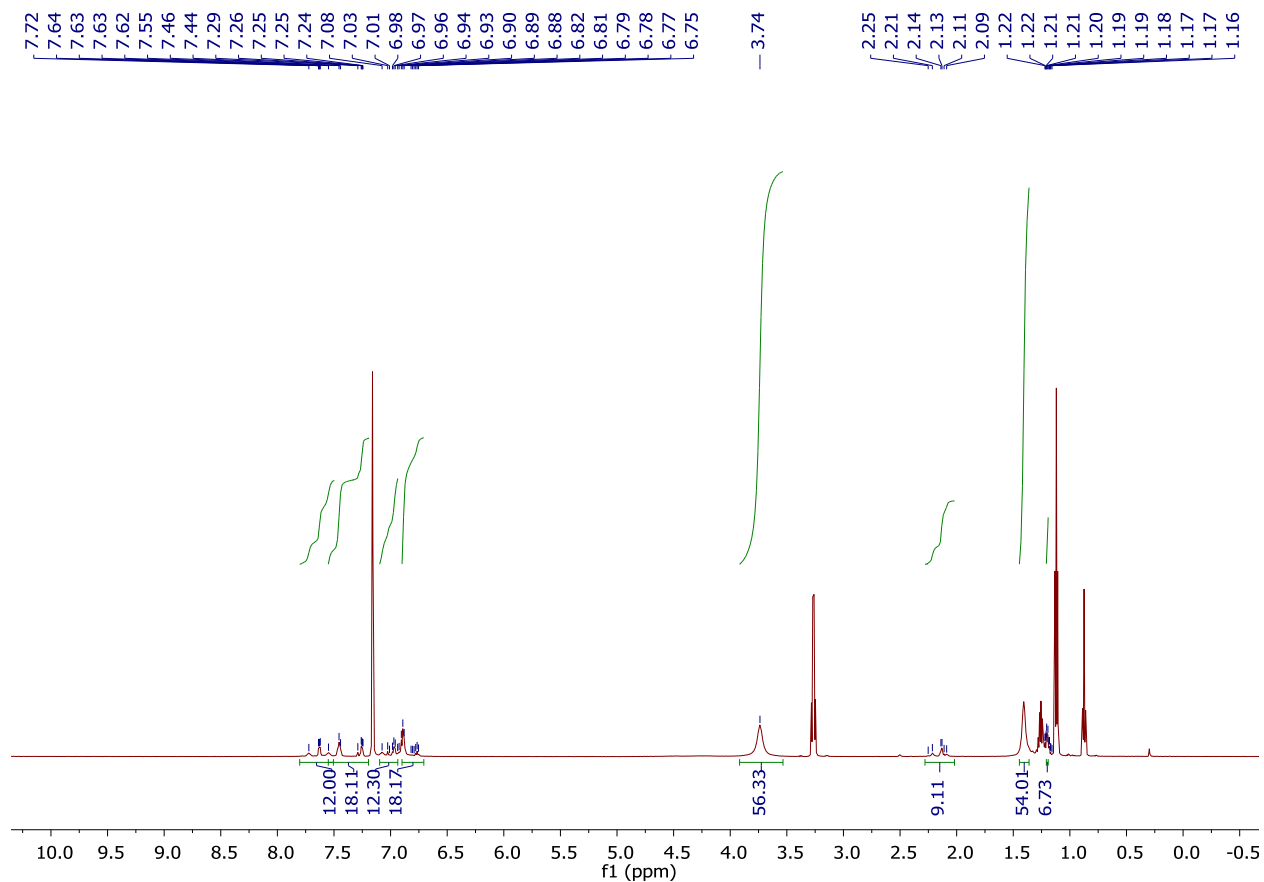
Figure B4a. ^{1}H NMR spectrum of **Co'$_2$-Mg** in benzene-d_6.
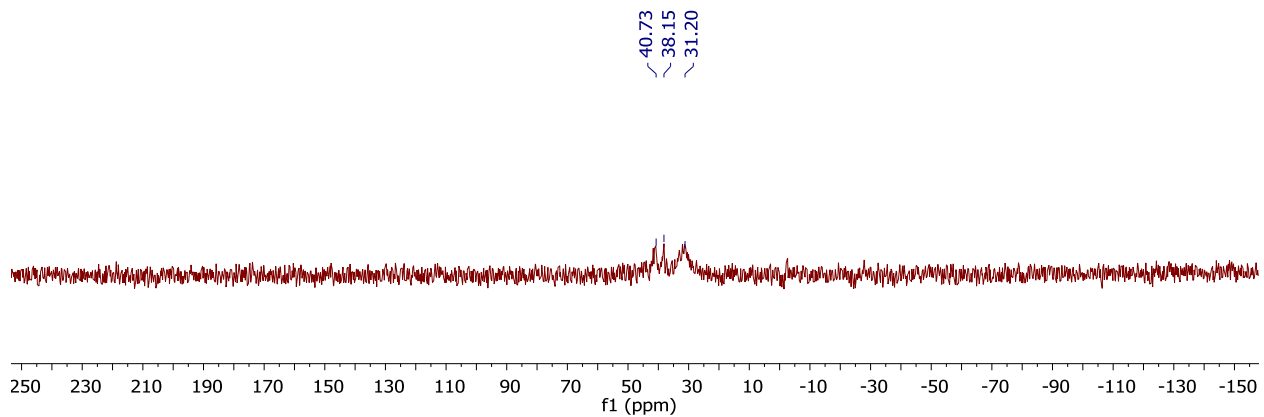
Figure B4b. ^{31}P{^{1}H} NMR spectrum of **Co'$_2$-Mg** in benzene-d_6.
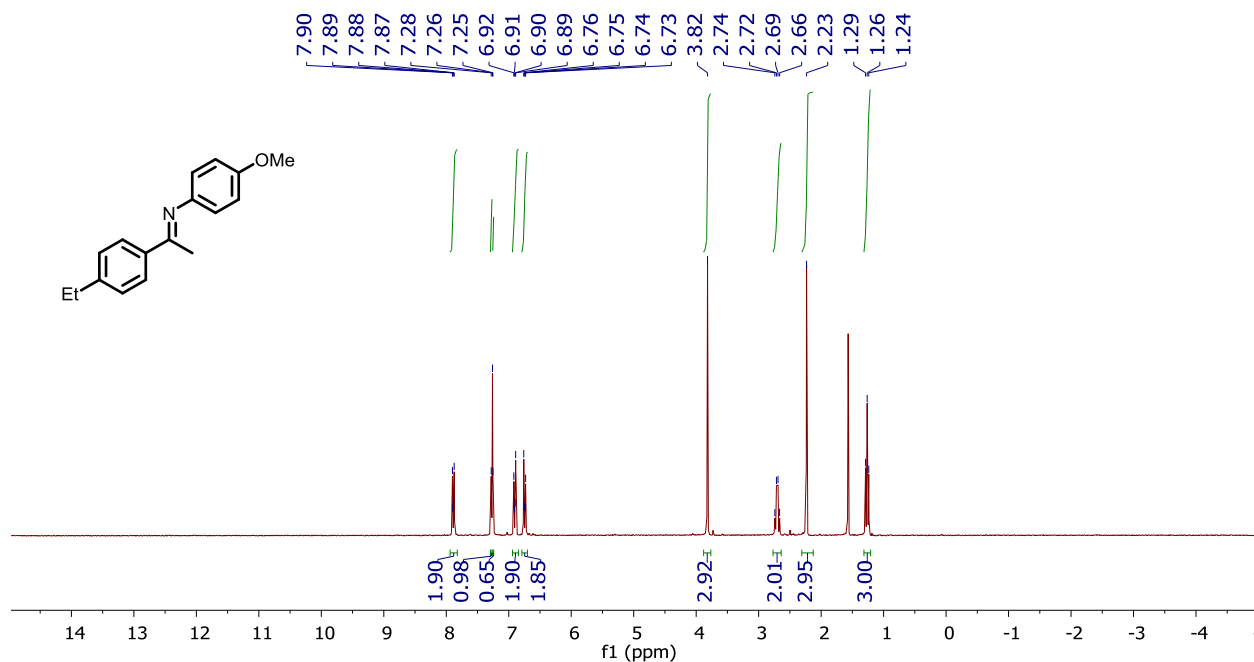
Figure B5a. ^{1}H NMR spectrum of **1a** in chloroform-*d*.
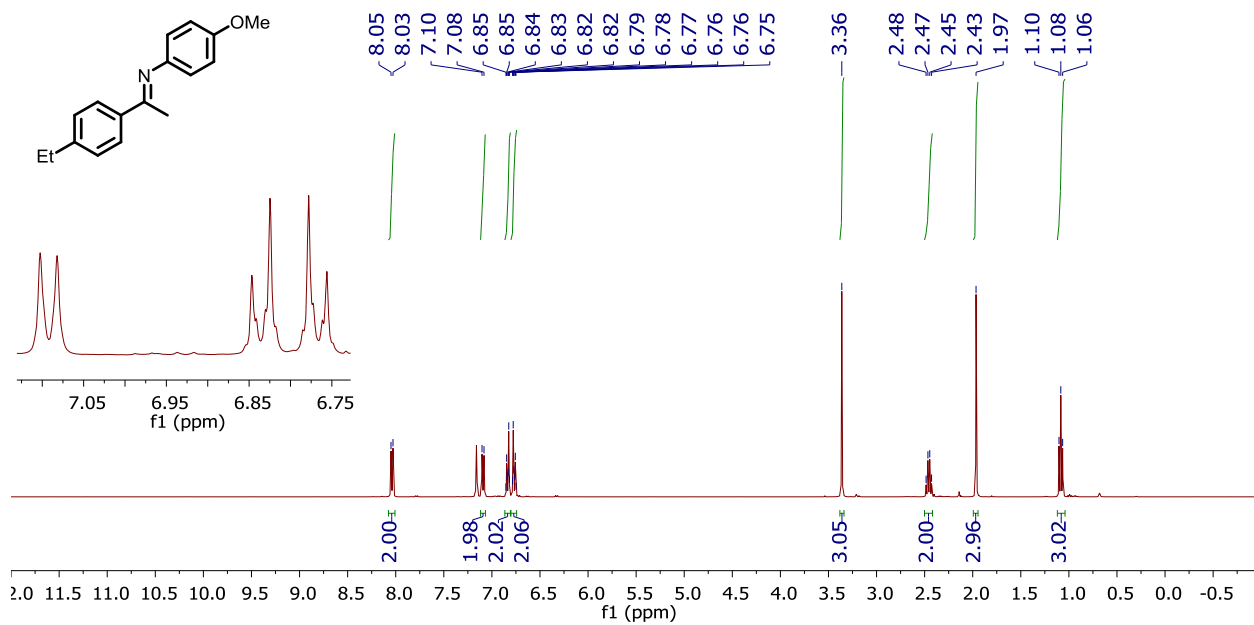
Figure B5b. ^{1}H NMR spectrum of **1a** in benzene-*d*$_6$.
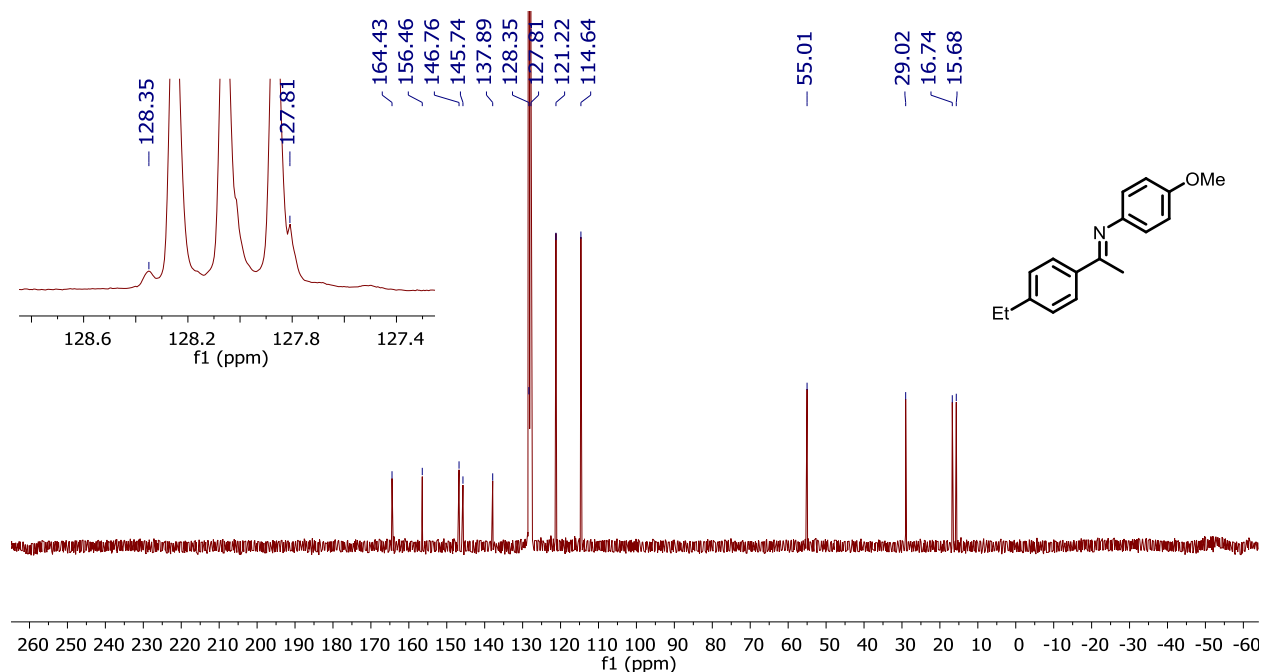
Figure B5c. $^{13}C\{^{1}H\}$ NMR spectrum of **1a** in benzene-d_6.
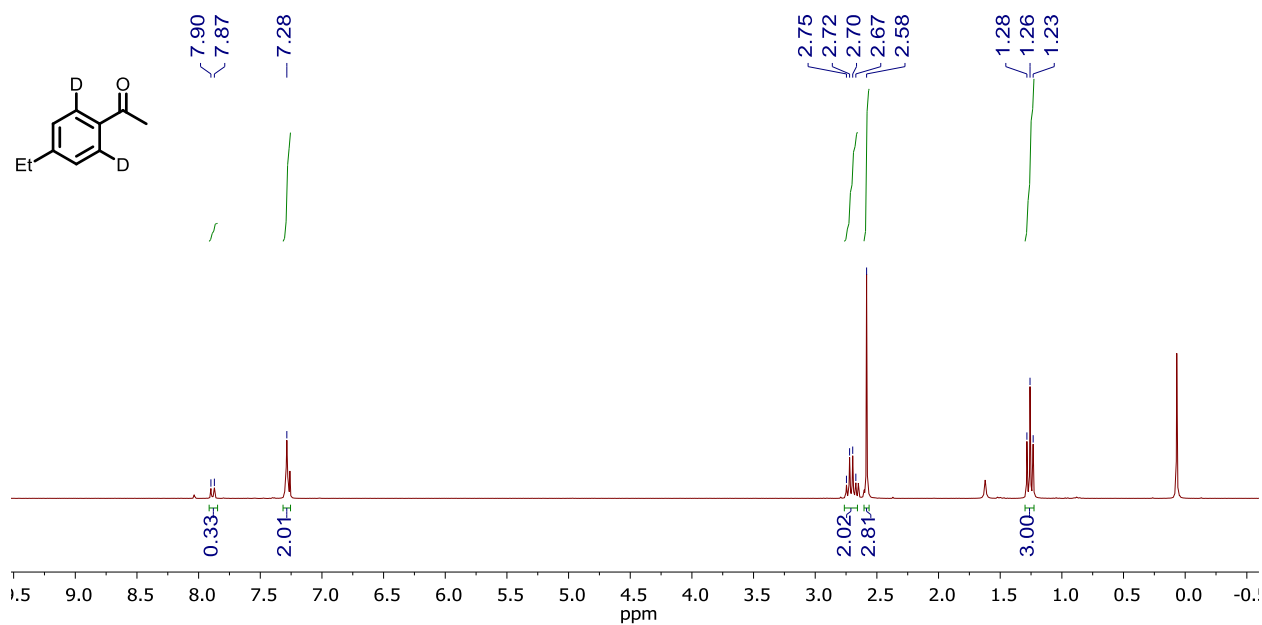
Figure B5d. ^{1}H NMR spectrum of 4'-ethylacetophenone-(2',6'-d_2) in chloroform-d. Note residual 4'-ethyacetophenone-(2'-d) is detectable at 7.90 ppm.
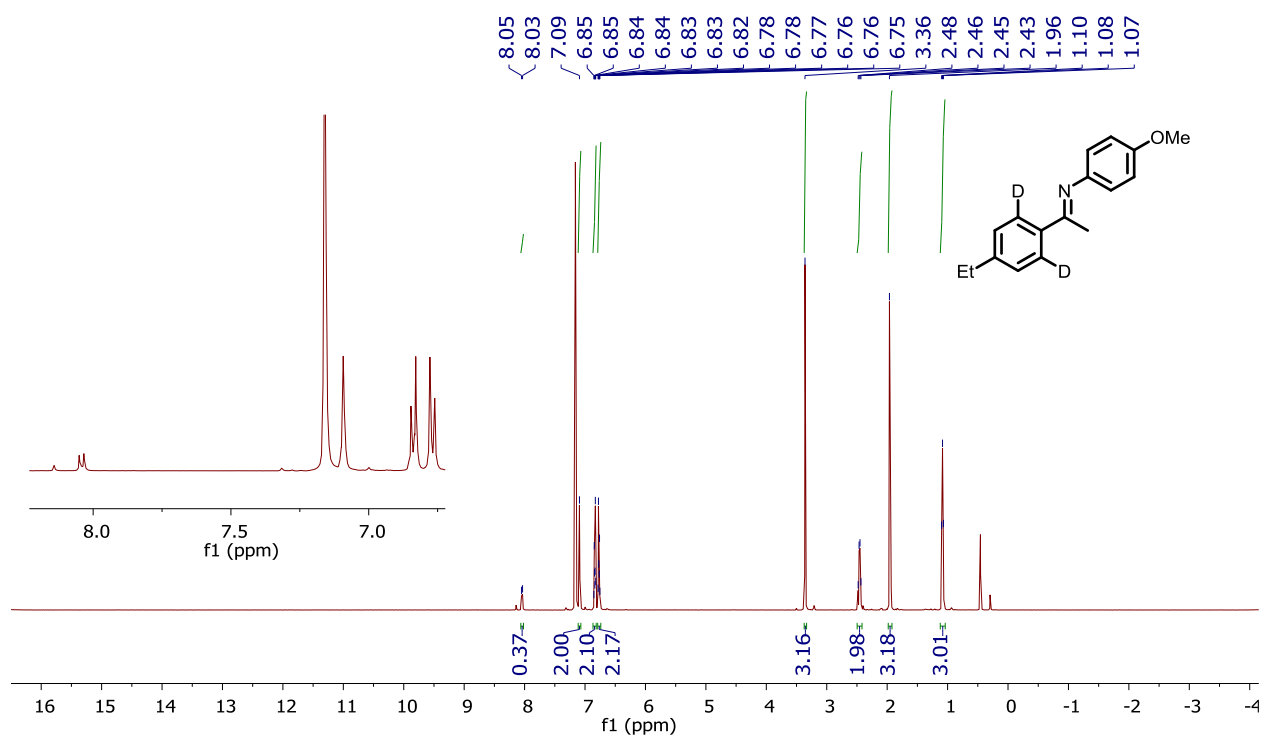
Figure B6a. ^{1}H NMR spectrum of **1a-d_2** in benzene-d_6.
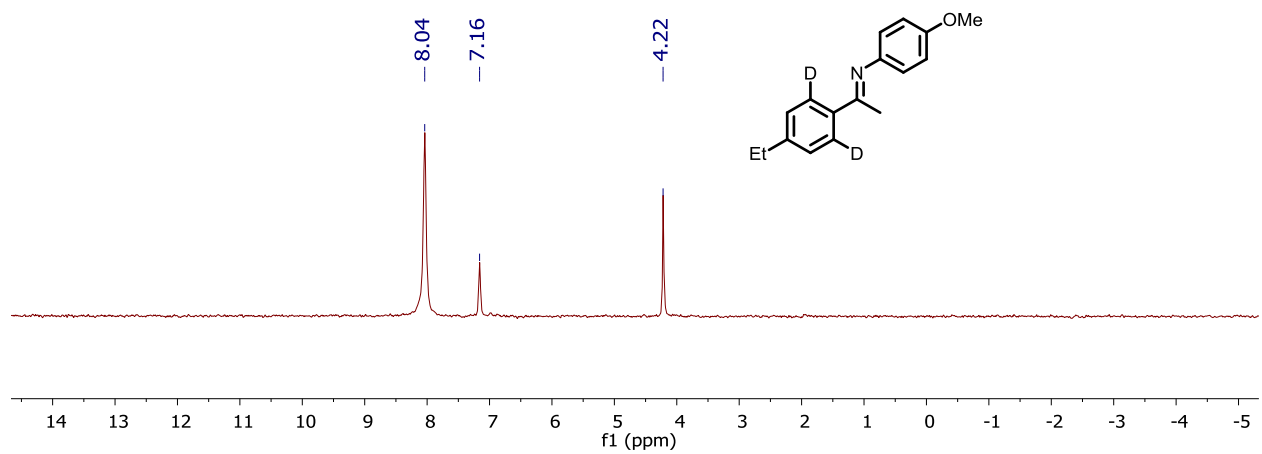
Figure B6b. ^{2}H NMR spectrum of **1a-d_2** in benzene-d_0. Note that residual CD_2Cl_2 exists at 4.22 ppm.
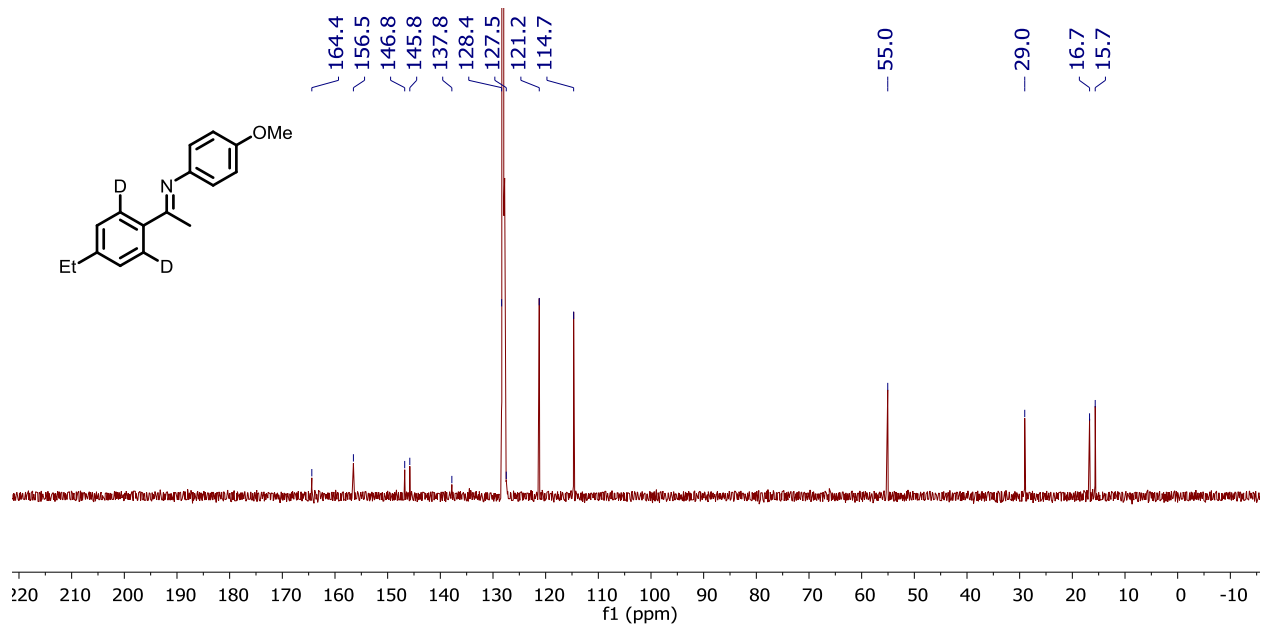
Figure B6c. $^{13}C\{^1H\}$ NMR spectrum of **1a-d_2** in benzene-d_6.
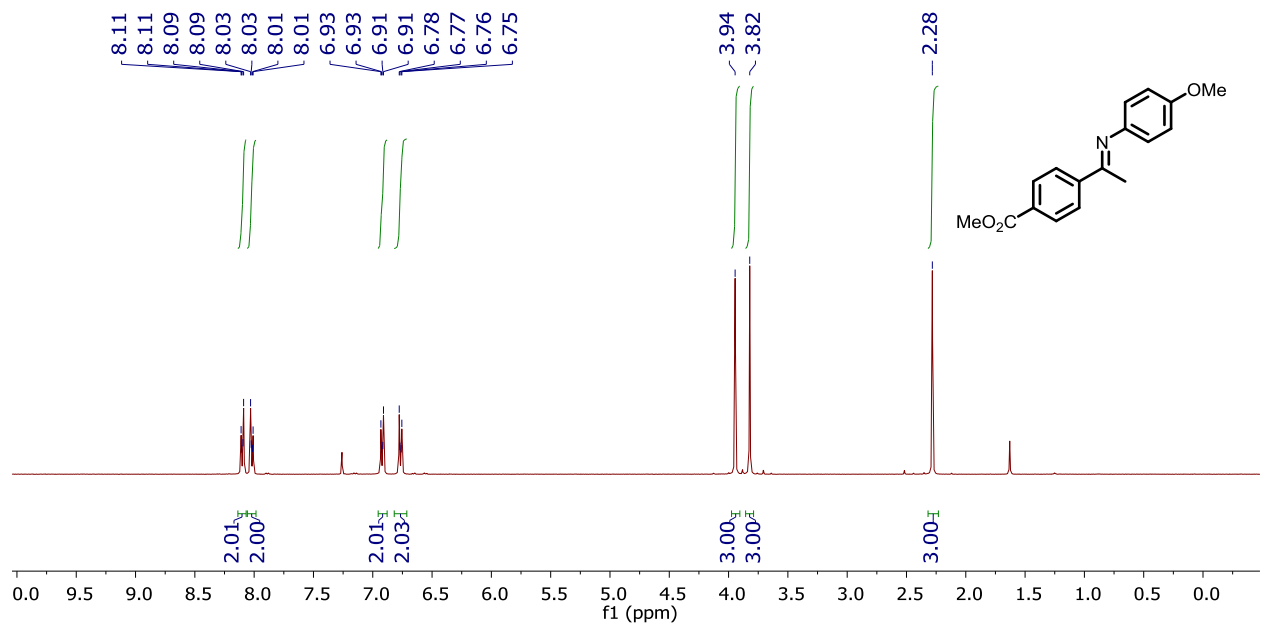
Figure B7. ^1H NMR spectrum of **1b** in chloroform-d.
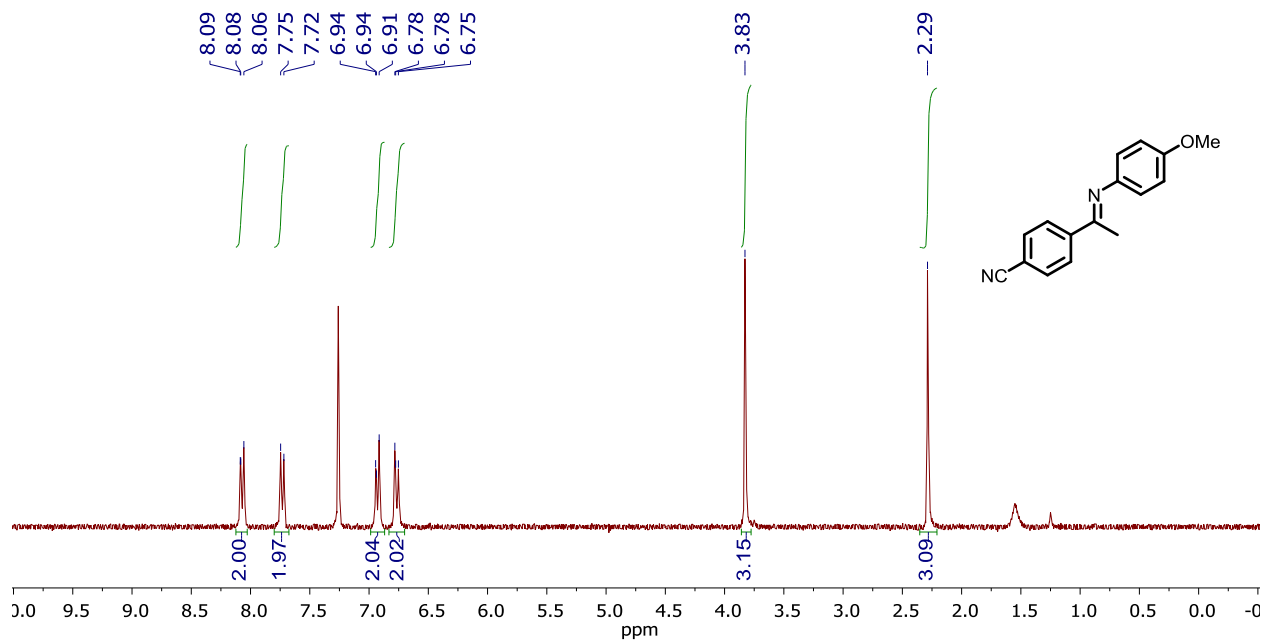
Figure B8. ^{1}H NMR spectrum of **1c** in chloroform-*d*.
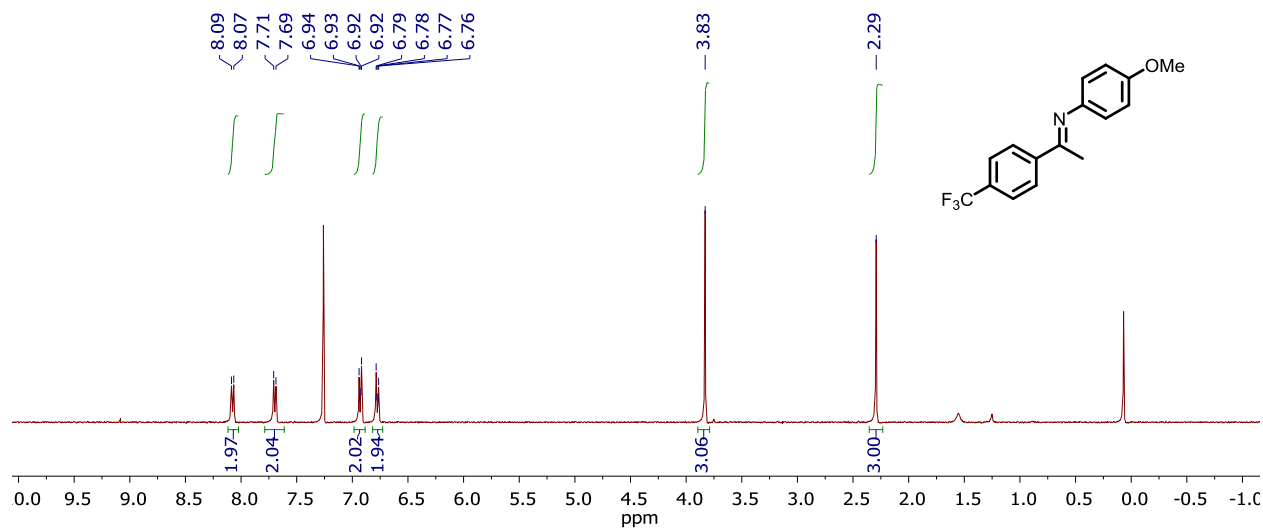
Figure B9a. ^{1}H NMR spectrum of **1d** in chloroform-*d*.
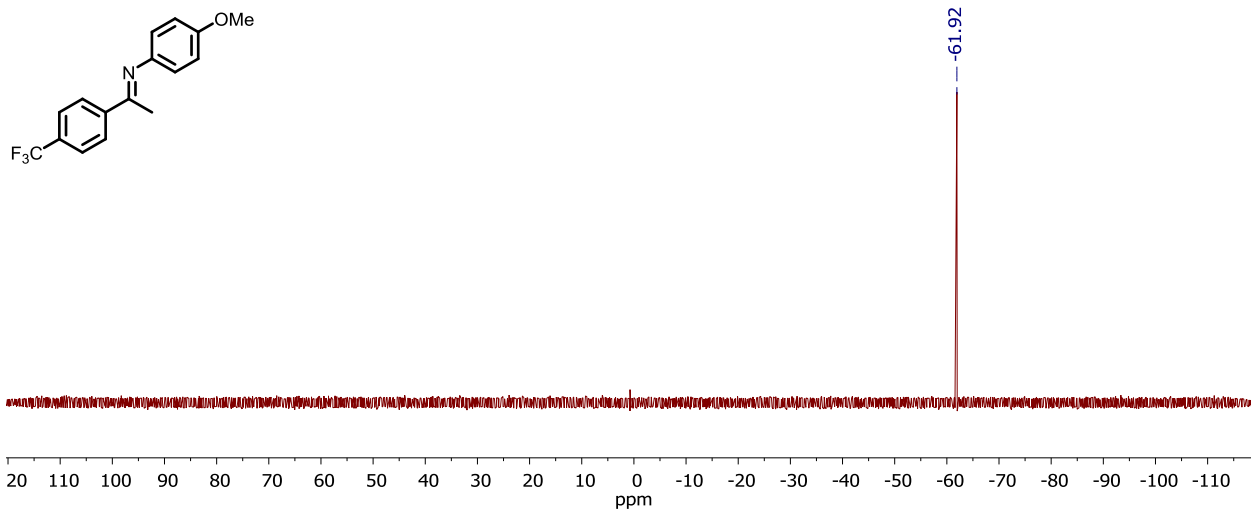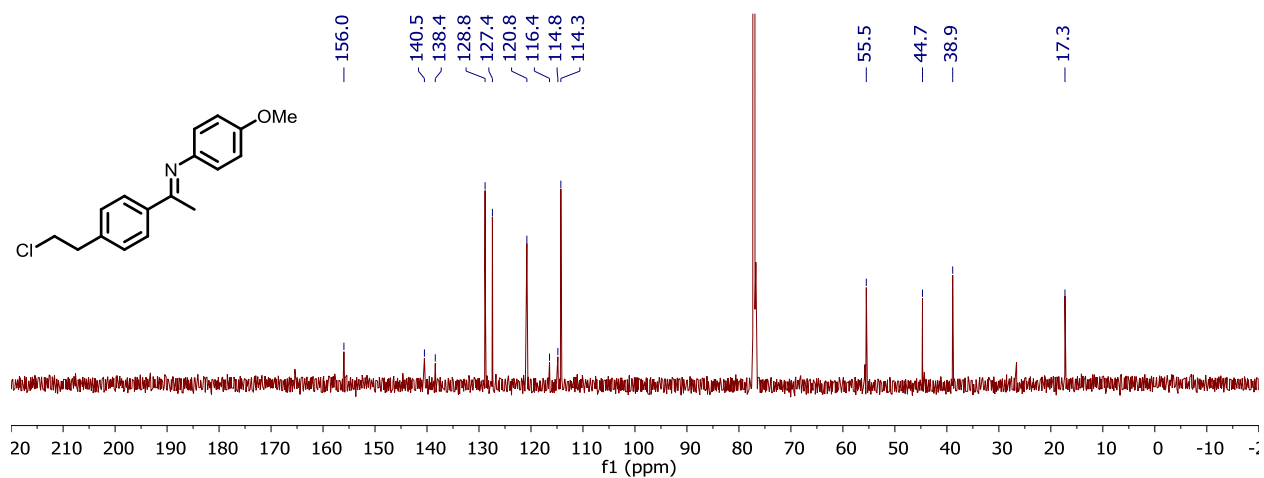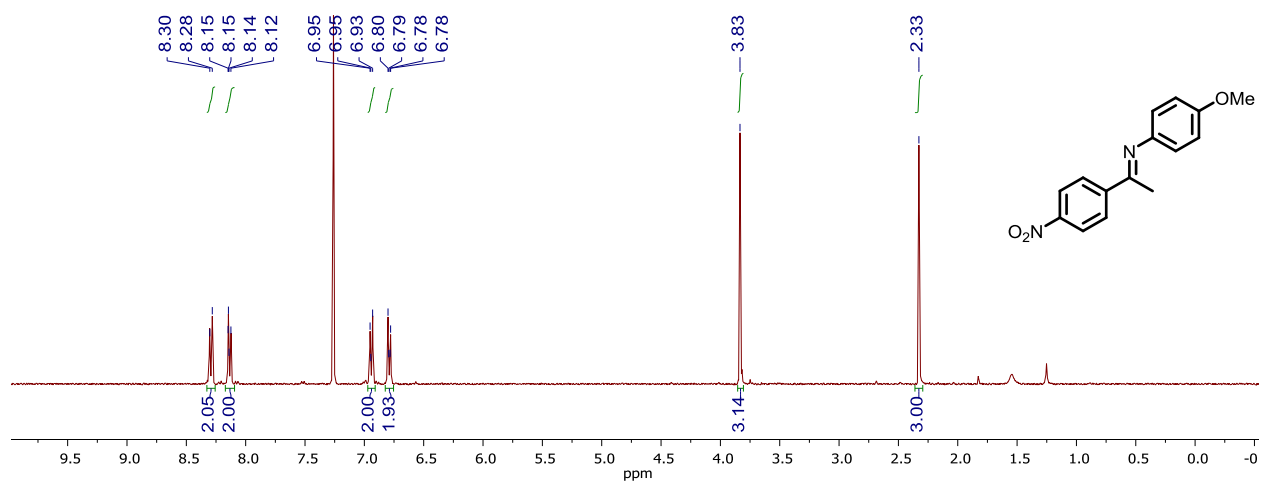
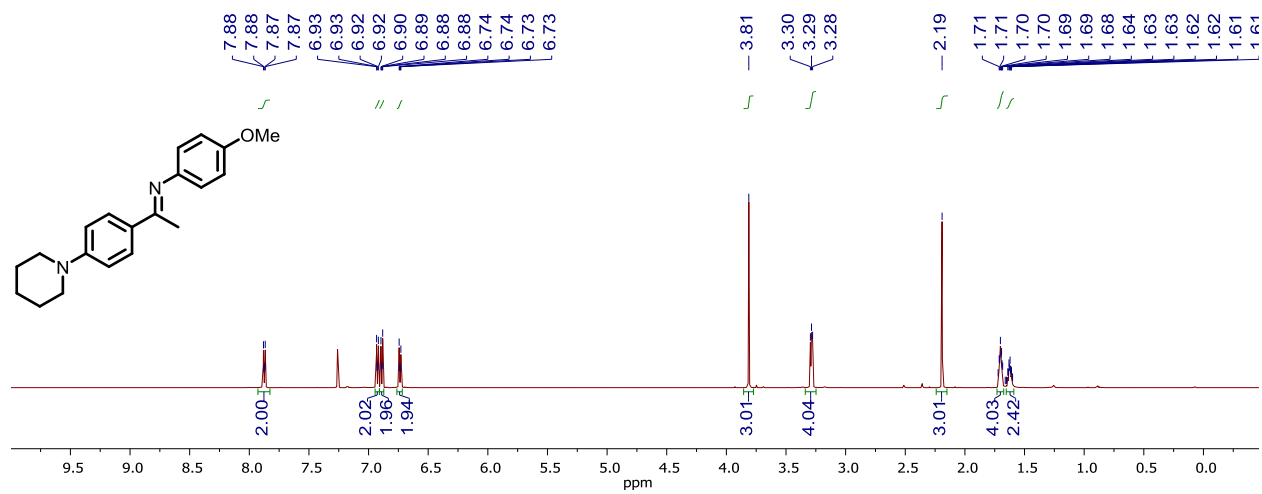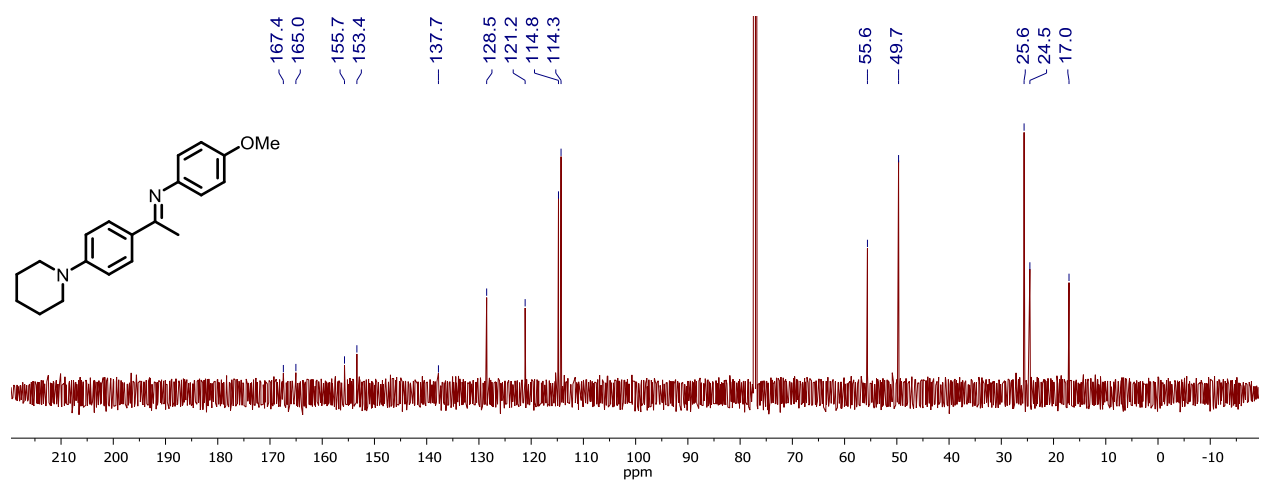**Figure B9b.** $^{19}\text{F}\{^1\text{H}\}$ NMR spectrum of **1d** in chloroform-*d*.
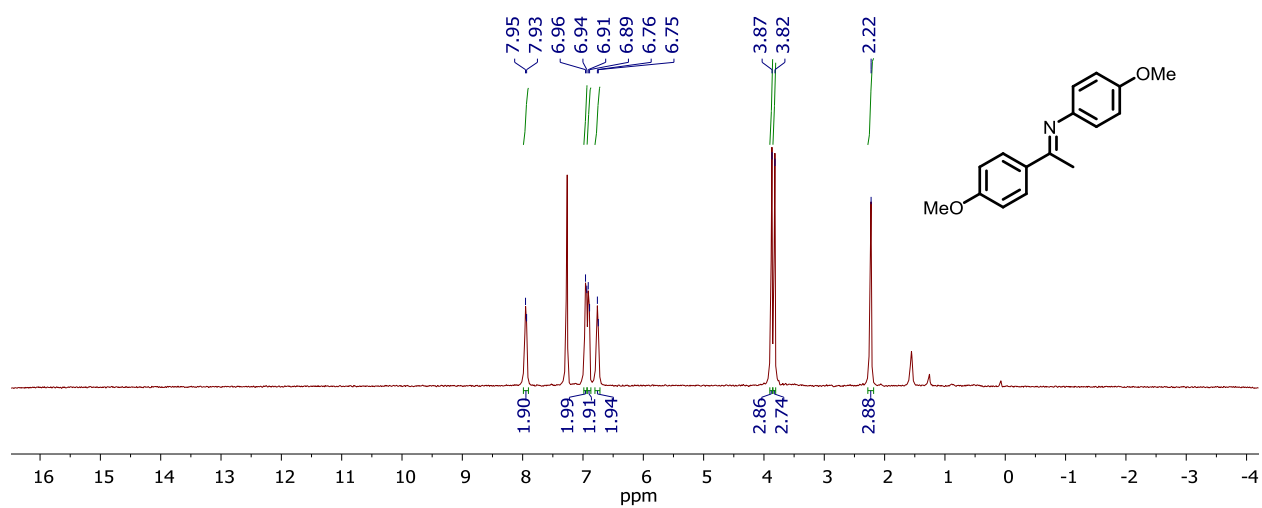
Figure B10. ^1H NMR spectrum of **1e** in chloroform-*d*.
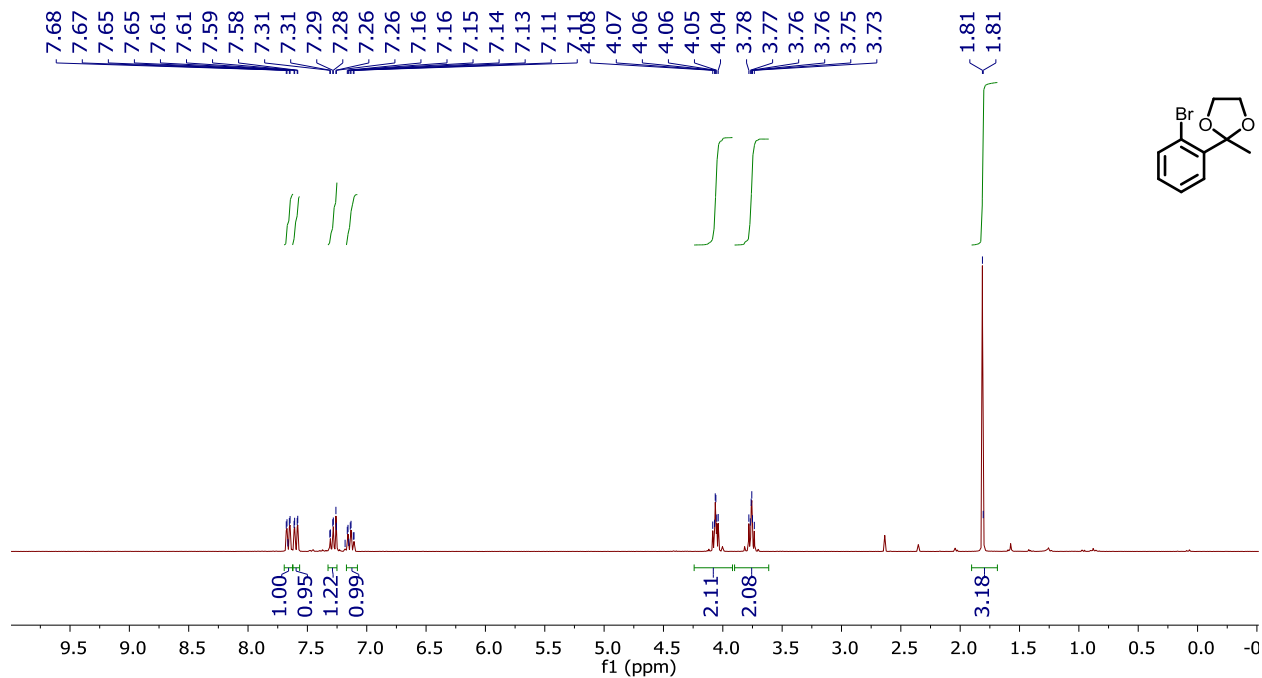
**Figure B11.** ^{1}H NMR spectrum of 2-(2-bromohenyl)-2-methyl-1,3-dioxolane in chloroform-*d*.
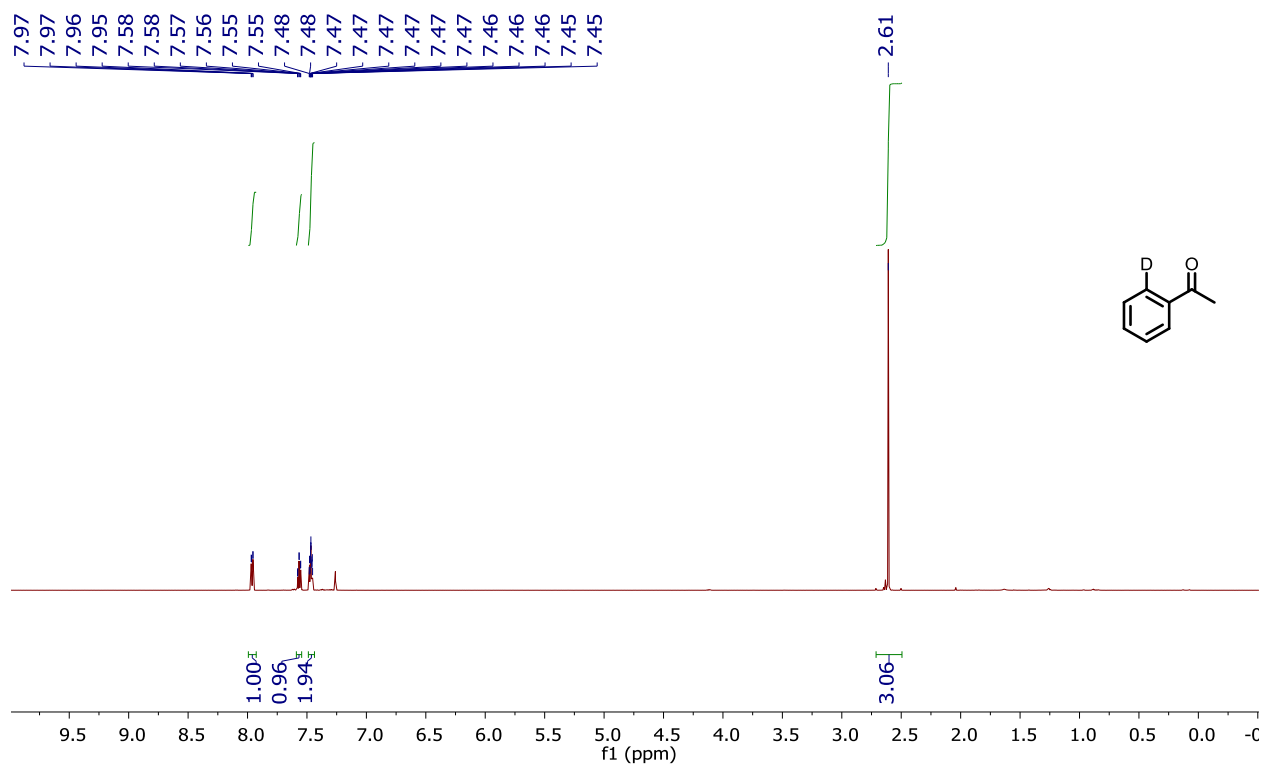
Figure B12. ^{1}H NMR spectrum of acetophenone-(2'-*d*) in chloroform-*d*.
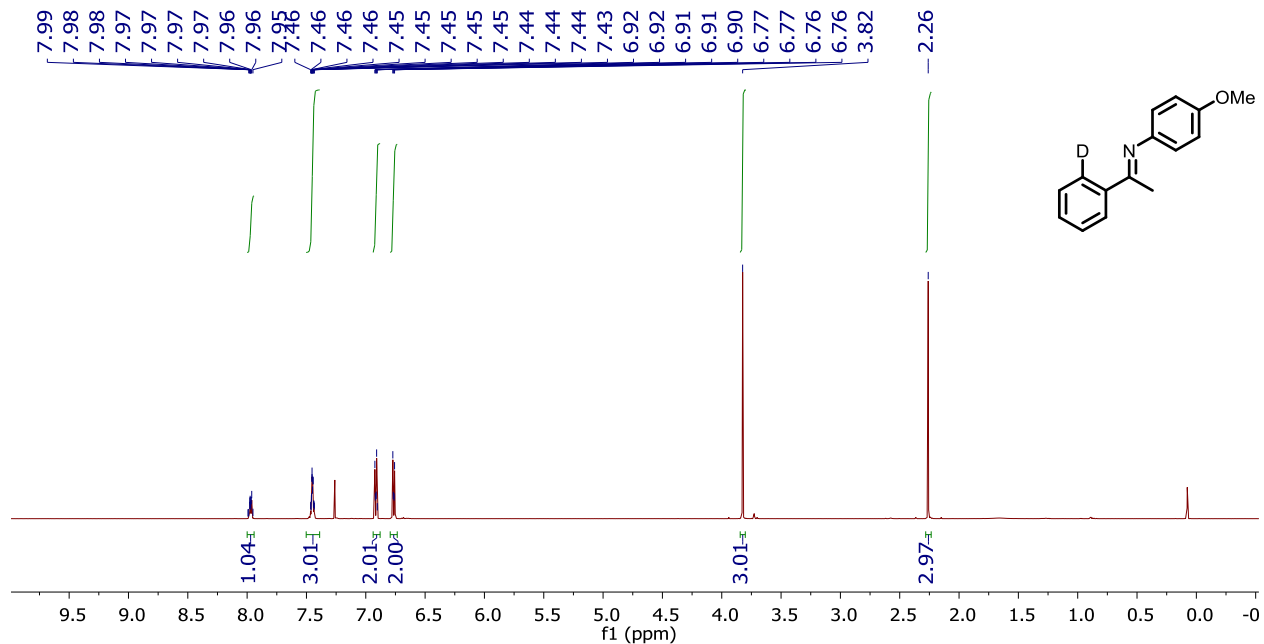
Figure B13a. ^{1}H NMR spectrum of **1f-*d*₁** in chloroform-*d*.
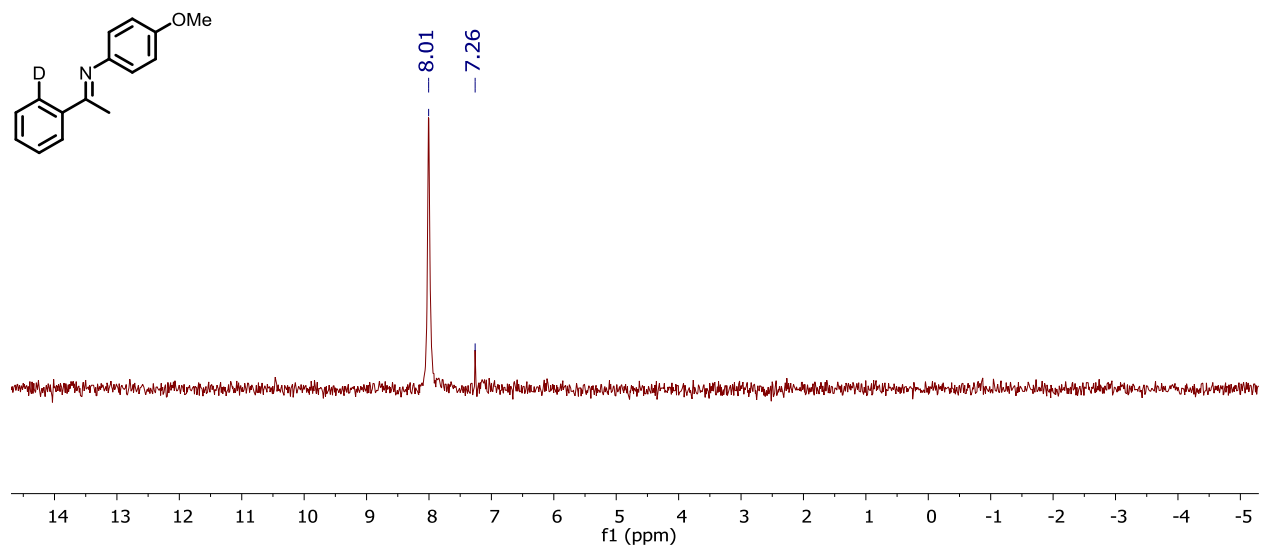
Figure B13b. ^{2}H NMR spectrum of **1f-*d*₁** in chloroform-*d*₀ with added chloroform-*d* as an internal reference.
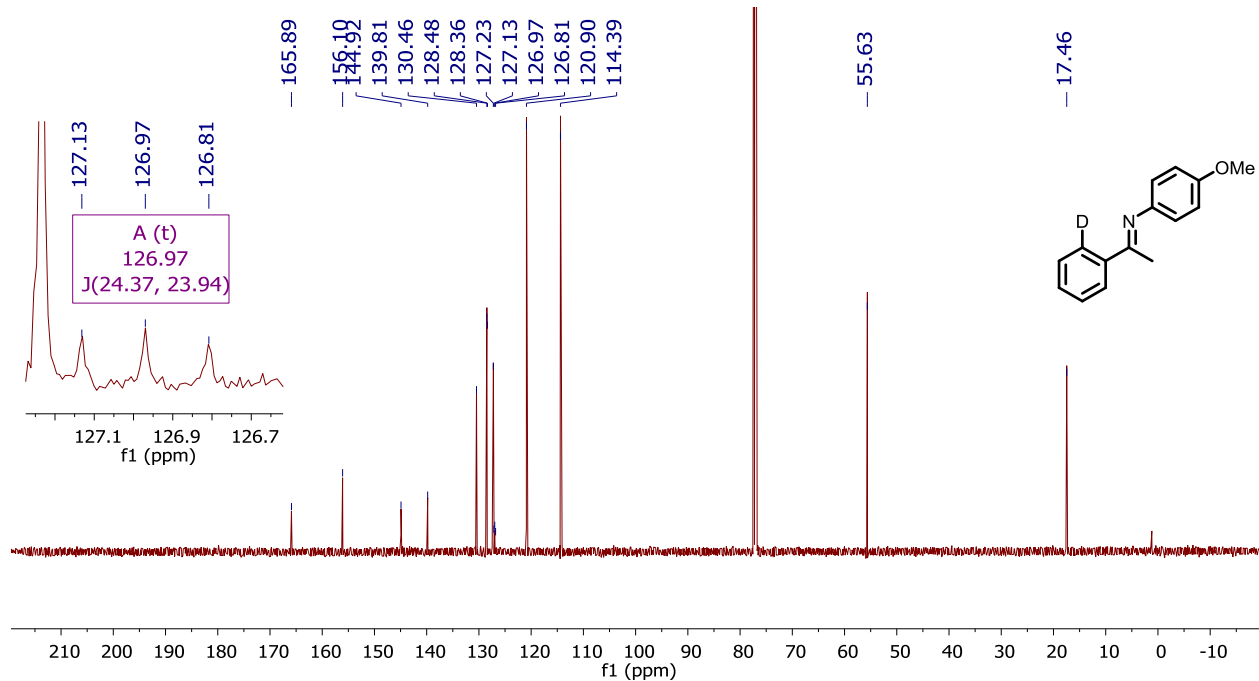
Figure B13c. $^{13}C\{^1H\}$ NMR spectrum of **1f-d_1** in chloroform-d.
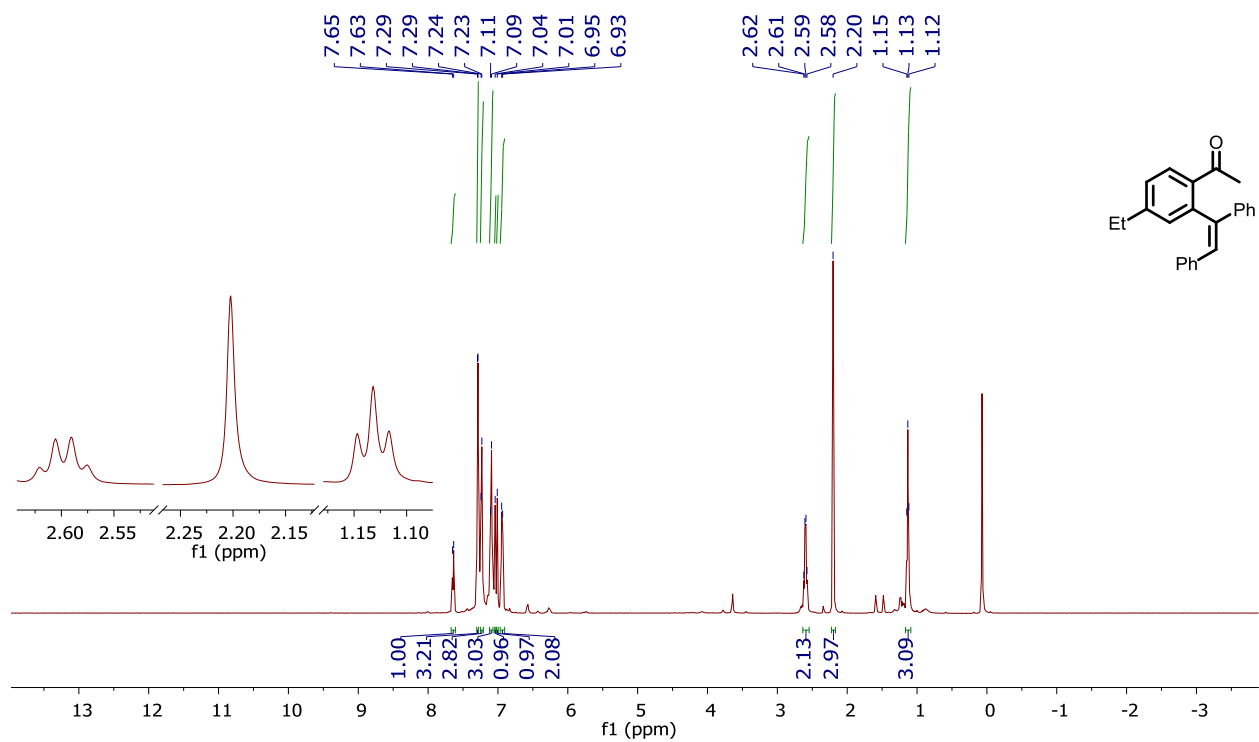
Figure B14a. ^1H NMR spectrum of **Z/E-2a** in chloroform-d.
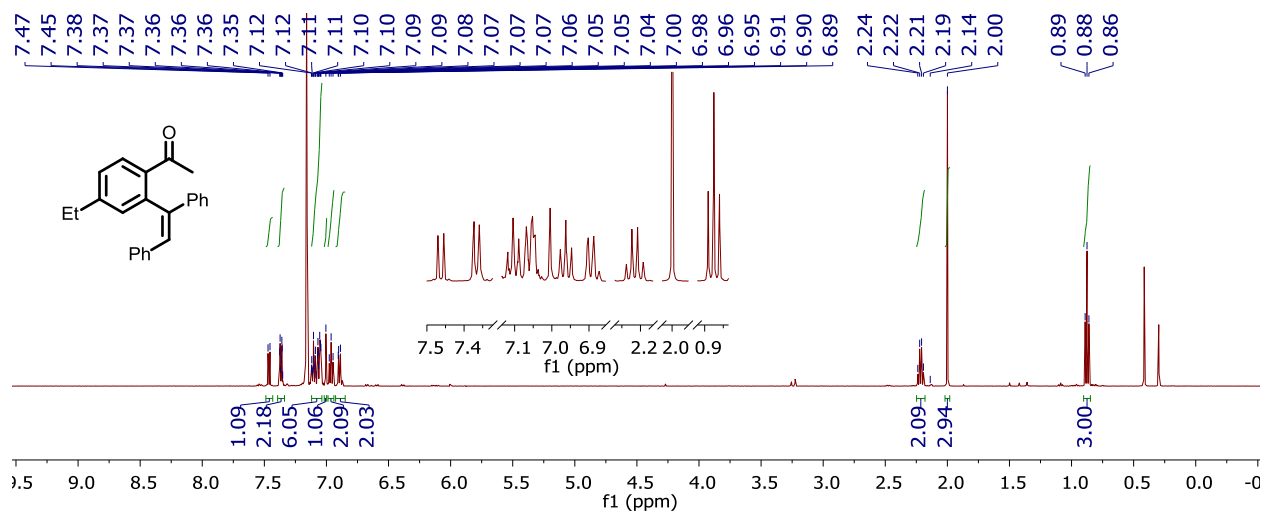
Figure B14b. ^{1}H NMR spectrum of **Z/E-2a** in benzene-d_6.
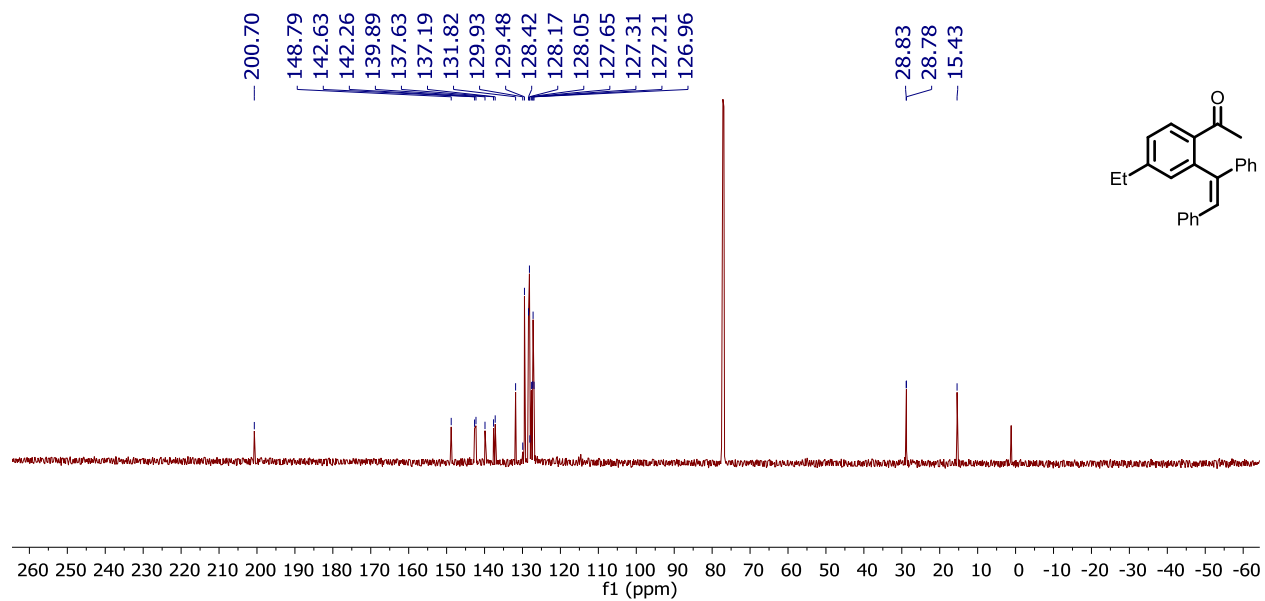
Figure B14c ^{13}C{^{1}H} NMR spectrum of **Z/E-2a** in chloroform-d.
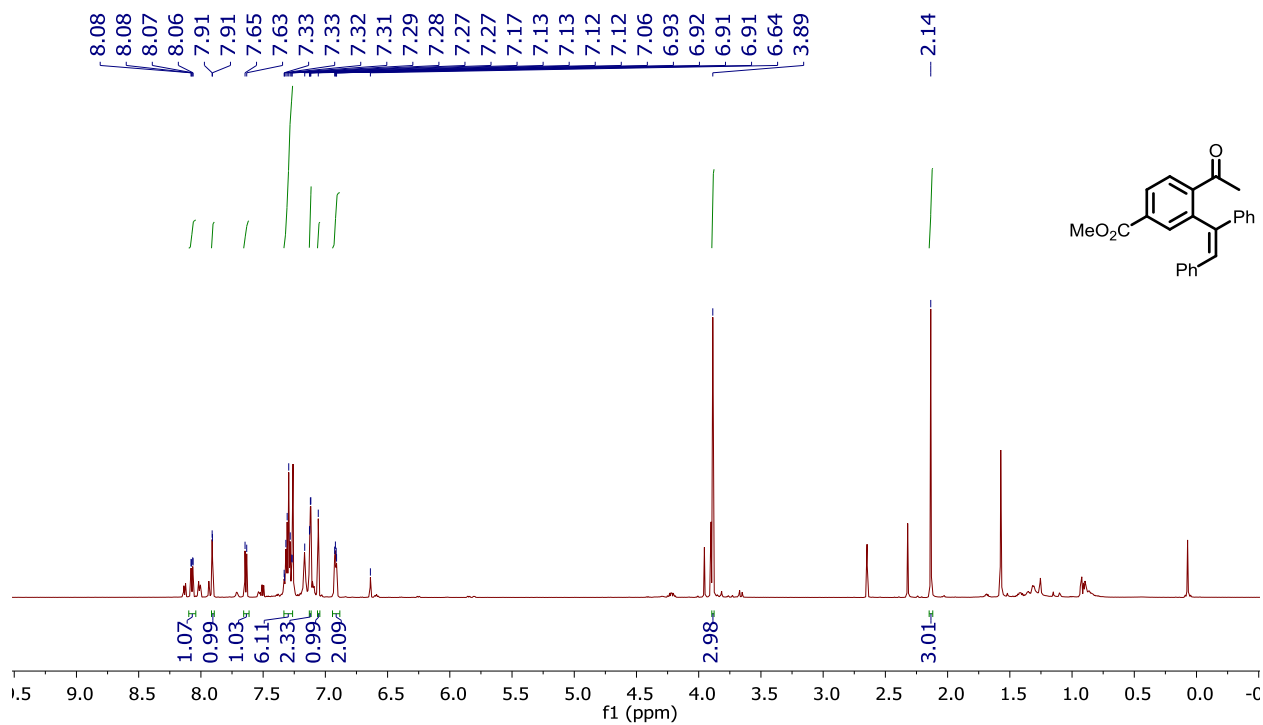
Figure B15a. ¹H NMR spectrum of **Z/E-2b** in chloroform-*d*. Note that highlighted peaks are for the *Z*-isomer. For *E*-isomer, see Figure B15b below.
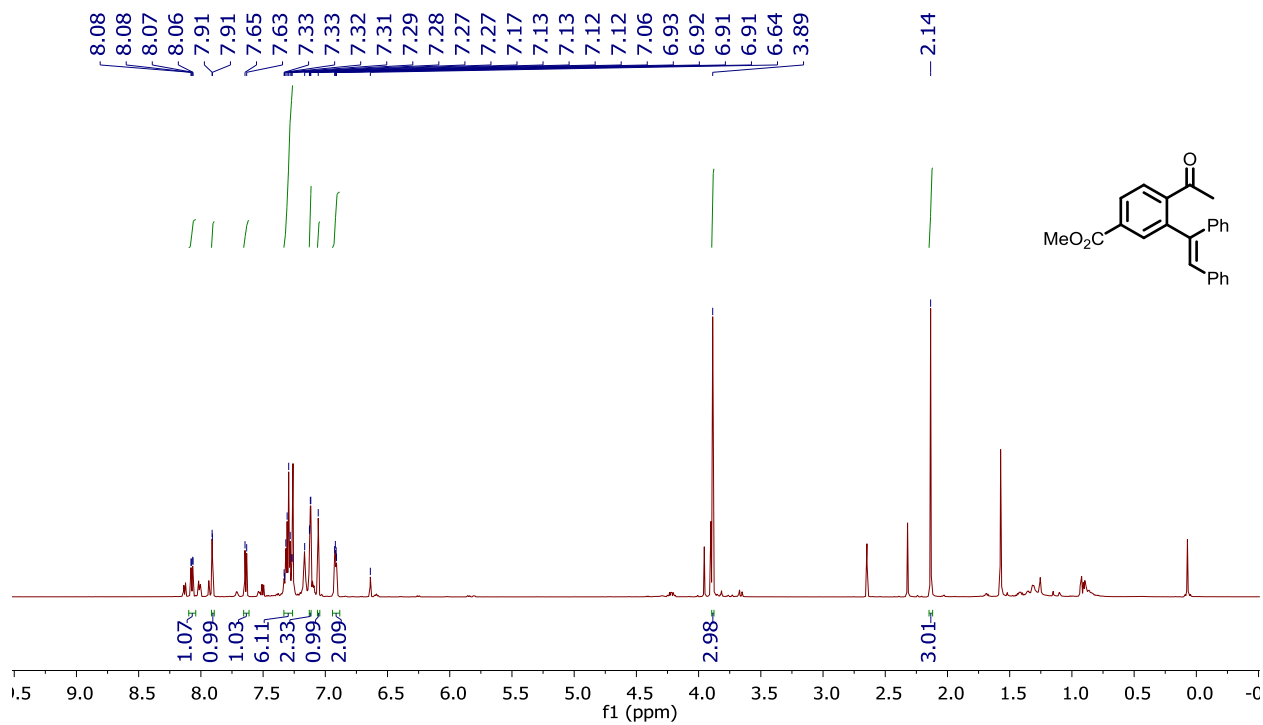
Figure B15b. ¹H NMR spectrum of **Z/E-2b** in chloroform-*d*. Note that highlighted peaks are for the *E*-isomer. For *Z*-isomer, see Figure B15a above.
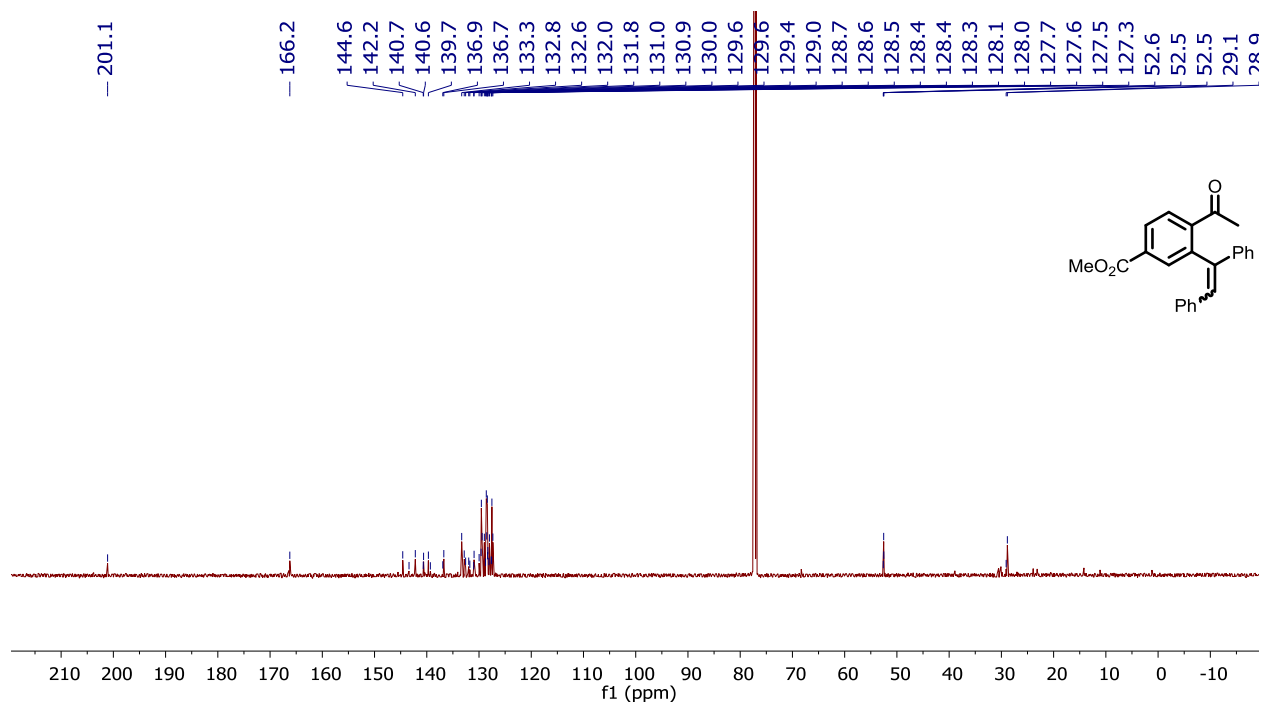
Figure B15c. $^{13}C\{^1H\}$ NMR spectrum of **Z/E-2b** in chloroform-*d*. Note that highlighted peaks are correspond to both the *Z/E*-isomers and are difficult to differentiate. Also note that residual EtOAc was identified.
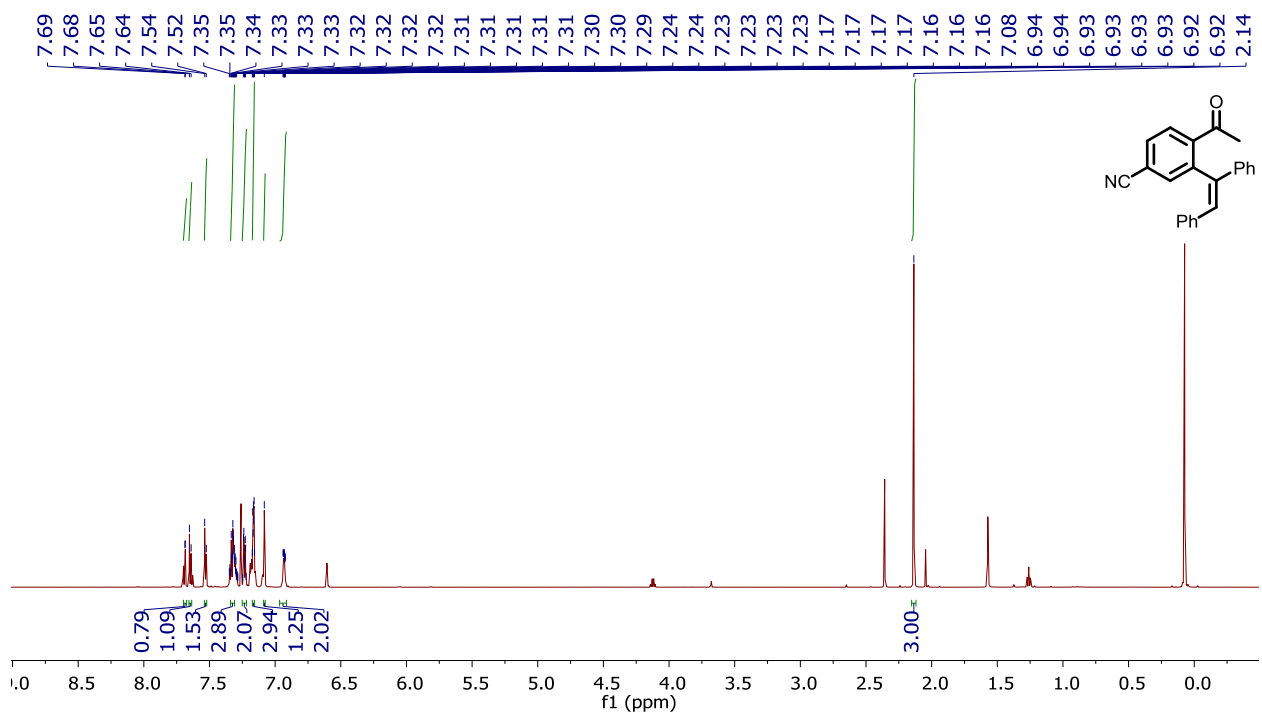
Figure B16a. ^1H NMR spectrum of **Z/E-2c** in chloroform-*d*. Note that highlighted peaks are for the *Z*-isomer. For *E*-isomer, see Figure B16b below.
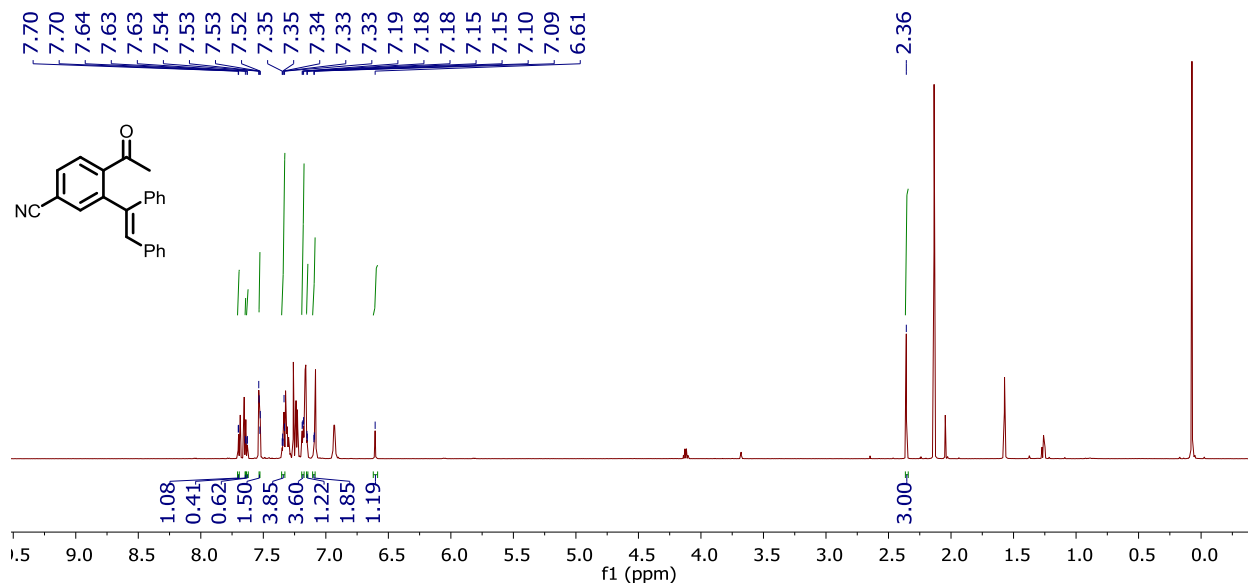
Figure B16b. ^{1}H NMR spectrum of **Z/E-2c** in chloroform-*d*. Note that highlighted peaks are for the *E*-isomer. For *Z*-isomer, see Figure B16a above.
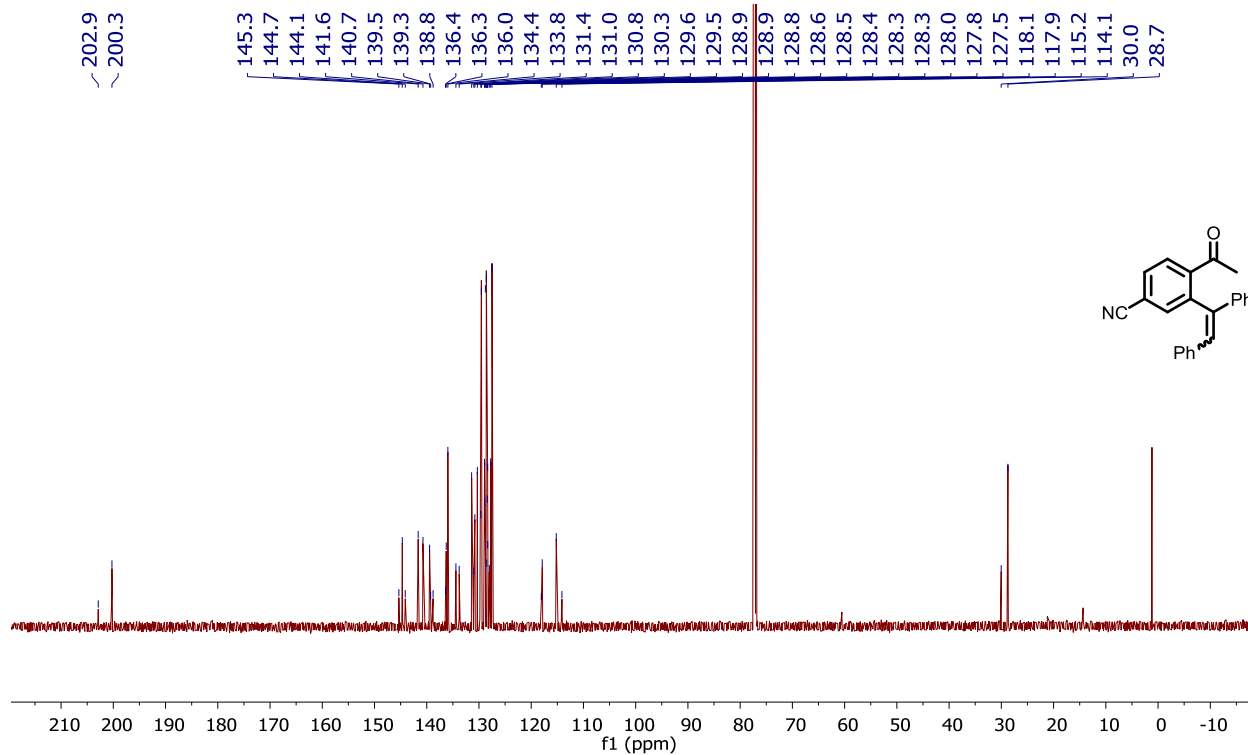
Figure B16c. ^{13}C{^{1}H} NMR spectrum of **Z/E-2c** in chloroform-*d*. Note that highlighted peaks are correspond to both the *Z/E*-isomers and are difficult to differentiate.
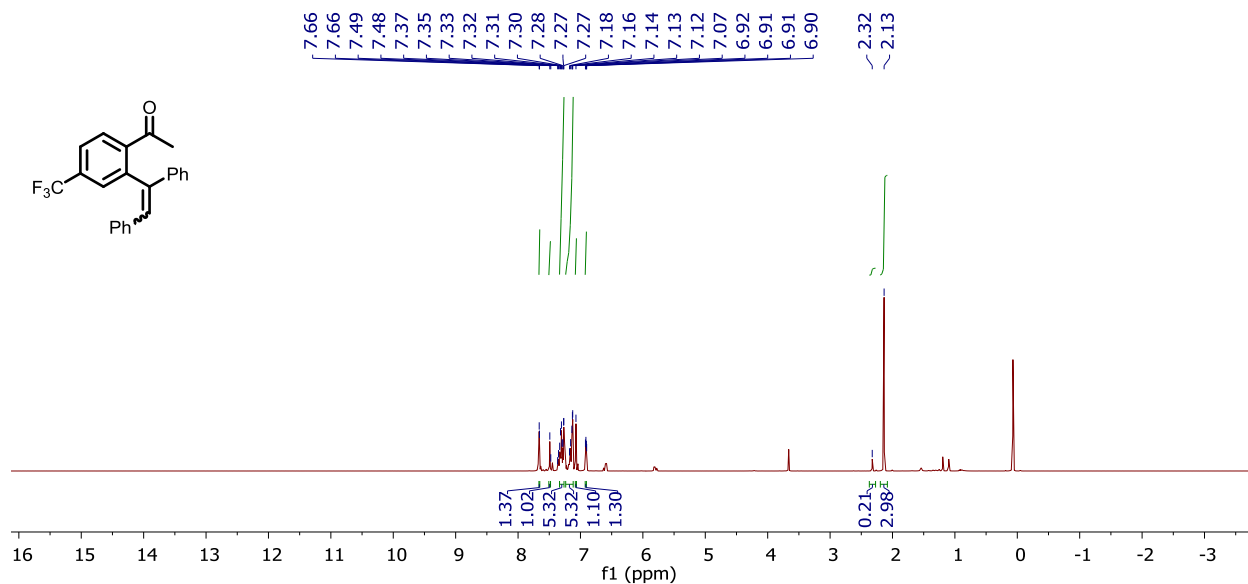
Figure B17a. ^{1}H NMR spectrum of **Z/E-2d** in chloroform-*d*. Note that residual *p*-anisidine (< 5%) exists.
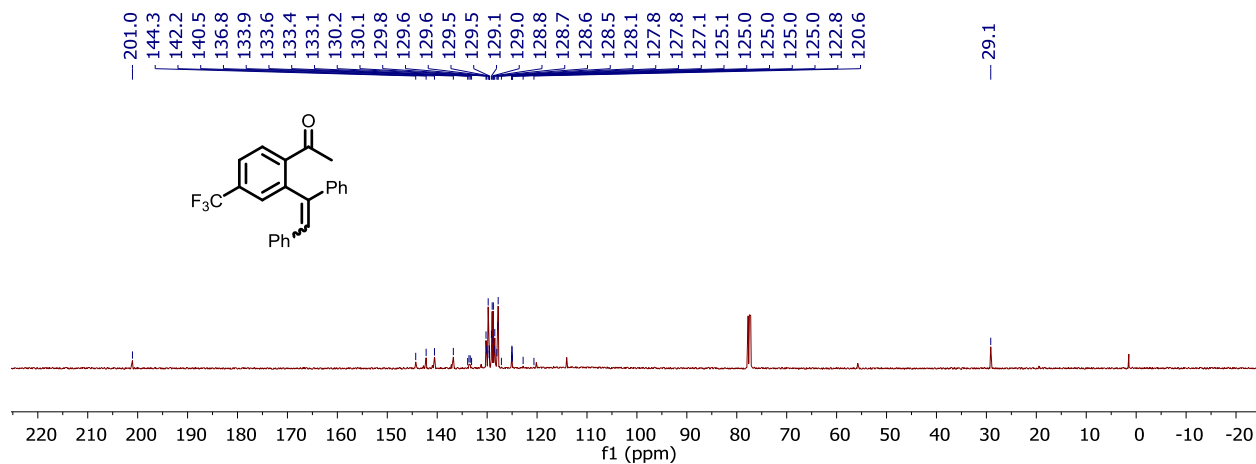
Figure B17b. ^{13}C{^{1}H} NMR spectrum of **Z/E-2d** in chloroform-*d*. Note: residual *p*-anisidine (< 5%) exists.
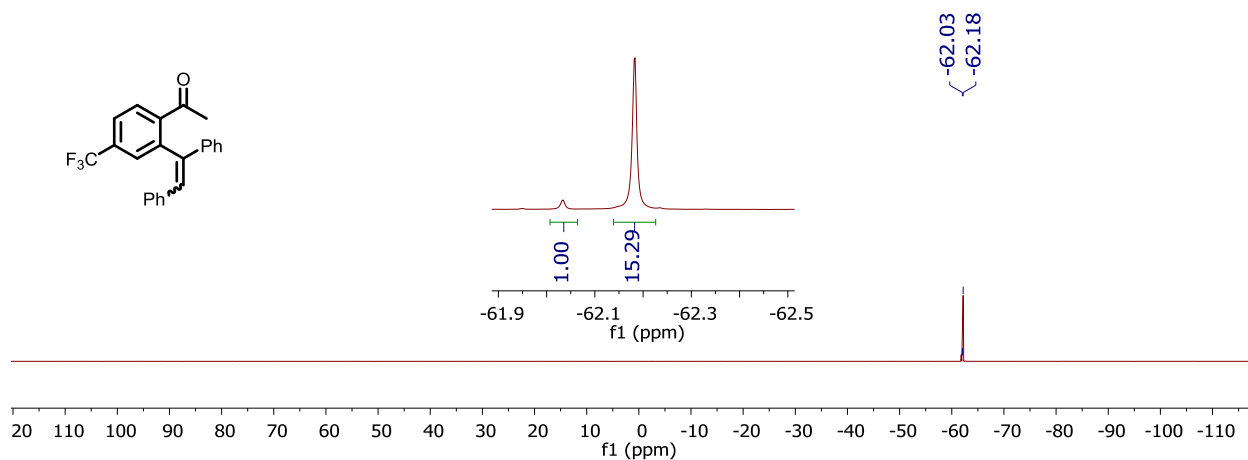
Figure B17c. ^{19}F{^{1}H} NMR spectrum of **Z/E-2d** in chloroform-*d*.
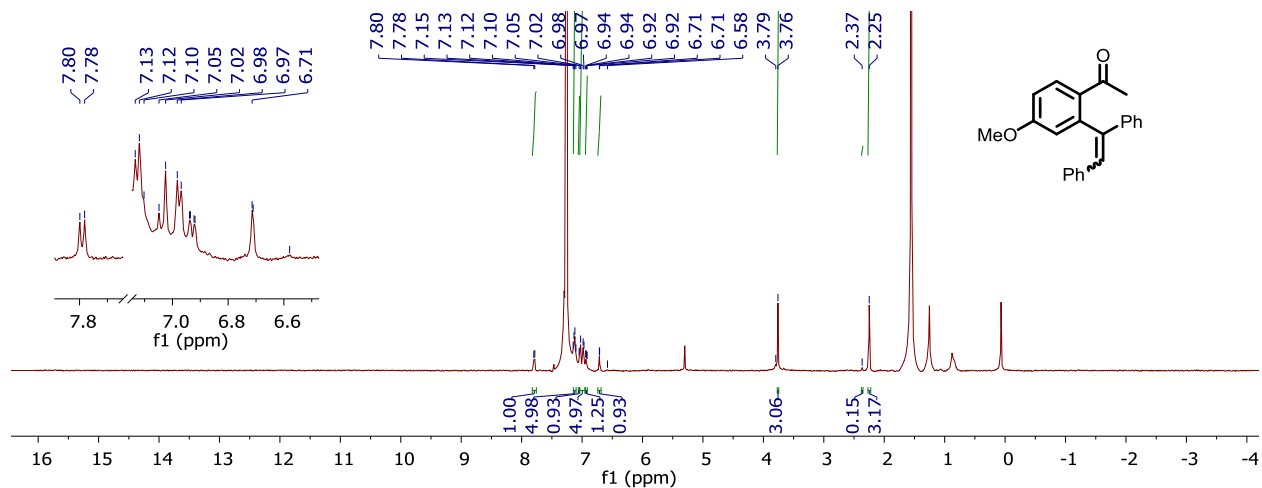
Figure B18a. ^{1}H NMR spectrum of *Z/E*-**2e** in chloroform-*d*.
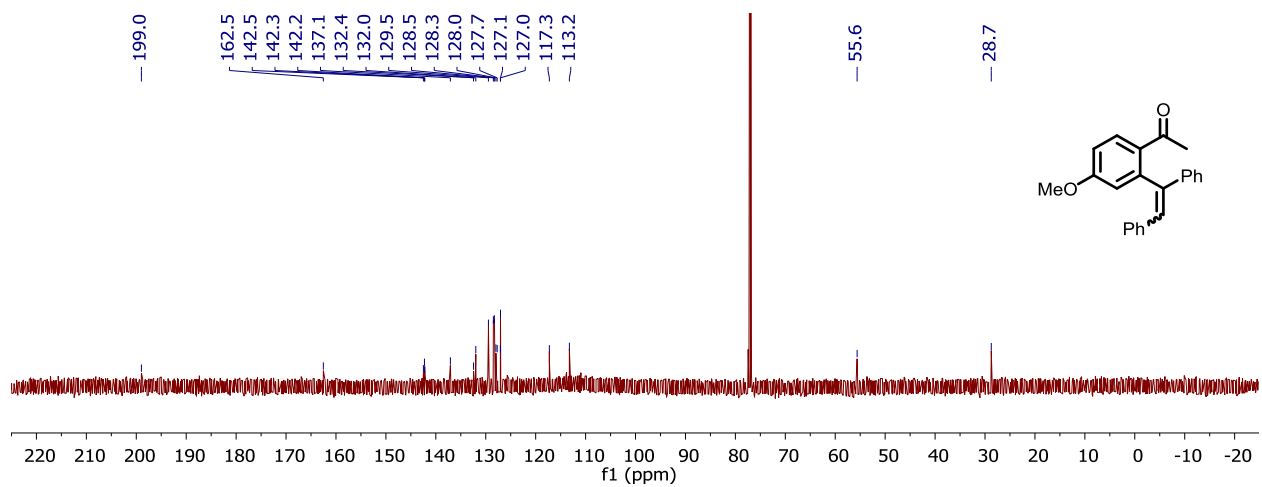
Figure B18b. ^{13}C{^{1}H} NMR spectrum of *Z/E*-**2e** in chloroform-*d*.
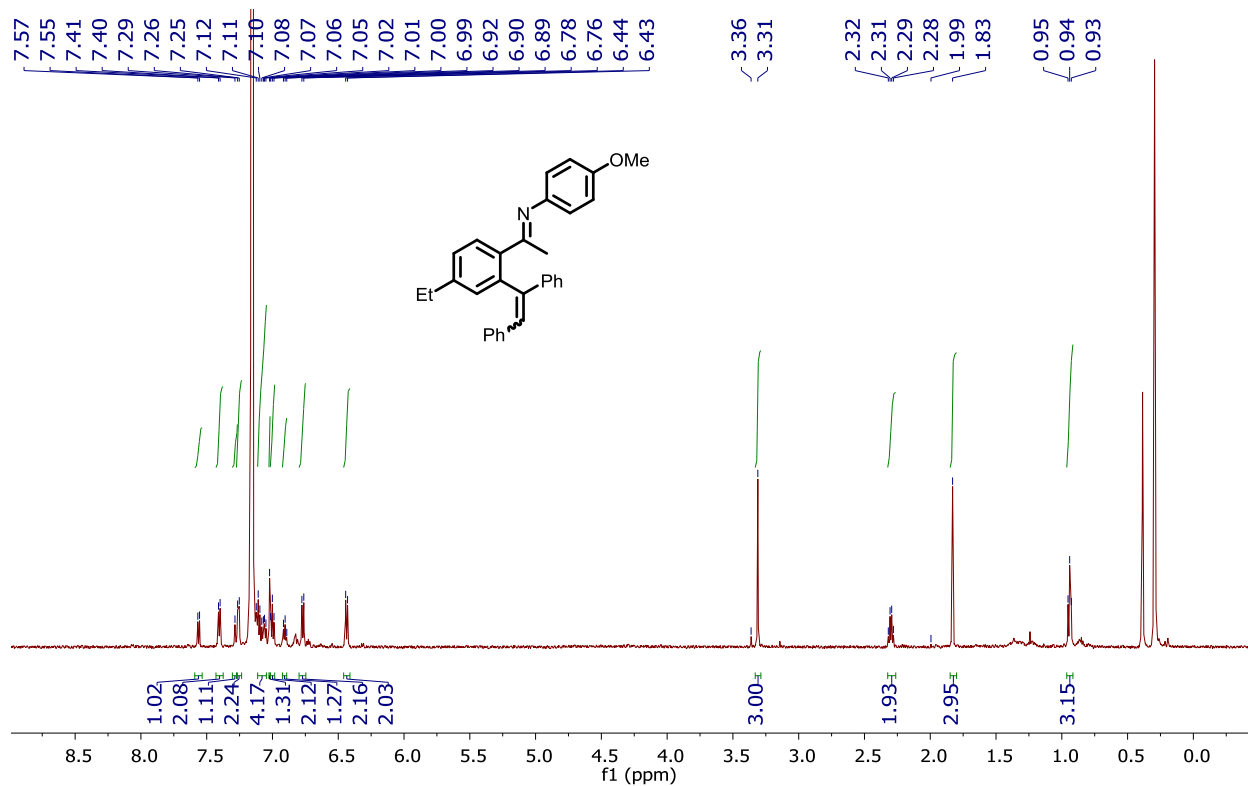
Figure B19a. ^{1}H NMR spectrum of **Z-3a** in benzene-d_6.
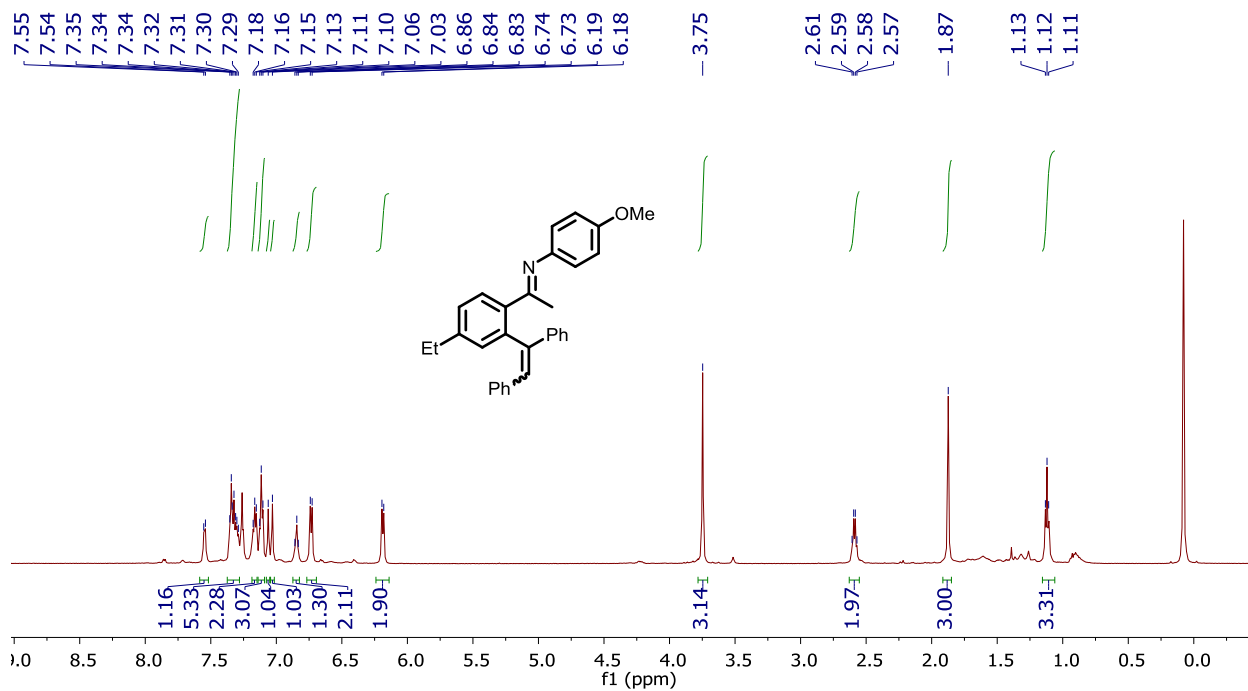
Figure B19b. ^{1}H NMR spectrum of **Z-3a** in chloroform-d.
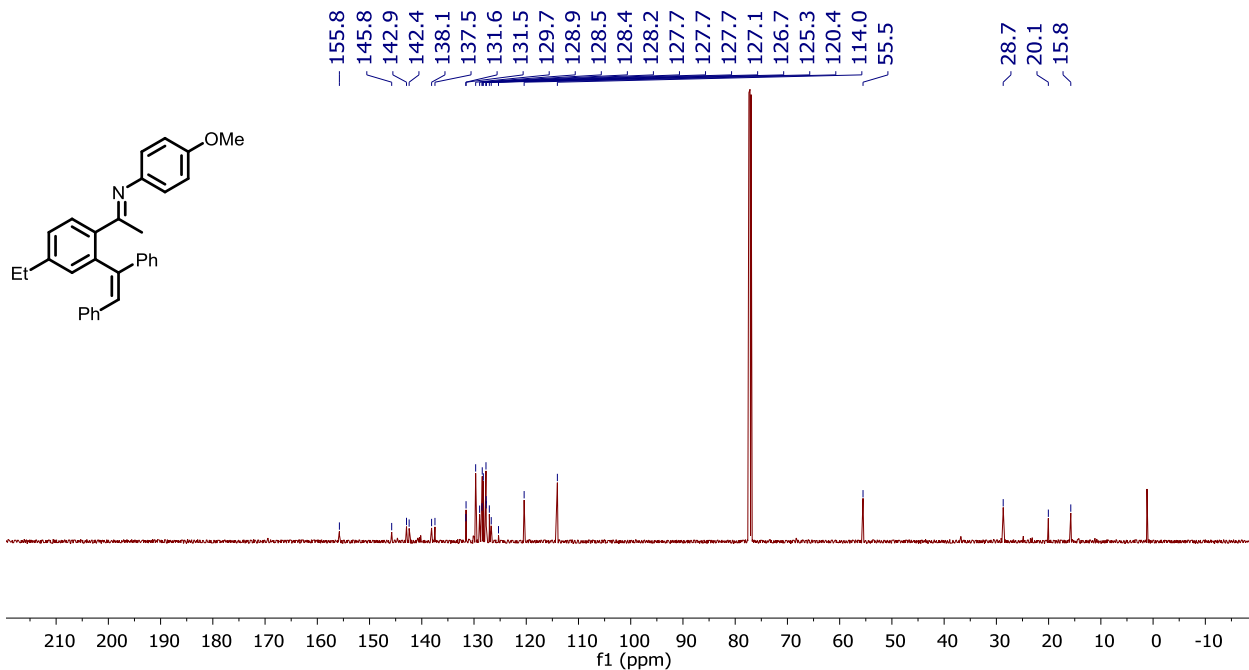
Figure B19c. $^{13}C\{^1H\}$ NMR spectrum of **Z-3a** in chloroform-*d*.
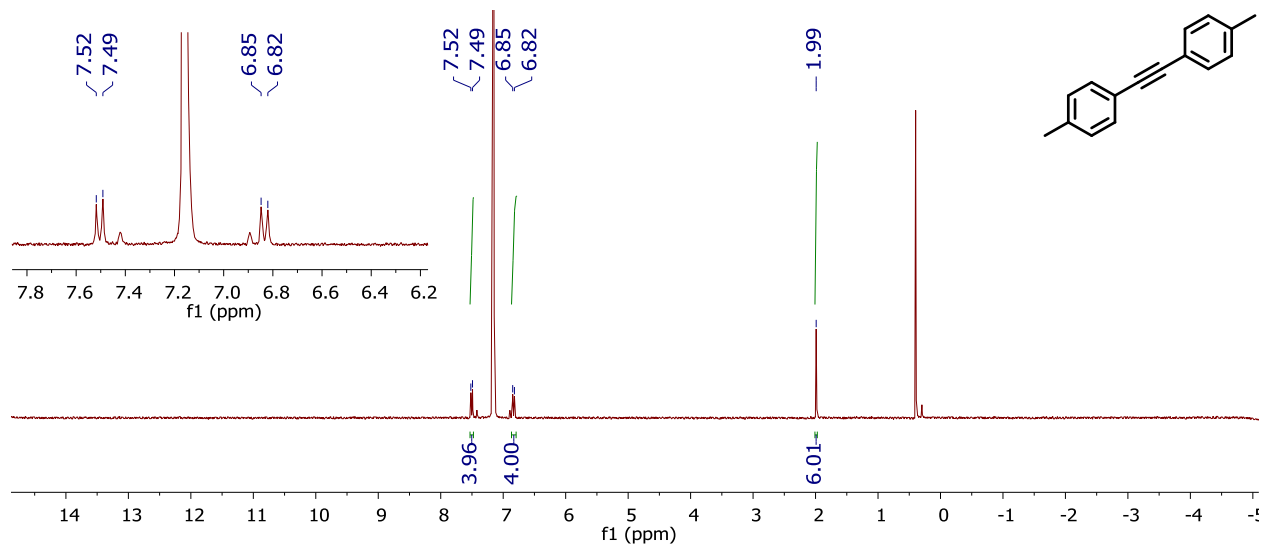
Figure B20. ^1H NMR spectrum of bis(*p*-tolyl)acetylene in benzene-*d*$_6$.

IR Spectral Data
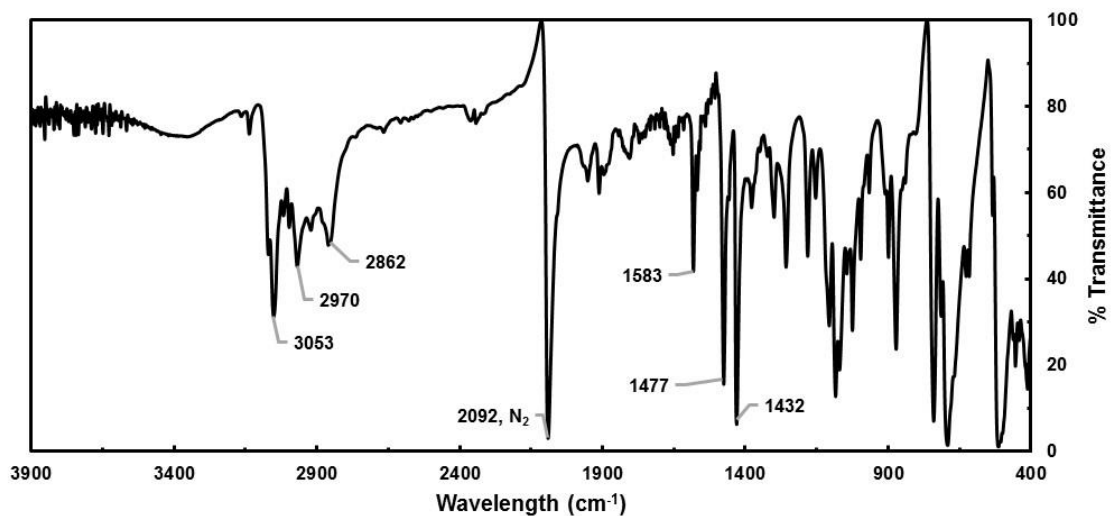
Figure B21. IR spectrum of **Co-H** (KBr).
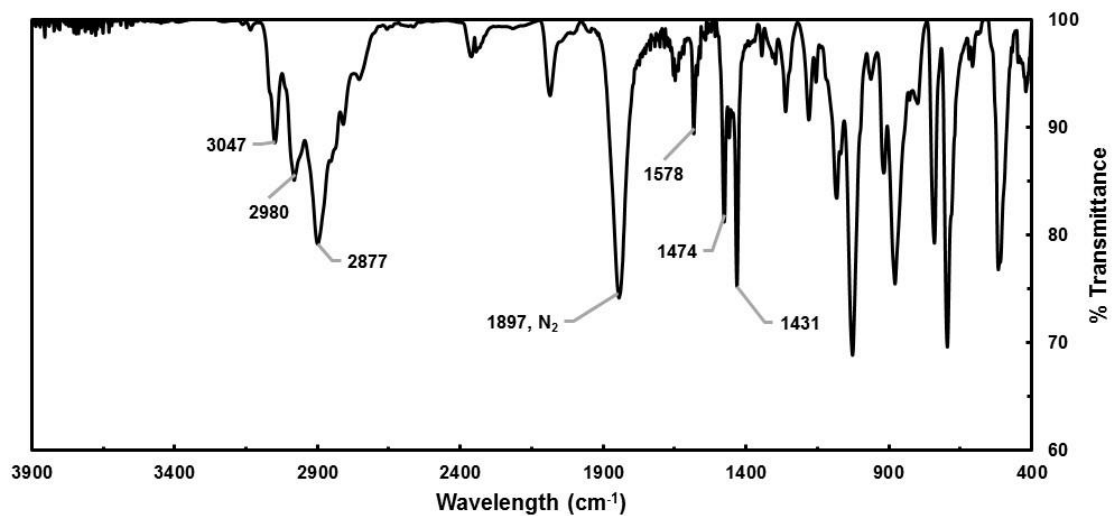
Figure B22. IR spectrum of **Co-Li** (KBr). Residual **Co-H** was observed as evidence by the existence of the corresponding N_2 peak. This was attributed to slow solid-state decomposition of **Co-Li** in the KBr pellet by adventitious reactivity with ambient H_2O.
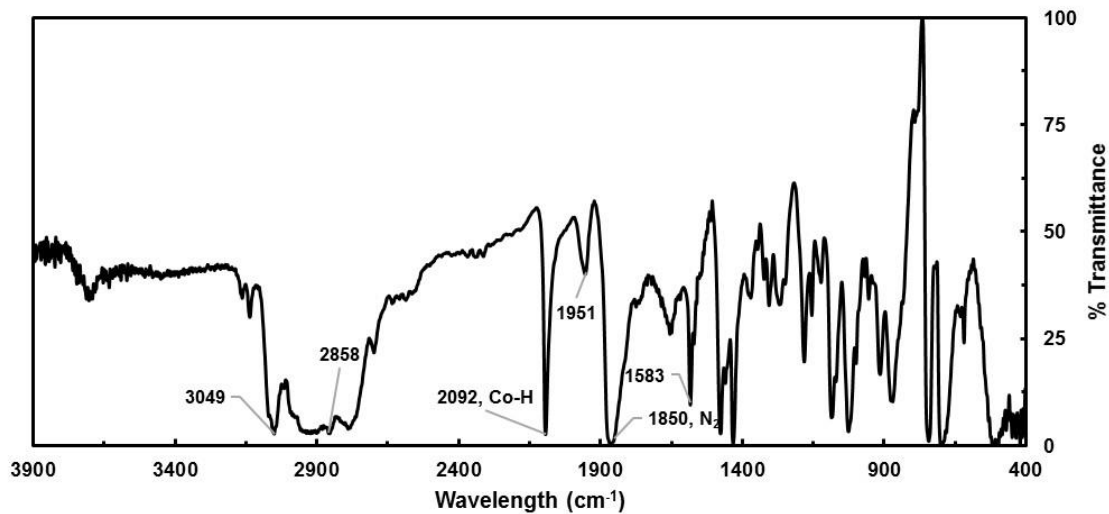
Figure B23. IR spectrum of **Co₂-Mg** (KBr). Residual **Co-H** was observed as evidence by the existence of the corresponding N_2 peak. This was attributed to slow solid-state decomposition of **Co-Li** in the KBr pellet by adventitious reactivity with ambient H_2O.
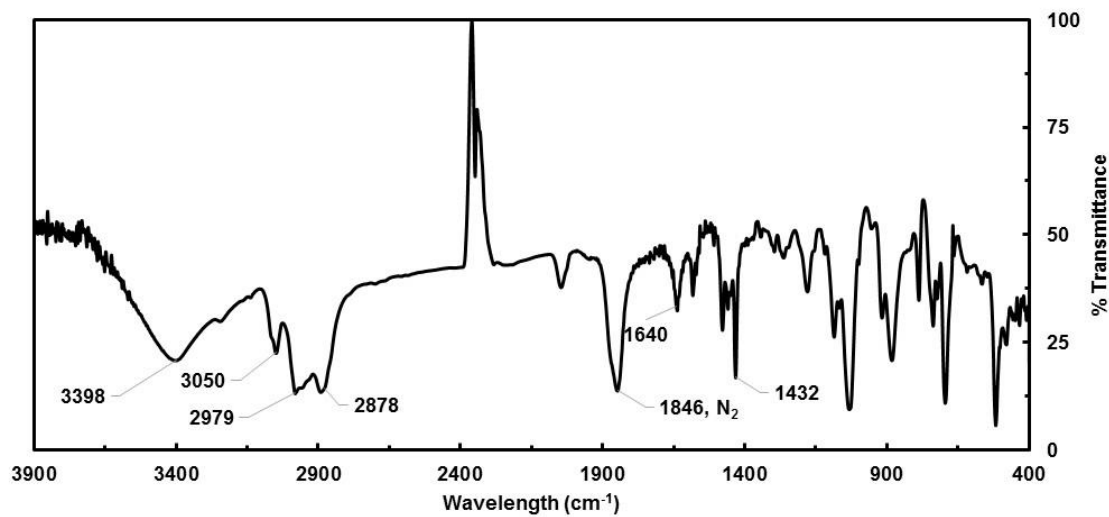
Figure B24. IR spectrum of **Co'₂-Mg** (KBr). Residual CO_2 is observed at ca 2400 cm^{-1}.

Appendix C

NMR

Spectral Data

from

Chapter Four:

Olefin Hydroarylations Catalyzed by a
Single-Component Cobalt(-I) Complex

NMR SPECTRA OF (*N*-ARYL) IMINE SUBSTRATES AND PRECURSORS
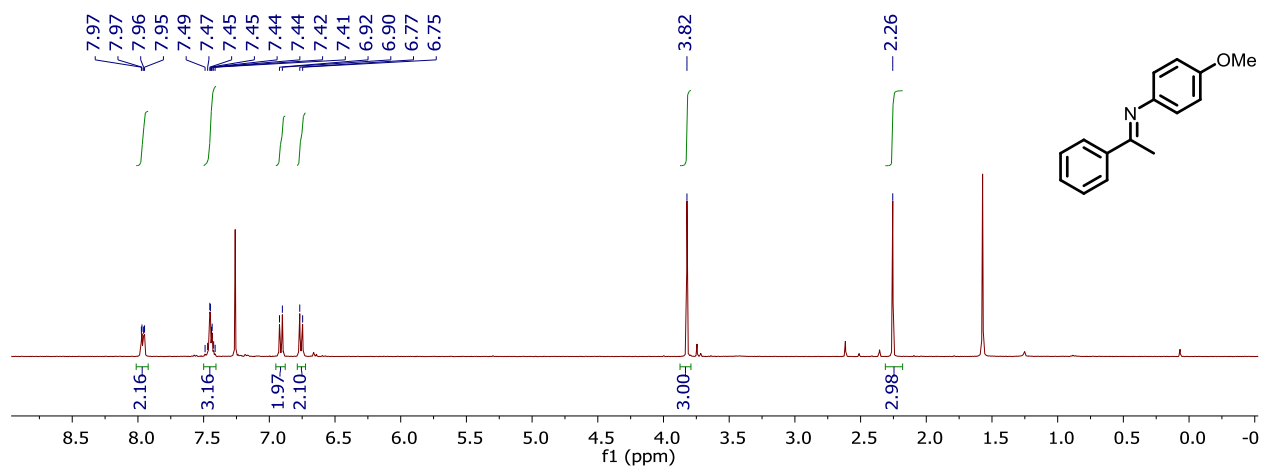
Figure C1. ^{1}H NMR spectrum of **1A** in chloroform-*d*.
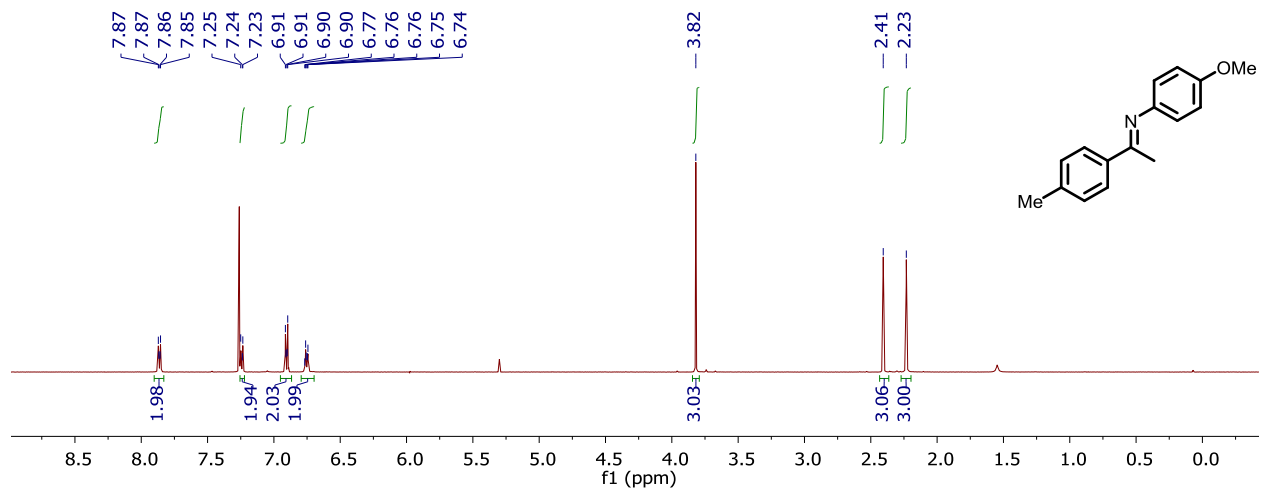
Figure C2. ^{1}H NMR spectrum of **1B** in chloroform-*d*.
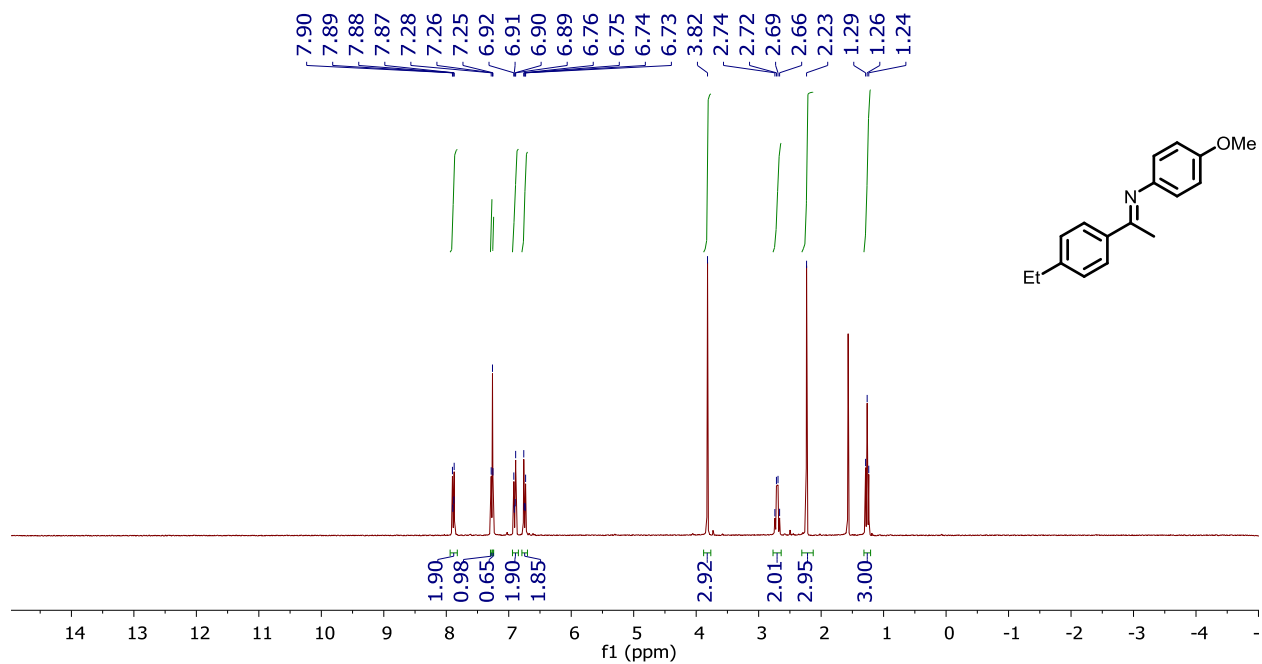
Figure C3. ¹H NMR spectrum of **1C** in chloroform-*d*.
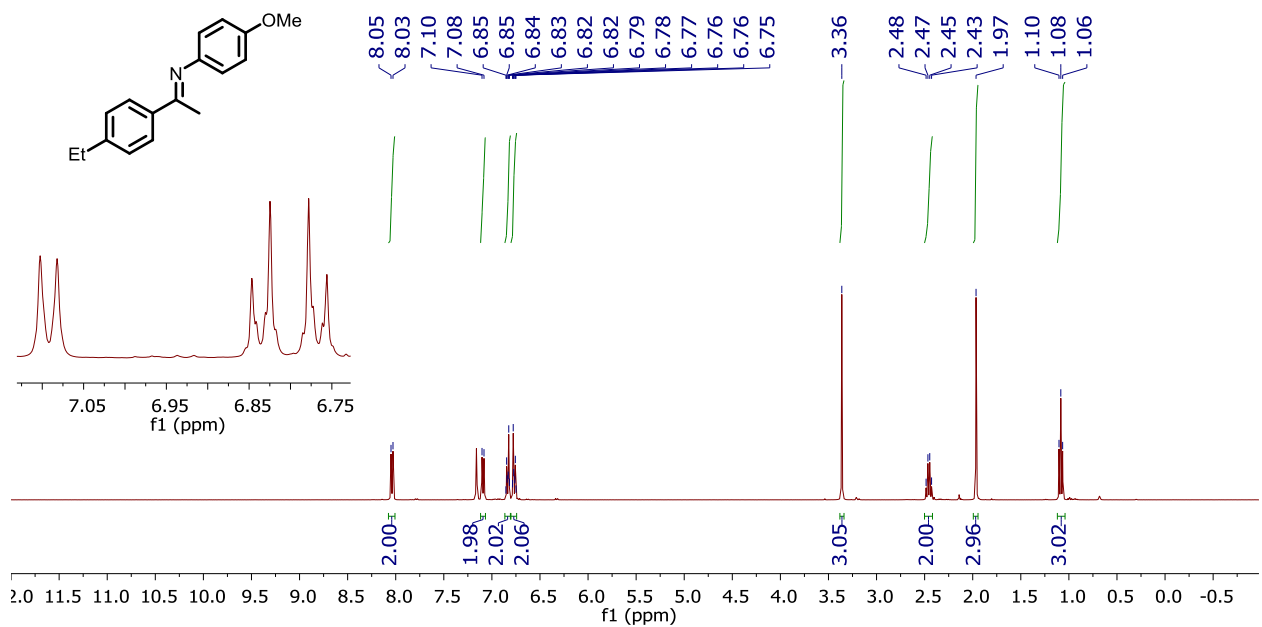
Figure C4. ¹H NMR spectrum of **1C** in benzene-*d₆*.
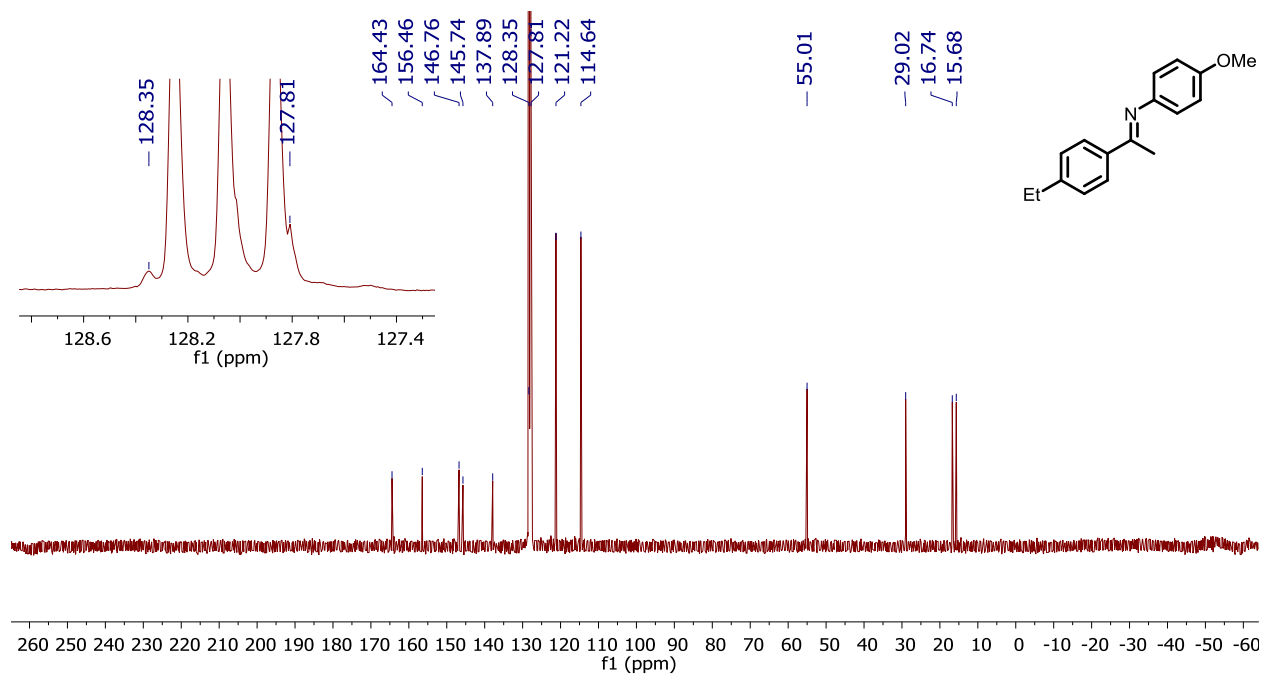
Figure C5. $^{13}C\{^{1}H\}$ NMR spectrum of **1C** in benzene-d_6.
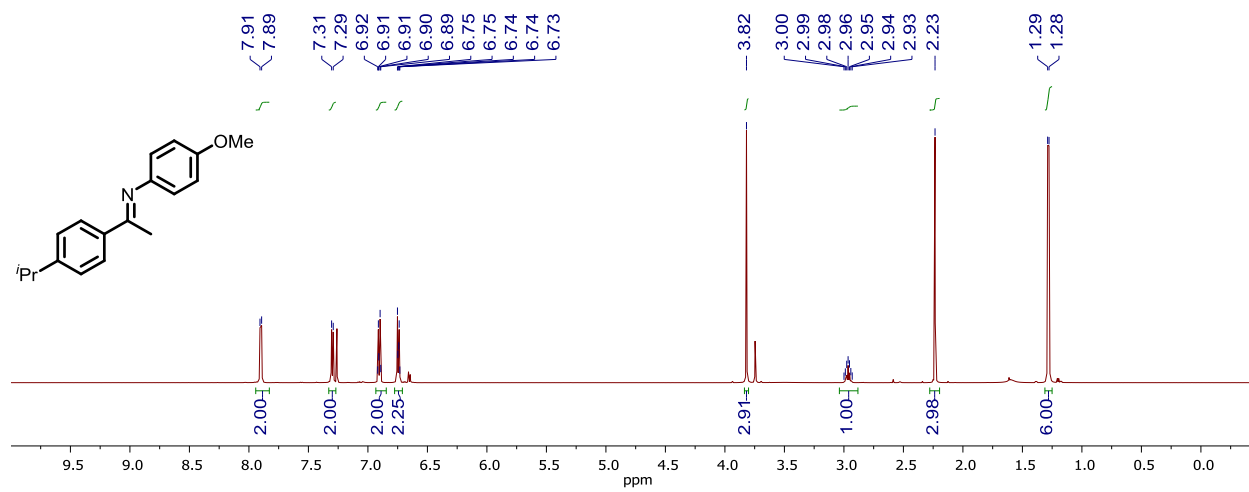
Figure C6. ^{1}H NMR spectrum of **1D** in benzene-d_6.
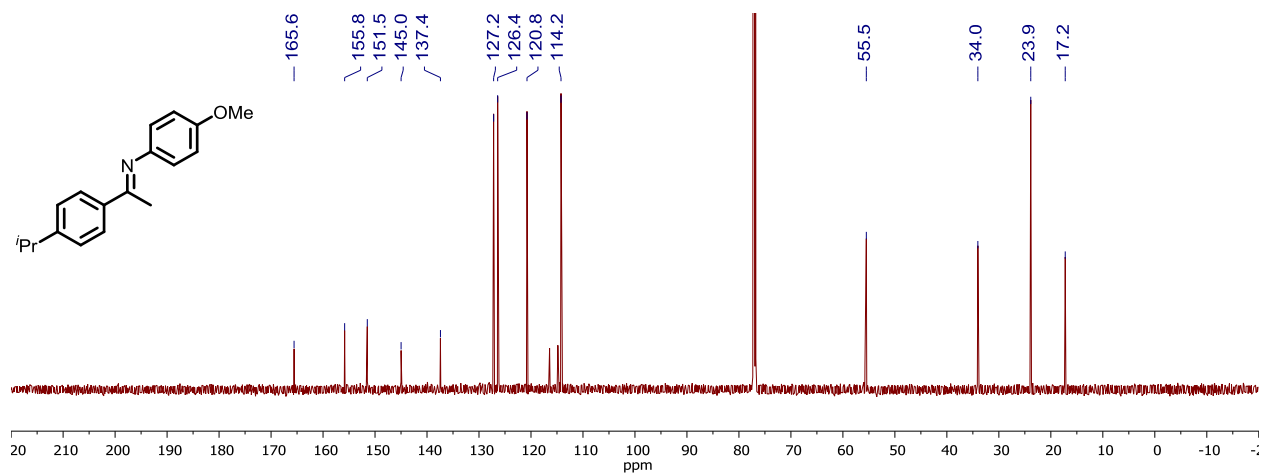
Figure C7. $^{13}C\{^1H\}$ NMR spectrum of **1D** in benzene-d_6.
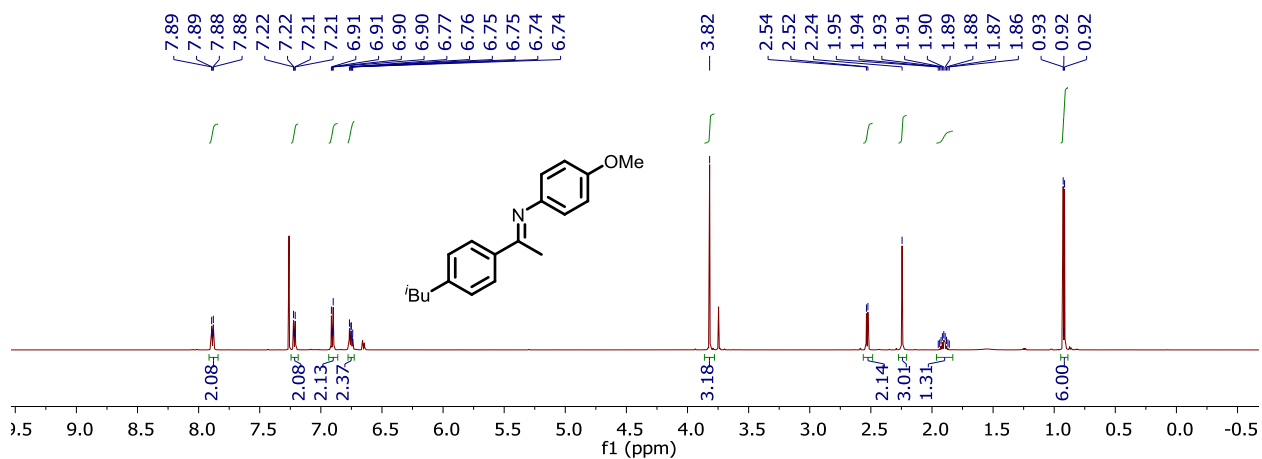
Figure C8. ^1H NMR spectrum of **1E** in chloroform-d.
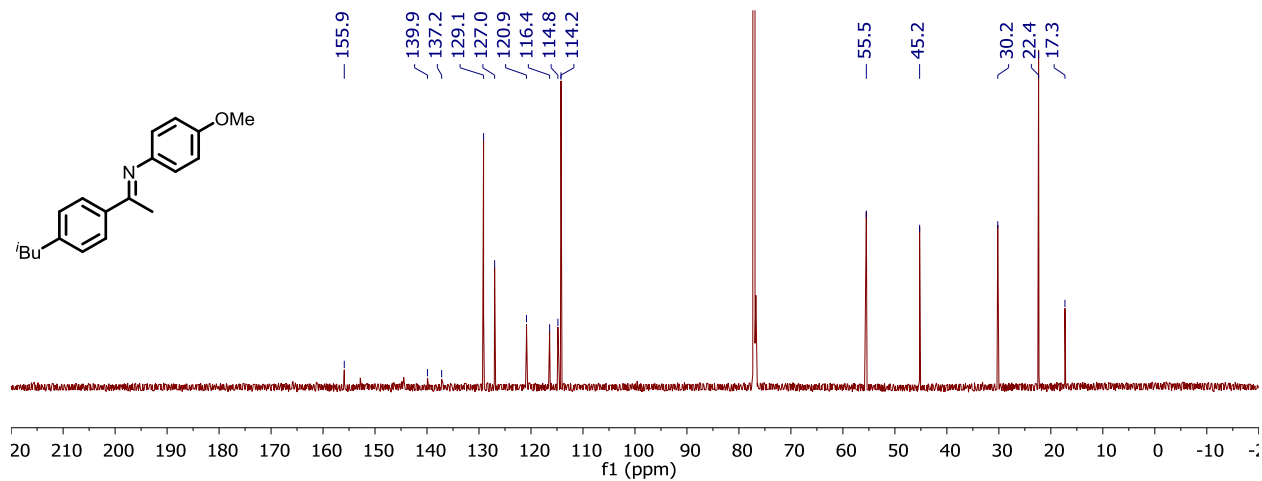
Figure C9. $^{13}C\{^1H\}$ NMR spectrum of **1E** in chloroform-d.
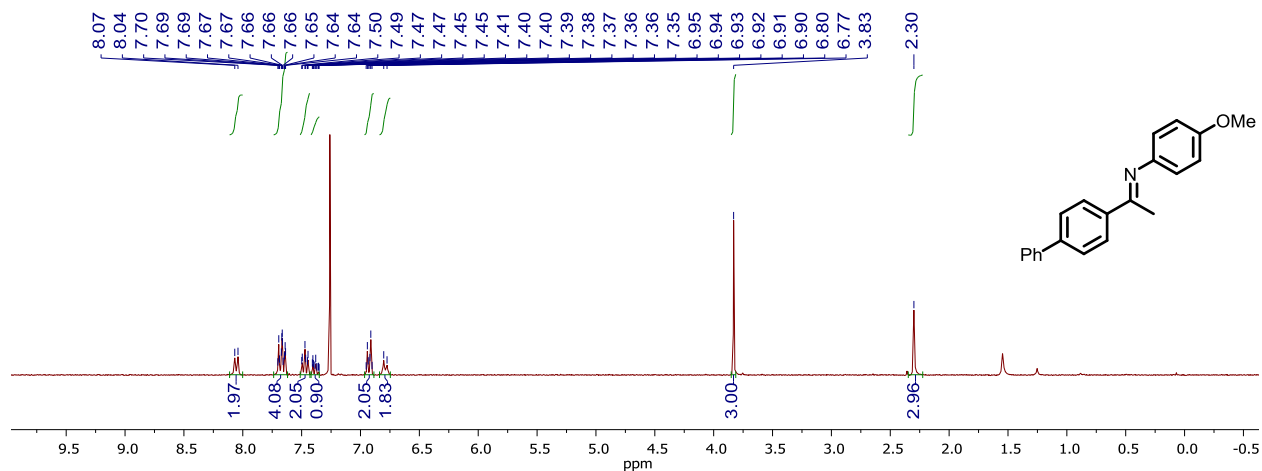
Figure C10. ^{1}H NMR spectrum of **1F** in chloroform-*d*.
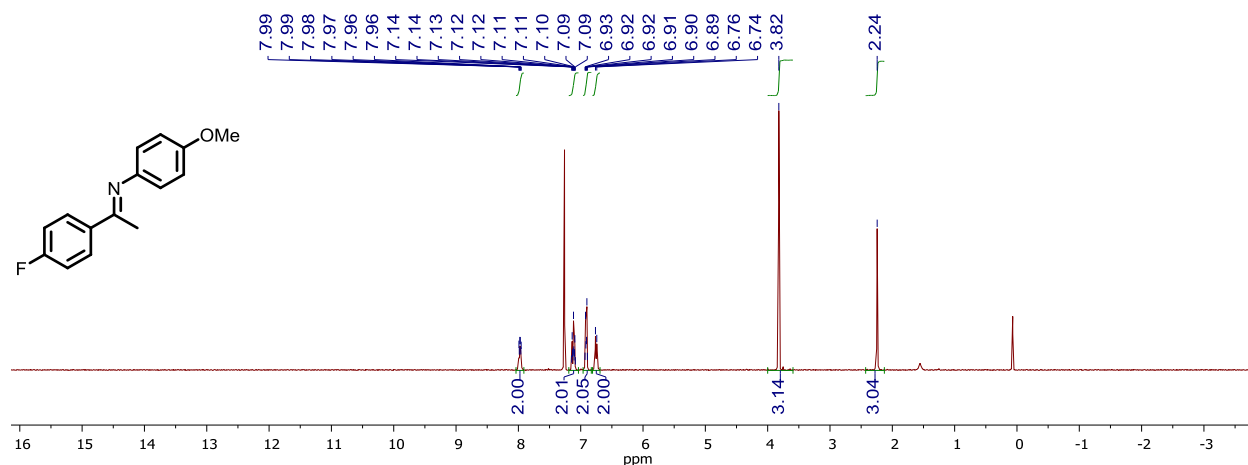
Figure C11. ^{1}H NMR spectrum of **1G** in chloroform-*d*.
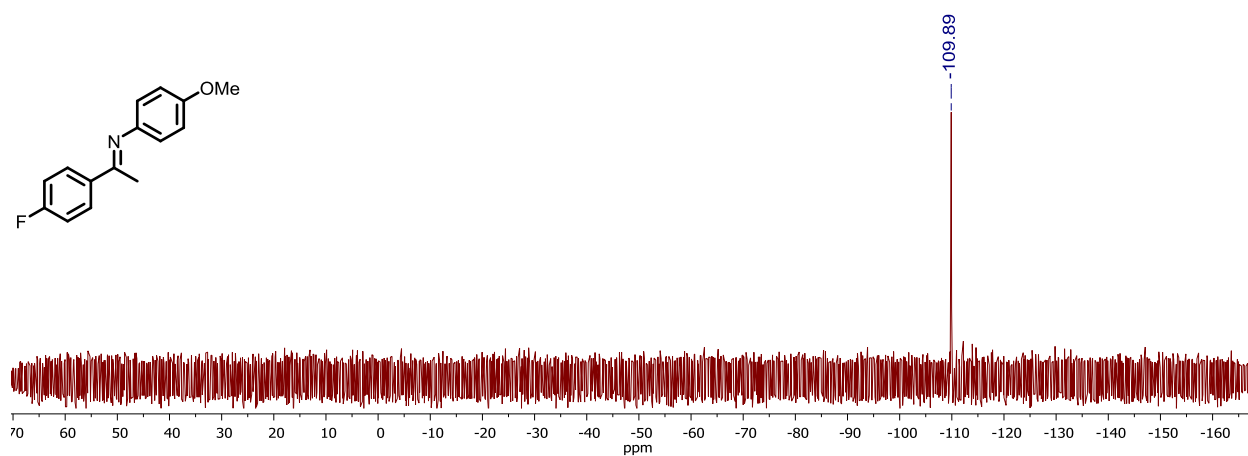
Figure C12. ^{19}F{^{1}H} NMR spectrum of **1G** in chloroform-*d*.
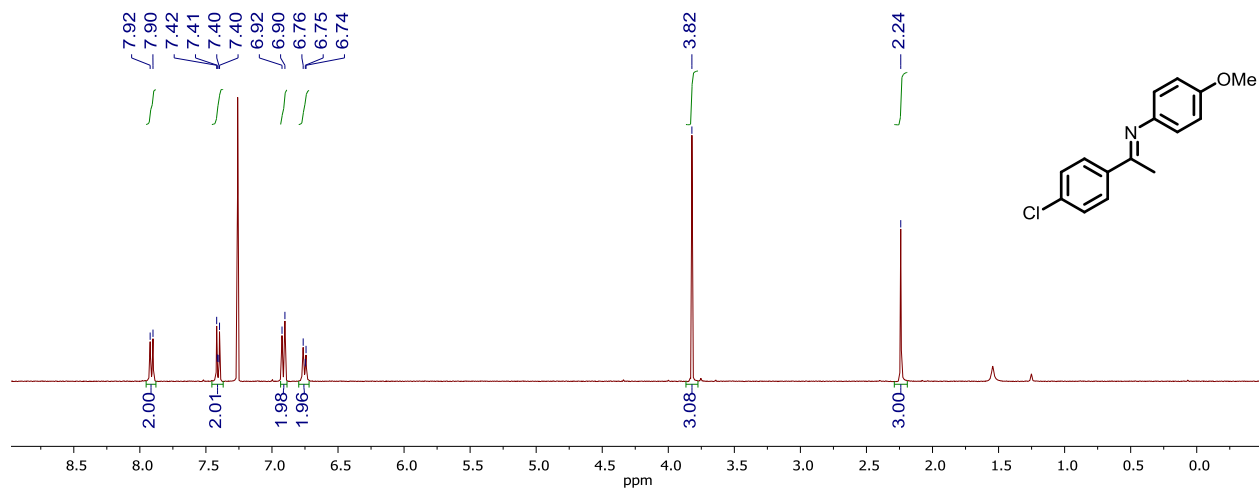
Figure C13. ^{1}H NMR spectrum of **1H** in chloroform-*d*.
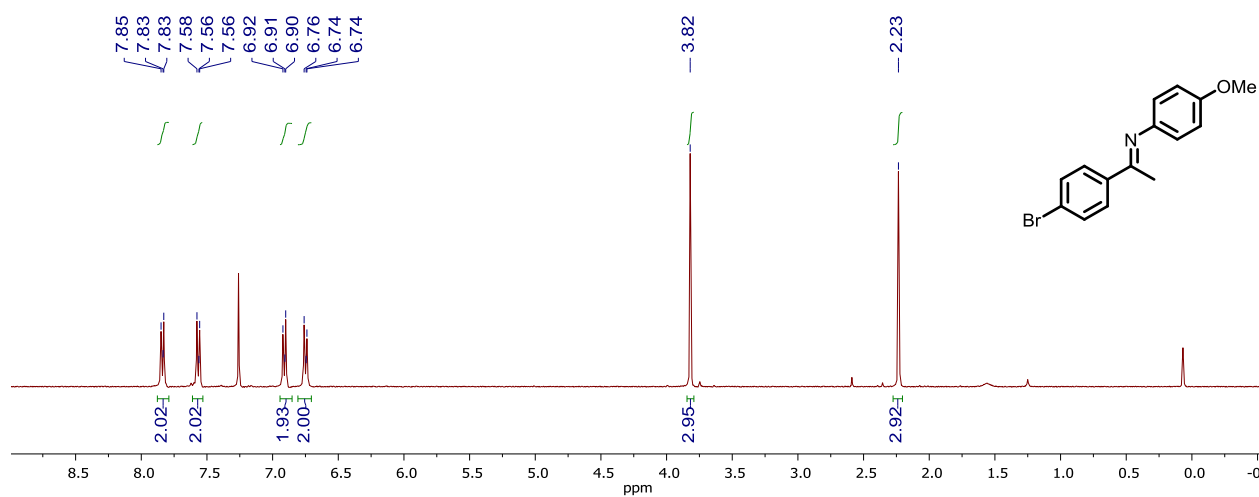
Figure C14. ^{1}H NMR spectrum of **1I** in chloroform-*d*.
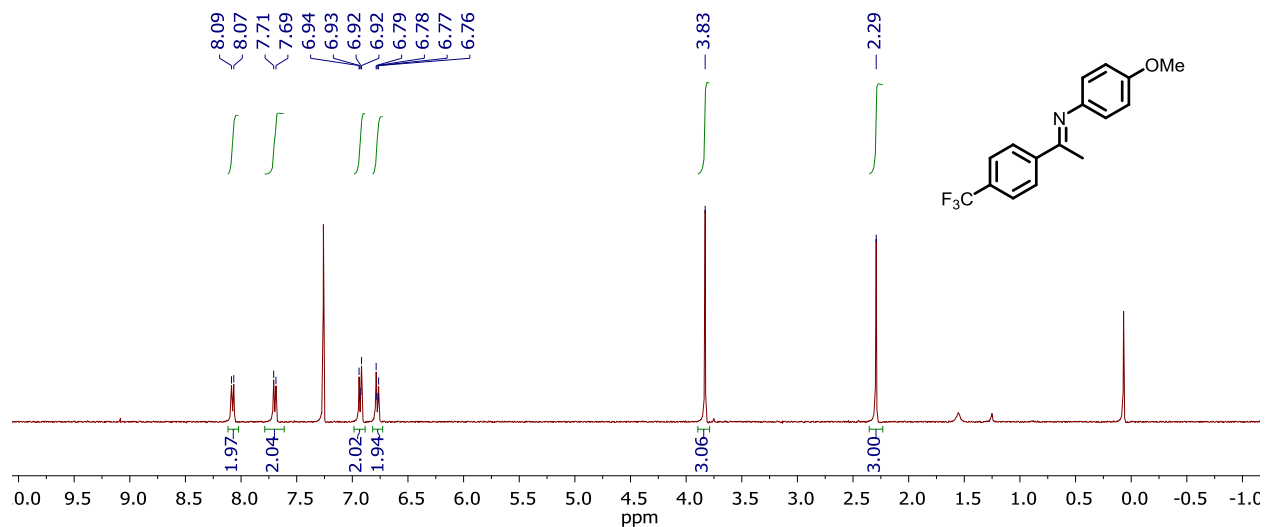
Figure C15. ^{1}H NMR spectrum of **1J** in chloroform-*d*.
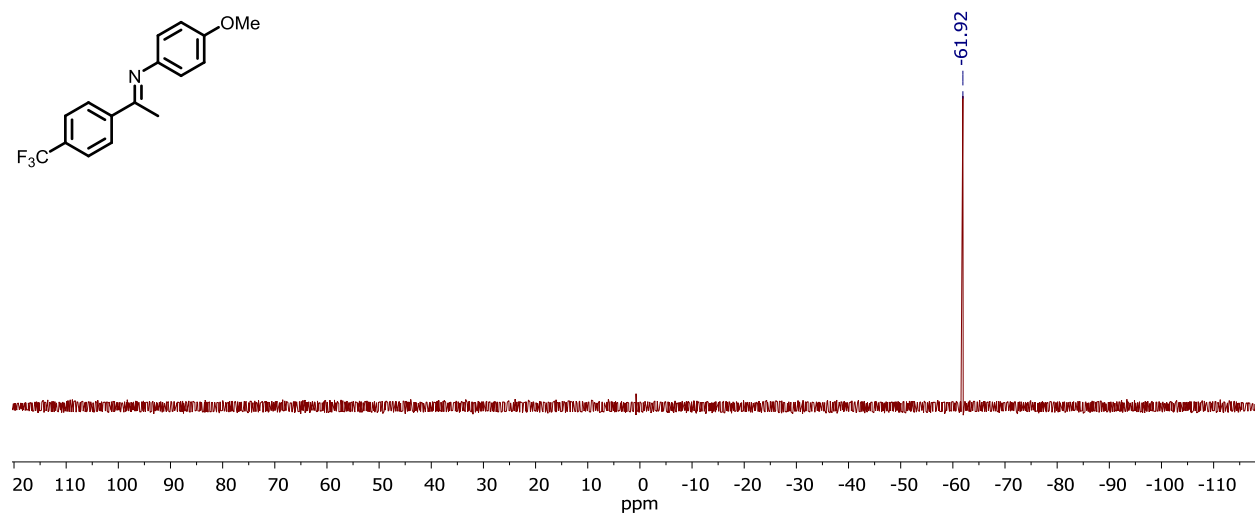
Figure C16. $^{19}F\{^{1}H\}$ NMR spectrum of **1J** in chloroform-*d*.
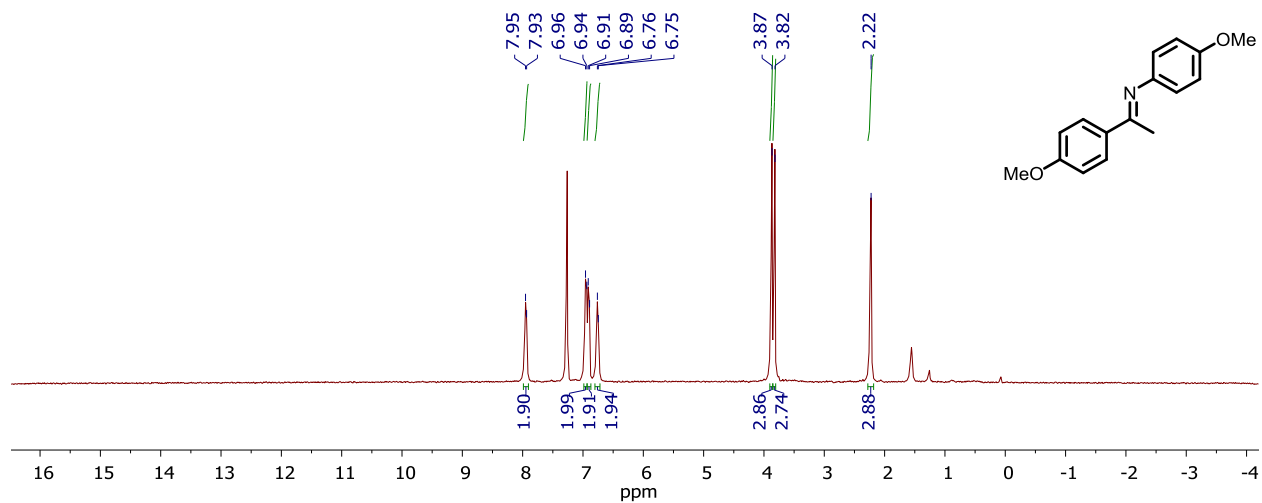
Figure C17. ^{1}H NMR spectrum of **1K** in chloroform-*d*.
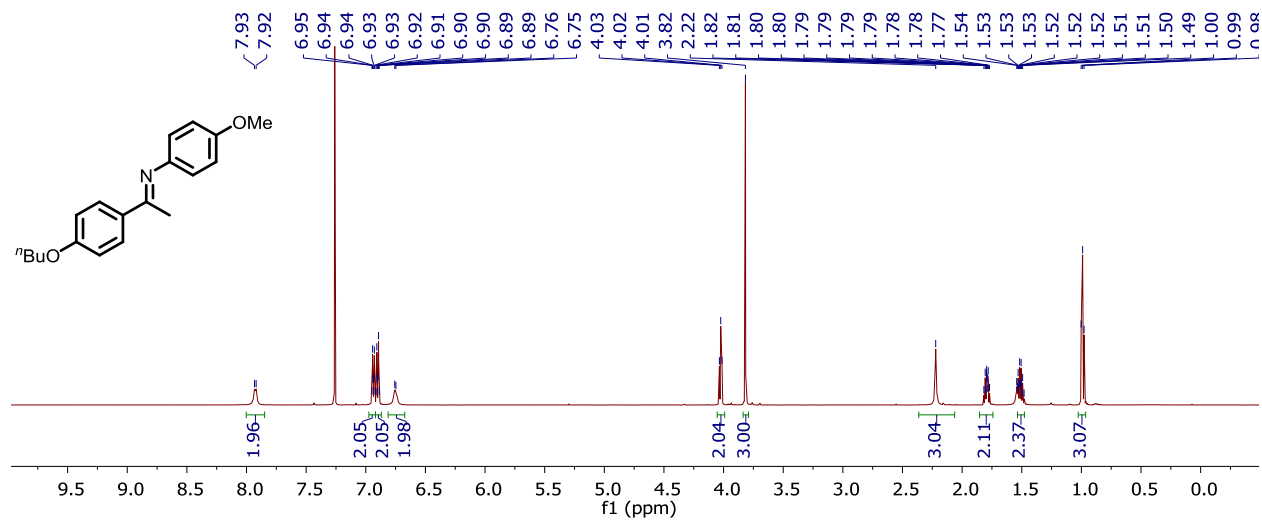
Figure C18. ^{1}H NMR spectrum of **1L** in chloroform-*d*.
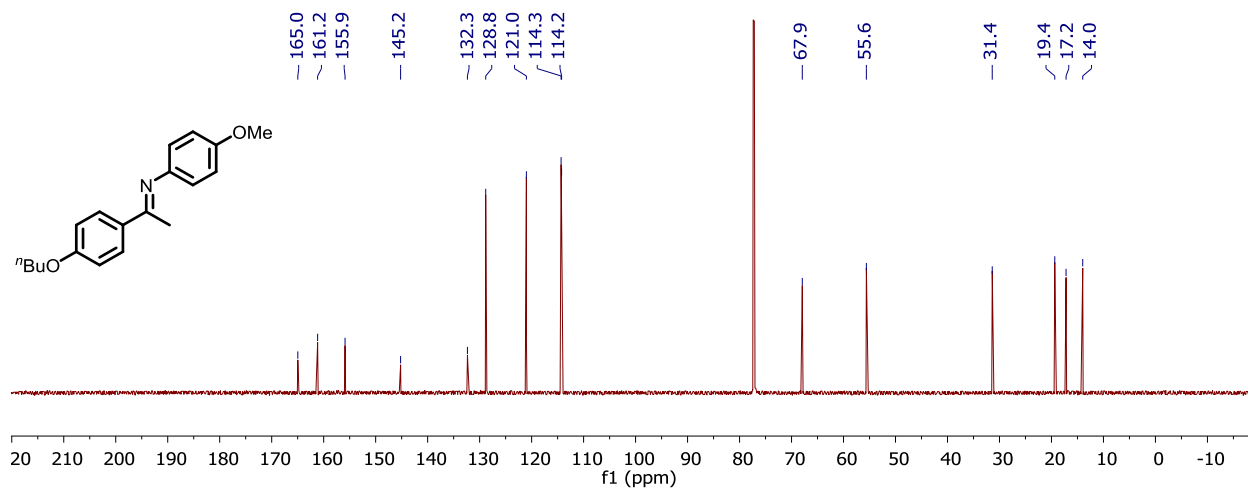
Figure C19. $^{13}C\{^1H\}$ NMR spectrum of **1L** in chloroform-*d*.
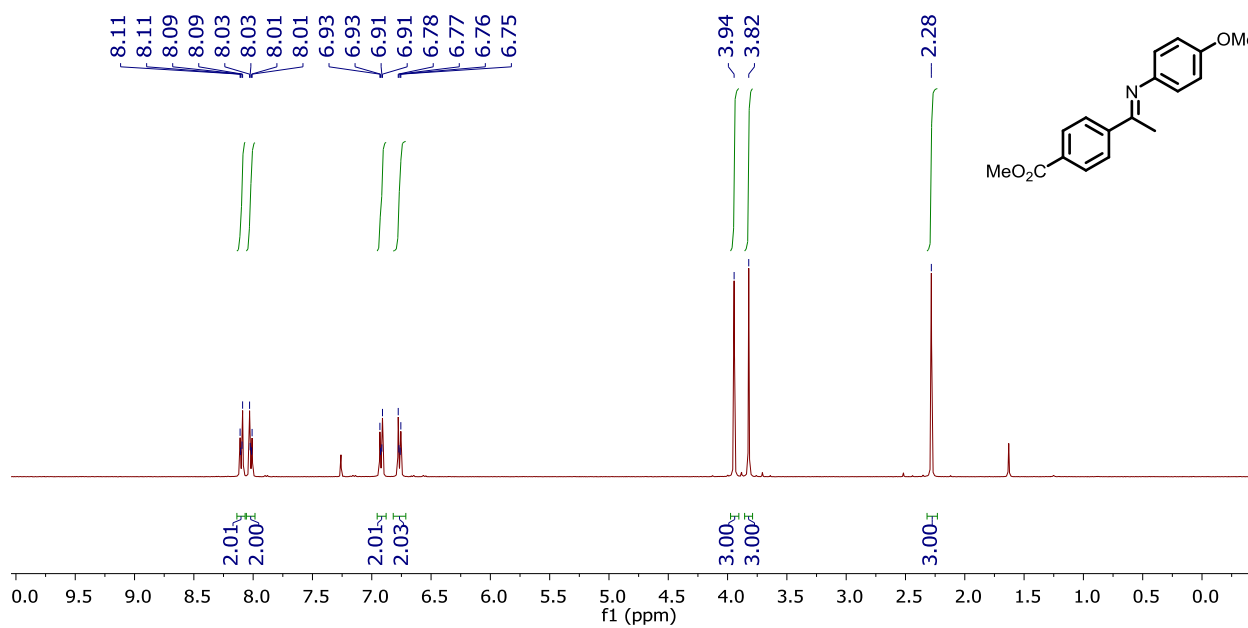
Figure C20. ^1H NMR spectrum of **1M** in chloroform-*d*.
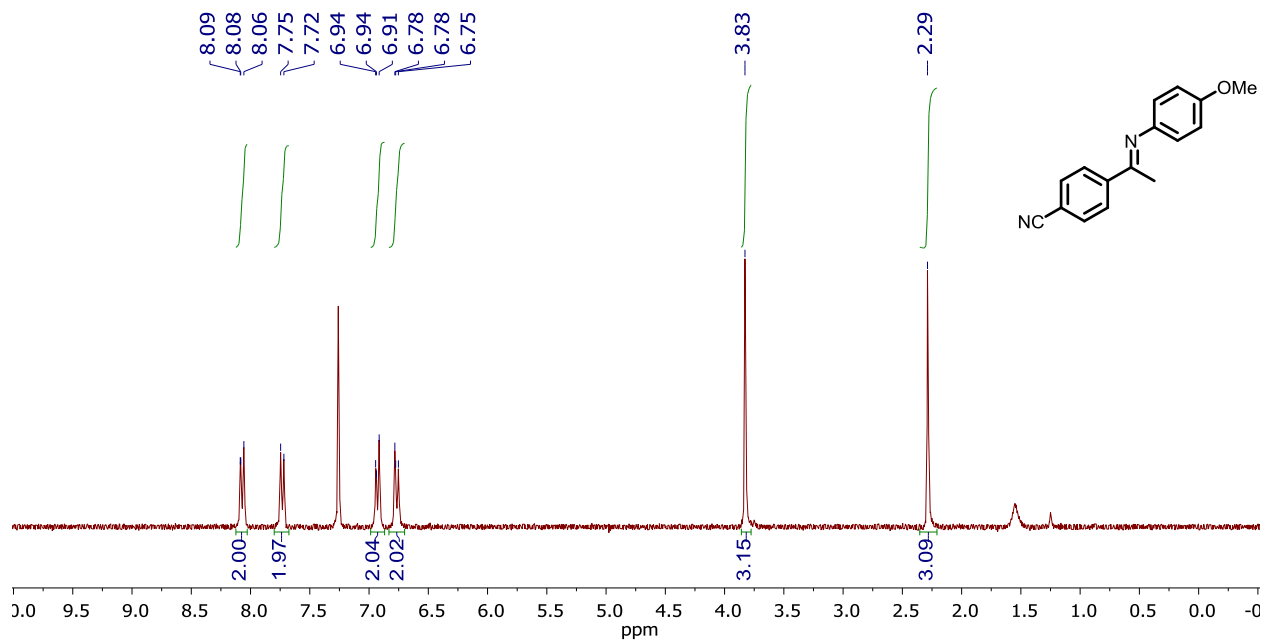
Figure C21. ^{1}H NMR spectrum of **1N** in chloroform-*d*.
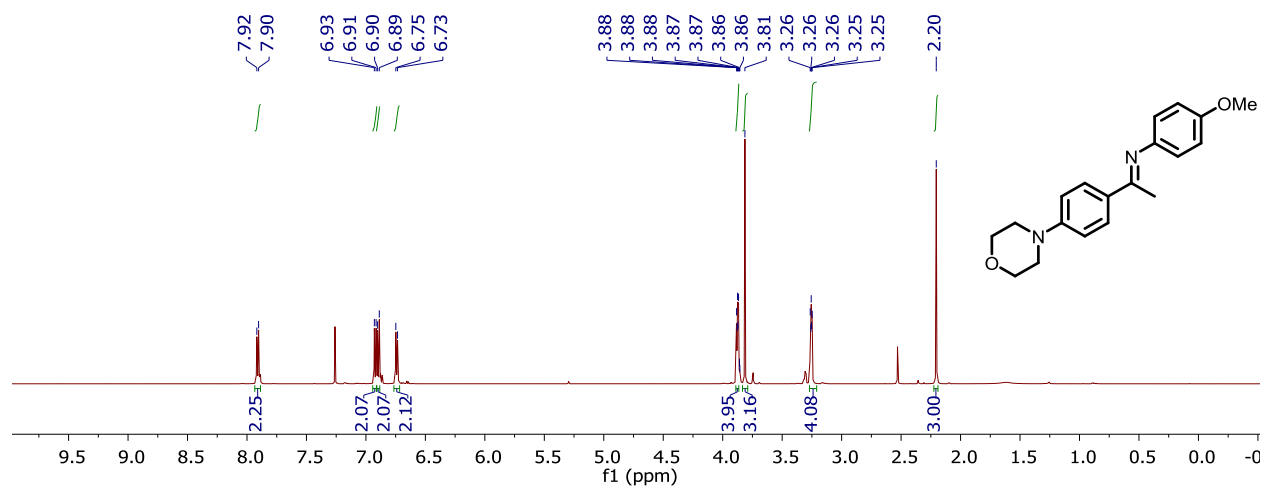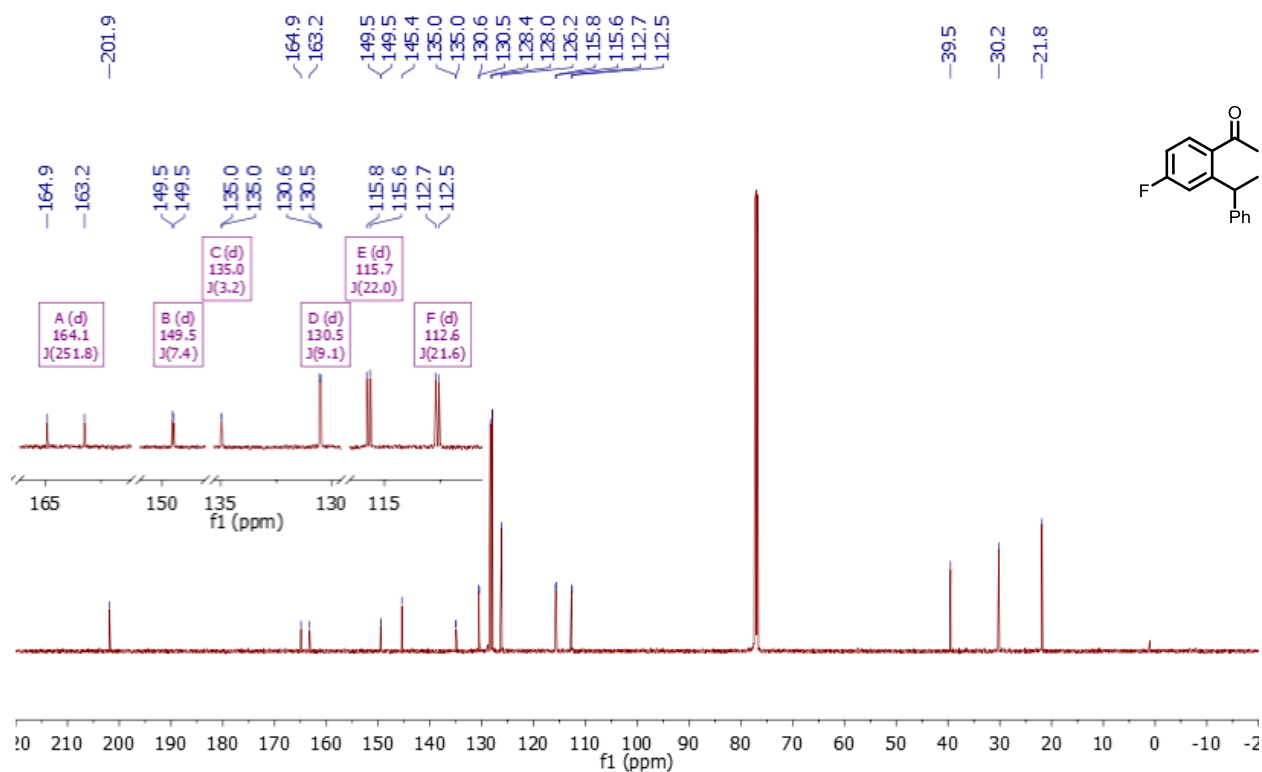

Figure C22. ^{1}H NMR spectrum of **1O** in chloroform-*d*.
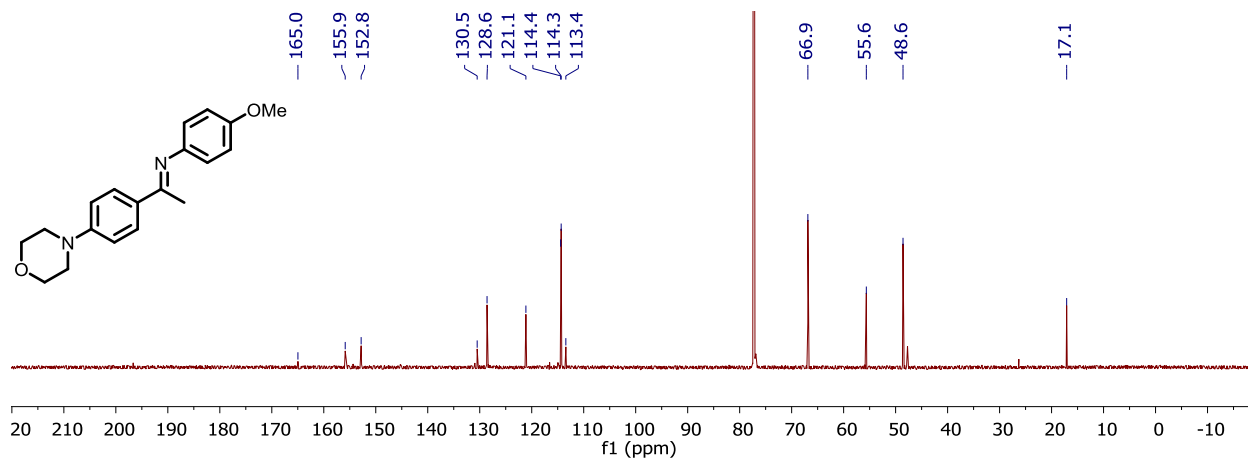
Figure C23. $^{13}C\{^1H\}$ NMR spectrum of **1O** in chloroform-*d*.
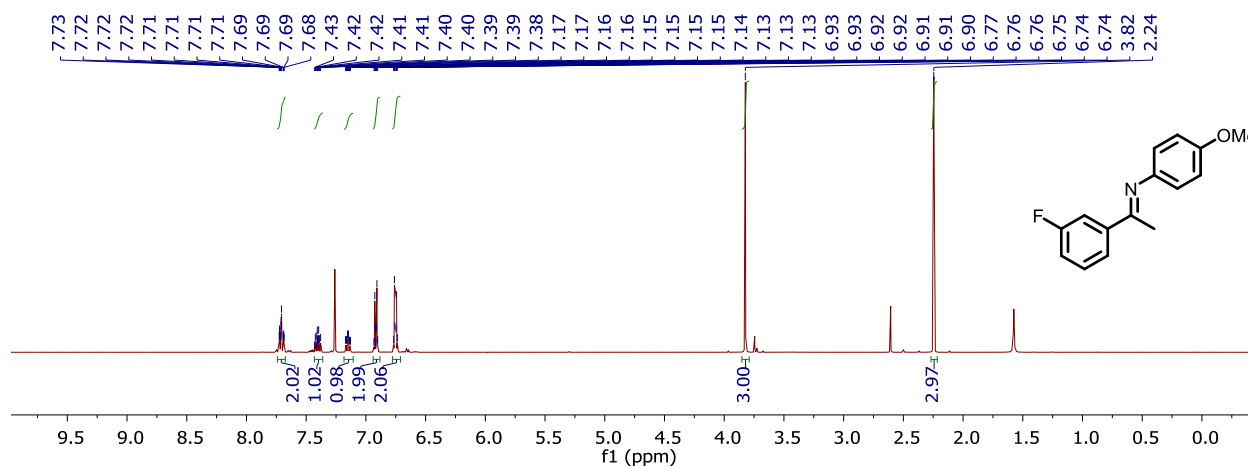
Figure C24. ^1H NMR spectrum of **1P** in chloroform-*d*.
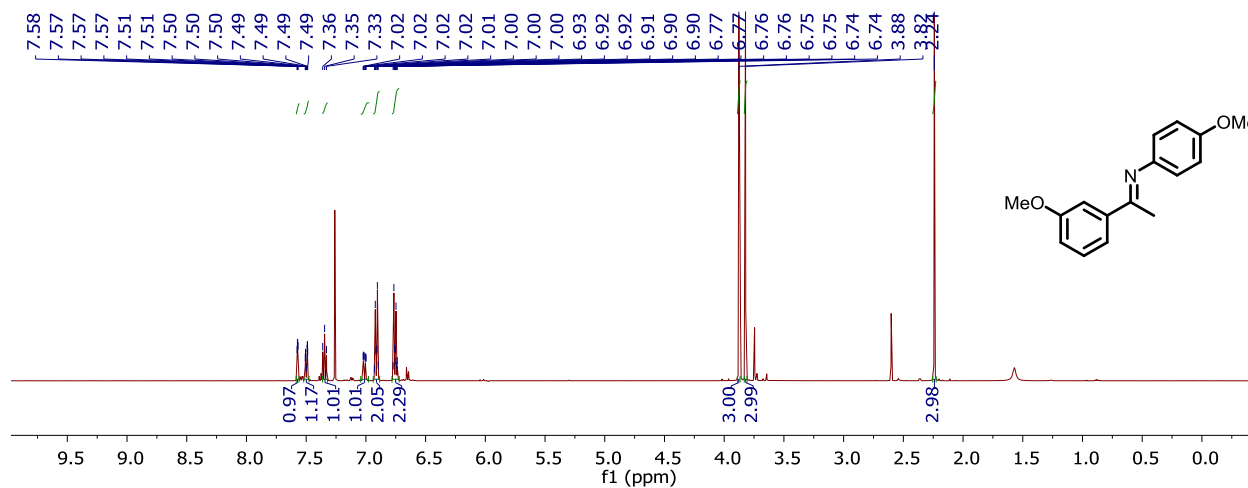
Figure C25. ^1H NMR spectrum of **1Q** in chloroform-*d*.
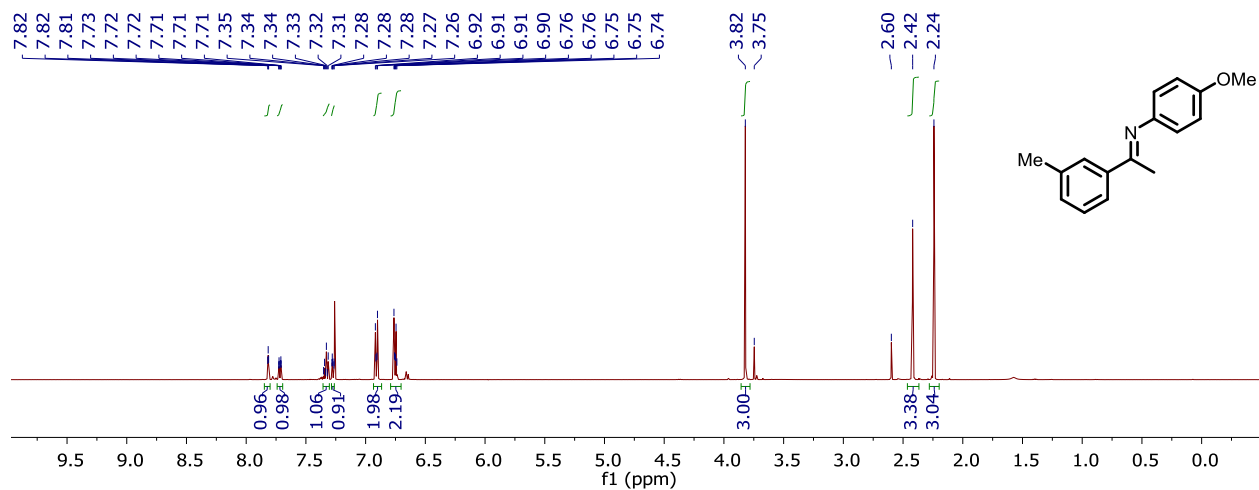
Figure C26. ^{1}H NMR spectrum of **1R** in chloroform-*d*.
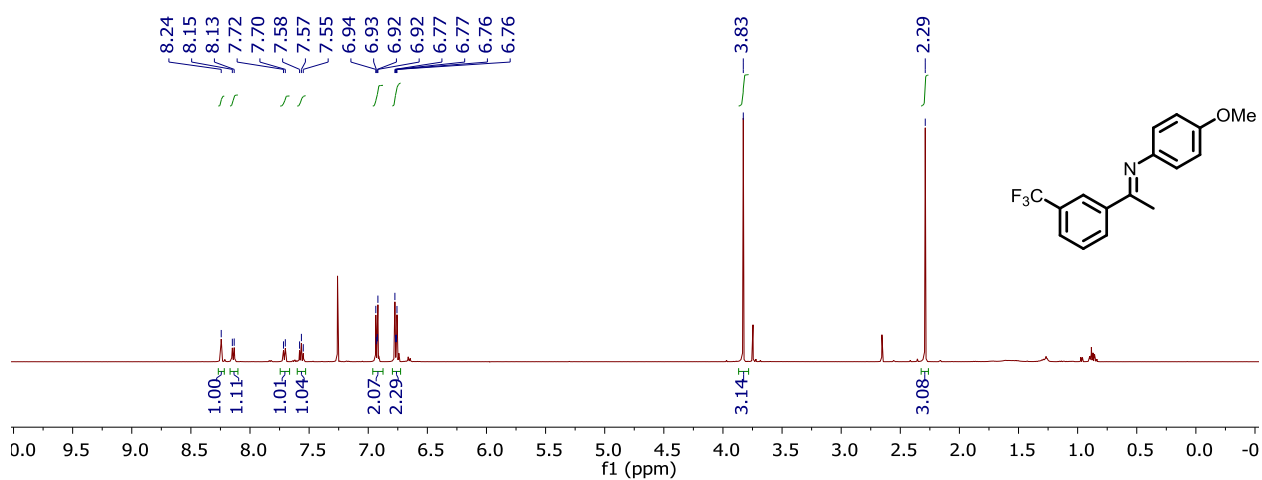
Figure C27. ^{1}H NMR spectrum of **1S** in chloroform-*d*.
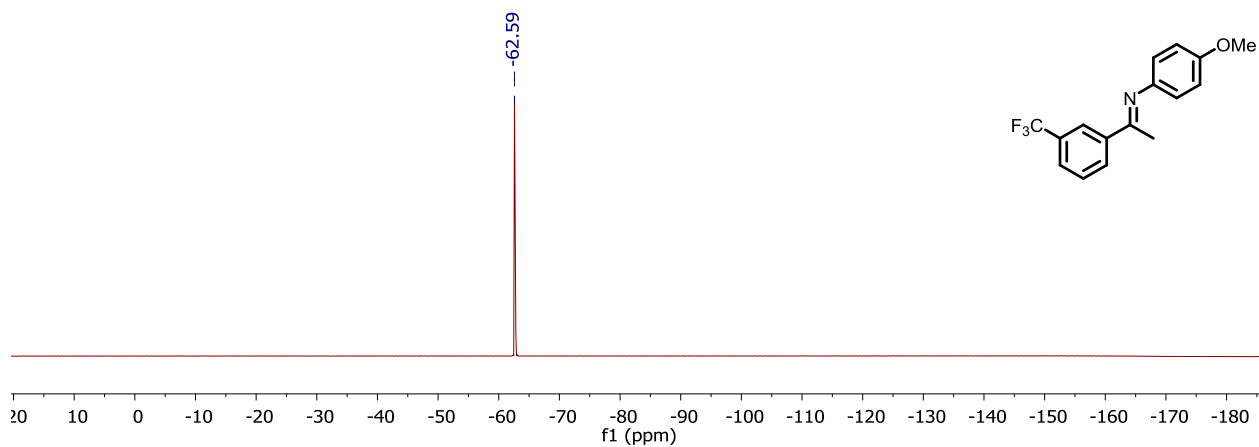
Figure C28. ^{19}F{^{1}H} NMR spectrum of **1S** in chloroform-*d*.
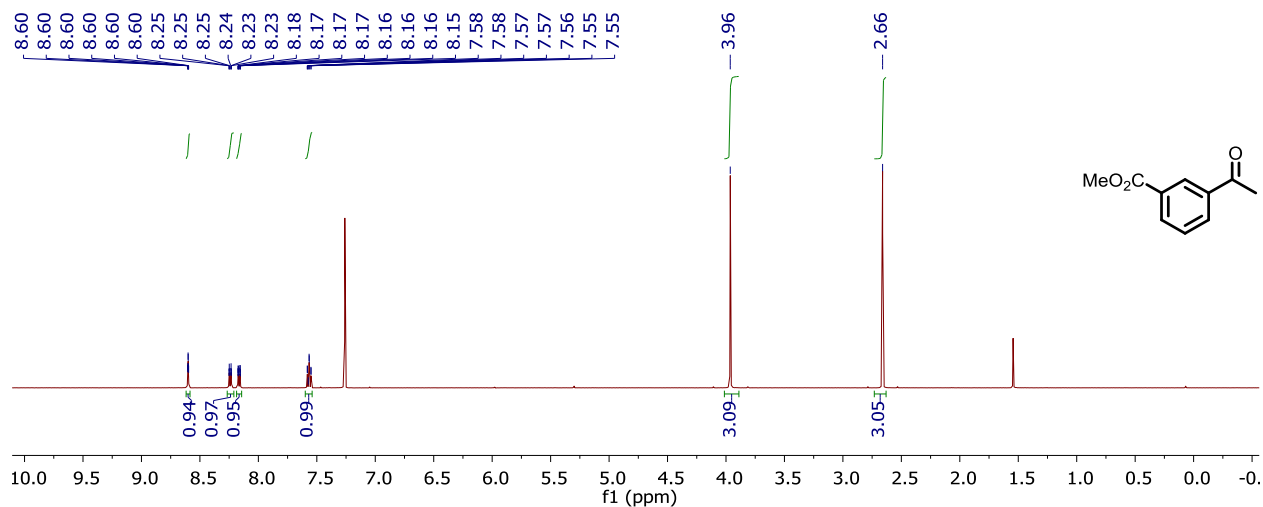
Figure C29. ¹H NMR spectrum of methyl 3-acetylbenzoate in chloroform-*d*.
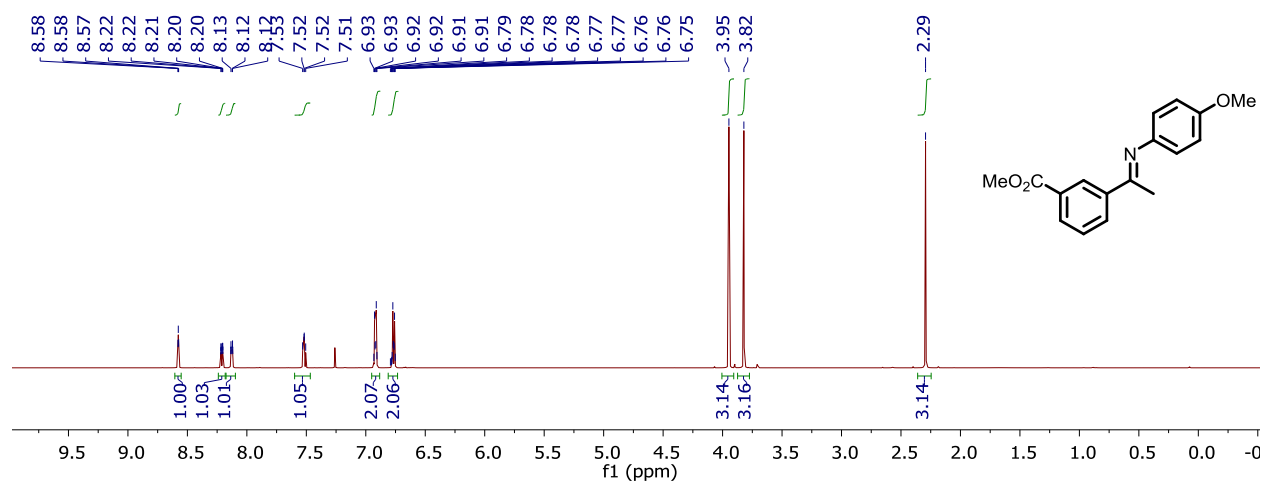
Figure C30. ¹H NMR spectrum of **1T** in chloroform-*d*.
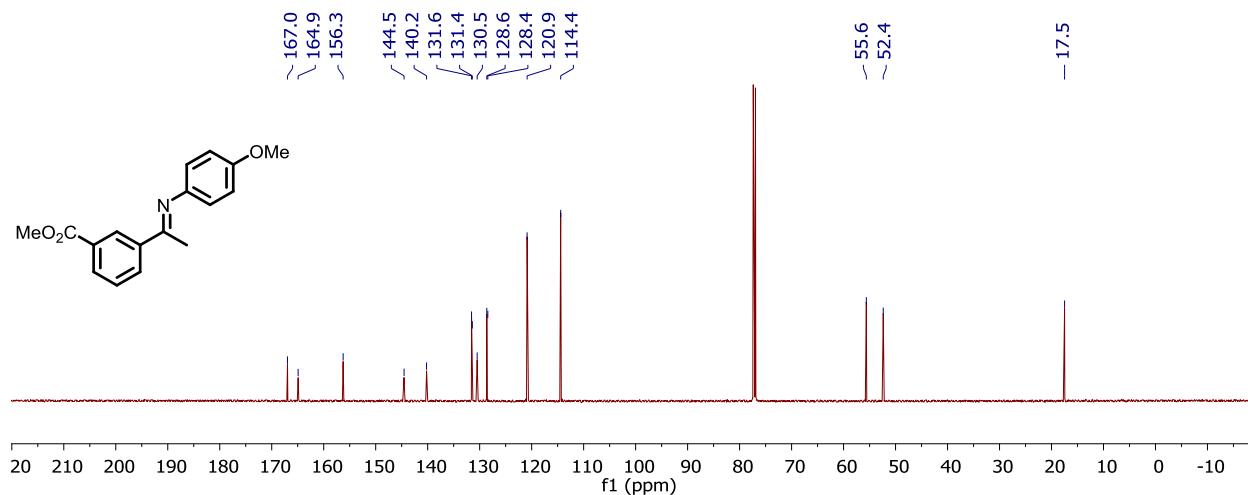
Figure C31. $^{13}C\{^1H\}$ NMR spectrum of **1T** in chloroform-*d*.
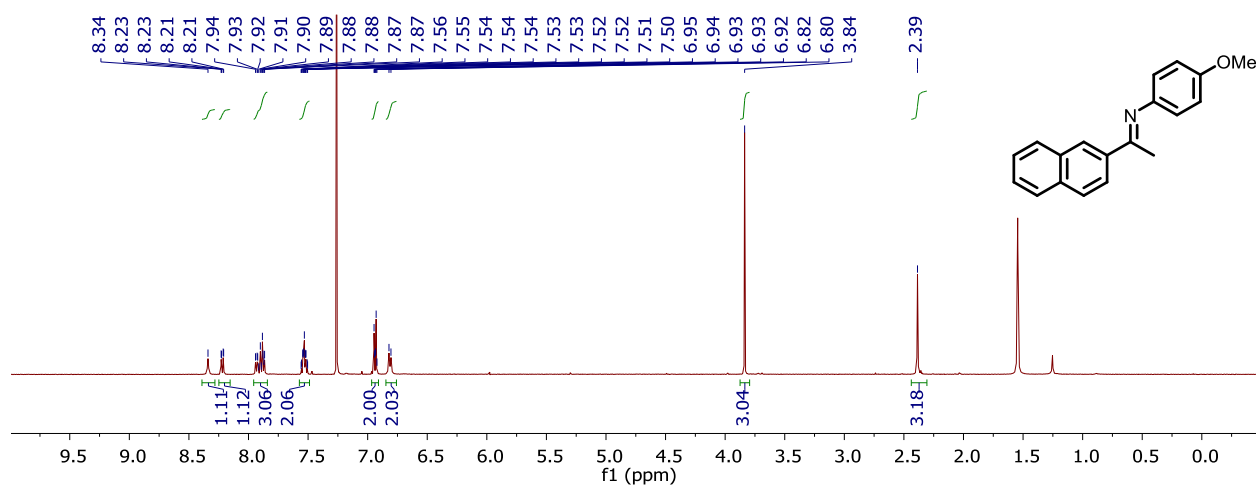
Figure C32. ^1H NMR spectrum of **1U** in chloroform-*d*.
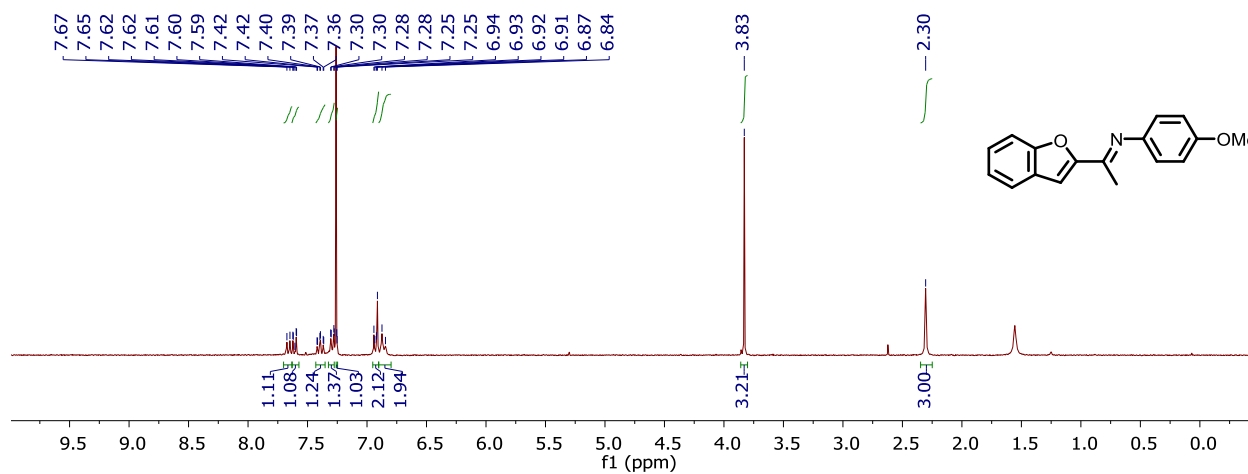
Figure C33. ^1H NMR spectrum of **1V** in chloroform-*d*.
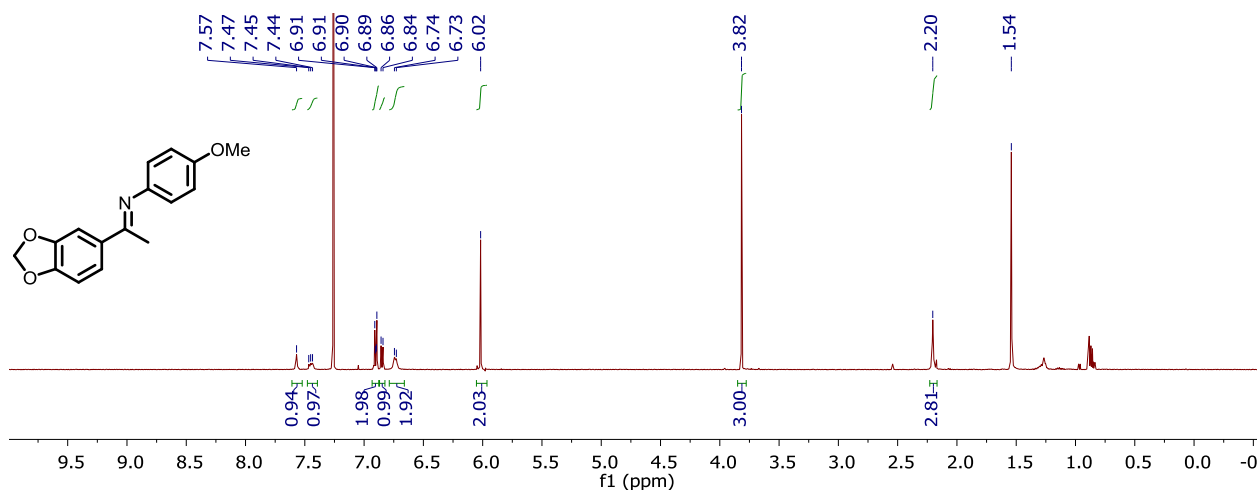
Figure C34. ^{1}H NMR spectrum of **1W** in chloroform-*d*.
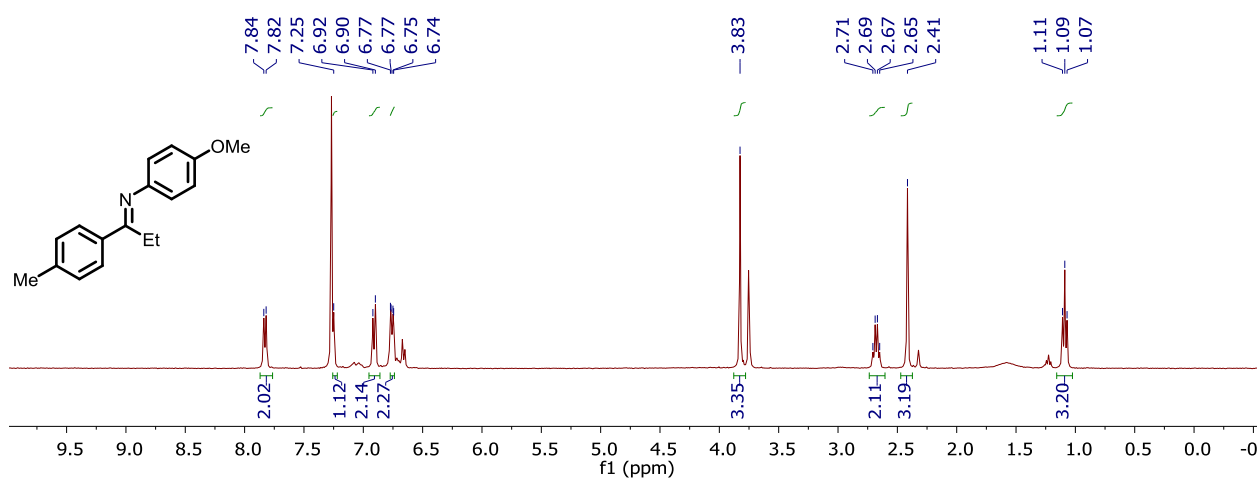
Figure C35. ^{1}H NMR spectrum of **1X** in chloroform-*d*.
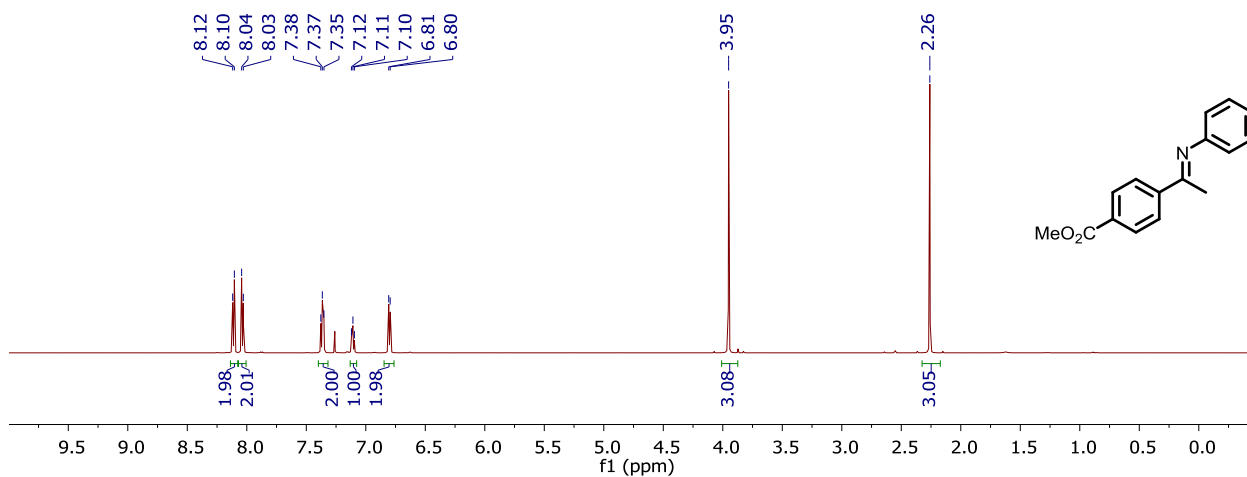
Figure C36. ^{1}H NMR spectrum of **5** in chloroform-*d*.
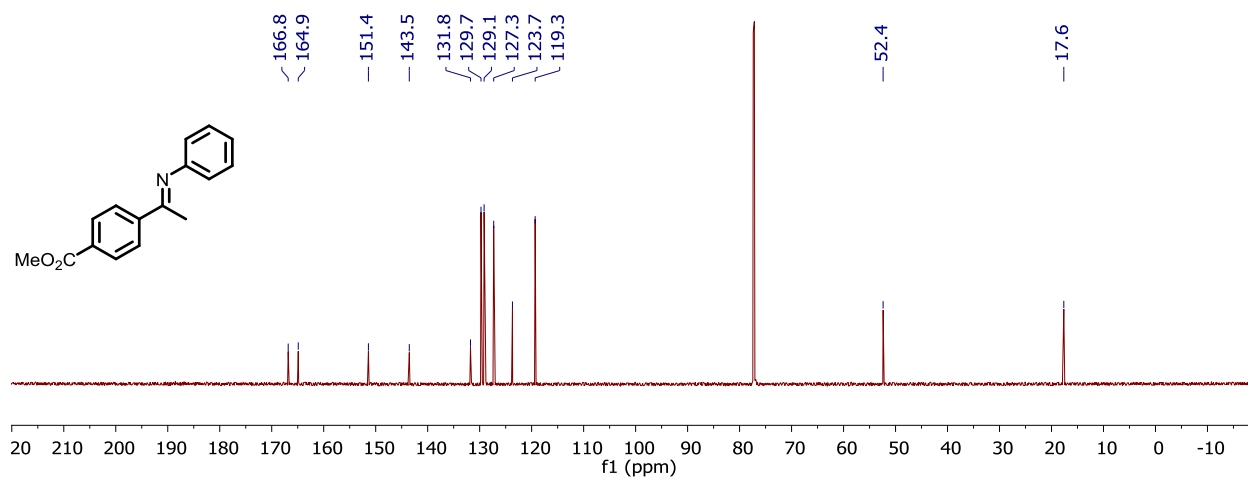
Figure C37. $^{13}C\{^{1}H\}$ NMR spectrum of **5** in chloroform-*d*.
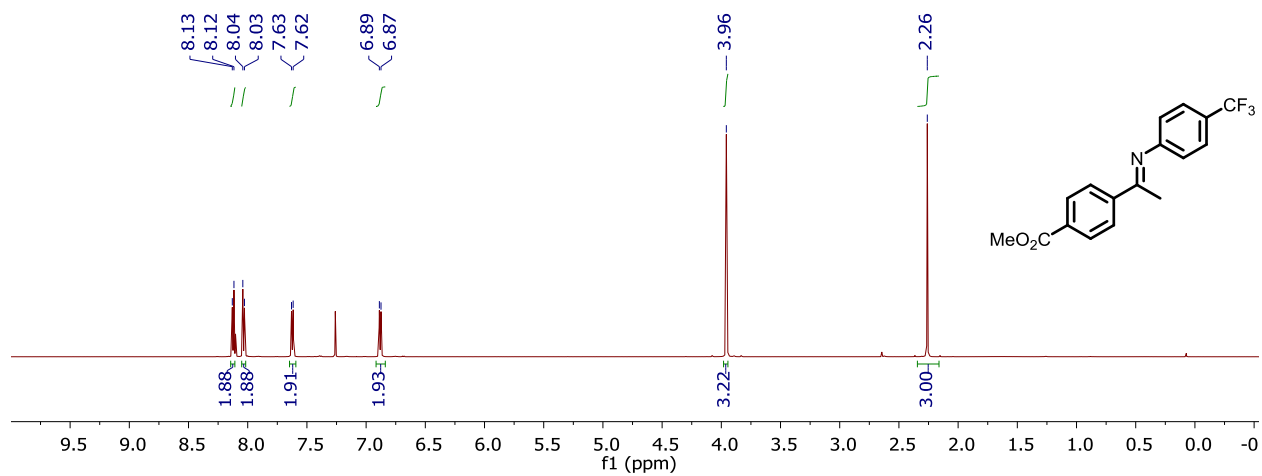
Figure C38. ^{1}H NMR spectrum of **6** in chloroform-*d*.
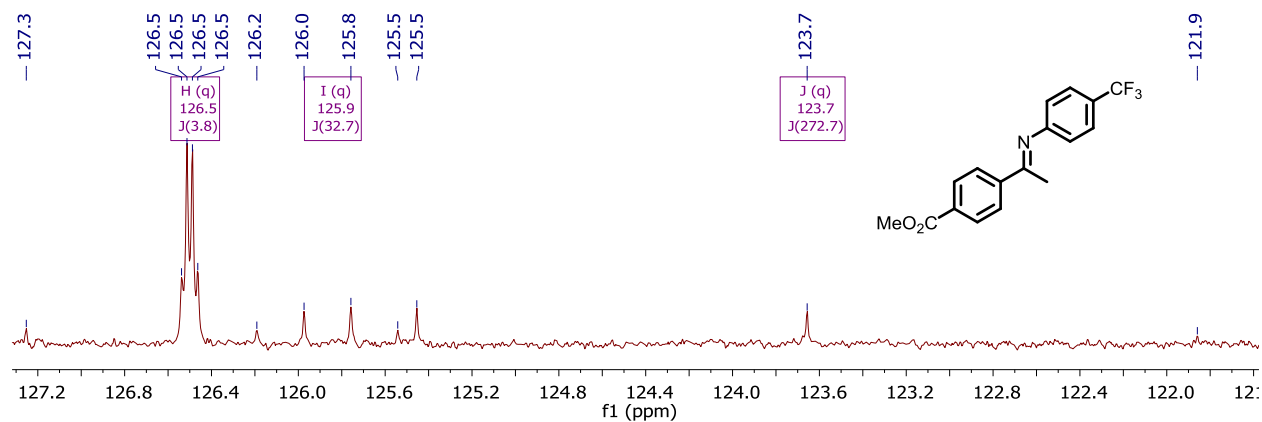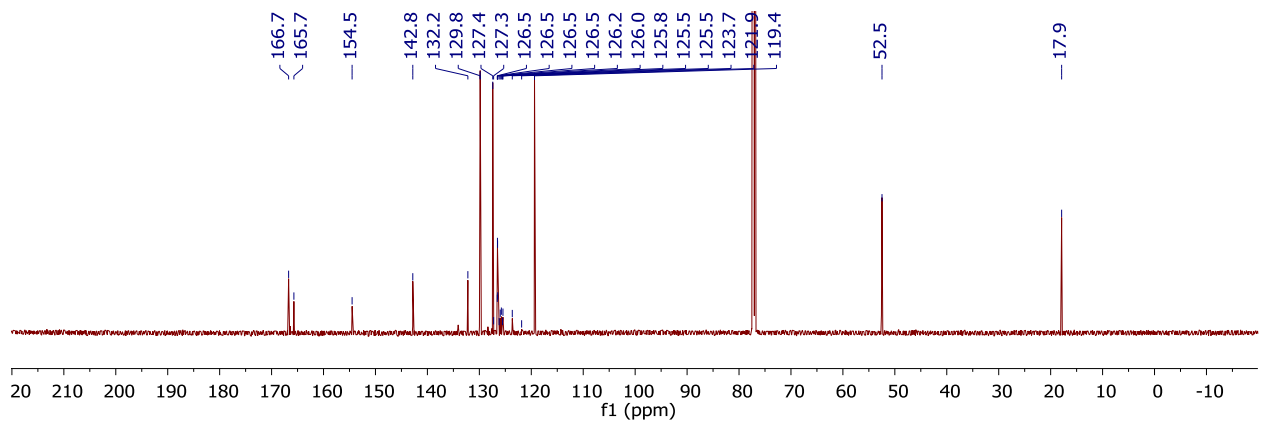
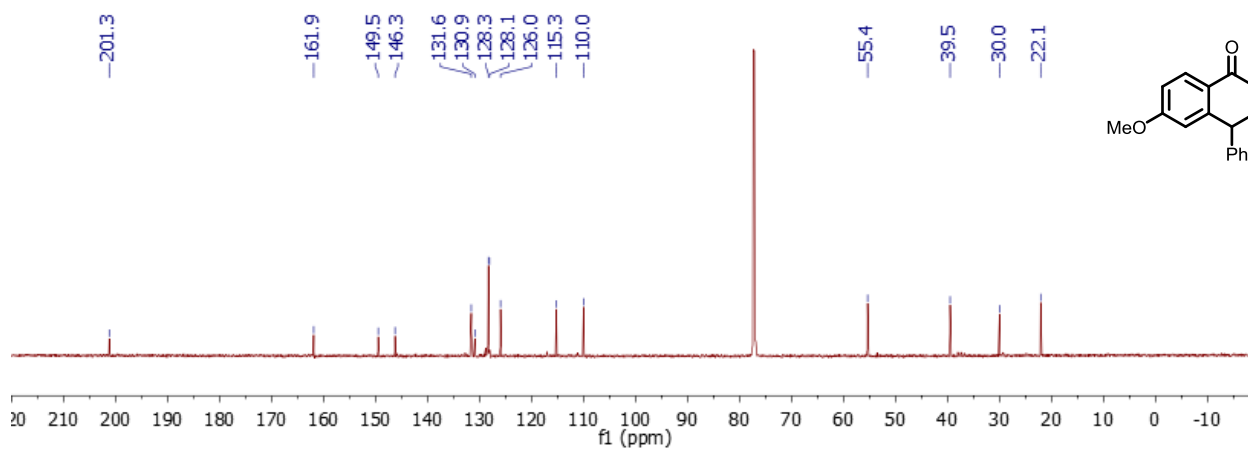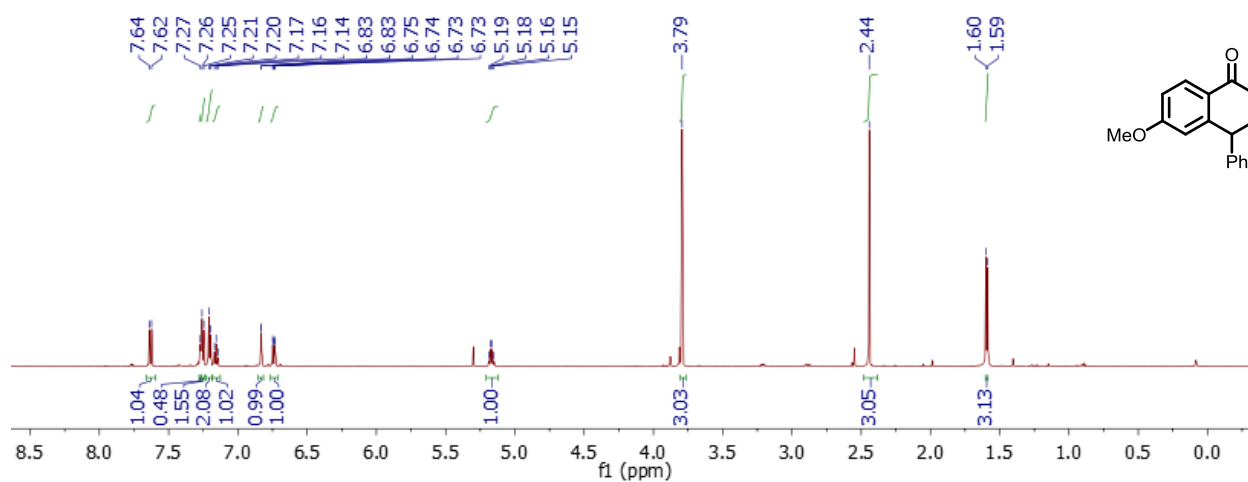**Figure C39.** $^{13}C\{^1H\}$ NMR spectrum of **6** in chloroform-*d*. **Top:** Full spectra. **Bottom:** expansion of peaks with $^nJ_{CF}$ couplings (n = 1, 2, or 3).
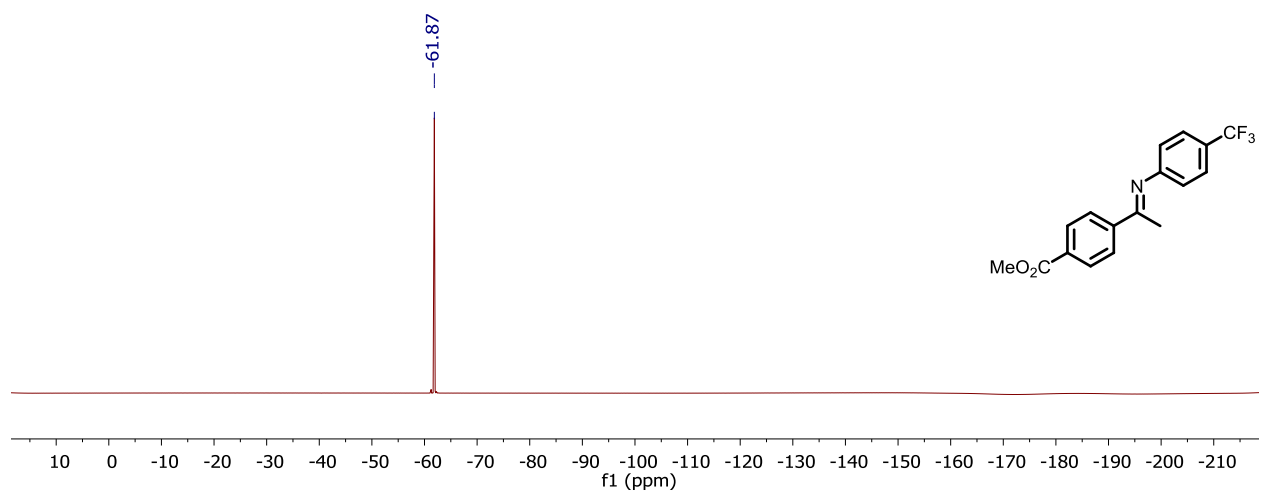
Figure C40. ^{19}F NMR spectrum of **6** in chloroform-*d*.
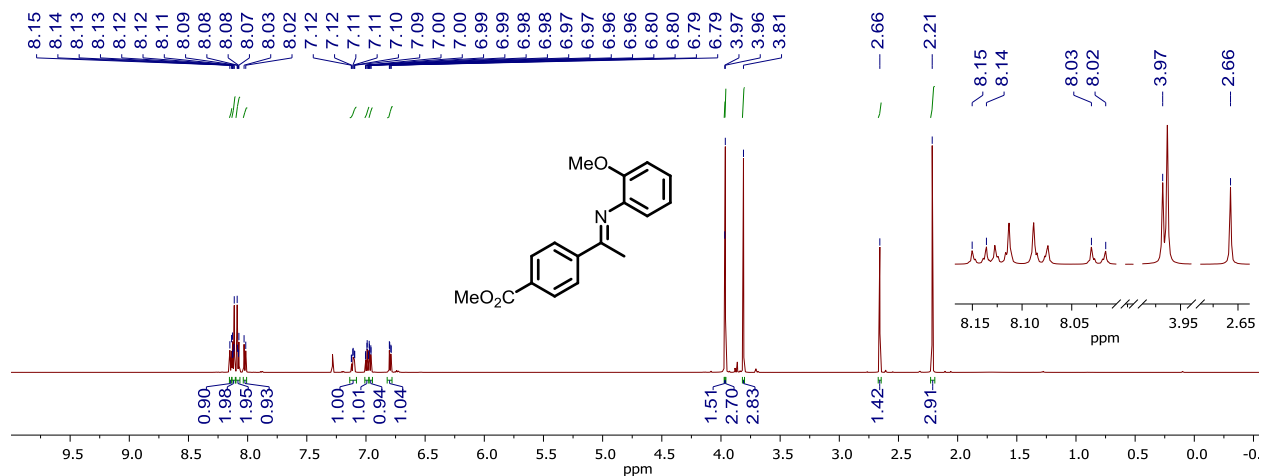
Figure C41. ^{1}H NMR spectrum of **7** in chloroform-*d*. Residual methyl 4-acetylbenzoate was identified and purification attempts were unable to remove it. **Inset:** resonances corresponding to the ca. 30% methyl 4-acetylbenzoate impurity.
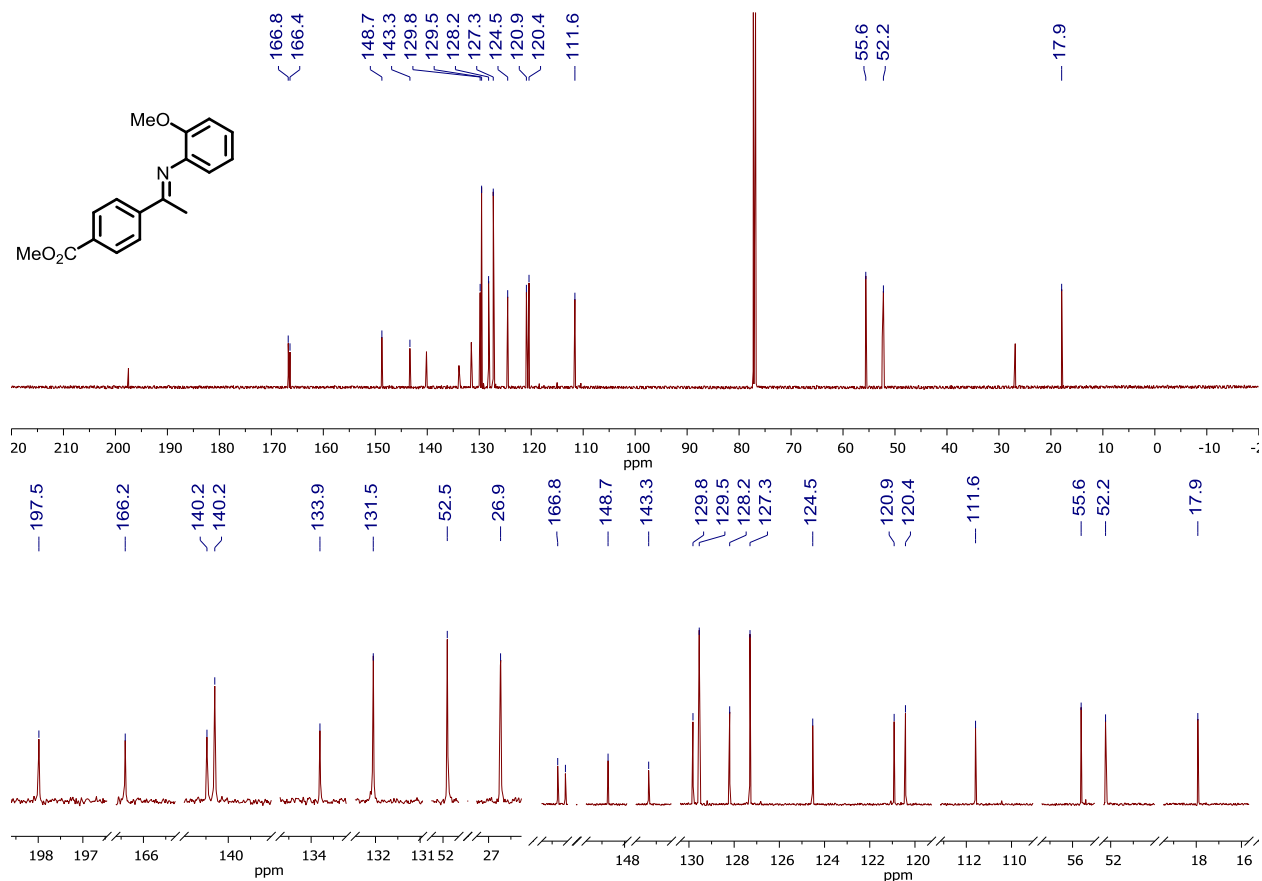
Figure C42. ^{13}C{^{1}H} NMR spectrum of **7** in chloroform-*d*. **Top:** full spectra. **Bottom Left:** peaks corresponding to the methyl 4-acetylbenzoate impurity. **Bottom Right:** peaks corresponding to the imine product, **7**.
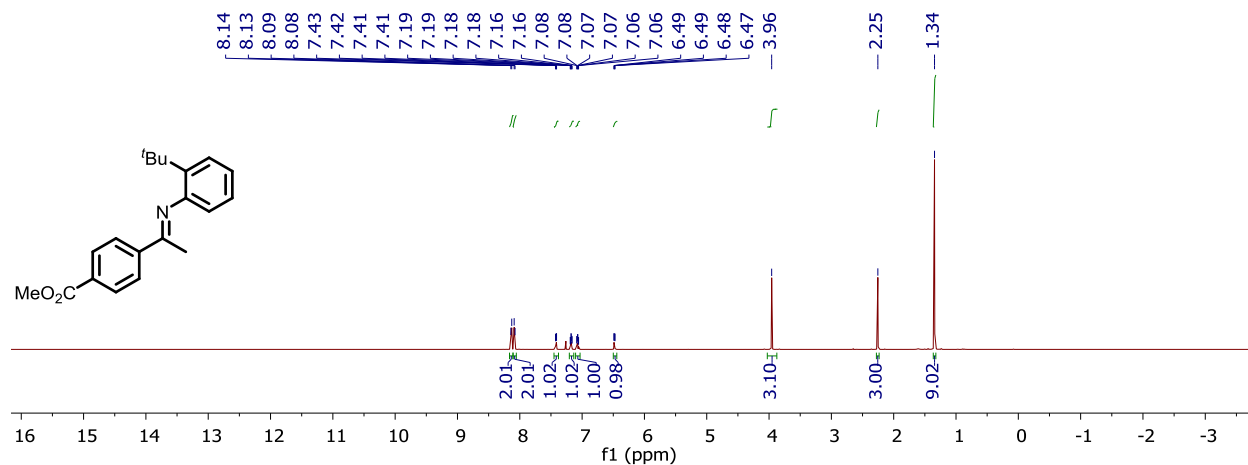
Figure C43. ^{1}H NMR spectrum of **8** in chloroform-*d*.
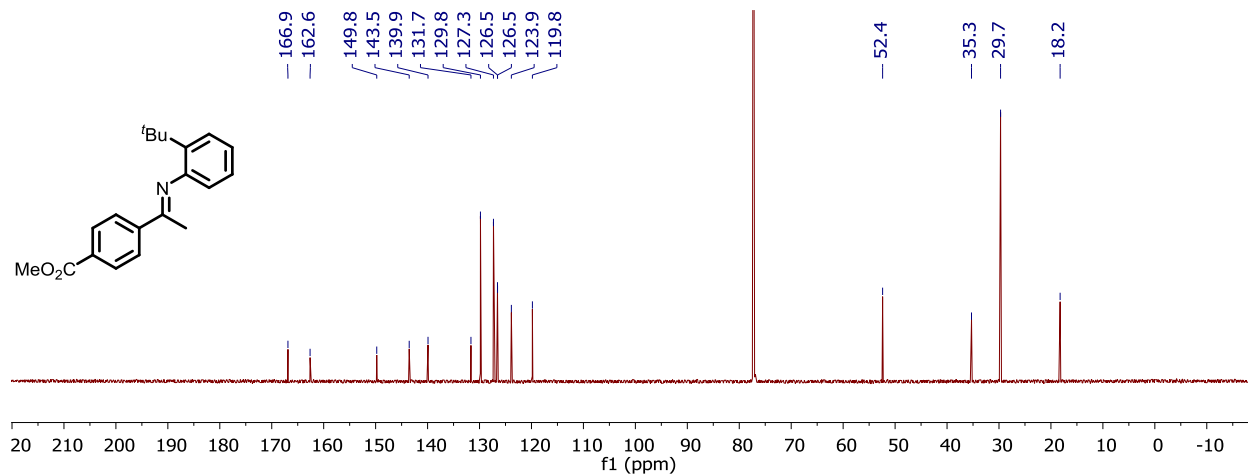
Figure C44. ^{13}C{^{1}H} NMR spectrum of **8** in chloroform-*d*.
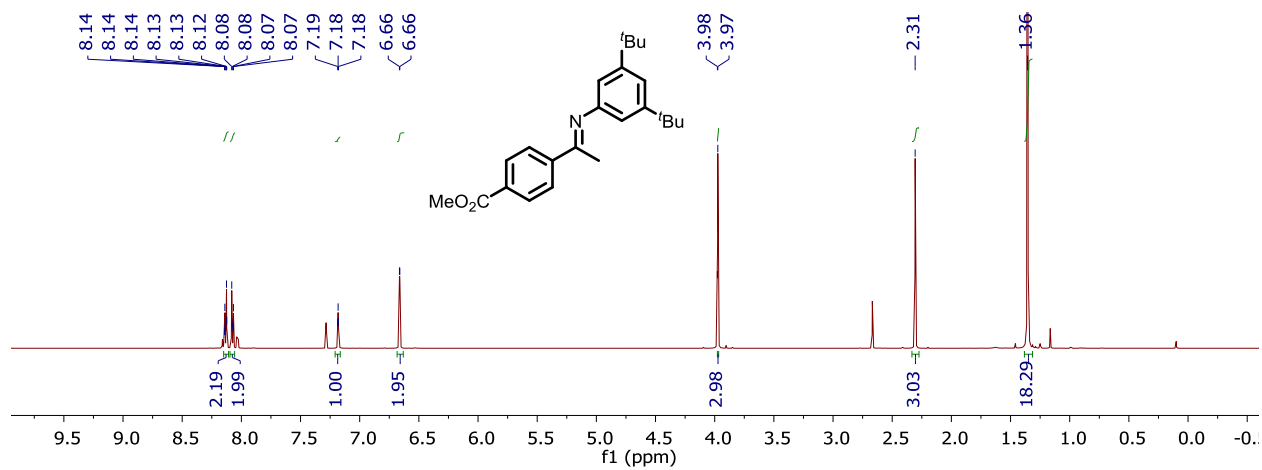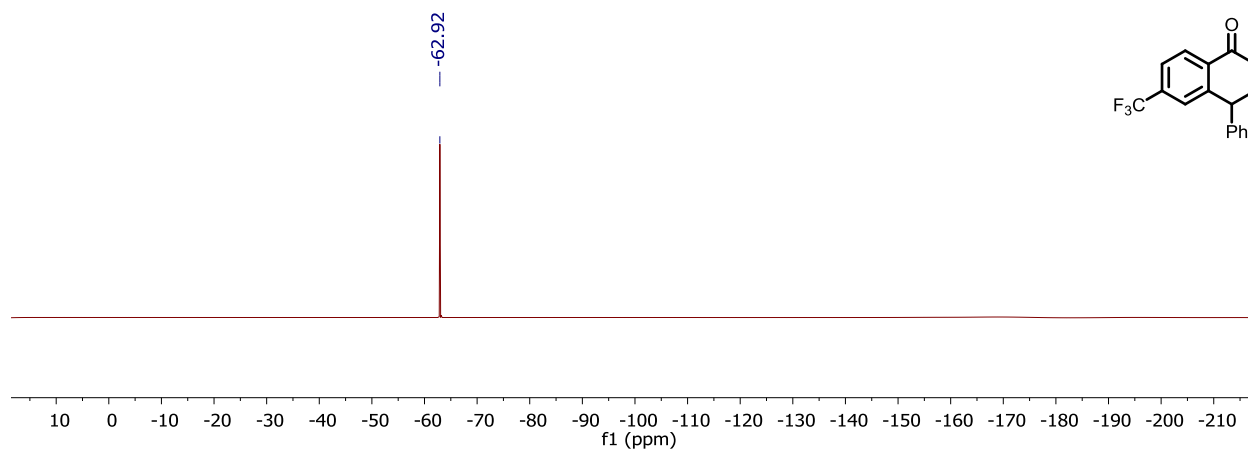

Figure C45. ^{1}H NMR spectrum of **9** in chloroform-*d*.
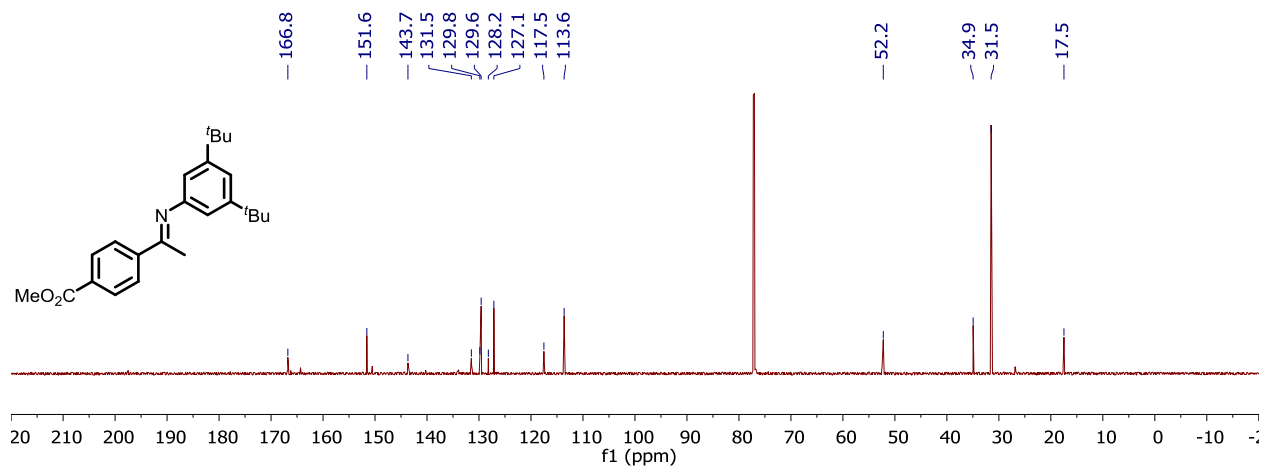
Figure C46. $^{13}C\{^{1}H\}$ NMR spectrum of **9** in chloroform-*d*.
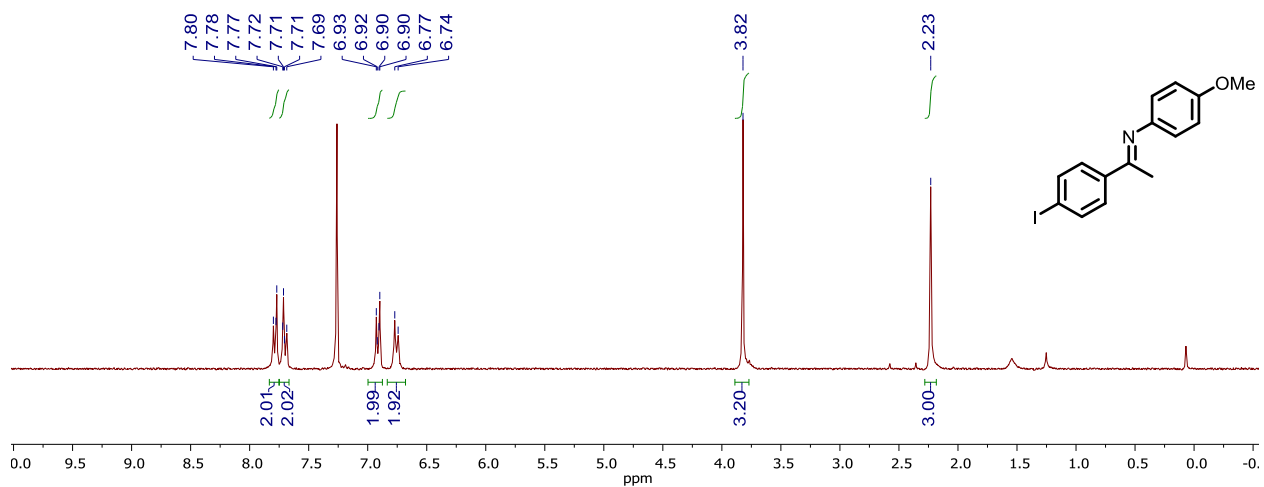
Figure C47. ^{1}H NMR spectrum of **S1** in chloroform-*d*.
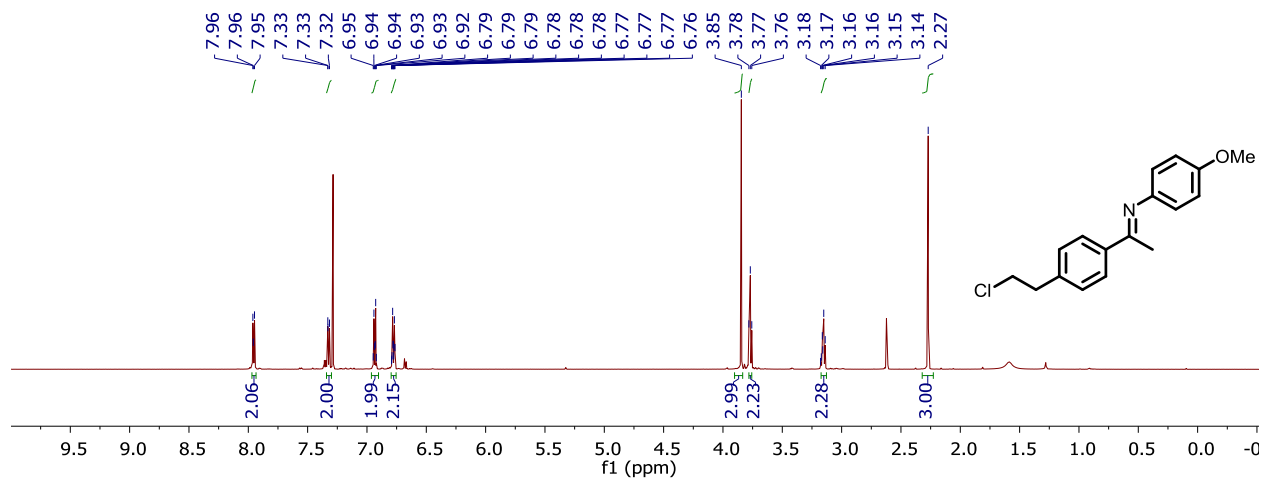
Figure C48. ^{1}H NMR spectrum of **S2** in chloroform-*d*.

Figure C49. ^{13}C{^{1}H} NMR spectrum of **S2** in chloroform-*d*.

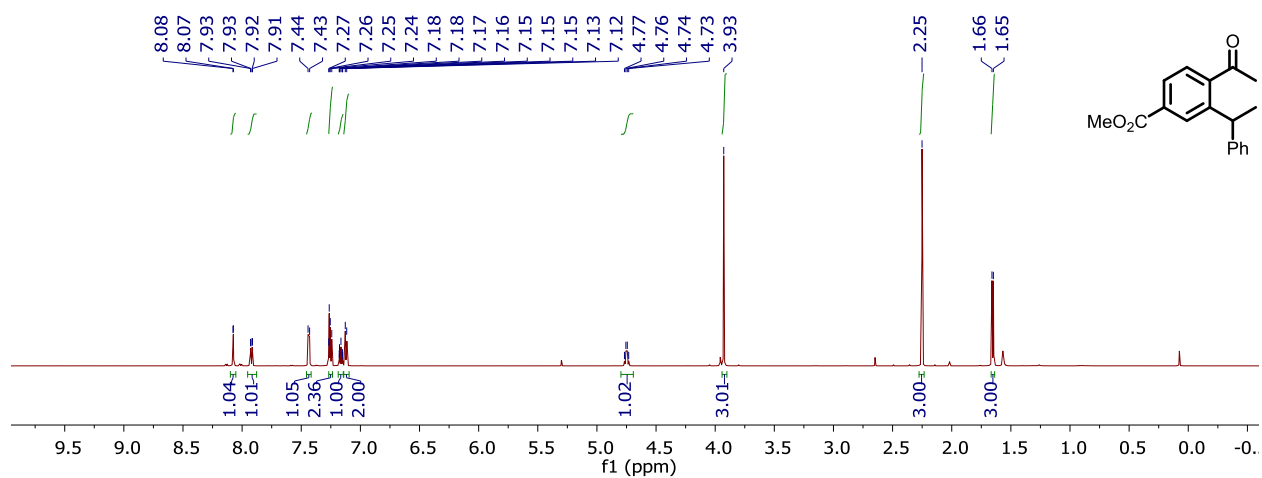**Figure C50.** ^{1}H NMR spectrum of **S3** in chloroform-*d*.

Figure C51. ^{1}H NMR spectrum of **S4** in chloroform-*d*.

Figure C52. ^{13}C{^{1}H} NMR spectrum of **S4** in chloroform-*d*.
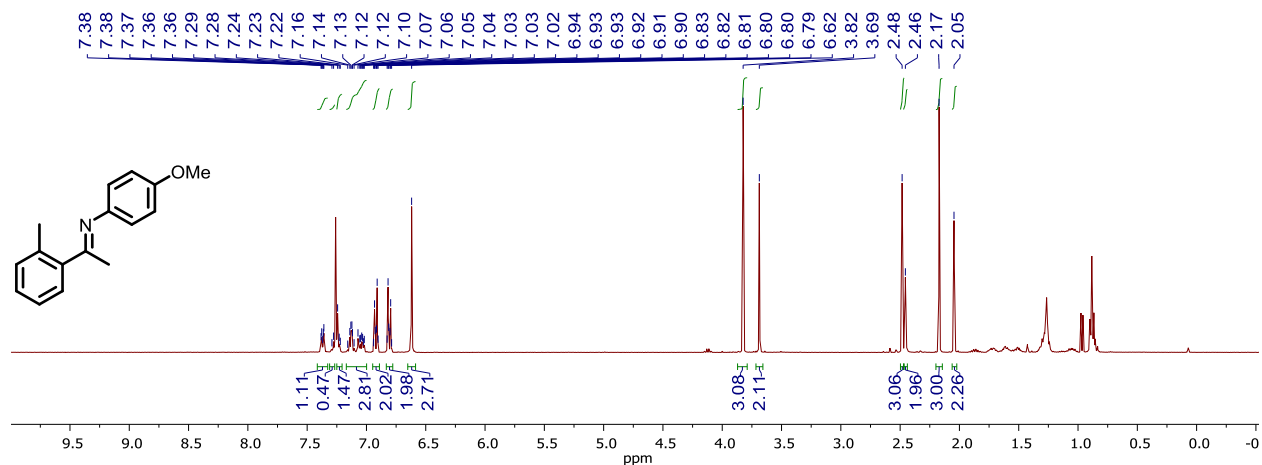
Figure C53. ^{1}H NMR spectrum of **S5** in chloroform-*d*. Note that a 1.4:1.0 mixture of *E/Z*-isomers exists.
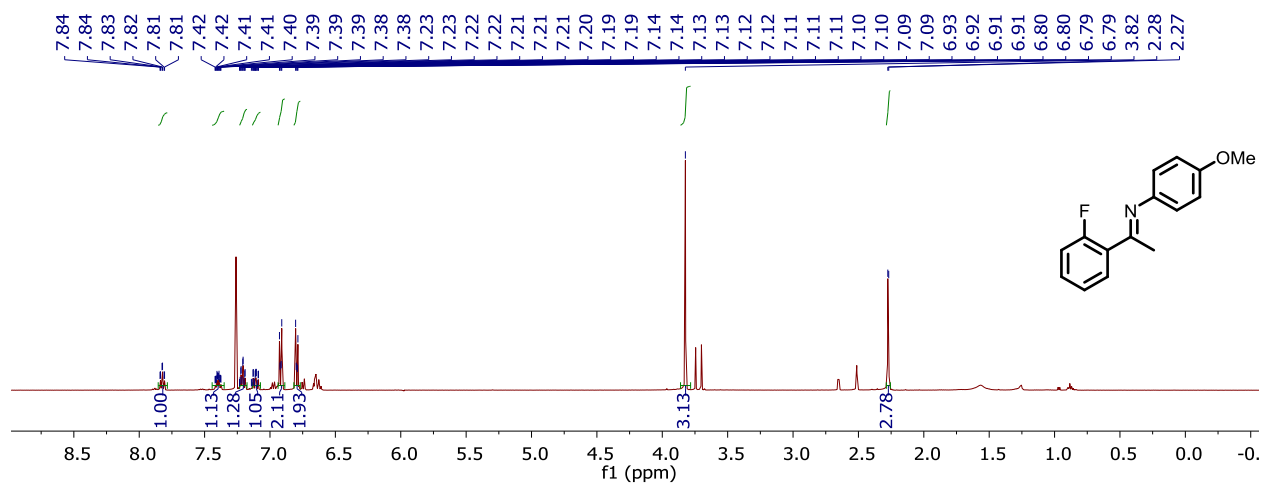
Figure C54. ^{1}H NMR spectrum of **S6** in chloroform-*d*.
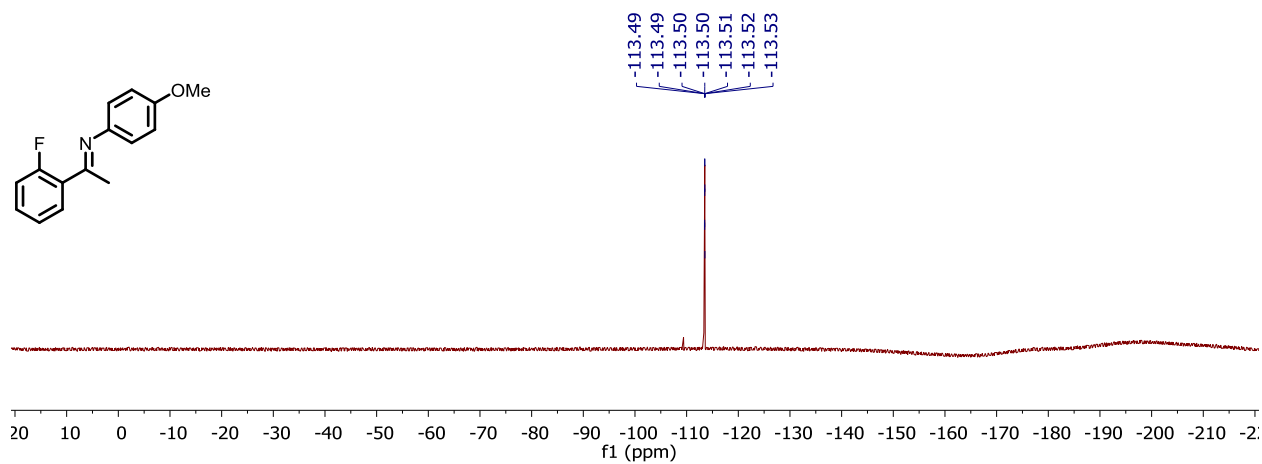
Figure C55. ^{19}F NMR spectrum of **S6** in chloroform-*d*.
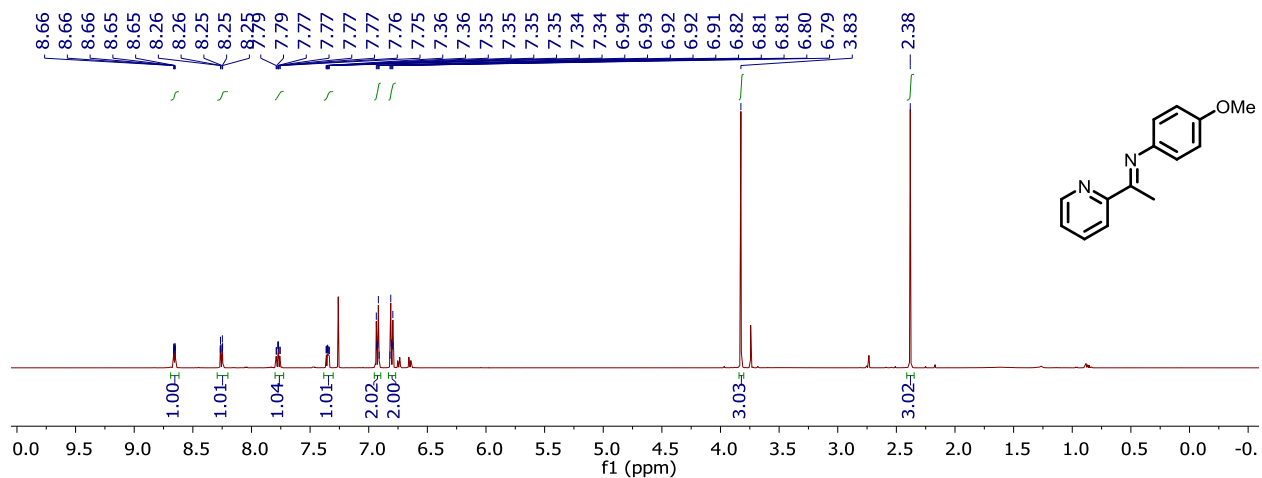
Figure C56. ^{1}H NMR spectrum of **S7** in chloroform-*d*.
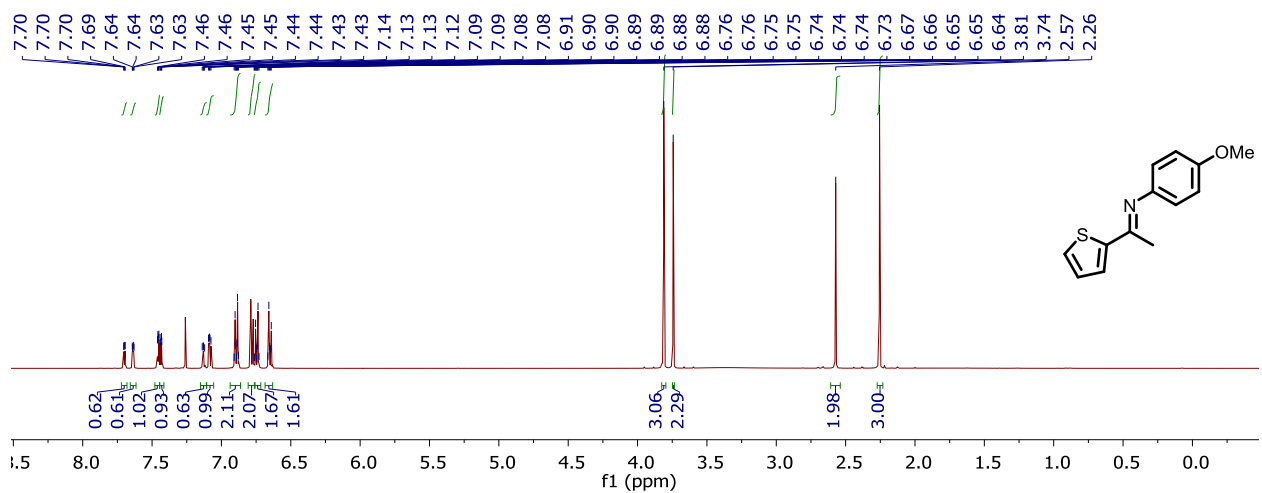
Figure C57. ^{1}H NMR spectrum of **S8** in chloroform-*d*.

NMR SPECTRA OF SYNTHESIZED SUBSTITUTED STYRENE SUBSTRATES
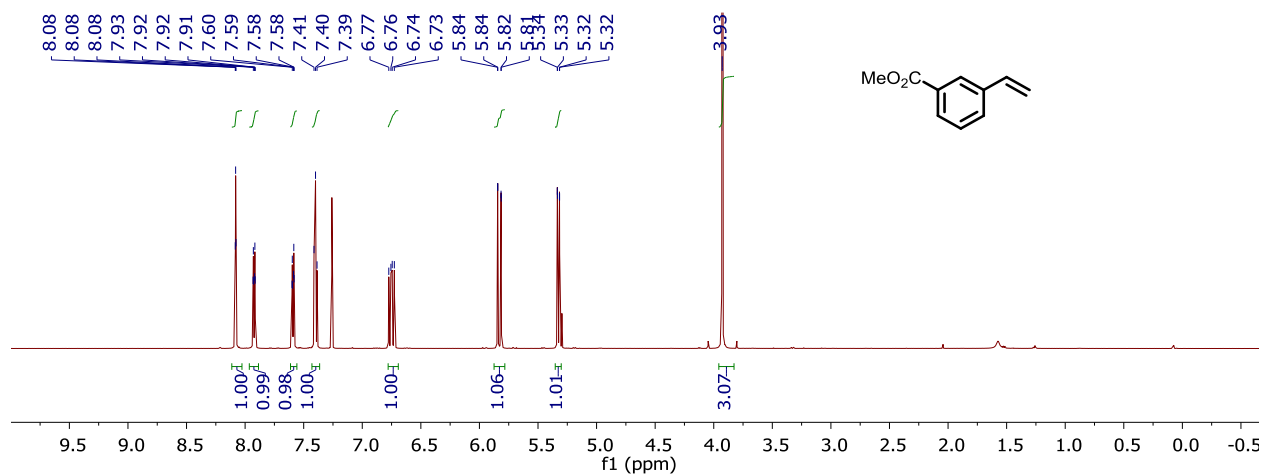
Figure C58. ¹H NMR spectrum of methyl 3-vinylbenzoate (**2k**) in chloroform-*d*.
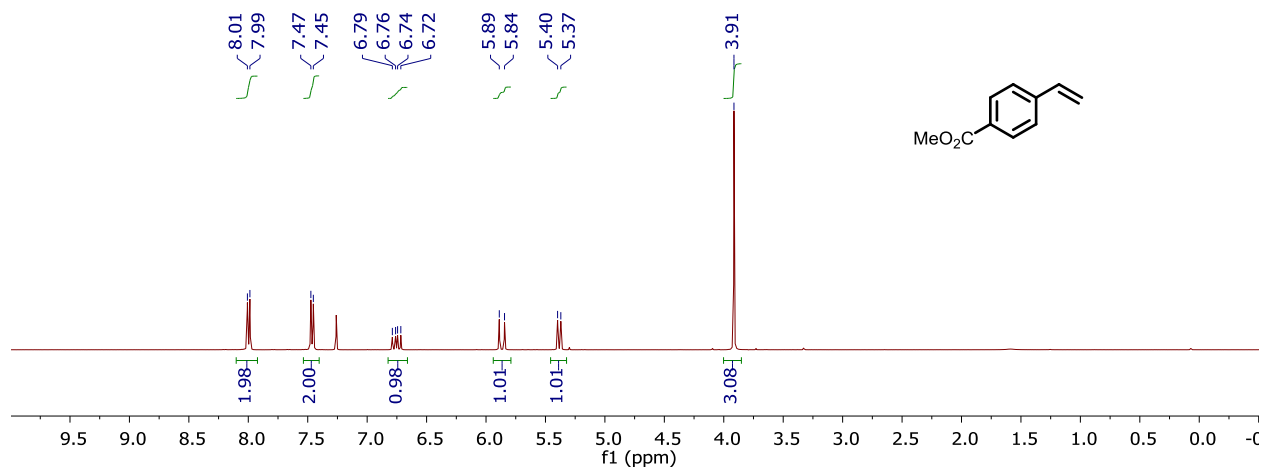
Figure C59. ¹H NMR spectrum of methyl 4-vinylbenzoate (**2l**) in chloroform-*d*.
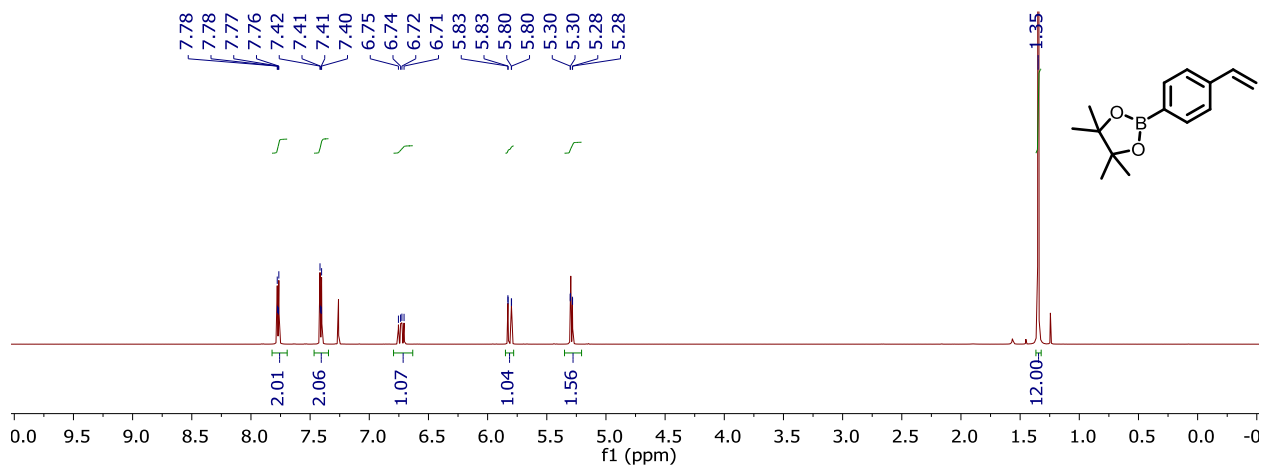
Figure C60. ¹H NMR spectrum of **2m** in chloroform-*d*.

NMR SPECTRA OF HYDROARYLATION PRODUCTS
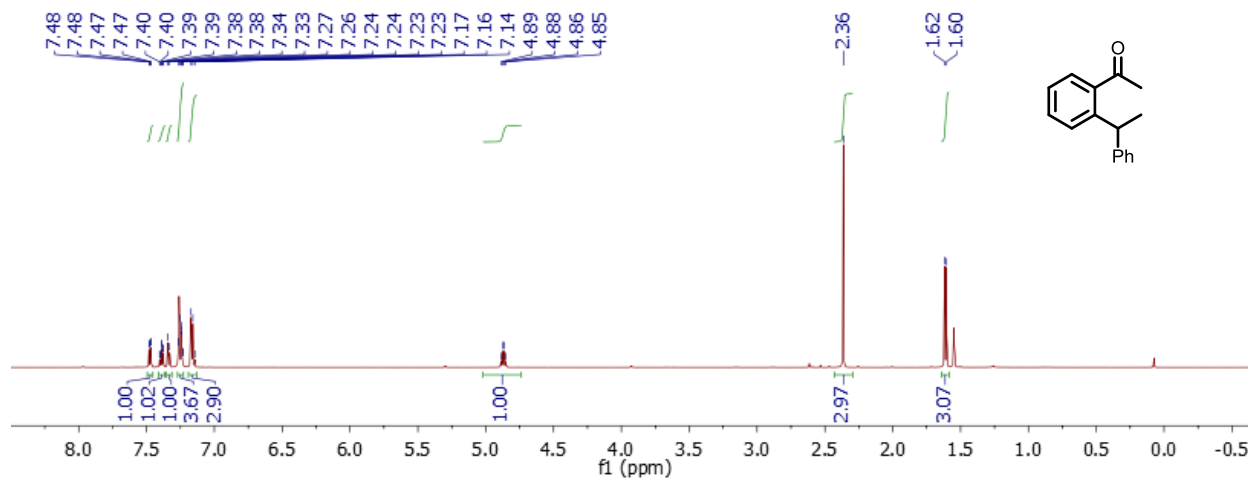
Figure C61. ¹H NMR spectrum of **3Aa** in chloroform-*d*.
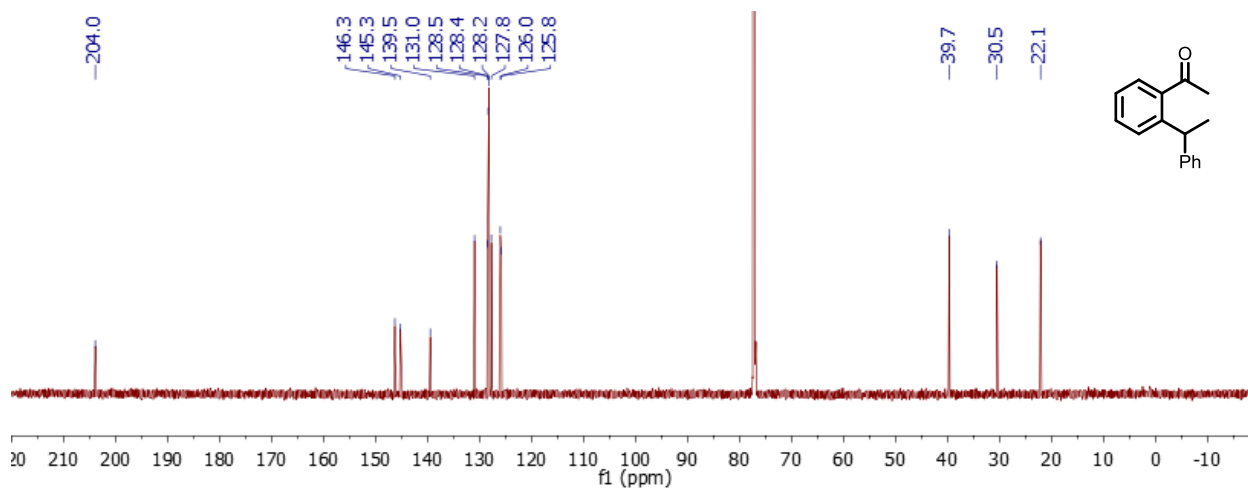
Figure C62. ¹³C{¹H} NMR spectrum of **3Aa** in chloroform-*d*.
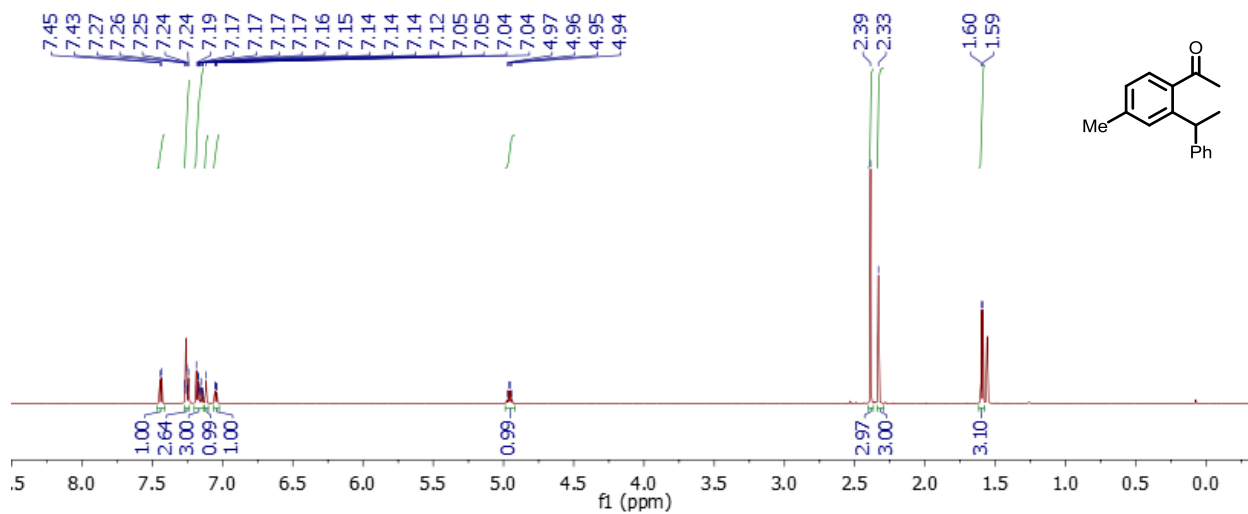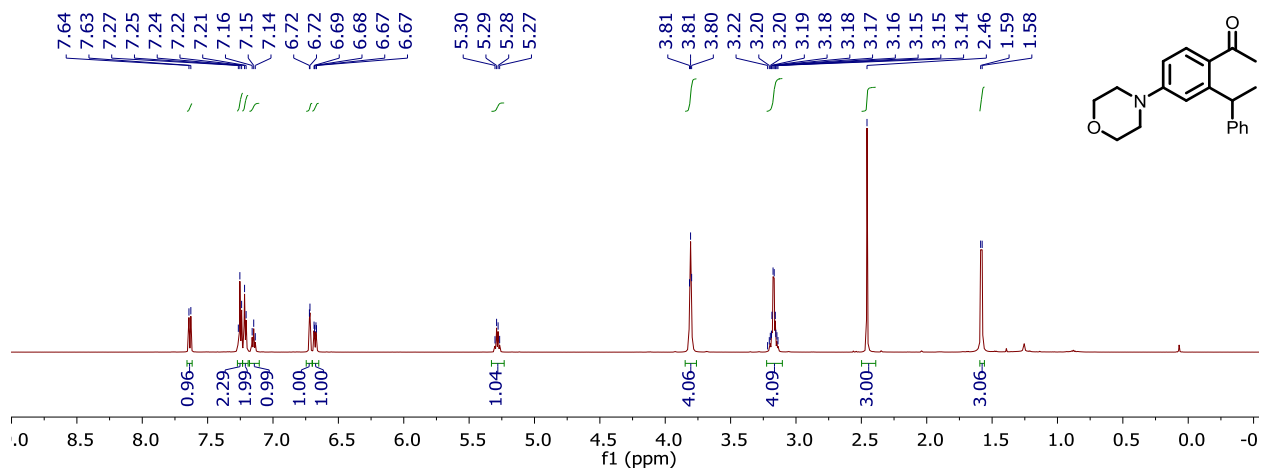

Figure C63. ¹H NMR spectrum of **3Ba** in chloroform-*d*.
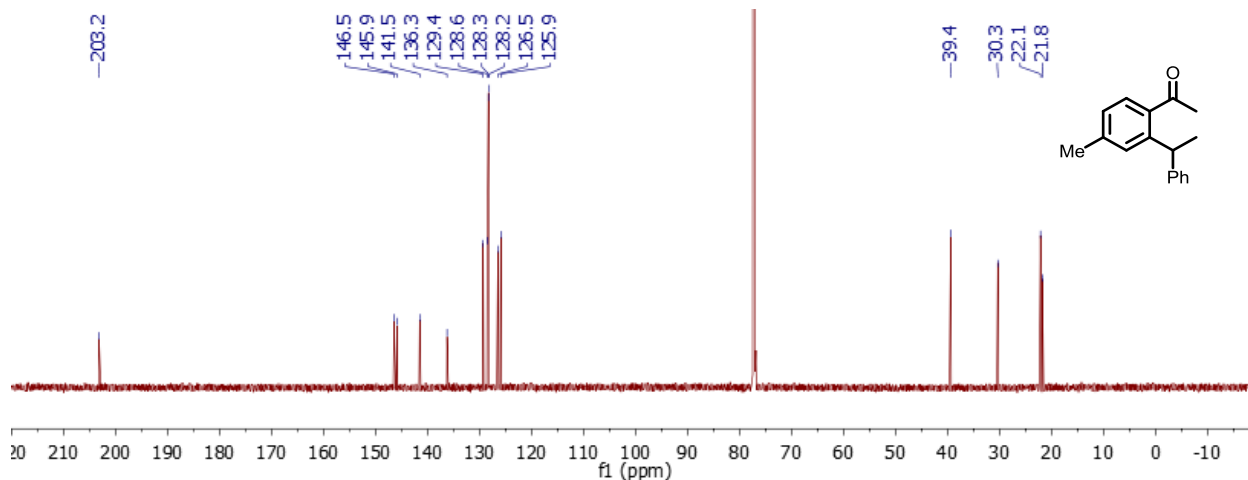
Figure C64. ^{13}C{^{1}H} NMR spectrum of **3Ba** in chloroform-*d*.
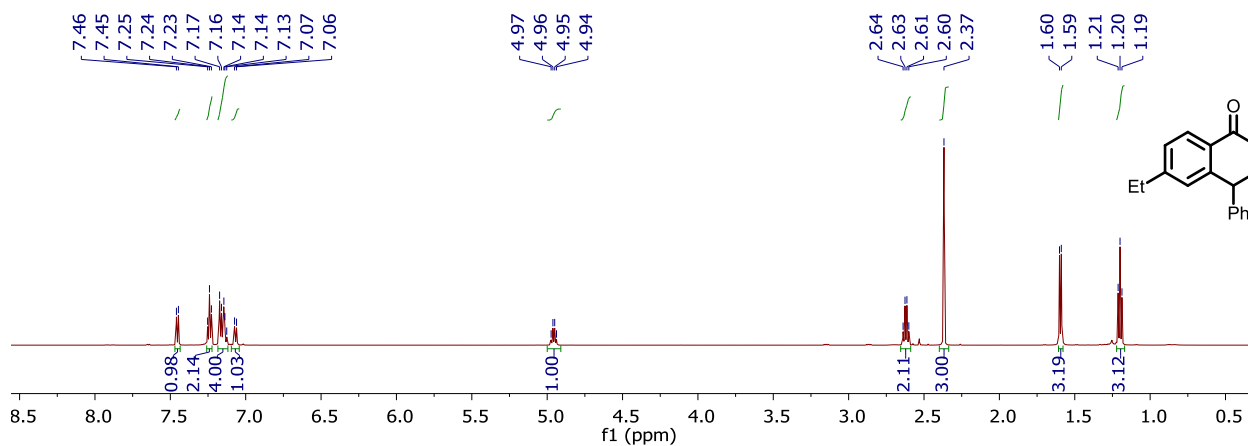
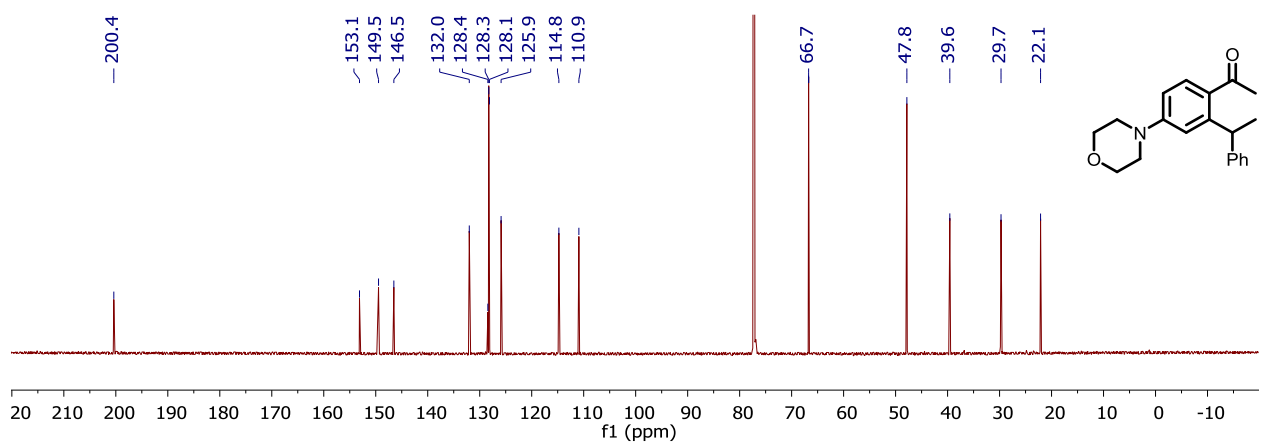**Figure C65.** ^{1}H NMR spectrum of **3Ca** in chloroform-*d*.
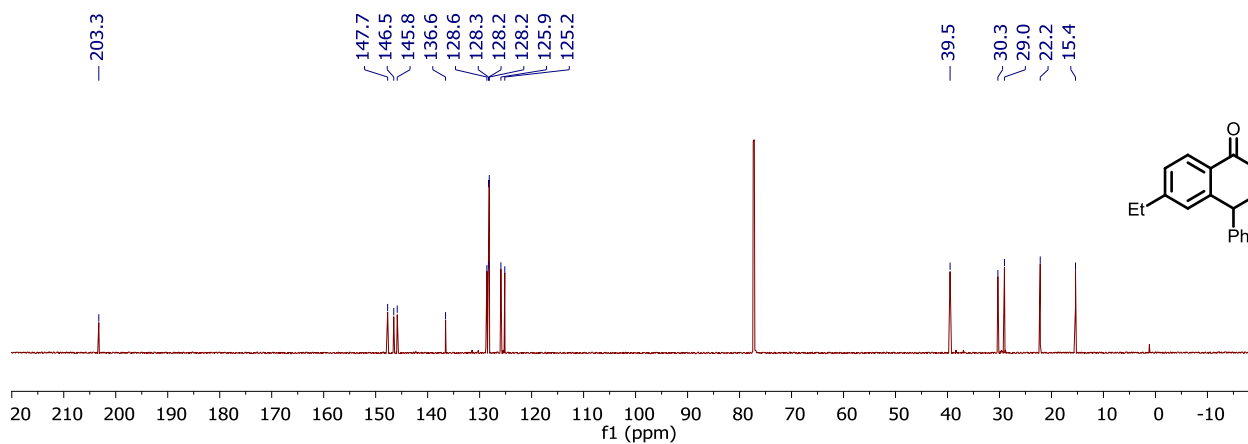
Figure C66. ^{13}C{^{1}H} NMR spectrum of **3Ca** in chloroform-*d*.
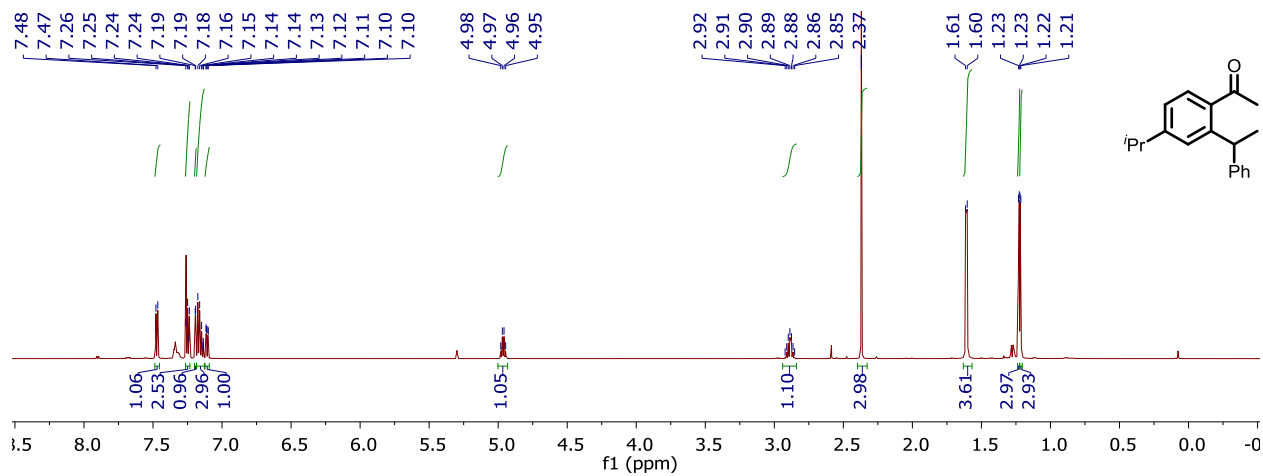
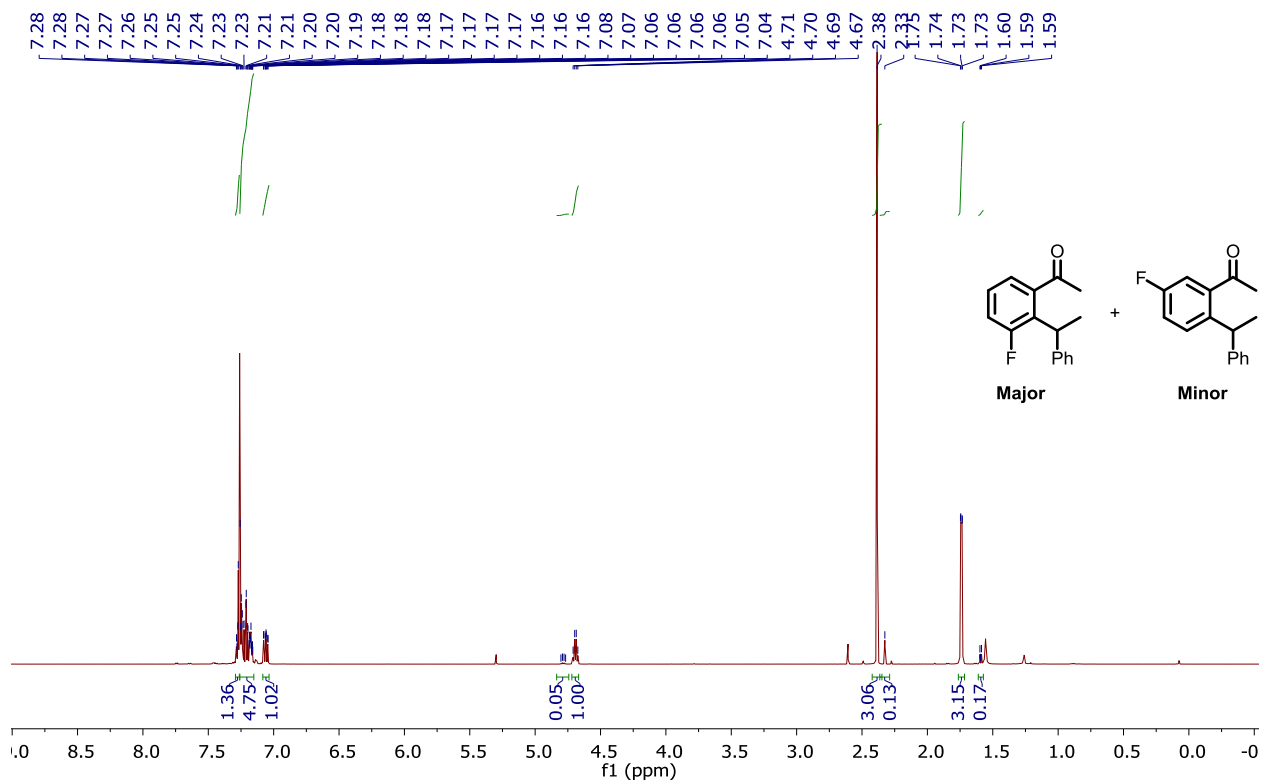**Figure C67.** ^{1}H NMR spectrum of **3Da** in chloroform-*d*.
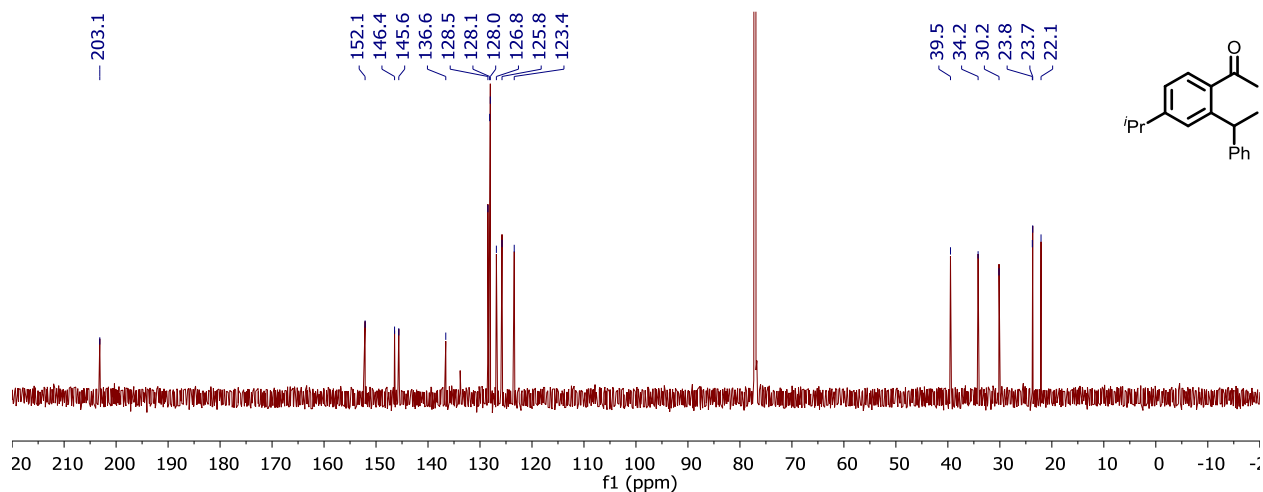
Figure C68. ^{13}C{^{1}H} NMR spectrum of **3Da** in chloroform-*d*.
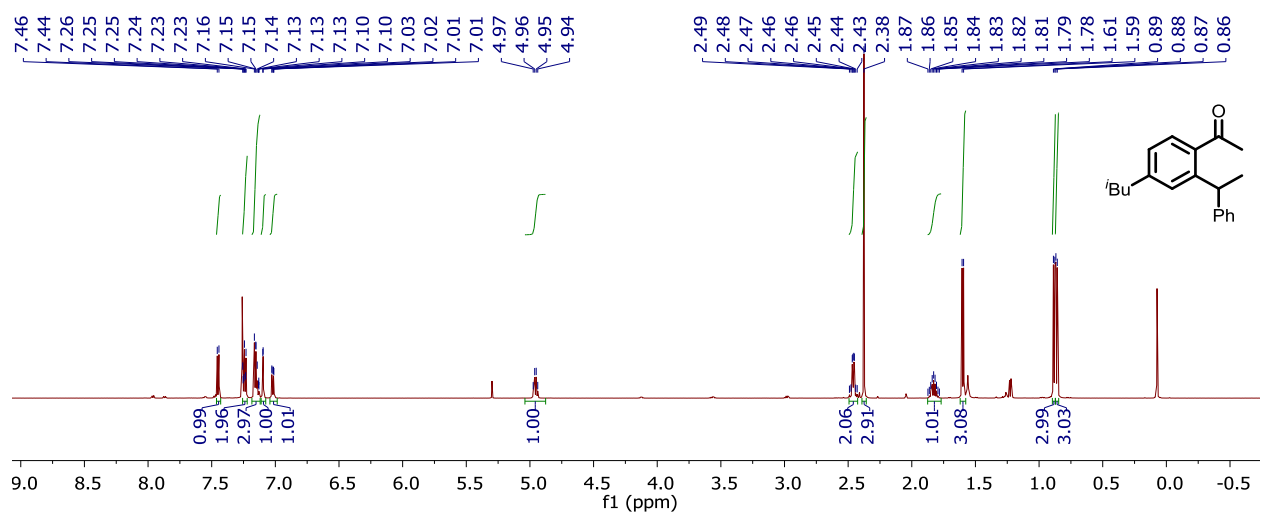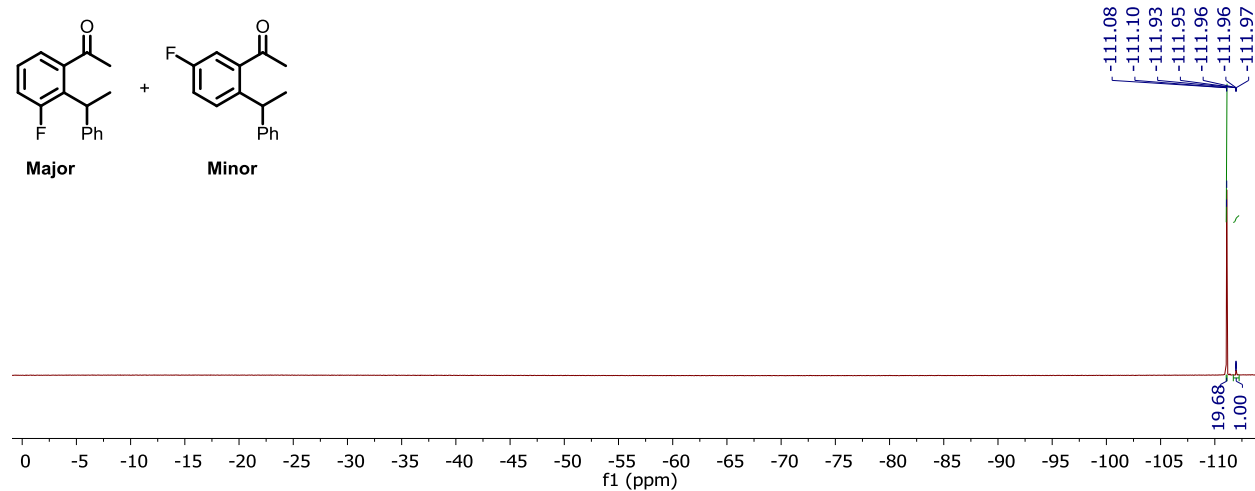

Figure C69. ^{1}H NMR spectrum of **3Ea** in chloroform-*d*.
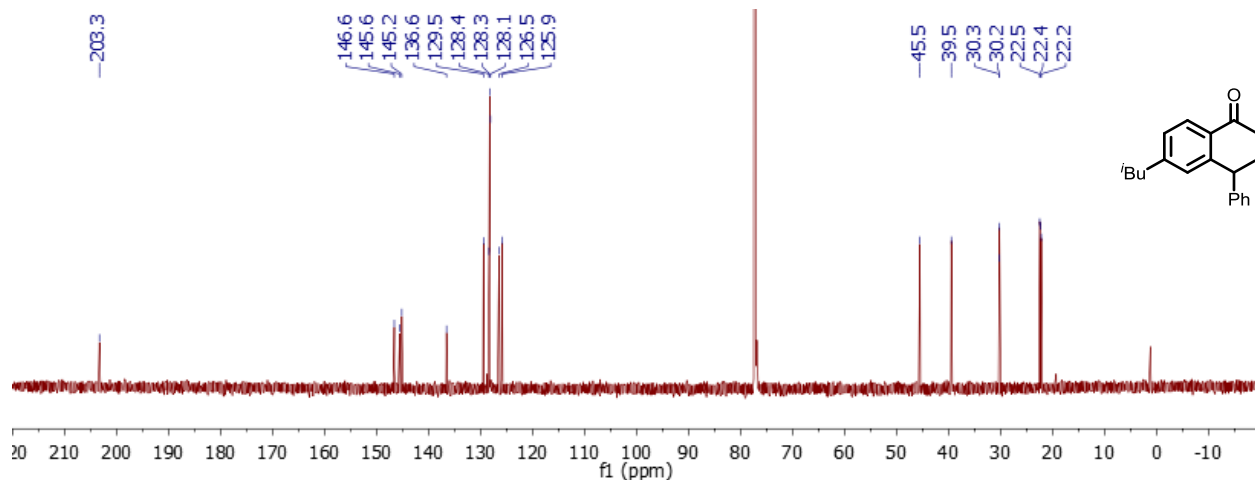
Figure C70. $^{13}C\{^1H\}$ NMR spectrum of **3Ea** in chloroform-*d*.
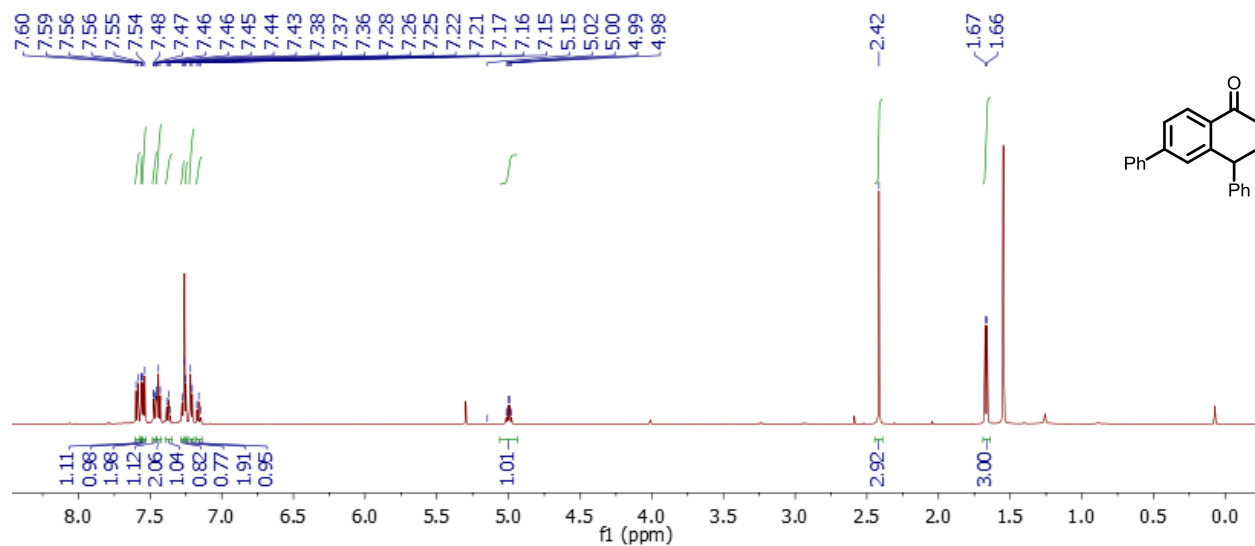
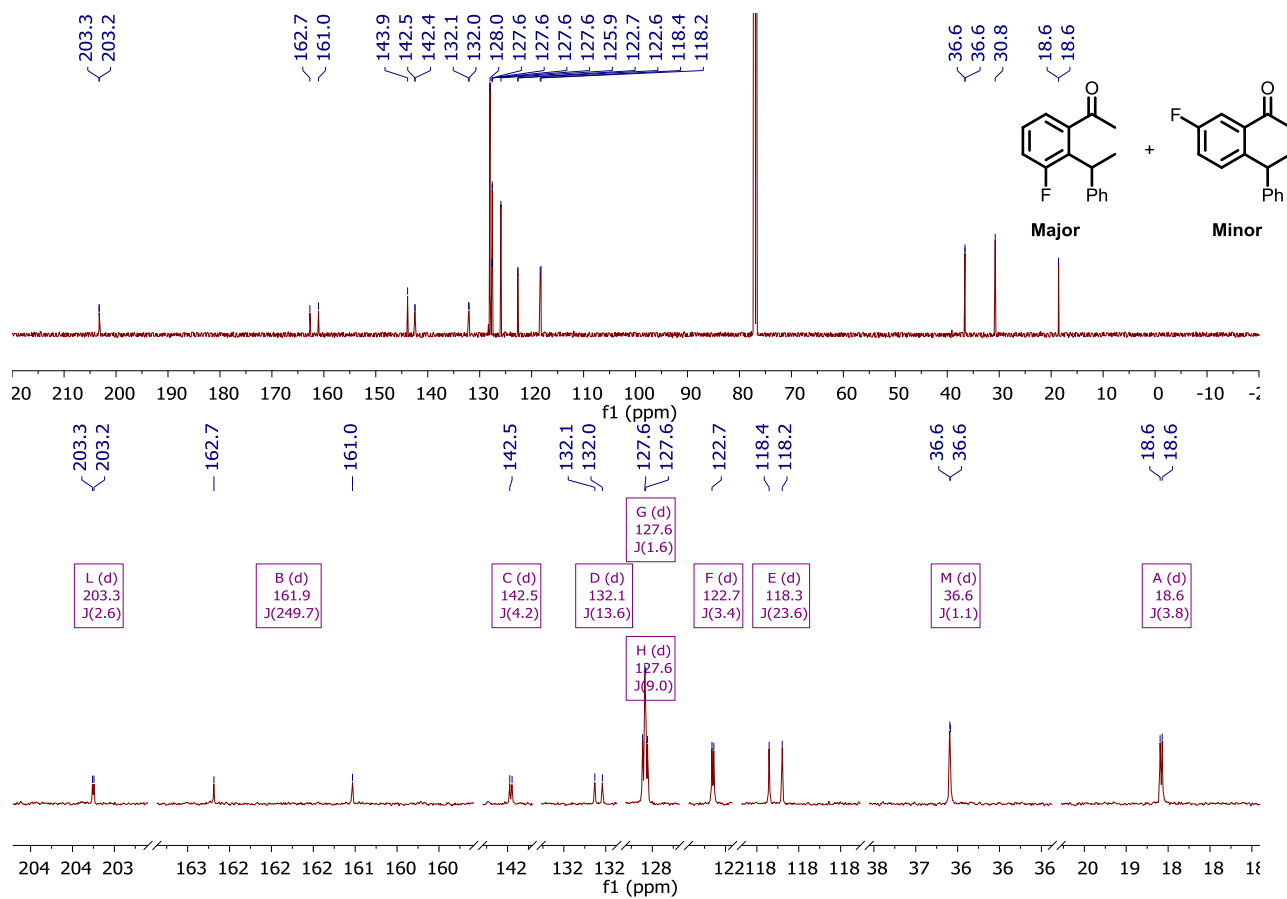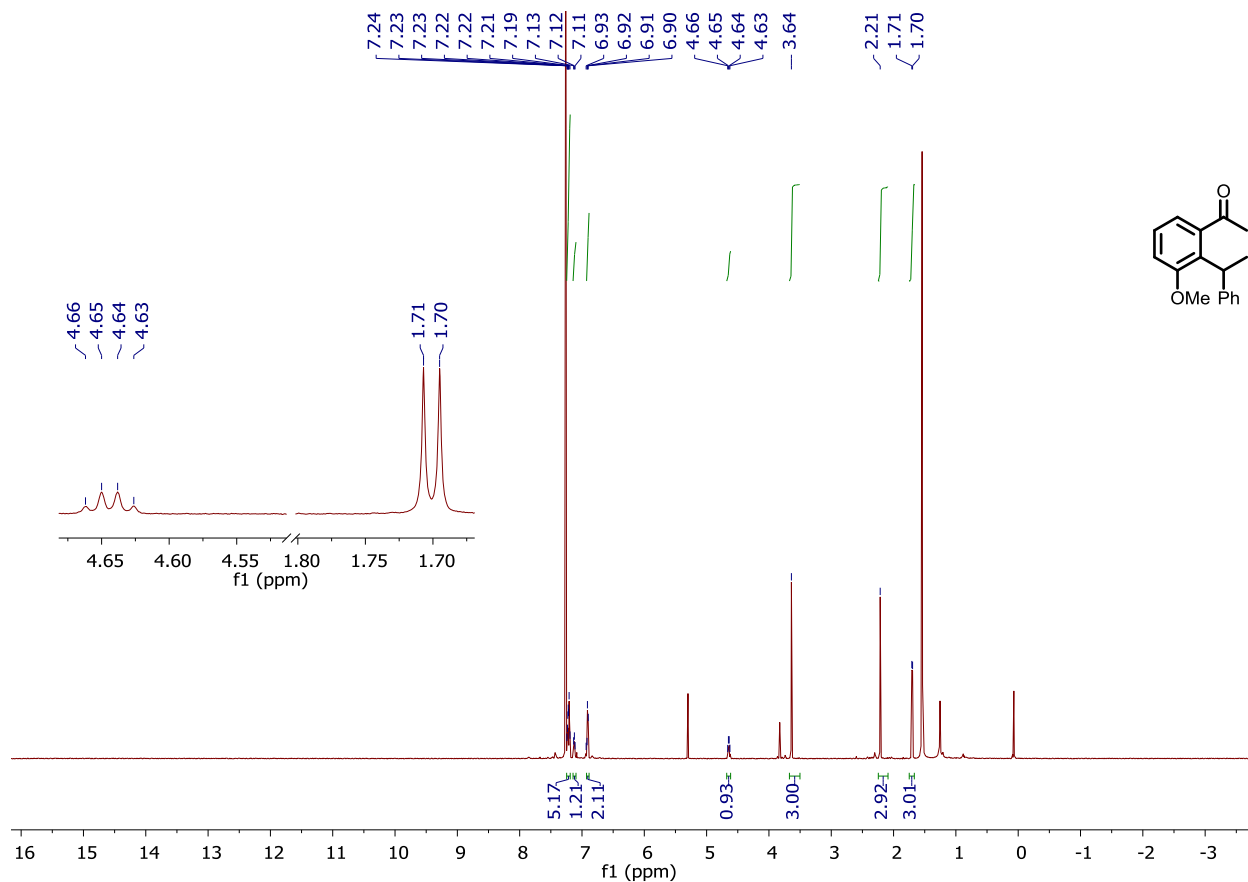**Figure C71.** ^1H NMR spectrum of **3Fa** in chloroform-*d*.
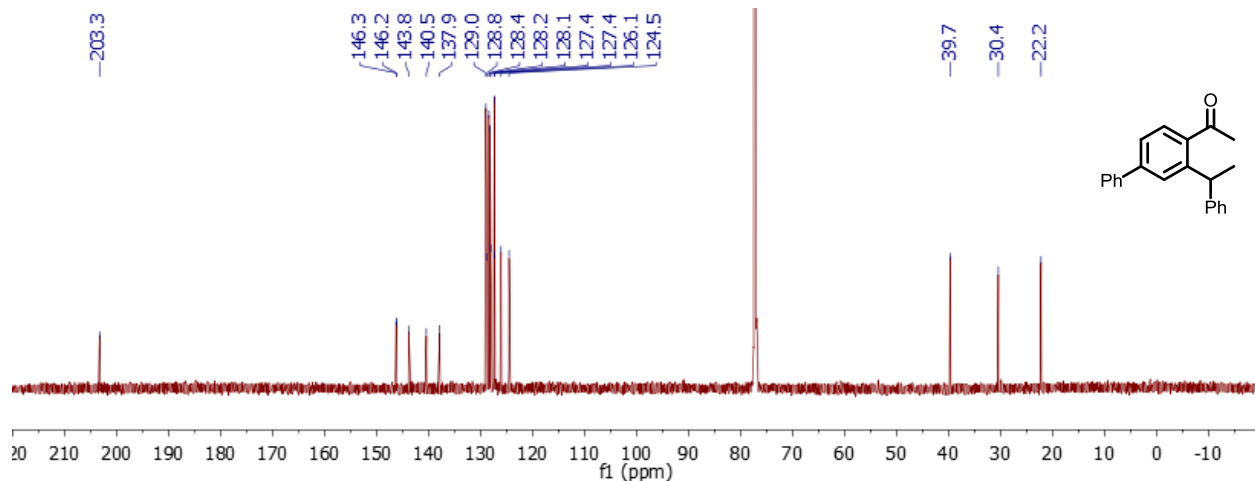
Figure C72. $^{13}C\{^1H\}$ NMR spectrum of **3Fa** in chloroform-*d*.
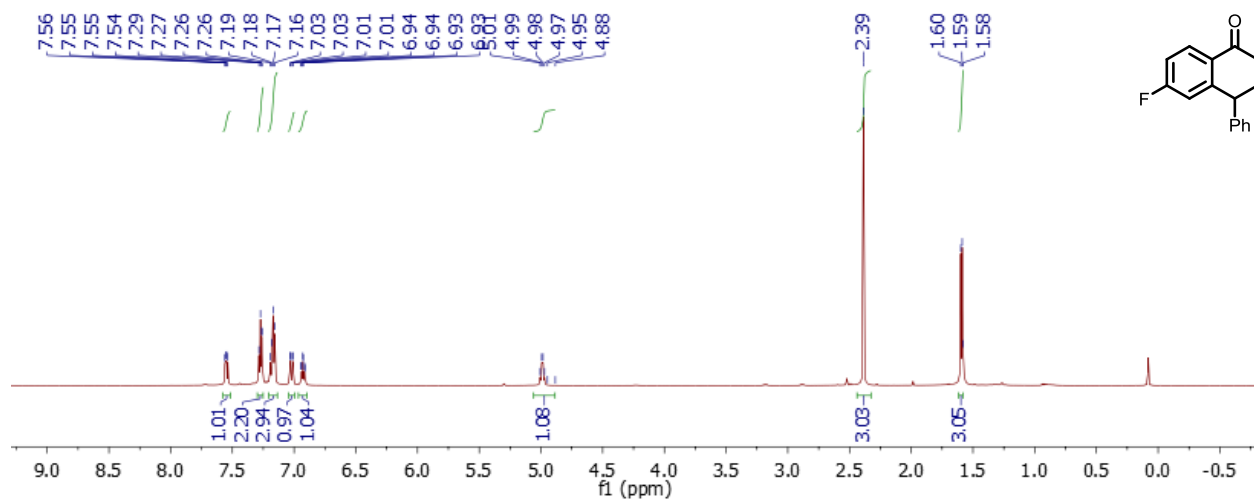
Figure C73. ¹H NMR spectrum of **3Ga** in chloroform-*d*.

Figure C74. ¹³C{¹H} NMR spectrum of **3Ga** in chloroform-*d*. **Inset**: expansion of peaks with $^nJ_{CF}$ couplings (n = 1, 2, 3, or 4).
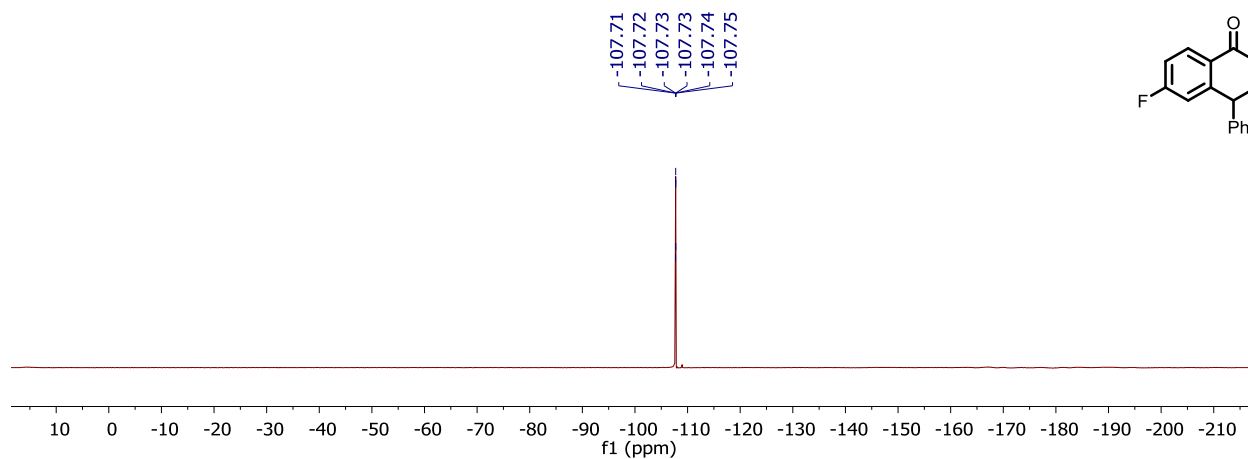
Figure C75. ^{19}F NMR spectrum of **3Ga** in chloroform-*d*.
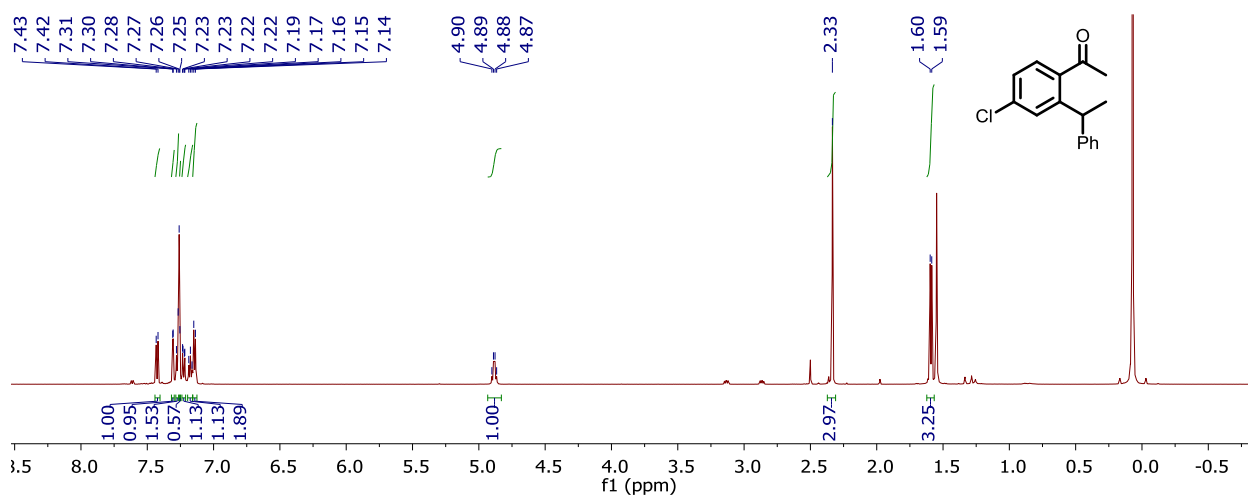
Figure C76. ^{1}H NMR spectrum of **3Ha** in chloroform-*d*.
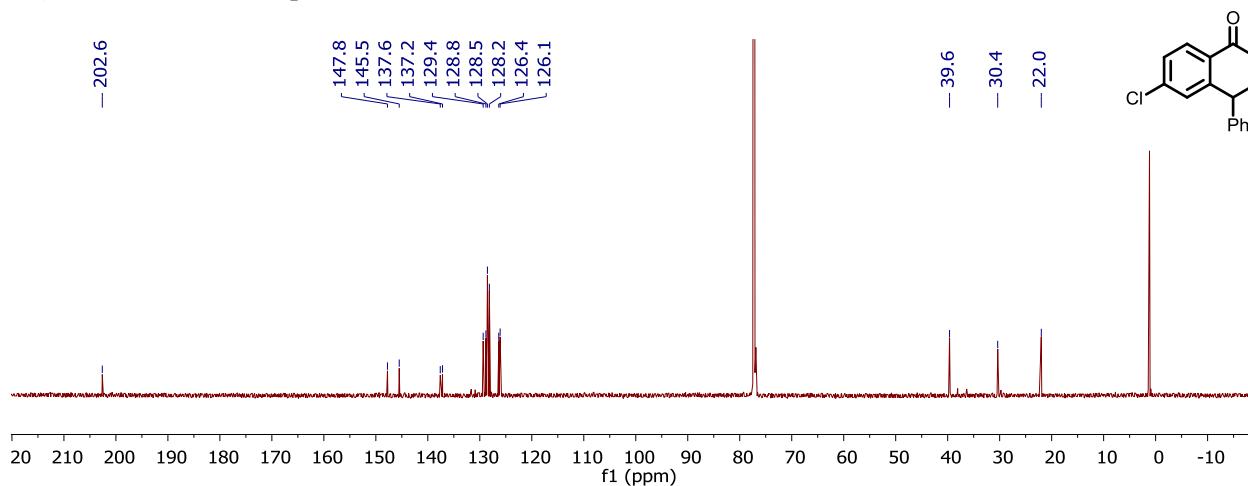
Figure C77. ^{13}C{^{1}H} NMR spectrum of **3Ha** in chloroform-*d*.
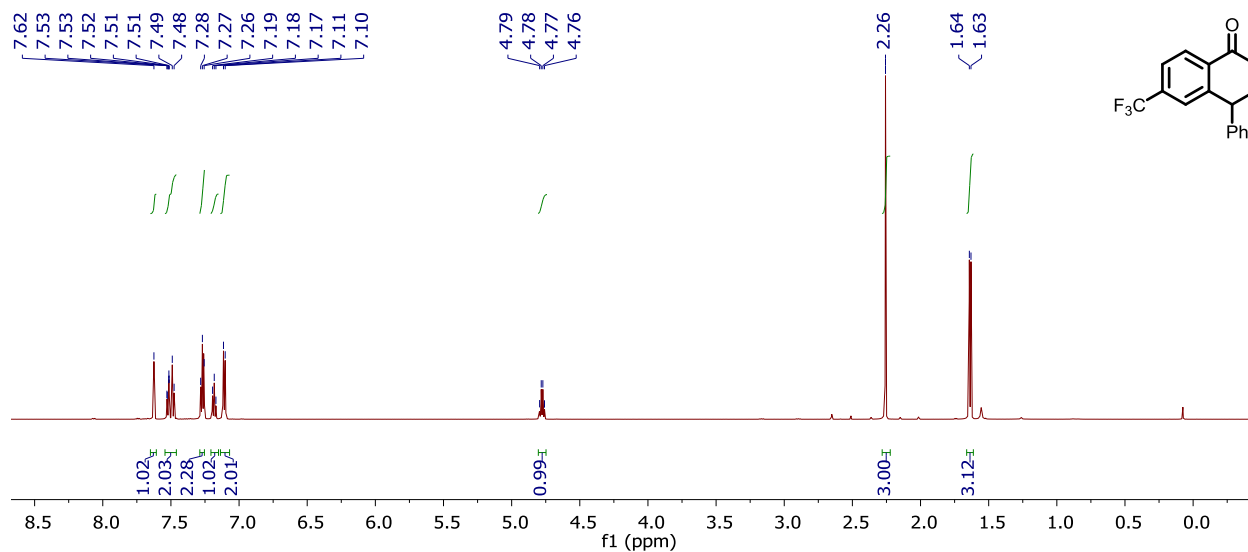
Figure C78. ¹H NMR spectrum of **3Ja** in chloroform-*d*.
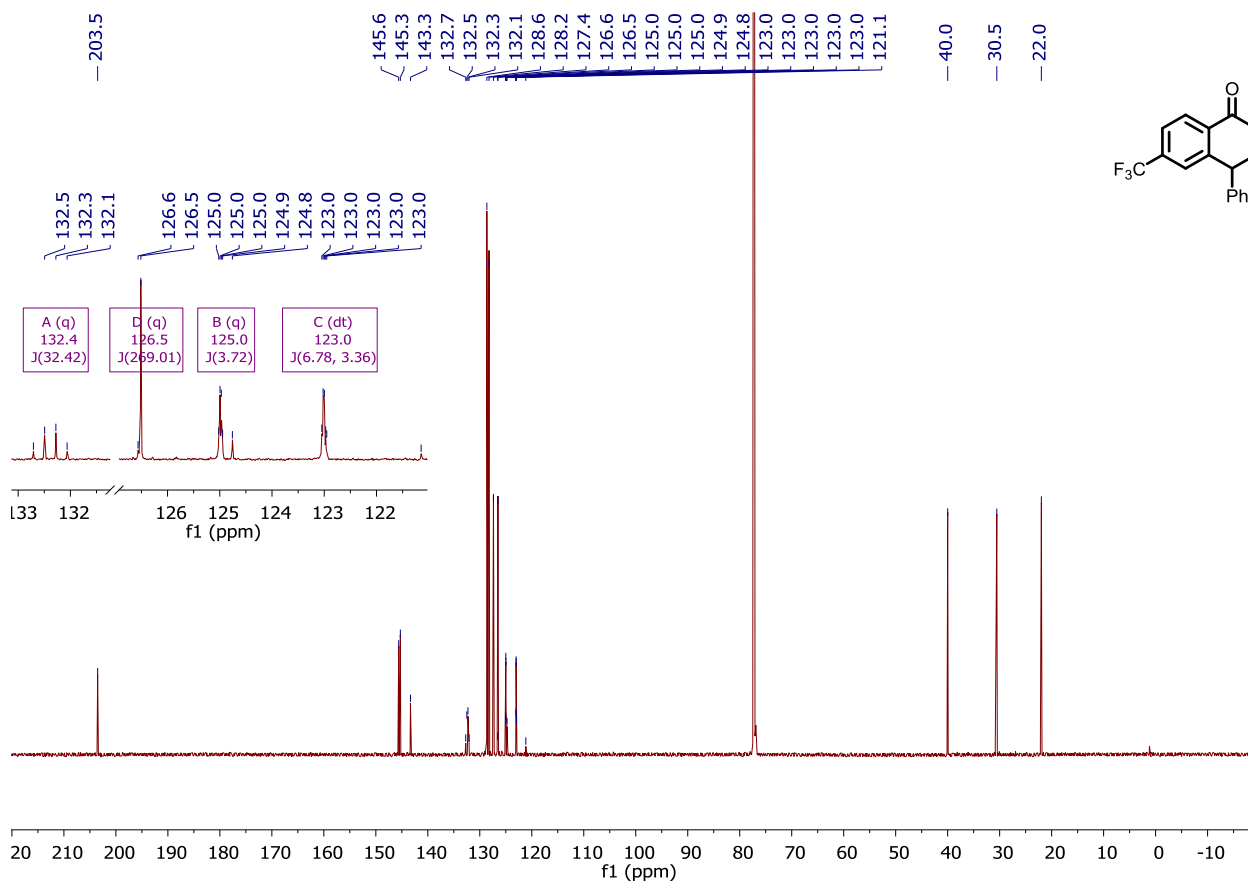
Figure C79. ¹³C{¹H} NMR spectrum of **3Ja** in chloroform-*d*. **Inset**: expansion of peaks with $^nJ_{CF}$ couplings (n = 1, 2, or 3).

Figure C80. ^{19}F NMR spectrum of **3Ja** in chloroform-*d*.

Figure C81. ^{1}H NMR spectrum of **3Ka** in chloroform-*d*.

Figure C82. ^{13}C{^{1}H} NMR spectrum of **3Ka** in chloroform-*d*.
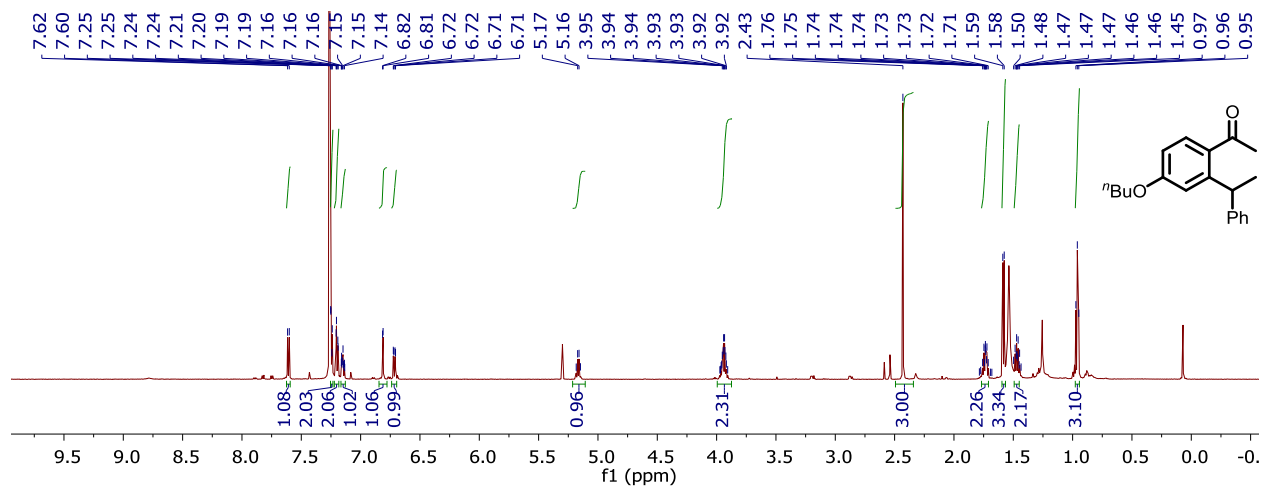
Figure C83. ^{1}H NMR spectrum of **3La** in chloroform-*d*.
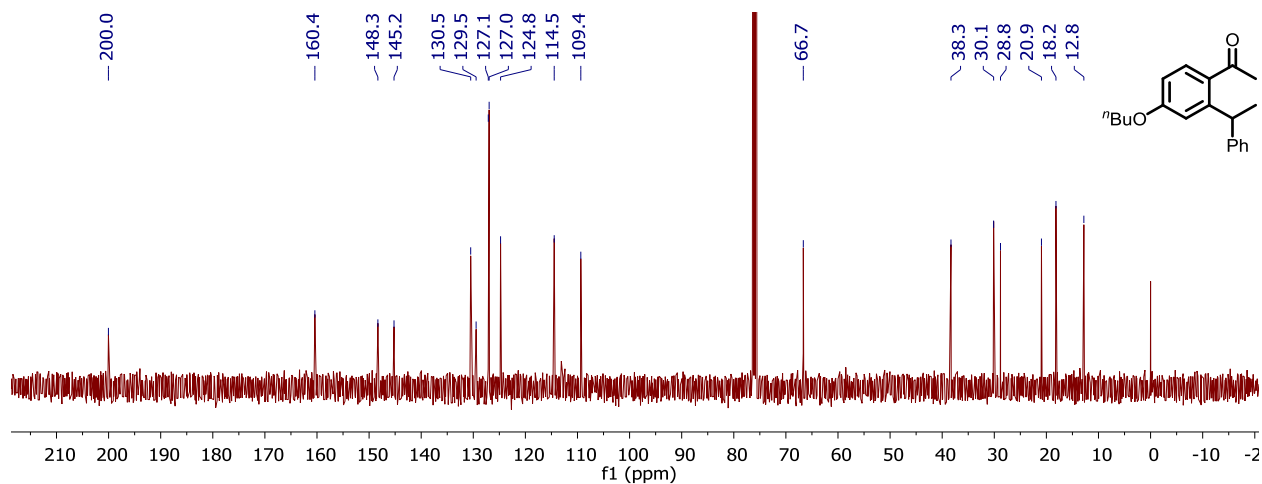
Figure C84. ^{13}C{^{1}H} NMR spectrum of **3La** in chloroform-*d*.

Figure C85. ^{1}H NMR spectrum of **3Ma** in chloroform-*d*.
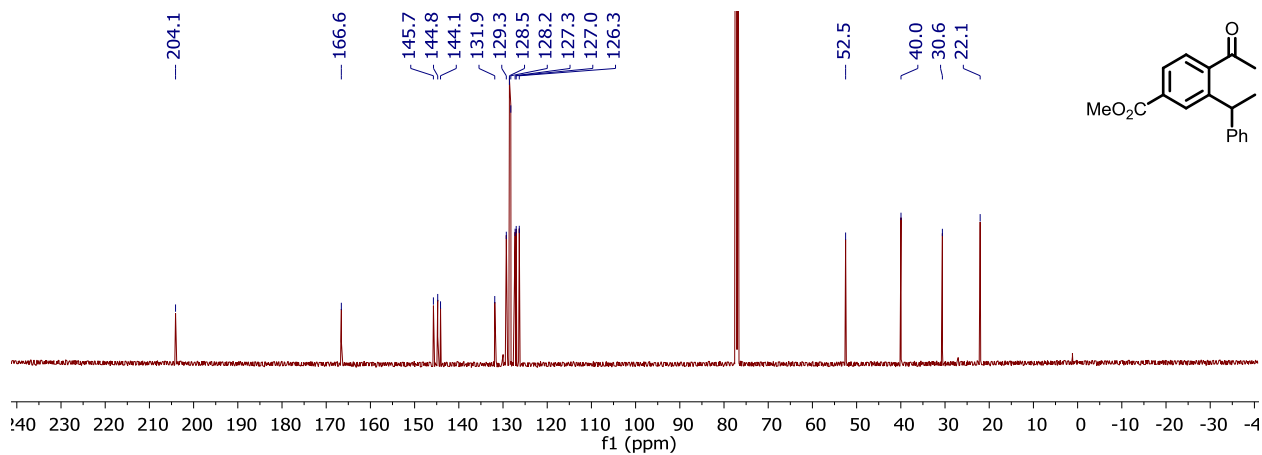
Figure C86. $^{13}C\{^1H\}$ NMR spectrum of **3Ma** in chloroform-*d*.
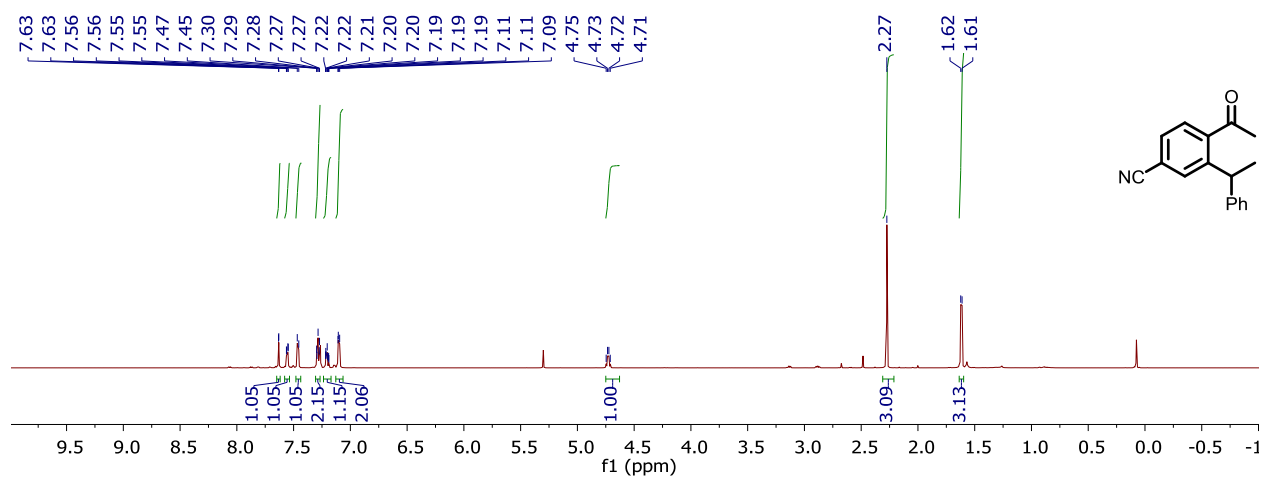
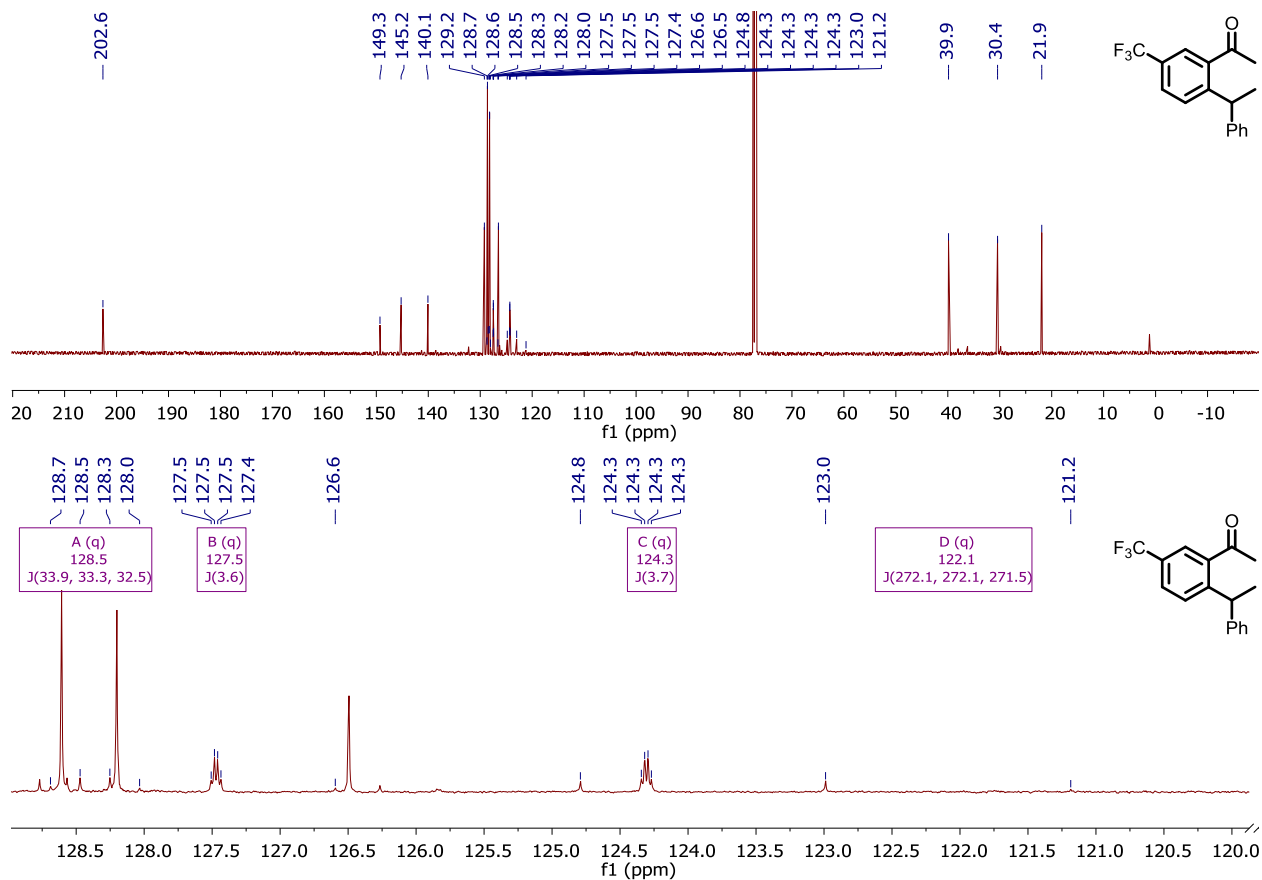**Figure C87.** ^1H NMR spectrum of **3Na** in chloroform-*d*.
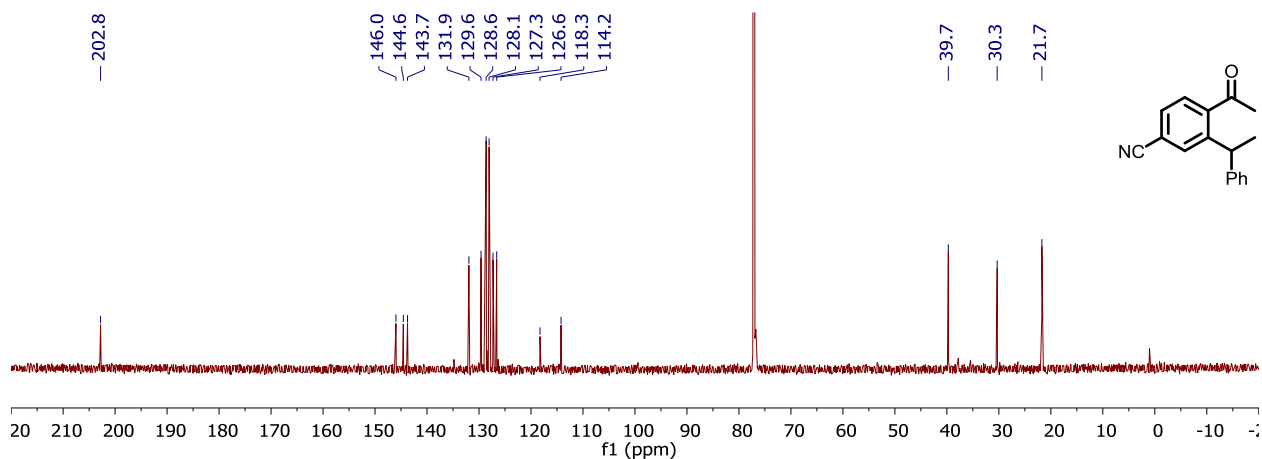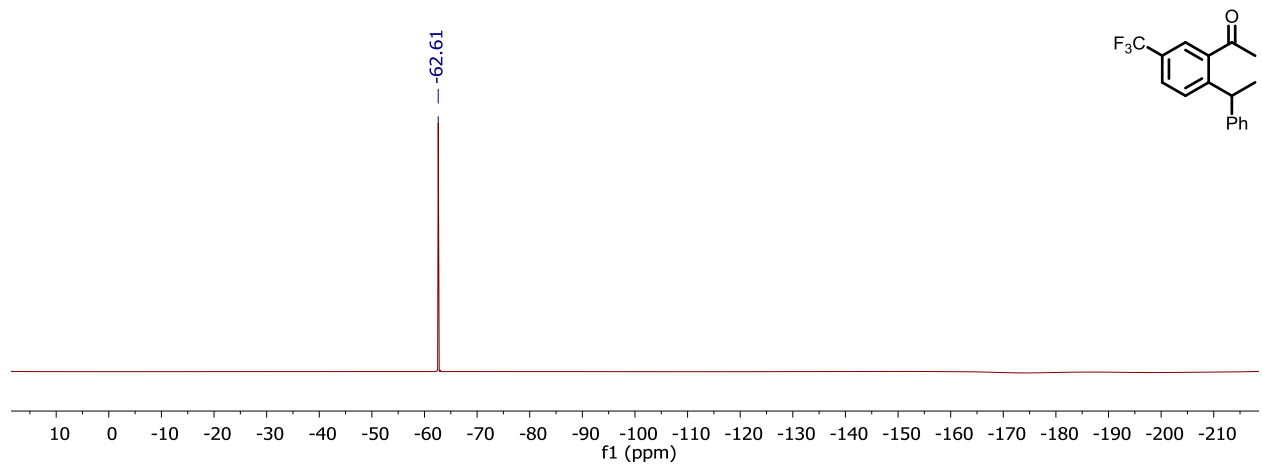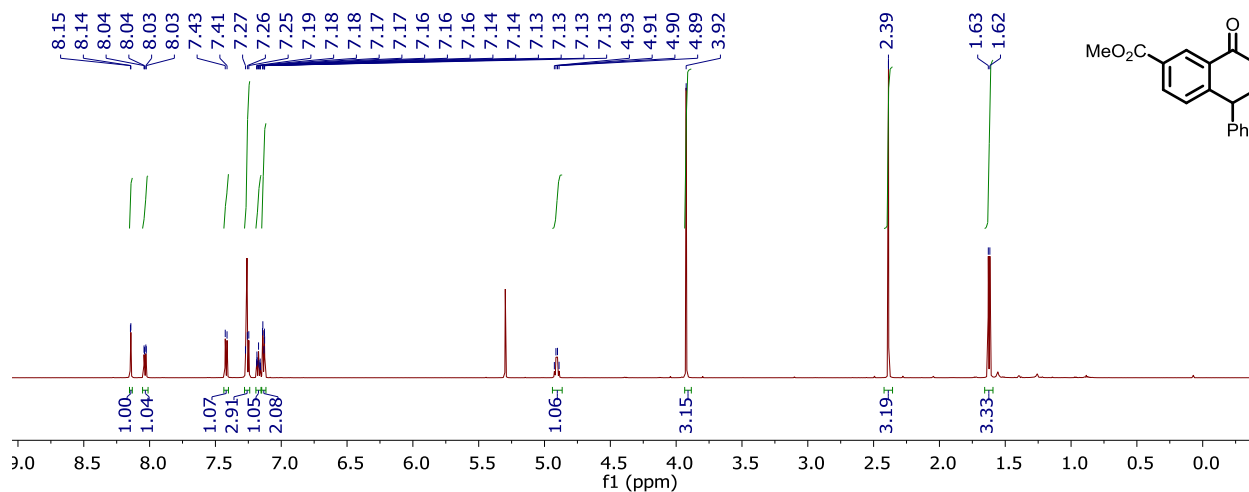

Figure C88. $^{13}C\{^1H\}$ NMR spectrum of **3Na** in chloroform-*d*.

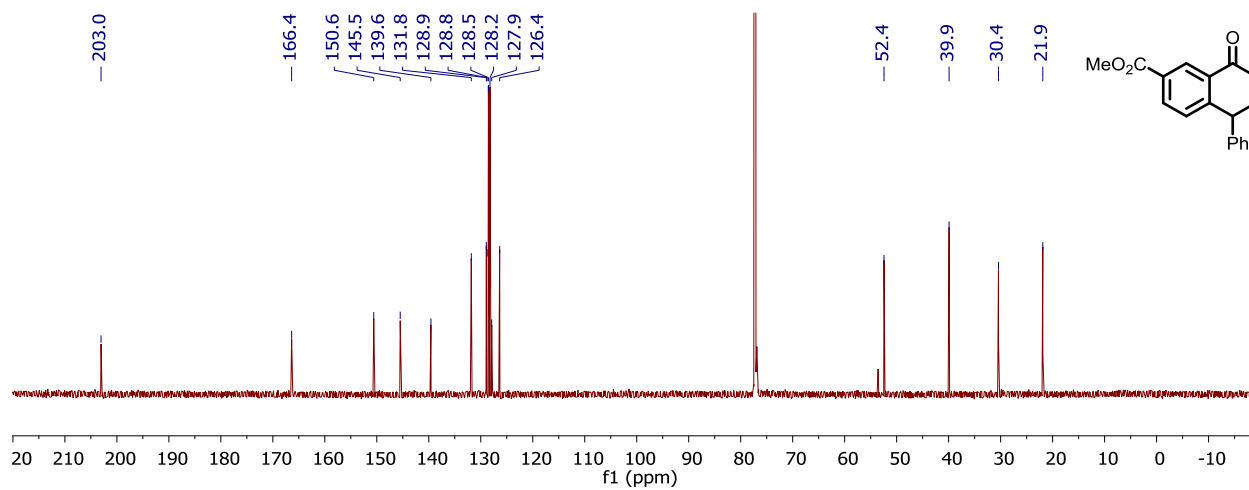**Figure C89.** ^{1}H NMR spectrum of **3Oa** in chloroform-*d*.

Figure C90. ^{13}C{^{1}H} NMR spectrum of **3Oa** in chloroform-*d*.

Figure C91. ¹H NMR spectrum of **3Pa** and **3Pa'** in chloroform-*d* as a mix of two isomers resulting from C–H activation at either the 2' or 6' aryl position.

Figure C92. $^{13}C\{^1H\}$ NMR spectrum of **3Pa** and **3Pa'** in chloroform-*d*. **Bottom**: expansion of peaks with $^nJ_{CF}$ couplings (n = 1, 2, 3, or 4).

Figure C93. ^{19}F NMR spectrum of **3Pa** and **3Pa'** in chloroform-*d*.

Figure C94. Crude ¹H NMR spectrum of **3Qa** in chloroform-*d*. **Inset:** Expansion of resonances corresponding to the phenylethyl aliphatic methine and methyl protons of **3Qa**.
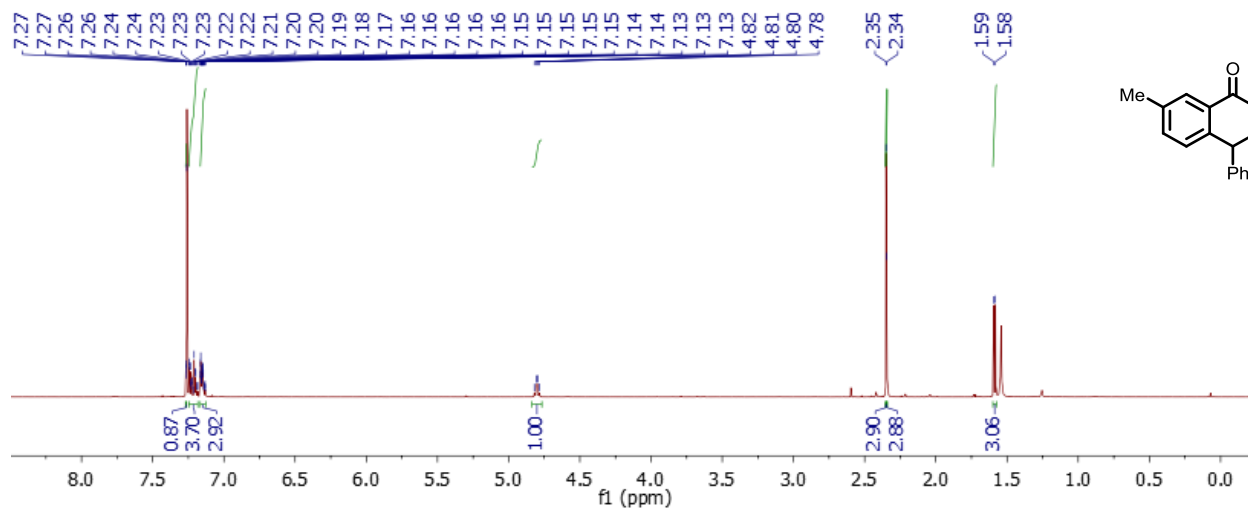
Figure C95. ¹H NMR spectrum of **3Ra** in chloroform-*d*.
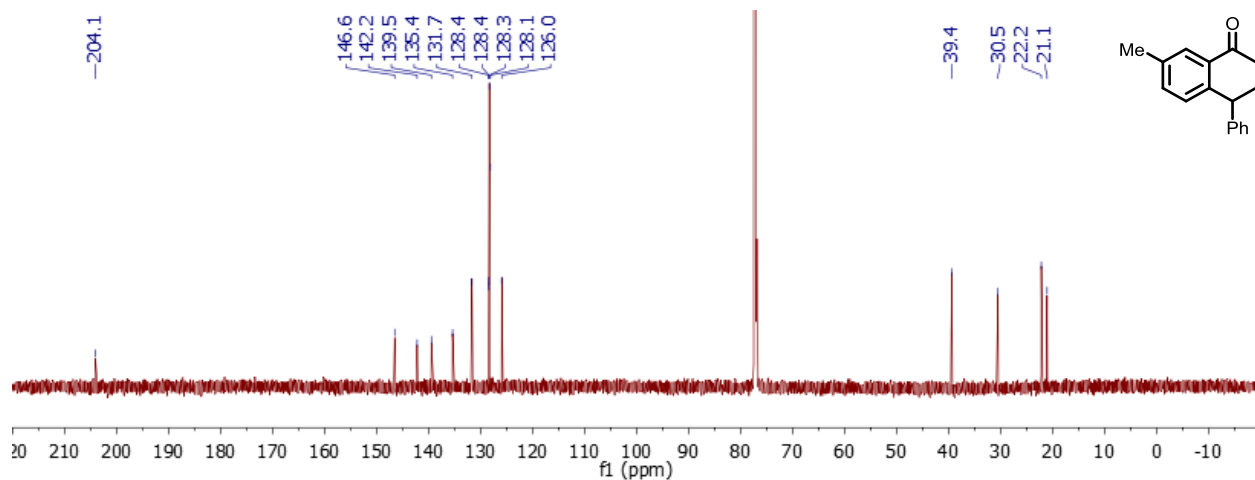
Figure C96. $^{13}C\{^1H\}$ NMR spectrum of **3Ra** in chloroform-*d*.
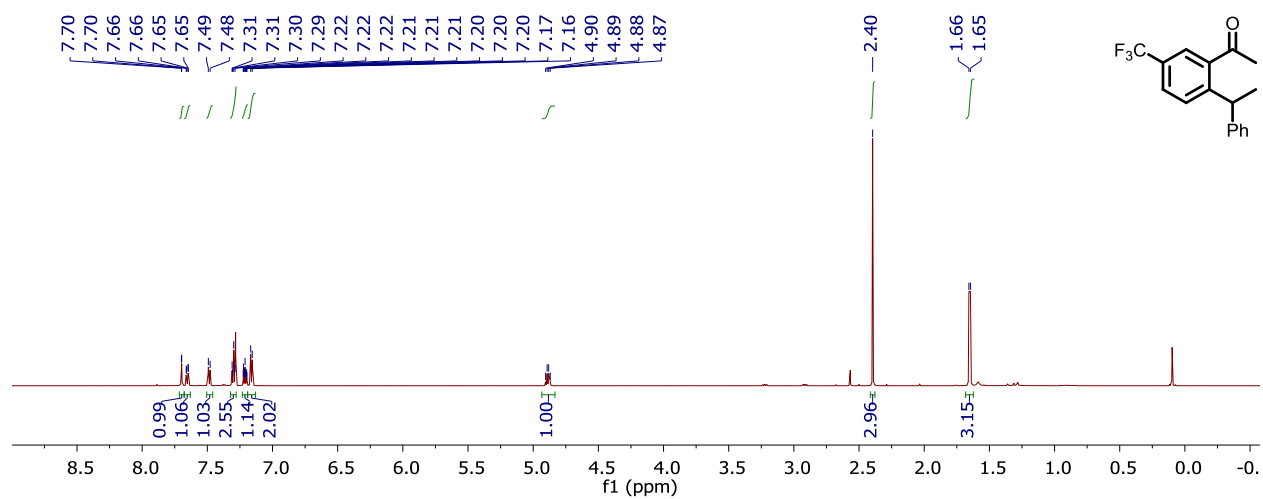
Figure C97. ^1H NMR spectrum of **3Sa** in chloroform-*d*.

Figure C98. $^{13}C\{^1H\}$ NMR spectrum of **3Sa** in chloroform-*d*. **Bottom**: expansion of peaks with $^nJ_{CF}$ couplings (n = 1, 2, or 3).
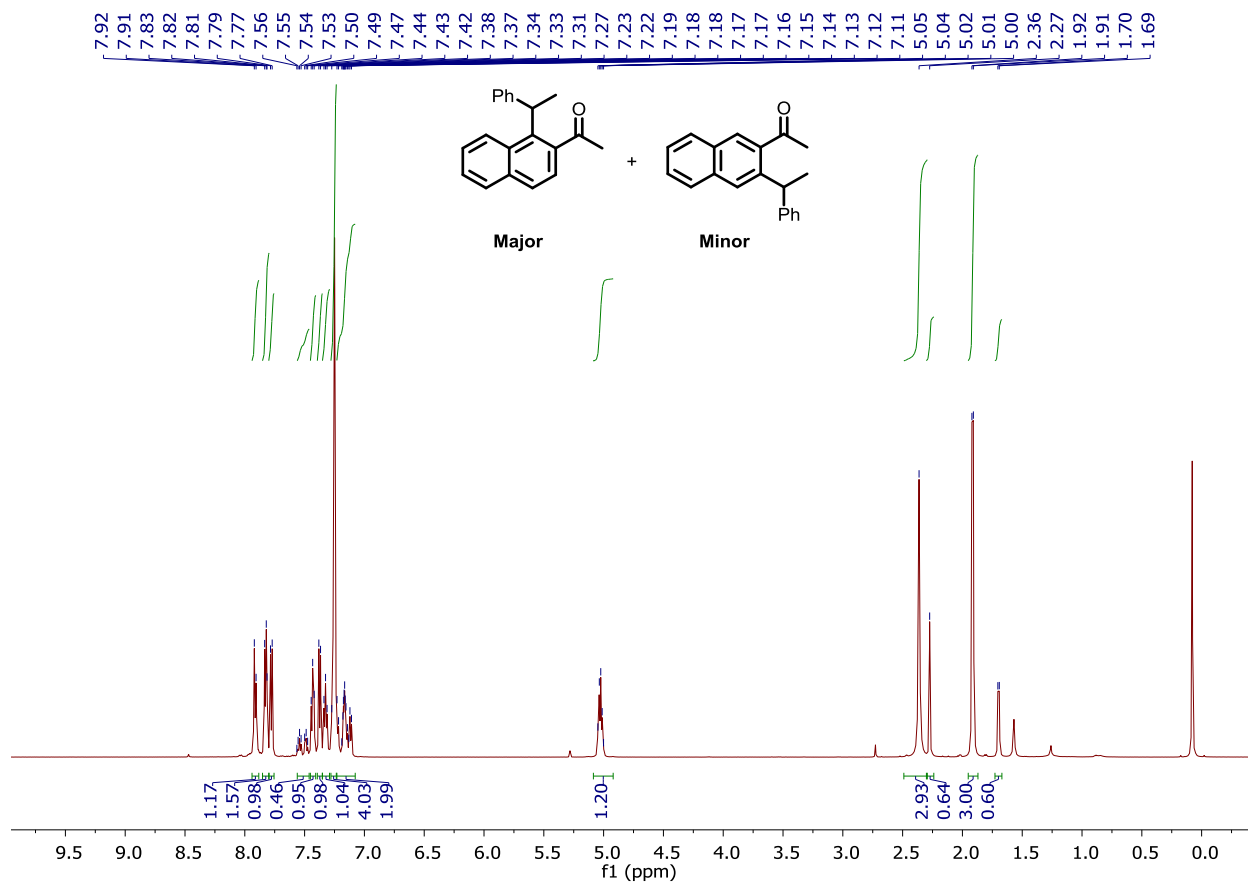

Figure C99. ^{19}F NMR spectrum of **3Sa** in chloroform-*d*.

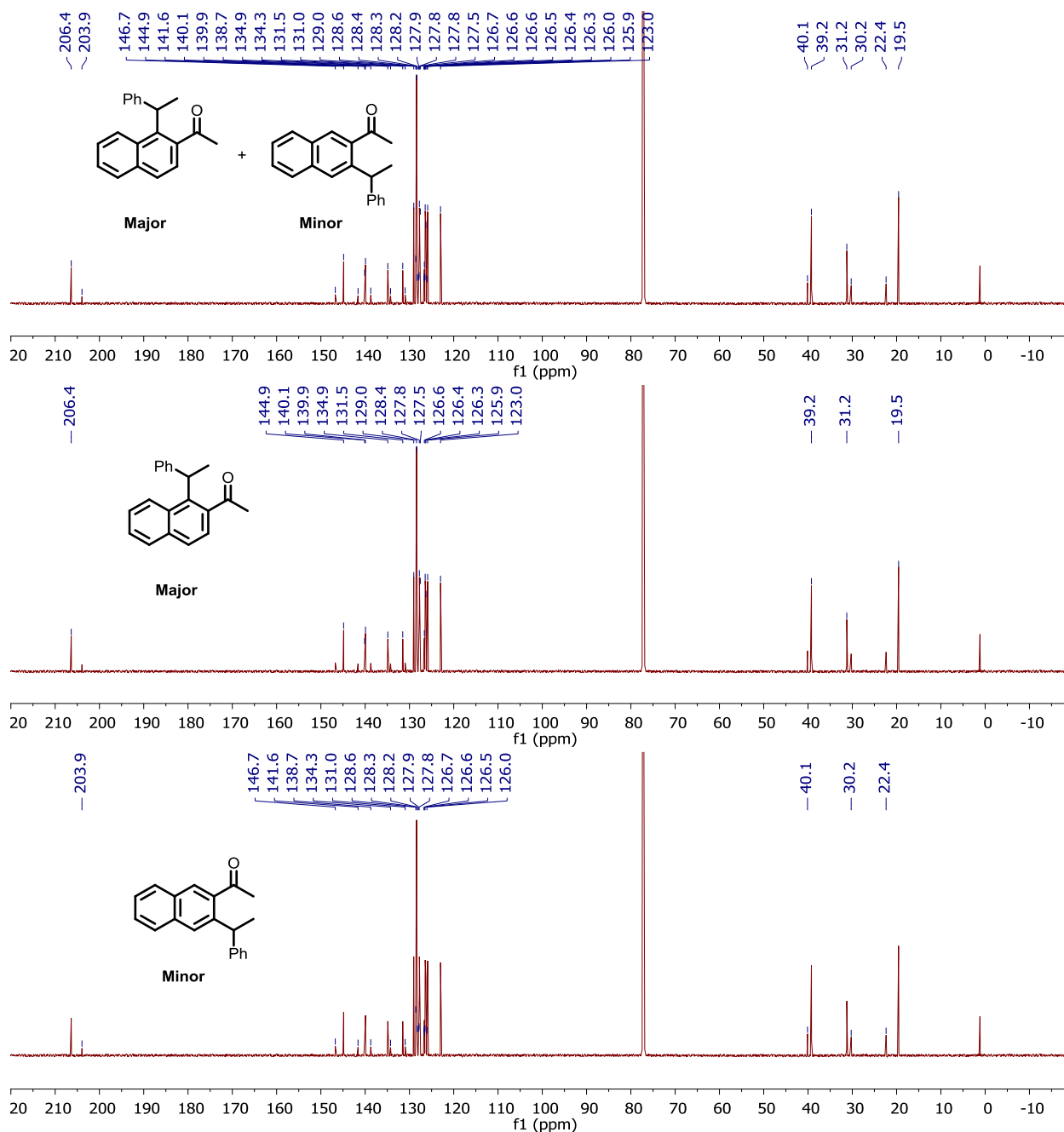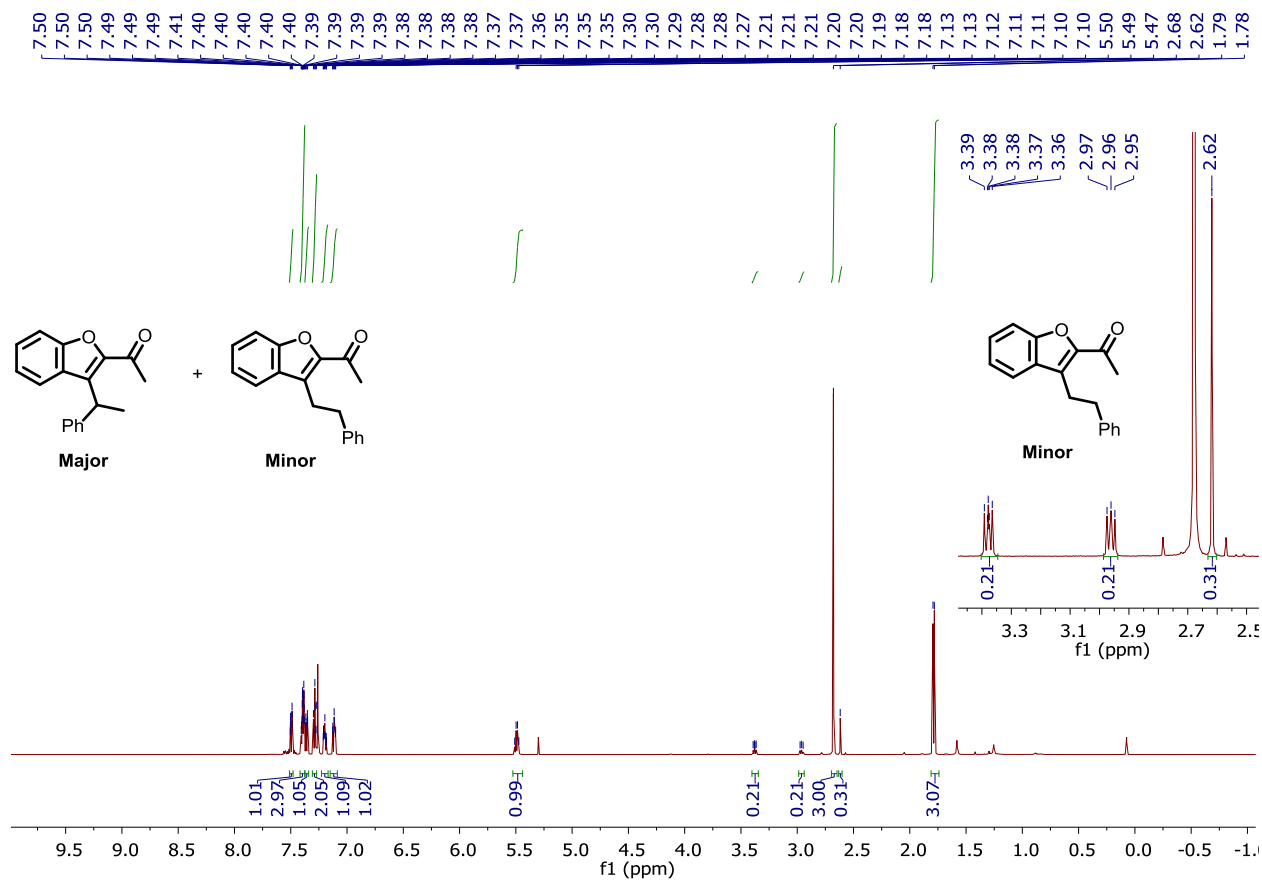**Figure C100.** ^{1}H NMR spectrum of **3Ta** in chloroform-*d*.

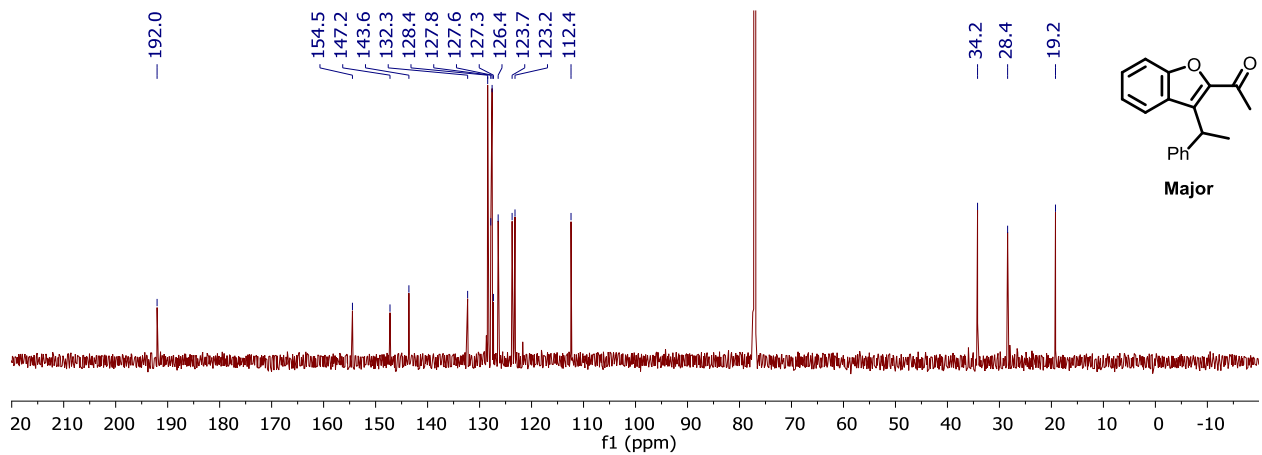**Figure C101.** ^{13}C{^{1}H} NMR spectrum of **3Ta** in chloroform-*d*.

Figure C102. ^{1}H NMR spectrum of **3Ua** and **3Ua'** in chloroform-*d*. Two isomers exist corresponding to C–H activation at the 1 or 3 position of the arene.

Figure C103. $^{13}C\{^1H\}$ NMR spectrum of **3Ua** and **3Ua'** in chloroform-*d*. **Top**: Full spectra with peaks identified for the major and minor isomers. **Middle:** spectra with peaks labeled for only the major isomer (**3Ua**). **Bottom:** spectra with peaks labeled only for the minor isomer (**3Ua'**).

Figure C104. ^{1}H NMR spectrum of **3Va** and **4Va** in chloroform-*d*. **Inset:** Expansion of the resonances corresponding to the minor, linear hydroarylation product **4Va**.

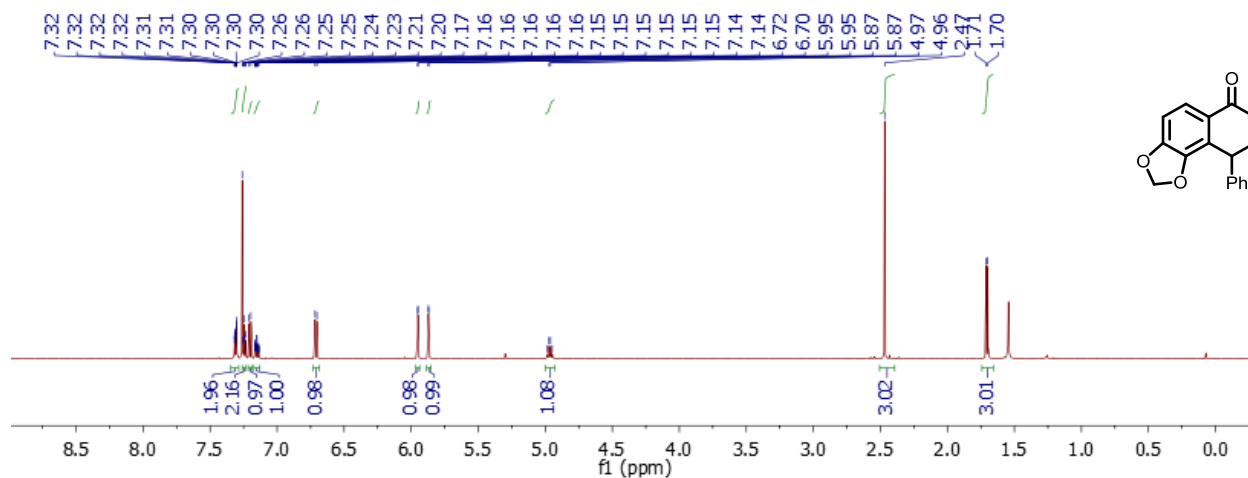**Figure C105.** ^{13}C{^{1}H} NMR spectrum of **3Va** in chloroform-*d*.

Figure C106. ¹H NMR spectrum of **3Wa** in chloroform-*d*.

Figure C107. ¹³C{¹H} NMR spectrum of **3Wa** in chloroform-*d*.
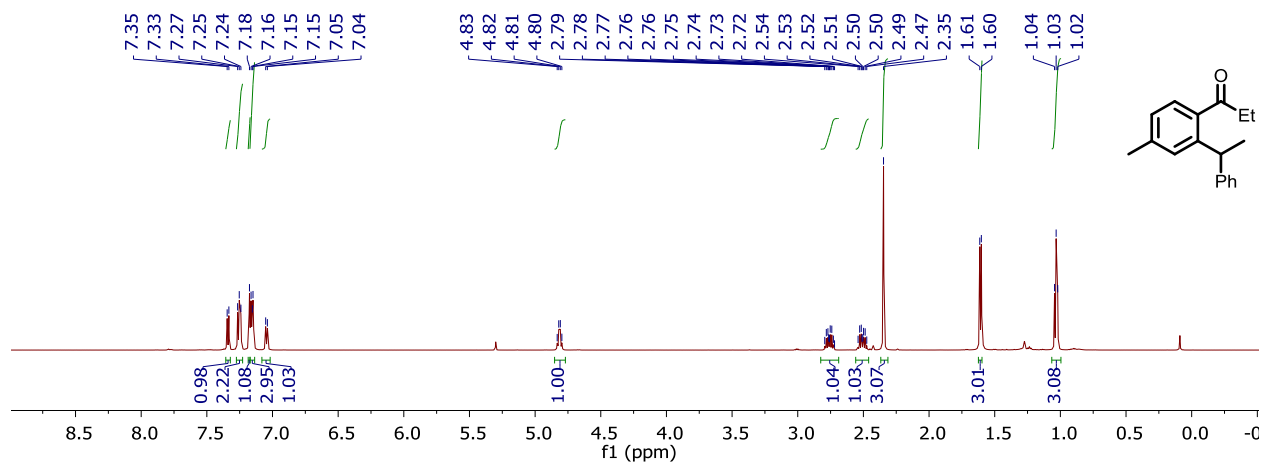
Figure C108. ¹H NMR spectrum of **3Xa** in chloroform-*d*.

Figure C109. $^{13}C\{^1H\}$ NMR spectrum of **3Xa** in chloroform-*d*.
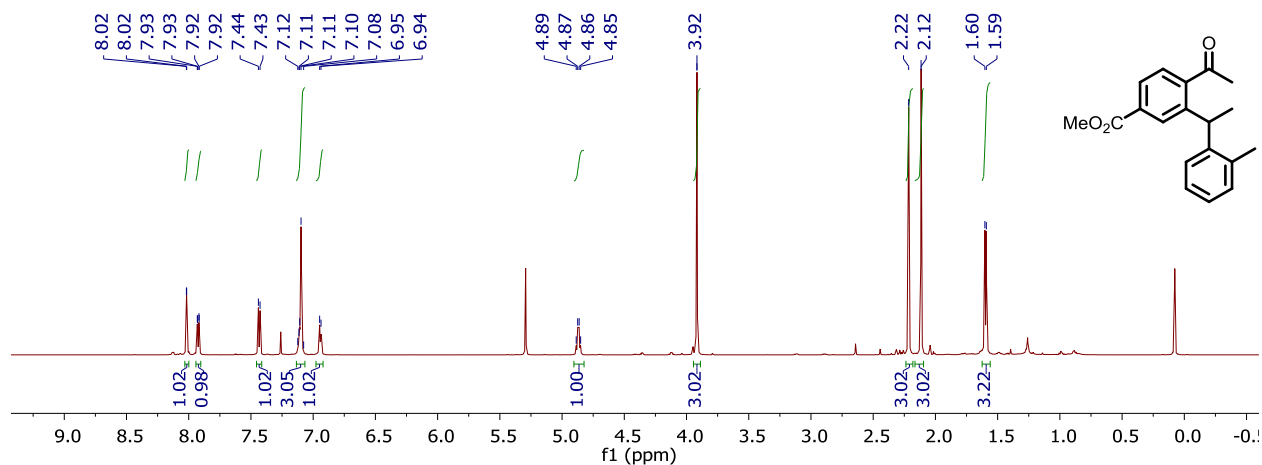
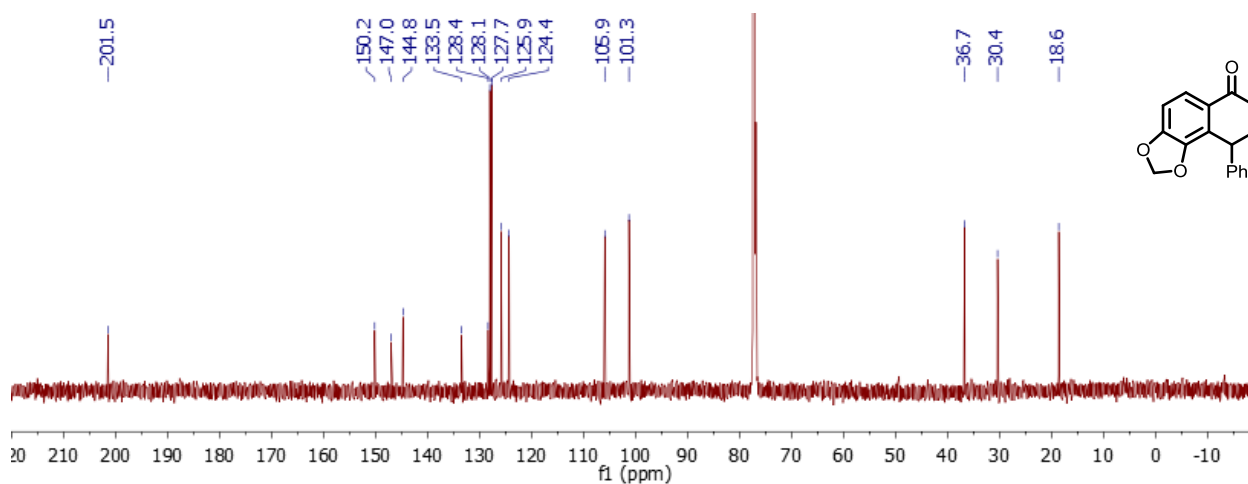**Figure C110.** ^1H NMR spectrum of **3Mb** in chloroform-*d*.
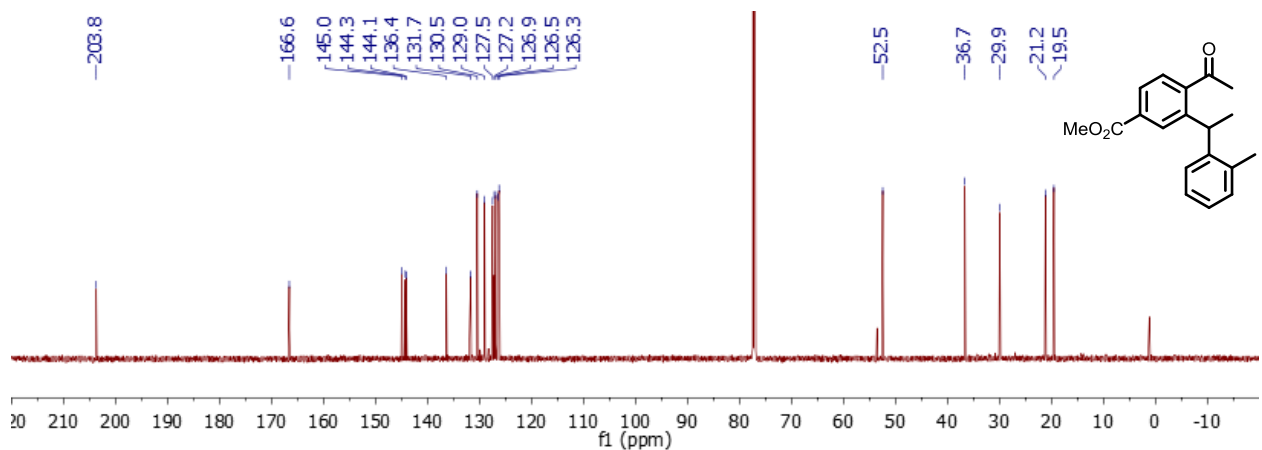
Figure C111. $^{13}C\{^1H\}$ NMR spectrum of **3Mb** in chloroform-*d*.
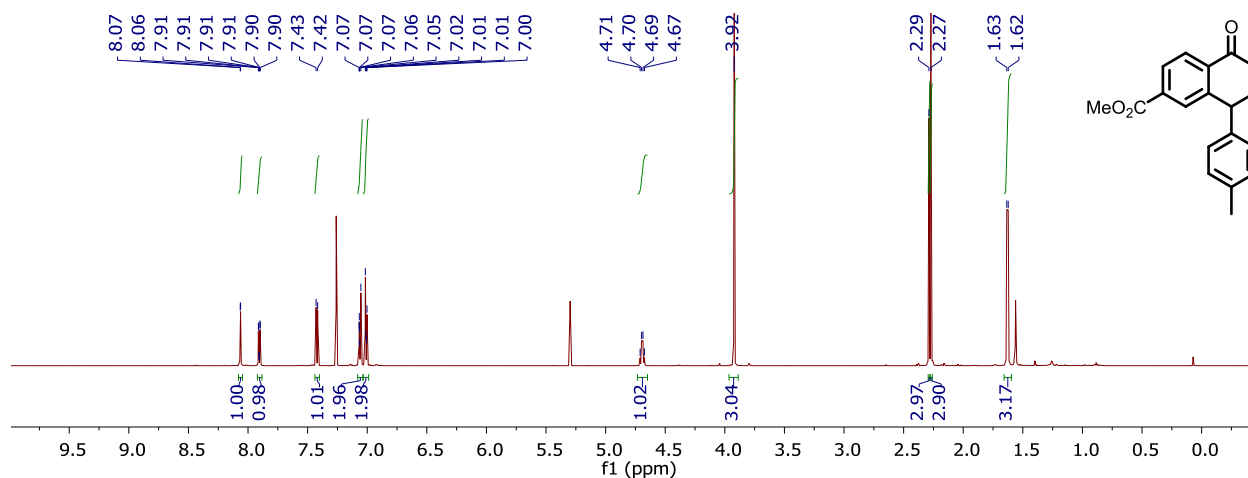
Figure C112. ^{1}H NMR spectrum of **3Mc** in chloroform-*d*.
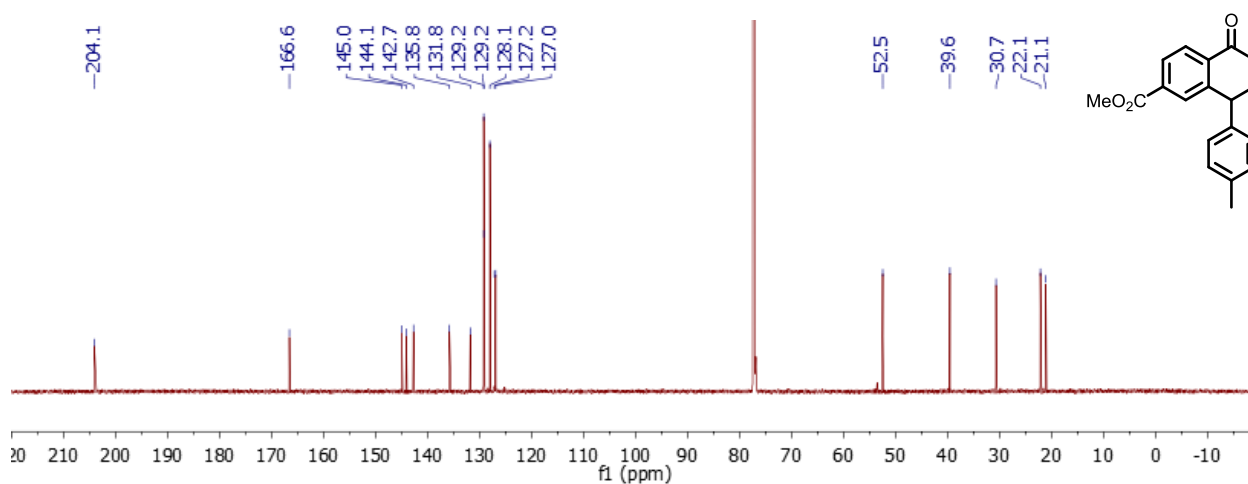
Figure C113. ^{13}C{^{1}H} NMR spectrum of **3Mc** in chloroform-*d*.
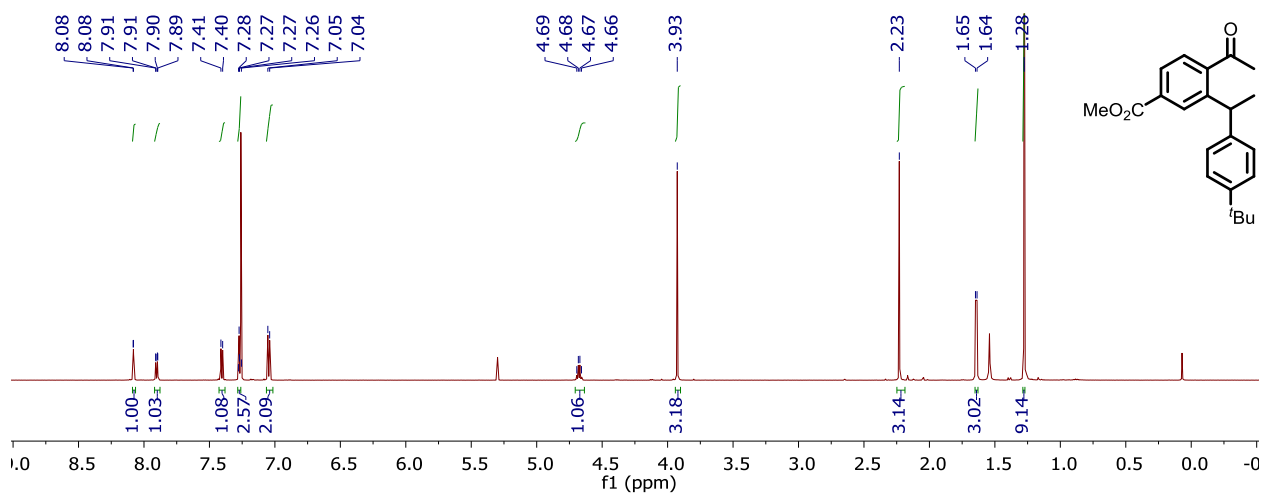
Figure C114. ^{1}H NMR spectrum of **3Md** in chloroform-*d*.

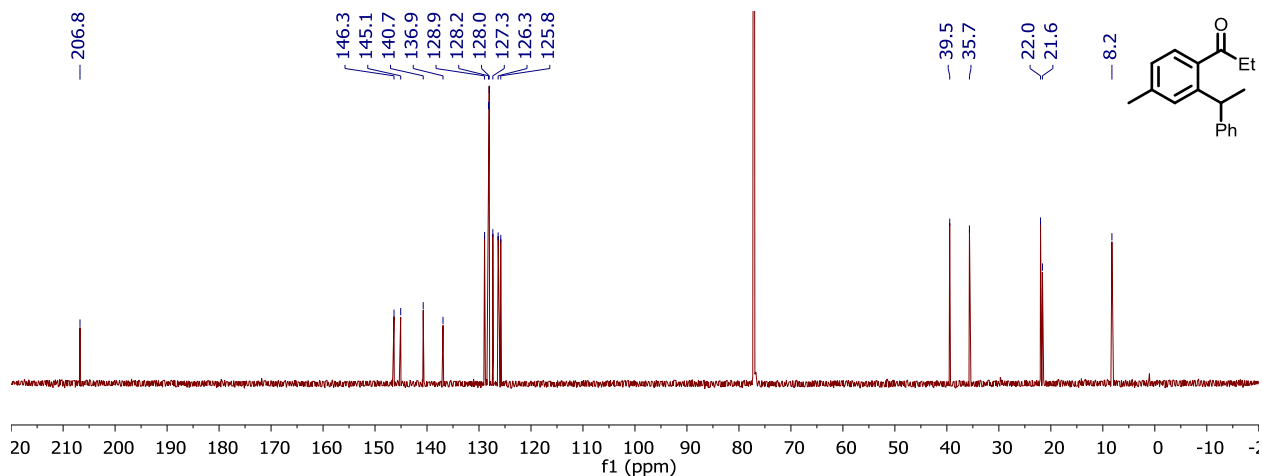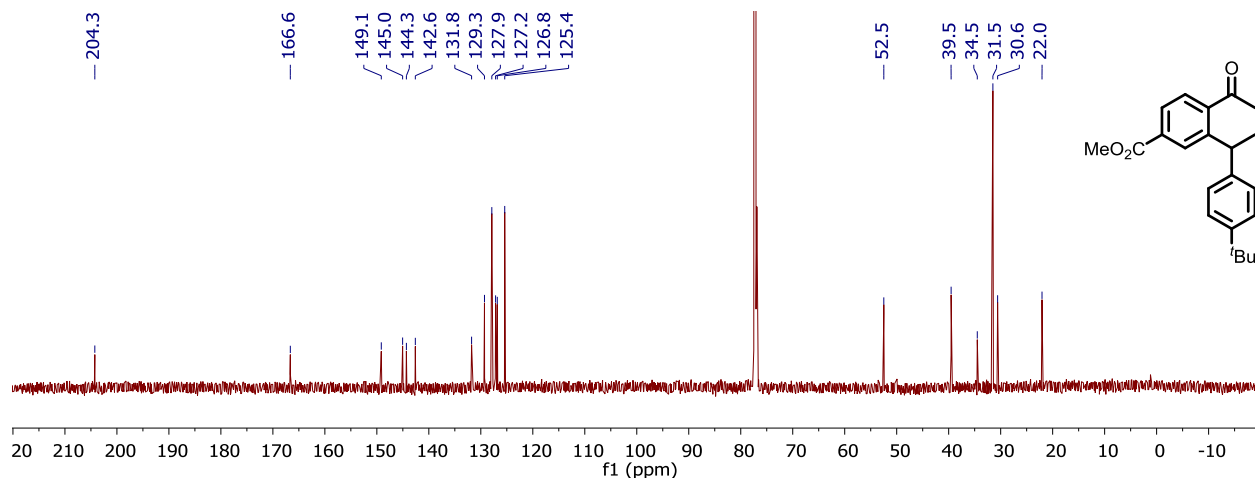**Figure C115.** $^{13}C\{^1H\}$ NMR spectrum of **3Md** in chloroform-*d*.
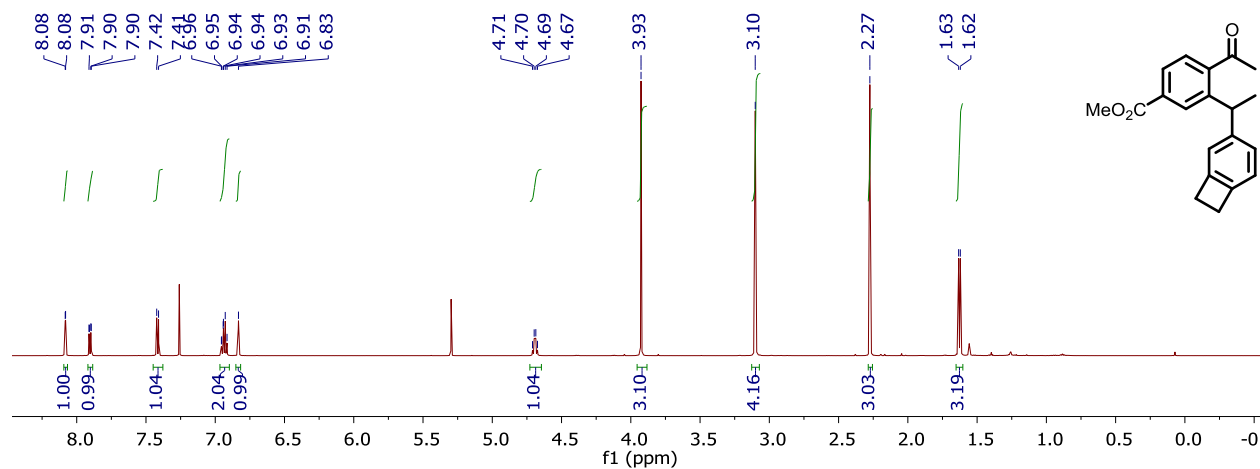
Figure C116. ^1H NMR spectrum of **3Me** in chloroform-*d*.
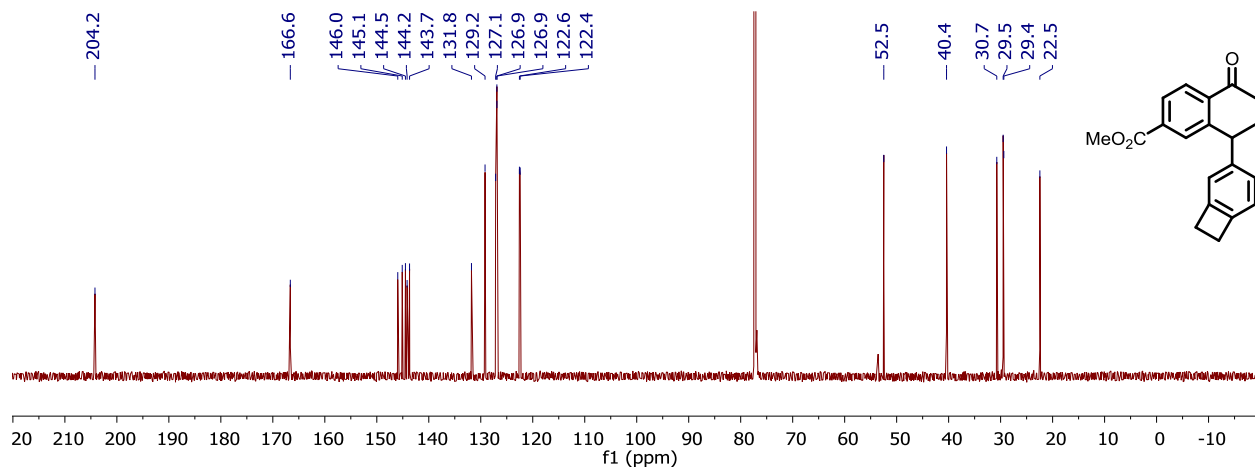
Figure C117. $^{13}C\{^1H\}$ NMR spectrum of **3Me** in chloroform-*d*.

Figure C118. ^{1}H NMR spectrum of **3Mf** in chloroform-*d*.
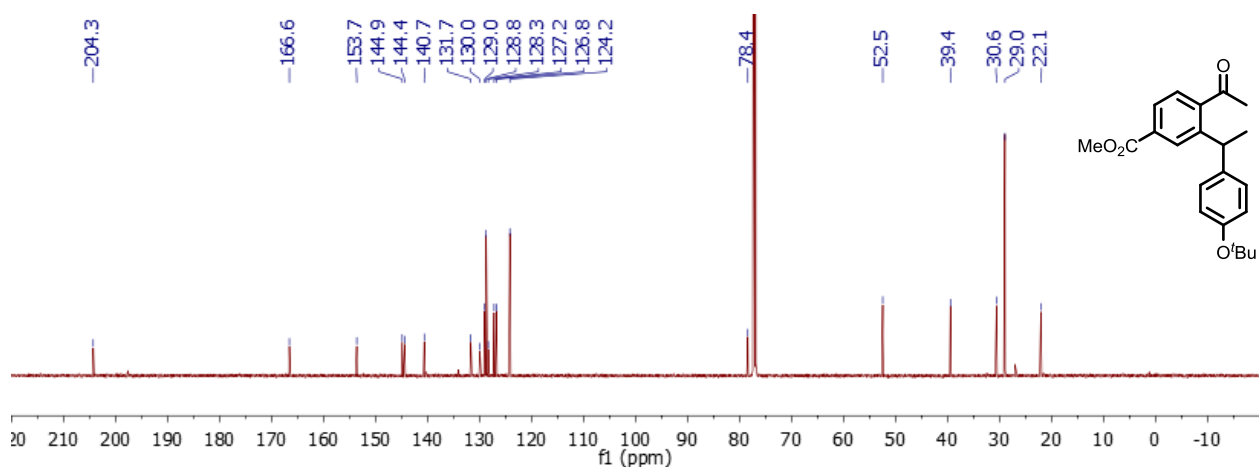
Figure C119. ^{13}C{^{1}H} NMR spectrum of **3Mf** in chloroform-*d*.
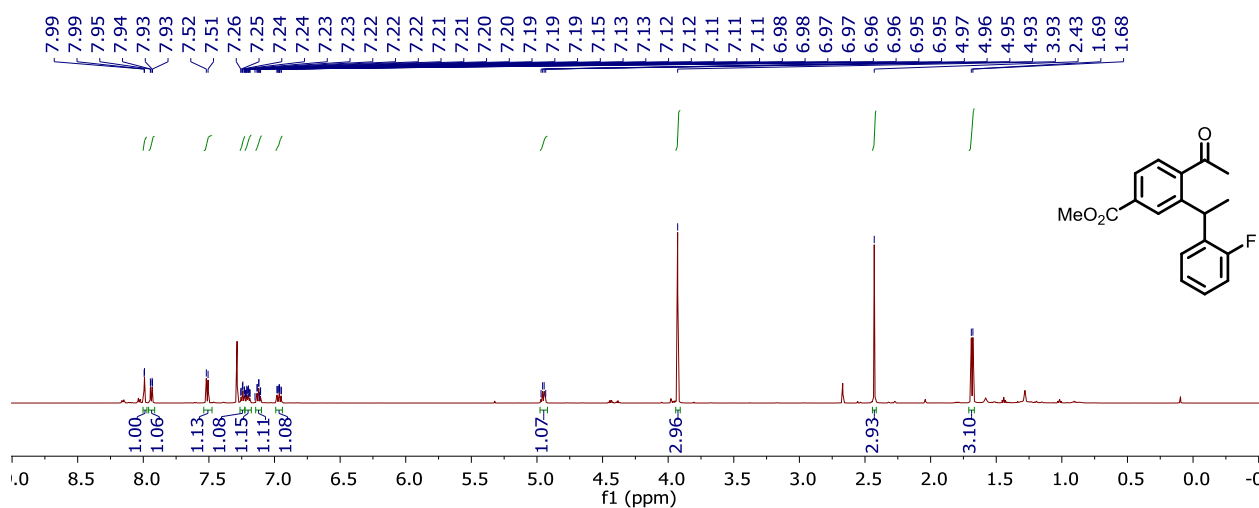
Figure C120. ^{1}H NMR spectrum of **3Mg** in chloroform-*d*.

Figure C121. Top: $^{13}C\{^1H\}$ NMR spectrum of **3Mg** in chloroform-*d*. **Bottom**: expansion of peaks with $^nJ_{CF}$ couplings (n = 1, 2, 3, or 4).

Figure C122. ^{19}F NMR spectrum of **3Mg** in chloroform-*d*.

Figure C123. ^{1}H NMR spectrum of **3Mh** in chloroform-d.

Figure C124. ^{13}C{^{1}H} NMR spectrum of **3Mh** in chloroform-d. **Inset**: expansion of peaks with $^nJ_{CF}$ couplings (n = 1, 2, 3, or 4).
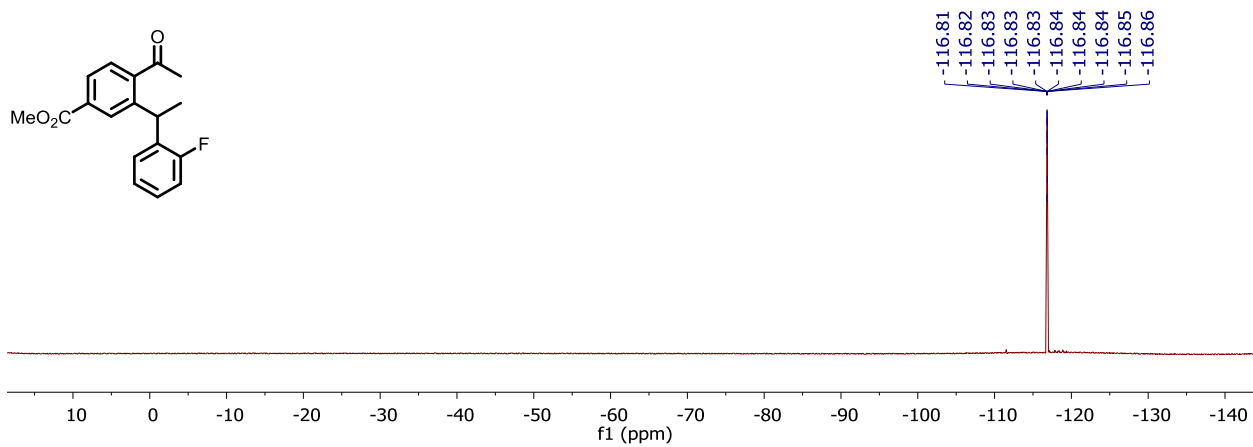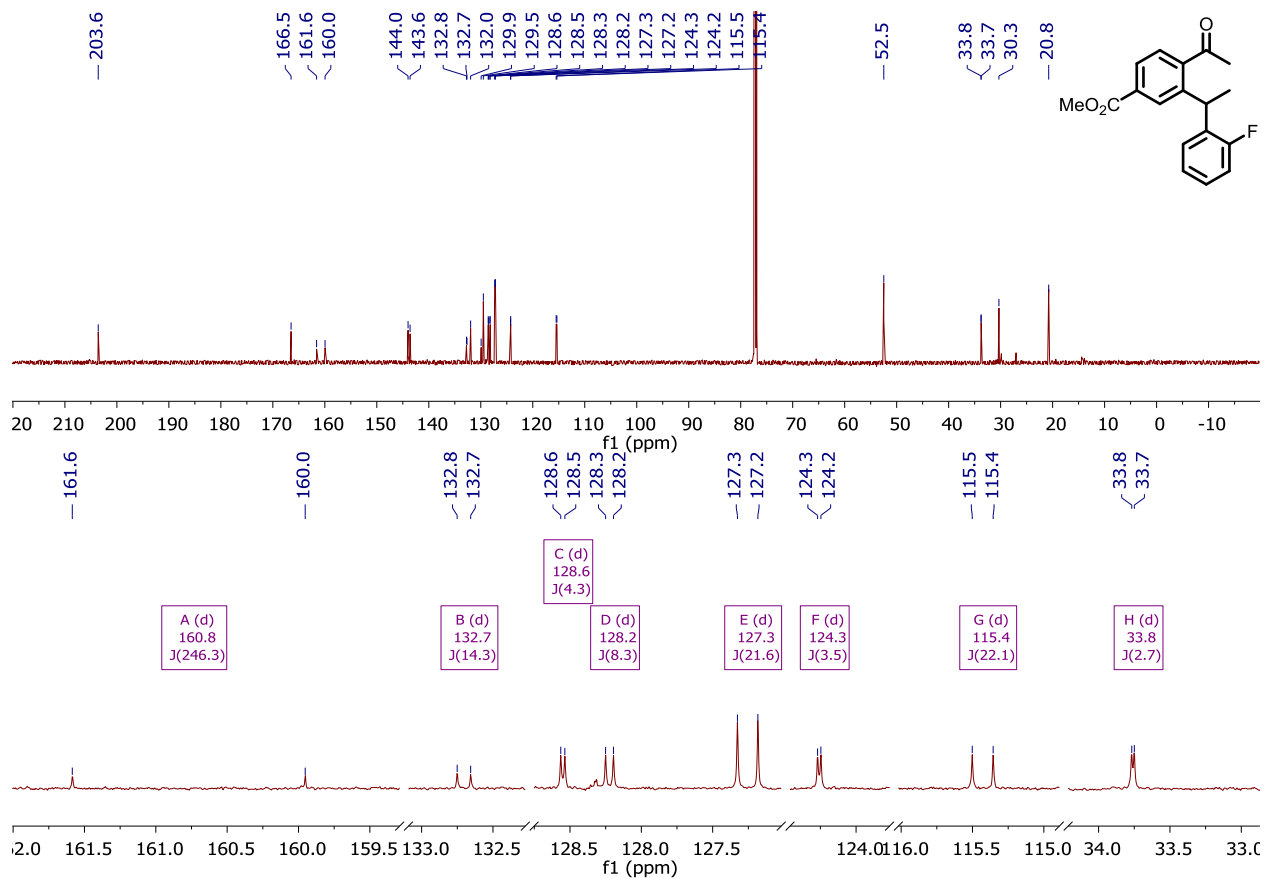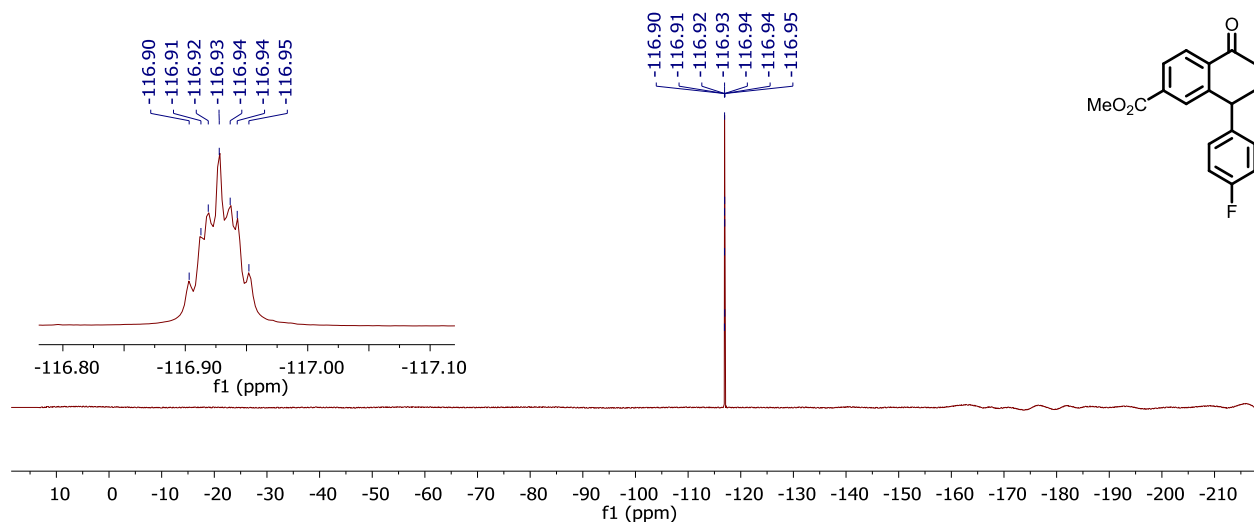
Figure C125. ^{19}F NMR spectrum of **3Mh** in chloroform-*d*. **Inset**: expansion of the ^{19}F peak.
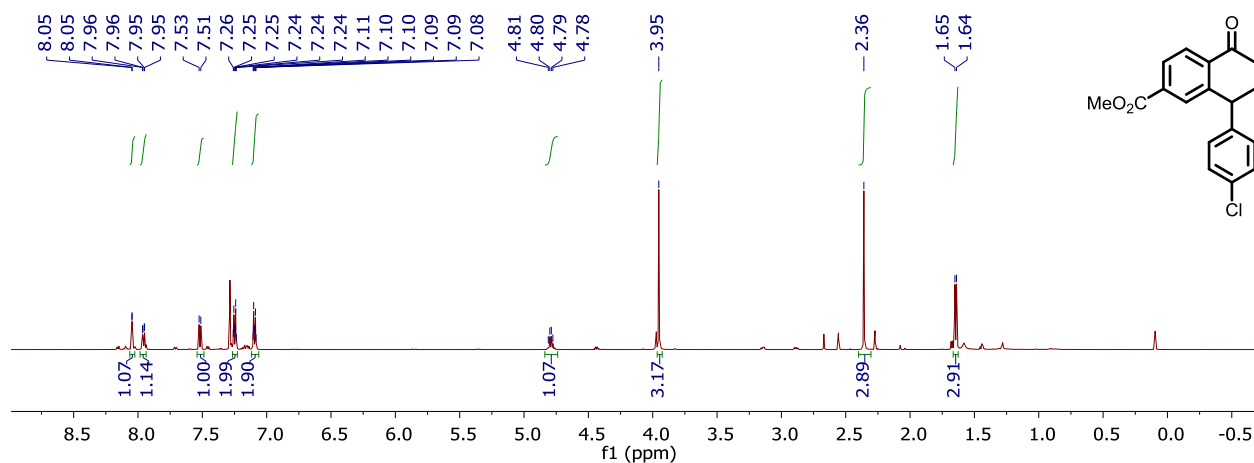
Figure C126. ^{1}H NMR spectrum of **3Mi** in chloroform-*d*.
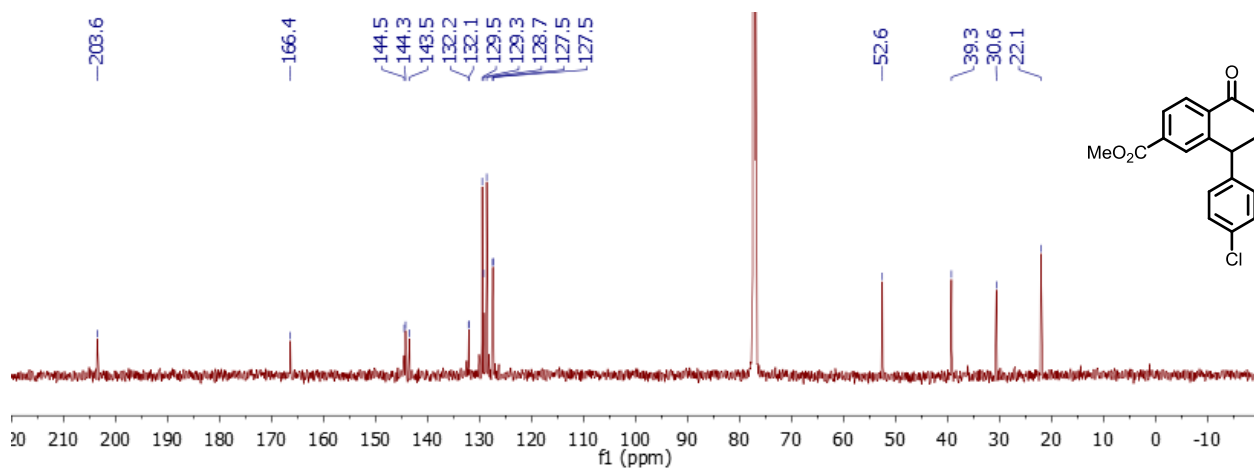
Figure C127. ^{13}C{^{1}H} NMR spectrum of **3Mi** in chloroform-*d*.

Figure C128. ^{1}H NMR spectrum of **3Mj** in chloroform-*d*.

Figure C129. Top: ^{13}C{^{1}H} NMR spectrum of **3Mj** in chloroform-*d*. **Bottom**: expansion of peaks with $^nJ_{CF}$ couplings (n = 1, 2, or 3).

Figure C130. ^{19}F NMR spectrum of **3Mj** in chloroform-*d*.

Figure C131. ^{1}H NMR spectrum of **3Mk** in chloroform-*d*. Note that residual CH$_2$Cl$_2$ exists as evidenced by the peak at 5.30 ppm.

Figure C132. ^{13}C{^{1}H} NMR spectrum of **3Mk** in chloroform-*d*. Note that residual CH$_2$Cl$_2$ exists as evidenced by the peak at 53.5 ppm.

Figure C133. ^{1}H NMR spectrum of **3Ml** in chloroform-d. Note that residual CH_2Cl_2 exists at 5.30 ppm.
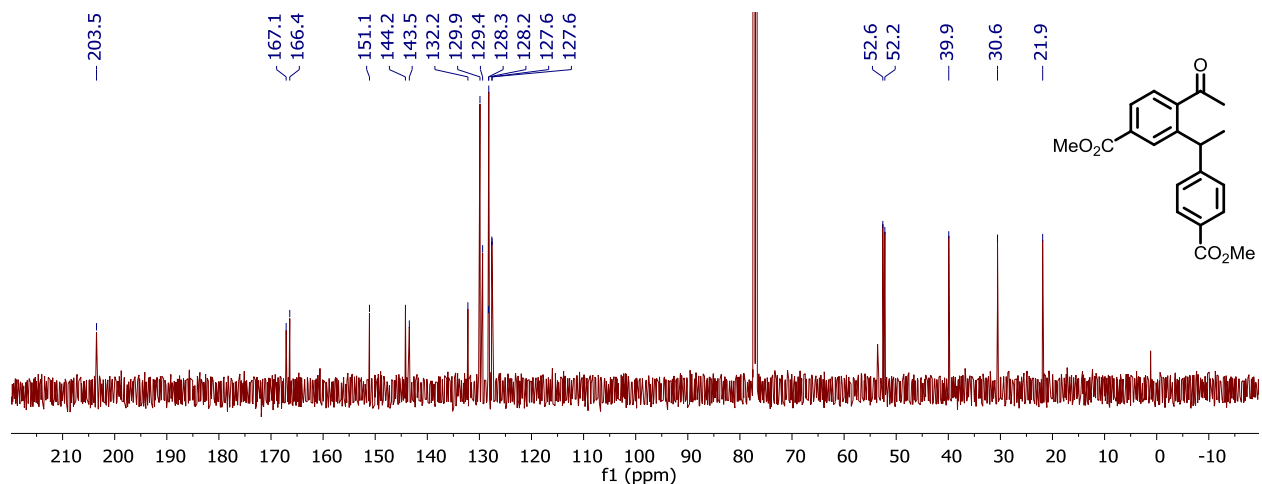
Figure C134. ^{13}C{^{1}H} NMR spectrum of **3Ml** in chloroform-d.
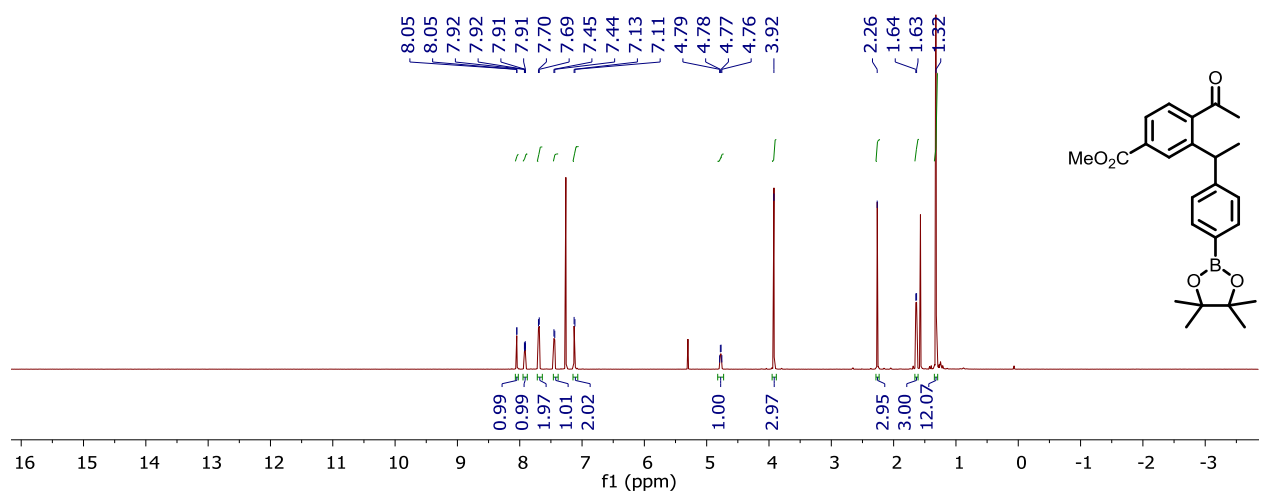
Figure C135. ^{1}H NMR spectrum of **3Mm** in chloroform-d.
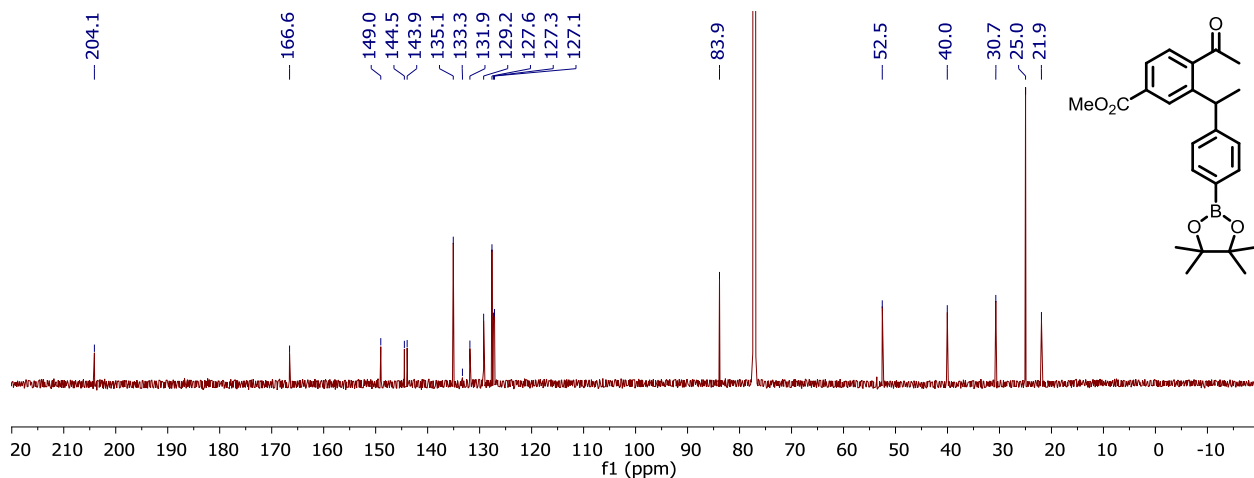
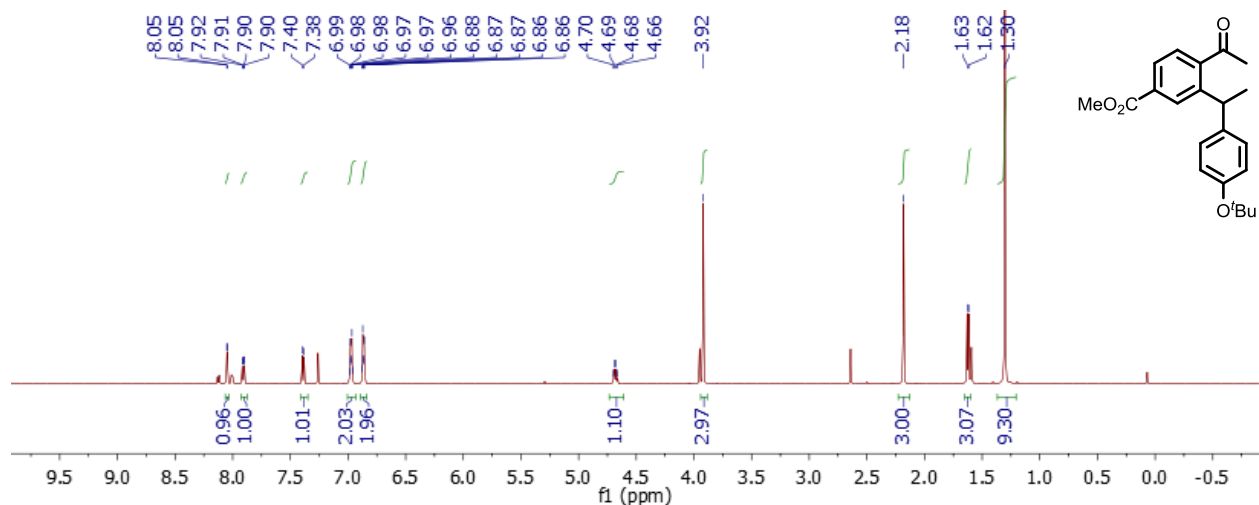**Figure C136.** ^{13}C{^{1}H} NMR spectrum of **3Mm** in chloroform-*d*.
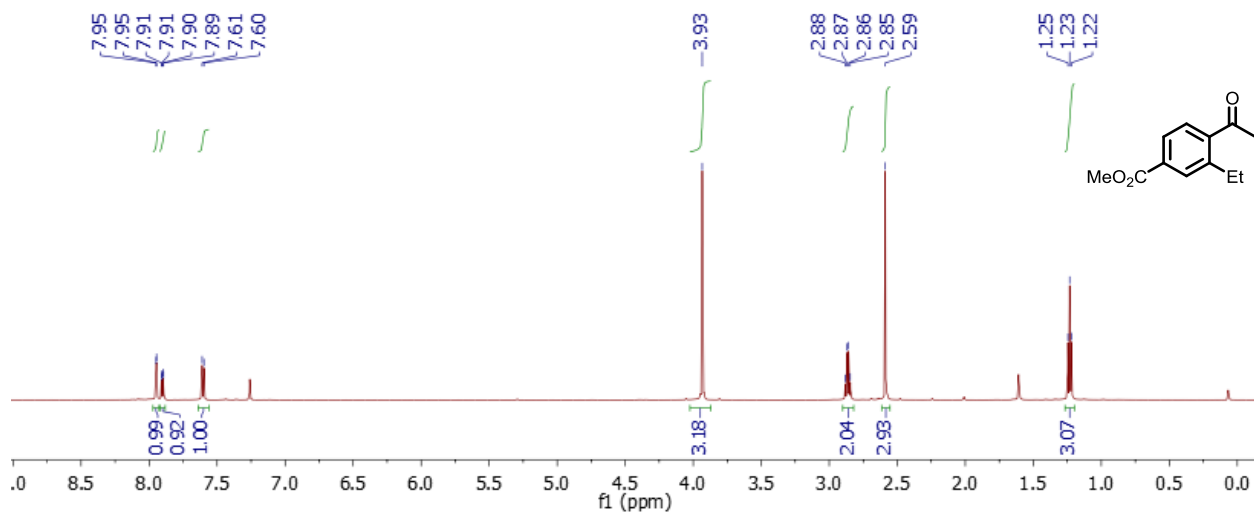
Figure C137. ^{1}H NMR spectrum of **4Mn** in chloroform-*d*.
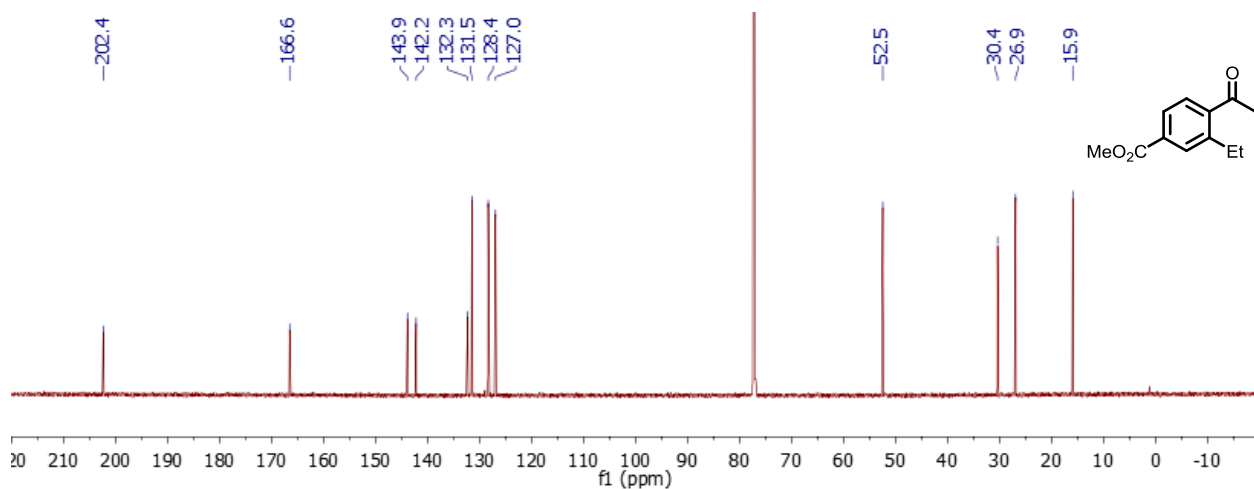
Figure C138. ^{13}C{^{1}H} NMR spectrum of **4Mn** in chloroform-*d*.
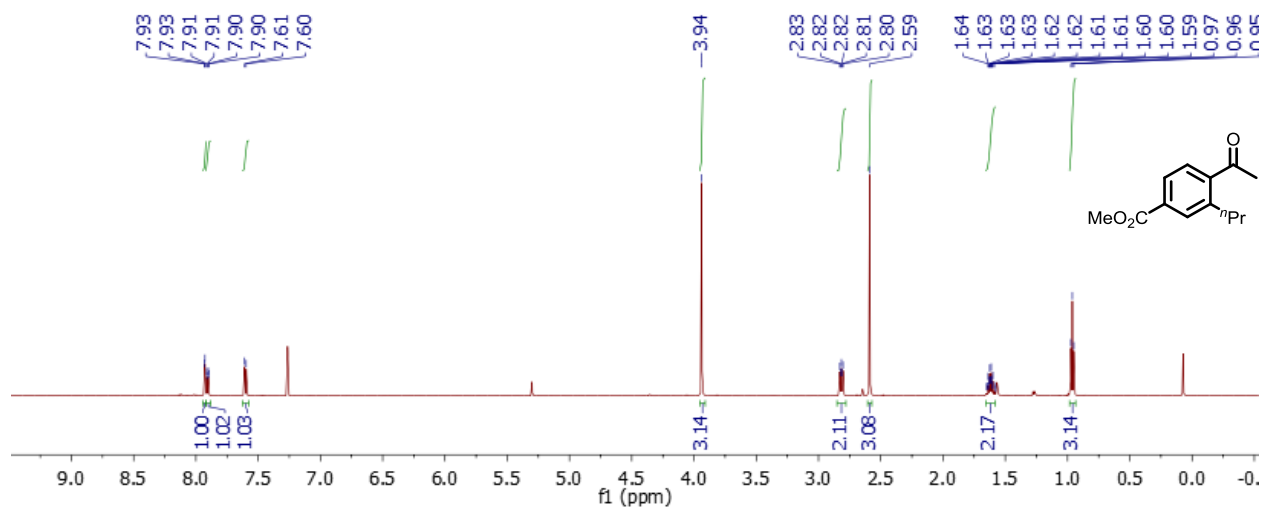
Figure C139. ^{1}H NMR spectrum of **4Mo** in chloroform-*d*.
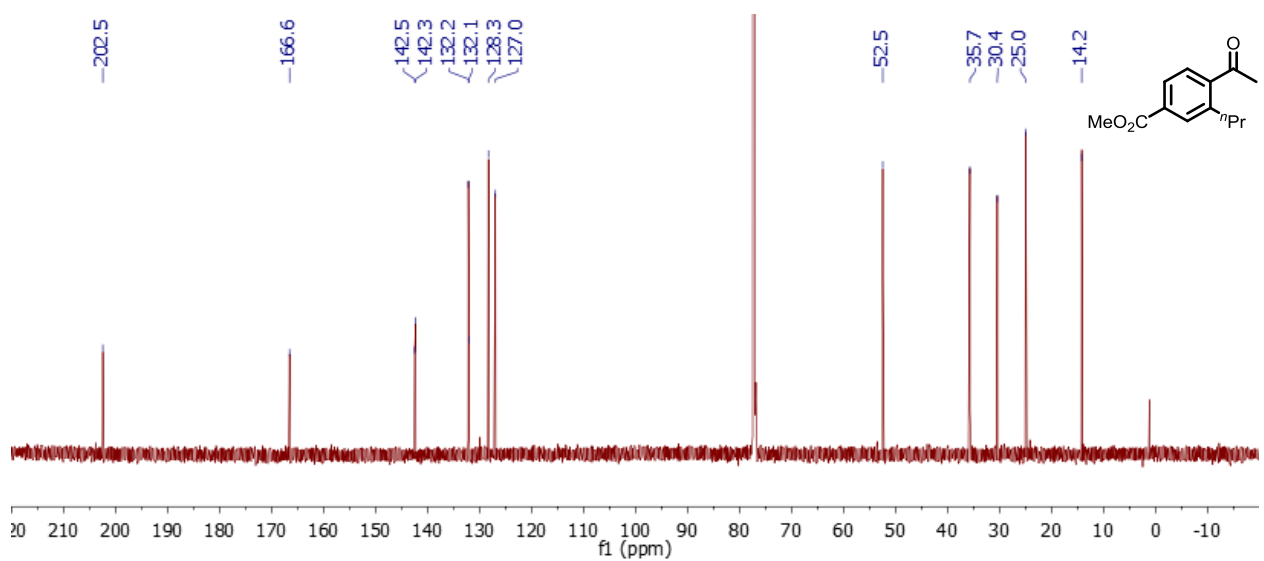
Figure C140. ^{13}C{^{1}H} NMR spectrum of **4Mo** in chloroform-*d*.
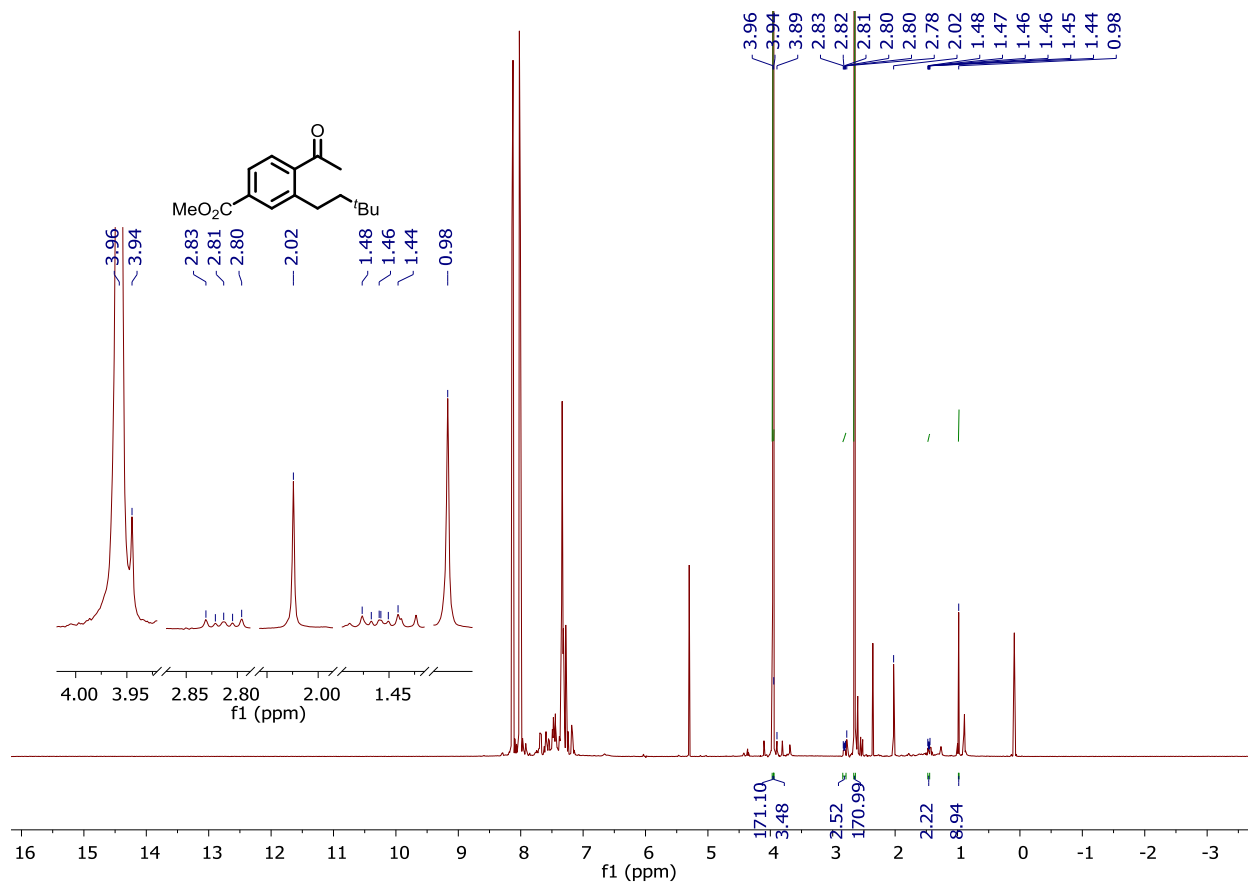
Figure C141. Crude ^{1}H NMR spectrum of **4Mp** in chloroform-*d*. **Inset:** Expansion of the resonances corresponding to the methyl ester, methylene, and *tert*-butyl protons of **4Mp**.
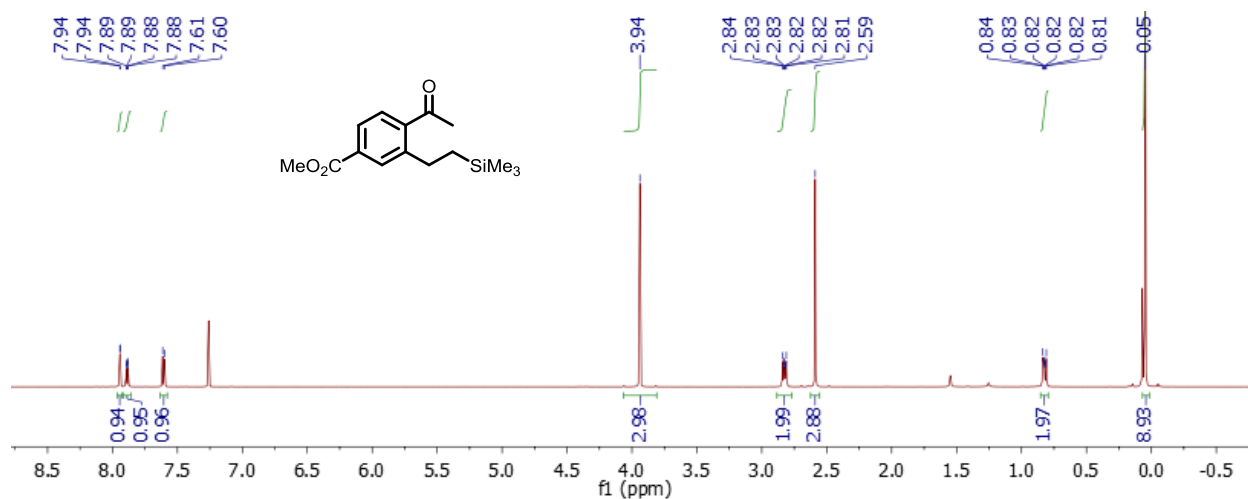
Figure C142. ^{1}H NMR spectrum of **4Mq** in chloroform-*d*.

Figure C143. $^{13}C\{^1H\}$ NMR spectrum of **4Mq** in chloroform-*d*.

Figure C144. ^1H NMR spectrum of **4Mr** in chloroform-*d*.

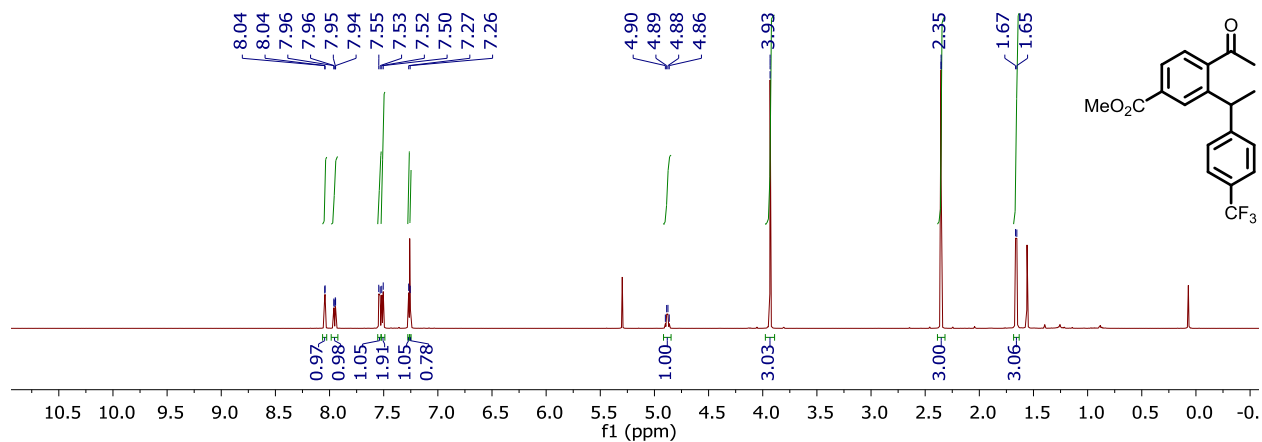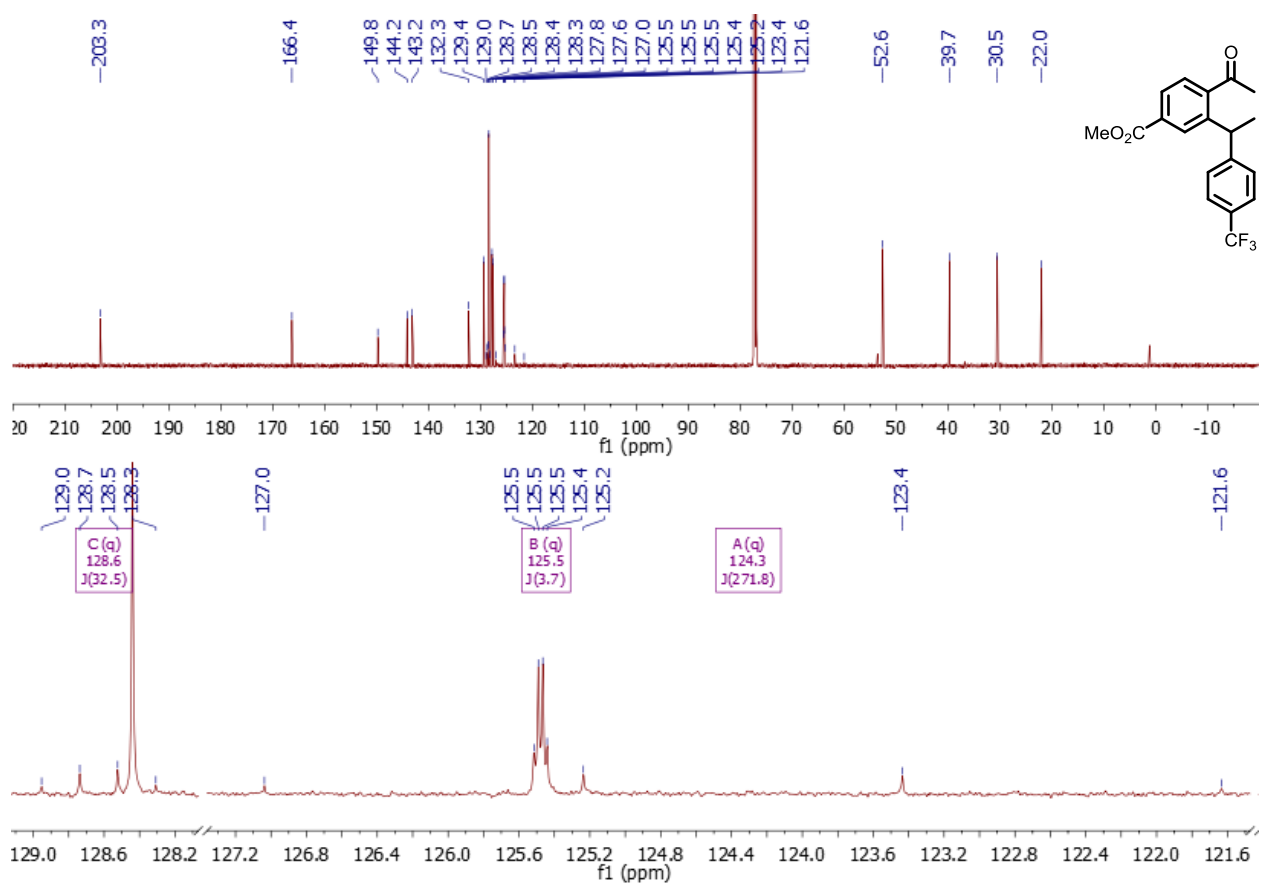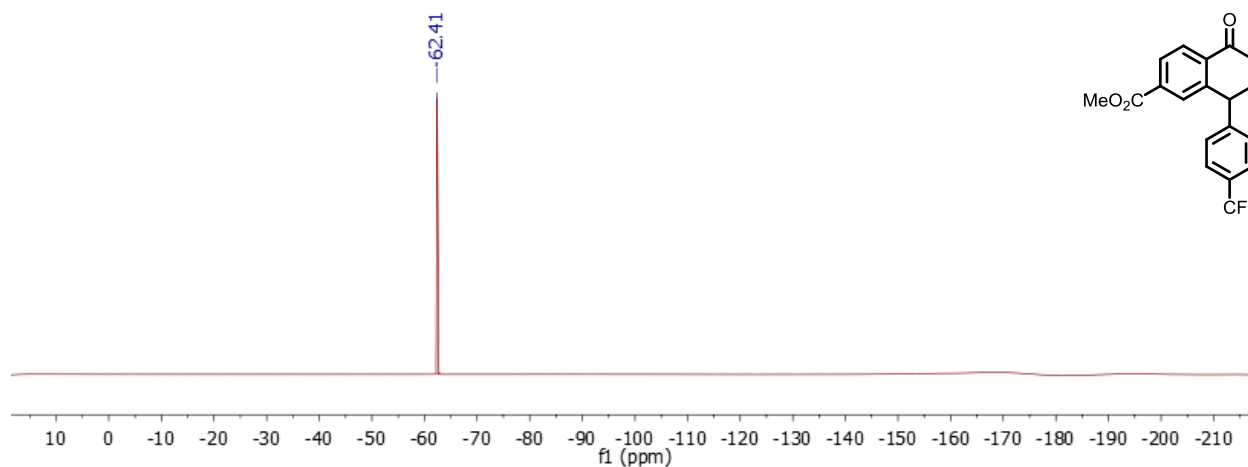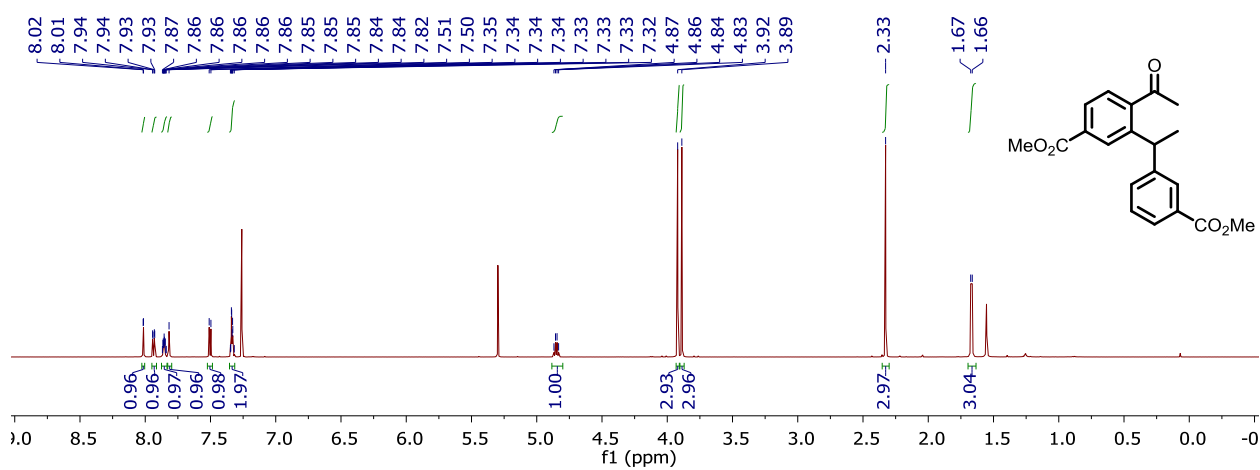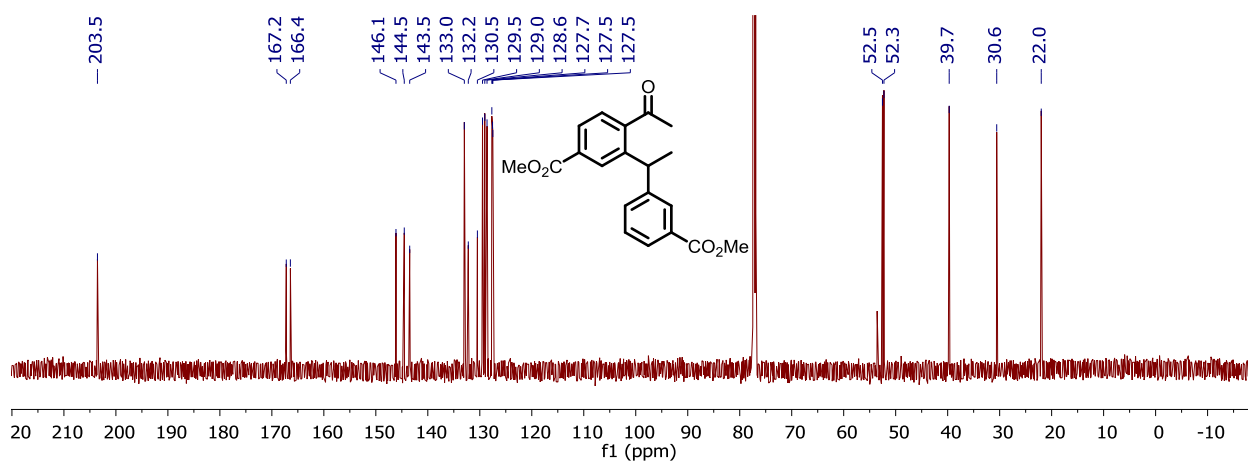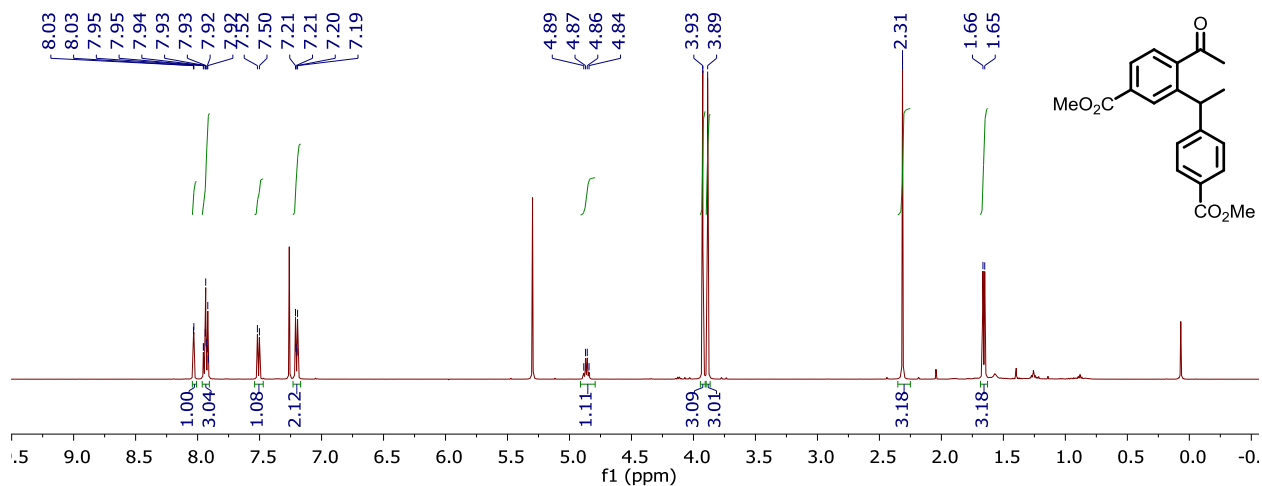**Figure C145.** $^{13}C\{^1H\}$ NMR spectrum of **4Mr** in chloroform-*d*.

Appendix D
Guide to Processing Kinetics Data
In MNova and Excel

Preface: While Excel (and other MSOffice programs) typically cannot outcompete specialty software in terms of sheer capability and user-interface, Excel can none-the-less be a powerful tool to generate professional looking figures. This documents function is to outline the process (and settings) to create a sleek plot (Part I) in the context of processing reaction kinetics by ^{1}H NMR spectroscopy (Part II).

This document assumes that MSExcel (v. 1910, Build 12130.20410) and MNova (v. 11.0) are used.

Note One: Get rid of the base settings on all MSOffice software. The default settings were designed with the average user (luddite) in mind. As a STEM graduate student/post-doc, you likely do not fit into this category. Below I have a list of settings that I think work best.

Axis Title: Arial, 12 pt, bold, black	Plot Area Frame: 2 pt thickness, black
Axis Labels: Arial, 10 pt, bold, black	Chart Area: no gridlines
Axis Line: 2pt width, black	Chart Area: no border line
Axis: 2 minor tick marks per major tick	Data Series: marker, no border, fill solid, marker size 5. Darker, highly contrasting colors work best (*i.e.*, dark red, dark blue, purple).
Axis: ~4 major tick marks per plot	No Chart Title
Axis: tick marks "inside"	Data Labels: Bold, 10 pt, arial. Same color as the data set.

Note Two: There are many useful functions/calls in Excel that are worth being aware of. They are tabulated below.

1. **$** is used to prevent the enumeration of cell values during autofill. This is especially useful when you have a static definition (*e.g.,* the value of the concentration of the internal standard). This can be used for the letter portion ($A5; A is static, but 5 will be enumerated), the number portion (A$5) or both portions ($A$5).
2. **''!** is a very useful call back function. This will search for any tab within your document with the name within the string. After the ! a cell number is given which will return *the value of that string in that subtab*. This saves lots of time by avoiding copy/pasting from multiple tabs. It will also auto-update the value if you change the original cell value.
   Example usage: Assume that in cell A5 in the subtab named 'TAB NAME' a value of 15.3 exists. Using the call function, 'TAB NAME'!$A$5, in a new tab titled 'EG' will return 15.3. If we change the original definition of A5, it will update in the 'EG' tab as well as 'TAB NAME'.
3. **Linest(y_values, x_values, set intercept to 0 if false)**. This will return the slope of the linear regression generated from the y/x input values. If the third input value is 'FALSE', the regression will force an x,y-intercept of (0,0). This usually is used as a two cell output, where the first cell is the slope and the second is the y-intercept.
4. **Slope(y_values, x_values)**. This is similar to linest, but will only return the slope.
5. **Intercept(y_values, x_values)**. This is similar to linest, but will only return the y-intercept.
6. **RSQ(y_values, x_values)**. This returns the R^2 of the linear regression generated from the y/x input values.
7. **Average(values)**. This returns the average value for the input data.
8. **Stdev.p(values)**. This returns the standard deviation for the average generated by the input values.

Part I: "How Do I Even Make a Publishable Quality Graph in Excel?"

Let's suppose that we have a generic data set (Figure D1) with some "x" and "y" value. First select the desired "x axis" data and then the "y axis" data *while holding the CTRL key*. This will ensure that the first values are fixed to the x-axis. A simple plot (scatter, bar, pie, etc.) can then easily be obtained under the "Insert" tab. For simple scatter plots, I typically prefer to display the data without connecting lines (i.e. the highlighted choice). The resultant graph ("raw") is not particularly appealing. We will address this later.
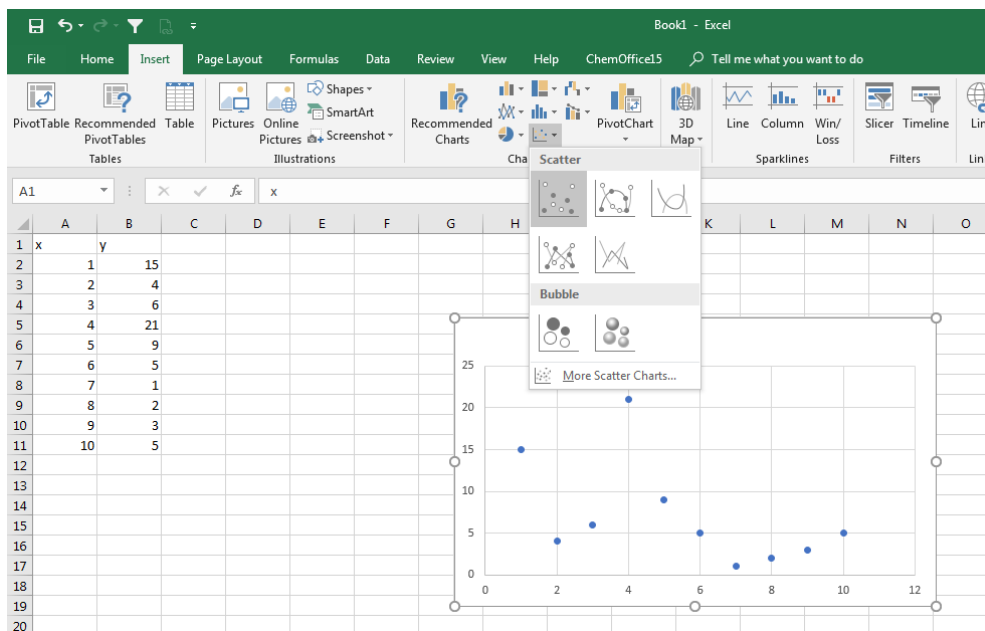
Figure D1. Generation of a plot from generic data.

Now suppose that we wish to a plot with *multiple* data sets but all of which have the same "x" value. Using a similar method to that described above, we can generate our desired plot. First select the "x" axis data then while holding CTRL, select *all the desired "y" axis data for all of your data sets*. The resulting graph will contain all of the data that was input; however, it will often be illegible until further processing (Figure D2).
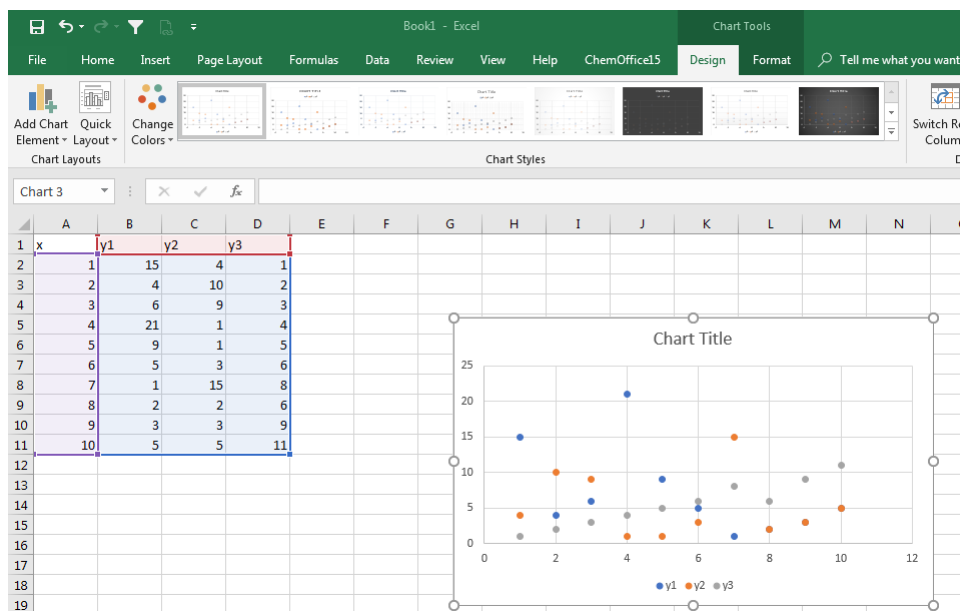
Figure D2. Scatter plot of multiple data sets with the same "x" values.

In real data sets, often we do not have the luxury of having exactly the same "x" values. Suppose we are running a kinetics experiment and plotting a concentration ([y]) versus time (t). Now suppose that our times for the multiple data sets are slightly different. If we naively plot the data by selecting all our data sets, Excel will interpret *each column as an independent "y" value* (Figure D3). Clearly this graph is not the intended plot! This is a highlight of the (non)intelligence of Excel.
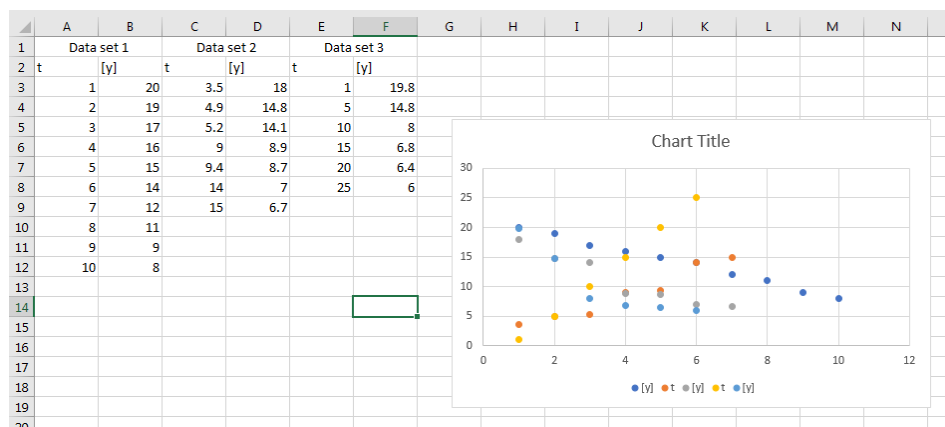
Figure D3. Excel's interpretation of plotting three data sets.

To circumvent this issue, generate a plot of just one of the data sets and *then* add in the other data sets each with their own defined "x" and "y" values (Figure D4). First right click the plot and select the "Select Data…" option. This will open up the "Select Data Source" panel where additional data entries can be added by clicking "Add." Here the other data sets can be added easily by selecting the "x", "y", and "series name" values; this will then add the new data set(s) to the plot.
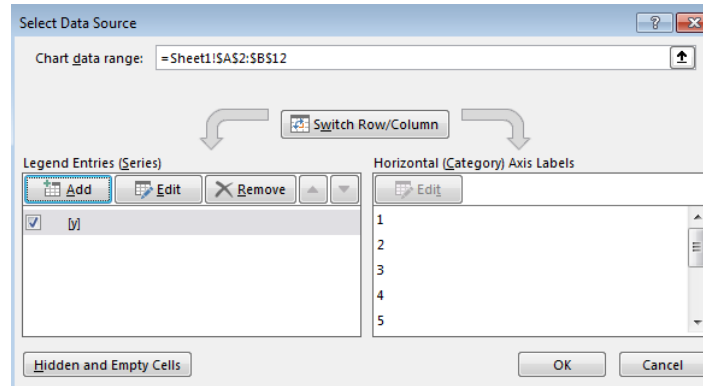
Figure D4. Select Data Source menu. Here new data sets can be added or edited.
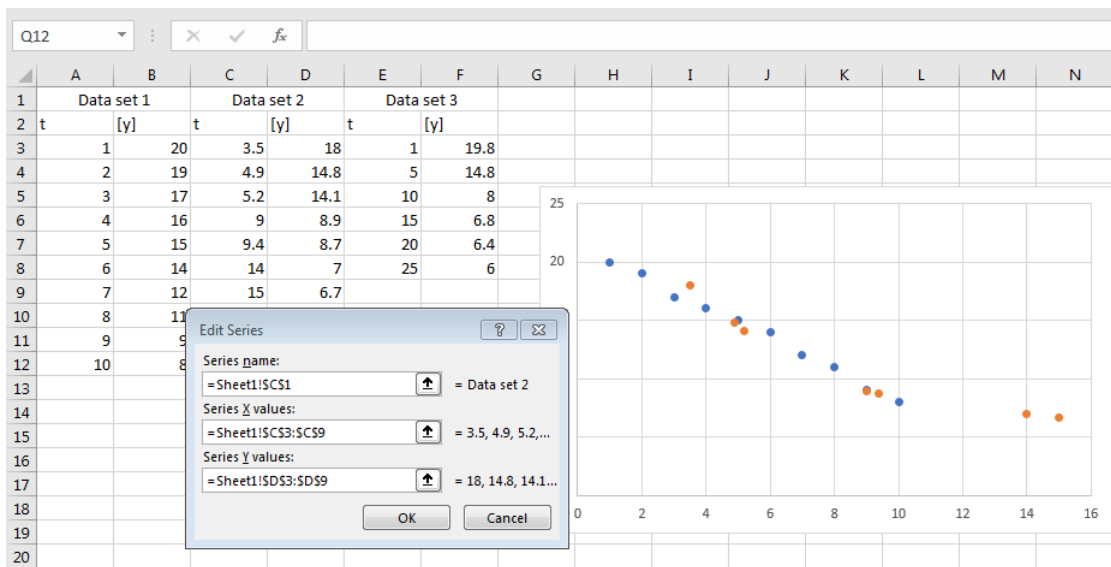
Figure D5. Plot with the second data set added.

Finally, the overall settings on this plot can be tuned to make this figure publishable quality! Most of these can be accessed by right clicking on the relevant portion of the plot (*e.g.,* the chart area parameters can be accessed by right clicking on the area within the plot. All possible sections can be accessed by right clicking on the chart and selecting the chart element which you wish to change (Figure D6). New chart elements can be accessed under the "Add Chart Element" button on the upper right corner under the "Design" subtab menu (*e.g.,* Axis Titles, Legends, Trendlines, Error Bars, etc.).
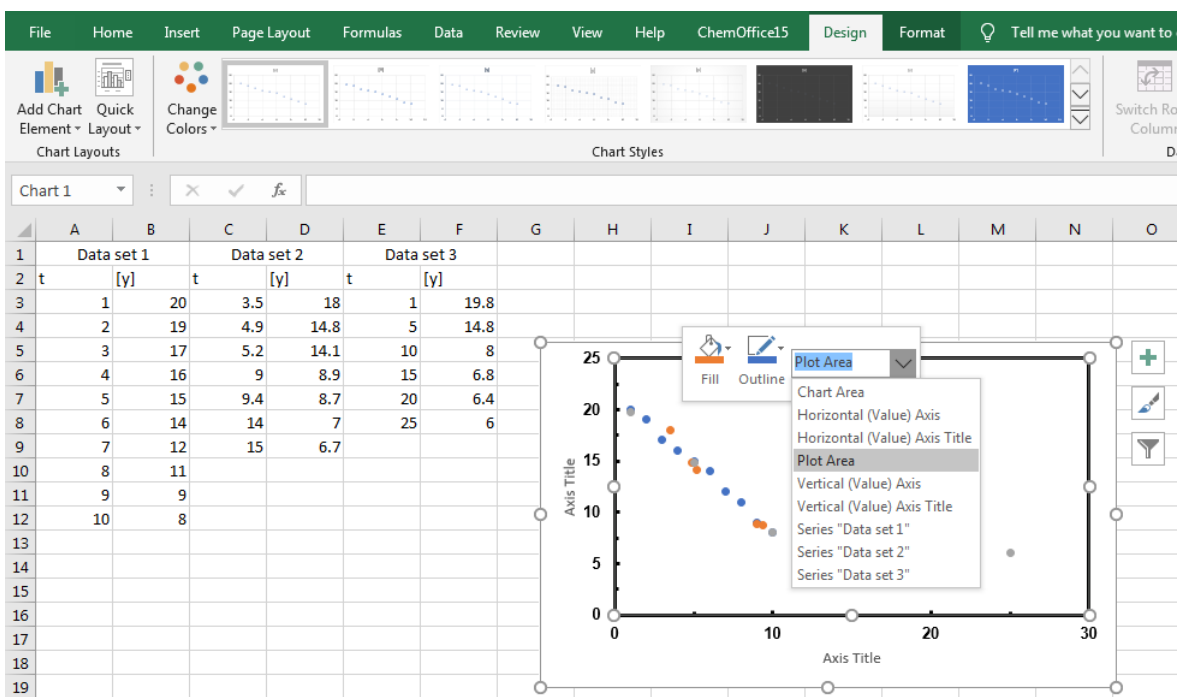
Figure D6. Adding chart elements and selecting chart elements to edit can be done by right clicking the plot.

Legends usually do not look particularly sleek; I find that adding in a single data label works better (right click only one data point and add a single data label). Color coding is your friend. Bolded letters and thick lines draw the reader to the center of the plot. Darker but contrasting colors for varied data sets work best. Use marker shapes in addition to this to create very easily distinguishable data sets. **Always add units to your axes.** Overall, your plot should look something like Figure D7, if you followed the settings described at the beginning of this guide. Usually plot titles are superfluous and distracting; most journals require figure captions which contain the plot titles. Notice how much prettier and visually engaging Figure D7 is when compared to the default plot generated (Figure D3). Generally, directly copy/pasting from Excel into Microsoft Word will generate an annoying editable figure. I prefer to past into Word as a .tiff or .jpg (or .bmp) file.
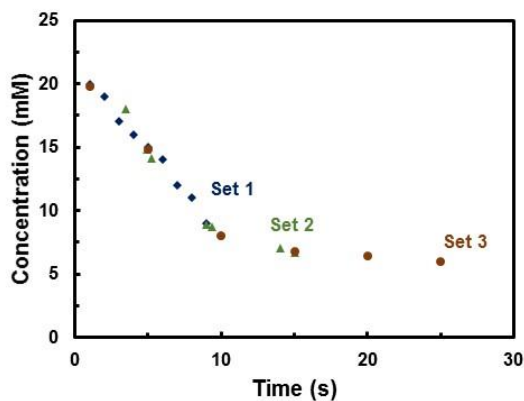
Figure D7. Final plot of the three data sets. More detail about the plot would go here, in the figure's caption.

Part II: Processing ¹H NMR Kinetics in MNova and Excel

Now that we have mastered the art of making pretty Excel plots on "fake" data, let's examine a real kinetics data set. For the purposes of this document, it is assumed that the NMR data has already been collected for the system of interest. Further, it is assumed that an internal standard has been added to ensure accurate integrations of the peaks of interest. In this example, $Si(SiMe_3)_4$ has been added as a standard. The two peaks of interest are given at 1.99 (starting material) and 2.07 ppm (product). After importing the data directly into MNova (drag and drop works just fine), the data should look something like Figure D8.
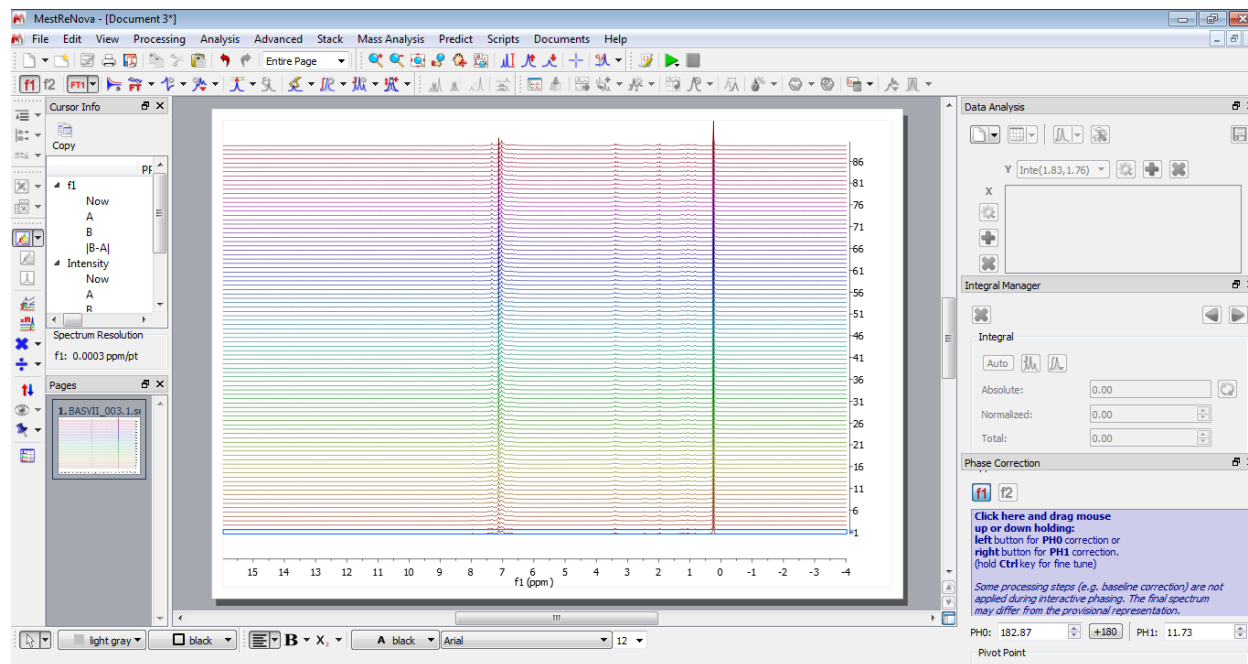
Figure D8. Stacked ¹H NMR spectra obtained from monitored kinetics experiments.

While the rainbow effect is visually intriguing, this view is not particularly effective at displaying the data for processing. To change the stack setting, click the stacked button on the right-hand menu bar (Figure D9, left). For the purposes of processing the data, superimposed works the best (Figure D9, right).
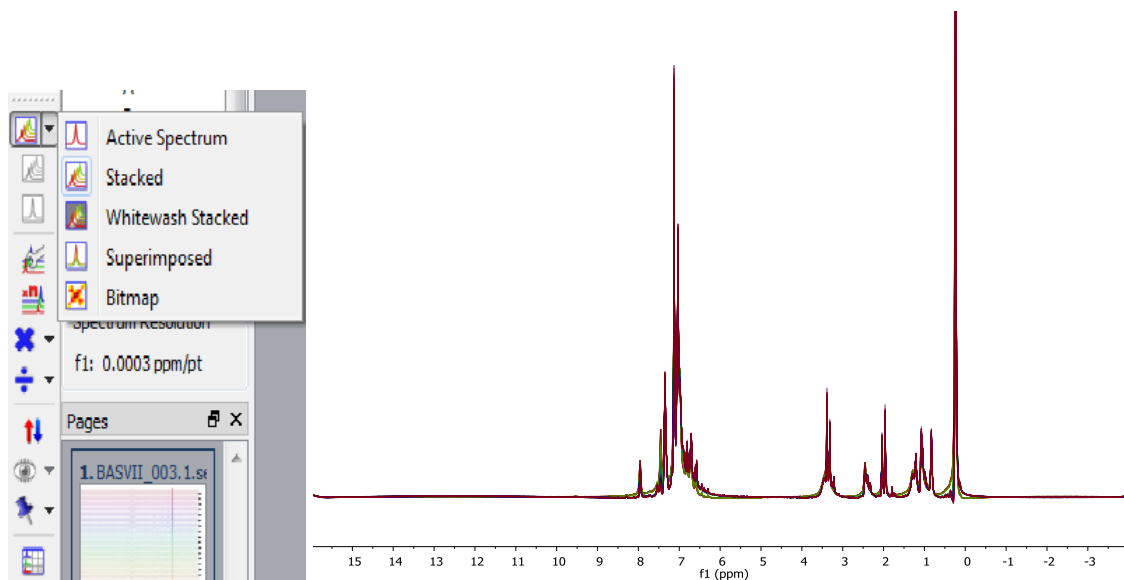
Figure D9. Left: Stack settings button. Superimposed (4th option from the top) makes data processing easier. **Right**: The resultant data is now superimposed.

From this view, reference the data to the residual solvent peak (this one is in benzene-d_6), automatically phase (unless you prefer by hand, but the automatic works well enough), and automatically baseline correct the data. Open the "Data Analysis" panel, which can be accessed under the "Panels" drop-down submenu on the "View" menu (Figure D10).
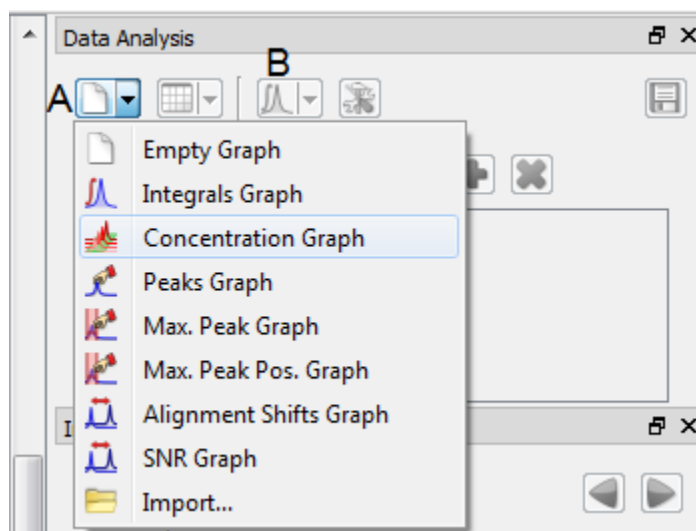
Figure D10. Data Analysis submenu. Under the pulldown menu labeled **A**, select "Integrals Graph" to create a new data series. The **B** button accesses an integral cursor so that new regions can be integrated.

In this menu, select the drop-down menu **A** and click the "Integrals Graph" option to switch to an integral cursor. Select a peak of interest and integrate it. This will generate a y/x plot above the spectra (Figure **D11**). In this example, peak "Y" corresponds to the $Si(SiMe_3)_4$ resonance.
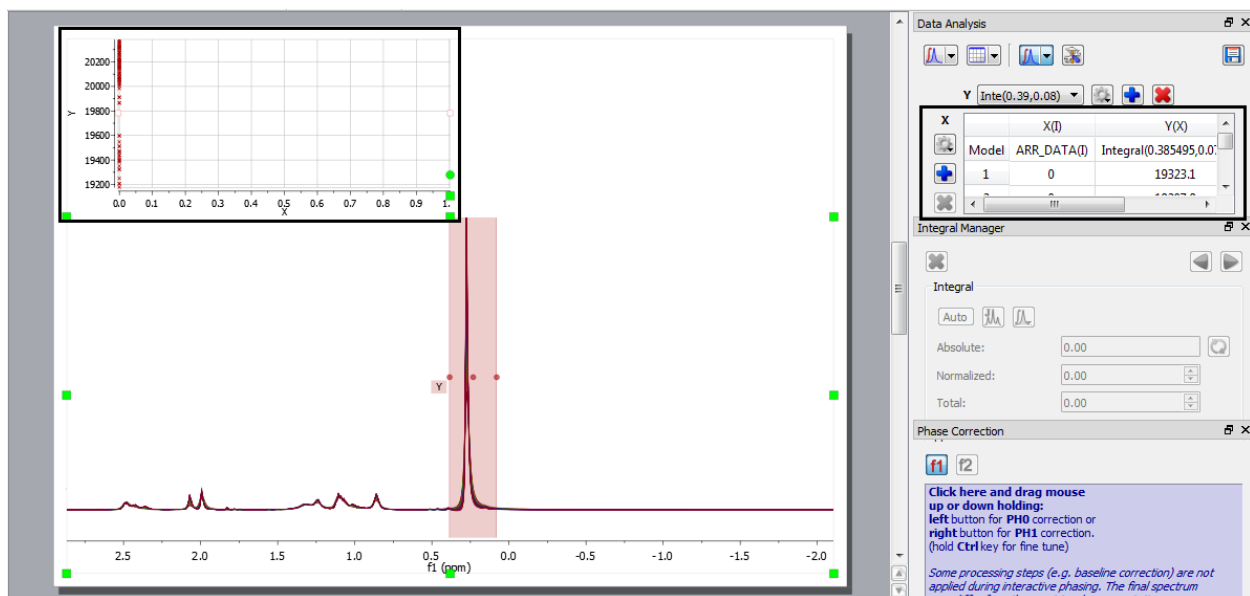
Figure D11. Integral graph and data table (highlighted with a black box) generated by integration of the Si(SiMe₃)₄ resonance at ca. 0.25 ppm.

Integrate all product or starting material resonances of interest by clicking the button labeled **B** in Figure D10. Clicking the **A** button again will only generate a new integrals graph and will not add another integral to the existing graph. *All integrations must be performed using the Data Analysis panel.* After all the relevant peaks have been integrated, the resultant spectra will appear similar to that described in Figure D12. In this example, peak "Y1" corresponds to a resonance in the starting material and "Y2" corresponds to a resonance in the product. While crude data manipulations can be performed in MNova, Excel (or an equivalent spreadsheet software) are better suited for the task. The data can be copied from MNova by selecting the "Report Table to Clipboard" option under the **C** menu in the Data Analysis panel.
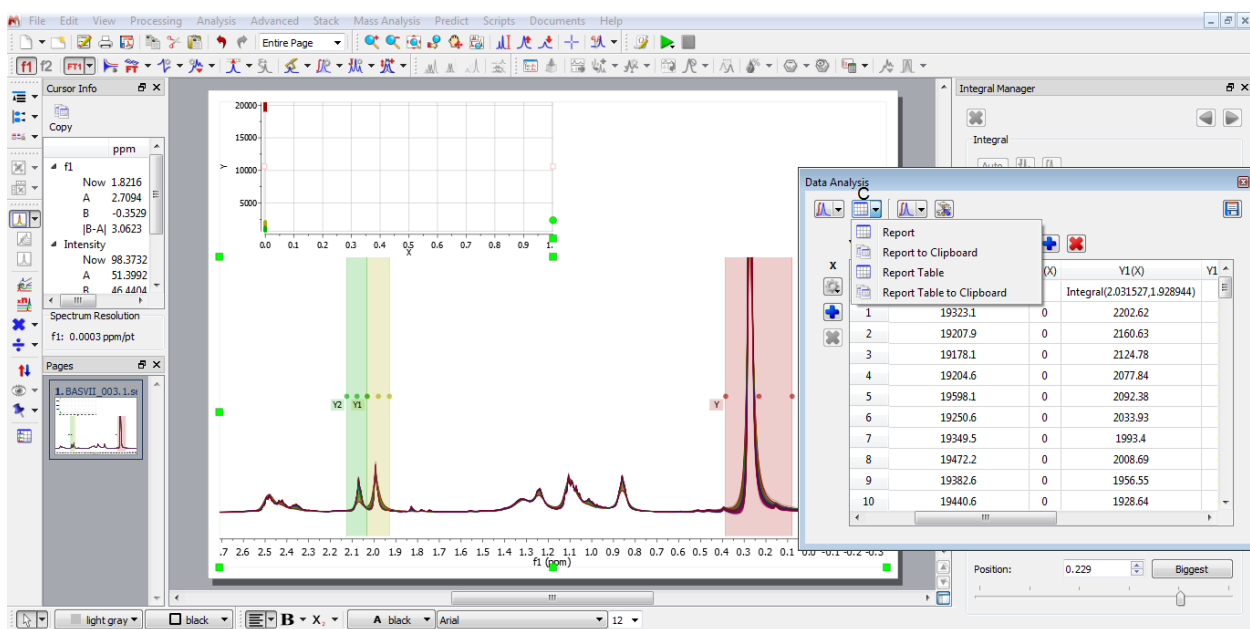
Figure D12. Final processed spectra with relevant product or substrate peaks integrated in the Data Analysis panel. Button **C** accesses a submenu where the data table may be copied to a clipboard to be pasted into Excel.

Paste (ctrl-p) the data directly into excel. Depending on how the data was acquired on the NMR spectrometer, the "X" column may have non-zero values. These correspond to the "time-stamp" on each of the stacked spectra. In this example, a long-multi pulse sequenced ^{1}H NMR experiment was performed; no "time-stamp" is added to the individual spectra, so it is essential to know the delay time between each scan (*i.e.*, d7 in the 1H kinetics parameter). In this experiment, a scan was taken every 20 seconds. The values in the generated table are absolute integration value; there is no physical meaning to these values on their own. Given that the concentration of the standard is a known, **and constant** value (*i.e.,* [Si(SiMe₃)₄]), the relative concentrations of any other species can be inferred. A relative integration can be calculated for each of the resonances of interest, as depicted in Figure D13. The form of each of these equations is depicted in line 2 of the spread sheet. ***It is vitally important that the number of protons corresponding to each resonance be known!*** In this example, the resonances for the starting material and product correspond to 3H each. The standard, Si(SiMe₃)₄, contains a 36H resonance.

A	B	C
time (s)	Relative Integral for Y1	Relative Integral for Y2
=G7*20	=(K7/3)/(I7/36)	=(M7/3)/(I7/36)
20	1.367870525	0.460301488
40	1.349837528	0.505911609
60	1.329503279	0.549209501
80	1.298333752	0.529810464
100	1.281170887	0.530249026
120	1.267861412	0.54613287
140	1.236253543	0.55654148
160	1.237884437	0.592624988
180	1.211325853	0.584409733
200	1.190480239	0.56146804
220	1.181116246	0.600046046
240	1.15480735	0.58266264
260	1.157972214	0.629650074
280	1.140676998	0.61248719
300	1.134160894	0.612275087
320	1.115909492	0.63518876
340	1.106266071	0.647686924
360	1.093548799	0.601455881
380	1.094417971	0.645111358
400	1.083273003	0.675460574

		Standard		Starting Matieral		Product	
#	X(I)	Y(X)	Y'(X)	Y1(X)	Y1'(X)	Y2(X)	Y2'(X)
Model	ARR_DATA(I)	Integral(0.385,0.080)		Integral(2.032,1.929)		Integral(2.125,2.032)	
1	0	19323.092	0	2202.624	0	741.204	0
2	0	19207.885	0	2160.627	0	809.791	0
3	0	19178.146	0	2124.784	0	877.735	0
4	0	19204.649	0	2077.837	0	847.902	0
5	0	19598.135	0	2092.38	0	865.991	0
6	0	19250.634	0	2033.928	0	876.117	0
7	0	19349.458	0	1993.403	0	897.398	0
8	0	19472.186	0	2008.693	0	961.642	0
9	0	19382.593	0	1956.553	0	943.948	0
10	0	19440.615	0	1928.639	0	909.607	0
11	0	19324.357	0	1902.026	0	966.292	0
12	0	19471.892	0	1873.857	0	945.462	0
13	0	19462.353	0	1878.072	0	1021.206	0
14	0	19419.678	0	1845.965	0	991.192	0
15	0	19400.221	0	1833.581	0	989.856	0
16	0	19548.123	0	1817.828	0	1034.729	0

Sheet1 | **Sheet2** | ⊕

Figure D13. Relative integrations for starting materials (column B) and products (column C) can be easily computed in Excel using the formulae given in line 2.

With the initial concentration of the standard known, the concentrations of starting material and product can be determined, as per the equations given in Figure D14. In this example, the concentration of [Si(SiMe₃)₄] was 12.5 mM (cell G2) and the initial concentration of "Y1" was 23 mM (cell K2).

| M3 | | fx | | |

	A	B	C	D	E	F	G	H	I	J	K	L	M	N
1	time (s)	Relative Integral for Y1	Relative Integral for Y2	[Y1], M	[Y2], M		Concentration of Si(SiMe3)4, M				Initial Concentration of Y1, M			
2	=G7*20	=(K7/3)/(I7/36)	=(M7/3)/(I7/36)	=B3*$G$2	=B3*$G$2		0.0125				0.023			
3	20	1.367870525	0.460301488	0.017098	0.005754									
4	40	1.349837528	0.505911609	0.016873	0.006324					Standard	Starting Matieral		Product	
5	60	1.329503279	0.549209501	0.016619	0.006865		#	X(I)	Y(X)	Y'(X)	Y1(X)	Y1'(X)	Y2(X)	Y2'(X)
6	80	1.298333752	0.529810464	0.016229	0.006623		Model	ARR_DATA(I)	Integral(0.385,0.080)		Integral(2.032,1.929)		Integral(2.125,2.032)	
7	100	1.281170887	0.530249026	0.016015	0.006628		1	0	19323.092	0	2202.624	0	741.204	0
8	120	1.267861412	0.54613287	0.015848	0.006827		2	0	19207.885	0	2160.627	0	809.791	0
9	140	1.236253543	0.55654148	0.015453	0.006957		3	0	19178.146	0	2124.784	0	877.735	0
10	160	1.237884437	0.592624988	0.015474	0.007408		4	0	19204.649	0	2077.837	0	847.902	0
11	180	1.211325853	0.584409733	0.015142	0.007305		5	0	19598.135	0	2092.38	0	865.991	0
12	200	1.190480239	0.56146804	0.014881	0.007018		6	0	19250.634	0	2033.928	0	876.117	0
13	220	1.181116246	0.600046046	0.014764	0.007501		7	0	19349.458	0	1993.403	0	897.398	0
14	240	1.15480735	0.58266264	0.014435	0.007283		8	0	19472.186	0	2008.693	0	961.642	0
15	260	1.157972214	0.629650074	0.014475	0.007871		9	0	19382.593	0	1956.553	0	943.948	0
16	280	1.140676998	0.61248719	0.014258	0.007656		10	0	19440.615	0	1928.639	0	909.607	0
17	300	1.134160894	0.612275087	0.014177	0.007653		11	0	19324.357	0	1902.026	0	966.292	0
18	320	1.115909492	0.63518876	0.013949	0.00794		12	0	19471.892	0	1873.857	0	945.462	0
19	340	1.106266071	0.647686924	0.013828	0.008096		13	0	19462.353	0	1878.072	0	1021.206	0
20	360	1.093548799	0.601455881	0.013669	0.007518		14	0	19419.678	0	1845.965	0	991.192	0
21	380	1.094417971	0.645111358	0.01368	0.008064		15	0	19400.221	0	1833.581	0	989.856	0
22	400	1.083273003	0.675460574	0.013541	0.008443		16	0	19548.123	0	1817.828	0	1034.729	0

Sheet1 Sheet2

Figure D14. Concentrations of starting materials (column D) and products (column E) are calculated using the initial concentration of standard and the relative integrals calculated in Figure D13.

The kinetic profile of the reaction described in this example can be generated using Part I of this guide (Figure D15). The slope generated from this is an approximation of the observed rate, $k_{initial}$. A detailed value can be obtained by applying the linest command. In this example, we use =linest(D3:D30, A3:A30, true) which will return a value of -7.87E-06. Recall that rates must be positive and this is a decay rate, so the value we have actually calculated is 7.8×10^{-6} M s^{-1}.

y = -8E-06x + 0.0167
R² = 0.96
Substrate
Product
Concentration (M) vs Time (s)
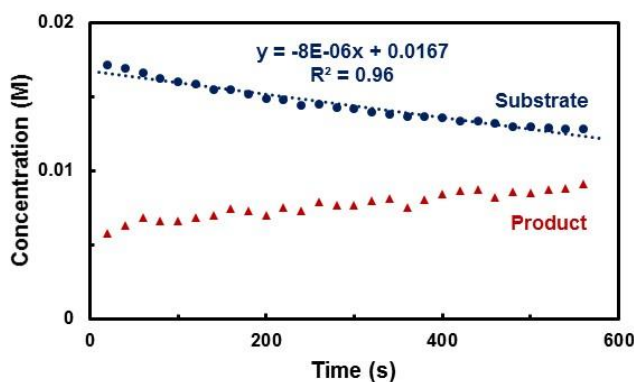
Figure D15. The resultant kinetic profile generated by the data described in this guide. The dotted blue line is the linear fit of the data described here.

Part III: Compiling Multiple Kinetics Data Sets and Extracting Rate Constants with Excel

With Parts I and II mastered, we shall apply it to a real data set (namely, the isomerization of *cis*-stilbene to *trans*-stilbene catalyzed by [(PPh$_3$)$_3$Co(N$_2$)]Li as described in Chapter Three). For the purposes of this guide, it is assumed that all the data has already been processed (see Part II). The kinetics data presented in this portion of the guide, the initial rate of isomerization was calculated at several different [*cis*-stilbene]$_0$ but at fixed [catalyst]$_0$ at 298 K with Si(SiMe$_3$)$_4$ as the standard. The initial rates were obtained from the linear fits of the kinetic profiles at initial time points (similar to that described in Figure D15). Using the data from each of these experiments, the rate constant k_{obs} can be determined (Figure D16). Two cells in each of the subtabs (labeled 007 data, 008 data, etc.) are required to generate a plot of $k_{initial}$ vs [*cis*-stilbene]$_0$.

The first cell is O1, where I have defined the initial *cis*-stilbene concentration. To directly call this value, use the equational form given in cell C2, but instead of '0xx data' apply the specific name of the data set in question (i.e. those given in column B). The second value is the $k_{initial}$ for each sub tab which is stored in cell L4 for each data set and can be called by the equation given in D4. However, this data was collected with units of 'min', so a simple conversion (and multiplication of 10^6) returns the desired value of $k_{initial}$ x 10^{-6} M s^{-1}.

	G11	f_x				
	A	B	C	D	E	F	G

	A	B	C	D	E	F	G
1			[*cis*-stilbene]$_0$, (M)	k_{init}, (M/min)	k_{init} x 10^{-6} (M/s)		
2		Data Set	='0xx data'!$O$1	='0xx data'!$L$4*-1	=D3*10^6/60	Equation Form	
3		007 data	0.065	6.36086E-06	0.106014348		
4		008 data	0.089	1.21224E-05	0.202039661		
5		009 data	0.180	1.97822E-05	0.329703171		
6		010 data	0.277	4.04194E-05	0.673656607		
7		011 data	0.494	8.78846E-05	1.464743494		
8							
9							
10		Equation Form	Returned Value	Units			
11	slope	=slope(E3:E7,C3:C7)		3.14 x 10^{-6} s^{-1}			
12	intercept	=intercept(E3:E7,C3:C7)		-0.14 x 10^{-6} M s^{-1}			
13	rsq	=RSQ(E3:E7,C3:C7)		0.98			
14							
15							
16							
17							
18							
19							

| ... | error | conc v kobs | 007 data | 008 data | 009 data | 010 data | 011 data | Sheet1 | ⊕ |

Figure D16. Compiled data for the isomerization of *cis*-stilbene to *trans*-stilbene. Note that the equation forms described in cells C2 and D2 the value of '0xx data' is replaced with the relevant tab name as given in the Data Set column, B.

A slope, intercept, and R^2 value are calculated from the data in C3:C7 and E3:E7 as described in the equations in B11, B12, and B13, respectively. The units have been added in manually. The plot of this data is given in Figure D17.
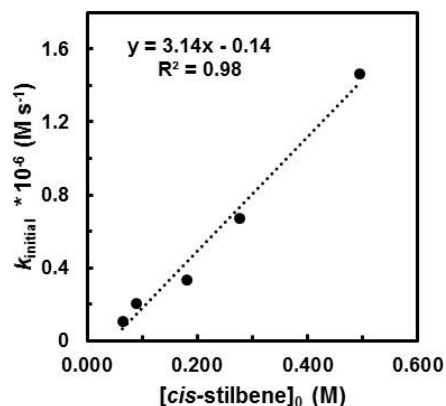
Figure D17. The relation between the initial rate and the initial concentration of *cis*-stilbene as calculated in this guide.

There exists one last feature of Excel that is useful for these purposes. This is the 'Regression' feature under in the Data Analysis package. First, the Data Analysis plugin needs to be installed. Fortunately, it comes default with Excel! Unfortunately, it needs to be activated. Open the 'Options' menu which is located at the bottom left corner under the 'File' tab of Excel. In the 'Options' menu, select the 'Add-ins' tab. This will open up the list of all active and inactive add-ins that are installed with your Excel program. From here, select the 'Go…' option (Figure D18).
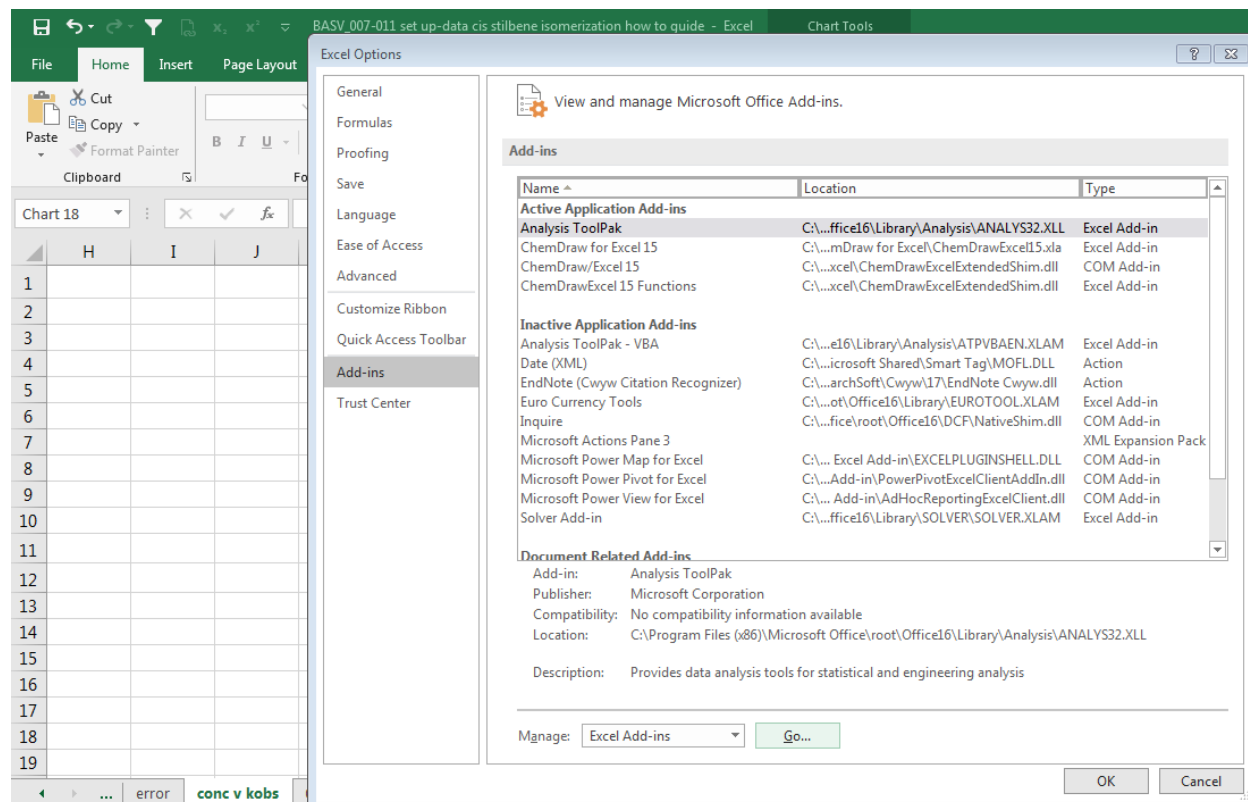
Figure D18. Excel 'Options' Menu with the 'Add-ins' tab active.

This will open a new option menu which displays all available add-ins. Select the 'Analysis ToolPak' option (Figure D19) then press OK.
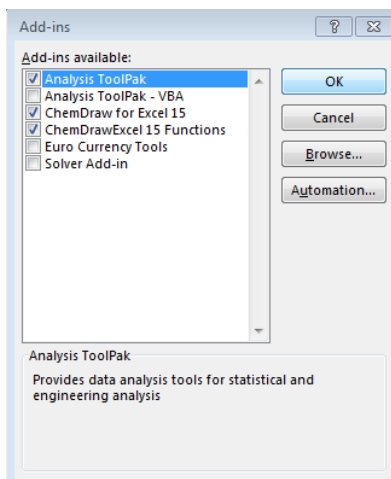
Figure D19. The 'Add-ins' Menu.

With the 'Analysis ToolPak' enabled, a new option under the 'Data' tab will appear (Figure D20). Press the 'Data Analysis' option and a new menu will open. This package has lots of fun statistical programs, but for this guide we will only use the 'Regression' option. Click OK and this will open a new prompt.
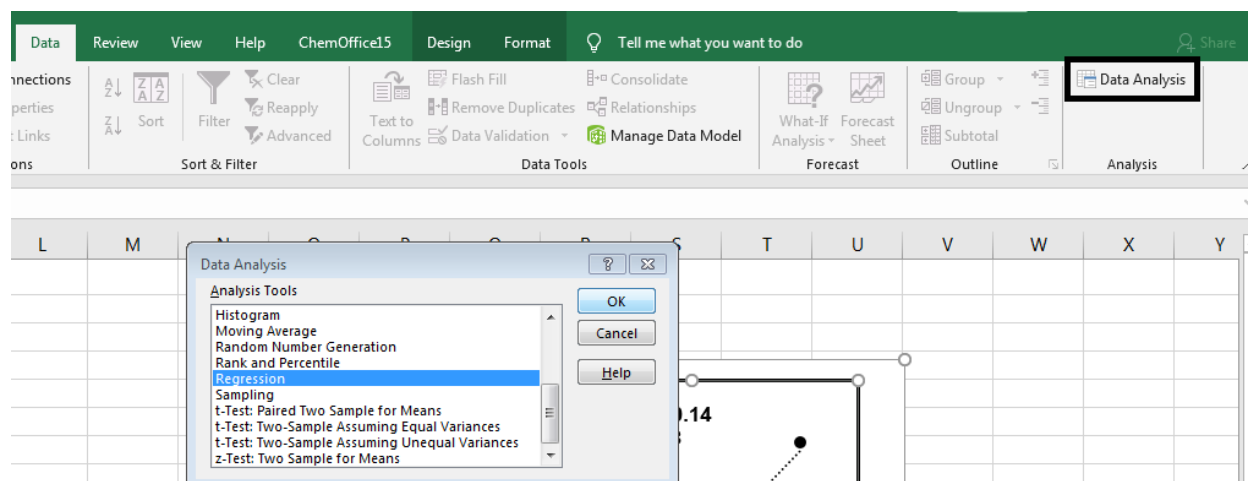
Figure D20. 'Data Analysis' Menu. Lots of fun statistical options exist, but for the purposes of this guide, only the 'Regression' option will be used.

In the new menu prompt (Figure D21) there are several parameters to be input in order to get out the desired regression data. There are lots of options that can be employed in the regression calculations, so feel free to explore all of them. Once ready, press OK.

C	D	E
[*cis*-stilbene]$_0$, (M)	k_{init}, (M/min)	k_{init} x 10^{-6} (M/s)
='0xx data'!$O$1	='0xx data'!$L$4*-1	=D3*10^6/60
0.065	6.36086E-06	0.106014348
0.089	1.21224E-05	0.202039661
0.180	1.97822E-05	0.329703171
0.277	4.04194E-05	0.673656607
0.494	8.78846E-05	1.464743494

Returned Value	Units
3.14	x 10^{-6} s^{-1}
-0.14	x 10^{-6} M s^{-1}
0.98	

Regression dialog:

Input
Input Y Range: $E$3:$E$7
Input X Range: $C$3:$C$7
☐ Labels   ☐ Constant is Zero
☑ Confidence Level: 95 %

Output options
○ Output Range:
◉ New Worksheet Ply:
○ New Workbook

Residuals
☐ Residuals   ☐ Residual Plots
☐ Standardized Residuals   ☐ Line Fit Plots

Normal Probability
☐ Normal Probability Plots

[OK] [Cancel] [Help]

Figure D21. The 'Regression' Menu. The data input are the calculated initial rates ($E$3:$E$7, and $C$3:$C$7).

A new Excel sheet is generated with LOTS of statistical information about the linear regression. The most important of these have been highlighted in Figure D22 in light blue. The R^2 and number of data points included are given in cells B5 and B8, respectively. The Y-i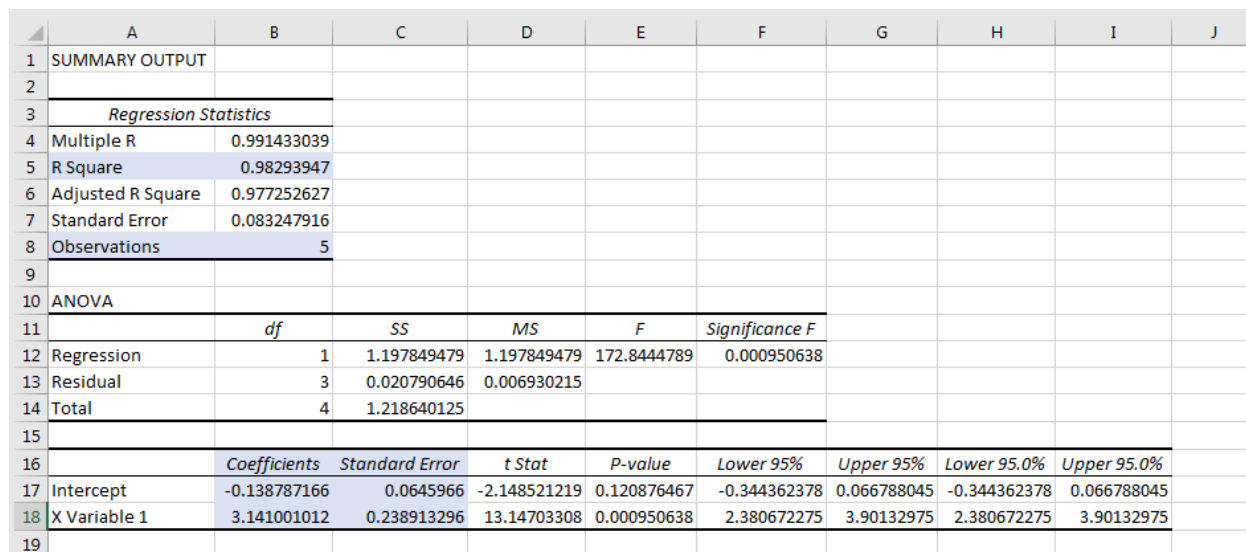ntercept and slope are given in cells B17 and B18. Notice how they match the values calculated using the 'slope' and 'intercept' functions. The standard errors of these values are given in cells C17 and C18. Therefore, our k_{obs} value has been calculated to be 3.14(24) x 10^{-6} s^{-1} with the error given in parenthesis. Pretty neat, huh!

	A	B	C	D	E	F	G	H	I	J
1	SUMMARY OUTPUT									
2										
3	*Regression Statistics*									
4	Multiple R	0.991433039								
5	R Square	0.98293947								
6	Adjusted R Square	0.977252627								
7	Standard Error	0.083247916								
8	Observations	5								
9										
10	ANOVA									
11		*df*	*SS*	*MS*	*F*	*Significance F*				
12	Regression	1	1.197849479	1.197849479	172.8444789	0.000950638				
13	Residual	3	0.020790646	0.006930215						
14	Total	4	1.218640125							
15										
16		*Coefficients*	*Standard Error*	*t Stat*	*P-value*	*Lower 95%*	*Upper 95%*	*Lower 95.0%*	*Upper 95.0%*	
17	Intercept	-0.138787166	0.0645966	-2.148521219	0.120876467	-0.344362378	0.066788045	-0.344362378	0.066788045	
18	X Variable 1	3.141001012	0.238913296	13.14703308	0.000950638	2.380672275	3.90132975	2.380672275	3.90132975	
19										

Figure D22. Regression statistics for the linear fit of the data in this guide.

"So Long, and Thanks for All the Fish"
–   **Douglas Adams**